SCHOLARLY PUBLICATIONS

A CURRENT AWARENESS BULLETIN
OF RESEARCH OUTPUT

@DTU

(25th Edition)

JANUARY 2015

BY: CENTRAL LIBRARY

DELHI TECHNOLOGICAL UNIVERSITY
(FORMERLY *DELHI COLLEGE OF ENGINEERING)*
GOVT. OF N.C.T. OF DELHI
SHAHBAD DAULATPUR, MAIN BAWANA ROAD
DELHI 110042

PREFACE

This is the **Twenty fifth** Issue of Current Awareness Bulletin started by Delhi Technological University, Central Library. The aim of the bulletin is to compile, preserve and disseminate information published by the faculty, students and alumni for mutual benefits. The bulletin also aims to propagate the intellectual contribution of Delhi Technological University (DTU) as a whole to the academia.

The bulletin contains information resources available in the internet in the form of articles, reports, presentations published in international journals, websites, etc. by the faculty and students of DTU. The publications of faculty and student which are not covered in this bulletin may be because of the reason that the full text either was not accessible or could not be searched by the search engine used by the library for this purpose.

The learned faculty and students are requested to provide their uncovered publications to the library either through email or in CD, etc to make the bulletin more comprehensive.

This issue contains the information published during **January 2015**. The arrangement of the contents is alphabetical. The full text of the article which is either subscribed by the university or available in the web is provided in this bulletin.

Central Library

CONTENTS

1. A High-Fidelity, Computationally Efficient Model for Interior Permanent Magnet Machines Considering the Magnetic Saturation, Spatial, Harmonics and Iron Loss Effect, Xiao Chen, Jiabin Wang, ***8.1.Bhaskar Sen***, Panagiotis Lazari, and Tianfu Sun

2. A Novel Method of Modeling Wireless Sensor Network Using Fuzzy Graph and Energy Efficient Fuzzy Based, k-Hop Clustering Algorithm, ***7.1.Aarti Jain***, Electronics and Communication, DCE. and B. V. Ramana Reddy

3. An Ontology based Framework for Automatic Detection and Updation of Requirement Specifications, MPS Bhatia, Rohit Beniwal and ***3.Akshi Kumar***, Computer Engineering, DTU

4. Assessing Nutraceutical Alpha Ketoglutarate for Its Effectiveness: 99m Technetium-Mebrofenin Nuclear Imaging in CCl4 Induced, Hepatotoxic Animal Model, Lalita Mehra, Amit Kumar, Aseem Bhatnagar, ***3.Yasha Hasija***, and Gaurav Mittal

5. Cancerous Cell Detection Using Histopathological Image Analysis, Aashna Jain, ***8. Shwetal Atey***, Satender Vinayak, Varun Srivastava, Computer Science, DTU

6. Characterization of Signed Graphs whose Iterated Signed Line Graphs are Balanced or S□ Consistent, Deepa Sinha and ***3. Mukti Acharya***, Applied Mathematics, DTU

7. COMMODITY FUTURES MARKET EFFICIENCY AND RELATED ISSUES: A REVIEW OF EXISTING LITERATURE, ***3. Archana Singh***, DSM

8. Energy and Exergy Analysis of Organic Rankine Cycle Using Alternative Working Fluids, Deepak Tiwari, Akhilesh Arora, ***3. Naushad Ahmad Ansari*** and Dr. A. F. Sherwani, Mechanical Engineering, DTU

9. E-Waste characteristic and its disposal, M. C. Vats and ***3. S. K. Singh***, DTU

10. Facile Synthesis of 2-Dimensional Transparent Graphene Flakes for Nucleic Acid Detection, Maumita Das Mukherjee Chetna Dhand Neeraj, Dwivedi Baijnath P. Singh Gajjala Sumana Ved V. Agarwal Jai, S. Tawale and ***3. Bansi D. Malhotra***, Biotechnology, DTU

11. FemA gene in Indian isolates of methicillin resistant Staphylococcus aureus – isolation and amplification through real time PCR, ***3. Shashank Kr. Singh***, Saleha Anwar, Hemant Kr. Sharma, Upendra Chaudhary and Sunil Kr. Verma, Biotechnology, DTU

12. Hydrodynamic Stability of Complaint Pipe for Normal Complaince, ***3. S. Anbukumar*** and ***3. Munendra Kumar***, Civil Engineering, DTU

13. In silico Designing and Optimization of EPO Mimetic Using Combinatorial Library ***3. Vimal Kishor Singh, 6. Neeraj Kumar, 6. Manisha Kalsan IB*** and ***6. Abhishek Saini***, Biotechnology, DTU

14. Induced Pluripotent Stem Cells: Applications in regenerative medicine, disease modelling and drug discovery, ***3.Vimal Kishor Singh, 3. Manisha Kalsan, 3. Neeraj Kumar, 3. Abhishek Saini,*** Biotechnology, DTU and Ramesh Chandra

15. National Conference on Advances in Materials Science for Energy Applications **(NO2 Sensing Properties of WO3 Thin Films Deposited by Rf-Magnetron Sputtering)** (from page no. 27 onwards) **by** ***3. Savita Sharma*****,** Monika Tomar**,** ***3. Nitin K. Puri*** and Vinay Gupta**,** Applied Physics, DTU

16. NOx Sensing properties of Barium Titanate thin films, ***3. S. Sharma***, A. Sharma, M. Tomar, ***3. N. K. Puri*** and V. Gupta, Applied Physics, DTU

17. On the significance of Non-Extensivity for the Dynamic Growth of Hidden-Layer Neurons, ***3. Seba Susan*** and ***3. Mayank Dwivedi***, Information Technology, DTU

18. Optical studies of Sm3+ ions doped Zinc Alumino Bismuth Borate glasses, K. Swapna, Sk. Mahamuda, ***3.A. Srinivasa Rao***, Applied Physics, DTU, S. Shakya, T. Sasikala, D. Haranath, G. Vijaya Prakash

19. Optimization of Production and Performance of Biodiesel through Optimization Techniques: A Review, Ashok Kumar Yadav, ***3. Amit Pal***, Mohd. Emran Khan, Mechanical Engineering, DTU

20. Phase Shifting Transformers can Optimizes the Transmission Infrastructure, Reduces the Losses, Improves Grid Stability, Reduces Congestion, Changes the Active & Reactive Power flow both in Magnitude and Direction, ***6. Shagufta Khan***, DTU and M.I. Khan

21. POLICY FOR MINIMIZATION OF SCRAP IN A PRODUCTION LINE WITH IMMEDIATE FEEDBACK AND MULTI SERVER WORKSTATIONS Abhimanu S. and ***3.1. Datta C.K***, Production Engineering, DTU

22. Review of the Concentrated Solar Thermal Technologies: Challenges and Opportunities in India, ***3. Dr. J.P Kesari, 3. Mohit Gupta, 3. Aadish Jain***, Mechanical Engineering, DTU and A.K Ojha

23. Simulation Modelling and Analysis of Network Design for Closed-Loop Supply Chain: A Case Study of Battery Industry, A. Jayanta, ***3. P.Gupta*** and S.K.Garg, Mechanical Engineering, DTU

24. STATISTICAL CONVERGENCE FOR GENERAL BETA OPERATORS, ***3. Naokant Deo***, Applied Mathematics, DTU, Mehmet Ali Ozarslan, and Neha Bhardwaj

25. Steady State Thermal Analysis of Gas Turbine Power Plant Cycles at Higher Temperatures, A Kumar, S S Kachhwaha and ***3. R S Mishra***, Mechanical Engineering, DTU

26. Supervised Pixel Classification into Arteries and Veins of Retinal Images, ***3. Smriti Chhabra*** and ***3. Bharat Bhushan***, Electrical Engineering, DTU

27. THEFT DETECTION SCHEMES FOR SMART GRID APPLICATION, ***3. Palak Kalra,*** Electrical Engineering, DTU

28. TOPSIS-AHP Based Approach for Selection of Reverse Logistics Service Provider: A Case Study of Mobile Phone Industry, A. Jayanta, P.Gupta, ***3. S.K.Garg***, M.Khan, Mechanical Engineering, DTU

29. Trait association analysis for yield and yield attributing traits in niger germplasm, (In-vitro propagation of endangered medicinal herb Chlorophytum borivilianum Sant and Fern., ***3. Nupur Jauhari, K. Lavanya, Navneeta Bharadvaja*** and Neelam Sharma) (from page no. 43 onwards), Biotechnology, DTU

30. Variation in Parameters of Ambient Air Quality in National Capital Territory (NCT) of Delhi (India), ***3.Anunay A. Gour, 3.Santosh K. Singh,*** Sushil K. Tyagi, ***3.Anubha Mandal***, Environmental Engineering, DTU

1. Vice Chancellor	***1.1. Ex Vice Chancellor***
2. Pro Vice Chancellor	***2.1. Ex Pro Vice Chancellor***
3. Faculty	***3.1. Ex Faculty***
4. Teaching-cum-Research Fellow	
5. Alumni	
6. Research Scholar	***6.1. Ex Research Scholar***
7. PG Scholar	***7.1. Ex PG Scholar***
8. Undergraduate Student	***8.1. Ex Undergraduate Student***

This article has been accepted for publication in a future issue of this journal, but has not been fully edited. Content may change prior to final publication. Citation information: DOI 10.1109/TIE.2014.2388200, IEEE Transactions on Industrial Electronics

A High-Fidelity, Computationally Efficient Model for Interior Permanent Magnet Machines Considering the Magnetic Saturation, Spatial Harmonics and Iron Loss Effect

Xiao Chen, *Student Member, IEEE*, Jiabin Wang, *Senior Member, IEEE*, Bhaskar Sen, *Student Member, IEEE*, Panagiotis Lazari, *Student Member, IEEE*, and Tianfu Sun

***Abstract*—Interior Permanent Magnet (IPM) machines exhibit relatively large spatial harmonics in phase voltages and high non-linearity in torque production due to both the presence of reluctance torque and the magnetic saturation in stator and rotor cores. To simulate the real electromagnetic behavior of IPM machines, this paper proposes a high-fidelity and computationally efficient machine model considering the magnetic saturation, spatial harmonics and iron loss effect, based on the inverse solution of the flux linkages extracted via Finite Element Analysis (FEA). Neither FEA nor derivative computation is involved in the time-stepping simulation, and thereby the proposed model is computationally efficient and numerically robust. The high fidelity of the proposed machine model is validated by both the FEA and experimental results.**

***Index Terms*—Finite element analysis, interior permanent magnet machines, machine modeling, magnetic saturation, spatial harmonics, iron loss effect.**

NOMENCLATURE

i_d	d-axis current
i_q	q-axis current
J	Rotor inertia
L_d	d-axis inductance
L_q	q-axis inductance
m	Number of phases
p	Number of pole pairs
R_s	Synchronous resistance
s	Derivative operator
t	time
T_{em}	Electromagnetic torque
T_L	Load torque
V_d	d-axis voltage
V_q	q-axis voltage
θ	Rotor position angle
Ψ_d	d-axis flux linkage
Ψ_q	q-axis flux linkage
Ψ_m	Permanent magnet flux linkage
ω	Angular speed in mechanical degree
ω_e	Angular speed in electrical degree

Manuscript received July 21, 2014; revised November 2, 2014; accepted November 29, 2014.

Copyright (c) 2014 IEEE. Personal use of this material is permitted. However, permission to use this material for any other purposes must be obtained from the IEEE by sending a request to pubs-permissions@ieee.org.

The authors are with the Department of Electronic and Electrical engineering, The University of Sheffield, Sheffield, S1 3JD United Kingdom (e-mail: x.chen.1988@ieee.org; j.b.wang@sheffield.ac.uk; elp11bs@sheffield.ac.uk; panos.lazari@sheffield.ac.uk; tianfu.sun@foxmail.com).

I. INTRODUCTION

PERMANENT Magnet Synchronous Machines (PMSMs) exhibit high torque density and high energy efficiency due to the fact that the magnetic field which facilitates electromechanical energy conversion is mainly produced by permanent magnets [1, 2]. Therefore, they have increasingly been employed in a variety of applications [3-5], such as industrial drives, hybrid and electric vehicles, wind turbine, aerospace, marine, and domestic appliances, etc.

In PMSMs, Surface-mounted Permanent Magnet (SPM) machines only have alignment torque component which results from the interaction of the permanent magnet field with armature currents [6]. The effective air-gap seen by the stator winding is relatively large, being equal to the sum of the air-gap and magnet thickness and hence the armature reaction is not very significant. Further, the winding inductance is virtually independent of rotor position. Therefore, it is relatively simple to model and control SPM machines. However, the magnet usage in SPM machines tends to be large due to absence of reluctance torque contribution [7]. SPM machines are less favored in applications which require a wide constant power operating range [8].

To improve field weakening capability and to reduce demand on permanent magnets, Interior Permanent Magnet (IPM) machines, including both conventional IPM machines with rare-earth materials and the Permanent Magnet Assisted Synchronous Reluctance Machines (PMA-SynRMs), have been employed [9, 10]. However, the presence of reluctance torque in IPM machines not only results in the non-linear relationship between the electromagnetic torque and the armature current, but also leads to more spatial harmonics in

0278-0046 (c) 2013 IEEE. Personal use is permitted, but republication/redistribution requires IEEE permission. See http://www.ieee.org/publications_standards/publications/rights/index.html for more information.

This article has been accepted for publication in a future issue of this journal, but has not been fully edited. Content may change prior to final publication. Citation information: DOI 10.1109/TIE.2014.2388200, IEEE Transactions on Industrial Electronics

phase voltages due to the inherently large variation in magnetic energy with rotor position [11, 12]. Therefore, the conventional model using constant *d*- and *q*-axis inductances cannot accurately represent the IPM machine behavior if the spatial harmonics and the magnetic saturation effect in stator and rotor cores are neglected [13], particularly in the field weakening region where the phase voltage harmonics will result in distorted current waveforms due to the limited DC link voltage.

To improve the IPM model fidelity, the circuit-field coupled co-simulation was employed in [13-15]. This approach is, however, very time-consuming due to the involvement of numerical Finite Element (FE) analysis. To avoid the FE computation in the simulation process, the *d*- and *q*-axis flux linkage variations with *d*- and *q*-axis currents and the rotor position were established via Finite Element Analysis (FEA) and the results were treated as curve fitted functions in the drive system simulation in [16]. However, it was necessary to compute the derivatives of the flux linkages with voltage inputs, resulting in the algebraic loop and numerical instability, particularly in a drive simulation system with switching devices. To avoid the derivative computation, the *d*- and *q*-axis current variations with *d*- and *q*-axis flux linkages and the rotor position were obtained by performing the inverse of the flux linkages as functions of currents and rotor position computed from FEA in [17-19]. However, the cross-coupling saturation effect was not included in [17], the order of the spatial harmonics considered in flux linkages was limited to 3 in [18], and the resultant torque was not validated in [19]. Moreover, the iron loss effect on the machine electromagnetic behavior has not been considered in these models [13-19], thereby compromising the model fidelity, particularly in the field weakening region where the iron loss is significant and the voltage is limited.

This paper proposes a high-fidelity and computationally efficient model for IPM machines considering the magnetic saturation in the stator and rotor cores, spatial harmonics in phase voltages, and the influence of iron loss on the machine electromagnetic behavior, based on the inverse solution of the flux linkages extracted via FEA. It has been shown that the torque ripple of an IPM machine drive will be significantly increased in field weakening operation due to large current control error with limited available voltage, and this performance deterioration cannot be predicted by conventional modeling approaches.

II. Conventional IPM Machine Model

In literature, the conventional approach to modeling a PMSM is based on the *d*- and *q*-axis voltage and torque equations shown in (1). The corresponding machine model schematic is illustrated in Fig. 1.

$$\begin{aligned} V_d &= L_d \frac{di_d}{dt} + R_s i_d - \omega_e L_q i_q \\ V_q &= L_q \frac{di_q}{dt} + R_s i_q + \omega_e \left(\Psi_m + L_d i_d \right) \\ T_{em} &= \frac{m}{2} p \left[\Psi_m i_q + \left(L_d - L_q \right) i_d i_q \right] \end{aligned} \tag{1}$$

where, *d*-axis inductance L_d, *q*-axis inductance L_q and permanent magnet flux linkage Ψ_m are the functions of both *d*-axis current i_d and *q*-axis current i_q, to take into account the magnetic saturation effect.

However, the conventional machine model only captures the effect of fundamental components whereas harmonic fields resulting from the combination of the magnetic saturation, slotting and permeance variation with rotor position are neglected. Secondly, the separation of $L_d i_d$ and Ψ_m from FE-predicted or measured *d*-axis flux linkage cannot be performed accurately under saturation since the superposition principle is no longer valid. Inaccurate machine model not only affects the performance prediction of the drive system, but also seriously compromises the quality of model-based control for maximum torque per ampere (MTPA) and field weakening operations.

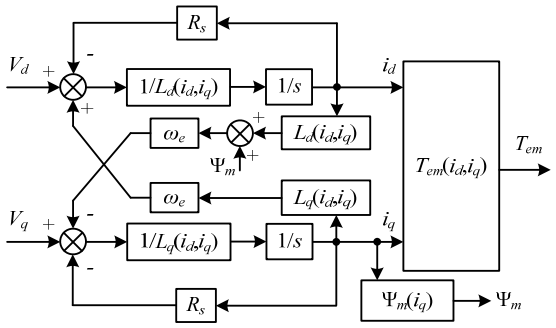


Fig. 1. Conventional IPM machine model schematic.

III. Proposed IPM Machine Model

A. Proposed IPM Machine Model

To address the problems associated with the conventional model as discussed in section II, a flux linkage-based machine model, as described by (2), (3) and (4), is employed.

$$\begin{aligned} V_d &= \frac{d\Psi_d}{dt} + R_s i_d - \omega_e \Psi_q \\ V_q &= \frac{d\Psi_q}{dt} + R_s i_q + \omega_e \Psi_d \end{aligned} \tag{2}$$

$$\begin{aligned} \Psi_d &= f\left(i_d, i_q, \theta \right) \\ \Psi_q &= g\left(i_d, i_q, \theta \right) \end{aligned} \tag{3}$$

$$T_{em} = \frac{m}{2} p \left(\Psi_d i_q - \Psi_q i_d \right) \tag{4}$$

where, *d*- and *q*-axis flux linkages Ψ_d, Ψ_q are the functions of the *d*- and *q*-axis currents i_d, i_q and the rotor position θ. Thus, the effects of both magnetic saturation and the spatial harmonic fields are inherently included in the above flux linkage functions.

Furthermore, to avoid the derivative calculation, the *d*- and *q*-axis flux linkages can be obtained by integration given in (5).

$$\begin{aligned} \Psi_d &= \int \left(V_d - R_s i_d + \omega_e \Psi_q \right) dt \\ \Psi_q &= \int \left(V_q - R_s i_q - \omega_e \Psi_d \right) dt \end{aligned} \tag{5}$$

By performing inverses of (3) at a given rotor position, the *d*- and *q*-axis currents are determined by (6).

0278-0046 (c) 2013 IEEE. Personal use is permitted, but republication/redistribution requires IEEE permission. See http://www.ieee.org/publications_standards/publications/rights/index.html for more information.

This article has been accepted for publication in a future issue of this journal, but has not been fully edited. Content may change prior to final publication. Citation information: DOI 10.1109/TIE.2014.2388200, IEEE Transactions on Industrial Electronics

$$i_d = f^{-1}\left(\Psi_d, \Psi_q, \theta\right)$$
$$i_q = g^{-1}\left(\Psi_d, \Psi_q, \theta\right) \quad (6)$$

To capture all the torque components, including cogging torque which is present even with zero currents [20], the electromagnetic torque computed from FEA can be written as a function of *d*- and *q*-axis currents i_d, i_q and the rotor position θ in (7).

$$T_{em} = T\left(i_d, i_q, \theta\right) \quad (7)$$

All the functions in (6) and (7) can be established by either 3-D lookup tables or curve fitting. The electromagnetic part of the proposed machine model schematic is illustrated in Fig. 2.

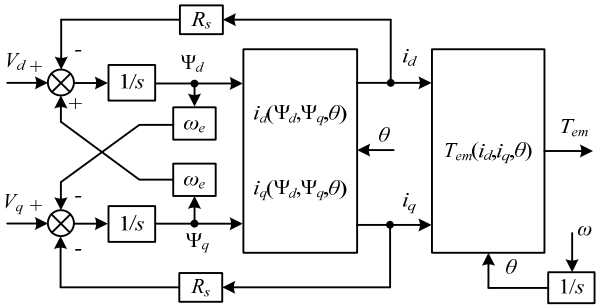


Fig. 2. Schematic of proposed electromagnetic model of IPM machines.

As shown in Fig. 2, for a given voltage, the *d*- and *q*-axis flux linkages Ψ_d and Ψ_q are calculated by the integrals in (5). Subsequently, the *d*- and *q*-axis current i_d and i_q are obtained from the functions $i_d(\Psi_d,\Psi_q,\theta)$ and $i_q(\Psi_d,\Psi_q,\theta)$ with the *d*- and *q*-axis flux linkages Ψ_d, Ψ_q, and rotor position θ as the inputs. The resultant electromagnetic torque is acquired from $T_{em}(i_d,i_q,\theta)$. Finally, the angular speed and position of the rotor can be calculated via the mechanical motion equations. It should be noted that the proposed model includes all effects due to magnetic saturation in the stator and rotor cores and spatial harmonics in the magneto-motive force (MMF), as well as torque ripple from variation of magnetic co-energy with rotor position.

To accurately represent the electromagnetic behavior of a PMSM machine, all the variations of *d*- and *q*-axis flux linkages and torque with *d*- and *q*-axis currents and rotor position, viz. $\Psi_d(i_d,i_q,\theta)$, $\Psi_q(i_d,i_q,\theta)$ and $T_{em}(i_d,i_q,\theta)$, are obtained via FEA or measurements. However, to implement the proposed model shown in Fig. 2, the *d*- and *q*-axis currents, viz. $i_d(\Psi_d,\Psi_q,\theta)$ and $i_q(\Psi_d,\Psi_q,\theta)$, as functions of Ψ_d, Ψ_q, and θ need to be obtained through the inverse of $\Psi_d(i_d,i_q,\theta)$, $\Psi_q(i_d,i_q,\theta)$. This process is described in the following section.

B. Inverse Solution of Currents versus Flux Linkages

Without loss of generality, a 36-slot 6-pole IPM machine prototype is employed to demonstrate the process and the effectiveness of the proposed modeling technique. The machine specifications and design parameters are listed in Table I and the schematic is shown in Fig. 3.

The *d*- and *q*-axis flux linkages and torque $\Psi_d(i_d,i_q,\theta)$, $\Psi_q(i_d,i_q,\theta)$ and $T_{em}(i_d,i_q,\theta)$ as functions of i_d, i_q, and θ are obtained via FEA by varying i_d, i_q and θ in the ranges of -140~140A, -240~240A and 0~120° (0~360° in electrical degree), respectively. The i_d, i_q and θ samples in FE calculation are 15, 25 and 97 respectively, and hence the total FE steps are 36,375. The off-line computation time to set up $\Psi_d(i_d,i_q,\theta)$, $\Psi_q(i_d,i_q,\theta)$ and $T_{em}(i_d,i_q,\theta)$ is approximately 32 hours on a quad-core 3.1GHz PC. The computation time also depends on the periodicity condition and mesh density of the FE model.

TABLE I
SPECIFICATIONS AND DESIGN PARAMETERS OF THE MACHINE PROTOTYPE

Quantity	Unit	Value
Peak torque	Nm	70
Rated torque	Nm	35.5
Base Speed	r/min	1350
Max Speed	r/min	4500
Peak power	kW	9.9
Rated power	kW	5
DC link voltage	V	120
Peak current	A	125
Number of pole-pairs	--	3
Number of slots	--	36
Active stack length	mm	118
Stator outer diameter	mm	150
Rotor outer diameter	mm	80

The *d*- and *q*-axis flux linkages and torque maps versus *d*- and *q*-axis currents at 0° rotor position referred to phase *A* axis are shown in Fig. 4, whilst the variations of the *d*- and *q*-axis flux linkages and torque with rotor position at i_d=-40A and i_q=60A are illustrated in Fig. 5. The magnetic saturation effect is evident in Fig. 4 and the spatial harmonics in the flux linkages and torque can be observed in Fig. 5. It should be noted that torque ripple exists even with constant *d*- and *q*-axis currents or sinusoidal phase currents. This ripple is present in a real IPM machine, but cannot be predicted by the conventional model in (1).

Based on the $\Psi_d(i_d,i_q,\theta)$ and $\Psi_q(i_d,i_q,\theta)$ maps at a given θ, i_d and i_q can be uniquely found. The solution to the inverse problem, viz., equation (6), can be obtained via the minimization of the residual flux linkage magnitude Ψ_{eq}, defined in (8).

$$\Psi_{eq} = \left|\Psi_d\left(i_d, i_q, \theta_0\right) - \Psi_{d0}\right| + \left|\Psi_q\left(i_d, i_q, \theta_0\right) - \Psi_{q0}\right| \quad (8)$$

where, the Ψ_{d0} and Ψ_{q0} are the given *d*- and *q*-axis flux linkages at θ_0, and Ψ_d and Ψ_q are obtained from the flux linkage maps with iterative solutions of the *d*- and *q*-axis currents as the inputs at the same rotor position.

To minimize Ψ_{eq}, the unknown i_d and i_q are found through an iterative process until the objective function Ψ_{eq} reduces to the required tolerance. During this process, $\Psi_d(i_d,i_q,\theta_0)$ and $\Psi_q(i_d,i_q,\theta_0)$ are calculated via the 2-D interpolation on the original flux linkage maps. The employed minimization algorithm is the interior-point method [21]. The computation time needed to build (6) is approximately 1 hour on a quad-core 3.1GHz PC.

The resultant *d*- and *q*-axis current variations are shown in Fig. 6 and Fig. 7. Fig. 6 depicts the *d*- and *q*-axis current maps versus *d*- and *q*-axis flux linkages at 0° rotor position , whilst Fig. 7 shows the *d*- and *q*-axis current variations with rotor position at Ψ_d = 0.083Wb and Ψ_q = 0.105Wb.

To validate the accuracy of the inverse, the resultant *d*-axis and *q*-axis currents at given *d*- and *q*-axis flux linkages and rotor position are used to obtain *d*- and *q*-axis flux linkages

0278-0046 (c) 2013 IEEE. Personal use is permitted, but republication/redistribution requires IEEE permission. See http://www.ieee.org/publications_standards/publications/rights/index.html for more information.

This article has been accepted for publication in a future issue of this journal, but has not been fully edited. Content may change prior to final publication. Citation information: DOI 10.1109/TIE.2014.2388200, IEEE Transactions on Industrial Electronics

from the original *d*- and *q*-axis flux linkage maps shown in Fig. 4, and the results are compared with the flux linkages that are used to generate the *d*- and *q*-axis currents from the inverse maps shown in Fig. 6. The resulting *d*- and *q*-axis flux linkage error maps are shown in Fig. 8. It can be observed that maximum error of the *d*-axis flux linkage is 1.5×10^{-5}% whilst that of the *q*-axis flux linkage is 1.0×10^{-6}%. Flux linkage errors at other rotor positions were also checked and they are of the similar order of magnitude.

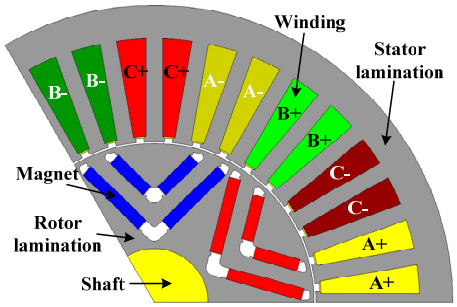


Fig. 3. Schematic for IPM 36-slot 6-pole machine prototype (one-third model).

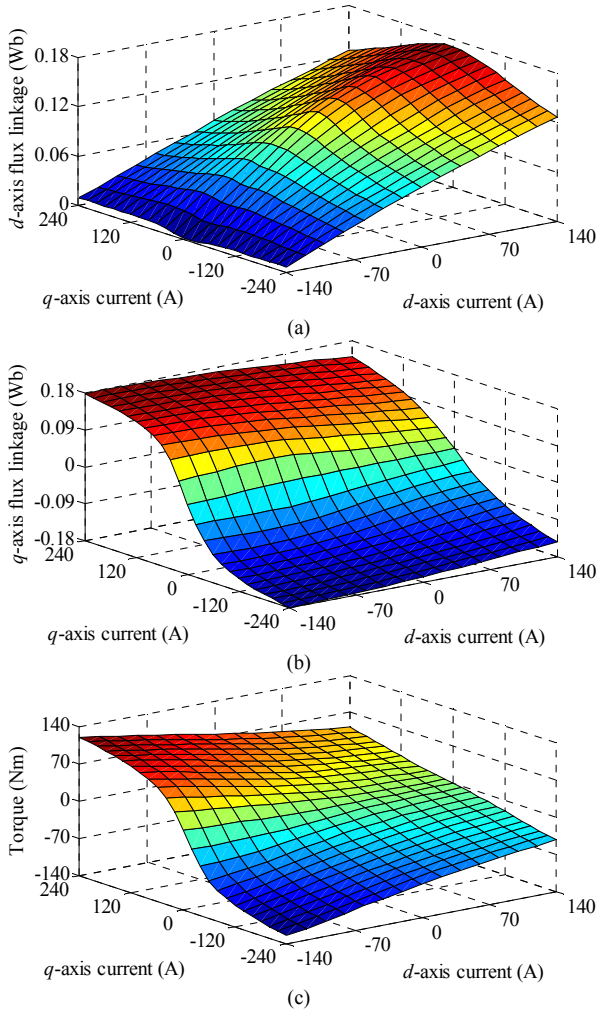


Fig. 4. Flux linkage and torque maps versus *d*- and *q*-axis currents at rotor position = 0°. (a) *d*-axis flux linkage. (b) *q*-axis flux linkage. (c) Torque.

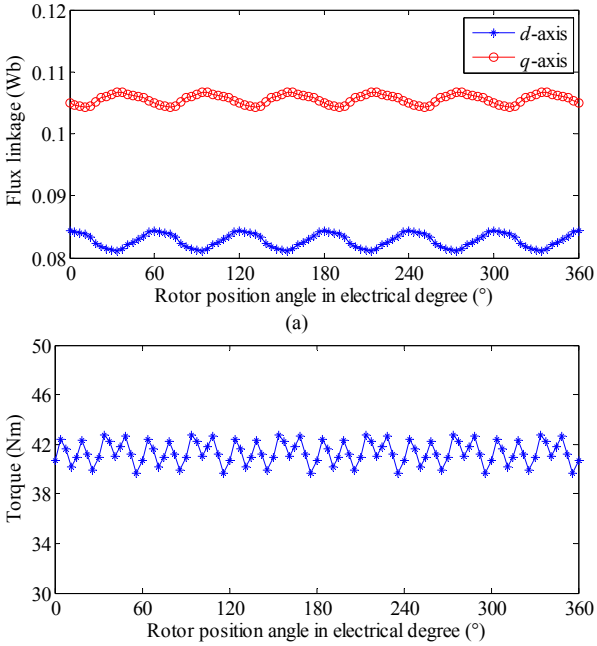


Fig. 5. Flux linkage and torque variations with rotor position at i_d=-40A, i_q=60A. (a) *d*- and *q*-axis flux linkages. (b) Torque.

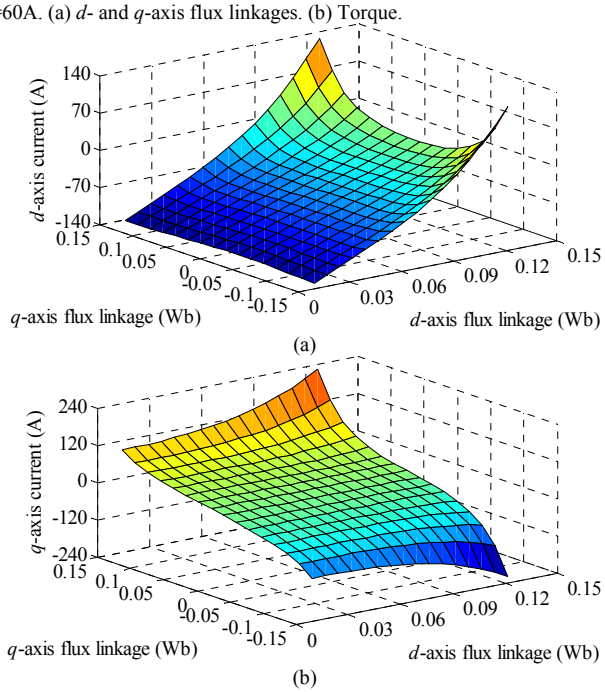


Fig. 6. Current maps versus *d*- and *q*-axis flux linkages at rotor position =0°. (a) *d*-axis current. (b) *q*-axis current.

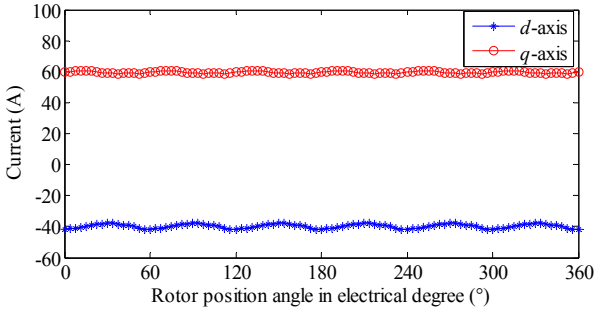


Fig. 7. *d*- and *q*-axis current variations with rotor position at Ψ_d=0.083Wb and Ψ_q=0.105Wb.

0278-0046 (c) 2013 IEEE. Personal use is permitted, but republication/redistribution requires IEEE permission. See http://www.ieee.org/publications_standards/publications/rights/index.html for more information.

This article has been accepted for publication in a future issue of this journal, but has not been fully edited. Content may change prior to final publication. Citation information: DOI 10.1109/TIE.2014.2388200, IEEE Transactions on Industrial Electronics

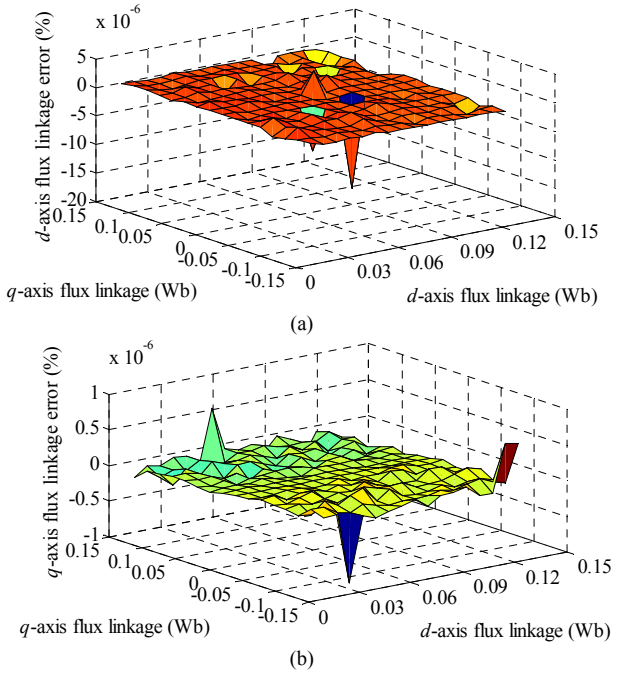


Fig. 8. Flux linkage error maps versus *d*- and *q*-axis flux linkages at rotor position =0°. (a) *d*-axis flux linkage error. (b) *q*-axis flux linkage.

IV. Inclusion of Iron Loss

A. Iron Loss Circuit Model

The iron loss in electrical machines increases or decreases active power depending on whether they operate as motor or generator, and hence affects the phase currents at a given supply voltage.

To consider the iron loss effect on the machine electromagnetic behavior at different load conditions in a computationally efficient manner, the iron loss model presented in [22, 23] is employed, which can be described by (9).

$$p_{Fe_oc} = a_h \frac{V_m}{2\pi\Psi_m} + a_e \left(\frac{V_m}{2\pi\Psi_m}\right)^2 + a_x \left(\frac{V_m}{2\pi\Psi_m}\right)^{1.5}$$
$$p_{Fe_sc} = b_h \frac{V_{da}}{2\pi\Psi_m} + b_e \left(\frac{V_{da}}{2\pi\Psi_m}\right)^2 + b_x \left(\frac{V_{da}}{2\pi\Psi_m}\right)^{1.5} \quad (9)$$

where, the iron loss coefficients (a_h, a_e, a_x) and (b_h, b_e, b_x) are determined by FE analysis at no-load (open-circuit) and short-circuit operations, respectively. The total iron loss at a given operation is the sum of p_{Fe_oc} and p_{Fe_sc}. The voltage magnitude V_m and the voltage due to armature reaction of the *d*-axis current V_{da} can be calculated by (10).

$$V_m = \omega_e \sqrt{\Psi_d^{\,2} + \Psi_q^{\,2}}$$
$$V_{da} = -\omega_e \left(\Psi_d - \Psi_m\right) \quad (10)$$

where, Ψ_m is obtained by the Ψ_d at i_d=0 while i_q equals to the on-load *q*-axis current.

The iron loss can be further decomposed into the components associated with the *d*- and *q*-axis flux linkages, as expressed by (11).

$$p_{Fe_d} = \frac{\Psi_q^{\,2}}{\Psi_d^{\,2} + \Psi_q^{\,2}} p_{Fe_oc} + p_{Fe_sc}$$
$$p_{Fe_q} = \frac{\Psi_d^{\,2}}{\Psi_d^{\,2} + \Psi_q^{\,2}} p_{Fe_oc} \quad (11)$$

In motoring operation, the iron loss consumes power from electrical supply, whereas it reduces electrical output power in generator mode. Therefore, if the iron loss effect is considered as the equivalent currents which incur losses in the equivalent resistors across the *d*- and *q*-axis induced voltages, as shown in Fig. 9, the influence of the iron loss on the *d*- and *q*-axis currents is given in (12).

$$i_{da} = i_d \mp \frac{p_{Fe_d}}{V_d - R_s i_d}$$
$$i_{qa} = i_q \mp \frac{p_{Fe_q}}{V_q - R_s i_q} \quad (12)$$

where, i_{da} and i_{qa} are the *d*- and *q*-axis currents which are associated with the armature reaction, "-" is for the motoring mode, and "+" is for the generator mode.

The schematic of the IPM model that integrates the iron loss model is shown in Fig. 10.

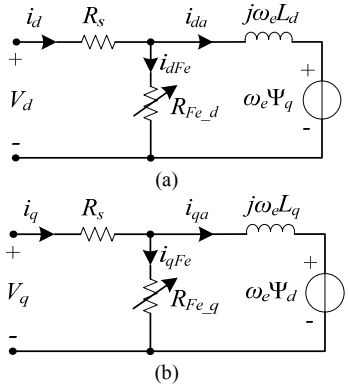


Fig. 9. Circuit model with equivalent iron loss components. (a) *d*-axis circuit model. (b) *q*-axis circuit model.

B. Iron Loss Influence on Electromagnetic Behavior

The influence of iron loss on the electromagnetic behavior of the IPM machine is studied using the developed model shown in Fig. 10. Fig. 11 compares the *d*- and *q*-axis currents at peak torque over the operating speed range in the motoring mode. If the iron loss is neglected, i_d=i_{da}; i_q=i_{qa}. Otherwise, they will be different. It can be seen that in the constant torque region where the machine operates at the MTPA condition with the current limit, the amplitudes of both *d*- and *q*-axis currents, i_{da} and i_{qa}, associated with electromechanical energy conversion are slightly reduced in the motoring mode when the iron loss is included. Consequently, the electromagnetic torque will be slightly lower. However, in the constant power region where the machine operates under the field weakening condition, the influence of iron loss on the *d*-axis current is more pronounced with increase in operating speeds. This is because the iron loss increases more than proportionally as the speed increases. It can also be seen that in the field weakening region the influence of iron loss on *q*-axis current is much less than that on the *d*-axis

0278-0046 (c) 2013 IEEE. Personal use is permitted, but republication/redistribution requires IEEE permission. See http://www.ieee.org/publications_standards/publications/rights/index.html for more information.

This article has been accepted for publication in a future issue of this journal, but has not been fully edited. Content may change prior to final publication. Citation information: DOI 10.1109/TIE.2014.2388200, IEEE Transactions on Industrial Electronics

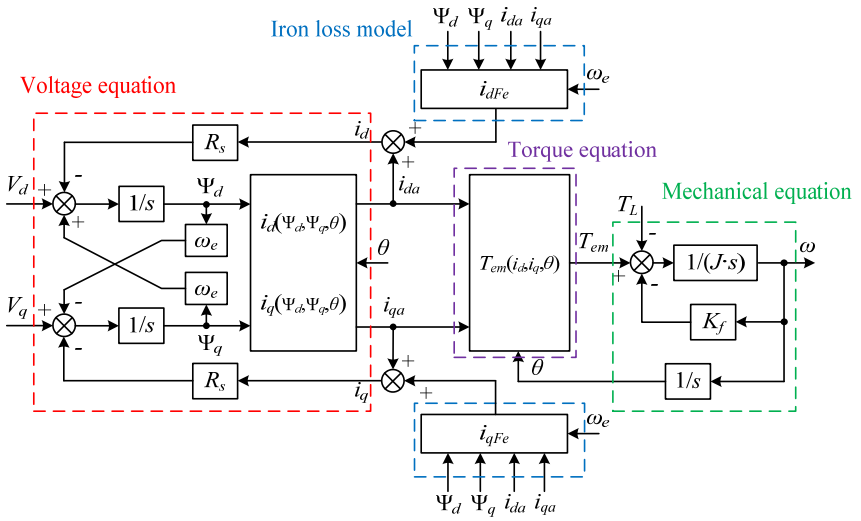


Fig. 10. Proposed IPM machine model schematic with iron loss effect.

current since the *d*-axis flux linkage has been weakened and becomes smaller than that of the *q*-axis at high speeds.

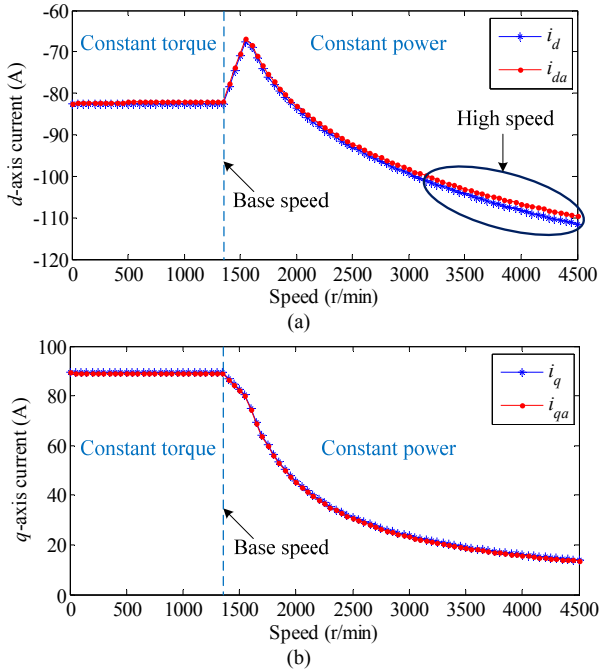


Fig. 11. Iron loss influence on *d*- and *q*-axis currents at the peak envelope in the motoring mode. (a) *d*-axis current. (b) *q*-axis current.

V. Model Validation

The proposed machine model has been implemented in Matlab/Simulink environment and validated by both FE analysis and experiments, as described in the following sections.

A. FE Validation

In most commercial electromagnetic FE tools, iron loss is usually evaluated in post process. Therefore, in the following FE validation, both the Simulink model and FE model do not consider the iron loss influence.

A number of representative points are compared for the purpose of validations. Since the ripples on flux linkages and torque are more significant at high speeds where the machine operates in a deep field weakening region, the comparisons are illustrated for the operating point at 18Nm and 4500r/min.

First, the drive system modeled with the proposed approach in the Simulink environment is simulated at a specific operating point and the resulting current waveforms, as shown in Fig. 12, are extracted. The current waveforms are then injected into the FE model under the same load condition. Figs. 13 and 14 compare Simulink and FE-predicted torque and voltage waveforms, respectively.

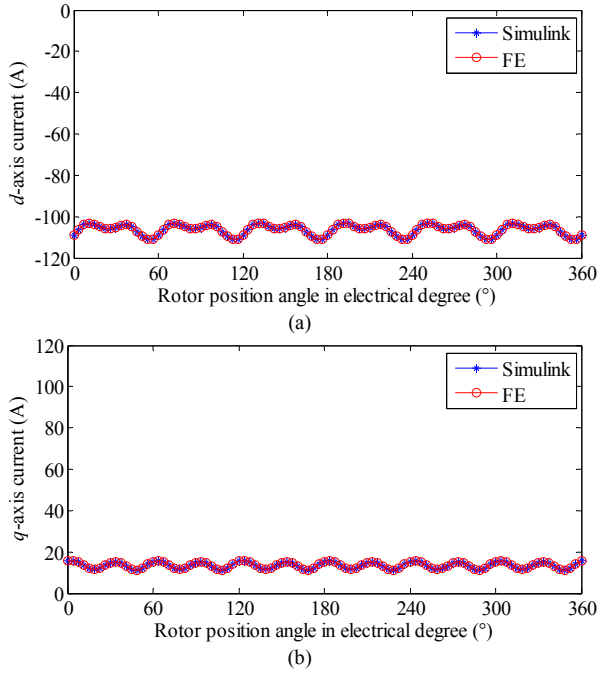


Fig. 12. Comparisons of *d*- and *q*-axis current waveforms used in Simulink and FE models. (a) *d*-axis current. (b) *q*-axis current.

0278-0046 (c) 2013 IEEE. Personal use is permitted, but republication/redistribution requires IEEE permission. See http://www.ieee.org/publications_standards/publications/rights/index.html for more information.

This article has been accepted for publication in a future issue of this journal, but has not been fully edited. Content may change prior to final publication. Citation information: DOI 10.1109/TIE.2014.2388200, IEEE Transactions on Industrial Electronics

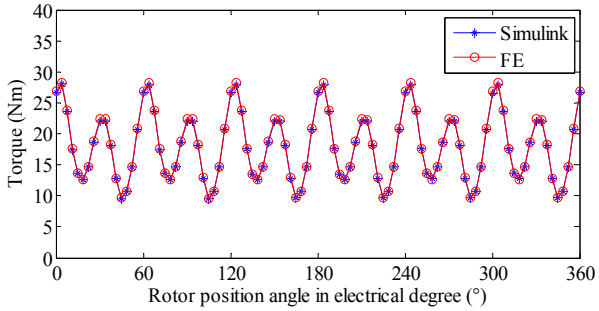


Fig. 13. Comparison of Simulink and FE-predicted torque waveform.

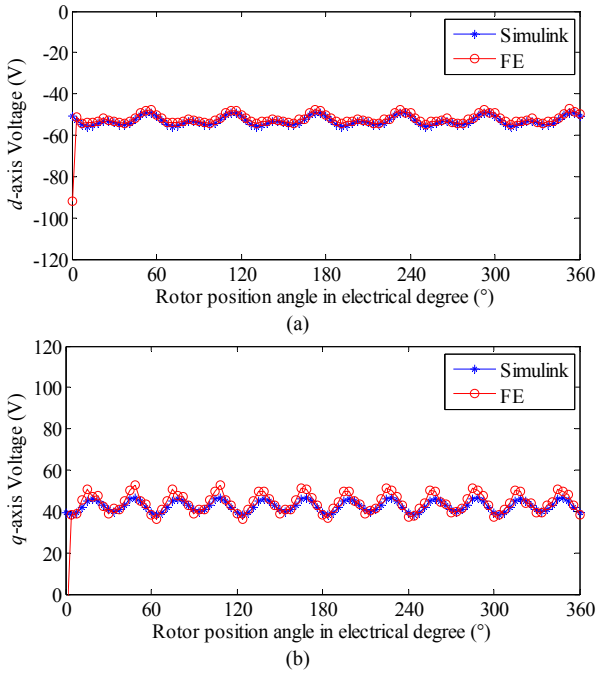


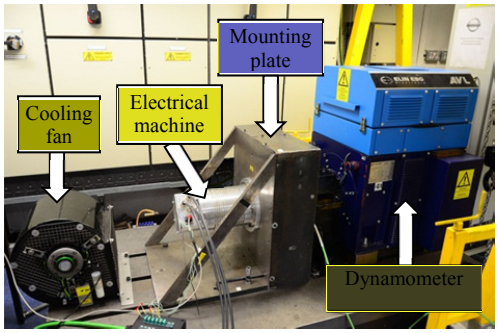
Fig. 14. Comparisons of Simulink and FE-predicted *d*- and *q*-axis voltage waveforms. (a) *d*-axis voltage. (b) *q*-axis voltage.

It can be observed that the torque waveforms predicted by Simulink and FE models coincide because the electromagnetic torque depends on the flux linkage and current. The injected currents in the FE model are identical to those of the Simulink model and the flux linkage error between the proposed and FE model is virtually negligible as illustrated in Fig. 8. Therefore, the FE-predicted torque waveform can be completely reproduced by the Simulink model.

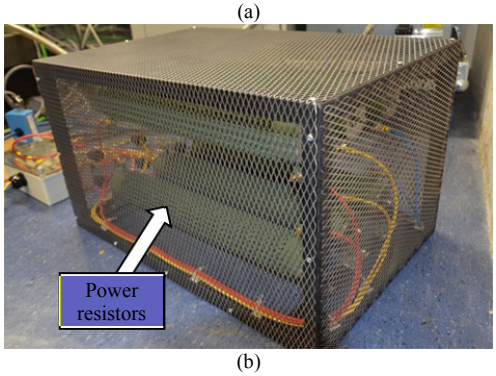
As shown in Fig. 14, the voltage waveforms predicted by the two models are slightly different since the voltage in FE analysis is calculated from the derivatives of the flux linkages. The accuracy largely depends on the size of transient steps; this can be understood by the fact that the smaller the step size, the better the FE-predicted voltage accuracy.

B. Experimental Validation in Generator Mode

To avoid any uncertainties introduced by an inverter, the machine prototype is driven by a dynamometer and operates in the generator mode with a resistive load for the validation of the proposed machine model. The experimental set-up, including the machine prototype, dynamometer and resistive load are shown in Fig. 15.



(a)



(b)

Fig. 15. Generator mode experimental set-up. (a) Electrical machine prototype and dynamometer. (b) Resistive load.

First, the no-load test is performed and the FE-predicted and measured phase back-EMF waveforms at 1350r/min are compared in Fig. 16. It is worth noting that the predicted phase back-EMF with ideal 2-D FE model of the machine is approximately 9% higher than the measured value due to the 3-D effect, manufacture tolerance (e.g., assembly gaps between magnets and rotor core), and difference in material properties, etc. The difference between the prediction and measurement is removed by a calibration procedure in which the magnet remanence is adjusted so that the fundamental phase back-EMF of the FE result coincides with the measurement. The calibrated FE model is used to compute the flux linkage and torque maps for the construction of the proposed Simulink model. From Fig. 16 (b), it can be observed that after calibration, the measured and predicted phase back-EMF waveforms match very well except for some high order harmonics.

On-load tests are performed against four load conditions with load resistance at 0.6875Ω, 1.0Ω, 2.2Ω and 3.2Ω, respectively. For each load condition, the speed varies from 500r/min to the speed at which the maximum power is reached. The measured and Simulink model-predicted voltage and current waveforms as well as the average torque are compared. Good agreements are observed for all four operating points between the predictions and measurements.

By way of example, Fig. 17 and Fig. 18 compare the measured and predicted line-to-line voltage and phase current respectively, at 1350r/min with 0.6875Ω load. It can be seen that both the predicted line-to-line voltage and phase current agree well with the experimental results. The errors in fundamental line-to-line voltage and current are 1.6% and 0.7%, respectively, which might result from the load resistance variation due to temperature rise and/or measurement errors.

0278-0046 (c) 2013 IEEE. Personal use is permitted, but republication/redistribution requires IEEE permission. See http://www.ieee.org/publications_standards/publications/rights/index.html for more information.

This article has been accepted for publication in a future issue of this journal, but has not been fully edited. Content may change prior to final publication. Citation information: DOI 10.1109/TIE.2014.2388200, IEEE Transactions on Industrial Electronics

The comparison of the predicted and measured torque is shown in Fig. 19. Due to the bandwidth limit of the torque transducer, the instantaneous torque waveform cannot be captured, and thereby only the mean torque value of the experimental result is shown in Fig. 19. The error in the mean torque value is 0.4%.

Therefore, the proposed model exhibits high-fidelity for predicting the electromagnetic behavior of the IPM machine even under heavy load conditions.

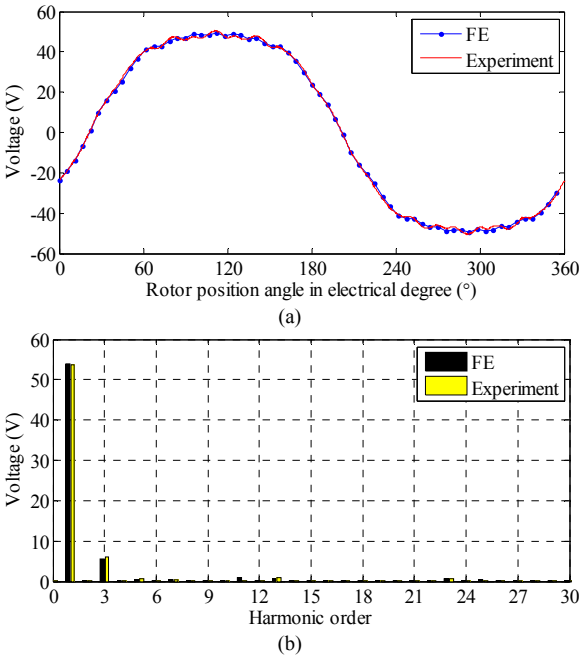


Fig. 16. Comparison of measured and FE-predicted phase back-EMF at 1350r/min. (a) Waveforms. (b) FFT spectra.

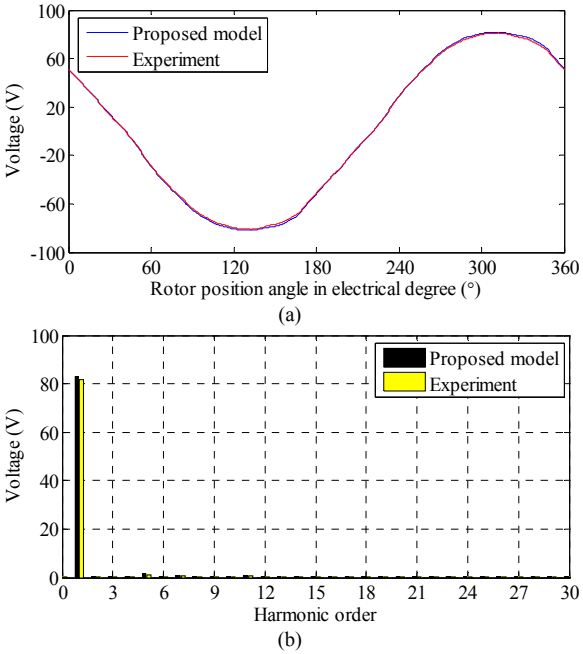


Fig. 17. Comparison of measured and predicted line-to-line voltage at 1350r/min with 0.6875Ω load. (a) Waveforms. (b) FFT spectra.

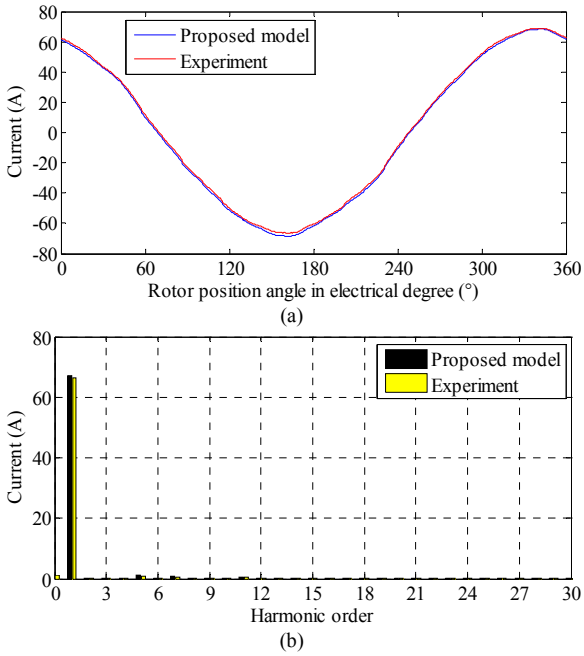


Fig. 18. Comparison of measured and predicted phase current at 1350r/min with 0.6875Ω load. (a) Waveforms. (b) FFT spectra.

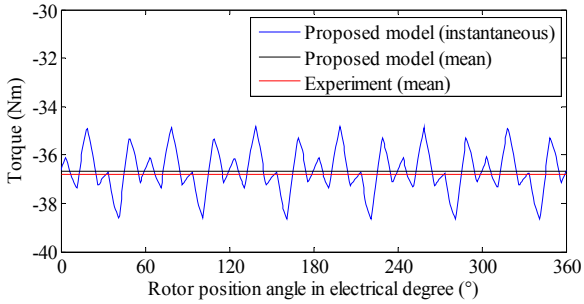


Fig. 19. Comparison of the measured and predicted torque at 1350r/min with 0.6875Ω load.

C. *Experimental Validation in Motoring mode*

Tests in inverter-fed motoring operation have also been performed to validate the proposed model. The prototype machine is driven by a 10kW voltage-fed inverter with an 8kHz switching frequency. The experimental set-up is illustrated in Fig. 20. The three-phase voltages and currents are captured by high band-width voltage and current transducers.

The measured three-phase voltage waveforms in one electrical cycle at 10Nm and 2700r/min (field weakening region) were filtered by a 10 kHz low pass filter, and the filtered voltages are shown in Fig. 21. The filtered voltages are applied to the proposed models with and without inclusion of the iron loss model, and the resultant phase *A* current waveforms and their spectra are compared with the measurement in Fig. 22 (a) and (b). Compared to the measured amplitude, 63.49A, of the fundamental current, the model-predicted current amplitudes with and without the iron loss inclusion are 63.32A (-0.3% error) and 61.47A (-3.2% error), respectively, as shown in Table II and Table III.

The comparison of currents in the *d*-*q* system is shown in Fig. 23, Tables II and III. It can be seen that the inclusion of iron loss in the model reduces the model errors in the mean *d*- and *q*-axis currents from -3.1% and -6.9% to -0.2% and -0.6%,

0278-0046 (c) 2013 IEEE. Personal use is permitted, but republication/redistribution requires IEEE permission. See http://www.ieee.org/publications_standards/publications/rights/index.html for more information.

This article has been accepted for publication in a future issue of this journal, but has not been fully edited. Content may change prior to final publication. Citation information: DOI 10.1109/TIE.2014.2388200, IEEE Transactions on Industrial Electronics

respectively, and hence improve model fidelity. The level of improvement will be dependent on operation conditions. At high speeds, iron loss becomes more significant, and hence neglecting iron loss may result in large error. For efficiency assessment and thermal evaluation, inclusion of iron loss in the model is indispensable.

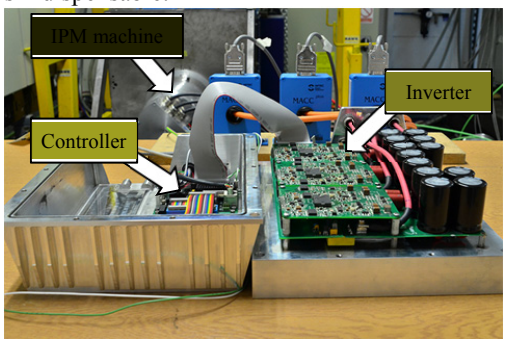


Fig. 20. Motoring mode experimental set-up.

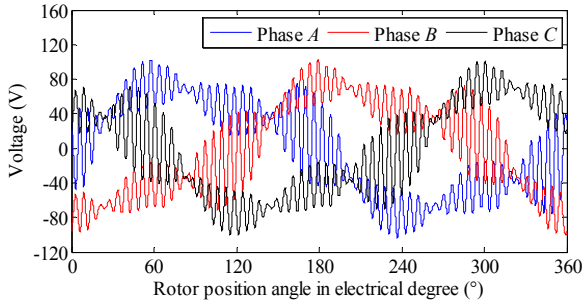


Fig. 21. Waveforms of measured three-phase voltages at 10Nm and 2700r/min filtered by a 10 kHz low pass filter.

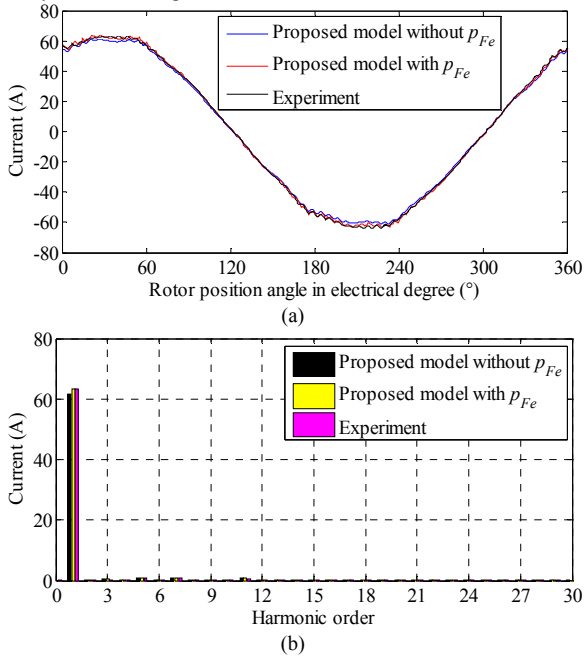


Fig. 22. Comparison of measured and predicted phase current at 10Nm and 2700r/min (field weakening region). (a) Waveforms. (b) FFT spectra.

TABLE II
COMPARISON OF MEASURED AND PREDICTED CURRENTS AT 10NM AND 2700R/MIN (FIELD WEAKENING REGION)

Quantity	Without p_{Fe}	With p_{Fe}	Experiment
Fundamental phase current (A)	61.47	63.32	63.49
Mean *d*-axis current (A)	-60.65	-62.47	-62.60
Mean *q*-axis current (A)	9.68	10.33	10.39

TABLE III
RELATIVE ERRORS IN PREDICTED CURRENTS AT 10NM AND 2700R/MIN (FIELD WEAKENING REGION)

Quantity	Without p_{Fe}	With p_{Fe}
Error in fundamental phase current (%)	-3.2%	-0.3%
Error in mean *d*-axis current (%)	-3.1%	-0.2%
Error in mean *q*-axis current (%)	-6.9%	-0.6%

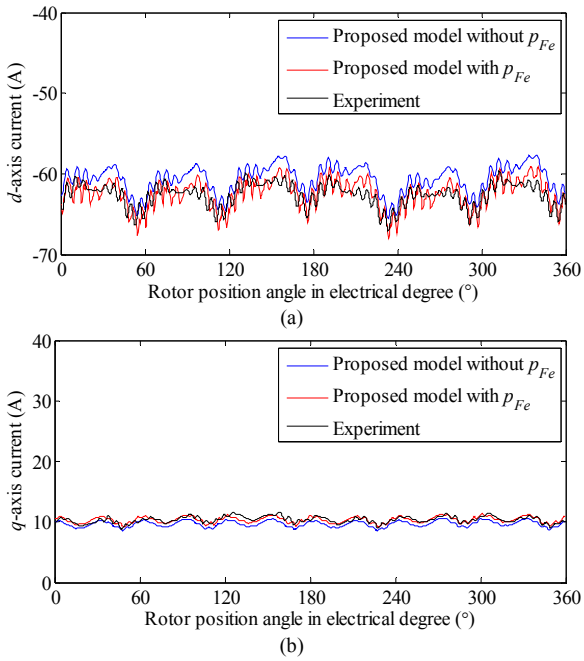


Fig. 23. Comparison of measured and predicted *d*- and *q*-axis current at 10Nm and 2700r/min (field weakening region). (a) *d*-axis current. (b) *q*-axis current.

VI. COMPARISON WITH CONVENTIONAL MODEL

The utility of the proposed model is studied in a drive system with the field-oriented control strategy in both constant torque and field weakening regions, and the results are compared with those obtained from the conventional model given in (1) under the same operating conditions.

If the current control bandwidth is high and the currents can be controlled close to sinusoidal, the resultant differences in flux linkage and voltage waveforms between the proposed and conventional models are quite significant. By way of example, Fig. 24 compares the flux linkage trajectories predicted by the conventional and proposed models in the field weakening region. The *d*- and *q*-axis currents are -62.6A and 10.4A, respectively, which correspond to the experimental working point in field weakening region in section V-C.

It can be seen that the flux linkage trajectory predicted by the proposed model is no longer a circle and exhibits fluctuation in magnitude. This fluctuation results in a large distortion in the voltage trajectory, as shown in Fig. 25.

0278-0046 (c) 2013 IEEE. Personal use is permitted, but republication/redistribution requires IEEE permission. See http://www.ieee.org/publications_standards/publications/rights/index.html for more information.

This article has been accepted for publication in a future issue of this journal, but has not been fully edited. Content may change prior to final publication. Citation information: DOI 10.1109/TIE.2014.2388200, IEEE Transactions on Industrial Electronics

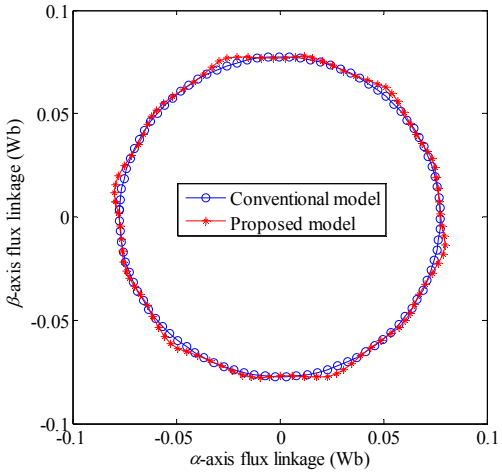


Fig. 24. Flux linkage trajectory comparison between proposed and conventional models under ideal sinusoidal current excitation.

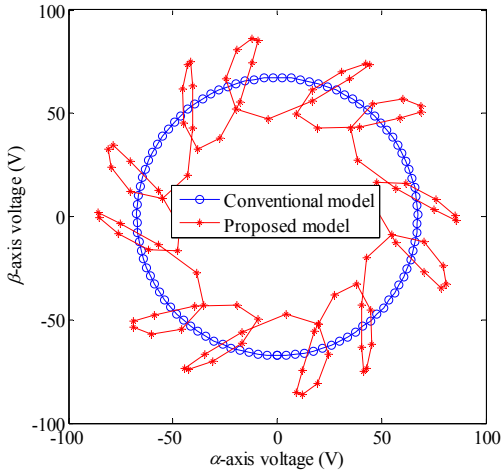


Fig. 25. Voltage trajectory comparison between proposed and conventional models under ideal sinusoidal current excitation.

If the currents can be controlled as purely sinusoidal, the voltage will exhibit enormous distortion in the field weakening region. However, the drive has a limited current control bandwidth and is usually fed by a voltage-source inverter with its maximum available voltage being limited. As a result, the current trajectory becomes distorted, as can be seen in Fig. 26. All the three current trajectories are obtained at the same load condition, viz., 10Nm and 2700r/min. It can also be observed that the current trajectory of the proposed model is very close to the measurement. However, the conventional model can neither predict accurately the current amplitude due to neglecting the iron loss nor capture the current ripples resulting from the MMF spatial harmonics.

Due to the current waveform being distorted as shown in Fig. 26, the proposed model predicts a very high torque ripple, which cannot be presented by the conventional machine model, as illustrated in Fig. 27. The harmonic distribution of the torque predicted by the proposed model, as shown in Fig. 27 (b), suggests that the dominant ripple harmonic is of the 12th order. It is mainly contributed by the 12th harmonic in the *d*- and *q*-axis currents, shown in Fig. 28, which interact with the DC components of the *q*- and *d*-axis flux linkages respectively.

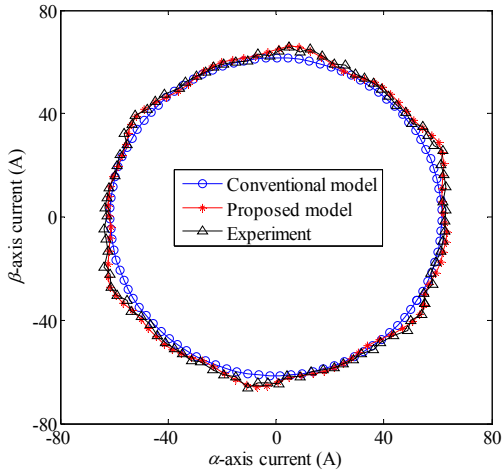


Fig. 26. Comparisons of measured and predicted current trajectories with voltage-source inverter at 10Nm and 2700r/min.

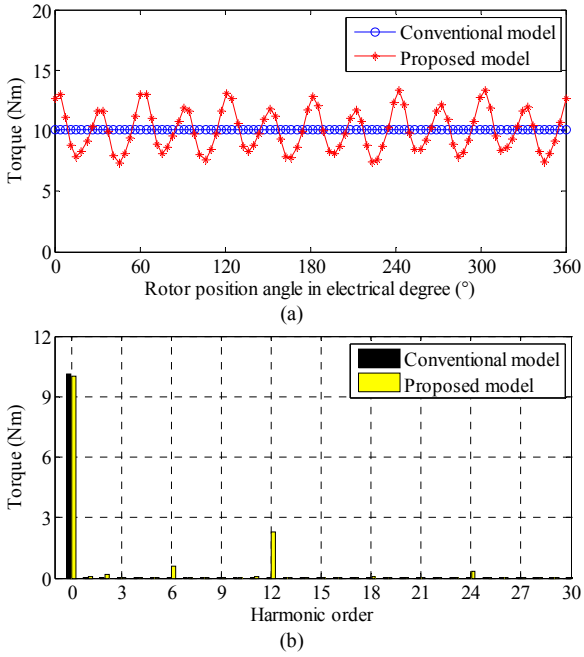


Fig. 27. Torque waveform and spectrum comparison for the proposed and conventional models with voltage-fed converter.

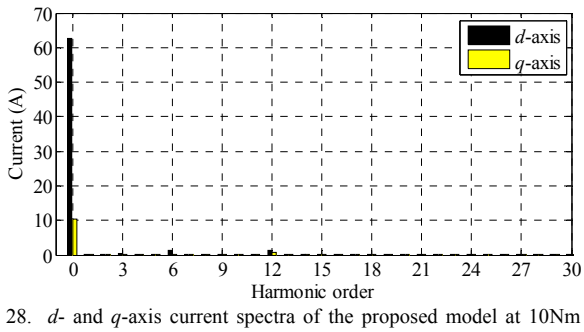


Fig. 28. *d*- and *q*-axis current spectra of the proposed model at 10Nm and 2700r/min.

In the constant torque region, the predicated current waveforms obtained from the proposed model are close to sinusoidal when the current control bandwidth is relatively high. However, the distortions in the flux linkages and voltages are still significant although the torque ripple is lower than that

0278-0046 (c) 2013 IEEE. Personal use is permitted, but republication/redistribution requires IEEE permission. See http://www.ieee.org/publications_standards/publications/rights/index.html for more information.

This article has been accepted for publication in a future issue of this journal, but has not been fully edited. Content may change prior to final publication. Citation information: DOI 10.1109/TIE.2014.2388200, IEEE Transactions on Industrial Electronics

observed in the field weakening region. Nevertheless, no distortion is seen in the predicted voltages, currents and flux linkages by the conventional model in both constant torque and field weakening regions.

In summary, the conventional inductance-based model neglecting spatial harmonics, position dependent *d*- and *q*-axis flux linkages and the iron loss effect cannot reflect the real machine behavior in the simulation, particularly in the field weakening region where the iron loss influence will be large and significant harmonics in current waveforms will be present due to current control error under the voltage limit.

In contrast, the proposed machine model includes the iron loss effect and captures all these effects in the form of 3-D flux linkage and torque lookup tables or curve fitted functions. Therefore, the proposed model exhibits high fidelity in predicting the real machine behavior.

Compared to the circuit-field coupled co-simulation, the order of magnitude of the computation time for the proposed model is reduced from days [13] to seconds. For a 0.5s simulation with 10μs time step, the computation time is 10s on a quad-core 3.1GHz PC.

VII. Conclusion

A high fidelity, computationally efficient model for IPM machines has been described. The model captures all significant effects associated with the electromagnetic behavior of the machines, including magnetic saturation, spatial harmonics and iron loss effect, and has been validated by both FE analysis and experiments. The proposed model provides an accurate means of assessing the drive performance of an IPM machine. It has been shown that torque ripple may increase significantly in the field weakening region due to current waveform distortions resulting from the inverter voltage limit. It is important to capture these adverse effects in drive system simulations in order to develop a robust control for high efficiency operations in both constant torque and field weakening regions.

References

[1] M. W. Brainard, "Synchronous Machines with Rotating Permanent-Magnet Fields; Part I. Characteristics and Mechanical Construction [includes discussion]," *Power Ap. Syst., Part III. Trans. Am. Inst. Elect. Eng.,* vol. 71, 1952.

[2] T. M. Jahns, G. B. Kliman, and T. W. Neumann, "Interior Permanent-Magnet Synchronous Motors for Adjustable-Speed Drives," *IEEE Trans. Ind. Appl.,* vol. IA-22, pp. 738-747, 1986.

[3] I. Boldea, L. N. Tutelea, L. Parsa, and D. Dorrell, "Automotive Electric Propulsion Systems With Reduced or No Permanent Magnets: An Overview," *IEEE Trans. Ind. Electron.,* vol. 61, pp. 5696-5711, 2014.

[4] D. Dorrell, L. Parsa, and I. Boldea, "Automotive Electric Motors, Generators, and Actuator Drive Systems With Reduced or No Permanent Magnets and Innovative Design Concepts," *IEEE Trans. Ind. Electron.,* vol. 61, pp. 5693-5695, 2014.

[5] J. Linni, K. T. Chau, and J. Z. Jiang, "A Magnetic-Geared Outer-Rotor Permanent-Magnet Brushless Machine for Wind Power Generation," *IEEE Trans. Ind. Appl.,* vol. 45, pp. 954-962, 2009.

[6] J. Wang, X. Yuan, and K. Atallah, "Design Optimization of a Surface-Mounted Permanent-Magnet Motor With Concentrated Windings for Electric Vehicle Applications," *IEEE Trans. Veh. Technol.,* vol. 62, pp. 1053-1064, 2013.

[7] K. Sung-Il, K. Young-Kyoun, L. Geun-Ho, and H. Jung-Pyo, "A Novel Rotor Configuration and Experimental Verification of Interior PM Synchronous Motor for High-Speed Applications," *IEEE Trans. Magn.,* vol. 48, pp. 843-846, 2012.

[8] G. Pellegrino, A. Vagati, P. Guglielmi, and B. Boazzo, "Performance Comparison Between Surface-Mounted and Interior PM Motor Drives for Electric Vehicle Application," *IEEE Trans. Ind. Electron.,* vol. 59, pp. 803-811, 2012.

[9] S. Morimoto, O. Shohei, Y. Inoue, and M. Sanada, "Experimental Evaluation of a Rare-Earth-Free PMASynRM With Ferrite Magnets for Automotive Applications," *IEEE Trans. Ind. Electron.,* vol. 61, pp. 5749-5756, 2014.

[10] H. Cai, B. Guan, and L. Xu, "Low-Cost Ferrite PM-Assisted Synchronous Reluctance Machine for Electric Vehicles," *IEEE Trans. Ind. Electron.,* vol. 61, pp. 5741-5748, 2014.

[11] L. Parsa and H. Lei, "Interior Permanent Magnet Motors With Reduced Torque Pulsation," *IEEE Trans. Ind. Electron.,* vol. 55, pp. 602-609, 2008.

[12] X. Chen, J. Wang, P. Lazari, and L. Chen, "Permanent Magnet Assisted Synchronous Reluctance Machine with fractional-slot winding configurations," in *Proc. IEEE IEMDC*, 2013, pp. 374-381.

[13] L. Di Leonardo, F. Parasiliti, M. Tursini, and M. Villani, "Transient analysis of PM synchronous motor drives by finite element model co-simulation," in *Proc. IEEE IECON*, 2013, pp. 6834-6840.

[14] F. Parasiliti, M. Villani, and A. Tassi, "Dynamic Analysis of Synchronous Reluctance Motor Drives Based on SimulinkÂ® and Finite Element Model," in *Proc. IEEE IECON*, 2006, pp. 1516-1520.

[15] W. Liang, J. Wang, T. Lu, and W. Fang, "A New Method for Multiple Finite-Element Models in Cosimulation With Electrical Circuit Using Machine Multiloop Modeling Scheme," *IEEE Trans. Ind. Electron.,* vol. 61, pp. 6583-6590, 2014.

[16] Y. Kano, K. Watanabe, T. Kosaka, and N. Matsui, "A Novel Approach for Circuit-Field-Coupled Time-Stepping Electromagnetic Analysis of Saturated Interior PM Motors," *IEEE Trans. Ind. Appl.,* vol. 45, pp. 1325-1333, 2009.

[17] O. Wallmark and J. Galic, "Prediction of dc-link current harmonics from PM-motor drives in railway applications," in *Proc. ESARS*, 2012, pp. 1-8.

[18] M. Boesing, M. Niessen, T. Lange, and R. De Doncker, "Modeling spatial harmonics and switching frequencies in PM synchronous machines and their electromagnetic forces," in *Proc. IEEE ICEM*, 2012, pp. 3001-3007.

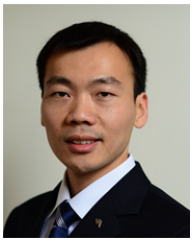
[19] G. Weidenholzer*, et al.*, "A flux-based PMSM motor model using RBF interpolation for time-stepping simulations," in *Proc. IEEE IEMDC*, 2013, pp. 1418-1423.

[20] N. Bianchi and L. Alberti, "MMF Harmonics Effect on the Embedded FE Analytical Computation of PM Motors," *IEEE Trans. Ind. Appl.,* vol. 46, pp. 812-820, 2010.

[21] F. A. Potra and S. J. Wright, "Interior-point methods," *J. Comput. Appl. Math.,* vol. 124, pp. 281-302, 2000.

[22] P. H. Mellor, R. Wrobel, and D. Holliday, "A computationally efficient iron loss model for brushless AC machines that caters for rated flux and field weakened operation," in *Proc. IEEE IEMDC*, 2009, pp. 490-494.

[23] J. Goss, P. H. Mellor, R. Wrobel, D. A. Staton, and M. Popescu, "The design of AC permanent magnet motors for electric vehicles: A computationally efficient model of the operational envelope," in *Proc. IET PEMD*, 2012, pp. 1-6.



Xiao Chen (S'13) born in Taian, China, in 1988, received B.Eng. degree in electrical engineering from Harbin Institute of Technology at Weihai, Weihai, China, in 2009, and received M.Eng. degree in electrical engineering from Harbin Institute of Technology, Harbin, China, in 2011, respectively. Since 2012, he has been an assistant in the School of Electrical Engineering and Automation in Harbin Institute of Technology, Harbin, China. Now he is working towards the Ph.D degree in the Dept. of Electronic and Electrical Engineering, The University of Sheffield, UK. His current research interests include the modeling, design and analysis of permanent-magnet synchronous machines for traction applications.

0278-0046 (c) 2013 IEEE. Personal use is permitted, but republication/redistribution requires IEEE permission. See http://www.ieee.org/publications_standards/publications/rights/index.html for more information.

This article has been accepted for publication in a future issue of this journal, but has not been fully edited. Content may change prior to final publication. Citation information: DOI 10.1109/TIE.2014.2388200, IEEE Transactions on Industrial Electronics



Jiabin Wang (S'94–A'96–M'01–SM'03) received the B.Eng. and M.Eng. degrees from Jiangsu University of Science and Technology, Zhenjiang, China, in 1982 and 1986, respectively, and the Ph.D. degree from the University of East London, London, U.K., in 1996, all in electrical and electronic engineering.

Currently, he is a Professor in Electrical Engineering at the University of Sheffield, Sheffield, U.K. From 1986 to 1991, he was with the Department of Electrical Engineering at Jiangsu University of Science and Technology, where he was appointed a Lecturer in 1987 and an Associated Professor in 1990. He was a Postdoctoral Research Associate at the University of Sheffield, Sheffield, U.K., from 1996 to 1997, and a Senior Lecturer at the University of East London from 1998 to 2001. His research interests range from motion control and electromechanical energy conversion to electric drives for applications in automotive, renewable energy, household appliances and aerospace sectors.

He is a fellow of the IET and a senior member of IEEE.



Bhaskar Sen (S'11) received the B.E. degree from Delhi College of Engineering, Delhi, India in 2003 and the M.Tech. degree from Indian Institute of Technology, Kanpur, India in 2006. From 2006 to 2011, he was with GE Global Research, Bangalore, India. Since 2011 he has been working toward the Ph.D. degree in the University of Sheffield, UK. His current research interests include electrical machine fault modelling, machine fault detection and fault tolerant drives.



Panagiotis Lazari (S'13) was born in Limassol, Cyprus, in 1986. He received the B.Eng. degree in 2010 from the Department of Electronic and Electrical Engineering, The University of Sheffield, UK, where he is currently working towards the Ph.D. degree on the development of traction machines for EV applications.



Tianfu Sun was born in China. He received B.Eng. degree in mechanical engineering and M.Sc. degree in civil engineering from Dalian University of Technology, Dalian, China, in 2009 and 2012, respectively. He is currently pursuing the Ph.D. degree in electronic and electrical engineering at The University of Sheffield, U.K. His current research interests include electric/hybrid vehicle drives, modeling of electric vehicle power-trains, vehicle dynamics, power-electronic control of electric machines, sensorless drives and optimal control for electric machine drive.

0278-0046 (c) 2013 IEEE. Personal use is permitted, but republication/redistribution requires IEEE permission. See http://www.ieee.org/publications_standards/publications/rights/index.html for more information.

Wireless Pers Commun
DOI 10.1007/s11277-014-2201-5

A Novel Method of Modeling Wireless Sensor Network Using Fuzzy Graph and Energy Efficient Fuzzy Based k-Hop Clustering Algorithm

Aarti Jain · B. V. Ramana Reddy

© Springer Science+Business Media New York 2015

Abstract Clustering is one of the widely used methods to save energy, increase spatial re usability, and scalability. In this paper, we have proposed a new fuzzy graph based modeling approach for wireless sensor network which takes into account the dynamic nature of network, volatile aspects of radio links and physical layer uncertainty. The fuzzy graph constructs fuzzy neighborhoods which are used to identify all the prospective member nodes of a cluster. For computation of optimum centrality of a cluster, we have defined a new centrality metric namely *fuzzy k-hop centrality*. The proposed centrality metric considers residual energy of individual nodes, link quality, hop distance between the prospective cluster head and respective member nodes to ensure better cluster head selection and cluster quality. Finally, a new computationally inexpensive clustering algorithm has been developed. The simulation results demonstrate that the proposed algorithm resulted in prolonged network lifetime in terms of clustering rounds, scalability, higher energy efficiency and uniform cluster head and cluster members distribution, as compare to LEACH-ERE and CHEF.

Keywords Fuzzy graph · k-Hop centrality · Possibility measure · Cluster head selection · Energy efficiency · Modeling

1 Introduction

The main task of wireless sensor network (WSN) is to efficiently sense and collect information, process it and finally relay it to the base station. The sensor nodes in WSN are battery powered and in most of the cases, it is not practically possible to recharge or change batteries. Thus energy efficiency to prolong the network lifetime becomes a vital design criterion for Wireless sensor networks. In addition to limited energy, high deployment density leads to

A. Jain (✉)
Ambedkar Institute of Advanced Communication Technologies and Research, Delhi, India
e-mail: rtjain2001@gmail.com

B. V. Ramana Reddy
Guru Gobind Singh Indraprastha University, Delhi, India

Published online: 10 January 2015

communication failures due to contention for shared communication medium. Moreover, broadcasting nature of sensor nodes leads to high probability of data redundancy which in turn leads to scalability as another important factor in system design [1–5].

To address these issues various probabilistic as well as fuzzy logic based clustering methods have been proposed. However, in most of the clustering methods emphasis is given on the selection of cluster heads (CHs) without paying much attention to the overall efficiency of the cluster. LEACH [6], is Low Energy Adaptive Clustering Hierarchy protocol which uses a probabilistic model to select CHs and rotates CHs periodically in order to balance energy consumption. However, being a pure probabilistic model, some CHs may be very close each other or may be located at the edge of WSN leading to inefficient clustering. LEACH-C, described in [7], is a probabilistic approach that uses a centralized algorithm to form clusters. LEACH-C requires location information of all nodes of the network which incurs additional communication overhead. In [8] Ferng et al. has proposed method of defining static clusters with dynamic structures. This method utilizes virtual points in a corona-based WSN. In Linked Cluster Algorithm [9], a node becomes the CH if it has the highest identity among all nodes within one hop of itself or among all nodes within one hop of one of its neighbors. The Weighted Clustering Algorithm (WCA) [10] elects a node as a CH on the basis of node degree, sum of distances to all neighbors, speed of node, and cumulative time the node has served as a CH. Nodes with the smallest weights, in their respective neighborhoods, are chosen as CH(s). In [11], a load balanced CH selection method using dynamic GAs has been proposed. Fitness of a CH is evaluated on the basis of balanced node degree. The major drawback of the above mentioned algorithms [6–11] is that they aim at generating 1-hop clusters which in turn leads to excessive number of clusters. This factor is more apparent in case of large-scale WSNs. Also, residual energy of nodes (both CHs and member nodes) is not considered while selecting cluster, which may lead to smaller network lifetime. In this paper we have proposed a fuzzy logic based energy aware *k-hop* clustering method which does not require the knowledge of whole topology and results in better energy efficiency of CH(s) as well as overall cluster.

HEED [12] is a distributed clustering scheme which considers a hybrid of energy and intra cluster communication cost when selecting CHs. However, HEED requires several iterations to form clusters. During each iteration, a lot of control messages are exchanged, which in turn leads to high overhead. Also, in HEED implementation, the nodes which are not covered by any CH are forced to become a CH. These CHs may lie in range of other CHs and also lead to higher number of CHs. Distributed Weight-based Energy-efficient Hierarchical Clustering protocol (DWEHC), proposed by Ding et al. [13], is a clustering algorithm similar to HEED. DWEHC is proposed to improve HEED by maintaining balanced cluster sizes and optimizing the intra-cluster topology using location awareness of the nodes. However, similar to HEED, the iterative nature of DWEHC produces a relatively high control message overhead. Our proposed algorithm is not iterative in nature and is computationally inexpensive leading to low control overheads. Further, the algorithm ensures that no two nodes which are in each other's communication range are selected as CHs.

Methods proposed by Gupta et al. [14], CHEF [15], CHEATS [16], Anno et al. [17] and LEACH-ERE [18], Taheri et al. [19], Mhemed et al. [20] are fuzzy logic based CH selection methods. In these methods Fuzzy Rule Based system is used for blending different clustering parameters. However, for energy sensitive wireless sensor nodes executing a large number of rules leads to high computational complexity and delay. Also, in related literature no emphasis is given for deriving the parameters required for clustering and their Automatic adjustment as the clustering process progresses. No modeling of the network is presented to derive defined parameters and parameters are not mapped into a single domain for observing

their actual impact. To address these issues, we have modeled the WSN by a fuzzy graph and for CH selection only fuzzy membership functions are used as compared to Fuzzy Rule Based system. Fuzzy logic is used to derive all necessary parameters i.e. link quality and metrics (*Fuzzy k-hop centrality* proposed in paper) required for clustering and their automatic adjustment. Further, the proposed model has been built in a manner so that it can be applied to dynamic, semi-dynamic and static clustering environment.

In wireless networks, nodes can control their transmission power on the basis of received signal strength [6,7,14–17]. As such the primary nodes (nodes which are within[1] cluster radius of a (CH)) consume overall less power as compared to secondary nodes (nodes which are not within cluster radius and connected to CH either through other nodes or by extension of their power). In case of extension of power by secondary nodes, due to sensors' RF characteristics, there is a maximum level up to which the power can be extended. In terms of energy efficiency, direct transmission between member nodes and their respective CHs is more preferable [21]. However, the overall life span of the network can be further increased, if the directly connected nodes after decrease in their energy levels can become *k-hop* ($k > 1$) secondary nodes. Unlike, the existing literature [6,7,14–18,22,23], these issue has been addressed in the proposed work by defining a fuzzy set and set membership function with respect to permissible transmission power and residual energy.

In existing literature, in most of the CH(s) selection methods [12–20,22–24] residual energy is considered as sole criteria for the selection of CH(s). In WSNs, during initialization of network, all nodes start with almost equal initial energy and is eligible for becoming CH. Many methods [14–20,22–24] are proposed in literature to break ties in CH selection, resulting from equal energy. However, these methods seldom consider the effect of initial selection of CH(s) on later rounds and overall energy efficiency of resulted cluster. One initial bad selection of cluster will repeatedly affect the later clustering rounds and hamper the lifetime of network [21,25]. Centrality measures have been used in literature as a metric for resolving ties and better CH selection. Degree centrality [26], which is the number of nodes that a given node is directly connected and closeness centrality, which is total geodesic distance from a given node to all other nodes [26,27] has been used in literature. In [14] a centralized approach using degree and closeness centrality has been proposed wherein Base station has to collect three fuzzy variables (concentration, energy and centrality) from all sensor nodes and then to elect a CH based on the collected information. Kim et al. [15] has also proposed a fuzzy logic based localized election mechanism (CHEF) that uses two fuzzy descriptors; residual energy and node closeness centrality with respect to immediate neighbourhood. In [17], author has used different fuzzy descriptors, the residual energy, node degree (centrality), distance from cluster centroid (closeness centrality), network traffic, and have evaluated their performance. LEACH-ERE [18] proposed by Lee et al., is also a fuzzy logic based selection criteria to elect CH. In addition to the residual energy, the expected residual energy (ERE), which considers node degree, has been considered to act as a fuzzy descriptor during CH selection process. In [19], degree centrality and in [20] local closeness centrality has been used as one of the input parameter for fuzzy rule based system. Gao et al. in [24] has proposed novel fuzzy multiple criteria decision making approach to elect CHs. Degree centrality is used as one of the metric to define evaluation value of a CH. When the degree centrality of a node is equal to the optimal number, the evaluation value is considered as 1. Energy-Efficient Cluster Head Selection (NECHS) [22] is a mechanism where number of neighbor nodes and remaining energy are the input variables of fuzzy system. In [23], each node calculates its distance from the area centroid, thus centrality of a

[1] Communication Radius of Cluster Head.

node is with respect to area centroid and not with respect to a particular cluster i.e. cluster centroid. This leads to overall high energy consumption in the network for other nodes to transmit data through the selected node. However in all of the methods, centrality of a node is calculated either with respect to entire topology—centralized method (closeness) or with respect to immediate neighbourhood—local method (degree). For sensor networks, in which nodes have limited resources and are randomly and densely deployed, maintaining record of whole topology by any node is not possible. At the same time employing a centralized authority to maintain network topology records and for taking decisions is not an energy efficient solution. In case the centrality is dependent upon nodes directly connected, it does not present a good comparison due to fact that cluster radius is not restricted to single hop (direct neighbourhood). As such CH has to address all the nodes which are closer to it than other selected CH(s) both *i.e.* direct and indirect. In view of the above there is a need of a centrality method which takes into account all the nodes *i.e.* both direct neighbours and k-hop neighbours. In this paper we have proposed a new centrality measure named as *fuzzy k-hop centrality* metric. The proposed metric computes the centrality of the node with respect to k-hop neighbourhood and addresses the problems of both the scenarios of considering the entire topology and being dependent only on the direct connections. In [28,29] k-hop clustering is proposed, but in those methods CHs are randomly selected and member nodes up to k–hops join them. No attention is paid towards the quality of CH. So these methods are entirely different from the random clustering approach followed by in the proposed work.

We summarize the main contribution of this paper as follows:

- Modeling of Wireless sensor network using Fuzzy Graph for Automatic adjustment of clustering parameters with respect to clustering rounds. Our modeling approach considers residual energy and geodesic distance between respective nodes to address dynamic characteristics of network. We also discussed the limitations of modeling of WSNs using Geometric Graph.
- Deriving the parameters for clustering and to address the constraints related to link quality, residual energy and maximum possible transmission range extension.
- Deriving a new centrality metric for better cluster formations throughout the lifetime of network. Our defined centrality metric ensures energy efficiency of resulted cluster, minimizes communication cost.
- A stand-alone distributed clustering algorithm has been developed that considers both energy and cluster communication cost. The proposed algorithm provides a method to prolong network life time with minimal computational complexity and control overhead, while identifying well distributed CH(s) within the existing constraints. We also discuss how our proposed algorithm is better than other clustering methods.
- The proposed method is simulated using MATLAB. The simulation results demonstrate that the proposed algorithm resulted in prolonged network lifetime in terms of clustering rounds, increased scalability, higher energy efficiency and uniform cluster head and cluster members distribution, as compare to LEACH-ERE and CHEF.

Thus unlike existing work [6–8,11–20,22–24], which addresses one issue at a time, the proposed work addresses all these issues in an integrated manner. The rest of the paper is organised as follows. Section 2 describes network architecture of a cluster based WSN and presents the main objectives of proposed clustering method. Section 3 explains the network modeling through fuzzy graph and derivation of all related parameters. Section 4 defines and derives *the fuzzy k- hop centrality* metric. Section 5 discusses the new clustering algorithm. Section 6 evaluates the effectiveness of the proposed approach via simulations. Finally, Sect. 7 contains concluding remarks and directions for future work.

2 Cluster Based Wireless Sensor Network

2.1 Network Architecture

In cluster based wireless sensor networks nodes are partitioned into a number of small groups called clusters. Certain node(s) in cluster(s) are selected as 'cluster heads', remaining nodes are termed as member nodes. CH(s) need to collect data from all the member nodes, control data communication and then transmit the aggregated packets to the base station. Nodes which are selected as CHs need to spend more energy than member nodes. In order to balance energy consumption among sensor nodes the whole data collection in clustered architecture is divided into periodic rounds. Each round consists of setup phase and steady phase. During setup phase selection of CH(s) is done and during steady phase data collection by CH(s) and final transmission to base station takes place [6–8,14–18]. In order to ensure low set up overhead, steady state time interval T_{OT} is kept very long than setup phase time interval T_{SP} i.e. $T_{OT} \gg T_{SP}$. The duration of steady state cycle is divided into slots and each sensor is assigned one slot for transmission of data. Between clusters there is negligible interference. This is achieved by assigning non overlapping frequency bands to adjacent clusters. For a cluster based WSN, whether multihop (indirect) or direct transmission should be used between sensors and cluster heads depends on multiple factors, including sensors' RF characteristics and the placement of CHs. However, in terms of energy efficiency, direct transmission between member nodes and their respective cluster heads is suitable [21,25].

2.2 Objectives of Proposed Clustering Method

In order to utilize energy resources uniformly and efficiently residual energy of a node is considered as the key parameter in selection of CH(s). Along with residual energy there is a need for another decision metrics for better cluster(s) selection to ensure the following:

- Better Network lifetime by efficient and minimum utilization of resources.
- Scalable and adaptive to change the relative importance of different parameters at different stages of network life.
- Low System complexity and control overhead
- Low computational time.
- Well distributed cluster(s).
- Transmission power control, while considering maximum allowable transmission range of node.

In our paper; we have addressed the above concerns by modeling WSN using fuzzy vertex and edge graph. For clustering we have defined two metrics *residual energy* and *fuzzy k*-hop *centrality*. *Residual energy* of a node has been defined as fuzzy set and associated fuzzy membership function so as address constraints related to points 1, 3 and 4 and *fuzzy k-hop centrality* is a fuzzy function to address the constraints related to point 2, 5, and 6.

3 Modeling of Wireless Sensor Network

3.1 Selection of Modeling Approach

Wireless sensor network can be modeled as directed geometric graph $G = (V, E)$, $V = \bigcup_{i=1}^{n} v_i$ and $E \subseteq V \times V$, where V represents the set of n alive nodes, v_i represents ith

node belonging to V and E represents set of edges. Each node $v_i \in V$ uses its radio link to create a point to point communication link with other nodes (neighbours) present in its communication range. For a network, let $V_{v_i}^k \subseteq V$ represents the set of neighbour nodes of v_i up to k-hops and $v_j^k \in V_{v_i}^k$ represents any particular k-hop neighbour node of v_i. Node v_i could define a subset, $V_{v_i}^1 \subseteq V_{v_i}^k$, a subset composed of nodes of $V_{v_i}^k$ which receive a minimal power of v_i's radio signal, where v_j^1 represents any 1-hop neighbour node of v_i. When this received power is exceeded above threshold (δ), the radio link (connectivity) between nodes v_i and v_j^1 is established. In the graphical representation of the network it leads to an edge binding between two nodes. The said geometric graph can be defined as follows:

Definition 1 (*Directed Geometric Graph*). For a wireless network modeled as directed geometric graph $G = (V, E)$, $V = \bigcup_{i=1}^{n} v_i$ and $E \subseteq V \times V$. Where V represents the set of n alive nodes, v_i represents ith node belonging to V and E represents set of edges. Node v_i defines a subset $V_{v_i}^k \subseteq V$, which composed of nodes $v_j^k \in V_{v_i}^k$, where $V_{v_i}^1$ represents the set of primary nodes v_i and $V_{v_i}^k - V_{v_i}^1$ represents the set of secondary nodes of node v_i, connected up to k-hops.

However, in WSNs, random placement of sensor nodes and transmission power control (TPC) mechanism [6] leads to non-binary connectivity relationship between directly connected sensor nodes i.e. between v_i and $V_{v_i}^1$. This non binary relationship is represented as edge weight. The nodes v_j^1 which receive high signal strength from v_i (low distance in-between) have higher edge weight as compared to pair of nodes which receives low signal strength.

For cluster based architecture of WSN, each node $v_i \in V$ is mapped to exactly one cluster v_c, where $1 \leq c \leq n_c$, $n_c \leq n$, n_c represents number of clusters and v_c represents any elected CH. A node can communicate with its CH directly (via single hop) or indirectly (via multi hop) depending upon the maximum available transmission power.

The transmission power of the nodes can be determined on the basis of their edge weights with the respective CH. The node v_j which can not connected directly to any CHs but can connected through *k-hops*, i.e. for which $v_c \in V_{v_i}^k$, relay their data to their respective nearest CH via other intermediate nodes. These secondary nodes choose their relay/intermediate nodes in such that sum total of edge weights of the relay/intermediate nodes is maximum.

Though the modeling by Geometric Graph addresses the random deployment of nodes and transmission power control mechanism but it does not addresses the constraints arising due to dynamic nature of the network. Firstly, the nodes which also act as relay nodes for other secondary nodes, consume more power due to transmission of data of these secondary nodes leading to non uniform consumption of energy which in turn affects the overall life span of the network. This constraint can be addressed by making residual energy as one of the parameters for determining edge weight so that with the consumption of energy of the relay nodes, the availability of alternate relay nodes having better residual energy can be explored. Secondly, as the clustering rounds progresses and the residual energy of the nodes gets consumed and a stage is reached when the residual energy of nodes (having high transmission power requirement due to their geographical location) is not sufficient even for a single round of clustering. The overall life span of the network can be increased if the edge weight takes into accounts the residual energy in such a manner that these nodes after reaching this stage become eligible as indirectly connected secondary nodes. In other words, 1-hop communication radius shall get deflated to increase the life span of the network.

These two issues have been addressed through edge membership functions defined by Definitions 6 and 8 and 9 of Sect. 3.2 and 4 respectively. These edge membership functions

are dependent upon two independent variables i.e. residual energy and geometric distance, which needs expert knowledge that can be imbibed in the system by defining fuzzy set and set membership functions for both residual energy and [2]received signal strength. We have incorporated this concept by using fuzzy vertex and edge graph.

3.2 Modeling of WSN Using Fuzzy Graph

For modeling of WSN we have extended fuzzy vertex and edge graph [30] which allows the attachment of fuzzy membership degrees to both vertices and edges. In addition issues discussed in the previous section, the representation with the fuzzy graph provides a solution to compute various performance metrics, which is not the case with other similar solutions [14–20,22–24]. Our proposed fuzzy vertex and edge graph $G'(\tilde{V}, \tilde{E}, \mu(v), \mu(e))$ has been derived from the geometric graph, $G(V, E)$. In the derived fuzzy graph $G'(\tilde{V}, \tilde{E})$, to every vertex V and each edge e of $G(V, E)$, a fuzzy membership degree is attached from [0, 1].

Definition 2 (*Fuzzy Vertex and Edge Graph*). The graph $G'(\tilde{V}, \tilde{E}, \mu(v), \mu(e))$ will be called a fuzzy vertex and edge graph on V and E where, $\mu(v_i) : V \rightarrow [0, 1]$ stands for membership level of each node v_i and $\mu(e_{i,j}) : E \rightarrow [0, 1]$ stands for the membership level of each link between node v_i and v_j. The final Arc Binding function (final edge weight) i.e. $\mu^e_{i,j}$ between nodes can be derived from $\mu(v)$, $\mu(e)$ using fuzzy relationship *T-norms* [31].

In the proposed work, the membership degree attached to each node (vertex) and membership degree attached to each edge are adopted in a way to approximate the capacity of the nodes to stay alive in a cluster and required transmission power respectively. In this paper, for each node $v_i \in V$, a linguistic variable *Residual Energy* and a fuzzy set *High Lifetime* $(\tilde{A})$ are defined. A fuzzy membership function is designed to map a value of the residual energy to its corresponding Fuzzy Lifetime membership degree $\mu(v_i)$ in the fuzzy set *High Lifetime*. The set membership functions are assigned to prioritize nodes according to their residual energy.

Definition 3 [32,33] (*Fuzzy Set*). If X is a collection of objects denoted by x, then a fuzzy set $\tilde{X}$ in X is a set of ordered pairs: $\tilde{X} = \left\{\left(x, \mu_{\tilde{X}}(x)\right) | x \in X\right\}$. $\mu_{\tilde{X}}(x)$ is called the membership function of x in $\tilde{X}$ that maps X to the membership space M. The range of the membership function is a subset of the non-negative real numbers whose supremum is finite. The membership function is not limited to values between 0 and 1 but if $sup_x(\mu_{\tilde{X}}(x)) = 1$, the fuzzy set $\tilde{X}$ is called normal i.e. $\mu_{\tilde{X}} : X \rightarrow [0, 1]$

Fuzzy sets allow an object to be a partial member of a set and membership function represents a "Degree of Belongingness" for each object to a fuzzy set, and provides a mapping of objects to a continuous membership value in the interval [0, 1]. When a membership value is close to the value 1 $(\mu_A(x) \rightarrow 1)$, it means that input x belongs to the set A with high degree, while small membership values $(\mu_A(x) \rightarrow 0)$, indicates that set A does not suit input x very well. The most commonly used membership functions are triangular, trapezoidal, piecewise linear and Gaussian [34]. These membership functions provide simple formulas and computational efficiency and have been used extensively, especially in real-time implementations. However, the selection of these membership functions does not have significant impact on the behavior of the system [35].

[2] More the received signal strength lesser is the transmission power required to establish link.

Definition 4 (*Fuzzy Set High Lifetime*). If V is a set of sensor nodes denoted by v, then a fuzzy set *High Lifetime* $(\tilde{A})$ in V is a set of ordered pairs: $\tilde{A} = \{(v_i, \mu(v_i)) | v \in V\}$. $\mu(v_i)$ is called the membership function of v_i in $\tilde{A}$ and is given by following equations:

$$\mu(v_i) = \begin{cases} 1 & for \quad E_R \geq E_{\max} - \xi \\ (E_R - \xi)/(E_{\max} - 2\xi) & for \quad E_{\max} - \xi \geq E_R \geq \xi \\ 0 & for \quad E_R < \xi \ and \ E_R > E_{\max} \\ & \forall v_i \in V \end{cases} \tag{1}$$

where, E_{R} is the current residual energy associated with a node, E_{max} is the maximum available energy and ξ is the calculated maximum energy required by a member node to remain functional for a single steady state cycle of clustering. In order to incorporate manufacturing imperfection in implanted batteries and so as to give equal importance to all nodes at the starting rounds of clustering, Residual energy above $E_{\max} - \xi$ is assigned membership value equal to 1.To calculate ξ, sensors are assumed to be randomly distributed i.e. as per a homogeneous spatial Poisson process of intensity λ in 2-dimensional space. In random clustering process any node can become a cluster head with some probability p. Thus, both cluster heads and member nodes can be assumed to be distributed as per independent homogeneous spatial process PP1 and PP0 of intensity $\lambda_1 = p\lambda$ and $\lambda_0 = (1-p)\lambda$ respectively [36,37]. Each member node joins the cluster of the closest cluster head to form a Voronoi tessellation [38]. The plane is thus divided into zones called the Voronoi cells and each Voronoi cell corresponding to a PP1 process point and a fraction of PP0 process points in each Voronoi cell. If n_α is the random variable denoting the number of PP0 process points in each Voronoi cell and R_{max} is the maximum possible distance at which a PP0 process point can be from its nucleus point PP1, then according to results in [37],

$$E[(n_\alpha | N = n) \approx E[n_\alpha] = \frac{\lambda_0}{\lambda_1} \tag{2}$$

$$R_{\max} = R_{\alpha_p} \leq \sqrt{\frac{-.917 \ln(\alpha_p)}{p_R \lambda_1}} \tag{3}$$

where, R_{α_p} is the value of distance such that probability $(\mathrm{p_R})$ of distance between a PP0 process points and its corresponding PP1 point process greater than R_{max} is less than α_p, where α_p is a very small value and $p_R \leq 7\exp(-1.09\lambda_1 R^2)$

Thus using Eqs. 2 and 3, ξ is given by:

$$\xi(l, d) = N_{frame} \times E_{Tx}(l, R_{\max}) \tag{4}$$

where,

$$N_{frame} = \frac{T_{OT}}{n_\alpha \times t_{slot} + t_{chtoBs}} \tag{5}$$

T_{OT} is the operation time of the steady-state phase, t_{slot} is the slotted time required for the transmission from a member node to the CH, and t_{chtoBs} is the time required for the transmission from CH to the base station. $E_{Tx}(l, R_{\max})$ is the energy consumed by a node to transmit one packet of size l-units at a distance of R_{max} [39,40] and is given by:

$$E_{Tx}(l, d) = \begin{cases} l * E_{elec}^{tx} + l * \varepsilon_{fs} * d^2, & d < d_0 \\ l * E_{elec}^{tx} + l * \varepsilon_{amp} * d^4, & d \geq d_0 \end{cases} \tag{6}$$

$$d_0 = \sqrt{\frac{\varepsilon_{fs}}{\varepsilon_{amp}}} \tag{7}$$

where E_{elec}^{tx} is the energy consumption per bit in the transmitter circuit and ε_{fs} and ε_{amp} are the energy consumption factor of amplification for the free space and multipath radio models, respectively.

In order to incorporate minimum transmission cost for a cluster, another linguistic variable *Received Signal Power* for a edge $e(v_{i,}v_j)$, and a corresponding fuzzy set *Low Energy Consumption* ($\tilde{B}$) are defined. A fuzzy membership function is proposed to map a value of a variable Received Signal Power to its corresponding Minimum Transmission Power membership degree $\mu(e)$ in the fuzzy set *Low Energy consumption*. In Clustered WSNs, this received signal power provides approximation to minimum requisite transmission power by member nodes for establishing link with CH. The low value of required transmission power indicates better proximity with CH and hence indicates energy efficient cluster. However with availability of transmission power control and thereby range extension possibility available with nodes, received signal power between nodes can be represented with a Fuzzy set and set membership functions. The fuzzy set representation incorporates different range extension facilities and addresses the limitation of imprecision in signal strength measurement [41].

Definition 5 (*Fuzzy Set Low Energy Consumption*) If E is a set of edges between sensor nodes, then a fuzzy set *Low Energy Consumption* ($\tilde{B}$) in E is a set of ordered pairs: $\tilde{B} = \left\{\left(e(v_i, v_j), \mu\left(e_{i,j}\right)\right) | e(v_i, v_j) \in E\right\}$. $\mu(e)$ is called the membership function of edge $e(v_{i,}v_j)$ in $\tilde{B}$ and is given by following equations:

$$\mu(e) = \begin{cases} 0 & for \quad R < \delta \\ (R-\delta)/(\gamma-\delta) & for \quad \delta \leq R \leq \gamma \\ 0 & for \quad R > \gamma \\ & \forall e(v_i, v_j) \in E \end{cases} \tag{8}$$

where, δ is the threshold value defined on receiver's sensitivity, γ is the minimum transmission power used by all nodes for constructing a connected geometric graph [42] and R is the actual received signal strength. For a sensor node, the minimum threshold value of received signal strength δ is dependent upon receiver's sensitivity, which is different for different manufactures.

By using fuzzy set and assigning fuzzy membership values between 0 to 1, residual energy and received signal power which have different measurement units have been made comparable so as to ensure optimal and objective conclusions. Also, all the membership degrees corresponding to residual energy and received signal power below a certain threshold value (ξ, δ) are assigned '0' importance so as to omit these nodes and edges for modeling the network which in turn increases the reliability.

For the computation of the resultant arc binding function $\mu_{i,j}^{e}$ of an directed edge $e'(v_i, v_j)$ of graph $G'(\tilde{V}, \tilde{E})$ between two connected nodes, a fuzzy relationship T-norm function is computed using *Fuzzy Lifetime* membership degree $\mu(v)$ and *Minimum Transmission Power* membership degree $\mu(e)$.

Definition 6 (*Resultant Arc Binding Fuzzy Membership Function*) For given two vertices and a connecting edge, the degrees associated with vertices represent its corresponding Fuzzy Lifetime membership degree $\mu(v)$ in the fuzzy set *High Lifetime*. Independent degree associated with edge represents its corresponding Minimum Transmission Power membership degree $\mu(e_{i,j})$ in the fuzzy set *Low Energy consumption*, where $i \neq j, 0 \leq \mu(v) \leq 1$ and $0 \leq \mu(e_{i,j}) \leq 1$. The resultant arc binding fuzzy membership function belonging to fuzzy edge $e'(v_i, v_j)$ is represented by $\mu_{i,j}^{e}$ and is given by:

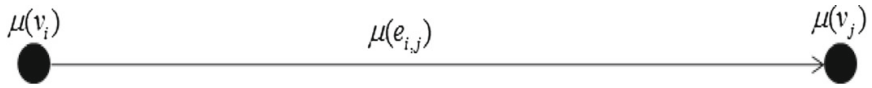


Fig. 1 Membership Degrees assigned in Fuzzy Vertex and Edge Graph

$$\mu^e_{i,j}(v_i, v_j) = f(\mu(v_j), \mu(e_{i,j})) \tag{9}$$

The resultant arc binding fuzzy membership function belonging to fuzzy edge $e'(v_j, v_i)$ is represented by $\mu^e_{j,i}$ and is given by:

$$\mu^e_{j,i}(v_j, v_i) = f(\mu(v_i), \mu(e_{j,i})) \tag{10}$$

where, $f(\mu(v_j), \mu(e_{i,j}))$ is a function expressing the degree of the existence of a edge $e'(v_i, v_j)$ and is usually realized by Fuzzy relationship *T-norm*. A directed edge of a fuzzy vertex and edge can be shown by Fig. 1.

Definition 7 [31] (*Fuzzy relationship T-norms*). Fuzzy relationship Triangular norms (T-norms) are monotone, commutative and associative functions $[0, 1] \times [0, 1] \rightarrow [0, 1]$ which are eligible for fuzzy set intersection. Although a number of T-norm operators have been proposed in the literature, as a useful set of operators which are good representatives of the range of possible T-norm functions, [43] proposes following T-norms:

$$\begin{aligned} T_1(x, y) &= max(0, x + y - 1) \\ T_2(x, y) &= xy \\ T_3(x, y) &= min(x, y) \end{aligned} \tag{11}$$

In the proposed method, fuzzy relationship *min* T-norm is used to calculate the final arc binding membership function. *Min* T-norm has been used as during preliminary rounds of clustering, each node has sufficient and equal energy and the signal strength will be the sole determining factor for connection strength/weight of edge between nodes. However, during each round there is energy consumption by nodes which in turn leads to non uniform energy level of nodes in later rounds. Thus during later rounds the connection strength/weight of edge will be dominated by residual energy so as to ensure that cluster is formed by nodes with sufficient residual energy. Hence the proposed methodology automatically caters to dynamic characteristics of the network. Mathematically, $\mu^e_{i,j}$ may be represented as

$$\mu^e_{i,j}(v_i, v_j) = min(\mu(v_j), \mu(e_{i,j})) \tag{12}$$

The above concept of deriving value of arc connection between two nodes in fuzzy vertex and edge graph is illustrated with the following example.

Example 1 For the given values of $\mu(v_i) = .7$, $\mu(v_j) = .5$ and $\mu(e_{i,j}) = .8$, the computed value of directed edge $e'(v_i, v_j)$ binding v_i to v_j i.e. $\mu^e_{i,j}$ for Fig. 2a is $= min(.5, .8) = .5$ and is represented in Fig. 2b.

The following example illustrates the computation of different parameters required for modeling of a wireless sensor network and explains the choice of relay node using fuzzy vertex and edge graph.

Example 2 For the given values of $E_{max} = 2$ J, $\xi = .15$ mJ, $\delta = -88$ dbm and $\gamma = 20$ dbm, the computed values of $\mu(v_i)$, $\mu(v_j)$, $\mu(e_{i,j})$, $\mu^e_{i,j}$ and the choice of relay node (v_j) by node v_i is given in Table 1.

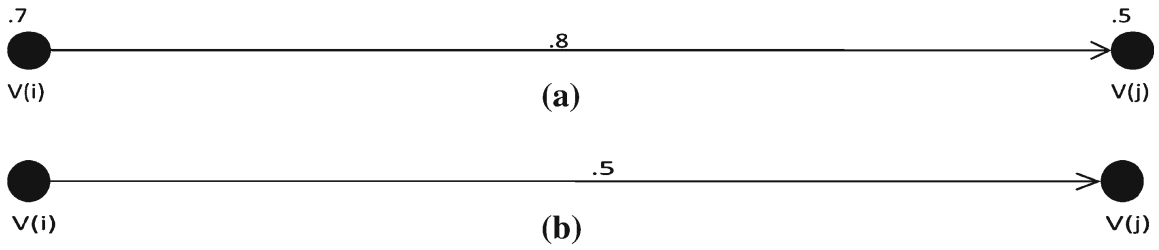


Fig. 2 Calculation of final arc binding function for fuzzy vertex and edge graph

Table 1 Arc binding membership function of an edge

For $E_{max} = 2$ J and $\xi = .15$ mJ			$\delta = -88$ dbm, $\gamma = 20$ dbm			$\mu^e_{i,j}(v_i, v_j) = min(\mu(v_j), \mu(e_{i,j}))$
Node (v_j)	Residual energy E_R *(assumed)*	Calculated membership degree $\mu(v_i)$	$e(v_i, v_j)$	Received Signal Strength R *(assumed)* (dbm)	Calculated membership degree $\mu(e_{i,j})$	Calculated arc binding membership function $\mu^e_{i,j}$
v_a	1.6J	.7961	(v_i, v_a)	0	.8148	.7961
v_b	.8J	.3823	(v_i, v_b)	10	.9074	.3823
v_c	1.1 J	.5588	(v_i, v_c)	−80	.3518	.3518

In the above example, though node **b** has highest value of received signal strength, node **a** has been selected as relay node due to higher arc binding membership function which is dependent upon on both residual energy and received signal strength.

4 Fuzzy k-Hop Centrality

In a CWSN, cluster head is responsible for handling communication of primary nodes ($k = 1$) and nodes up to k-hops ($k \geq 2$) (secondary nodes). However, in related literature, centrality of a CH does not consider these secondary nodes or it is assumed that all nodes which are closer to a cluster head than other cluster heads will communicate with the closer cluster head directly. These assumptions adversely affect the optimum selection of clusters as secondary nodes are also important for efficient clustering and all the secondary nodes are not able to communicate directly with the cluster head due to their constraints in respect of residual energy and available transmission range. To address this issue, we have derived fuzzy logic based membership functions for computing the possibility with which a node can directly communicate with cluster head along with the possibility of a node to get connected through multi hopping. Each node v_i maintain two lists, one for primary and secondary nodes which can be directly connected and another for secondary nodes which can be reached through multi hopping along with respective possibility values.

Definition 8 (*Possibility Function for Direct Connection*). The possibility with which nodes are directly connected to CH is given by following membership function.

$$\mu^{dir}_{i,j} = \min_{v_i \in V} \left\{ \left\{ \mu(v_i) + \mu(e_{i,j}) - 1 \right\}, \mathrm{A} \right\} \tag{13}$$

where,

$$\mathrm{A} = \underset{\substack{v_j \in V_{v_i}^k \\ i \neq j \neq l}}{max} \left\{ \mu_{i,j}^{e}, \underset{v_l \in V_{v_i}^k}{max} \left\{ \underset{\substack{e'(v_l, v_j) \in \widetilde{E} \\ \mu_{i,l}^{dir} > 0}}{max} \left\{ 0, \mu_{i,l}^{e} + \mu_{l,j}^{e} - 1 \right\} \right\} \right\} \tag{14}$$

This membership function is considered at the time of CH selection while calculating fuzzy k-hop centrality metric of tentative CHs.

Definition 9 (*Possibility Function for Indirect Connection*). The possibility with which secondary nodes can connected to CH indirectly through multi hopping is given by following membership function.

$$\mu_{i,j}^{indir} = \underset{\substack{v_j \in V_{v_i}^k \\ i \neq j \neq l}}{max} \left\{ \mu_{i,j}^{e}, \mathrm{B} \right\} \tag{15}$$

where

$$\mathrm{B} = \underset{v_l \in V_{v_i}^k}{max} \left\{ \underset{\substack{e'(v_l, v_j) \in \widetilde{E} \\ \mu_{i,l}^{dir} > 0}}{min} \left\{ \mu_{i,l}^{e}, \mu_{l,j}^{e} \right\} \right\} \tag{16}$$

This membership function is used by member nodes when no direct connection with final CH(s) is possible.

In has been analysed in [25], that clusters with directly connected member nodes, both primary and secondary, performs best for a large spectrum of different network sizes, node densities and number of base stations. To apply this concept we have defined a new metric *fuzzy k-hop* centrality which has been derived by using k-hop centrality. The measure of k-hop centrality C^k of node v_i is taken as the sum total of possibility values $\mu_{i,k}^{dir}$ with which it is directly connected to other nodes (both primary and secondary). Mathematically,

$$C^k(v_i) = \sum_{\substack{j=1 \\ j \neq i \\ v_j \in V_{v_i}}}^{n} \mu_{i,j}^{dir}(v_i, v_j) \tag{17}$$

where

$$k = \frac{R_{\max}}{d_{hop}} \tag{18}$$

R_{max} is as given by Eq. (3) and d_{hop} is the one hop communication radius calculated in respect to minimum transmission power γ used by all nodes for constructing a connected geometric graph [42]. If we use Eq. (17) as CH selection metric, even a large number of weak connections i.e. for small value of $\mu_{i,j}^{dir}$ can add up to appear as a strong connection. This problem has been addressed by using a fuzzy α-level-set representation for the centrality i.e. $C_{\alpha}^{k}(v_i)$ which is the sum total of arc binding membership function with which nodes are connected to v_i with at least α membership function value [44] and is computed as under

$$C_{\alpha}^{k}(v_i) = \sum_{\substack{j=1 \\ j \neq i \\ v_j \in V_{v_i}}}^{n} \mu_{i,j}^{dir}(v_i, v_j) \quad for \quad \mu_{i,j}^{dir}(v_i, v_j) \geq \alpha \tag{19}$$

Definition 10 [34] (*Fuzzy* $\boldsymbol{\alpha}$*-level set*). A set A_α is a α-level set of a fuzzy set if it is made up of members whose membership is not less than α i.e. $A_\alpha = \left\{x \in X | \mu_{\tilde{A}}(x) \geq \alpha\right\}$, Here, α is any arbitrary value on the interval [0, 1]. The centrality metric $C_\alpha^k(v_i)$ can be normalized as under and the *fuzzy k-hop centrality* is given by:

$$\tilde{C}_\alpha^k(v_i) = 1 - \bigcup_{\alpha \in [0,1]} \left\{ \frac{\alpha}{C_\alpha^k(v_i)} \right\} \tag{20}$$

Definition 11 (*Fuzzy k-hop Centrality*). Fuzzy k-hop centrality $\tilde{C}_\alpha^k(v_i)$ can be used to select optimum clusters along with suitable CHs and is derived from the sum total of arc binding membership function, $C_\alpha^k(v_i)$ with which nodes are directly connected to v_i with at least α membership function value.

The concept and application of fuzzy k-hop centrality has been illustrated with the following example.

Example 3 [3] Assume three candidate nodes ***a***, ***b*** and ***c*** with almost equal residual energy and are competing for becoming CHs as shown in Fig. 3. By using only degree centrality [26], node ***b*** has precedence over node ***a*** **and** ***c***, as it is connected with 5 direct links, whereas ***a***, ***c*** are connected with 4 links. As already discussed, this method has limitations as it does not consider secondary nodes for computation of centrality. If we use closeness centrality, while treating links between nodes in discrete manner i.e. 1 if link exist, 0 otherwise, ***a*** and ***c*** has the same centrality value and has precedence over node ***b***. As already discussed, the calculation of closeness centrality [27] requires knowledge of whole topology, which puts strain on computational and power resources.

The third method is *k*-hop centrality, considering 2-hop centrality node ***a*** would be a better choice since it can reach 15 nodes in addition to itself while node ***c*** can only reach 13 nodes whereas node ***b*** can only reach 9 nodes. This is despite the fact that most of the member nodes of node ***a*** are connected to it with weak strength which in turn would require member nodes to transmit at higher transmission powers to reach and deliver data to node ***a*** (cluster head). At the same time, node ***c*** is connected to 13 nodes and all member nodes are connected to it with very high signal strength.

However, as both node degree and connectivity strength are important to calculate centrality of a node, node ***c*** should be the optimum choice. As indicated in Table 2, the proposed *fuzzy k-hop centrality* metric overcomes the constraints of the other centrality methods and provides the optimal solution.

5 Proposed Clustering Approach

This paper considers a WSN with a large number of sensor nodes randomly deployed over a 2-D planer area having identical computational capabilities and the same amount of initial battery energy. After deployment all sensor nodes and the base station are stationary. The sensor nodes can communicate with each other through short-range radios. The received signal strength is measurable and hence node can adjust their transmission range. Intra cluster MAC and the routing of packets is coordinated by the CH nodes so that packet transmissions and receptions within each cluster are synchronized.

[3] For simplicity this example assumes symmetric links.

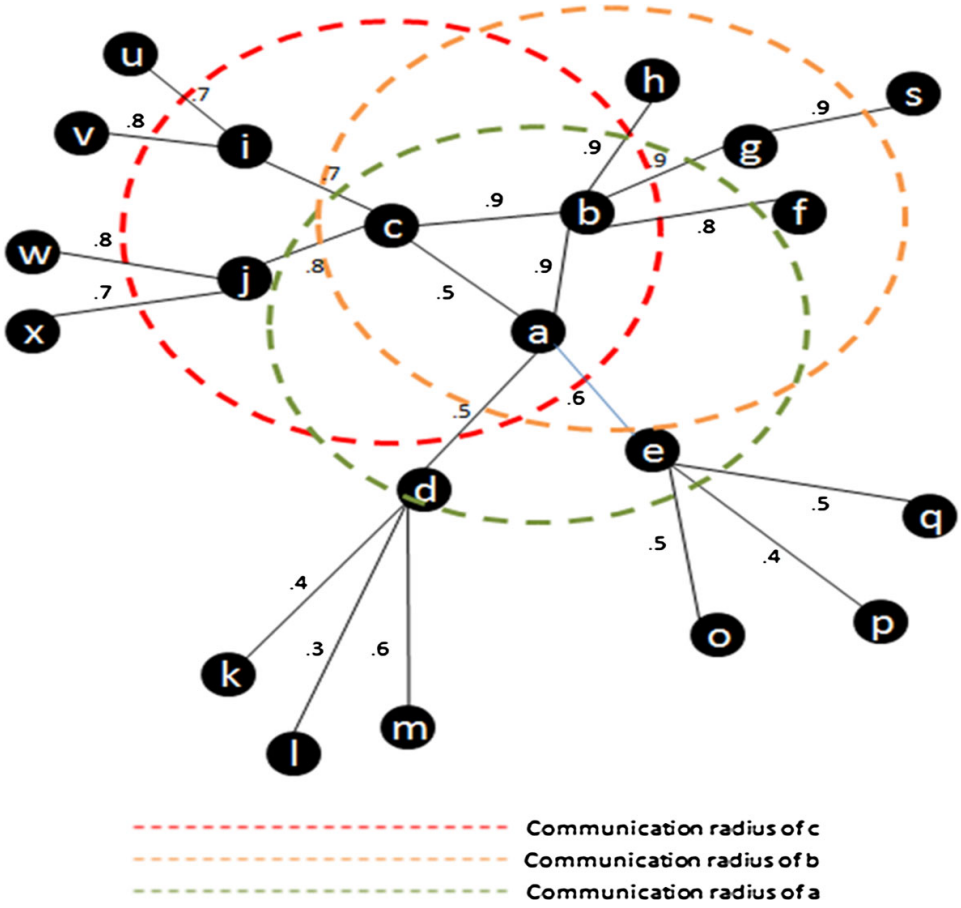


Fig. 3 Graphical representation of numerical example

Table 2 Fuzzy 2-hop centrality calculation for example given in Fig. 3

$\alpha = .3$				$\alpha = .4$		
Node (x_i)	$C^k(v_i)$	$C^k_\alpha(v_i)$	$\widetilde{C^k}(v_i)$	$C^k(v_i)$	$C^k_\alpha(v_i)$	$\widetilde{C^k_\alpha}(v_i)$
a	9.3	9	.9666	9.3	8.2	.9512
b	7	7	.9571	7	7	.9428
c	9.6	9.6	.9687	9.6	9.6	.9583

5.1 Selection of Candidate Cluster Heads

In the proposed method two clustering parameters i.e. Residual Energy and *fuzzy k-hop* Centrality of a node have been considered for cluster head selection. In order to balance energy consumption among sensor nodes, the method configures clusters in every round. During preliminary rounds of clustering, all nodes have equal and sufficient energy to become CH(s) and as such centrality of a node is the vital factor. However, during subsequent rounds as the residual energy starts decreasing, it becomes another important factor in selection of CHs.

In literature various Fuzzy Inference based clustering algorithms [14–18,22,23] are proposed, in which Fuzzy Rule Based System is used for blending different clustering parameters to select CHs. The Fuzzy Rule-Based System is most useful in modeling complex systems that can be observed by humans as it makes use of linguistic variables as its antecedents and

consequents, which can be represented by fuzzy sets and logical connectives of these sets. The rule based fuzzy system finds its utility where input parameters are non-linear in nature and relationship between these parameters is complex. Based on the number of rules, these systems execute large set of computations, which in turn leads to high response time and more energy consumption.

The present network has been modeled as fuzzy graph wherein the calculated centrality is a fuzzy number. Thus non-linear nature of the various parameters has been addressed by modeling the network through the fuzzy graph and fuzzy set membership values. Requisite residual energy for becoming a CH can be represented as fuzzy set where each node calculates its fitness μ_r corresponding to its residual energy during round r by using following membership function:

$$\mu_r(v_i) = \begin{array}{ll} 1 & for \quad E_R(v_i) \geq E_f \\ \frac{E_R(v_i)}{E_f} & for \quad 0 \leq E_{r(v_i)} \leq E_f \end{array} \tag{21}$$

and

$$E_f = E_{\max} - r \times \zeta \tag{22}$$

where, E_r is the current residual energy of node v_i and r denotes current clustering round. ξ is the maximum possible energy consumed by a member node for executing a single clustering round and has been approximated from Eq. 4. E_f is a variable to select energy abundant nodes and is updated in every round by using Eq. (22).

Each sensor node generates a random number *rand*() between 0 and 1. For any node v_i, if the generated random number and calculated $\mu_r(v_i)$ is greater than α_c, the node v_i, becomes a CH candidate (v_c).

$$i.e.\, v_i = v_c \; if \; rand(v_i) \;\&\&\; \mu_r(v_i) > \alpha_c \tag{23}$$

The parameter α_c plays an important role in the proposed clustering algorithm. Increasing α_c will shrink the number of candidate CH nodes and increase the weightage of residual energy but decreases the importance of centrality metric. Decreasing α_c will lead to decrease in importance of residual energy and will result in inefficient clustering. The per round average energy consumption by cluster heads and member nodes along with first node die metric are used as performance metrics to measure the efficiency of network operation. We analyze the effect of α_c on the network performance through simulations by fixing network topology and then varying α_c between 0 to 1. The average total energy consumption per round by member nodes and cluster head(s) is normalized by maximum energy cost and are denoted by E_{CH} and E_{MEM} . Each result is averaged on all possible clustering rounds and further for 100 different random network topologies. First Node Die (FND) [45] is averaged by maximum number of round for random topologies. It has been observed from results obtained from simulation (Fig. 4) that there exists a maximum FND value corresponding to an optimal value of α_c. Around this α_{opt} energy cost incurred by member nodes (E_{MEM}) as well energy cost for CHs (E_{CH}) is also minimum. This is mainly due to sufficient energy and optimum centrality value, which leads to efficient clustering. The optimum point for network performance is between ranges $.58 \leq \alpha_{opt} \leq .7$

By taking into consideration the energy consumed by member nodes during a round for computation of E_f it is ensured that sufficient number of nodes are eligible for the selection of CH. Also the nodes elected as CHs in recent rounds will not be eligible for re-selection as the energy consumed by a CH (E_c) is always much greater than energy consumed by a member node (E_m) i.e $E_c \gg E_m$. However, in subsequent rounds, the nodes which earlier

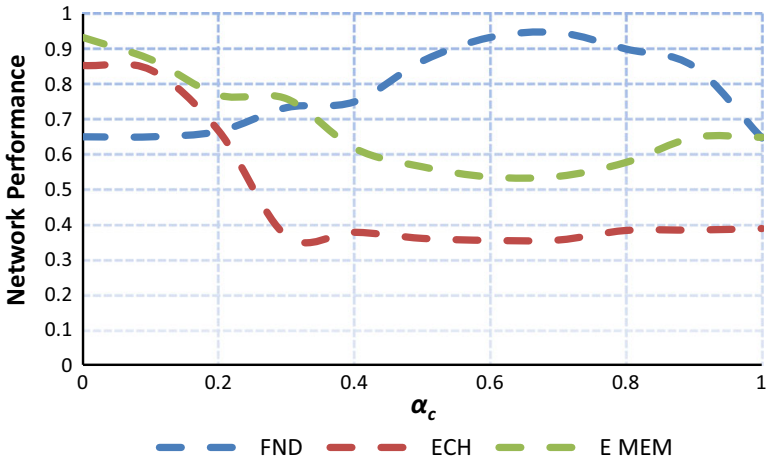


Fig. 4 The effect of α_c on the network performance

served as CH will again become eligible, as the value of $E_{f,}$ which is decreasing in each round, will become comparable to their respective residual energy (E_r).

The selection of CHs among these candidate nodes is based on *fuzzy k- hop centrality* $\breve{C}^k(v_i)$. The candidate CH(s) having high values of $\breve{C}^k(v_i)$ with respect to their competitors nodes becomes final CH(s). In most of the clustering algorithms in existing literature [6,7,9,13–17], a node after becoming a CH cannot become a CH again up to fixed clustering rounds, due to which the available number of nodes eligible for becoming CH(s) keep on decreasing with each passing round and as such selected CHs of later rounds are not true representatives of entire topology. This limitation has been addressed by selecting candidate nodes on the basis of residual energy. All nodes having energy more than α_c are eligible for becoming candidate nodes and hence sufficient number of nodes is always there for selection of CHs. As compared to other probabilistic as well as fuzzy inference based methods, the proposed method is computationally inexpensive, faster and does not introduce high delay for cluster(s) setup.

5.2 Proposed Clustering Algorithm

Similar to [6], the proposed clustering method configures clusters in every round. The pseudo code of the clustering method in described as Algorithm 1. For every round (lines 3–25), during set up phase each node calculates a membership function with respect to its residual energy and generates a random number. If this membership function and random number is more than a predefined threshold (line 6), the particular node(s) become candidate(s) for current CH(s) selection round. The candidate nodes calculate *fuzzy k-hop centrality* value (line 9) and then broadcast the candidate message with the centrality value. After advertising a candidate-message, these nodes wait candidate messages from other nodes. Subsequently, the candidate node(s) with highest values of centrality broadcasts the final CH-message up to k-hops indicating the selection of CH(s).

On the basis of same the non CH nodes selects their respective cluster heads. In case of multiple CH messages, the sequence of priority for CH selection will be that first preference will be given to the directly connected node over that of indirectly connected node. In case of CH nodes falling under same category, the one having higher membership function will get the precedence. If a node does not receive any final CH message, it declares itself as a separate CH. Finally member node sends a JOIN-REQ request to the respective head.

ALGORITHM 1. Clustering process

Input:
N: a wireless sensor network
v_i: a node of N
V: {v_c | v_c is v_i's *vicinity* node which is CH candidate}
α_c: a α- cut value to become a CH candidate
r: current clustering round
Output:
CH(v_i): the cluster head of the node v_i
isClusterHead(v_i): true if CH(v_i)=v_i
Function:
Broadcast (data, destination, no of hops)
Send (data, destination)
$\mu_r(v_i) = f(E_f, \xi, E_{r(v_i)})$
Network Initialization:
1. isClusterHeads(v_i) = false
2. $r \leftarrow 0$
Main:
/* for every clustering round */
3. $r = r+1$
4. $E_f = E_{max} - r \times \xi$;
5. $\mu_r(v_i) = f(E_f, \xi, E_{r(v_i)})$
6. **if** $\mu_r(v_i)$ && $rand(0,1) > \alpha_c$
7. CH(v_i) $\leftarrow v_i$
8. cent(v_i) $\leftarrow \widetilde{C^k}(v_i)$ // calculate fuzzy k-hop centrality
9. Broadcast (cent(v_i), id,1) //Candidate-Message broadcast their centrality value
10. On receiving Candidate-Messages from CH candidates
11. **for** each v_c *in* V
12. **if** $(cent(v_i) < cent(v_c))$
13. $CH(v_i) \leftarrow v_c$
14. **else** isClusterHead(v_i) $\leftarrow$ true
15. **end if**
16. **end if**
17. **if** (isClusterHead (v_i) == true)
18. broadcast (fin-CH-Message, V, k)
19. **else**
20. On receiving fin-CH-Message
21. **if** $(\mu_{i,c}^{dir} > 0)$,
22. Send JOIN-REQ messages to the closest CH
23. **else if** $(\mu_{i,c}^{indir} > 0)$
24. Send JOIN-REQ messages to the closest CH
25. **else**
26. CH(v_i)=v_i
27. **end if**
28. **end if**
29. **end if**

An illustrative example of showing CH(s) selection is presented as follows.

Example 4 Illustration of "algorithm for clustering" while considering 5 sensor nodes lying in each other's communication range and parameters $E_{max} = 1\,\text{J}, \xi = .003\,\text{mJ}, r = 60$, then $E_f = .82\,\alpha_c = .7$. The results on the basis of same are given in Table 3.

In the above example, initially node **1** and node **3** are selected as tentative CHs as both has μ_r and rand() number greater than equal to $\boldsymbol{\alpha_c}$. Subsequently on the basis of fuzzy k-hop centrality node **1** is elected as final CH.

Table 3 Final cluster head selection

$E_{max} = 1\,\text{J}, \xi = .003\,\text{mJ}, r = 60$, then $E_f = .82\alpha_c = .7$

S.no.	Residual energy (E_r)	μ_r	rand(0,1)	Candidate CH	Fuzzy k-hop centrality	Final CH
1	.85	1	.7	1	.67	1
2	.52	.634	.8	0	–	0
3.	.7	.853	.9	1	.59	0
4.	.48	.585	.9	0	–	0
5.	.79	.963	.6	0	–	0

6 Performance Evaluation

In this section, we have evaluated the performance of proposed clustering algorithm using fuzzy graph based modeled wireless sensor network through simulations. The simulation metrics and implementation are described in Sect. 6.1. In Sect. 6.2, on the basis of metrics discussed in Sect. 6.1, performance of the proposed method is compared with LEACH-ERE [18] and CHEF [15].

6.1 Metrics and Methodology

The implementation and evaluation of the proposed clustering approach is done through MATLAB simulations. For comparison with LEACH-ERE and CHEF, we use the same energy model and cluster rotation time as adopted in [6]. According to this model, transmission and receiving costs are characterized by the following equations:

$$E_{Tx}(l,d) = \begin{cases} l * E_{elec}^{tx} + l * \varepsilon_{fs} * d^2, & d < d_0 \\ l * E_{elec}^{tx} + l * \varepsilon_{amp} * d^4, & d \geq d_0 \end{cases} \tag{24}$$

$$E_{Rx}(l) = l * E_{elec}^{Rx} \tag{25}$$

where, l is the number of bit per packet, d is the distance from the sender node to the receiver node, E_{elec} *is* per bit energy dissipation in transmitting or receiving circuitry. ε_{fs} and ε_{amp} are the energy consumption factor of amplification for the free space and multipath radio models respectively. Simulations are done using the values 50 nJ/bit, 10 pJ/bit/m^2 and .0013 pj/bit/m^4 for E_{elec}, ε_{fs} and ε_{amp} respectively.

Evaluation of the performance of our proposed method is done in terms of: (I) Network life time, FND and Half Node Die (HND) metrics. Network lifetime is defined as the distribution of sensor nodes with respect to each round. FND is the estimated number of the rounds in which the first node dies and HND defines estimated the number of rounds in which half of the sensor nodes dies [45]. (II) Average energy dissipation by a CH, by all elected cluster head(s) and member nodes in a single round of clustering. (III) Node density, the term *node density* can be comprehended in two ways. On the one hand, the node density could be the average number of nodes per unit area of the sensing field. This way, with a fixed size of the sensing field, the node density depends on the total number of sensor nodes. On the other hand, the nodes are scattered randomly in the sensing field. The nodes may be dense in some areas, and sparse in others. Therefore, the node density varies inside the field [46].

The simulation is based on the following scenario: a random network consists of 500 nodes is deployed in an area of 200 m × 200 m. The sink is assumed to be situated at (100, 100) m of the above specified area. Each sensor node starts with initial energy equals to 2 J,

has maximum communication radius of 75 m and a sensing range of 20 m. For the present simulation 10 % data aggregation ratio has been assumed.

6.2 Performance Comparison

The performance of the proposed clustering algorithm is compared to LEACH-ERE and CHEF in terms of performance metrics discussed in Sect. 6.1. LEACH-ERE [18] proposed by Lee et al., is a recently proposed fuzzy logic based selection criteria to elect CH. In addition to the residual energy, the expected residual energy (ERE) has been introduced to act as a fuzzy descriptor during CH selection process. By using [18], workload among sensor nodes is evenly distributed and network lifetime has been outperformed as compare to LEACH [6]. ERE incorporates distance of the CH to the base station. Hence edge nodes would have lesser probability to become CHs than other nodes. Thus lesser the distance between node and base station and high residual energy, more the probability that it would become CH. In LEACH-ERE both residual energy as well as ERE has been taken as selection parameter. But proposed fuzzy rules have given more weightage to residual energy. Also, in ERE selection parameters may lead to selection of CHs with lesser number of neighbor nodes which may not result in optimum clustering. [15], a widely used method, has proposed a fuzzy logic based approach (namely CHEF: Cluster Head Election mechanism using Fuzzy logic). The method proposed by them is localized election mechanism using two fuzzy descriptors (residual energy and local distance). As the method considers local distance (sum total of distance between CH and directly connected nodes) and residual energy, this method identifies good CHs. However, this method is not suitable for sensor networks with very high density of sensor nodes. As the clustering process progresses and nodes batteries started exhausting, the clusters with member nodes with sufficient energy are required to form clusters. However this method only considers local distance and resulted into inefficient clustering.

For comparison identical wireless network characteristics has been considered. Same random seed has been used to generate the identical WSN topology. The simulation results are shown in Figs. 5, 6, 7 and 8. As per Fig. 5, the proposed method outperforms LEACH-ERE, CHEF in terms of network lifetime. In LEACH-ERE, during initial rounds of clustering a large number of nodes are eligible as candidate nodes. Also high computational cost due to fuzzy inference rules, leads to excessive overhead for choosing final CH and hence results in high energy consumption. Figure 6 shows the rounds in which first node and half of the nodes die for each algorithm and results shows that although there is not substantial improvement in FND, but HNA has substantially improved. Overall results indicate that proposed method results in prolonging the operational network lifetime.

Figures 7 and 8 shows the average energy consumed for the data transmission and reception by CHs and member nodes respectively and indicates that there is considerable energy savings in our algorithm. In Table 4 we have calculated the average energy, variance and standard deviation of the energy consumed per clustering by CHs during 100 randomly selected rounds. Our proposed method has resulted in steady energy consumption by the cluster heads. In our method *k-hop* consideration has successfully balanced the energy consumption between cluster heads. This in turn makes nearly constant energy consumption by cluster heads during a round and results in least variance and standard deviation.

Node density i.e. average number of nodes per unit area of the sensing field has been varied to evaluate the performance of the algorithm in respect to FND, HND, standard deviation of number of member nodes per cluster, and standard deviation in number of resulted clusters per clustering round. For calculating standard deviation in of number of cluster heads per clustering round, we simulate the 50 different topologies for a given fixed node density i.e.

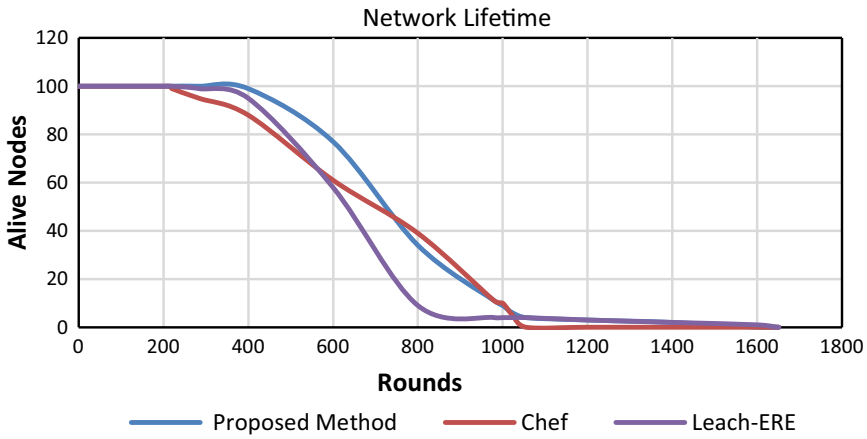
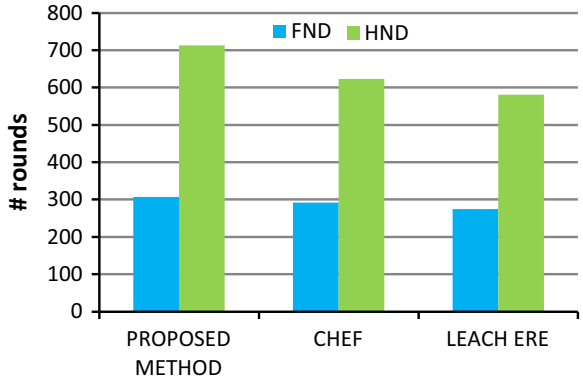


Fig. 5 Number of Alive nodes

Fig. 6 Number of rounds in which first node and half of the nodes dies



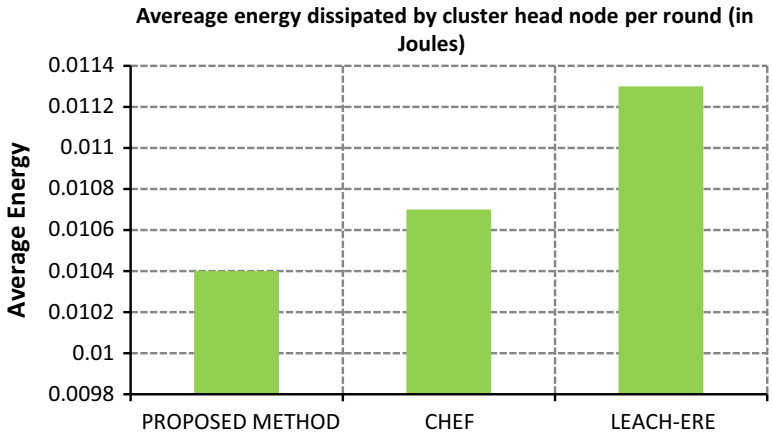


Fig. 7 Per round energy consumption by cluster heads

from 100 to 1,000, and obtain number of clusters per clustering round. In the simulations, the maximum possible communication range is fixed at 75 m and the sensor density is varied from 100 to 1,000. Cluster radius is calculated the same way as calculated by Kim et al. [15]. Nodes are randomly deployed in the sensing field. Figures 9, 10, 11 and 12, shows that our proposed method works well in lower or higher node density.

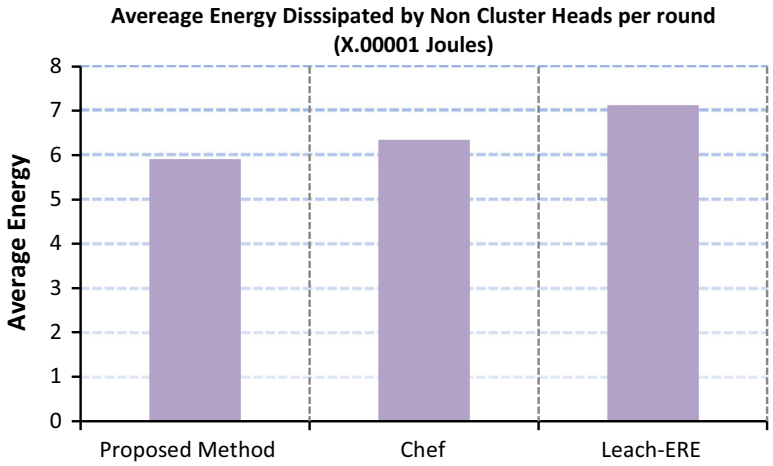


Fig. 8 Per round average energy consumed by member nodes

Table 4 Energy consumed by all cluster heads in a round

	LEACH-ERE	CHEF	Proposed method
Average	0.183	0.168	0.162
Variance	0.001334444	0.000778889	0.000306667
STD deviation	0.036530049	0.027908581	0.017511901

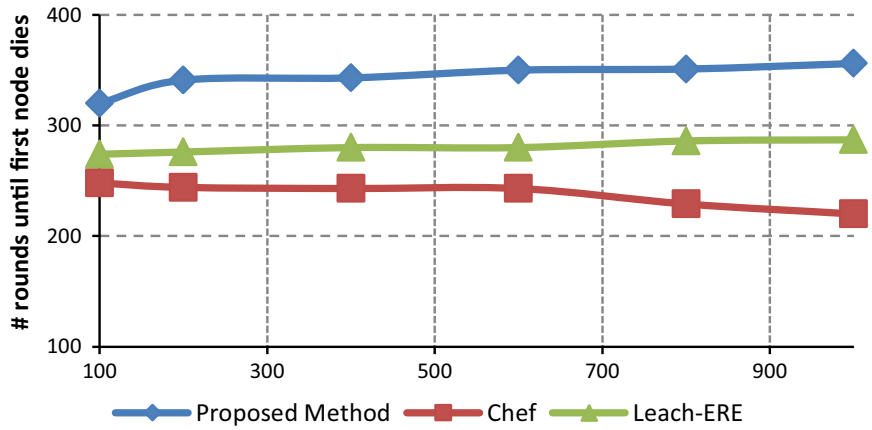


Fig. 9 Impact of node density on FND

7 Conclusion and Future Work

In this paper, we have proposed a new method for modeling and *k-hop* clustering for WSNs which results in better scalability, balancing of energy consumption of nodes and longer network life time. Fuzzy vertex and edge graph has been used for modeling WSN, to consider the residual energy as well as required transmission power by member nodes of a cluster. The proposed modeling by fuzzy graph addresses the issues arising from the dynamic nature of the WSNs i.e. non uniform energy consumption and depletion of energy levels of certain nodes to an extent that they cannot execute a single round of clustering. These issues have been addressed by selection of relay nodes in each round based upon residual energy and connectivity strength and considering energy depleted nodes as indirectly connected secondary nodes. Further, for achieving better and efficient clustering in WSN, we have defined a new

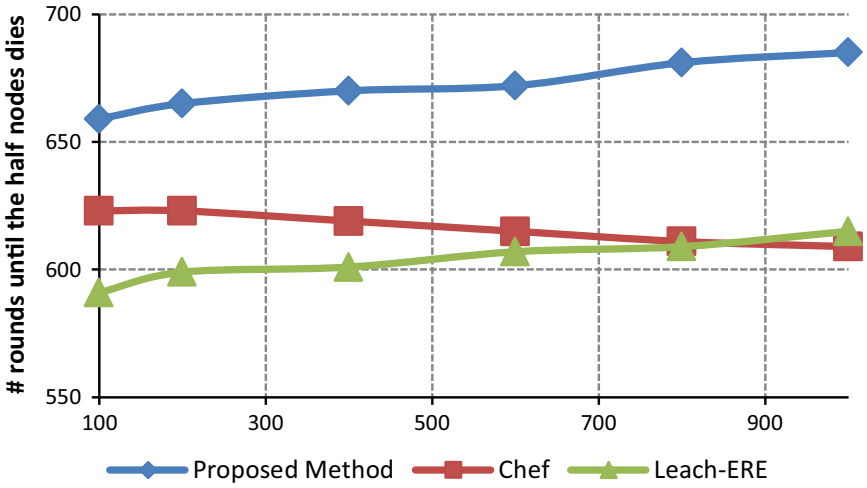


Fig. 10 Impact of node density on HND

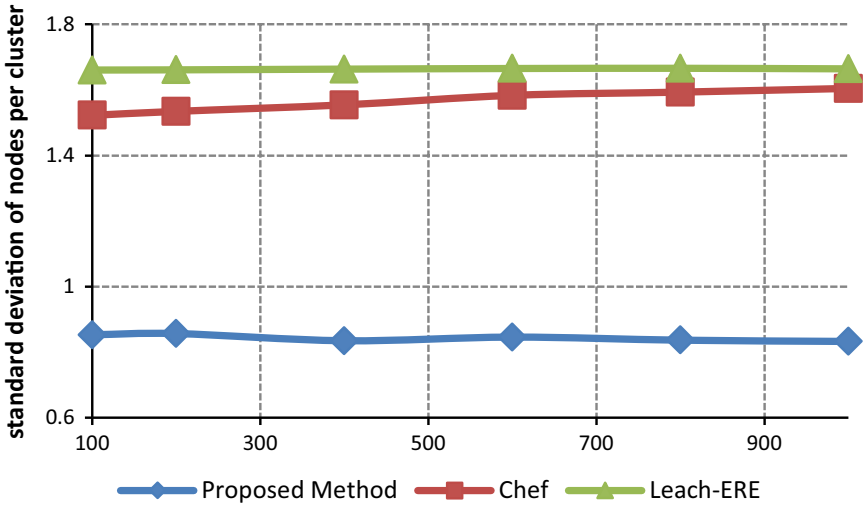


Fig. 11 Impact of node density on ratio of member nodes to cluster heads

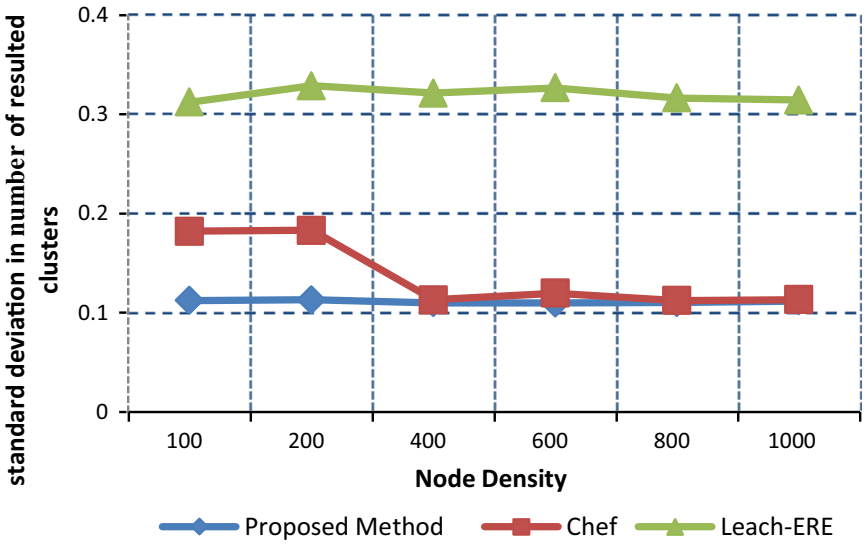


Fig. 12 Impact of node density on number of clusters per clustering round

metric *fuzzy k-hop centrality* which considers both residual energy and connectivity strength and addresses the limitations of degree centrality, closeness centrality and k-hop centrality. The proposed modeling technique has been evaluated by developing a computationally inexpensive clustering algorithm and simulating the same. The results suggest better performance of the proposed technique as compared to existing available methods LEACH and CHEF. The proposed method can be applied for design of several types of sensor networks that require energy efficiency, scalability, prolonged network lifetime, and load balancing. This work can be further extended for quasi stationary and mobile sensor networks and can be used for optimized routing in wireless mesh networks.

References

1. Akyildiz, I. F., Su, W., Sankarasubramaniam, Y., & Cayirci, E. (2002). Wireless sensor networks. A Survey. *Computer Networks*, *38*(2), 393–422.
2. Manap, Z., Ali, B. M., Ng, C. K., Noordin, N. K., & Sali, A. (2013). A review on hierarchical routing protocols for wireless sensor networks. *Wireless Personal Communications*, *72*(2), 1077–1104.
3. Yick, J., Mukherjee, B., & Ghosal, D. (2008). Wireless sensor network survey. *Computer Networks*, *52*(12), 2292–2330.
4. Mhatre, V., & Rosenberg, C. (2004). Design guidelines for wireless sensor networks: Communication, clustering and aggregation. *Ad Hoc Networks*, *2*(1), 45–63.
5. Troubleyn, E., Moerman, I., & Demeester, P. (2013). QoS challenges in wireless sensor networked robotics. *Wireless Personal Communications*, *70*(3), 1059–1075.
6. Heinzelman, W. R., Chandrakasan, A. & Balakrishnan, H. (2002). Energy-efficient communication protocol for wireless microsensor networks. In *Proceedings of the 33rd Hawaii international conference on system sciences* (pp. 3005–3014).
7. Heinzelman, W. R., Chandrakasan, A., & Balakrishnan, H. (2002). An application-specific protocol architecture for wireless microsensor networks. *IEEE Transactions on Wireless Communications*, *1*, 660–670.
8. Ferng, H. W., Tendean, R., & Kurniawan, A. (2012). Energy-efficient routing protocol for wireless sensor networks with static clustering and dynamic structure. *Wireless Personal Communications*, *65*(2), 347–367.
9. Baker, D. J., & Ephremides, A. (1981). The architectural organization of a mobile radio network via a distributed algorithm. *IEEE Transactions on Communications*, *29*(11), 1694–1701.
10. Chatterjee, M., Das, S. K. & Turgut, D. (2002). WCA: A weighted clustering algorithm for mobile ad hoc networks. *Journal of Cluster Computing, Special issue on Mobile Ad hoc Networking, 5*, 193–204.
11. Cheng, H., Yang, S., & Cao, J. (2013). Dynamic genetic algorithms for the dynamic load balanced clustering problem in mobile ad hoc networks. *Expert Systems with Applications.*, *40*, 1381–1392.
12. Younis, O., & Fahmy, S. (2004). HEED: A hybrid, energy-efficient, distributed clustering approach for ad hoc sensor networks. *IEEE Transactions on Mobile Computing*, *3*(4), 366–379.
13. Ding, P., Holliday, J. & Celik, A. (8–10 June 2005). Distributed energy efficient hierarchical clustering for wireless sensor networks. In *Proceedings of the 8th IEEE international conference on distributed computing in sensor systems (DCOSS)* (pp. 322–339). CA, USA: Marina Del Rey.
14. Gupta, I., Riordan, D. & Sampalli, S. (2005). Cluster-head election using fuzzy logic for wireless sensor networks. In *Proceedings of the Annual Conference Communications Network Services Research* (pp. 255–260).
15. Kim, J., Park, S., Han, Y. & Chung, T. (2008): CHEF: Cluster head election mechanism using fuzzy logic in wireless sensor networks. In *Proceedings of the international conference advanced communications and technology* (pp. 654–659).
16. Pires, A., Silva, C., Cerqueira, E., Monteiro, D., & Viegas, R. (2011). CHEATS: A cluster-head election algorithm for WSN using a Takagi-Sugeno fuzzy system. In *Communications (LATINCOM), 2011 IEEE Latin-American conference* (pp. 1–6).
17. Anno, J., Barolli, L., Durresi, A., Xhafa, F., & Koyama, A. (2008). Performance evaluation of two fuzzy-based cluster head selection systems for wireless sensor networks. *Mobile Information Systems*, *4*(4), 297–312.
18. Lee, J. S., Member, S., & Cheng, W. L. (2012). Fuzzy-logic-based clustering approach for energy predication. *IEEE Sensors Journal*, *12*(9), 2891–2897.

19. Taheri, H., Neamatollahi, P., Younis, O. M., Naghibzadeh, S., & Yaghmaee, M. H. (2012). An energy-aware distributed clustering protocol in wireless sensor networks using fuzzy logic. *Ad Hoc Networks*, *10*(7), 1469–1481.
20. Mhemed, R., Aslam, N., Phillips, W., & Comeau, F. (2012). An energy efficient fuzzy logic cluster formation protocol in wireless sensor networks. *Procedia Computer Science*, *10*, 255–262.
21. Hoang, A. T., & Motani, M. (2007). Collaborative broadcasting and compression in cluster-based wireless sensor networks. *ACM Transactions on Sensor Networks (TOSN)*, *3*(3), 1–34.
22. Hu, Y., Shen, X., & Kang, Z. (2009). Energy-efficient cluster head selection in clustering routing for wireless sensor networks. In *Proceedings of the IEEE 5th international conference on wireless communications, networking and Mobile Computing* (pp. 1–4).
23. Liang, Q. (2003). Clusterhead election for mobile ad hoc wireless network. In *Proceedings of the 14th IEEE international symposium on personal, indoor and mobile radio communications* (pp. 1623–1628).
24. Gao, T., Jin, R. C., Song, J. Y., Xu, T. B., & Wang, L. D. (2012). Energy-efficient cluster head selection scheme based on multiple criteria decision making for wireless sensor networks. *Wireless Personal Communications*, *63*(4), 871–894.
25. Förster, A., Förster, A., & Murphy, A. L. (2010). Optimal cluster sizes for wireless sensor networks: An experimental analysis. In *Ad Hoc networks, LNICST* (vol. 28, pp. 49–63). Berlin: Springer.
26. Freeman, L. C. (1978). Centrality in social networks: Conceptual clarification. *Social Networks*, *1*, 215–239.
27. Bonacich, P. (1987). Power and centrality: A family of measures. *American Journal of Sociology*, *92*, 1170–1182.
28. Chen, Q., Ma, J., Zhu, Y., Zhang, D., & Ni, L. (2007). An energy-efficient k-hop clustering framework for wireless sensor networks. *Wireless Sensor Networks,* 17–33.
29. Garcia, F., Solano, J. & I. Stojmenovic, I. (2003). Connectivity based k-hop clustering in wireless networks. *Telecommunication Systems, 22*(1–4), 205–220.
30. Koczy, L. T. (1992). Fuzzy graphs in the evaluation and optimization of networks. *Fuzzy sets and systems*, *46*, 307–319.
31. Gupta, M., & Qi, J. (1991). Theory of T-norms and fuzzy inference methods. *Fuzzy Sets Systems*, *40*, 431–450.
32. Klir, G., & Yuan, B. (1995). *Fuzzy sets and fuzzy logic: Theory and applications*. Upper Saddle River, NJ: Prentice Hall.
33. Zimmermann, H. (1991). *Fuzzy set theory and its applications* (2nd ed.). Dordrecht: Kluwer Academic.
34. Ross, T. (2004). *Fuzzy logic with engineering applications* (2nd ed.). Chichester: Wiley.
35. Aboelela, E., & Douligeris, C. (1998). Fuzzy multiobjective routing model in B-ISDN. *Computer Communications*, *21*, 1571–1584.
36. Bandyopadhyay, S., & Coyle, E. J. (2003). An energy efficient hierarchical clustering algorithm for wireless sensor networks. *IEEE INFOCOM*, *3*, 1713–1723.
37. Foss, S. G., & Zuyev, S. A. (1996). On a Voronoi aggregative process related to a bivariate Poisson process. *Advances in Applied Probability*, *28*(4), 965–981.
38. Okabe, A., Boots, B., Sugihara, K. & Chiu, S. N. *Spatial tessellations: Concepts and applications of Voronoi diagrams*, 2nd edn. New York: Wiley.
39. Karl, H., & Willig, A. (2005). *Protocols and architectures for wireless sensor networks*. New York: Wiley.
40. Rappaport, T. S. (1998). *Wireless communications: Principles and practice* (2nd ed.). Englewood Cliffs, NJ: Prentice-Hall.
41. Issaad, O., Pierre, S., Ivascu, G. I., & Garcia, O. (2008). A novel approach to modeling and flooding in ad-hoc wireless networks. *Journal of Computer Science*, *4*(12), 967–975.
42. Narayanaswamy, S., Kawadia, V., Sreenivas, R. S., & Kumar, P. (2002). Power control in ad-hoc networks: Theory, architecture, algorithm and implementation of the COMPOW protocol. In *European wireless conference*.
43. Bonissone, P. P., & Keith, S. D. (1986). Selecting uncertainty calculi and granularity. *Machine Intelligence Pattern Recognition*, *4*, 17–247.
44. Yager, R. R. (2010). Concept representation and database structures in fuzzy social relational networks. *Systems, Man and Cybernetics, Part A: Systems and Humans, IEEE Transactions on*, *40*(2), 413–419.
45. Handy, M.J., Haase M. & Timmermann D. (2002). Low energy adaptive clustering hierarchy with deterministic cluster-head selection. In *Proceedings of the international workshop mobile wireless communication networks* (pp. 368–372).

46. Wu, Y., Zhang, L., Wu, Y., & Niu, Z. (2009). Motion-indicated interest dissemination with directional antennas for wireless sensor networks with mobile sinks. *IEEE Transactions on Vehicular Technology*, *58*(2), 977–989.



Aarti Jain graduated with a B.Tech degree in Electronics and Communication Engineering from Beant Govt. Engineering College, Punjab, India in June 2002. Then she obtained her M.E. degee in Electronics and Communication from Delhi College of Engineering, University of Delhi, India in 2009. Currently, she is working as Asst. Prof. at the Department of Electronics and Communication Engineering, Ambedkar Institute of Advanced Communication Technology and Research. She is currently working towards the Ph.D. degree from Guru Gobind Singh Indraprastha University, Delhi. Her current research interests are in Energy and quality management for wireless sensor networks.



B. V. Ramana Reddy is Professor of USICT G.G.S. Indraprastha University, Dwarka. He obtained his ME and Ph.D (ECE) degrees during 1991 and 1998 respectively. He served in various capacities and has about 20 years of experience in teaching and research. Before joining this University he served as Asstt. Professor at NIT Hamirpur. He has about 25 publications in journals and International Conferences to his credit. He is a Fellow of IETE and a member of other professional bodies such as IE, IEEE, ISTE and SEMCEI. He has guided few scholars leading to M. Tech and Ph.D's. He has currently 6 students registered for Ph.D. His current research interest includes Wireless communications which include mobile, Adhoc and sensor based networks, computer communication networks, Semiconductor and VLSI circuits and microwave and optical communications.

An Ontology based Framework for Automatic Detection and Updation of Requirement Specifications

MPS Bhatia[1] and Rohit Beniwal [3]
Department of Computer Engineering,
Netaji Subhas Institute Of Technology, NSIT
Delhi- 78, India
mpsbhatia@nsit.ac.in[1], rohitbeniwal@yahoo.co.in[3]

Akshi Kumar[2]
Department of Computer Engineering
Delhi Technological University, DTU
Delhi - 42, India
akshi.kumar@gmail.com[2]

Abstract— **In recent years, integration among research field of Software Engineering and Semantic Technologies took place due to the presence of vendors at different geographical and virtual locations. This integration also resulted in various issues and challenges that are still need to be addressed. Issues and challenges, which will keep this collaborated field dynamic and lively for years to come. Among such issues, one is to automate the process of detection and updation of requirements specifications using ontologies during maintenance phase. This paper presents a framework approach for the above issue. Further it provides a metric suite that can be used to evaluate effectiveness of the approach.**

Keyword— Ontology, Semantic Web, Software Engineering, Deletion, Updation, Requirement Specifications

I. INTRODUCTION

In recent years, integration among research field of Software Engineering and Semantic Technologies took place. The reason for integration was to find mechanism for 'reusing' and 'sharing' software engineering knowledge when vendors are present at different geographical and virtual locations. Without reusing and sharing software engineering knowledge, the development led to the generation of inconsistent information followed by the development of undesired software. Research overcame this problem by applying semantic techniques to the field of software engineering, which addressed the reusing and sharing problem. In this regard, Ontologies, which are formal and explicit specification of a shared conceptualization [1], played the vital role for solving many issues that aroused due to this integration. However, this integration still has many issues and challenges that will keep this collaborated field dynamic and lively for years to come [2], [3]. Among such issues, one is to automate the process of detection and updation of requirements specifications using ontologies during maintenance phase.

When software system is in maintenance phase, developers generally update the software system without updating Software Requirements Specifications (SRS). In such a situation, as time goes by, it becomes more and more difficult to maintain the system as it lacks proper documentation. When we have ontology based source code implementation, which is generally done through consecutive use of Application Domain Ontology, Object Oriented Design Ontology (OO Design Ontology) and Object Oriented Source Code (OO Source Code) Ontology, any change in these ontologies that leads to changes in functional requirements, which in turn changes the external behaviour of the software system, can be populated back to requirements specifications for their updation. Application Domain Ontology represents the concepts of domain model and relationships that exist between different concepts [4], [5], [6], [7], [8]. OO Design Ontology defines the object oriented design concepts such as class, subclass, method, interface, objects, etc. [9], [10]. OO Source Code Ontology contains all concepts related to Object Oriented Programming (OOP). This ontology defines properties such as Abstraction, Inheritance, Polymorphism, and encapsulation [11], [12], [13]. This research paper presents a framework approach for solving the above mentioned issue followed by evaluation approach.

This paper is organised as follows: section II discusses the current approach (state of the art); section III discusses the framework; section IV discusses the evaluation approach for framework and section V concludes the paper.

II. CURRENT APPROACH

To the best of our knowledge, we have not seen any work done in this direction using ontology and semantic web techniques. However authors [Charrada, Koziolek, and Glinz, 2012] [14] have presented a heuristic based approach for detecting out-dated requirements, but they haven't proposed any approach for updating them. They also lack in terms of evaluation of their work. So, here in this paper, we provide an updation as well as an evaluation approach also.

III. FRAMEWORK

The framework is divided into five phases namely development phase, maintenance phase, comparison phase, deletion phase and addition phase.

A. Development Phase

Fig. 1 shows the framework for development phase. It consists of four steps. In first step, domain model is built by developing Application Domain Ontology from SRS. Once this ontology is developed, it establishes the traceability links to the SRS i.e. each requirement of SRS can be traced

978-1-4799-6629-5/14/$31.00 ©2014 IEEE

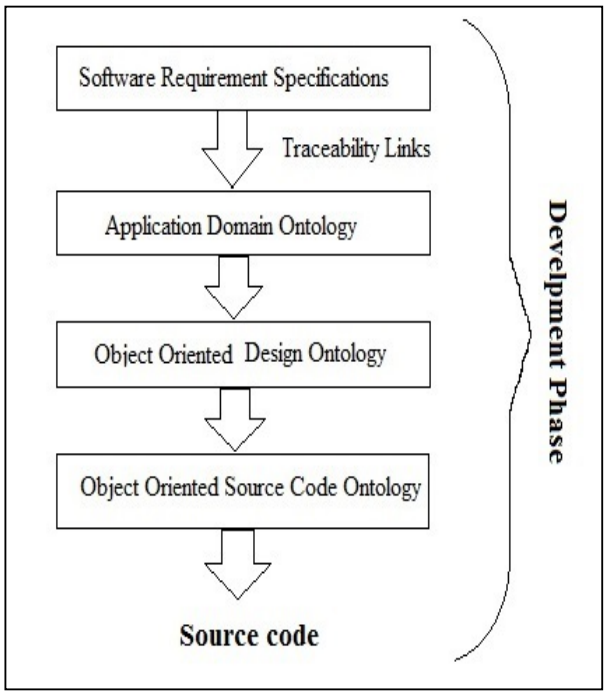


Fig. 1 Development Phase

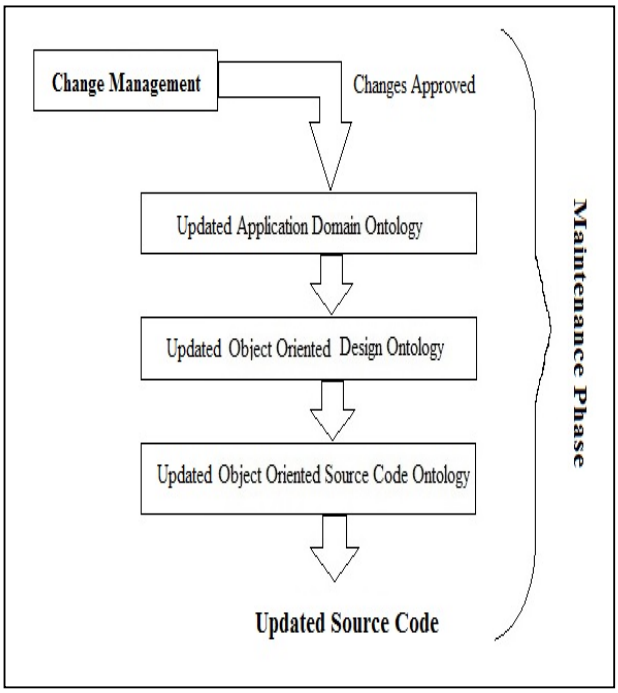


Fig. 2 Maintenance Phase

to the concepts of Application Domain Ontology. In second step, OO Design Ontology is developed with the help of Application Domain Ontology. In third step, OO Source Code ontology is developed with the help of OO Design Ontology. To develop these ontologies, various ontology editor tools are available for download on the web at AI[3] [Adaptiva Information, Adaptiva Innovation, Adaptiva Infrastructure] on www.mkbergman.com [15], few popular tools with their features/ limitations are shown in [3]. In fourth and last step, OO Source Code Ontology is converted into Executable Source Code. After all these steps, we assume that testing took place and then the software system is delivered to the customer for his use.

B. Maintenance Phase

Fig. 2 shows the framework for maintenance phase. Once the system is delivered to the customer, it comes into operation and maintenance phase. Now, let's assume that a change request comes and is granted by the change management. However due to schedule and cost constraint, maintenance team directly update the software system without updating SRS. Then this maintenance phase consists of four steps. In first step, Application domain ontology is updated representing the updated domain model. In second step, OO Design Ontology is updated with the help of Application Domain Ontology. In third step, OO Source Code ontology is updated with the help of OO Design Ontology. In fourth and last step, OO Source Code Ontology is converted into Updated Source Code.

C. Comparison Phase

Fig. 3 shows the framework for comparison phase. This phase consist of Comparison System, which compares two ontologies. Here, Original and Updated Application Domain Ontologies are taken inputs to the Comparison System. The Comparison System is implemented using either Protégé or Semantic Web Ontology Overview and Perusal (SWOOP). Using any of ontology editors, we compare old and new ontologies that result in added and deleted entities. Added entities represent the concepts of added source code, which is further divided in newly, modified and renamed entities. Deleted entities represent the concepts of deleted source code.

D. Deletion Phase

Fig. 4 shows the framework for deletion phase. This phase consist of Deletion System, which deletes obsolete requirements in SRS. Here, deleted entities and original SRS are taken inputs to the Deletion System. Deletion system is implemented using programming environment of Jena or OWL API. The deleted entities of Original Application domain Ontology have already traceability links to the SRS. In programming environment, the code is written in such a way as to delete obsolete requirements corresponding to deleted entities of application domain ontology. This results in updated SRS having deleted obsolete requirements.

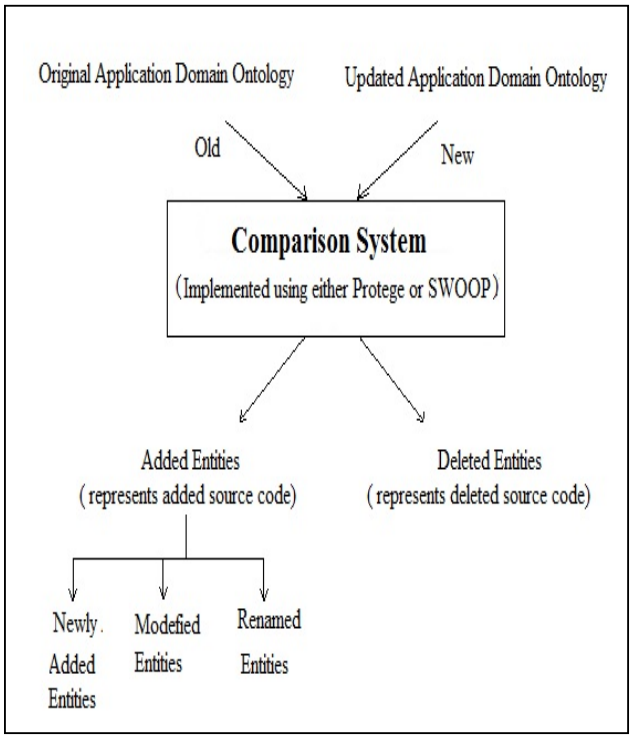


Fig. 3 Comparison Phase

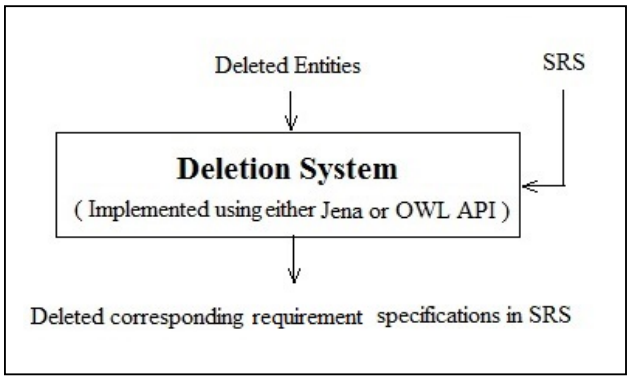


Fig. 4 Deletion Phase

E. Addition Phase

Fig. 5 shows the framework for addition phase. This phase consist of Addition System. Here, Added entities and original SRS are taken inputs to the Addition System. Addition System is implemented in two ways. The first one is Semi-automatic and the second is entirely Manual.

1) *Semi-automatic Approach*

In this approach, we decode the added entities. Added entities are first decoded in Axioms. Axioms are then decoded into General Concepts. At last General concepts are decoded into General Terminology. This General

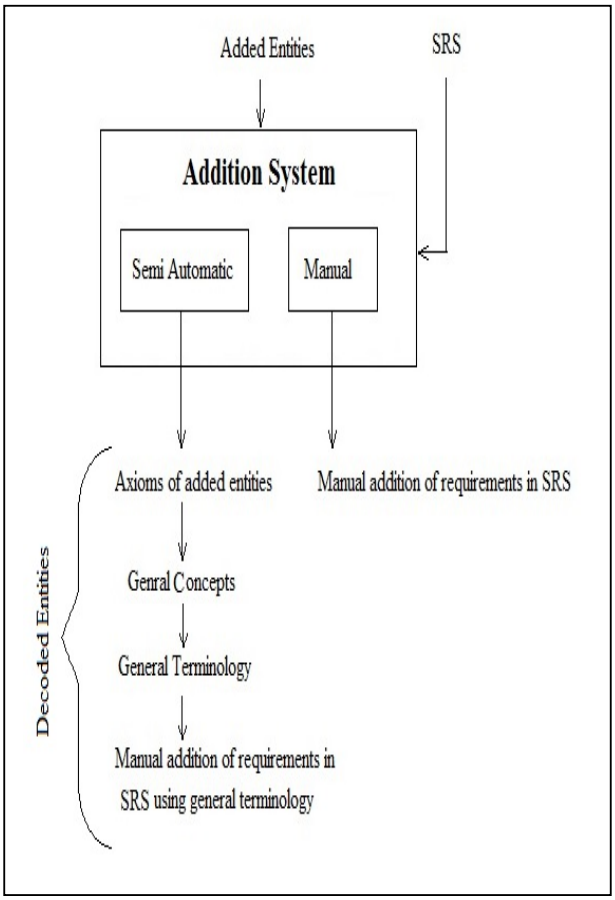


Fig. 5 Addition Phase

Terminology is then used to add requirements manually to SRS.

2) *Manual Approach*

In Manual approach, we manually add requirements to the SRS.

IV. EVALUATION APPROACH

To evaluate effectiveness our approach, we can use the following metric suite.

A. Average time taken to delete one obsolete requirement, T_d

$$T_d = \frac{\sum_{i=1}^{n} T_i}{n} = \frac{Total\ time\ taken\ to\ delete\ n\ obsolete\ requirements}{No.of\ requirements}$$

B. Average time taken to add one new requirement Semi-automatically, T_{as}

$$T_{as} = \frac{\sum_{j=1}^{n} T_j}{n} = \frac{Total\ time\ taken\ to\ add\ n\ new\ requirements\ Semi-automatically}{No.of\ requirements}$$

C. Average time taken to add one new requirement manually, T_{am}

$$T_{am} = \frac{\sum_{k=1}^{n} T_k}{n} = \frac{Total\ time\ taken\ to\ add\ n\ new\ requirements\ manually}{No.of\ requirements}$$

D. Average no. requirements added per entity added, N_a

$$N_a = \frac{\sum R_a}{\sum E_a} = \frac{Total\ no.\ of\ requirements\ added}{Total\ no.of\ entities\ added}$$

E. Average no. requirements deleted per entry deleted, N_d

$$N_d = \frac{\sum R_d}{\sum E_d} = \frac{Total\ no.\ of\ requirements\ deleted}{Total\ no.of\ entities\ deleted}$$

F. Percentage of requirements updated in SRS, P_u

$$P_u = \frac{\sum R_a - \sum R_d}{\sum R_o} * 100 = \frac{Total\ no.of\ requiremtns\ added - Total\ no.of\ requirements\ deleted}{Total\ no.of\ original\ requirements} * 100$$

The proposed metric suite is a very preliminary work carried out in this direction. The metric suite needs to be applied on large data sets and more evaluation needs to be done before its universal acceptance in research and practice.

Though this metric suite is a preliminary work, but we intend to compare our work with other's relevant and related work.

V. CONCLUSION

Here In this paper we have presented ontology based framework for automatic detection and updation of requirements specification followed by the metric suite that can be used to evaluate effectiveness of our approach. However to really know its effectiveness, framework must be first implemented followed by the evaluation by metric suite.

REFERENCES

[1] R. Studer, R. Benjamins, and D. Fensel, "Knowledge engineering: Principles and methods," Data & Knowledge Engineering 25, no.1, pp. 161–198, 1998.

[2] Y. Zhao, J Dong and T Peng, "Ontology classification for semantic-web-based software engineering," Services Computing, IEEE Transactions on Services Computing, Vol. 2, No. 4, pp. 303-317, 2009.

[3] M.P.S. Bhatia, A. Kumar, R. Beniwal, "Ontologies for Software Engineering: Past, Present and Future," unpublished.

[4] S. Thaddeus and S.V.K. Raja, "Ontology-Driven Model for Knowledge-Based Software Engineering," Proc. 18th Int'l Conf. Software Eng. and Knowledge Eng., pp. 337-341, July 2006.

[5] A.P. Ambro´sio, D.C. de Santos, F.N. de Lucena, and J.C. de Silva, "Software Engineering Documentation: An Ontology-Based Approach," Proc. WebMedia and LA-Web Joint Conf. 10th Brazilian Symp. Multimedia and the Web Second Latin Am. Web Congress, pp. 38-40, 2004.

[6] B. Antunes, P. Gomes, and N. Seco, "SRS: A Software Reuse System Based on the Semantic Web," Proc. Third Int'l Workshop Semantic Web Enabled Software Eng., June 2007.

[7] J.C. Caralt and J.W. Kim, "Ontology Driven Requirement Query," Proc. 40th Ann. Hawaii Int'l Conf. System Sciences, p. 197c, Jan. 2007.

[8] H.-J. Happel, A. Korthaus, S. Seedorf, and P. Tomczyk, "KOntoR: An Ontology-Enabled Approach to Software Reuse," Proc. 18th Int'l Conf. Software Eng. and Knowledge Eng., pp. 349-354, July 2006.

[9] J. Dietrich and C. Elgar, "A Formal Description of Design Patterns Using OWL," Proc. Australian Software Eng. Conf., pp. 243-250, 2005.

[10] D. Hyland-Wood, D. Carrington, and S. Kaplan, "Toward a Software Maintenance Methodology Using Semantic Web Techniques," Proc. Second Int'l IEEE Workshop Software Evolvability, pp. 23-30, Sept. 2006.

[11] C. Kiefer, A. Bernstein, and J. Tappolet, "Analyzing Software with iSPARQL," Proc. Third Int'l Workshop Semantic Web Enabled Software Eng., June 2007.

[12] R. Witte, Y. Zhang, and J. Rilling, "Empowering Software Maintainers with Semantic Web Technologies," Proc. Fourth European Semantic Web Conf., pp. 37-52, June 2007.

[13] Y. Zhang, R. Witte, J. Rilling, and V. Haarslev, "An Ontology-Based Approach for Traceability Recovery," Proc. Third Int'l Workshop Metamodels, Schemas, Grammars, Ontologies for Reverse Eng., 2006.

[14] E Ben Charrada, A Koziolek, and M. Glinz, "Identifying outdated requirements based on source code changes." In Requirements Engineering Conference (RE), 2012 20th IEEE International, pp. 61-70. IEEE, 2012.

[15] AI3 [Adaptiva Information, Adaptiva Innovation, Adaptiva Infrastructure]: http://www.mkbergman.com/

Assessing Nutraceutical Alpha Ketoglutarate for Its Effectiveness: ^{99m} Technetium-Mebrofenin Nuclear Imaging in CCl_4 Induced Hepatotoxic Animal Model

Lalita Mehra, Amit Kumar, Aseem Bhatnagar, Yasha Hasija, and Gaurav Mittal

***Abstract*---**Alpha Ketoglutarate (AKG), the active metabolite nutraceutical have been available in market and has been demonstrated to have anti-oxidant properties previously. Newer metabolic functioning of this novel metabolite have been under covered recently in microbial studies, indicating there is more to α-KG, and it might be an evolutionary molecule and a common linking metabolite which acts to help cell survive when it is exposed to various stressors. The current study assess its hepatoprotective effectiveness in a well-established CCl_4 induced acute hepatotoxic animal model, which are now known to have both lipid peroxidation dependent and independent pathways causing liver injury. Parameters assessed included, Biochemical (Liver functioning tests, oxidative stress, antioxidant levels) and histopathological assessment. ^{99m}Tc-Mebrofenin Nuclear (functional imaging) of animals were done, it provides objective validation of other parameters assessed, provides in-vivo quantification of liver functioning and parameters assessed can quantify oxidative and inflammatory pathways to liver injury and intervention response distinctly.

***Keywords*---**Alpha-Ketoglutarate (AKG), Carbon Tetrachloride (CCl_4), Hepatotoxicity, ^{99m} Technetium-Mebrofenin

I. Introduction

In past decade or so nutraceutical have generated great deal of consumer interest, largely on account of reported beneficial potential of these novel bioactives to treat chronic conditions with fewer to no side effect profile. Scientific research supporting the biological activities of these nutraceuticals in, *in-vitro* and in-vivo experimental models lack stringent validating criterion. Also inability to undercover the most active metabolite among the various polyphenols; scarce and inconclusive human trials; lack of long term studies, have led low confidence and criticism from the clinical fraternity [1]. Thus there is a need for stringent scientific validation of prophylactic and therapeutic utility of these class of agents.

Alpha-ketoglutarate (AKG), non-essential amino acid, have been marketed for some time now with various reported benefits, most important being its anti-ageing and anabolic properties which have been ascribed largely to its antioxidant properties. Biochemically AKG has been described for its ability to convert ammonia to non-toxic amino acids like glutamine, non-enzymatic oxidative decarboxylation of hydrogen peroxide and as such suppresses free radical generation and prevention of lipids peroxidative damage [2]. AKG is shown to inhibit oxidative stress induced by H_2O_2 in erythrocytes and cultured neurons [3], [4]. In addition to its protective activity on redox homeostasis, AKG is shown to have chelating properties by forming, active complexes with iron in brain homogenates [5]. As such AKG is known to have anti-oxidant properties. In past AKG has been shown to be effective as an antidote against cyanide poisoning [6], reducing oxidative stress caused by sodium valproate [7], ethanol [8], and ammonium acetate [2]. More novel roles that AKG might have in a cell than merely having antioxidant properties are being under-covered. Recent mechanistic studies showed newer molecular mechanisms of this metabolite. α-KG inhibits ATP synthase and leads to reduced ATP content, decreased oxygen consumption and increased autophagy, in both *C. elegans* and mammalian cells and also shown to prevent mtDNA damage. Thus α-KG might be an evolutionary molecule and a common linking metabolite which acts to help cell survive when it is exposed to various stressors [9].

Carbon- tetrachloride (CCl_4) is a well-known potent hepatotoxin, which has been used since seventies to create in-vivo models of acute and chronic liver injuries. The critical mechanism and signaling pathways for pathogenesis in well perfused liver and isolated or cultured hepatocytes have been elucidated [10]. Now there is a growing body of evidence to suggest that CCl_4 toxicity is, rather a mutifactorial process, unlike as previously thought. Earlier, much of CCl_4 hepatotoxicty, had been attributed to its activation by mitochondrial cytochrome P450 (CYP) 2E1, and very marginally by other CYPs (CYP2B and CYP3A), resulting in formation of trichloromethyl ($CCl_3^{\cdot}$) and trichloromethylperoxy radical ($CCl_3OO^{\cdot}$). Both free radicals

Lalita Mehra, Amit Kumar, Aseem Bhatnagar, Gaurav Mittal, INMAS, DRDO, India. Email id: lalita.mehra@ymail.com
Yasha Hasija, Delhi Technological University, India

being highly reactive species cause subsequent lipid peroxidation, resulting in cellular and intra-cellular membrane lysis, leading to hepatocytic necrosis [10]-[13]. However, more recent studies have shown that, lipid peroxidation-independent mechanisms, also seem to be involved in CCl_4 induced hepatotoxicity. CCl_4 intoxication induced a severe decrease in mitochondrial respiratory chain complex IV activity; mitochondrial DNA (mtDNA) alterations, reduced glutathione (GSH) depletion, decreased aconitase activity and macromolecular ultrastructural alterations [13]. As such CCl_4 induced liver injury is not merely a free radical reactive species hepatotoxicity model. Studies in rats treated with CCl_4 showed that cytokines (TNF-α and IL-6) caused perturbation in bile acid and organic anion transporters [14] which was objectively demonstrated by ^{99m}Tc-Mebrofenin hepatobiliary scan in a carbon tetrachloride–induced liver injury model [15].

In the current study, the animal model of CCl_4-induced acute liver injury is employed, meanwhile apart from serum transaminases, free radical, antioxidant, mitochondrial and histopathological parameters, in-vivo physiological liver functioning is assessed using, ^{99m}Tc-mebrofenin nuclear (functional) imaging modality. It provides better objective validation to other parameters assessed as serum level of various substances produced by the liver, including albumin, bilirubin, alkaline phosphatase, and transaminase are indirect indicators of liver function whereas measurement of radioactivity emitted from the liver serves as a direct indicator of the physiological status of the hepatocyte [16].

Also, since a previous ^{99m}Tc-Mebrofenin hepatobiliary scan [15], in a carbon tetrachloride–induced liver injury model, showed derangement, which were described to be cytokine mediated rather than oxidative stress mediated. This modality parameter was included in the study.

II. Materials And Methods

A. Ethics Statement

All the procedures and care managed to the animals has been approved by the Committee for the Purpose of Control and Supervision of Experiments on Animals (CPCSEA) regulations and the study protocol was approved by the Institutional Animal Ethics Committee of the Institute (INM/IAEC/2009/06/009), INMAS, DRDO, and Delhi, India.

B. Chemicals

Alpha Ketoglutarate (AKG) (Fluka chemika, buchs, Switzerland) and CCl_4 (Merck Ltd, India), Glutathione peroxidase kit and Glutathione reductase assay kit were procured from (Calibiochem, Merck, India), Lipid peroxidation (TBARS) colometric Assay kit, Superoxide Dimutase (SOD) Activity Assay kit, Alanine transaminase (ALT), Aspartate transaminase (AST), Alkaline Phosphatse Assay Kit, Albumin and Total Bilrubin kits were procured from (Biovision, India). All other chemicals used were of highest purity grade commercially available.

C. Experimental Animals

Male Sprague Dawley rats weighing (200 to 250 g) were obtained from the animal house of Institute of Nuclear Medicine and Allied Sciences (INMAS), DRDO, Delhi. All the animals were housed in polypropylene cages and were administered food (Hindustan Lever Ltd, Mumbai, India) and water *ad libitum* in the experimental animal care facility.

D. Experimental Protocol

AKG toxicity Study*:* The animals (n=6, each group) were administered variable doses of AKG, Group1 (G1): 0mg/kg, Group2 (G2): 1gm/kg, Group3 (G3): 2gm/kg, Group 4(G4): 4gm/kg orally by gavage for 2 weeks. Animals were observed for mortality and morbidity. Clinical symptoms and body weight were recorded daily throughout the study period. At the end of treatment animals were sacrificed.

Hepatotoxicity Model*:* For liver injury model, single injection CCl_4 was injected intraperitoneally at 2ml/kg body weight with and without orally administered AKG (2gm/kg bodyweight) for one week.

E. Nuclear Medicine Procedures

Radiopharmaceutical:^{99m} Technetium-Mebrofenin (MEB)

^{99m}Tc-sodium pertechnetate (BRITS, Mumbai, India), 185–222 MBq in 3 mL normal saline, was mixed with Mebrofenin (MEB) according to the manufacturer's instructions. This class of agent has gamma ray emitting properties of ^{99m}Tc which are acquired using gamma cameras. Mechanism of uptake of ^{99m} Tc-MEB by the hepatocyte is similar to those of organic anions such as bile acids or bilirubin [17]. It has high first pass extraction with hepatic uptake of ^{99m} Tc-MEB being 98% and it strongly resists displacement by a high bilirubin level [18]. Unlike bilirubin, ^{99mTc}-MEB is secreted into bile canaliculi in their native state, without undergoing any conjugation [19]. Thus it serves as an ideal in tracer for in-vivo quantification of hepatic functioning and delineation of hepatobiliary tree. 300 µci of radiopharmaceutical was administered in the present study. The dose not taken up by the liver is excreted through urine.

F. Image Acquisition: Gamma Camera

A gamma camera (Siemens) equipped with a low-energy, high-resolution, parallel-hole collimator and interfaced to a computer, was used for image acquisition. A 20% window centered on 140 keV was used for energy discrimination. Dorsal images were acquired for 60 min using a 64 × 64 × 16 matrix at a zoom factor of 2. Images were acquired for 1s per frame for 2 min, followed by 1 min per frame for 58 min.

G. Image Processing: Workstation

Data were analyzed using a conventional nuclear medicine workstation (Pegasys; ADAC Laboratories). Regions of interest were drawn over the liver, and hepatic time–activity curves were generated. The curves generated over the liver provide a measure of the rapidity of uptake and excretion of ^{99m} Tc-MEB. The time at which maximal hepatic activity of ^{99m}Tc-MEB occurred (T_{peak}) as well as the time required for peak ^{99m} Tc-MEB activity to decrease by 50% ($T_{1/2\ peak}$) were determined.

Management and husbandry conditions were identical in all groups with 12/12 h light/dark cycle at 21±2°C. Food and water were provided *ad libitum.* At the end of the experiment animals were sacrificed and blood samples were collected and serum was separated by centrifugation at 2000× *g* for 10 min and stored for biochemical estimations. Portions of liver tissue was placed in formaldehyde solution for routine histopathtological examination and one portion in liquid nitrogen for antioxidant status.

H. Measurement of Serum Parameters and Antioxidants

Leakage of intracellular enzymes as alanine aminotransferase (ALT) and Aspartate aminotransferase (AST), Alkaline Phosphatase (ALP) [20], Total Bilirubin and Albumin were determined by using semi-automatic biochemical analyzer (Krish Bio medicals, Delhi) using the commercially available kits according to the manufacturer's details.10% homogenate of liver was prepared by using IKA T25 digital Ultra Turrax at 4ºC in 0.15 M KCl. The homogenate was centrifuged (12,000 rpm for 45 min at 4ºC) in Remi cooling centrifuge to remove the debris and supernatant was used for enzyme assay. Lipid Peroxidation, MDA was evaluated by the thiobarbituric reactive oxygen substances (TBARS) by the method of Ohkawa [21]. The final concentration of MDA was expressed as nm/100g tissue. Catalase (CAT) activity was estimated by the method of Beers and Seizer [22] and is expressed as n moles of H_2O_2 decomposed/min/mg protein. Superoxide dismutase (SOD) activity was estimated by the method of Marklund [23] and is expressed as units/min/mg protein. Total reduced glutathione (GSH) was determined by the method of Ellman [24] and Glutathione peroxidase was determined by the method of Rotruck [25].

I. Histopathology Analysis of Liver

Tissues were processed by standard histopathological procedue and microscopic changes in liver were observed. Liver tissues were fixed in 10% formalin and embedded in paraffin and 5 µm size sections were cut. The sections were deparaffinized using xylene and ethanol and then washed with phosphate buffer saline (PBS) and with permeabilization solution (0.1 M citrate, 0.1% Triton X-100). The deparaffinized sections were stained with hematoxylin and eosin. Tissue histology was observed under the fluorescence microscope (Olympus BX 60).

III. Statistical Analysis

The statistical significance was determined by using one way analysis of variance (ANOVA) by Graph pad prism 5. Statistical significance value was set at $p < 0.05$.

IV. Results

A. AKG Toxicity Study

After 2 weeks effects of AKG on serum ALT, AST and ALP activities in rats treated with variable doses of AKG, Group1 (G1): 0mg/kg, Group2 (G2): 1gm/kg, Group3 (G3): 2gm/kg, Group 4(G4): 4gm/kg were evaluated. The clinical biochemistry analysis was performed at the end of exposure did not revealed any significant changes in any of the observed parameter however high dose terminal group animals revealed minor elevations in the level of ALT, AST and ALP. The administration of alpha Ketoglutarate at dose levels of 4g/kg body weight revealed significantly decreased mean body weight (data not shown). No mortality has been seen at these doses. No significant alterations has occured in the LFT at lower doses except elevations in ALP at high dose (Fig 1).

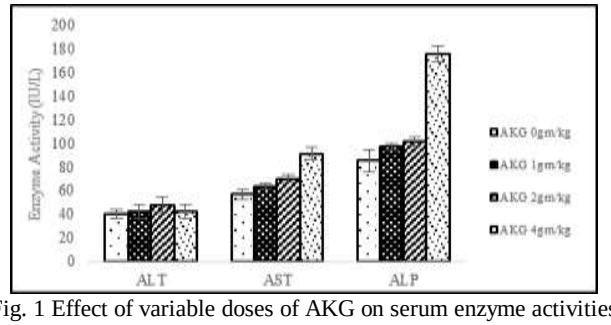


Fig. 1 Effect of variable doses of AKG on serum enzyme activities (G1: control, 0gm/kg, G2: low dose, 1gm/kg, G3: mid dose, 2gm/kg, G4: high dose, 4gm/kg). Data is expressed as Mean ±SD, $p<0.05$

B. Effect of AKG on CCl_4 Induced Liver Injury

The effect of AKG on liver injury administered by CCl_4 were examined. After 24 hrs there was a remarkable increment in ALT and AST levels while ALP and Bilirubin levels were not altered significantly. The oral administration of AKG attenuated the serum elevations and hence suggesting curative effect (Fig 2. & 3).

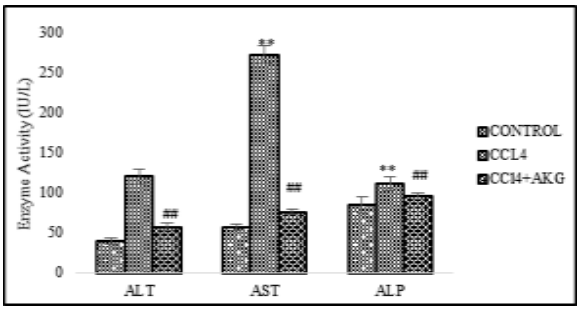


Fig. 2 Effect of AKG on serum enzyme activities in CCl_4 induced hepatotoxicity in rats. Data are expressed as Mean ±SD; n=6, $^{**}p<0.01$, when compared to control, $^{\#\#}p<0.01$, when compared to CCl_4 group

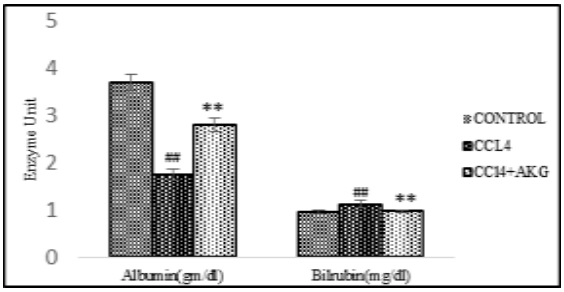


Fig 3: Effect of AKG on Albumin and Bilrubin in CCl_4 induced hepatotoxicity in rats. Data are expressed as Mean ±SD; n=6, $^{\#\#}p<0.01$, when compared to control, $^{**}p<0.01$, when compared to CCl_4 group.

C. *Effect of AKG on Hepatic Antioxidant Levels*

The levels of liver MDA, as product of lipid peroxidation, SOD showed increment in CCl_4 treatment group which are significantly higher than the control group animals. While AKG treatment reversed the alterations. In CCl_4 treatment group there is a significant reduction of hepatic GSH and Catalase as compared to normal control group. AKG supplementation elevated the GSH and Catalase activity as compared to the CCl_4 group.

TABLE I
EFFECT OF AKG ON LIVER ANTIOXIDANT STATUS AGAINST INDUCED CCL_4 TOXICITY IN RATS

Parameters	Control	CCl_4	CCl_4+AKG
TBARS (mM/100g tissue)	0.92±.23	2.34±0.20*	1.34±0.17**
SOD, Superoxide Dismutase (50% inhibition of NBT reaction/min/mg protein)	5.78±0.61	3.02±0.34*	4.02±0.39**
Catalase (µmoles/min/mg protein)	69.03±3.67	39.7±4.3*	59.45±5.40**
Glutathione Peroxidase (µg of GSHconsumed/min/mg protein)	6.23±0.14	4.52± 0.12*	5.01±0.17**
Reduced Glutathione (mg/g tissue)	44.83±4.82	20.82±5.67*	32.04±7.82**

Mean ±SD; n=6 , * p<0.05, when compared to control, **p<0.05, when compared to CCl_4 group

D. *Histopathology Analysis of Liver Tissues*

The histopathological examination showed that treatment with CCl_4 caused typical centribular hepatocytic steatosis (both macrovesicular and microvesicular) and cagulative necrosis especially in the periportal hepatocytes. While the AKG treated animal tissues showed almost normal histological profile of hepatocytes with mild congestion. Thus, histological examination clearly demonstrated the protection of AKG against CCl_4 hepatotoxicity.

FIG. 4 HISTOLOGICAL APPEARANCES OF THE LIVER (H&E STAINING)

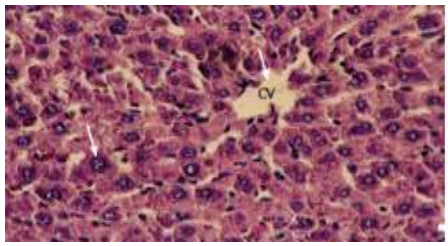


Fig. 4A. Control liver showing normal histological appearances

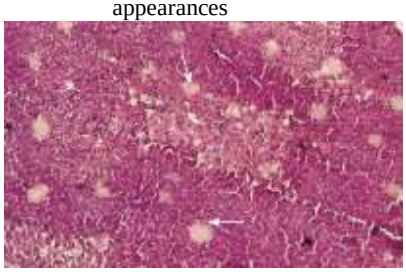


Fig. 4B. CCl_4 treated rats showing coagulative necrosis and the formation of vacuoles

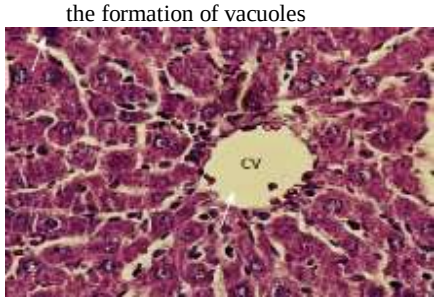


Fig. 4C AKG treatment group rats showing normal histological profile of hepatocytes. CV: Central vein.

E. *^{99m}Tc-Mebrofenin (MEB) Handling*

In control group rats, 99mTc-mebrofenin showed prompt uptake, uniform distribution and efficient tracer accumulation with rapid tracer clearance from the liver. For 300 microcurie of injected dose, peak counts stood at (400+/-120 counts/sec) with T_{peak} (148+/-40 sec) and T 1/2 peak (424+/- 56 sec) for the control group. In CCl_4 treatment group rats, 99mTc-mebrofenin did not showed delayed tracer uptake T_{peak} (223+/-52 sec; p not significant versus normal control), liver tracer clearance, though was markedly delayed in CCl_4-treated rats $T_{1/2\ peak}$ (1017+/- 130 sec; p significant versus normal control) and showed less efficient tracer accumulation; peak counts stood at (200+/-70 counts/sec). AKG, intervention in CCl_4 group, significantly reverted back

the deranged parameters. Peak counts stood at (430+/-126 counts/sec) with T_{peak} (153+/-48 sec) and $T_{1/2\ peak}$ (443+/- 70 sec) for the AKG intervention group.

FIG. 5 MEBROFENIN IMAGING SHOWS KINETICS OF HEPATIC MEBROFENIN UPTAKE AND EXCRETION IN REPRESENTATIVE RATS.

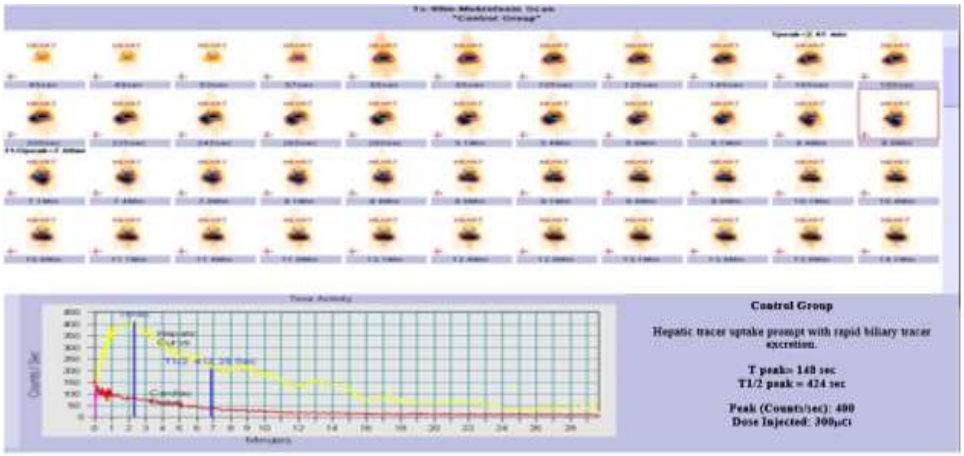


Fig. 5A. Control rat shows prompt mebrofenin clearance from liver.

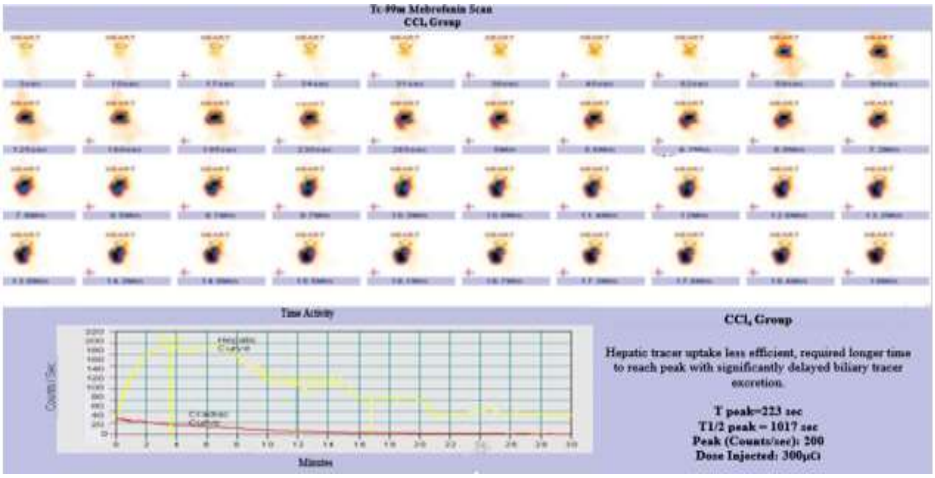


Fig. 5B CCl_4 rat shows considerably longer retention of mebrofenin activity in liver.

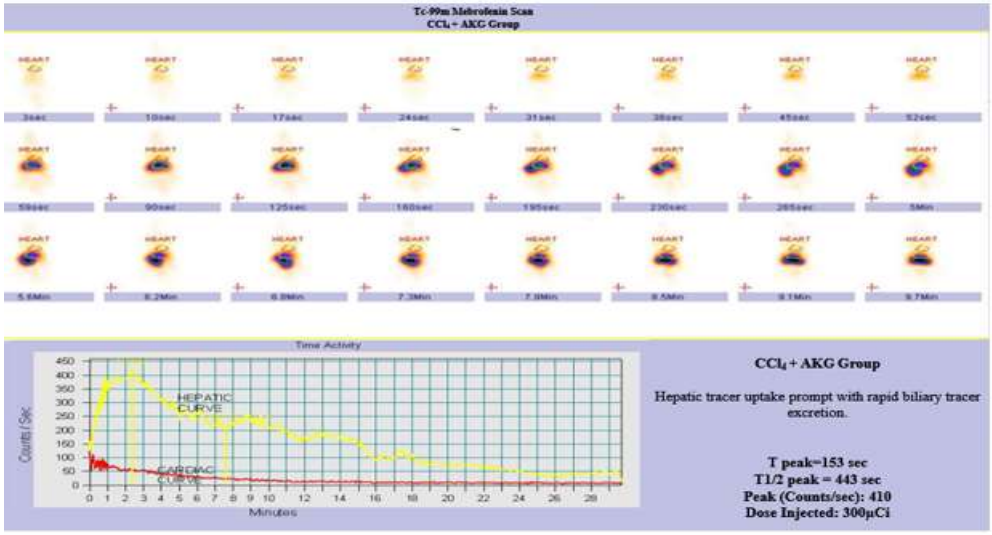


Fig. 5C. CCl_4+AKG shows prompt mebrofenin clearance from liver.

V. Discussion

The administration of AKG at higher doses revealed significantly decrease mean body weight and decreasing trend of mean body weight throughout the experiment. High concentration of AKG (4gm/kg b.w.) led diarrhea to animals while No observed adverse effect level (NOAEL) for AKG at lower doses is seen over two weeks experiment period..

The present study was conducted to evaluate the curative effect of AKG against CCl_4 induced hepatotoxicity in rat. This study gives some scientific evidences on the effect of AKG on enzymatic, antioxidant status, histological observations and nuclear functional imaging study. CCl_4 is used as hepatotoxic agent in animals for establishing acute and chronic hepatic injury models and to study the hepato-curative action of plants and other compounds [26], [27]. CCl_4 induced hepatic damage are related to its conversion into reactive toxic metabolites [28]. The mechanism of hepatic injury by CCl_4 involves lipid peroxidation of membrane bound fatty acids which result in destructing the cell membrane and the intracellular organelles of the hepatocyte [29]. Serum hepatobiliary enzymes such as AST, ALT and ALP are present in high concentrations in the liver under normal conditions and the elevations in serum enzymes indicates the hepatocytes membrane damage [30]. The present data revealed that serum AST, ALT, ALP and Bilirubin were significantly increased and albumin decreased in rats intoxicated with $CC1_4$ in comparison with control group. The treatment of AKG significantly ameliorated the toxic effects. Recent microbial studies on AKG had shed newer light to its antioxidant properties, are in agreement with our result.

Oxidative stress is a prominent feature in the pathophysiology in acute liver disease [31]. Oxidative stress occurs when reactive oxygen species (ROS) are not adequately neutralized by cellular antioxidant defense mechanisms [32]. Thiobarbituric acid reactive substances (TBARS), the final metabolites of peroxidized polyunsaturated fatty acids, have been used as biomarkers of oxidative stress [33] Antioxidant defense was evaluated by measuring glutathione (reduced GSH), glutathione peroxidase (GSHpx),superoxide dismutase(SOD) and catalase (CAT) [34]. In the present study CCl_4 treated rats have significantly higher levels of TBARS and significantly lower antioxidant levels. This is in agreement with CCL_4 induced hepatotoxic model [35].In hepatocytes CCl_4 undergo bioactivation by mitochondrial cytochrome P450 (CYP)2E1, resulting in formation of trichloromethyl (CCl3.) and trichloromethyl peroxy radical (CCl3OO.). Both free radicals being highly reactive species cause subsequent lipid peroxidation, as evident by significantly higher levels of TBARS, resulting in cellular and intra-cellular membrane lysis, leading to hepatocytic necrosis and decrease in hepatic antioxidant enzymes. The decreased concentration of antioxidants in CCl_4 liver may be due to NADPH reduction or their utilization in the exclusion of free radicals. The present study reveals that treatment with AKG has a critical role in abbrogating the oxidative stress-mediated toxicity of CCl_4. CCl_4 -induced raised TBARS and reduced anti-oxidant levels were significantly reverted to control levels with co-administration of AKG. These are in general agreement with previous study in which, administration of AKG prevented the rise in the TBARS and hydroperoxides levels in rats treated with sodium valproate. The likely explanation to these may be that AKG offer protection against oxidative damages, by participating in the non-enzymatic, NADPH independent oxidative decarboxylation in the hydrogen peroxide [7]. Ammonia is known to inhibit antioxidant enzymes, AKG by acting as a scavenger of amino groups transforms the ammonia to nontoxic amino acids like glutamate or glutamine [36]. AKG is also known be involved in GSH synthesis [37]. AKG as a strong ammonia and phosphate binding factor may indirectly stabilize redox state in organism [38]. The present study shows that AKG offers protection against oxidative damage caused by CCl_4.

99mTc-mebrofenin hepatobiliary scintigraphy is widely used for assessing overall physiological liver function and assessing hepatobiliary tree for the transit of bile. The two functional parameters measured as integral part of hepatobiliary imaging are T_{peak} and $T_{1/2\ peak}$. T_{peak} represents the efficacy of mebrofenin uptake by hepatocytes and $T_{1/2peak}$ reflects the dynamics between extraction, retention and clearance of biliary mebrofenin [39]. Thus T_{peak} and $T_{1/2\ peak}$ represents mebrofenin handling which involves the hepatocyte transporters. The specific transporters involved in the hepatic excretion of 99mTc-mebrofenin is not established. An earlier study of 99mTc-mebrofenin hepatobiliary scintigraphy in CCl_4 animal hepatotoxic model, observed no significant change in T_{peak} with significantely delayed $T_{1/2\ peak}$. The study opinioned that CCl_4 induced -inflammatory cytokine (TNF-α, IL-6) mediated the downregulation of receptors such as ATP–dependent proteins the bile canalicular transporters like, bile salt excretory pump (BSEP) and the multidrug resistance– related protein the basolateral exporters like MRP1 and MRP3. As such the downregulation of cytokine-regulated exporters resulted in significantly delayed $T_{1/2peak}$ without significantly affecting T_{peak}. Thus T_{peak} and $T_{1/2\ peak}$ represented the inflammatory cytokine mediated hepatic injury and not the direct oxidative hepatic necrosis. Mebrofenin accumulation (total radioactivity counts/sec at T_{peak}), represents functional parenchymal liver cell mass [40]. Thus depletion of parenchymal liver cell mass, as in CCl_4-induced peroxidative hepatic necrosis, causes reduced peak mebrofenin accumulation.

In the present study, CCl_4-induced hepatotoxic group, showed reduced peak mebrofenin accumulation (indicative of oxidative hepatic necrosis), significantly delayed $T_{1/2\ peak}$ with

no significant delay in T_{peak} (indicative of inflammatory cytokine mediated hepatocyte injury).The result were in agreement with two previous studies [41]. Treatment with exogenous AKG significantly reverted back such abnormal parameters. Thus AKG showed hepatoprotective effect as a potent antioxidant as well as prevented cytokine mediated inflammatory pathogenesis. Molecular underpinnings of its function in this regard needs to be explored further. It protective role in other inflammatory pathologies might be a potential research avenue.

VI. Competing Interest

The authors declare that they have no competing interest.

Acknowledgment

Authors are greatly indebted to INMAS and University Grant Commission (UGC), New Delhi, India whose financial and logistic support made this study possible.

Author's contribution

LM carried out experimental design, blood and liver sampling, statistical analysis and participated in drafting the manuscript. AK carried out nuclear medicine procedures. All authors read and approved the final manuscript.

References

[1] S.H. Zeisel, "Regulation of Nutraceuticals," Science, vol. 285, pp. 185-186, 1999.

[2] S. Velvizhi, B. Kadiyala, K.B. Dakshayani, "Effects of α-ketoglutarate on antioxidants and lipid peroxidation products in rats treated with ammonium acetate," Nutrition, vol. 18, pp. 747-750, 2002.

[3] M. Sokolowska, A. Oleszek, L. Wlodek, "Protective effect of alpha-ketoacids on the oxidative hemolysis," Pol J Pharmacol, vol. 51, pp. 429-434, 1999.

[4] S. Desagher, J. Glowinski, J. Premont, "Pyruvate protects neurons against hydrogen peroxide-induced toxicity," J Neurosci, vol. 17, pp. 9060-9067, 1997.

[5] R.L. Puntel, D.H. Roos, D. Grotto, S.C. Garcia, C.W. Nogueira, J.B. Rocha, "Antioxidant properties of Krebs cycle intermediates against malonate pro-oxidant activity in vitro: a comparative study using the colorimetric method and HPLC analysis to determine malondialdehyde in rat brain homogenates," Life Sci, vol. 8, pp. 51-62, 2007.

[6] L. Brendan, Mitchell, R.K. Bhandari, V.S. Bebarta, G. A. Rockwood, G. R. Boss, B. A. logue, "Toxicokinetics profiles of α-ketoglutarate cyanohydrin, a cyanide detoxification product, following exposure to potassium cyanide," Toxicology letters, vol. 222, pp. 83-89,2013.

[7] M. Vidya, P. Subramanian, "Effect of α-ketoglutarate on antioxidants and lipid peroxidation products in rats treated with sodium valproate," J. Appl. Biomed, vol. 4, pp. 141-46, 2006.

[8] S. Velvizhi, T. Nagalashmi, M.M. Essa, K.B. Dakshayani, P. Subramanian, " Effect of α-ketoglutarate on lipid peroxidation and antioxidant status during chronic ethanol administration in wistar rats," Polish Journal of Pharmacology, vol. 54, pp. 231-236, 2002.

[9] M. Randall, Chin, F. Xudong, Y. Melody, Pai et al, "The metabolite α-ketoglutarate extends lifespan by inhibiting ATP synthase and TOR," Nature, 2014.

[10] L.W. Weber, M. Boll, A. Stampfl, "Hepatotoxicity and mechanism of action of haloalkanes: carbon tetrachloride as a toxicological model," Crit Rev Toxicol, vol. 33, pp.105–136, 2003.

[11] M.K, M.Odin, D.A. Eastmond, "Postulated carbon tetrachloride mode of action: a review," J Environ Sci Health C Environ Carcinog Ecotoxicol Rev, vol. 25, pp. 185–209, 2007.

[12] R.O. Recknagel, E.A. Glendee, J.A. Dolak et al, "Mechanisms of carbon tetrachloride toxicity," PharmacolTher, vol. 43, pp. 139–154, 1989.

[13] Laetitia Knockaert, Alain Berson et al, "Carbon tetrachloride-mediated lipid peroxidation induces early mitochondrial alterations in mouse liver," Laboratory Investigation, vol. 92, pp. 396-410, 2012.

[14] Geier, C.G. Dietrich, S.Voigt et al, "Effects of proinflammatory cytokines on organic anion transporters during toxic liver injury and cholestasis," Hepatology, vol. 38, pp. 345–354, 2003.

[15] J. Brigid, K. Bhargava, G. Tronco et al, "Regulation of Hepatobiliary Transport Activity and Noninvasive Identification of Cytokine-Dependent Liver Inflammation," The journal of nuclear medicine, vol. 46(1), January 2005.

[16] G. T. Krishnamurthy, S. Krishnamurthy, "Nuclear Hepatology," A Textbook of Hepatobiliary Diseases, Second Edition, Page 129-130.

[17] L.R. Chervu , A.D. Nunn , M.D. Loberg, "Radiopharmaceuticals for hepatobiliary imaging," Semin Nucl Med, vol. 12, pp. 5–17, 1982.

[18] S.Krishnamurthy, G.T. Krishnamurthy, "Technetium-99m iminodiacetic acid organic anions: review of biokinetics and clinical application in hepatology," Hepatology, vol. 9, pp. 139–153, 1989.

[19] M.D. Loberg, M. Cooper, E. Harvey, P. Callery, W. Faith, "Development of new radiopharmaceuticals based on N-substitution of iminodiacetic acid," J Nucl Med, vol.7, pp. 633 – 638, 1976.

[20] S. Reitman, S. Frankel, "A colorimetric method for the determination of serum glutamic, oxaloacetic and glutamic pyruvic transaminases," Am J Clin Pathol, vol. 28(1), pp. 56-63, 1957.

[21] H. Ohkawa, N. Ohishi, K. Yagi, "Assay for lipid peroxides in animal tissues by thiobarbituric acid reaction," Anal Biochem, vol. 95(2), pp. 351-358, 1979.

[22] R. F Beers, I.W. Sizer, "A spectrophotometric method for measuring the breakdown of hydrogen peroxide by catalase," Boil Chem, vol. 195(1), pp. 133-140,1952.

[23] S.L. Marklund, G. Marklund, "Involvement of the superoxide anion radical in the autoxidation of pyragallol and a convenient assay for superoxide dismutase," Eur J Biochem, vol. 47, pp. 469-474, 1974.

[24] G.L. Ellman, "Tissue sulphydryl groups," Arch Biochem Biophys, vol. 82, pp.70-77, 1959.

[25] J.T. Rotruck , A.L. Pope, H.E. Ganther, A.B. Swanson, D.G. Hafeman, W.G. Hoekstra, "Selenium: biochemical role as a component of glutathione peroxidase," Science, vol. 179(4073), pp. 588-90, 1973.

[26] R. Aliyu, Z.S. Okoye, W.T.Shier, "The hepatoprotective cytochrome P450 enzyme inhibitor isolated from Nigerian medicinal plant Cochlospermum planchonni is a Zinc salt," J. Ethnopharmacol, vol. 48, pp. 89-97,1995.

[27] Bishayee, Sarkar A, Chatterjee M, "Hepatoprotective activity of carrot (Daucus carota L) against carbon tetrachloride intoxication in mouse liver," J. Ethnopharmacol, vol.47, pp. 69-74,1995

[28] B. Halliwell, J. Gutteridge, "Lipid peroxidation, oxygen radicals, cell damage and antioxidant therapy," Lancet, vol. 23, pp. 1396-1397, 1984.

[29] H. De-Groot and T. Noll, "The crucial role of low steady oxygen partial pressure in haloalkanes free radical induced lipid peroxidation. Possible implications in haloalkane liver injury," Biochem. Pharmacol, vol. 35, pp.15-19, 1986.

[30] R.B. Drotman, G.T. Lawhorn, "Serum enzymes as indicators of chemically induced liver damage," Drug ChemToxicol, vol. 1(2), pp. 163-171, 1978.

[31] C.S. Lieber, "Role of oxidative stress and antioxidant therapy in alcoholic and nonalcoholic liver diseases," Adv Pharmacol, vol. 38, pp. 601–28, 1997.

[32] E.C. Opara, "Oxidative stress," Dis Mon, vol. 52, pp. 183–98, 2006.

[33] Moselhy, F. Hamdy et al, "A Specific, Accurate, and Sensitive Measure of Total Plasma Malondialdehyde by HPLC," Journal of Lipid Research, vol. 54(3) pp. 852–858, 2013.

[34] B. Ragıp, D. Haluk, O. Hanefi et al, "Protective effects of antioxidants on the experimental liver and kidney toxicity in mice," Eur J Gen Med, vol.5(3),pp. 157-164, 2008.

[35] L.W. Weber, M. Boll, A. Stampfl, "Hepatotoxicity and mechanism of action of haloalkanes: carbon tetrachloride as a toxicological model," Crit Rev Toxicol, vol. 33, pp.105–136, 2003.

[36] M. Vidya, P. Subramanian,"Effect of α-ketoglutarate on antioxidants and lipid peroxidation products in rats treated with sodium valproate,"J. Appl. Biomed, vol. 4, pp. 141-46, 2006.
[37] P. Lasch , T. Petras , O. Ullrich O, J. Backmann, D. Naumann, T.Grune, "Hydrogen peroxide-induced structural alterations of RNAse," A. J. Biol. Chem, , vol. 276, pp. 9492–9502, 2001.
[38] T. Niemiec, J. Sikorskai,A. Harrison et al, "Alpha-ketoglutarate stabilizes redox homeostasis and improves arterial elasticity in aged mice," Journal of physiology and pharmacology, vol. 62(1), pp. 37-43, 2011
[39] G.B. Daniel, A. Bahr, J.A. Dykes, R. Denovo, K. Young, G.T. Smith, "Hepatic extraction efficiency and excretion rate of technetetium-99m-mebrofenin in dogs," J. Nucl. Med, vol. 37, pp. 1846-1849, 1996.
[40] J. Brigid, K. Bhargava, G. Gene, Tronco et al, "Regulation of Hepatobiliary Transport Activity and Noninvasive Identification of Cytokine-Dependent Liver Inflammation," The journal of nuclear medicine, vol. 46(1), pp. 146-152. 2005.
[41] H. Malhi, K.K. Bhargava, M. Afriyie et al, "99m-mebrofenin scintiscanning for evaluating liver disease in a rat model of Wilson's disease," J Nucl Med, vol. 43, pp. 246-252, 2002.

ISSN(Online): 2320-9801
ISSN (Print): 2320-9798

International Journal of Innovative Research in Computer and Communication Engineering

(An ISO 3297: 2007 Certified Organization)

Vol. 2, Issue 12, December 2014

Cancerous Cell Detection Using Histopathological Image Analysis

Aashna Jain[1], Shwetal Atey[2], Satender Vinayak[3], Varun Srivastava[4]

UG Student, Department of Computer Science, GGSIPU, BVCOE, Paschim Vihar, New Delhi, India[1,3]

UG Student, Department of Computer Science, Delhi Technological University, Bawana Road, New Delhi, India[2]

Assistant Professor, Department of Computer Science, GGSIPU, BVCOE, Paschim Vihar, New Delhi, India[4]

ABSTRACT: Histopathology refers to the examination of biopsy samples by a pathologist using a microscope for analysing and classifying diseases. In order to study the manifestations of a disease, the analysis of histopathological image is done manually by a pathologist and therefore the diagnosis is subjective and greatly dependent on the level of expertise of the professional. In order to overcome this problem of a possible erroneous diagnosis and for early stage detection, an automated computerized image processing system is needed for quantitative diagnosis of biopsy samples. In this paper we have proposed a model for early stage cancerous cell detection and have reviewed and summarized the phases involved, namely, Image Pre-processing, Image Segmentation, Feature Extraction and Classification**.**

KEYWORDS: Image Processing, Image Segmentation, Cancerous Cell Detection, Feature Extraction, Histopathological Image Analysis, Active Contour Model, Morphological Feature Extraction, Computer Assisted Diagnosis

I. INTRODUCTION

Early stage cancerous cell detection using histopathological images is characterized by the identification of abnormal uncontrolled cell. Damaged cells divide and multiply to form a tumor that may be benign (non-cancerous) or malignant (cancerous) [5]. The distortion in the shape of a cell and the density of cluster of cells are the signatures of the presence of malignity in a body tissue. The proposed automated system makes use of morphological feature analysis, i.e., cell shape analysis in order to detect and classify cells as cancerous or non-cancerous.

The entire process is divided into a number of phases, namely, Image Pre-processing, Image Segmentation, Feature Extraction and Classification.

Image Pre-processing largely comprises undesirable noise removal and enhancement of image in order to determine focal areas of the image. For this purpose, we have applied techniques such as dilation and erosion. Median filtering and thresholding techniques were also applied.

After pre-processing, Image segmentation is done in order to extract clear cell boundaries for further processing. Many segmentation methods exist of which some are region based, texture based, gradient contour based, active contour based etc. We have employed the Chan-vese implementation of theActive Contour Model [2]. Overlapping and connectedclustering of cells are the primary problems prevailing in the segmentation domain.

Feature extraction is performed on these segmented images. In this phase, we extracted and analysed both textural and morphological features. Textural features are extracted and analysed using Grey Level Co-occurrence Matrix (GLCM) which is amongst the most frequently used techniques for texture analysis.

Morphological Feature Analysis, i.e., cell shape analysis has become a necessity in cell image processing and pattern recognition. Its main aim is the quantitative characterization of cell morphology for abnormality identification and classification. It forms a major part of the early stage cancer detection procedure.

ISSN(Online): 2320-9801
ISSN (Print): 2320-9798

International Journal of Innovative Research in Computer and Communication Engineering

(An ISO 3297: 2007 Certified Organization)

Vol. 2, Issue 12, December 2014

The last phase deals with the classification of cells as cancerous or not. A number of supervised and unsupervised techniques are available for the classification/clustering of elements on the basis of extracted features. Few of the famous techniques are K-means, Fuzzy c-means, Super Vector Machine (SVM), Neural Networks, Decision trees etc. We have employed the General Classifier Neural Networks (GCNN) model for classification [1].

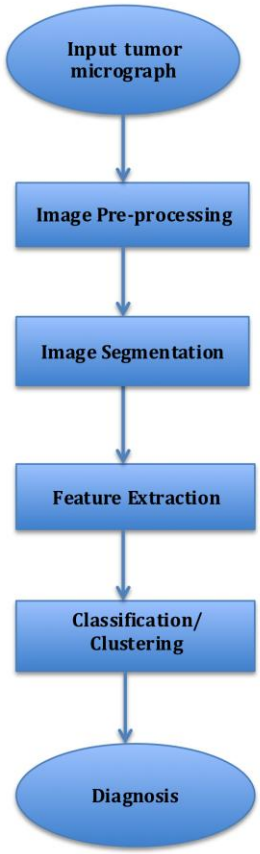


Fig 1. Various steps involved in cancerous cell detection process

II. RELATED WORK

Ahmad Chaddad et al [5], in April 2011, extracted Haralick's Texture Features and Morphological Parametersfrom Segmented Multispectrale Texture Bio-Images for Classification of Colon Cancer Cells. They made use of Probabilistic Neural Network (PNN), the activation function for which is a function that measures the distance of unknownvariable to all known class variables.

Baouchan Pang et al [8], in October 2010, proposed a machine learning technique for cell nucleus segmentation ofcolor histological image based on convolutional networks. They used gradient descent algorithm,convolutional network with 3 hidden layers and 8 feature maps per hidden layer for segmentation of cells from background.

ISSN(Online): 2320-9801
ISSN (Print): 2320-9798

International Journal of Innovative Research in Computer and Communication Engineering

(An ISO 3297: 2007 Certified Organization)

Vol. 2, Issue 12, December 2014

Akif Burak Tosun et al [9], in July 2008, proposed a homogeneity measure based on the distribution of the objects that are defined to represent tissue components. Using this measure, they demonstrated a new object-orientedsegmentation algorithm and therefore, implemented the Object-oriented texture analysis for the unsupervised segmentation of biopsy imagesfor cancer detection.

T.S. Furey et al [10], in May 2000, made use of Support Vector Machine (SVM) for classification and validation ofcancer tissue samples using microarray expression data.

M.Dhivya et al [11], in March 2014, used Support Vector Machine (SVM) Classifiers in order to detect cancer using histopathological image analysis.

A. D. Belsare et al [7], in August 2012, reviewed the various techniques used in computer assisted histopathology image analysis for cancer detection andclassification.

III. METHODOLOGY

A. IMAGE PRE-PROCESSING

Primary aim in this step is to remove the large amount of random noise present in the images in order to determine the focal areas on which mathematical operations need to be performed. For this median filtering is used for enhancing image quality, i.e., forincreasing the contrast between the foreground (areas of interest) and background, which is followed by the thresholding technique for noise reduction. In thresholding, the intensity matrix of an image is used for identifying pixels under a threshold value which are considered noisy. These threshold values can be determined automatically by using several computational techniques. We have employed the Otsu method for determining an optimal threshold valueto maximize the between-class variance [8].

B. IMAGE SEGMENTATION

Segmentation can be both region and boundary based. We employed both the approaches as each alone have their respective limitations.

The region based approach includes the thresholding technique which is used here to separate cells from the background but it does little to separate overlapping cells. For this, Watershed Algorithm is applied to detect the boundary lines between the overlapping cells.

Amongst the various boundary based techniques, Active Contour Model proves to be very powerful especially when irregular shapes such as cancerous cells are present within an image. In this method we begin with some initial contour, defined by a chosen function. We describe two major areas, namely, area inside contour and area outside contour. Then we evolve this contour on the basis of some level set function. Our target is to optimize this function by varying the parameters of the function. Chan-Vese segmentation [2] method has been used to optimally fit a two-phase piecewise constant model to the image. It is an excellent implementation of the Active Contour Model as unlike others, this method does not rely on edge detection. The segmentation boundary is represented using a level set function. Here, we used an energy fitting function as the level set function with the following four parameters:-

1. Variation of grey/RGB inside contour
2. Variation of grey/RGB outside contour
3. Length of contour
4. Area inside the contour

We applied penalties on the above four parameters. As all these parameters have a minimum value of zero, we optimized the function by varying these parameter values. We gave high percentage to the parameter which we wished to optimize the most and at the same time gave relaxation to the others. For example, to minimize the variation inside contour, i.e., to segment the area that is as uniform as possible in terms of RGB/Grey scale value then set its corresponding parameter's value accordingly giving high percentage value to it.Image is described as I, with domain Ω then ϕ: Ω ->IR, a function H(ϕ) is known as Heaviside function which is defined as,

$$H(\phi)=1, \text{ if } \phi >=0$$
$$=0, \text{ if } \phi <0$$

The level set function (i.e. energy fitting function) used:-

ISSN(Online): 2320-9801
ISSN (Print): 2320-9798

International Journal of Innovative Research in Computer and Communication Engineering

(An ISO 3297: 2007 Certified Organization)

Vol. 2, Issue 12, December 2014

$$F(\phi) = \mu \int (|\nabla H(\varphi)|dx)^p + \nu \int H(\varphi)dx + \lambda 1 \int |I - c1|^2 H(\varphi)dx + \lambda 2 \int |I - c1|^2 (1 - H(\varphi)dx$$

where term 1 is an integral term representing total length of contour and μ is the weight given to this parameter. Hence, the combined term describes the penalty on total length of the contour.
Similarly term 2 represents the penalty on the total area inside contour, term 3 represents the penalty on the variation of area inside contour and term 4 represents the penalty on variation of area outside the contour.

$$C1 = \frac{\int I.H(\varphi)dxdy}{\int H(\varphi)dxdy} \qquad C2 = \frac{\int I.(1-H(\varphi))dxdy}{\int (1-H(\varphi))dxdy}$$

The terms c1 and c2 represent the average value of area inside and outside the contour respectively.

Different types of initialization may be undertakensuch as single large circle, multiple circles etc. But one must keep in mind the fact that convergence of initial contour affects the final segmentation or output.

We initialized using a uniform continuous function:-

$$\phi_{x,y} = \sin\left(\pi.\frac{x}{10}\right).\sin\left(\pi.\frac{y}{10}\right)$$

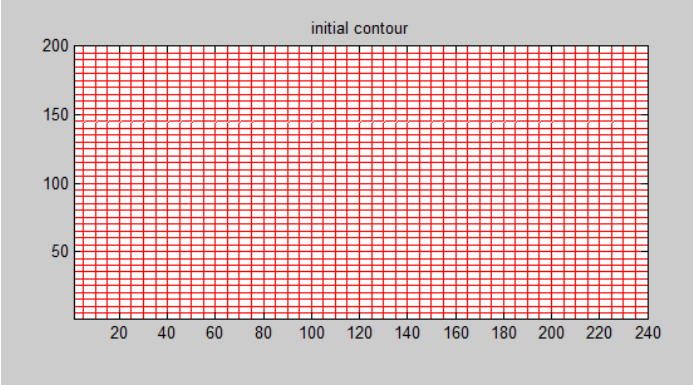


Fig. 2 shows the contour representation of selected value of $\phi_{x,y}$

Algorithm for segmentation using Chan-Vese method[2]:-

1. Initialize the value of ϕ
2. Repeat for a large number of iterations
3. Compute c1 and c2 for current value of ϕ
4. Update ϕ according to the new values obtained
5. Calculate the difference between ϕn and ϕn-1
6. If this difference is less than threshold
7. Then break the loop
8. Do reinitialization (optional)

ISSN(Online): 2320-9801
ISSN (Print): 2320-9798

International Journal of Innovative Research in Computer and Communication Engineering

(An ISO 3297: 2007 Certified Organization)

Vol. 2, Issue 12, December 2014

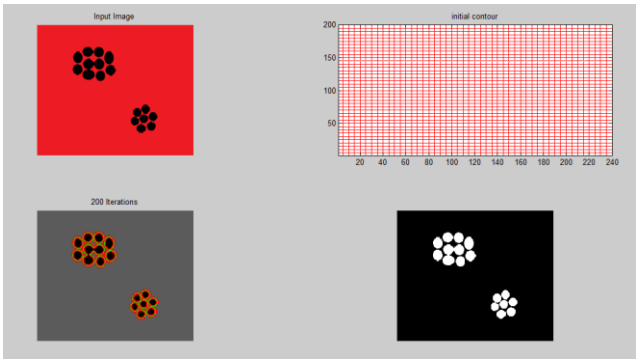


Fig 3. Cell segmentation of a random pattern of circles

In the above example clear segment boundaries are defined using Active Contour Model for a general image consisting of a random pattern of circles. Here, $\mu = 0.5$, $\lambda 1 = 1$, $\lambda 2 = 1$ and ν is kept constant. As value of μ is kept low, therefore the boundary is not fine or not much penalty is given to contour length. Hence, it segments individual cells.

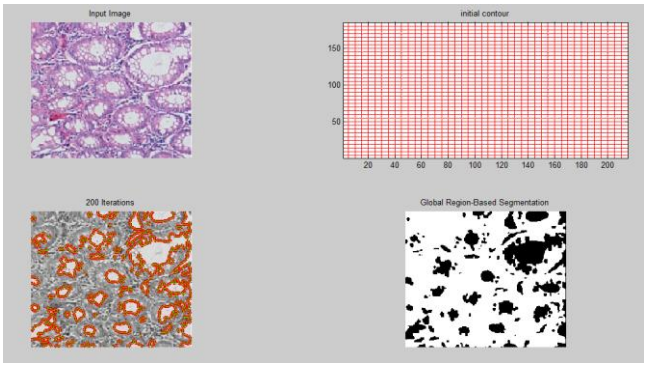


Fig 4. Image shows a failed case of cell segmentation

Using the same approach, we segmented individual cells which formed the primary input for feature analysis.

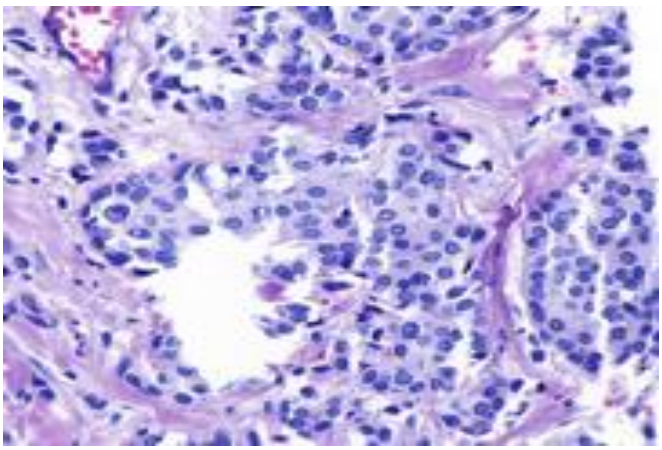


Fig. 5 Image showing a histopathological image taken as input

ISSN(Online): 2320-9801
ISSN (Print): 2320-9798

International Journal of Innovative Research in Computer and Communication Engineering

(An ISO 3297: 2007 Certified Organization)

Vol. 2, Issue 12, December 2014

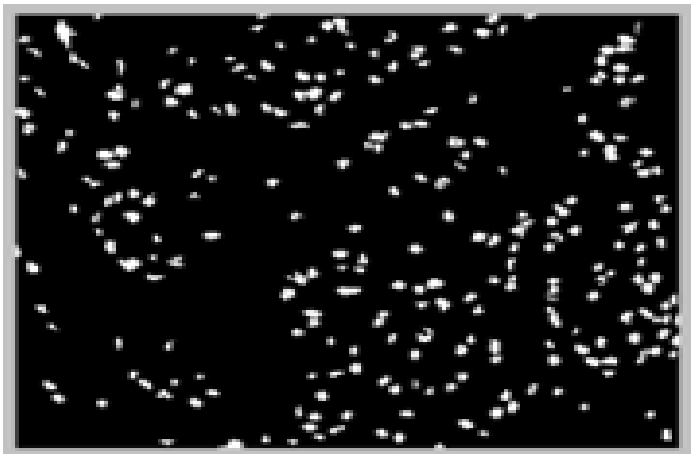


Fig. 6 Image showing the segmented output of image in fig. 5

Fig.5 shows a histopathological image which is taken as input and Fig.6 shows its corresponding segmented output.

C. FEATURE EXTRACTION

After segmentation of cells from the image we perform morphological analysis of these cells. Morphological features are geometric features. Eight morphological parameters were used to classify segmented cells. These parameters include the following:-

1. Area- The total number of pixels present in a cell.
2. Perimeter- The total number of pixels present in the boundary of a cell.
3. Xor cell-circle- It is applied between the cell and a circle having the same area and center of mass as of the cell
4. Xor cell-convex- It is applied between the cell and a convex which covers the cell.
5. Solidity- It is defined as the ratio of area of nucleus of a cell to its cell area. If the cell is abnormal then size of nucleus increases, hence, solidity also increases.
6. Xor cell-rectangle- It is applied between the segmented cell and a rectangle covering it.
7. Standard deviation along X-axis- If the cell is cancerous then cells distribution is disturbed and there is random distribution hence, if Std dev along any axis comes to be high then there is a possibility of cancer.
8. Standard deviation along Y-axis- *explanation same as above.*

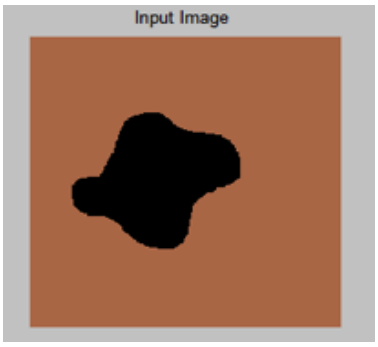


Fig. 7 Pattern taken as input image

ISSN(Online): 2320-9801
ISSN (Print): 2320-9798

International Journal of Innovative Research in Computer and Communication Engineering

(An ISO 3297: 2007 Certified Organization)

Vol. 2, Issue 12, December 2014

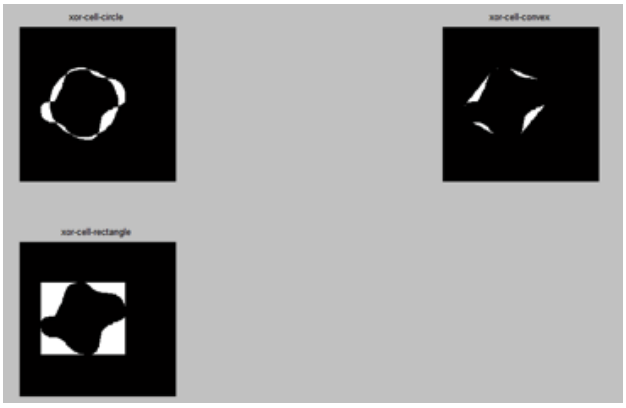


Fig. 8 Image shows xor-cell-circle, xor-cell-convex and xor-cell-rectangle for fig.7

Fig.7 shows a pattern taken as input and Fig.8 shows the corresponding xor-cell-circle, xor-cell-convex and xor-cell-rectangle outputs.

D. CLASSIFICATION

Classification is done on the basis of features extracted for each cell. We extracted eight morphological features for each cell and arranged each feature in a 2-D array with each column representing a cell and rows corresponding to the eight morphological features taken into account– Area, Perimeter, XOR cell-circle, XOR cell-convex, Solidity, XOR cell-rectangle, Standard deviation in x directionand Standard deviation in y direction. We employed the General Classifier Neural Network (GCNN) model [1] in order to classify different cells among cancerous and non-cancerous group.

GCNN is a radial basis function based classification neural network proposed by Buse Melis Ozyildirim and Mutlu Avci in the year 2012. The neural network makes use of the gradient descent algorithm based optimization on the smoothing parameter. It has 5 layers; input, pattern, summation, normalisation and output. For each pattern layer neuron, a smoothing parameter is allocated. Smoothing parameters are updated to converge squared error of winner neuron to global minimum [1]. GCNN makes use of target values for each pattern layer neuron and provides regression based effective classification.

IV. CONCLUSION

In some cases where the images contain high level of noise, the Active Contour Model fails to give clear segmented boundaries of cells. Also, as it works on the principle of optimization of energy function, there may be instances where area inside the cell and area outside the cell exhibit same value for a particular energy function thus ACM does not work accurately in such a case. Low resolution of the image, increased blurness and excessive overlapping of cells also pose a problem in cell segmentation process.

The Watershed algorithm along with the various thresholding and filtering techniques might lead to distortion of images in the form of blurring or unwanted removal of a few cells from the image. Also, there are cases where the cell and the background plazma both have the same value for particular measurement for a given feature such as the grey scale value. Here, there is no clear distinction between edge of the cell and that of the plazma, hence, may lead to inaccurate results.

Another problem faced during feature extraction phase was the inability of the system to discriminate between single-nucleus and multi-nuclei cells and therefore, both were treated as the same.

ISSN(Online): 2320-9801
ISSN (Print): 2320-9798

International Journal of Innovative Research in Computer and Communication Engineering

(An ISO 3297: 2007 Certified Organization)

Vol. 2, Issue 12, December 2014

GCNN proved to be comparable to other famous neural network models used for classification and clustering like Self-OrganisingMap (SOM), Probabilistic Neural Network(PNN), Generalised Regression Neural Network (GRNN), etc. Using the described methodology, we successfully segmented the images to indicate clear cell boundaries and also, classified each cell into their corresponding groups of cancerous and non-cancerous type on the basis of extracted features.

REFERENCES

1. Buse Melis Ozyildirim and Mutlu Avci, "Generalized classifier neural network," Elsevier,Neural Networks 39 (2013) 18–26 19.
2. T. Chan and L. Vese, "Active contours without edges," IEEE Trans Imag Proc, Vol.10, No.2, 2001, pp. 266-277.
3. Shengyong Chen, Mingzhu Zhao, GuangWu, Chunyan Yao, and Jianwei Zhang,Review Article on "Recent Advances in Morphological Cell Image Analysis," Hindawi Publishing Corporation, Computational and Mathematical Methods in Medicine, Volume 2012.
4. Vandana, B. S.; Antony, P. J., "Automated Segmentation using Histopathology Images as a Diagnostic Confirmatory Tool in Detection of Bone Cancer," International Journal of Computer Applications . 2012, Vol. 57, p48-55. 8p.
5. AHMAD.CHADDAD, CAMEL.TANOUGAST, ABBAS. DANDACHE and AHMED.BOURIDANE, "Extracted Haralick's Texture Features and Morphological Parameters from Segmented Multispectrale Texture Bio-Images for Classification of Colon Cancer Cells," Issue 2, Volume 8, April 2011.
6. Cigdem Demir and Bulent Yener, "Automated cancer diagnosis based on histopathological images: a systematic survey,"TECHNICAL REPORT, RENSSELAER POLYTECHNIC INSTITUTE, DEPARTMENT OF COMPUTER SCIENCE, TR-05-09.
7. A. D. Belsare and M. M. Mushrif, "HISTOPATHOLOGICAL IMAGE ANALYSIS USING IMAGE PROCESSING TECHNIQUES: AN OVERVIEW," Signal & Image Processing : An International Journal (SIPIJ) Vol.3, No.4, August 2012.
8. Baochuan Pang, Yi Zhang, Qianqing Chen, Zhifan Gao, Qinmu Peng and Xinge You,"Cell Nucleus Segmentation in Color Histopathological Imagery Using Convolutional Networks", 978-1-4244-7210-9/10, 2010 IEEE.
9. A. B. Tosun, M. Kandemir, C. Sokmensuer and C. Gunduz-Demir, "Object oriented texture analysis for the unsupervised segmentation of biopsy images for cancer detection", Pattern Recognition, Vol.42, No.6, 2009, pp. 1104-1112.
10. T.S. Furey, N. Cristianini, N. Duffy, D.W. Bednarski, M. Schummer and D. Haussler, "Support vector machine classification and validation of cancer tissue samples using microarray expression data", Bioinformatics 16(2000) 906-914.
11. M.Dhivya, S.Deepa, S.Anbumani and R.Kavin, "Detection and grading of cancer using histopathological image analysis", International Journal of Electronics and Communication Engineering (IJECE), 2014, Vol.3, Issue 2,59-68.

Asian Journal of Business and Economics
Volume 4, No.4.4 Quarter IV 2014
ISSN: 2231-3699

COMMODITY FUTURES MARKET EFFICIENCY AND RELATED ISSUES: A REVIEW OF EXISTING LITERATURE

Archana Singh
Assistant Professor, Delhi School of Management, Delhi Technological University, Delhi, India
Narinder Pal Singh
Assistant Professor, Guru Nanak Institute of Management, New Delhi, India

ABSTRACT

The study of market efficiency in commodity futures markets is important to both the government and the producers/marketers in India. In this paper, we review the available literature on commodity futures market efficiency and related issues viz. the effect of seasonality on commodity futures market efficiency, the inflationary impact of commodity futures trading and the impact of commodity futures trading on spot market volatility. The review shows that the results produced in available literature are often conflicting: the efficiency hypothesis is supported only for certain markets and only over some periods. Also there are very few studies on microstructure and macroeconomic issues in commodity futures market, and integration with other international markets. This forms further scope of research in this area. Keywords: Commodity futures, Efficient Market, Efficiency, Volatility, Cointegration etc

Introduction

Commodity futures market is a place where farmers/producers and traders can reduce their price risk. India has long history of trade in commodity derivatives. Organized commodity derivatives in India started as early as 1875, barely about a decade after they started in Chicago. Since 2003, when commodity futures' trading was permitted, commodity futures market in India has experienced an unprecedented boom in terms of the number of modern exchanges, number of commodities allowed for derivatives trading as well as the value of futures trading in commodities. There are 22 Commodity Exchanges (6 National and 16 Regional Exchanges) recognized by FMC in India where 113 commodities are traded. Six electronic multi-commodity national exchanges recognized by the Government of India are MCX Mumbai, NCDEX

Mumbai, NMCE Ahmedabad, ICEX Mumbai, ACE Mumbai & UCX Navi Mumbai. National Multi-Commodity Exchange of India, Ahmedabad (NMCE), was the first to trade in futures from November 2002, Multi Commodity Exchange of India Ltd, Mumbai (MCX) and National Commodity and Derivatives Exchange Ltd., Mumbai (NCDEX) started trading a year later. The national exchanges accounted for 99.7% of the turnover of commodity futures contracts traded in India during FY2012-13. MCX alone had a market share of 87.3% in FY 2012-13.

Efficient Market

An efficient market is one in which prices always "fully reflect" available information and where no traders in the market can make a profit with monopolistically controlled information (Fama, 1970). In other words, an efficient commodity futures market can provide effective signals for the spot market price and eliminates the possibility that profit can be guaranteed as part of the trading process. This price reflects the equilibrium value for suppliers and demanders in the market.

Efficient futures markets provide a mechanism for managing the risk associated with the uncertainty of future events. Out of the various aspects of these markets, futures market efficiency is one of the most extensively researched topics in the empirical literature. **Sewell (2011)** critically reviews literature available on EMH. The efficient market hypothesis (EMH) asserts that financial markets are efficient. Sewell says "On the one hand, the definitional 'fully' is an exacting requirement, suggesting that no real market could ever be efficient, implying that the EMH is almost certainly false. On the other hand, economics is a social science, and a hypothesis that is asymptotically true puts the EMH in contention for one of the strongest hypotheses in the whole of the social sciences. Strictly speaking the EMH is false, but in spirit is profoundly true. Besides, science concerns seeking the best hypothesis, and until a flawed hypothesis is replaced by a better hypothesis, criticism is of limited value".

Carter (1999) conducted a study on then available literature on different issues in commodity futures market. He pointed out some economic issues which should be addressed. In this research, we have focused on literature available on efficiency and related issues.

Literature Review

There are numerous empirical studies that analyze different aspects of futures markets in developed countries like the US. Out of the various aspects of these markets, futures market efficiency is one of the most extensively researched topics in the empirical literature. Most of the studies investigating the efficiency of commodity futures markets employ a conventional approach of regressing the cash price at maturity on a previous futures price. But, there are studies which used research techniques different from regression. **Samuelson (1965)** first analysed the role of futures prices as predictor of future spot prices for a given contract and found that it follows a martingale; in other words, today's futures prices are the best unbiased predictor of tomorrow's futures prices. However, **Danthine (1978)** *and* **Lucas (1978)** have both shown theoretically that periodical failure of the martingale property to hold is not evidence of the market inefficiency. **Danthine (1978)** first criticized Samuelson's (1965) argument that spot commodity prices may not follow a sub-martingale if they vary with such factors as the weather, which may be serially correlated. He went on to develop possible reasons why the link between a martingale process and efficiency in commodity markets could be problematic.

Rausser *and* **Carter (1983)** examined the efficiency of the soybean, soybean oil, and soybean meal futures markets using semi strong form test via structurally based ARIMA models. They emphasized that "unless the forecast information from the models is sufficient to provide profitable trades, then superior forecasting performance in a statistical sense has no economic significance".

Tomek (1997) stressed that if the futures market is efficient, then it should be able to out-forecast an econometric model. The development of co-integration theory by **Engle and Granger (1987)** provided a new technique for testing market efficiency. **Aulton, Ennew**, *and* **Rayner (1997)**, **Crowder and Hamed (1993), Fortenberry and Zapata (1993), Chowdhury (1991), Mckenzie and Holt (2002)** and many others accepted and used cointegration theory for testing market efficiency.

Later, Johansen co integration technique was developed. **Wang, H. Holly et al. (2005), Bhar and Hamori (2006), Sahi and Raizada (2006), Gupta and Ravi (2013)** and many others have used Johansen cointegration to test commodity market efficiency.

However, **Neil Kellard et al. (1999)** investigated the claim whether the cointegration existence between commodity spot and lagged futures rates should be accepted as long-run market efficiency. They studied the UK wheat futures contract traded at LIFFE. They concluded that "such tests are not wholly appropriate for evaluating commodity market efficiency".
Since the introduction of futures, there have been two way arguments about the efficiency of futures markets (both financial and commodity futures markets). So the literature has been presented separately on studies supporting efficiency and inefficiency.

Literature on Efficiency

Goss (1981) examined the unbiasedness hypothesis of futures prices of copper, tin, lead and zinc. The results showed copper and zinc futures markets as efficient. **Goss (1985)** revised his paper by introducing joint tests for the same metals of the LME extending the sample period to 1966-1984. He found contrary results. EMH was not rejected for lead and tin.
Roll (1984) found that price movements in the orange juice futures market could predict freezing temperatures in Florida better than the US national weather services could. However, *Roll* indicates that a 'puzzle' remains in the orange juices futures market because there is a large amount of inexplicable price volatility. **Canarella and Pollard (1986)** tested the hypothesis that the futures price was an unbiased predictor of the future spot price using both overlapping and non-overlapping data for the contracts of copper, lead, tin and zinc covering the period 1975-1983. Using three different estimation methods, they confirmed the unbiasedness hypothesis. **Fama and French (1987)** examined whether the futures prices for copper and other metals contain evidence of forecast power or systematic risk premiums for the period 1967-1984. They showed that the copper futures price contains suggestive evidence of both systematic risk premiums and forecasting power.

MacDonald and Taylor (1988a) tested the EMH for four metals in the LME covering the period 1976-1987. Copper and lead futures markets were found to be efficient. **Gross (1988)** examined unvaried LME prices for the period 1983-84. Based on the mean square error criterion, he provided evidence that the EMH is not rejected for the copper futures market. **Crowder and Hamed (1993)** examined the NYMEX crude oil contracts and concluded that accounting for the cointegration between spot and futures, one cannot reject the speculative efficiency hypothesis during the period March 1983 – September 1990.

Furstenberg and Zapata (1993) evaluated the relationship of the North Carolina corn and soybean markets with respect to the CBOT. Co-integration existed between any air of these markets and no strong evidence was found to reject the efficiency hypothesis. **Moore and Callen (1995)** examined the Speculative Efficiency of the LME for six base metals between 1985 and 1989. They showed that the long-run speculative efficiency cannot be rejected for the copper and other three metals. **Aulton, Ennew**, *and* **Rayner (1997)** re-investigated the efficiency of UK agricultural commodity futures markets using the co-integration methodology. They found that the market is efficient for wheat. Using monthly data, and the Phillips and Loretan (1991) approach, **Peroni and McNown (1998)** supported the speculative efficiency hypothesis for the WTI for the 1984-1996 period.

Gulen (2000) found that the futures price of light sweet crude oil traded at NYMEX plays a significant role in price discovery. i.e. the futures price is an unbiased predictor of the spot price. This observation was also supported by the widespread use of the futures price as a benchmark all over the world as well as by the decision of the U.S. Minerals Management Service to switch to the futures price from the posted price as the standard for calculating royalties. However, his paper explicitly dealt with the crash in 1986. **Murry and Zhu (2004)** investigated the impact of the introduction and exit of Enron Online (EOL) on the efficiency of the U.S. natural gas market. Using a conventional EGARCH model, he found little evidence that the introduction of EOL coincided with the reduction in the market price volatility. **Wang and Bingfan (2002)** studied the efficiency of the Chinese wheat and soybean futures markets using Johansen's cointegration approach. The results suggest a long-term equilibrium relationship between the futures price and

cash price for soybeans and weak short-term efficiency in the soybean futures market. **J B Singh (2004)** attempted to understand the price risk of agricultural and derived commodities for the period 1988-99 in India. He investigated the usefulness of futures market to discover prices, manage uncertainty and risk, and improve the performance of agricultural commodities. He found that among all commodities (pepper, custorseed, potato, gur, turmeric and Hessian), castorseed (Ahemdabad and Mumbai) and pepper futures markets are efficient and unbiased and also performs the role of risk management and hedging effectiveness.

Bhar and Hamori (2006) found that the prices of commodity futures traded on the Tokyo Grain Exchange (TGE) did not move together in the long run. They suggested that the cointegrating relation exists among commodity futures contract from 2000 to 2003 but not earlier during the 1990s i.e the price mechanism works better and the long run relationships among prices becomes more apparent as a market develops. **Bose (2006)** examined the efficiency of commodity futures market in India. He found that notional multi-commodity indices with higher exposure to metals and energy products behaved like the equity indices in terms of efficiency and flow of information. These futures and spot markets help in price discovery.

Lorne N. Switzer and Mario El-Khoury (2006) investigated the efficiency of the NYMEX Division light sweet crude oil futures contract market during recent periods of extreme conditional volatility. Crude oil futures contract prices were found to be cointegrated with spot prices, including over the period prior the onset of the Iraqi war and until the formation of the new Iraqi government on April 2005. **Xin Yu, Chen Gongmeng and Firth Michael (2006)** investigated the efficiency of the Chinese metal futures (i.e. copper and aluminum) traded on China's Shanghai Futures Exchange. Using random walk and unbiasedness hypotheses, they concluded that China's copper and aluminum futures markets were efficient during 1999–2004.

Pete Locke (2006) examined the transparency, liquidity and efficiency of the wholesale natural gas market in the United States, both in absolute terms and compared to other commodity markets. He concluded that natural gas futures were efficient. He found that natural gas prices were quick to reflect changes in information, reflecting great efficiency. On the surface, the

evolution to market prices might appear to increase volatility. **Lokare (2007)** found an evidence of co-integration in both spot and future prices, showing improved operational efficiency in pepper, mustard, gur, wheat, sugar (S), cotton, sesame seed, gold, copper, lead, tin and bent crude oil, rubber, sesame oil, aluminium, zinc, silver and furnace oil markets in India. **Sahoo and Kumar (2009)** examined the efficiency and futures trading-price nexus for gold, copper, petroleum crude, soya oil, and chana (chickpea) in commodity futures markets in India. They concluded that the commodity futures market is efficient for all five select commodities.

Kaur and Rao (2010) studied the weak form efficiency of guar seed, refined soya oil, chana and pepper futures markets in India. They used run test and autocorrelation analysis for testing weak form of efficiency. Using autocorrelation, they found that that all select commodities but refined soya oil futures markets were efficient. The results of run test showed that futures market for all the select commodities were efficient. **N P Singh (2010)** investigated efficiency of futures market of Guar Gum and Guar Seed in India using Error Correction Mechanism (ECM). He concluded that the futures markets for Guar Gum and Guar Seed were efficient in weak form.

Chakrabarty and Sarkar (2010) analysed long term equilibrium relationship between the multi-commodity spot market index (comdex spot) and the futures market index (comdex futures), agricultural commodity spot and futures index, & commodity spot index and Nifty 50. They also examined futures markets of potato, wheat, Masoor Grain and different types of rice at NCDEX. They concluded that commodity spot market indices are cointegrated with the futures market indices as well as Nifty. The price of different qualities of rice was found to be dependent on the recent news and not on the old news.

Ali and Gupta (2011) tested the efficiency of the futures market for twelve agricultural commodities traded at NCDEX. They used Johansen's cointegration analysis and Granger causality tests. They found that there was a long-term relationship between futures and spot prices for most of the select except for wheat and rice. Moreover, bi-directional relationships was found between spot and futures prices of some of the selected commodities in the short run. **Sehgal, Rajput and Dua (2012)** examined ten agricultural commodities futures market for a period from June 2003-March 2011 on NCDEX. They found that markets were efficient for all

but one commodity (Turmaric). Also their results showed bi-directional Granger lead relationship for all select commodities except Turmaric. They concluded that Indian commodity market is still is not competitive for some commodities.

Kristoufek and Vosvrda (2012) examined the market efficiency of 25 commodity futures across various groups like metals, energies, softs, grains and other agricultural commodities using a proposed efficiency Index. They found that the most efficient of all the analyzed commodities is heating oil, closely followed by WTI crude oil, cotton, wheat and coffee. They also inferred the efficiency for specific groups of commodities viz. energy commodities were found to be the most efficient and the other agricultural commodities the least efficient groups.

Murthy and Reddy (2012) studied the relationship between the futures price and spot prices and the farmer's participation. For chili and turmeric, they found that futures prices affect spot prices. Also, they found that "majority of the farmers are not aware of the commodity futures trading and hence do not participate in futures trading". **Gupta and Ravi (2013)** explored the efficiency between commodity futures and spot markets at MCX, NMCE and NCDEX for chana, guar seed, wheat, and potato and cotton seed oil cake. They found evidences of efficiency in most of the sample commodities.

Literature on Inefficiency

Elam (1978) developed a semi-strong test of efficiency. He estimated an econometric model of the US hog market and used it to generate price forecasts. These forecasts were in turn used in a fundamental trading strategy. His trading rule yielded profits over the period studied and led *Elam* to conclude that the hog futures market is not efficient. Similar results were found by **Leuthold and Hartmann (1979).** They tested the efficiency of the same market by estimating a simple two-equation, demand-supply model to forecast hog prices.

Goss (1981) examined the hypothesis that futures prices were unbiased predictors of the subsequent spot prices for the markets of copper, tin, lead and zinc, using daily price data from the LME for the period 1971-1978. He rejected the unbiasedness of futures prices for lead and tin. **Goss (1985)** revised his paper by introducing joint tests for the same metals of the LME

extending the sample period to 1966-1984. His results showed that the Efficient Market Hypothesis (EMH) was rejected for copper and zinc.

A simple linear regression model was used by **Bigman, Goldfarb, and Schechtman (1983)** to test the efficiency of wheat, corn and soybean trading at the CBOT. Based on F tests, they conclude that futures prices generally provide inefficient estimates of the spot price at maturity. Later, **Maberly (1985)**, **Elam and Dixon (1988)** *and* **Shen and Wang (1990)** pointed out the result is invalid based on such conventional F tests when the prices series are non-stationary. **MacDonald and Taylor (1988a)** tested and rejected the EMH for tin and zinc. **Graciela Kaminsky and Manmohan S. Kumar (1989)** used excess returns as a measure of efficiency in seven different commodity markets over the 1976-1988 period. Their results indicated that it is not possible to make any strong generalizations on the efficiency of the commodity futures market for short-term forecast horizons. For longer periods, however, it does appear that several of the markets may not be fully efficient.

Sephton and Cochrane (1990, 1991) examined the unbiasedness hypothesis in the LME with respect to six metals for the period 1976-1985. They concluded that the LME is not an efficient market. **Chowdhury (1991)** pointed out the problems of hypothesis testing in the futures market literature and suggested how the co-integration approach can be used to circumvent some of these difficulties. **Moosa and Al-Loughani (1994)** rejected futures market speculative efficiency for the West Texas Intermediate (WTI) contracts for the period January 1986-July 1990. The same hypothesis was rejected for the copper futures contract traded on the LME by **Beck (1994)**. However, **Peroni and McNown (1998)** noted that the Moosa and Al-Loughani conclusion may be unwarranted, as a result of the shortcomings of the test statistics employed.

Aulton, Ennew, *and* **Rayner (1997)** found that the market is not efficient for pigment and potatoes. **Kellard, et al. (1999)** examined the efficiency of several widely traded commodities in different markets, including soybeans on the CBOT and live hogs and live cattle on the Chicago Mercantile Exchange. The results showed that the long run equilibrium condition holds, but there

was evidence of short-run inefficiency for most of the markets studied. The degree of the inefficiency was measured based on the forecast error variances.

Mckenzie and Holt (2002) tested market efficiency and unbiasedness in four agricultural commodity futures markets – live cattle, hogs, corn, and soybean meal – using cointegration and error correction models with GQARCH-in-mean processes. They found that each market is unbiased in the long run, although cattle, hogs and corn futures markets exhibit short-run inefficiencies and pricing biases. Models for cattle and corn outperform futures prices in out-of-sample forecasting. **Wang and Bingfan (2002)** found that the futures market for wheat is inefficient in China, which may be caused by over-speculation and government intervention.

Ahmed El H. Mazighi (2003) checked the efficiency of futures markets for natural gas. He found that efficiency is almost completely rejected on the both the International Petroleum Exchange (IPE) in London (UK Market) and the New York Mercantile Exchange (NYMEX) the US market. **Kenourgios and Samitas (2004)** showed that the copper futures contract market on the LME is inefficient and did not provide unbiased estimates of future copper spot prices. They tested for both long-run and short-run efficiency using cointegration and error correction model.
J B Singh (2004) found that turmeric markets were inefficient and biased in India for the period 1988-99. **Wang, H. Holly et al. (2005)** studied the efficiency of the Chinese wheat and soybean futures markets. The results of Johansen's cointegration approach suggested a long-term equilibrium relationship between the futures price and cash price for soybeans and weak short-term efficiency in the soybean futures market. The over-speculation and government intervention were suggested reasons for wheat futures market inefficiency. **Qingfeng "Wilson" Liu (2005)** examined the relations among hog, corn, and soybean meal futures price series using the Perron (1997) unit root test and autoregressive multivariate cointegration models. Accounting for the significant seasonal factors and time trends, they found that inefficiency exists in these three commodity futures markets.

Easwaran and Ramasundaram (2008) analysed the efficiency and price volatility of select four commodities (castor, cotton, pepper and soya) on MCX and NCDEX. These markets were found

to be inefficient. They explained that the inefficiency was due to several factors like thin volume and low market depth, infrequent trading, lack of effective participation of trading members etc.

Soni and Singla (2012) analyzed the market efficiency of Guar gum futures market NCDEX using an error correction model and GARCH-M-ECM. They found Guar gum futures market was inefficient. They suggested over-speculation or market manipulation as the probable reason for inefficiency. **Inoue and Hamori (2012)** tested for weak form efficiency using MCX's spot and futures index-comdex for a period from Jan 2006 to March 2011. They used the dynamic OLS (DOLS) and the fully modified OLS (FMOLS) methods. They found that the commodity futures market was not efficient for the entire sample period but for the sub period July 2009 to March 2011. They concluded that commodity futures market exhibits weak form efficiency as the market size expands.

From above presented literature we can say that the results of these studies have been mixed and the efficiency hypothesis is supported only for certain markets and only over some periods. The findings of studies show that some commodity futures markets are efficient while others are inefficient.

Literature on Related Issues

There are various issues related to efficiency of commodity futures market. The one of such issues is the effect of seasonality on efficiency. **Newbold et.al. (1999)** investigated the effects of seasonality in testing efficiency over a range of commodities. Using quasi-ECM model, at both short and long forecast horizons they found evidence that the seasonal terms were significant i.e. the market was inefficient. The information about the seasonal pattern was not embodied in the basis and could be used by agents to predict future spot prices movements. **Sorenson** provided a framework for estimating model parameters, and especially seasonal parameters, using both the time-series characteristics and cross-sectional characteristics of agricultural commodity futures prices for the period 1972 to 1997. Estimation results were provided in the case of corn, soybeans, and wheat using weekly panel-data observations of futures prices from CBOT. He found that normal backwardation for soybeans and wheat while the situation for corn was mixed besides the estimated seasonal features. Also, he suggested normal backwardation to be the case for long contract maturities while contango be the case for short contract maturities.

The second related issue is inflationary impact of commodity futures. **Sahi and Raizada (2006)** investigated the efficiency of wheat futures market at NCDEX and analyzed its effect on social welfare and inflation in the economy. They used Johanson's Cointegration approach for different futures forecasting horizons ranging from one week to three months. Wheat futures market was found to be inefficient in short run and social loss statistic also indicated poor price discovery. The growth of commodity futures volume was found to have significant impact on the inflation in the economy. **Sahoo and Kumar (2009)** examined the impact of futures trading on inflation. They did not find sufficient evidence for inflationary impact of futures market. **Gupta and Ravi (2013)** explored the efficiency between commodity futures and spot markets at MCX, NMCE and NCDEX for chana, guarseed, wheat, potato and cotton seed oil cake. They found evidences of efficiency in most of the sample commodities. Further they examined the association between the spot price of commodities like Chana, Guarseed, Refsoyaoil, Gold and Silver, and WPI. Spot prices of commodities were found to be responsible for rise in WPI inflation.

The effect of commodity futures trading on volatility of commodity spot market is the third issue that has been discussed here. **Weaver and Banerjee (1990)** found that that futures trading for cattle and other related commodities did not lead to dynamic instability of cattle price despite the external information's role in determining cattle price. **Antoniou and Foster (1992)** analyzed the effect of futures trading on spot price volatility for Brent crude oil in UK. Using GARCH method they found that there was no volatility spillover from futures to spot market. **J B Singh (2004)** examined the hessian spot market price variability before and after (over the period 1988-97) the introduction of futures trading. He investigated the impact of futures market on inter-seasonal and intra-seasonal price volatility. He found that the cash market volatility, mainly inter-seasonal volatility, was has reduced after the introduction of hessian futures market. **Karande (2006)** in his doctoral thesis found that the introduction of castor seed futures market at Mumbai and Ahmedabad has had a beneficial effect on the castor seed spot price volatility. **Bose (2008)** used notional price indices of commodity markets covering metals, energy and agricultural products. Energy and metal indices exhibit informational efficiency of commodity futures market with stabilizing effect on volatility of underlying market.

Nath and Ligareddy (2008) found that futures trading had a destabilizing effect on spot market. Results of regression, correlation and Granger Causality indicated that introduction of futures trading led to increase in price of urad significantly. Spot prices of these commodities declined after the ban on futures trading was introduced. Price volatility was also increased during the period, when trading in futures was allowed. Wheat price increased in post futures period but the same was also coincided by steep fall in supply. **Dey, Maitra and Roy (2011)** studied cointegration and volatility spillover in Indian pepper futures market. They found a unidirectional causality from futures to spot prices of pepper. They concluded that the volatility of one market leads to another market. They found a bi-directional spillover effect under GARCH model but unidirectional under EGARCH i.e. from futures to spot.

Scope for Further Study in Commodity Futures Market

In view of literature reviewed, various concerns are raised in commodity markets that need to be addressed and investigated through research. Some of the research gaps that have been identified relate to integration with international markets, macroeconomic issues, microstructure issues of commodity futures market etc. These have been discussed below.

- No other market seems to have such extensive international macroeconomic linkages as does the commodity market. When commodities are emerging as an asset class-*earning superior risk adjusted returns* compared to stock markets or bond markets (*Domanski and Heath (2007) and Mishra (2008)*), there is dearth of studies on important issues like integration of Indian commodity market with foreign markets.
- In a developing market like Indian Commodity market, Market Microstructure has been ignored. Some studies were conducted on commodity market microstructure in India in the ’60s and ’70s. But these studies lacked the analytical quantitative rigour. Out of a few research papers on microstructure, Bhanumurthy (2004) is an important study on Indian foreign exchange market microstructure. Naes and Skjeltorp (2006) studied stock market microstructure. These studies are either in stock market or foreign exchange market. So microstructure research in commodity market in India has great scope.
- Futures market efficiency is one of the most extensively researched topics in the empirical literature. From the government policy point of view, an efficient market means

a better alternative to market interventions such as imposing price stabilization policies *(Sahadevan(2002), Thomas (2003), (Pavaskar and Ghosh, 2008), Chakrabarti and Ghosh (2009)*). The results produced are often conflicting: the efficiency hypothesis is supported only for certain markets and only over some periods. Although some of the conclusions reached in the literature reflect genuine efficiency or inefficiency, some of them may reflect the lack of attention paid to the institutional aspects governing the functioning of futures markets.

- The most relevant aspect for agro-commodities, although not yet extensively investigated, is seasonality. (Wang and Bingfan (2002), J B Singh (2004), Wang, H. Holly et al. (2005), (Newbold et al., 1999)). The study of the effect of seasonality on the efficiency of agro-commodities futures market becomes even more important in agriculture denominated country like India.
- In a country like India, where there have been allegations of inflation on commodity futures trading, an empirical investigation is utmost important and hence required. For instance, Govt. of India decided to suspend the futures trading in urad, tur and wheat in early 2007 due to the same reason. Moreover, the Expert Committee to study the impact of futures trading on agricultural commodity prices, chaired by *Abhijit Sen (2008)*, failed to arrive at any unanimous conclusion.

Conclusion

The study of market efficiency in commodity futures markets is important to both the government and the producers/marketers in India. Moreover there are some other important issues related to market efficiency viz. effect of seasonality in agro-commodities, inflationary impact of commodity futures and volatility spillover between spot and futures market. So in this paper, we have reviewed the available literature on commodity futures market efficiency and related issues mentioned above. The review showed that the results produced in available literature are often conflicting: the efficiency hypothesis is supported only for certain markets and only over some periods. Also from literature review, some areas have been identified that need attention of researchers. These are commodity market microstructure, macroeconomic issues in commodity futures market, inflationary impact of commodity futures market and

integration with other international markets and effect of sub-prime crisis. This forms further scope of research in this area.

REFERENCES

Abhijit Sen (2008), "Report on the Expert Committee to study the Impact of Futures Trading on Agricultural Commodity Prices", Ministry of Consumer Affairs, Food & Public Distribution, Govt. of India.

Ali J, Gupta K B, (2011) "Efficiency in agricultural commodity futures markets in India: Evidence from cointegration and causality tests", Agricultural Finance Review, Vol. 71 Iss: 2, pp.162 – 178

Antonios Antoniou and Andrew J Foster (June 1992) The effect of futures trading on spot price volatility: evidence for Brent crude oil using GARCH, *Journal of Business Finance and Accounting* 19(4) 473–484

Aulton A. J., C.T. Ennew and A.J. Rayner: Efficiency tests of Futures Markets for UK Agricultural Commodities, Journal of Agricultural Economics, Vol. 48, No. 3, 1997, pp. 408-423.

Bhanumurthy N R, "Microstructures in the Indian Foreign Exchange Market", Working paper series 2004, Institute of Economic Growth (India)

Bhar, R. and Hamori S., Linkages among Agricultural Commodity Futures Prices: Some further evidence from Tokyo, Applied Economics Lettters, Vol. 13, 2006, pp. 535-539.

Beck S E, "Cointegration and market efficiency in commodities futures markets", Applied Economics, Volume 26, Issue 3, 1994

Bigman, Goldfarb, and Schechtman, "Futures Market Efficiency and The time Content of the Information Sets", Journal of Futures Markets, No. 3, 1982, pp 321-334

Bose S, "Commodity Futures Market in India: A Study of Trends in the Notional Multi-Commodity Indices", *ICRA Bulletin-Money and Finance*, May 2008, pp 125-58

Canarella, G. and Pollard, S.K. (1986), "The Efficiency of the London Metal Exchange: A Test with Overlapping and Non-Overlapping Data," Journal of Banking and Finance, Vol. 10, 1986, p. 575-93.

Carter C. A., "Commodity Futures Market: A Survey" The Australian Journal of Agricultural and Resource Economics; 43:2, pp-209-247; 1999

Chakrabarti, S. and N. Ghosh (2009): "Intertemporal transfer of News and a Possible Asymmetry: Futures trading in Agro-commodities", Paper presented at the seminar on *Commodity Derivative Markets: Opportunities and Challenges*, organised by TAER and ISID, at ISID, New Delhi, October 30.

Crowder, W. J., and Hamed, A. (1993): "A Cointegration Test for Oil Futures Market Unbiasedness," Journal of Futures Market, 13: 933-941.

Danthine J P (1978), "Information, Futures Prices and Stabilizing Speculation" Journal of Economic Theory, Vol. 17, no.1, pp 79-98

Dey K, Maitra D and Roy S (2011), "Price Discovery, Market Efficiency and Volatility Revisited: Anecdotes from Indian Pepper Futures Markets",

Domanski & Heath (2007), "Financial investors and commodity markets", BIS Quarterly Review, March 2007, pp 53-67

Easwaran R S and Ramasundaram P, "Whether Commodity Futures Market in Agriculture is Efficient in Price Discovery?-An Econometric Analysis", Agricultural Economics Research Review, Vol. 21 (Conference Number) 2008, pp 337-344

Elam, E.(1978), "A Strong Form of the Efficient Market Model Applied to the US. Hog Futures market," Ph. D. Thesis (unpublished), University of Illinois.

Elam, E and Dixon, B. L., "Examining the validity of a test of futures market efficiency", Journal of Futures Markets, 8, pp 365-72

Engle, R.F. and C.W.J. Granger, Cointegration and Error Correction: Representation, Estimation, and Testing, Econometrica, 55, 1987, pp 251-276

Fama E F., "Efficient Capital Markets: A review of theory and empirical work", Journal of Finance, vol.25, no.2, 1970, pp 383-417

Fama, E.F.: Efficient Capital Markets: 11, Journal of Finance, 60(5), 1991, pp 1575-1617

Fama, E. and K. French: Commodity Futures Prices: Some Evidence on Forecast Power, Premiums and the Theory of Storage, Journal of Business, 60: 1, Jan. 1987, pp 55-73.

Fortenberry, T.Randall and H.O. Zapata: An Examination of Cointegration Relation between Futures and Local Grain Markets, The Journal of Futures Markets, 13(8), 1993, pp 921-932.

Goss, B.A.(1981), "The Forward Pricing Function of the London Metal Exchange," Applied Economics, Vol.13, 1981, p. 133-50.

Goss, B.A.(1985), "The Forward Pricing Function of the London Metal Exchange," in B.A. Goss, eds., Futures Markets: Their Establishment and Performance, London: Croom and Helm, 1985, p. 157-73.

Graciela Kaminsky and Manmohan S. Kumar , "Efficiency in Commodity Futures Markets" IMF Working Paper, WP/89/106, 1989

Gross, M.(1988), "A Semi-strong Test of the Efficiency of the Aluminum and Copper Markets at the LME," The Journal of Futures Market, Vol. 8, 1988, p. 67-77

Gulen, S.G., 1998. Efficiency in the crude oil futures market. Journal of Energy Finance and Development, 3, 13–21.

Gupta and Ravi , "Commodity Futures Market Efficiency in India and Inflationary Impacts", Working Paper, 2013

Inoue and Hamori, "Market Efficiency of Commodity Futures in India", IDE Discussion paper No. 370, Oct 2012

Karande K, "A Study of Castorseed Futures Market in India", Unpublished Doctoral Thesis 2007

Kaur and Rao (2010), "An Empirical study of select Agricultural Derivatives Traded on NCDEX", *Journal of Management Research, Vol. 10, No. 2, August 2010, pp 116-132*

Kenourgios D F, Samitas A G (2004), "Testing Efficiency of the Copper Futures Market: New Evidence from London Metal Exchange", *Global Business and Economics Review, Anthology* 2004, pp. 261-271.

Kellard, N., P. Newbold, T. Rayner and C. Ennew (1999), The Relative Efficiency of Commodity Futures Markets, The Journal of Futures Markets, Vol.19, pp 413-432.

Kristoufek L, Vosvrda M (2012), "Commodity futures and market efficiency", International Journal of Advancements in Research & Technology, Volume 1, Issue 5, October-2012

Kumar, Vashisht and Kalita, "Food Inflation: Contingent and Structural Factors", Economic & Political Weekly, Vol - XLV No. 10, March 6, 2010

Leuthold, R M and Hartmann P (1979), "A semi strong form evaluation of the efficiency of the hog futures market", American Journal of Agricultural Economics, 61(3), pp 482-89.

Lokare S M, "Commodity Derivatives and Price Risk Management: An Empirical Anecdote from India" Reserve Bank of India Occasional Papers, Vol. 28, No. 2, Monsoon 2007

Lucas R E J(1978), "Asset Prices in an Exchange economy", Econometrica Vol. 46, no 6, pp 1429-45

Maberly, E.D., Testing Futures Market Efficiency – A Restatement, The Journal of Futures Markets, Vol. 5, 1985, pp 425-432.

MacDonald, R. and Taylor, M.P., "Metal Prices, Efficiency and Cointegration: Some Evidence from the LME," Bulletin of Economic Research, Vol. 40, 1988a, p. 235-39

Mazighi A E H (2003), "The efficiency of Natural gas futures markets", OPEC Review 2003, 27(2), 143-158

Mckenzie, A. M. and M.T. Holt, "Market Efficiency in Agricultural Futures Markets", Selected Paper presented at American Agricultural Economics Association Annual Meeting, Salt Lake City. 2002

Mishra A K, "Commodity Futures Markets in India: Riding the Growth Phase", White paper, 2009, evalueserve

Moore, M.S. and Callen, U., "Speculative Efficiency on the London Metal Exchange," The Manchester School, Vol. LXIII, 1995, p. 235-56

Moosa, I.A. and Loughani, N.E., 1994. Unbiased and time varying risk premia in the crude oil futures market, Energy Economics, 16, 99–105

Murry D and Zhu Z (2004), "EnronOnline and Informational Efficiency in the US Natural Gas Market", The Energy Journal, Vol 25, No. 2, 2004

Murthy and Reddy, "Commodity Futures Market: A Necessity for the Indian Farmers", *Research Journal of Social Science and Management*, Volume: 02, Number: 02, June-2012, pp 100-109

Nath G C and Lingareddy T, "Impact of Futures Trading on Commodity Prices", Economic & Political Weekly, Vol - XLIII No. 03, January 19, 2008

Naes R and Skjeltorp J, "Is the Market Microstructure of Stock Markets Important?" *Economic Bulletin*, 77 (3), 2006), pp. 123–32.

Newbold P, Rayner T, Ennew C, Marrocu E, "Testing seasonality and efficiency in commodity futures markets", *Discussion Paper No. 99/33, School Of Economics*

Pavaskar M and Ghosh N (2008), "More on Futures trading and Commodity Prices", Economic & Political Weekly, Vol 43, Issue 10, March 2008.

Peroni, E., McNown, R.F., 1998. Non informative and informative tests of efficiency in three energy futures markets. Journal of Futures Markets 18, 936–964.

Pete Locke (2006), "Natural Gas Price Transparency and Liquidity" October 2006, Natural Gas Supply Association (NGSA)

Qingfeng "Wilson" Liu, "Price relations among hog, corn, and soybean meal futures", Journal of Futures Markets, vol. 25(5), pp 491 – 514, 03/2005Ravikumar P H, "Commodity Boom, the Good, the Bad and the Ugly", Charted Financial Analyst", June 2006

Rausser G C and Carter C., "Futures Market Efficiency in the Soybean Complex", Review of Economics and Statistics, Vol 65, no.3, 1983, 469-78.

Roll R, "Orange Juice and Weather", American Economic Review, Vol 74, no.5, 1984, pp 861-80.

Sahadevan K G, "Derivatives and Price Risk Management: A Study of Agricultural Commodity Futures in India", A Seed Money Project Report, IIM, Lukhnow; 2002

Sahi GS and Raizada G, "Commodity Futures Market Efficiency in India and Effect on Inflation", SSRN online papers

Sahoo and Kumar (2009), "Efficiency and Futures Trading-Price Nexus in Indian Commodity Futures Markets", Global Business Review, 2009, vol. 10, issue 2, pages 187-201

Samuelson P.A. (1965), "Proof that properly anticipated prices fluctuate randomly", Industrial Management Review, Volume 6, no.2, pp 41-49

Sehgal S, Rajput N and Dua R K, "Price Discovery in Indian Agricultural Commodity Markets", International Journal of Accounting and Financial Reporting, Vol. 2, No 2, 2012, pp 34-54

Sephton, P. S. and Cochrane, D. K. (1990), "A Note on the Efficiency of the London Metal Exchange," Economic Letters, 33, p.341-345.

Sephton, P. S., and Cochrane, D.K. (1991), "The Efficiency of the London Metals Exchange: Another Look at the Evidence," Applied Economics, 23, p.669-674.

Sewell M, "History of Efficient Market Hypothesis" *UCL Deptt of Computer Science*, Research Note RN/11/04, Jan 2011

Shen, C. and L. Wang, "Examining the Validity of a Test of Futures Market Efficiency: A Comment", The Journal of Futures Markets, 10, 1990, pp 195-196.

Singh J B, "Futures Market in the Management of Price Risks in Indian Agriculture", Unpublished Doctoral Thesis 2004

Singh N P, "Efficiency of Agro-Commodity Futures Market", Prabandhan-Journal of Management, 2010

Slade M E and Thille H (2004), "Commodity Spot prices: An Exploratory assessment of Market Structure and forward trading effects", Journal of Economic Literature, September.

Soni and Singla (2012), "A Study of the Efficiency and Unbiasedness in NCDEX: A Case Study of Guar Gum", XI Capital Markets Conference, 21-22 December 2012, Indian Institute of Capital Markets (UTIICM)

Sorensen C, "Seasonality in Agricultural Commodity Futures", e paper

Switzer L N and El-Khoury M (2007), "Extreme volatility, Speculative Efficiency and the Hedging Effectiveness of the Oil Futures Market", Journal of Futures Markets, Vol. 27, Issue 1, pp 61-84

Tomek, William G.: Futures Trading and Market Information: Some New Evidence, Food Research Institute Studies, Vol. 17, No. 3, 1979-80, pp 351-359.

Thomas, S. (2003), 'Agricultural Commodity Markets in India: Policy Issues for Growth', Indira Gandhi Institute for Development Research Working Paper , Mumbai.

Wang H H and Ke Bingfan, "Efficiency tests of agricultural commodity futures markets in China" The Australian Journal of Agricultural and Resource Economics; vol. 49(2), June 2005, pp 125-141

Weaver R D and Banerjee A, "Does futures trading destabilize cash prices? Evidence for U. S. live beef cattle" Journal of Futures Markets, Volume 10, Issue 1, pages 41–60, February 1990

Yang Jian, Brian Balyeat R and David J. Leatham (2005): "Futures trading Activity and Commodity cash price volatility", Journal f Business Finance Accounting, 32(1&2); 297-323.

Yu X, Gongmeng C and Michael F (2006), "Efficiency of Chinese Commodity Futures Market: Development and Empirical Evidence", China and World Economy 14 (2), pp 79-92

IOSR Journal of Mechanical and Civil Engineering (IOSR-JMCE)
e-ISSN: 2278-1684,p-ISSN: 2320-334X, Volume 12, Issue 1 Ver. II (Jan- Feb. 2015), PP 85-92
www.iosrjournals.org

Energy and Exergy Analysis of Organic Rankine Cycle Using Alternative Working Fluids

Deepak Tiwari[1], Akhilesh Arora[2], Naushad Ahmad Ansari[3],*Dr.A.F.Sherwani

Abstract: *The present study is based on parametric investigation in terms of thermal efficiency, exergetic efficiency and exergy destruction with the help mathematical modeling on different ORC models using different fluids. The Thermal efficiency of ORC model of Saturated, Trilateral is compared by using working fluids such as (HFO-1234yf,HFC-134a,HFC-245fa,Ethanol,Iso-pentane by varying expander inlet temperature (30-160°C),at fixed condensation temperature(30°C) assuming fixed expander isentropic efficiency (=0.75) and fixed isentropic pump efficiency(=0.60). The Thermal efficiency as well as exergetic efficiency has been observed best for theHFO-1234yf and found nearly close with HFC-134a. HFO-1234yf has good potential for working fluid for ORC application for low to medium temperature. It has zero global warming potential (GWP), zero Ozone layer depletion (ODP) and very Low evaporation Temperature. This paper provides a basis to compare the thermal and exergetic efficiency for various working fluids and exergy destruction in various component such as Expander, Evaporator,Condenser,Pump for saturated and Trilateral cycle when used with R-1234yf as working substance.*

Keywords: *Organic Rankine cycle models, Energy analysis& Exergy analysis, Exergy destruction; R-1234yf, R-134a, R-245fa, Ethanol, Isopentane.*

Biographical notes: Deepak Tiwari is pursuing Ph.D. From Department of Mechanical Engineering of Jamia Millia Islamia University, Delhi. His research area includes exergy analysis of thermal systems and alternative refrigerants.
Akhilesh Arora is working as an Associate Professor in the Department of Mechanical Engineering and Automation at Indira Gandhi Delhi Technological University for Women, Delhi, India. He obtained his PhD from the Indian Institute of Technology, Delhi in 2011. His research area includes alternate refrigerants, alternate refrigeration technologies and exergy analysis of thermal systems.
Naushad Ahmad Ansari is working as an Assistant Professor in Department of Mechanical Engineering at Delhi Technological University, Delhi. He obtained his Master of Technology (M. Tech) in Thermal Engineering from Aligarh Muslim University, Aligarh in 2000. His research area includes alternate refrigeration technologies, exergy analysis of thermal systems, fluid mechanics and computational fluid dynamics.
Dr. A.F.Sherwani is working as an Assistant Professor in Department of Mechanical Engineering of Jamia Millia Islamia University, Delhi. His research area includes alternate refrigeration technologies, exergy analysis of thermal systems and renewable, sustainable energy and life cycle analysis.

I. Introduction

Heat is recovered by organic Rankine cycles (ORC).Low grade heat is useful for operation of Organic Rankine cycle the Low grade heat is available from various heat sources such as solar ,ocean , thermal , geothermal, biomass, and available source of heat from engine exhaust or industrial process waste heat. The word ORC has been used from the fact that it is basically a Rankine cycle which runs organic Fluid as a working substance Serrano et al. [1] did the theoretical investigation and has suggested that possibility to introduce the concept of recovery of waste heat in heavy duty diesel engine of two stage turbocharged engine and introduced the best use of IC engine Exhaust waste heat coupling with simple water Rankine cycle. Wang.et al. [2] Proposed and designed a experimental set up of solar operated rankine cycle by using R-245fa as a working substance and used evacuated and Flat plate collector and found the efficiency of overall power generation of evacuated collector is 4.2% and with flat plate collector is 3.2%. DiGenova et al. [3] proposed a customized organic Rankine cycle based on the heat source from Fischer Tropsch plant reactor and found that the steam Rankine cycle may achieve 20.6% conversion efficiency using this heat source and by using hexane as a working substance in ORC the conversion efficiency may reach 20.6%. Wang et al. [4] proposed the concept of discontinuous waste heat recovery at low temperature and did the performance analysis with the effect of temperature at exit to the heat source on thermal efficiency, power consumption ,mass flow rate,expander outlet temperature, net power output,cycle irreversibility,exergy efficiency by using various working substances such as acetone,butane,isopentane,pentane,R-245fa,CF3l,R-414b,R-21 and found acetone shows the least exergy destruction and R-245fa shows maximum thermal efficiency at fixed pinch point temperature difference. Larjola [5] suggested the applicability of high speed (ORC) and found that the low temperature waste heat

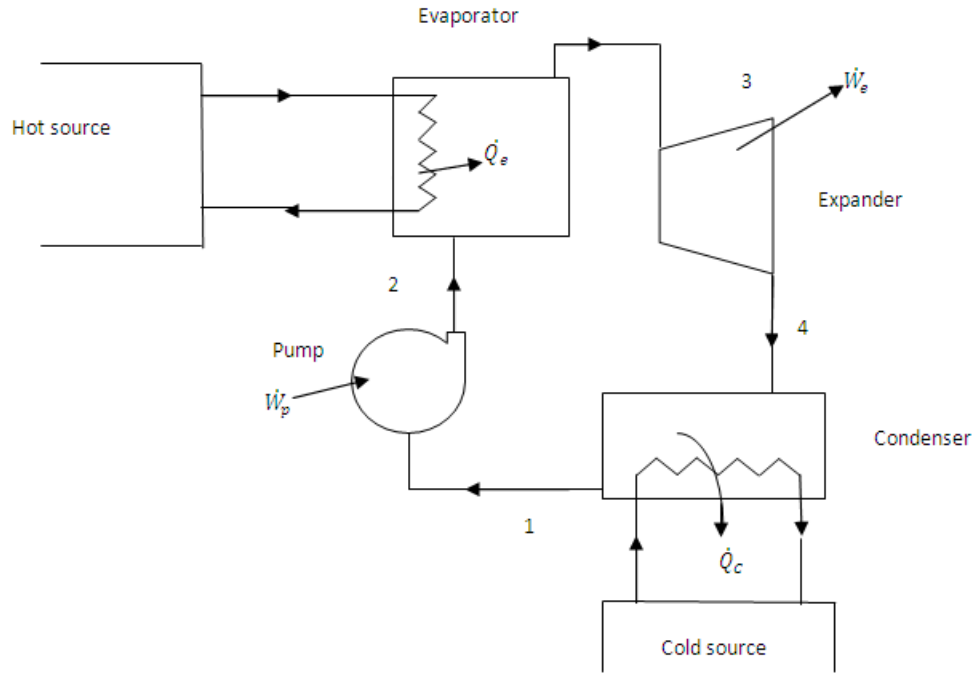
sources are such as combustion of I.C. engine blast furnace hot gases steel industries diesel engine exhaust gases, gas turbine can be converted into electricity with highest efficiency. Li et al. [6] Analyzed the effect of fouling in organic rankine cycle and concluded that convective and radiative heat losses increase with increase in operating temperature. Quoilin et al. [7] proposed the design optimization and performance of economical solar operated (ORC) to generate power for rural and remote area and found that overall efficiency of electricity can be reached 7to 8% . Heberle et al. [8] carried out the exergy analysis of a combined heat and power generating ORC using geo-thermal energy inlet source (>450^{0}k) and used four working fluids are such as isobutene,isopentane,R-227ea,R-245fa and found that R-227 shows highest second law efficiency for inlet temperature 353-423k and isobutene is best working fluid for higher temperature inlet source of geothermal water . Aleksandra& Borsukiewicz [9] has calculated pump work in ORC by using 18 working substance in subcritical organic rankine cycle plant and found that for lower critical temperature of the working substance and the pressure in the cycle will be more thus pumping power will be more.

Nobru et al. [10] presented Study on First Law efficiency(Energy analysis) by using HFO-1234yf as working substance for low to medium temperature range of Organic Rankine cycle and found that it is potential working substance having negligible ozone depletion potential, global warming potential and found highest thermal efficiency 8.8-11.4% for expander inlet temperature range of (180-160^0C) in SupercriticalOrganic Rankine cycle.Till now there is no study about exergy analysis and exergy destruction in various component expander,pump,condenser,and evaporator using HFO-1234yf as working substance in Organic Rankine cycle(ORC)

In this paper, the first and second law analysis of ORC have been carried out using working fluids as HFO-1234yf,HFC-134a,HFC-245fa,Ethanol,Iso-pentane.

II. Basic Organic Rankine Cycle

Fig.1. Shows schematic diagram of Organic Rankine cycle,It consist of following component are such as Evaporator,Expander, Condenser, Pump.



2.1 Working Fluids

There are five working fluids used in this simulation study: HFO-1234yf, HFC-134a, HFC-245fa, iso-pentane, and ethanol. The working substances HFC-245fa and iso-pentane are dry fluid used to utilize low-temperature heat source from industrial power plants waste.Ethanol and HFC-134a are wet fluids and Ethanol is in use now a days as a good automotive working fluid in organic rankine cycle because of it's' capability to perform best for medium-temperature range (200-300°C).The purpose of using organic substance as working fluids is because they have evaporation temperature which is found to be very low as compared to steam (water vapor) and has this tendency to change into vapor or superheated vapor by using low to medium-temperature heat source.The organic substances dry (HFC-245fa, Iso-pentane) and isentropic (HFC-1234yf) which may enhance the expander life more; The vapor gets expansion in the expander has tendency to remain in dry or either saturated or superheated vapor conditions.

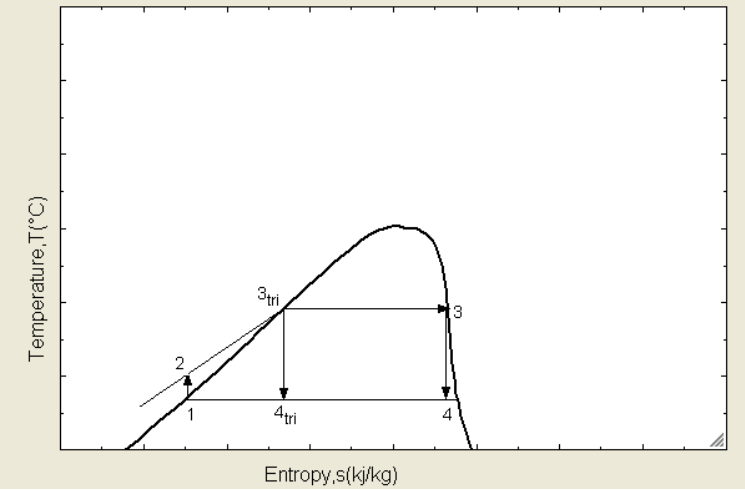
Working fluid	Flammability/ Toxicity	Type	Molecular mass(kg/kmol)	$T_{cri}\,(^0C)$	$T_{bp}\,(^0C)$	$P_{cri}\,(MPa)$	ODP	GWP(100yr)
HFO-1234yf	No	Isentropic	114.042[a]	94.7[a]	-29.45[b]	3.382[b]	~0	4
HFC-134a	No	Wet	102.03[b]	101[a]	−26.0745[b]	4.0593[b]	~0	1320[c]
HFC-245fa	No	Dry	134.05[b]	154[a]	15.14[b]	3.651[b]	~0	1020[c]
Isopentane	Yes	Dry	72.149[b]	187.2[a]	27.83[b]	3.387[b]	~0	~20[c]
Ethanol	Yes	Wet	46.068[b]	240.7[a]	78.24[b]	6.148[b]	na	Na
Acetone	No	Wet	58.08	3.60[a]	329.15	4.70[a]	~0	Na

Table-1 Comparative characterstic of working fluids (HFO-1234yf, HFC-134a, HFC-245fa, Isopentane, Ethanol, Acetone)

a. a Ref.Akasa et al
b. b REFPRP:Ref.Lemmon et al.[20]
c. c Ref.calm et al [21]

2.2 Saturated cycle model:

Fig.2 shows T-s diagram for wet fluids (such as HFC-134a,Ethanol)It is similar to trilateral cycle it is very compact design system can be used to obtain reasonable thermal efficiencies by recovering waste heat from low temperature level. The temperature-entropy (T-S) diagram for the saturated cycle is shown by the cycle path 1-2-3-4-1. The heat is supplied to evaporator (2-3) at isobaric condition. The process (1-2) is reversible adiabatic pumping the process (3-4) is reversible adiabatic expansion. The process (4-1) shows constant pressure heat rejection process



2.3 Trilateral cycle model:

Fig.3 Shows T-s diagram of ORC for isentropic fluid (HFO-1234yf) The trilateral organic rankine cycle seems to be triangular rankine cycle. It looks very simple cycle when compared with a conventional cycle, it shows very competitive performance when it is used for low temperature source of heat. It has low operating cost of same sized components.

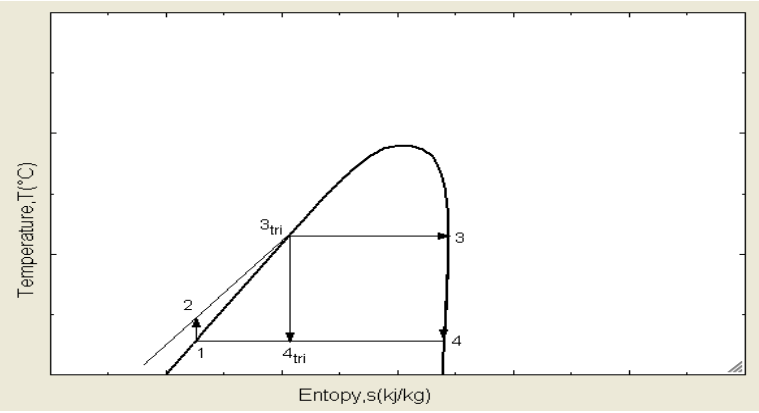
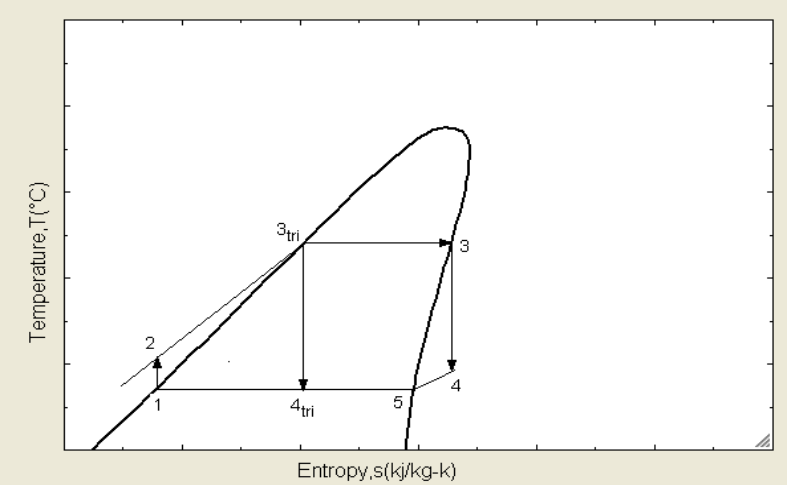


Fig 4 Shows T-s diagram of ORC for dry fluid (HFC-245fa,Isopentane)



The reason of using this cycle is that the temperature profile of working substance is matching perfectly to the heat source. Its' operating pressure is optimum, so it is used economically for where low powered heat application is required.

In this simulation work, T-s diagram for the trilateral ORC model is represented by cycle path 1-2-3-4-1. The pressure, at which pump is working which is same as evaporation pressure but practically it is lower than the critical pressure of the working fluid. The inlet temperature to the expander is maintained at saturated condition.

The cycle consists of reversible adiabatic (isentropic) pumping shown by state (1-2) of a working fluid then, followed by constant pressure heat supply to the working fluid (2-3),then isentropic expansion of the working fluid containing two-phase mixture at state (3-4) is then entered, for constant pressure heat rejection in condenser and finally return with two-phase mixture at saturated liquid state (4-1).The trilateral cycle is differed by conventional cycle where the working substance remains in the form of liquid when it exit from the evaporator. By keeping constant condenser temperature, the thermal efficiency substantially increases when operating inlet temperature varies from Tin=50°C to $170\pm10°C$ then falls slowly when the expander inlet temperature further reaches up to 200°C.

2.4 Energy Analysis

The following assumption are made during thermodynamic analysis of ORC

1) The process is steady -flow and steady state;2)There is no pressure drop in connecting pipes and heat exchanger:3)process in expander and pump is isentropic;4)There is no heat loss from equipments and pipes;5)The heat carrier of exhaust gas is non- corrosive and non-condensable in heat exchange process ;6)The isentropic expander efficiency 75%.) ;7)The isentropic pump efficiency is 60%.The fixed condensation temperature is 30°C.

The general energy balance equation for all existing cycle (Saturated, Trilateral, Supercritical, Superheated, and Subcritical) is as follow:

The isentropic pump efficiency &power

$$\eta_p = \frac{h_{2s}-h_2}{h_2-h_1} \quad (1)$$

$$W_P = \dot{m} * (h_2 - h_1) \quad (2)$$

For the expander

Isentropic efficiency

$$\eta_e = \frac{(h_3 - h_4)}{(h_3 - h_{4s})} \quad (3)$$

$$W_e = \dot{m} * (h_3 - h_4) \quad (4)$$

The amount of heat supplied to the working fluid into evaporator

$$Q_{in} = \dot{m} * (h_3 - h_2) \quad (5)$$

Thermal Efficiency Of the ORC cycle

$$\eta_{th}=\frac{W_e-W_P}{Q_{in}} \quad (6)$$

$$\eta_{th}=\frac{(h_3-h_4)-(h_2-h_1)}{Q_{in}} \quad (7)$$

2.5 Exergy Analysis

The second law of thermodynamics assists in evaluating the performance of the system based on exergy, which always decreases owing to irreversibility. Exergy is the measure of usefulness, quality or potential of a stream to cause change and an effective measure of the potential of a substance to impact the environment (Dincer, 2003). Exergy balance for a control volume undergoing steady state process is expressed as (Lee and Sherif, 2001).

$$\dot{E}D_i = \sum(\dot{m}e)_{in} - \sum(\dot{m}e)_{out} + \left[\sum\left(\dot{Q}(1-\frac{T_0}{T})\right)_{in} + \sum\left(\dot{Q}(1-\frac{T_0}{T})\right)_{out}\right] \pm \sum\dot{W}$$

Where EDi represents the rate of exergy destruction occurring in the process in the component under consideration

The first two terms on the right hand side represent exergy of streams entering and leaving the control volume. The third and fourth terms are the exergy associated with heat transfer Q from the source maintained at constant temperature T and is equal to work obtained by Carnot engine operating between T and T0. The last term is the mechanical work transfer to or from the control volume. Second law performance of the system can be measured in terms of exergetic efficiency.Exergetic efficiency can also be expressed in terms of total exergy destruction and exergy supplied to the system.

Exergy destruction in evaporator:

$$E_{devap} = (h_2-T_O*S_2)- (h_3-T_0*S_3)+q_s*[1-T_O/ (T_3+273)] \quad (8)$$

Exergy destruction in expander:

$$E_{dexp} = (h_3-T_O*S_3)- (h_4-T_O*S_4)- (h_3-h_4) \quad (9)$$

Exergy destruction in condenser:

$$(h_4-T_O*S_4)- (h_1-T_o*S_1) \quad (10)$$

Exergy destruction in pump:

$$E_{dpump}= (h_1-T_o*S_1)- (h_2-T_o*S_2)+ (h_2-h_1) \quad (11)$$

$$E_{dtotal} =E_{devap} +E_{dexp}+E_{dcond}+E_{dpump} \quad (12)$$

Exergetic Efficiency

$$\eta_{ex} =1-E_{dtotal}/E_{inpu} \quad (13)$$

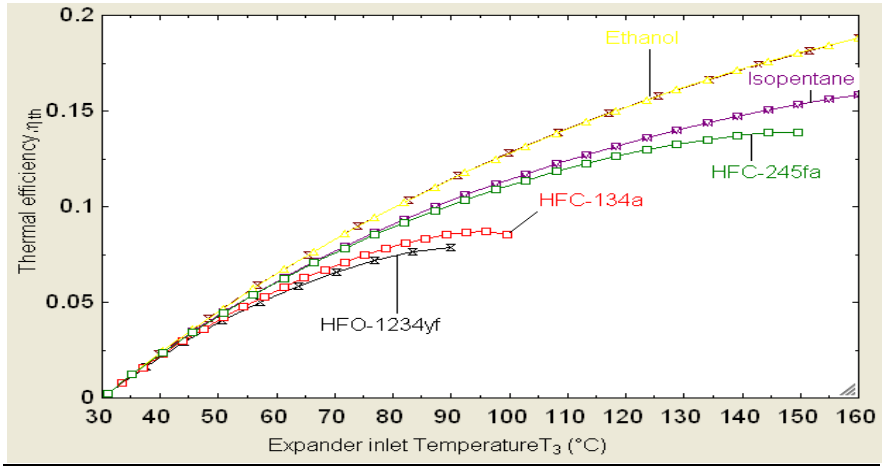
$$E_{input} =q_S*[1-T_O/ (T_3+273)]+W \quad (14)$$

$$\eta_{ex\,1} =W_T/E_{input} \quad (15)$$

III. Result And Discussion

This section deals with the result and discussion for simple ORC cycle with various working fluids at different Expander inlet temperature at fixed condenser temperature (30°C), Isentropic Expander efficiency (η_T=75%), IsentropicpumpEfficiency (η_P=60%).

Fig.5. Shows relative Comparison of Thermal Efficiency of Saturated by using various working fluid. In saturated Rankine cycle model by using HFO-1234yf shows Lowest Thermal Efficiency (7%) and ethanol shows highest thermal efficiency (20%) as compared to other working fluid in temperature Range (30-90°C).



Exergetic Efficiency Comparison of various Working Fluid in Saturated Cycle.

Fig.6. Exergetic efficiency for saturated ORC HFO-1234yf shows lower exergetic efficiency (52%) Ethanol shows higher Exegetic efficiency(60%) for expander inlet temperature (30-100°C).

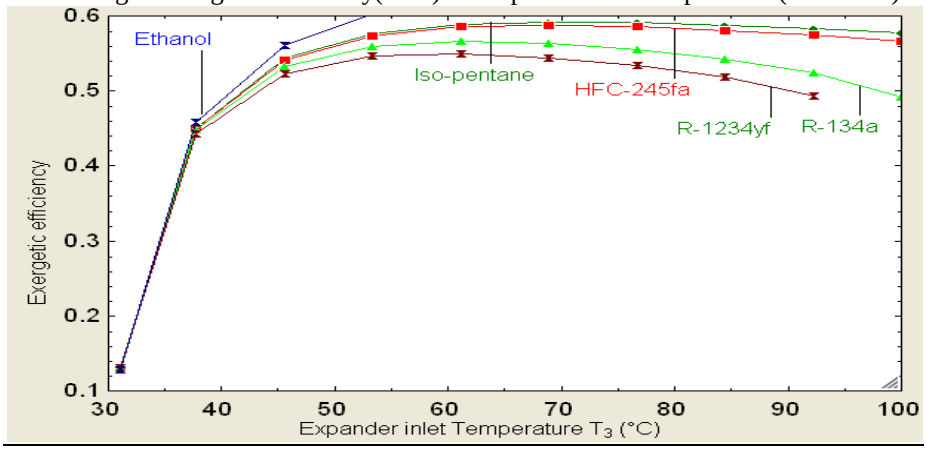


Fig.7. shows Comparison of Exergy Destruction in variour component (Expander, Evaporator, Pump, and Condenser) in Saturated cycle using R-1234yf

The exergy destruction (7kw) in evaporator is highest as compare to expander, pump, condense and pump shows the lowest exergy destruction(2kw) for temperature range of (30-100°C).

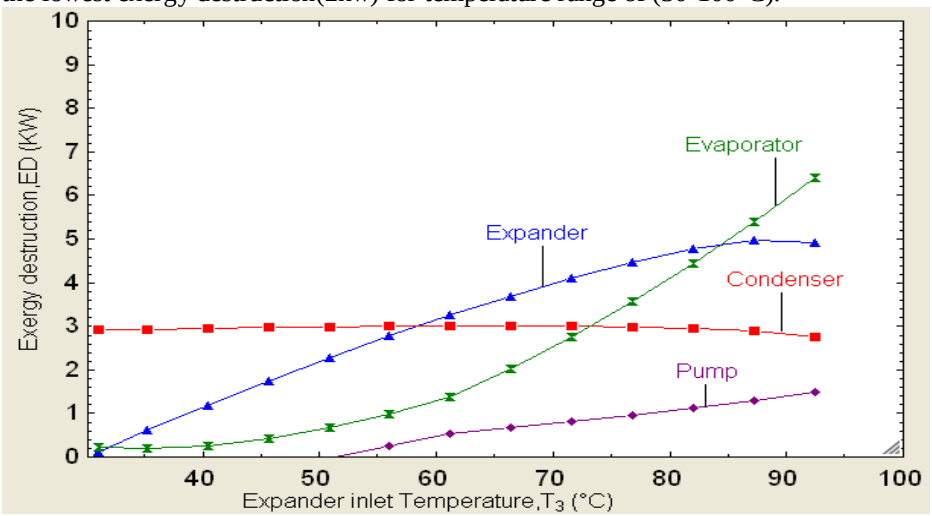


Fig.8.Shows relative Comparison of Thermal Efficiency with Expander inlet Temperature of Trilateral cycle by using various workingFluid .

It has been observed that Ethanol shows higher thermal efficiency (14%), HFO-1234yf lower thermal efficiency(5%) for expander inlet temperate (30-160°C).

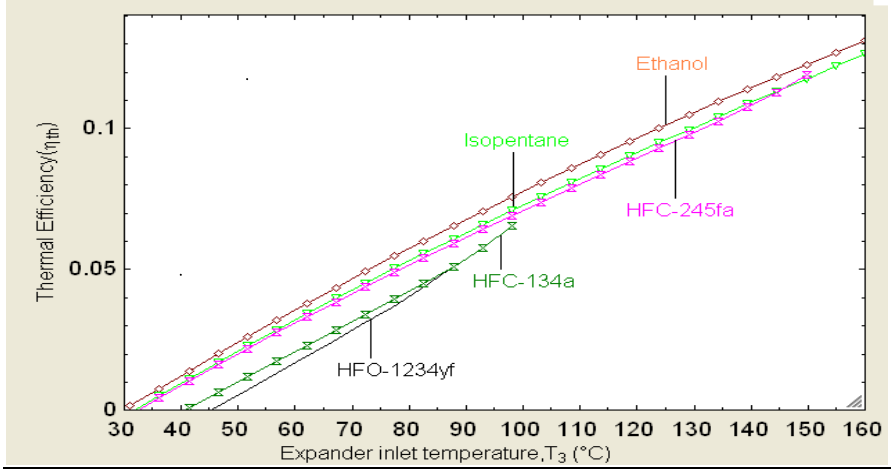


Fig.9 Shows. Exergetic Efficiency Comparison of various Working Fluid in Trilateral cycle HFC-134a shows highest exergetic efficiency(42%) is close to the exergetic efficiency(40%) when HFO-1234yf is used.

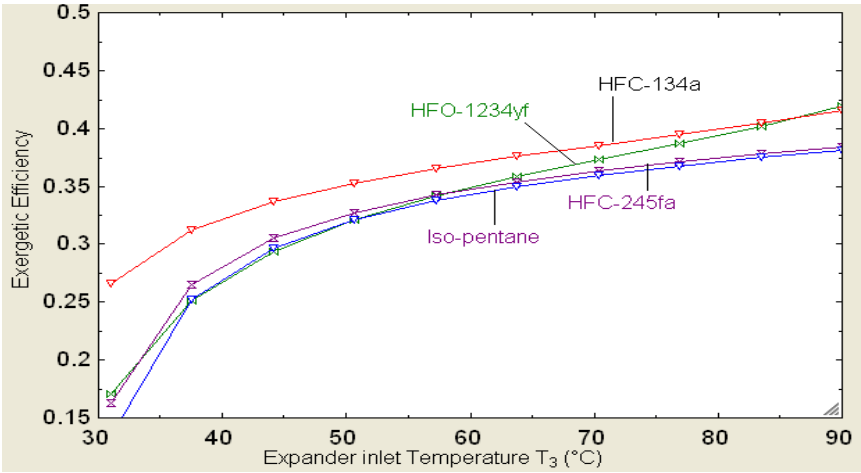
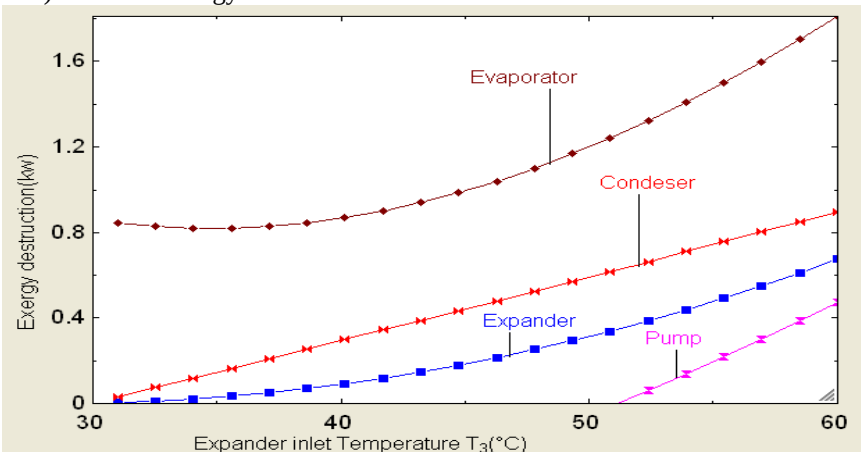


Fig.10. Shows relative Comparison of Exergy destruction of Trilateral cycle by using HFO-1234yf as working Fluid.

The exergy destruction in evaporator (1.8kw) is highest as compare to expander, pump, condenser and pump shows (0.6kw) the lower exergy destruction.



IV. Conclusions

The first law efficiency obtained in this section is similar to the result obtained by Nobru et.al. On the basis of result obtained from the thermodynamic model, the following conclusions are drawn:-HFO-1234yf is used as working fluid in two ORC models through first order simulation are Saturated, Trilateral cycle. The first law efficiency of HFO-1234yf has been compared with that of other working fluids (R-245fa, R-134a, Isopentane, and Ethanol). HFO-1234yf may be used for low-to medium-temperature ORC applications; Thermal efficiency is not always the best among the other simulated fluids depending on the temperature level of expander. So, the HFO-1234yf can be used as a good alternative working fluid for low to medium-temperature heat sources of ORC applications (at prescribed expander inlet temperature of up to 170°C) if ODP and GWP are considered within safe limit. Beyond the above work, in this paper the Exergetic efficiency and exergy destruction has been calculated and compared by using HFO-1234yf as working fluid with other working fluids(R-245fa, R- 134a,Isopentane, and Ethanol) which are as follows.

1) The exergetic efficiency of Ethanol is highest in saturated cycle (60%) when expander inlet temperature is from 30^0C-100^0C.
2) The exergetic efficiency of R-1234yf (9%) is found very close to exergetic efficiency of R-134a(10%) in saturated cycle.
3) The exergetic efficiency of R-134a(42%) when used in Trilateral cycle is close to the exergetic efficiency(40%) of R-1234yf as a working substance for expander inlet Temperature from 30^0C-90°C.
4) The exergy destruction in evaporator is highest (7kw) and Lowest in pump (2kw) when R-1234yf is used as working substance in saturated cycle for expander inlet temperature from 0°C-100°C.
5) The exergy destruction is highest (1.8kw) in evaporator and lowest in pump (0.18kw) for expander inlet temperature from 30^0C-60°C in Trilateral cycle.

References

[1]. Serrano J.R., Dolz V., Novella R., Garcia A. , 2011. HD Diesel engine equipped with a bottoming Rankine cycle as a Waste heat Recovery System. Applied Thermal Kevinj. Engineering 36 (2011) , 279-287.

[2]. Wang X. D. Zhao L. Wang J.L, Zhang W. Z. , Zhao X .Z., W. Wu. 2009. Performance evaluation of low-temperature Solar Rankine cycle system utilizing R245fa. Solar Energy84 (2010), 353-364.

[3]. DiGenova Kevinj. Botros Barbara B, Brisson J.G., 2012. Method For customizing on organic Rankine cycle to a complex heat source for efficient energy conversion, demonstrated on Fischer Tropsh Pant. Applied Energy 102 (2013) 746-754.

[4]. Wang Dongxiang, Ling Xiang, Peng Hao. 2012. Performance Analysis of double organic Rankine cycle for discontinuous low temperature Waste heat Recovery. Applied Thermal Engineering 48 (2012) 63-71.

[5]. Larjola j., 1994. Electricity from industrial waste heat using high-speed organic Rankine cycle. International journal of Production Economics 41 (1995) 227-235.

[6]. Li jing, Pei Gang, Li YunhuLI, Ji jie.,2012. Evaluation of External heat loss from small-scale expander used in organic Rankine cycle. Applied Thermal Engineering 31 (2011) 26942701.

[7]. Quilin S., Orosz M., Hemond H., Lemort V.,2012. Performance and design optimization of Low-cost solar organic Rankine cycle for remote Power generation. Solar Energy 85 (2011)955-966.85

[8]. Heberle Florian, Bruggemann Dieter., 2010. Exergy based fluid selection for geothermal organic Rankine cycle for combined heat and power generation. Applied Thermal Engineering 30 (2010).

[9]. Borsukiewiz-Gozdur Alesksandra .,2012. Pumping work in the organic Rankine .

[10]. Yamada Noboru, Mohamad Md Nor Anuar,Trinh Trung Kien .,2011. study on Thermal Efficiency of low to medium organic Rankine cycle using HFO-1234yf.Renewable Energy 41 (2012)368-375.cycle.Applied Thermal Engineering 51 (2013) 781-786.

Nomenclature

HFO	Hydro-fluro -Olefin
HFC	Hydro-fluro-carbon
EES	Engineering equation solver
Ed	Exergy destruction (kw)
H	Efficiency (%)
T	Temperature (°C)
Subscripts	
Cond	condenser
Exp	expander
Pump	pump
Evap	evaporator
Ex	exergetic
In	inlet to expander
1	Pump inlet state
2	Pump exit state
3	Expander inlet state
4	Expander exit state
Greek letters η	(efficiency)

International Journal of Ecological Science and Environmental Engineering
2014; 1(2): 49-61
Published online October 10, 2014 (http://www.aascit.org/journal/ijesee)



Keywords
E-Waste,
Hazardous,
Recycling,
Recovery,
E-Waste Disposal Techniques

Received: January 02, 2014
Revised: September 29, 2014
Accepted: September 30, 2014

E-Waste characteristic and its disposal

M. C. Vats[1], S. K. Singh[2]

[1]Technical Officer, DRDO, Delhi, India
[2]Prof and Dean Delhi Technological University Delhi, India

Email address
maheshchandervats@gmail.com (M. C. Vats), singhsk@email.com (S. K. Singh)

Citation
M. C. Vats, S. K. Singh. E-Waste Characteristic and Its Disposal. *International Journal of Ecological Science and Environmental Engineering.* Vol. 1, No. 2, 2014, pp. 49-61.

Abstract
E-waste contains both hazardous and non-hazardous substances in their components. Globally, the e-waste generation is estimated at 20 to 50 million tonnes annually. It represents 1 to 3% of the global municipal waste produced as 1636 million tonnes per year. The obsolete and EOL electrical and electronic equipment in large numbers made it a fast growing waste all over the world increasing at the rate of 3 to 5% per annum with respect to the municipal waste. The presence of organic toxic and hazardous substances in e-waste separates it from the normal municipal waste. These hazardous substances like plastic, lead, mercury, cadmium, arsenic etc. pose health hazards on the human being to the most when treated in uncontrolled condition via air, water and soil. The people engaged in the recycling and recovery from the e-waste is severely affected with chronic and acute diseases like cancer etc. The infrastructure to deal with abundant e-waste in the developing countries is insufficient in terms of technology, techniques is the root cause of concern as more than 90% e-waste is treated with rudimentary and primitive techniques adopted by informal agencies. The presence of these pollutants in the atmosphere creates various kinds of diseases. To prevent the human being and environment from contamination of these pollutants, it is desirable to study the characteristics of various hazardous materials in e-waste so that people are made aware about ill effects of e-waste treated in uncontrolled conditions. This paper will focus on the e-waste categories, composition of e-waste, hazardous components, various characteristics, ill effects of hazardous substances present in the e-waste, existing disposal methods of e-waste in developing Nations and new innovative disposal methods relevant to solve the existing e-waste treatment problems.

1. Introduction

A new waste stream has been created by EOL (End of Life), Obsolete Electrical and Electronic Equipment discarded in abundance in the past in both developing and developed Nations as the technology is changing every day. A generic word E-waste is globallyused for waste created this waste stream. It has been defined in various ways by various agencies. The glimpse of these definitions has been mentioned in Table 01.

In general, the equipment run by electricity (both AC and DC) having PCB to control/regulate the functional aspects of equipment either declared obsolete; EOL would be the e-waste. The developing countries like India and China are the emerging economies. They are facing a flow of huge quantity of e-waste in their countries via domestic generation as well as illegal imports. The e-waste offers a good business opportunity in terms of sale of second-hand electrical and electronic equipment as well fulfils the futuristic demand of recyclable material viz. components, metals, plastics etc. [R. Widmer et al.].In developed Nations, the environmental laws for the recycling,

recovery and disposal are very stringent and the ratio of e-waste treatment cost to recovery of materials from e-waste is quite high. This high ratio causes the flow of e-waste from developed Nations to developing Nations and increased manifolds and encouraged informal recycling in developing countries [R. Widmer et al.].To stop this practice, Basel convention incepted in 1989 and came into force in 1992- to stop the trans-boundary movement of hazardous materials from developed Nations to developing Nations [Basel Convention]. For the sake of e-waste treatment in developed Nations European Union [Comprised 17 developed countries] has taken a lead for this initiative. EU Directives has categorised e-waste in ten categories to keep them under single umbrella [EU, 2002a]. As nowadays, globally the use of electrical and electronic equipment has increased many folds in the industrial, commercial and household sectors and made it a fast growing waste. Besides the toxic and hazardous attributes of e-waste; the most of the people are dumping of this e-wasted equipment in municipal waste bins in developing countries. There are many reasons behind the generation of a huge quantity of e-waste like globalization, transfer of technology, abrupt changes in technology, affordable price of new equipment with more features than old one, decreased life-span of equipment, illegal dumping of e-waste from developed countries, varieties and availability low cost equipment .Also, the useful life of all consumer electronic devices is short relatively, and decreasing due to rapid changes in equipment features and capabilities [Kang and Schoenung, 2004]. For example, globally the average life span of mobile phone is less than two years; but in developing Nations like India; it is four years [Survey 2013]. Similarly, the lifespan of CPUs in computers dropped from 4 to 6 years in 1997 to 2 years in 2005 [Babu et al., 2007]. The exploration of constant need to replace the old equipment in the name of new technology with new features accumulated a huge quantity of e-waste in the developing Nations. For example, India is generating more than 8, 00,000 tonnes per annum [CPCB, 2008] with respect to the global production 20 to 50 million tonnes [UNEP, 2005]. It represents 1 to 3% of the global municipal waste produced as 1636 million tonnes per year which is a huge quantity [Robinson, 2009] and increasing at faster rate of 3% to 5% with respect to the municipal waste [BAN/SVTC, 2002], which is three times faster than municipal waste general growth [Arensman 2000] and in developing Nations like India, the rate of increase of e-waste generation has been anticipated as 15% per annum. The per capita e-waste generation in developing Nations like China and India is less than 1 Kg per annum with respect to the EU 14 to 24 Kg per capita per annum, which gives totally 10 million tonnes annually alone [Huismann et al.2007].

Table 01. *Overview of selected definitions of WEEE or e-waste.*

Reference	Definitions
EU WEEE Directive **[EU, 2002a]**	"Electrical or electronic equipment which is waste . . . including all components, sub-assemblies and consumables, which are part of the product at the time of discarding." Directive 75/442/EEC, Article 1(a) defines 'waste' as "any substance or object which the holder disposes of or is required to dispose of pursuant to the provisions of national law in force."
Basel Action Network **[Puckett and Smith, 2002].**	"E-waste encompasses a broad and growing range of electronic devices ranging from large household devices such as refrigerators, air conditioners, cell phones, personal stereos, and consumer electronics to computers which have been discarded by their users."
OECD [2001].	"Any appliance using an electric power supply that has reached its end of- life."
SINHA [2004].	"An electrically powered appliance that no longer satisfies the current owner for its original purpose."
StEP [2005].	E-waste refers to ". . .the reverse supply chain which collects products no longer desired by a given consumer and refurbishes for other consumers, recycles, or otherwise processes wastes."

Ref:- R. Widmer et al. / Environmental Impact Assessment Review 25 (2005) 436–458, 439

The voluminous generation of e-waste threatened the waste treating agencies as it contains hazardous metals (Heavy Metals and Persistent organic Pollutant) and inorganic and organic compounds : Lead(Pb), Mercury(Hg), Cadmium(Cd), Tin(Sn), Antimony(Sb),Arsenic(As), Asbestos(As), Barium(Ba), Beryllium(Be),Chromium(Cr-vi), Nickel(Ni), Selenium(Se), Yttrium(Y), Zinc(Zn),BFRs, PCDD/F,PCB etc, which is 1% of the total weight of the equipment[EU, 2002a].The hazardous substances explode while handling, recycling, and recovery of the recyclable material from the e-waste in uncontrolled condition. The people engaged in this trade in developing Nations are severely affected as they are not aware about and also there is no infrastructure or finance intensive infrastructure to deal with this waste and simply people started rudimentary and primitive methods like- open burning of e-waste to get the metals like copper, aluminium, steel in the developing countries. This practice covers more than 90% of the waste generated either indigenously or imported for recycling or illegally received from different sources. It is a diverse and complex nature of waste contains non-hazardous compounds also: Copper, Aluminium, Plastic, Silver, Gold, palladium etc. These can be recovered from e-waste by suitable techniques. However, an international effort: Basel Convention- to stop the trans-boundary movement of hazardous waste had been made in 1989[Basel Convention]. This research paper will meet the following objectives:

- It will help in establishing the ESM in the developing countries.
- It will warn the persons engaged in this profession regarding the ill effects of of e-waste, when treated in uncontrolled condition.
- It will disseminate awareness among people engaged in this profession for the use of new technologies in place of primitive and rudimentary methods used to recover and recycle the e-wasted components and

materials.

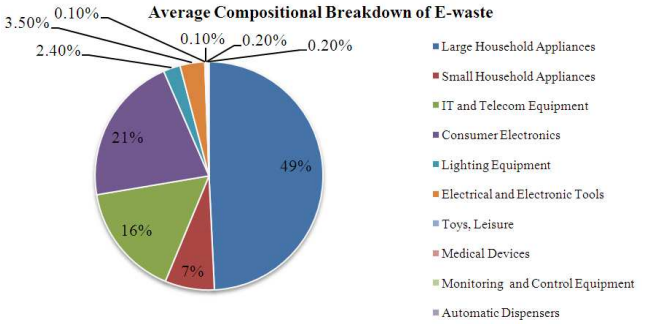
- It will prepare a road map for the recycling technologies are of a great futuristic concerned.
- It will facilitate the exploration of new profession for unemployed people.

This research paper is being organised in the following sections.

1. Section 1: It will describe E-waste categories used by the European Union and
2. Average compositional breakdown of e-waste.
3. Section 2: It will describe average composition of material found in e-waste.
4. Section 3: It will describe the hazardous components of e-waste, hazardous
5. compounds in e-waste.
6. Section 4: It will describe the e-waste disposal methods through Recycling in both
7. controlled and uncontrolled conditions.
8. Section 5: It will describe the health hazards associated with e-waste treatment through recycling, incineration, land filling.

2. E-Waste Categories

In this technological boom, both developing and developed are using EEEs in abundance in commercial, industrial and household sectors. The manufacturers are introducing new technologies as per day user demand in the equipments and obsolete the existing equipments, which are not only out featured but not compatible to the new technological requirements. This process accumulated a huge quantity of e-waste comprising numerous equipments small and large in size viz. washing machines, vacuum cleaner, VCR, Television, halogen lamps, electric Shaw, sports equipment, medical devices, monitoring and control equipments etc. The equipment construction and usage are almost similar world over. After EOL (End Of Life), obsoleting, these equipments are put in TSDF (Treatment Storage, Disposal Facility). The participation of each equipment in e-waste has been ensured by EU Directives so that their treatment may be planed as per their composition of material and size.



Ref:- Association of Plastics Manufacturer in Europe(APME): Plastics — Insight into Consumption and Recovery in Western Europe 2000, cited in International Copper Study Group, 2003).

Fig. 1. *Average Compositional Breakdown of E-waste.*

The equipments in e-waste are made of both hazardous and non-hazardous substances. In hazardous substances it has various toxic and hazardous substances like heavy metals-lead, mercury, cadmium and persistent organic compounds BFRs, and phthalates etc. in their components which are cause of concern as they releases while processing, recycling or disposal in uncontrolled condition and pose risk on human health [UNEP 2005]. The pollutants in the e-waste are estimated as 2.7% of the total by weight [Empa,*Swiss Federal Laboratories for materials testing and research*]. These constituents made it a complex waste as these are present in the material in hidden form such as mercury in switches, and it is very difficult to separate them in pure form from the waste. For their proper regulation and management of all equipment for disposal- recycling, recovery, EU has categorized them in ten categories with their respective contributed percentage in the e-waste generated in EU 27[Huismann et al.2007] as shown in Table 01.

Table 02. *E-waste categories used by the European Union and the average compositional breakdown*

Sr. No.	Category	%age of total e-waste	Sub-categories	%age of total e-waste
1.	Large household appliances Washing machines, dryers, refrigerators, air-conditioners etc.	**49**	**1A**. Large household appl. Excl. 1B and 1C **1B**. Cooling and freezing **1C**. Smaller items	**27.7** **17.7** **3.6**
2.	Small household appliances Vacuum cleaners, coffee machines, irons, toasters, etc.	**7.0**	-	**7.0**
3.	IT and telecom. equipment PCs, Laptops, cell phones, telephones, fax machines, copiers, printers, etc	**16**	**3A**. IT and telecom. equip. excl. 3B and 3C. **3B.** CRT monitors **3C.** LCD monitors	**8.0** **8.3** **0.0**
4.	Consumer electronics Televisions, VCR/DVD/CD Players, Hi-Fi sets, Radios, etc.	**21**	**4A** Consumers electronics excl. 4Band 4C **4B.** CRT TV's **4C.** Flat Panel TV's	**7.8** **13.3** **0.0**
5.	Lighting equipment Fluorescent tubes, sodium lamps etc. (Except: bulbs and halogen bulbs)	**2.4**	**5A.** Luminaries **5B.** Lamps	**0.7** **1.7**
6.	Electrical and electronic tools Drills, Electric saws, sewing Machines, lawn mower etc. (Except: large stationary tools/machines)	**3.5**	-	**3.5**

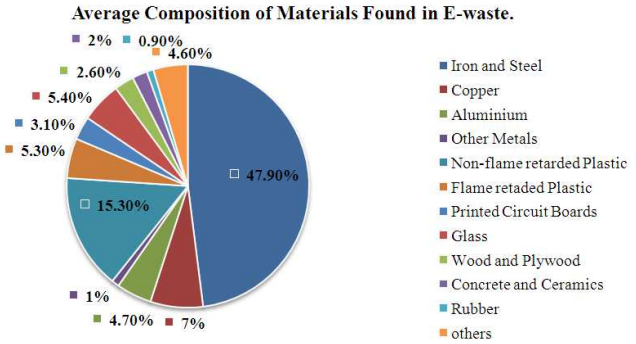
Sr. No.	Category	%age of total e-waste	Sub-categories	%age of total e-waste
	Toys, leisure and sports equipment			
7.	Electric train sets, coin slot machines treadmills, etc.	**0.1**	-	**0.1**
8.	Medical devices	**0.1**	-	**0.1**
9.	Monitoring and control equipment	**0.2**	-	**0.2**
10.	Automatic dispensers	**0.2**	-	**0.2**

Ref: E-waste generated by the EU 27 member states in 2005.

The Table 02 shows that the categories 1 to 4 account for almost 95% of the total e-waste generated and category 1 accounts for almost half the total weight. The least contribution is Medical devices i.e. 01%. In EEEs manufacturing more than thousand materials are used. However the schedule 1 has categorized e-waste in two categories viz IT and Telecommunication Equipment and Consumer Electrical and Electronics. IT and Telecommunication covers Centralized data processing: Mainframes, Minicomputers, Personal computing: Personal Computers (CPU with input and output devices)Laptop (CPU with input and output devices) Notebook, Notepad etc., Printers including cartridges Copying equipment Electrical and electronic typewriters Pocket and desk calculators and other products and equipment for the collection, storage, processing, presentation or communication of information by electronic means User terminals and systems ,Facsimile, Telex, Telephones, Pay telephones, Cordless telephones, Cellular telephones, Answering systems, And other products or equipment of transmitting sound, images or other information by telecommunications and in consumer electrical and electronics: Television sets (incl LCD, LED) Refrigerator, washing machine and air conditioners[Modified Draft Notification, the e-waste ((Management and Handling) Rules 2010 was published by the Government of India in the Ministry of Environment and Forests vide number S.O.1125 (E), dated 14thMay, 2010]. The composition of these constituents will be described in section 2.

3. Composition Of Material In E-Waste

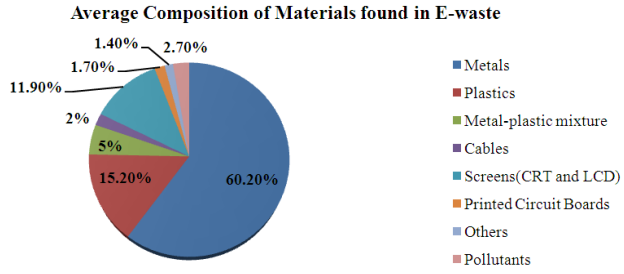
The most of the Electrical and electronic equipment are manufactured with the due control by PCBs which regulates the function of the equipment. However, various other parts are used in the manufacturing. With this e-waste has become a diverse and complex nature of waste having both hazardous and non-hazardous ingredients. Broadly e-waste may be classified in weightage proportions of materials recovered from the e-waste. Steel constitutes 50%, copper, aluminium and other metals 13% and plastics 21% [ETC/SCP], however e-waste is made of wide variety of substances in thousands. The hazardous and toxic metals constitute about 1% of the total weight and rest of the material like precious metals constitute gold 0.1%, Silver 0.2% and palladium 0.005% respectively. The recoverable precious metals play a pivotal role as it gives 95% financial support to the recycling infrastructure, however other metals and materials like lead, nickel and various plastics may worth after recovery from e-waste[He et al. 2006, Cui and Zhang 2008]. The availability of recoverable material made e-waste a resourceful of metals and materials.



[Ref: (ETC/SCP, Former ETC/RWM)Widmer et al. 2005]

Figure 2. *Weighted Percentage of Material in E-waste.*

However, similar kind of study conducted by Empa (Swiss Federal Laboratories for materials testing and research) reveals that all metals constitute 60.2%, Plastics 15.2%, Metal-plastic mixture5%, Printed Circuit Boards 1.7%, pollutants 2.7% etc. as shown in figure 3.



[Ref: (Empa, Widmer et *al*. 2005].

Figure 3. *Weighted Percentage of Material in E-waste.*

4. Hazardous Components And Compounds In E-Waste

The presence of heavy metals in e-waste made it indifferent to the municipal biodegradable waste as they not only hamper the bio-degradation process but harms the human health and environment also. People engaged in the-waste treatment process are directly exposed to these metals while doing recycling, recovery processes and are most affected. However, beyond threshold value these are toxic and hazardous, for example dibutyl phthalate anddiethylhexy1 phthalate are

considered "Toxic for Reproduction" at concentrations >=0.5%.[CPCB Guidelines 2008.]. Hazardous compounds are found in the components described in WEEE Directives Annex II, which are to be removed immediately from the e-wasted equipments[European Commission 2003a]. Mostly, these components are always available in e-waste [AEA 2004, EPS Canada 2006, and IGES 2009] and cause of concern of hazardousness in equipments. For example Capacitors containing polychlorinated biphenyls (PCBs), Mercury-containing components such as switches or backlighting lamps, Batteries, PC-boards of mobile phones and of other devices if the surface area of the circuit board is greater than 10 cm^2.The percentage of heavy metals depends upon the manufacturing requirements of the equipment, for example The copper traces are woven in layers in PC-board to facilitates the flow of current [AEA 2004, Eswaraiah et al 2008, IGES 2009]. The components connected in this circuitry arrangement are switches, resistors, capacitors. The connecting media is soldering having tin and lead in the ratio of 60/40 [Geibig&Socolof 2005]. The typical solder content in scrap of PC board ranges between 4 to 6% by weight or 50 g/ m^2 of PC board [AEA 2004].However, the solder contains other different substances also. Similarly, relay and switches often contain mercury but also contain small amount of cadmium for plated contacts. All components in e-wasted equipment are not hazardous. The table 2 will show the hazardous components with respective hazardous compound used and applications of the equipment.

Table 03. *Components and Electrical and electronicequipment containing hazardous compounds.*

Sr. No.	Components	Compounds of concern	Applications
1.	Printed circuit boards (PC-boards)	Pb, Sb in solder, Cd, Be in contacts and Switches Hg in switches and relays Ga,As in LEDsBFR in plastics	Ubiquitous, from beepers toPCs.
2.	Batteries	Ni and Cd in Ni-Cd batteries Pb in lead acid batteries Hg in Hg batteries	In various portable electronic devices.
3.	Various Hg containing components.	Hg.	Thermostats, sensors, relays, switches, gas discharge lamps, medical equipment and telecom equipment.
4.	Cathode ray tubes (CRTs)	Pb and Sb in CRT glass Various metals (e.g. Cd) in the glass phosphor Ba in electron gun getter.	Old TV sets, PC monitors, oscilloscopes.
5.	Liquid crystal displays (LCDs)	Liquid crystals in the screen	Most devices with a screen,e.g. cell phones, laptops etc.
6.	Plastics and polymers	PVC and Teflon as polymers BFRs, Cd, Pb, org-Sn and phthalates as additives	Wire insulation, plastic housing, circuit boards etc.
7.	PCB-containing capacitors	PCB	In various electronic circuits
8.	Refrigerating circuits	Freon	Refrigerators, freezers, air-conditioners.
9.	Toner cartridges	Toner, including carbon black	Laser printers, copying Machines, faxes.

Ref: SWEDISH ENVIRONMENTAL PROTECTION AGENCY REPORT 6417

The presence of all materials in equipment is in proportion to meet the designed perimeters. The construction of majority of equipment are PCB based which contains maximum numbers of hazardous compounds like lead, Stibium, Cadmium, mercury, beryllium, Gallium, Arsenic, and BFRs. However, OEMs are reducing these hazardous compounds in their manufacturing of equipments under the instruction of RoHS.

5. E-Waste Disposal Methods

The presence of worthwhile recyclable material in e-waste has attracted the informal recycling and recovery system much in the developing Nations. Also, the pressing need of modern technology in developing Nation thereby obsoleting the existing in huge quantity. For example, In India, a serious step has been taken to enact a law for the management and handling of e-waste and it is in place w.e.f. 01st May 2012[E-waste rule 2011]. The CPCB (Central pollution Control Board) has registered e-waste recyclers countrywide. But still, the users, manufacturers are not much aware about the far going ill effects of mishandled e-waste. In view of this, the users are either keep the EOL equipment in their possession or handover it to the corner side Kabaris as there is no curb side collection mechanism for these EEEs (Electrical and Electronic Equipments) as the informal recyclers disposing the e-waste in unorganized manner and throw the left over in the municipal waste bins. In India a huge quantity of e-waste are available and unfortunately 90 % of e-waste are treated by the informal agencies like kabaris, recyclers etc. They are greedy to extract the intended material like copper, aluminium, steel and leave behind or let burn in open the rest material of e-waste. The manufacturing of Electrical and Electronic Equipment has emerged as fast growing sector world over. For example in developing Nation like India, IT industries leaded and increased with annual growth of 42.4% per year between 1995 to 2000 and PC industries grown with compound annual growth rate 25%. In 2005-06 India had 4.64 million desktops, 431 thousands of note-books and 89 thousands servers [CPCB, Guidelines, 2008].The new law enacted, facilitated a compatible e-waste management system in India. It encompasses collection, storage, reuse, recycling, recovery from e-waste and incineration and land-filling. Presently, there is an increasing demand of advanced technology on regular basis. The presence of hazardous substances in e-waste indicates the careful handling of waste and processes it for reuse, recycle and recovery for all recyclable materials as this sector of recycling has a potential of components refurbishment. The recycling and recovery of materials from e-waste have become essential as they release

burden on natural resources, meet the virgin material requirement, prevent the release of hazardous materials from e-waste, reduce the volume of e-waste so that the land requirement in metropolitan city may be kept minimum for further expansion. Prior to incineration and land-filing the e-waste undergoes recycling, reuse and recovery options as shown in flow chart in fig 3. The informal recyclers are using primitive and rudimentary e-waste disposal methods like open burning for the recovery of metals: copper, aluminium, steel and put rest of the material plastics, PCBs, ceramics, asbestos, which are all hazardous in nature and during incineration/ open dump burning, these explode in the atmosphere. Some of the hazardous methods are shown in fig.4.



Figure 4. *Options Prior to Incineration.*

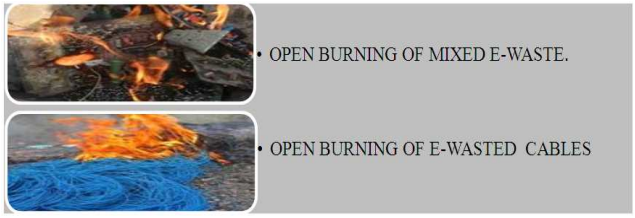


Figure 5. *Hazardous Methods of e-waste Disposal*

The environmentally sound e-waste recycling stressing the manual dismantling of e-waste which helps in recovery of recyclable metals, plastics, components and segregate the hazardous components need further treatment e.g. mercury and lead containing components: batteries, CRT-Glass and LCDs [Cui and Forsberg 2003, UNEP 2009]. For example mercury containing components are normally treated in specialized mercury recovery facilities or authorized hazardous waste incinerators having modern flue gas cleaning systems [OECD 2003].The other mechanical processes like shredding, grinding, magnetic and eddy current separation etc. are involved, which are the primary requirement of recovery shown in Fig 6.

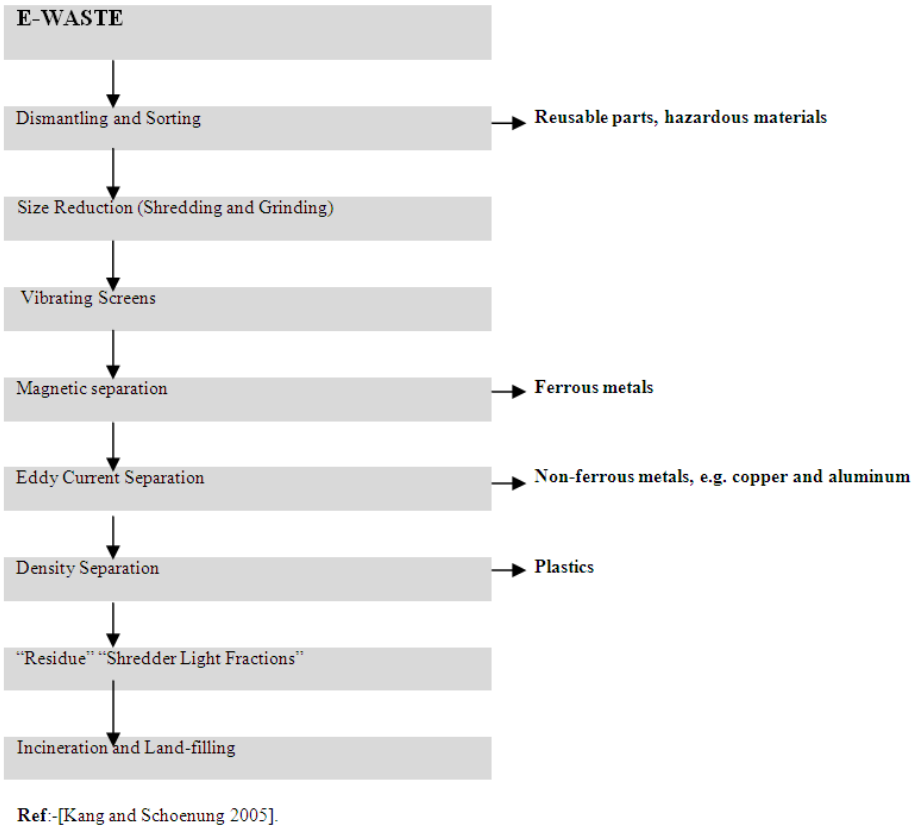


Fig. 6. *Schematic of the first steps in a typical e-waste recycling process.*

The profile for Dismantling and sorting varies according to the scale of the operations required as for small manual is applicable as in large automated operations are desirable to deal with the e-waste.

Ideally, for Further refining of metal fractions, initially the pyro-metallurgical process is used followed by hydro-

metallurgical processes. However, the hydro- metallurgical process may also be used as alternate process in place of pyro-metallurgical process since it consumes less energy and it is exact and more predictable and easy to control during process. Both processes are in use as since more than two decades and followed by electrolytic refining. For example, for the recovery of non-ferrous metals and precious metals pyro-metallurgical processes in copper smelter is used and further refining electrolytic process is used [Cui and Zhang 2008]. The recovery of metals achieved by this process is 99% and the remaining 0.9% in electrolyte is treated with acidic solution to recover the metals from electrolyte. This kind of smelters are in place in Boliden in Sweden, Umicore in Belgium, Noranda in Canada, NorddeutscheAffinerie AG in Germany [Allsopp et al 2006] and Dowa Eco-System in Japan [IGES 2009].How this integrated facility works shown in the Fig.7.These are the following main steps in hydo-metallurgical process treating the solid material with caustic or acids caused leaching of the material resulting the reduction in grain size of the material and facilitate more metal yields from the material. The leaching solvents are commonly used namely cyanide, thiourea, thiosulfate, and sodium hydroxide and acids such as aqua regia, sulphuric acid, nitric acid, and hydrochloric acid. After treatment, the metal of interest is isolated from the solution and concentrated by applying any of the suitable methods like the solvent extraction, precipitation, cementation, adsorption, ion exchange, filtration and distillation [Cui and Zhang 2008, Antrekowitsch et al 2006].

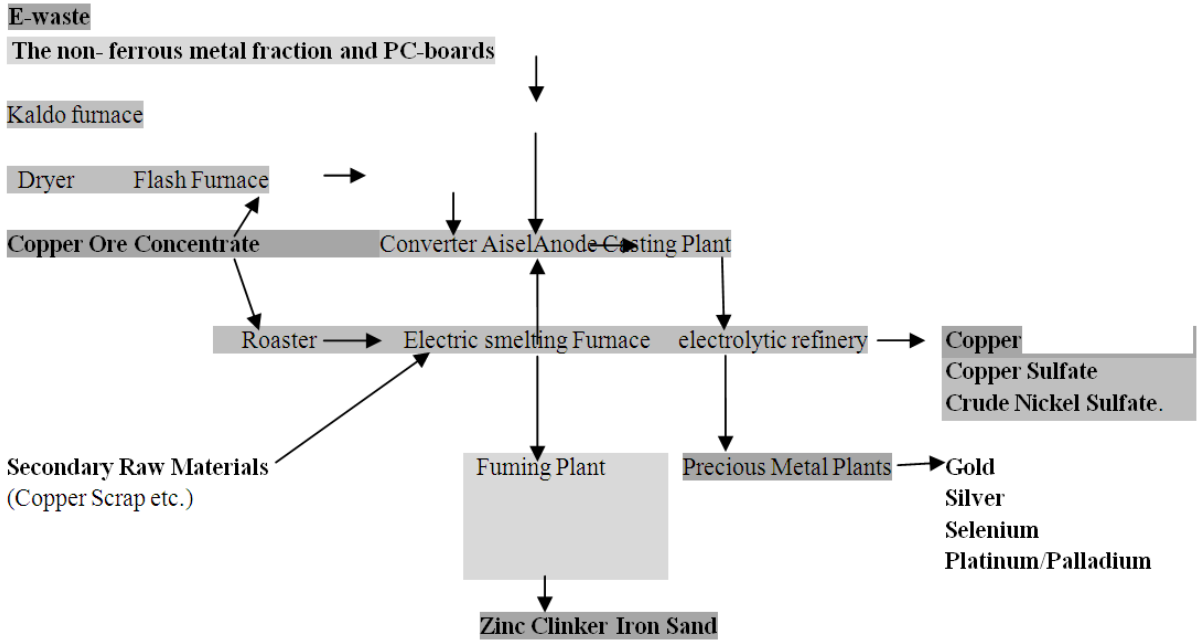


Fig. 7. *Schematic of the processes used to recover copper and precious metals from ore concentrate, copper Scrap and e-waste at Boliden's Rönnskär smelter in Sweden [Boliden 2010].*

For the recovery of plastics from e-waste is also essential like recovery of metals as plastics also have great potential of recycling value [Kang &Schoenung 2005]. Hardly 25% of plastics is being recycled since the presence of numerous polymers and additives made it very complex materials [Schlummer et al 2007]. The different products and quality of plastics are separated from the e-waste and subsequent separation is being made by using the following techniques like sieving, density separation (in various aqueous or non-aqueous media), electrostatic separation (e.g. triboelectric separation) and air-separation, in combination with various size reduction steps, such as grinding, milling and granulation [Kang &Schoenung 2005]. The foreign material in plastics is separated by performing the following techniques magnetic separation, eddy current separation and air-separation. The plastics so obtained are used in the manufacturing of new plastic products. However, the attempts are made to transform the plastics into coke, coke oven gas and other chemicals by using pyrolysis and depolymerisation techniques as alternative recycling methods [Kang &Schoenung 2005]. Also, the plastics is being used both for heat and energy recovery system and acts as a fuel and reducing agent in the smelter process and replaces some of the coke used for the purpose [Kang &Schoenung 2005, Schlummer et al. 2007]. However, it contradicts in the abatement of pollution resulting from the process as the formation of dioxin and furan in the ambience.

In the developing countries, the informal recyclers are inviting health hazards not only for engaged workers but to the environment also. During recycling they use rudimentary and primitive methods to recover the targeted metals like copper, steel, plastics, aluminium etc and leave behind the precious metals either in the waste or in ash due to lack of awareness about the recovery of precious materials by new technology and techniques. These activities are carried out in small workshops or just outdoors [BAN & SVTC 2002].They

do not have any control over the process/ emission generated from the combustion of e-waste.

5.1. Environmentally Sound E-Waste Treatment Technologies

These treatment technologies are used in three tier system i.e. 1st level treatment, 2nd level treatment and 3rd level treatment.

From the 1st level treatment Plastic is separated and the remaining items like CRT, Circuit boards, cables, hazardous waste, mercury switches are put as input in 2nd level treatment further to extract metals further.

From 2nd level treatment the plastic mixtures and plastic with flame retardants, glass, lead, are separated and the other metals are separated by using Magnetic and Eddy current separation of ferrous and non-ferrous metals like Fe and non Fe (Cu, Al, Au, Ag and other precious metals using the material physical properties like electric conductivity, magnetic properties and density. These are dry process based treatment are shown in the figure 8 and 9 respectively.

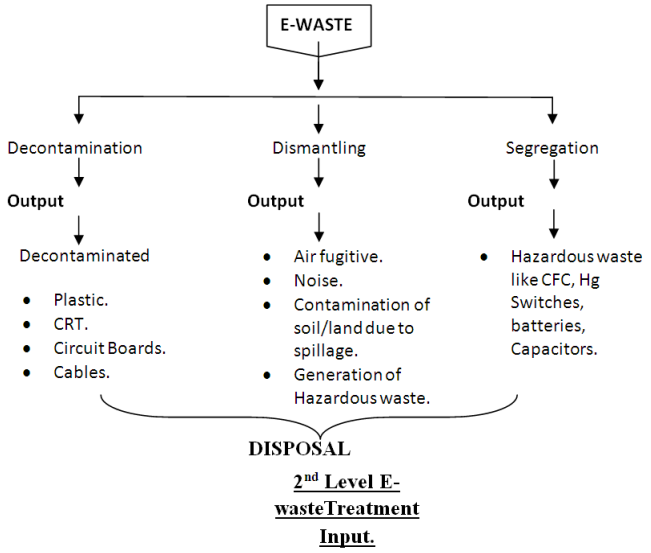


Fig. 8. *Flow Chart of 1st Level treatment.*

The pre-communicating of e-waste is essentially required to prepare a feed stock for magnetic and eddy current separation processes. It includes mill hammering, shear shredding and pulverisation of e-waste. Further, the material is screened and de-dusted followed by separation of valuable metal fraction of Copper, Aluminium and residual fractions of precious metals (Gold and Silver etc) by using electrostatic, gravimetric, eddy current technologies. Overall magnetic separation, eddy current separation, electrostatic separation, air tables, gravity air classifiers, air cyclones and shape screens are used among other processes also [Goosey and Kellner, 2003; Li et al., 2004; Kang and Schoenung, 2005; Hamos GmbH].However, the yield of these metals besides these technologies depends upon the particle size and shape, feeding rate, optimum operations also. For example eddy current separation for non-ferrous metals is best suited for granular metal of size more than 5 mm. Also eddy current separator ensures better separation of Aluminium fraction in comparison to the fraction of Copper, Silver and Gold. The grounded material having size less than 2 mm, electrostatic precipitation is used for copper recovery most of time [Zhang and Forssberg, 1997; luga et al., 1998; Li et al, 2004, Hamos GmbH; Kang and Schoenung, 2005]. However, electrostatic separation gives poor separation efficiencies at -100 µm fine sizes [Wills, 1997]. [Zhao et al. (2004)] compared with column air separator.

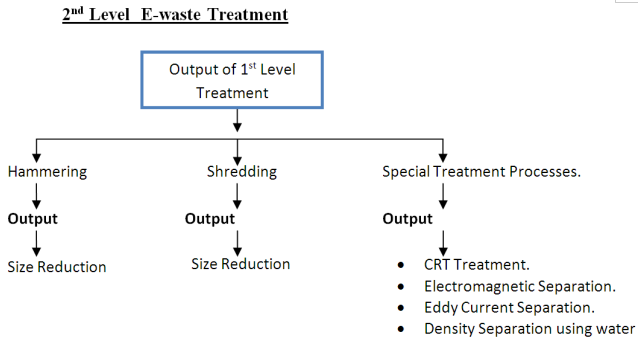


Fig. 9. *Flow chart of 2nd level e-waste treatment.*

A typical treatment process used for the treatment non-CRT e-waste is shown in figure 10. As more efficient treatment method denotes more recovery of metals/ materials from e-waste and less environmental loading.

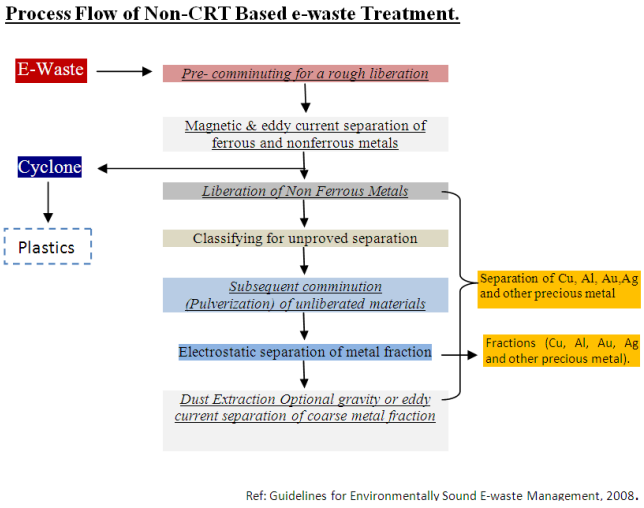


Fig. 10. *Now the feed stock is ready for recovery of various metals. It is the input for 3rd level treatment of e-waste.*

5.2. 3rd Level Treatment of E-Waste

The 3rd level treatment is based upon the input (residual fractions), technologies used and its final output. Apart from eddy current separation, magnetic separation etc. the e-waste feedstock is treated with incineration; refining, smelting and distillation to get heat energy and concentrated metals. The various processes of 3rd level treatment are input, unit operations and respective output is presented in the table 04.

Table 04. *Input/ Output and unit operations for 3rd level treatment of e- waste.*

Input/WEEE Residue.	Unit Operation/ Disposal / Recycling Technique.	Output.
Sorted Plastic	Recycling	Plastic Product
Plastic Mixture	Energy Recovery/Incineration	Energy Recovery
Plastic Mixture with FR	Incineration	Energy Recovery
CRT	Breaking/Recycling	Glass cullet
Lead Smelting	Secondary Lead Smelter	Lead
Ferrous Metal Scrap	Secondary steel/iron recycling	Iron
Non-ferrous metal Scrap	Secondary copper and aluminium smelting	Copper/Aluminium
Precious Metals	Au/Ag Separation(refining)	Gold/Silver/Platinum and Palladium
Batteries (Lead Acid/NiMH and LiION)	Lead recovery and smelting Re-melting and separation	Lead
CFC	Recovery/ Reuse and incineration	CFC/ Energy Recovery
Oil	Recovery/Reuse and incineration	Oil Recovery/ Energy
Capacitors	Incineration	Energy Recovery
Mercury	Separation and Distillation.	Mercury

Ref:- Ref: Guidelines for Environmentally Sound E-waste Management, 2008

The techniques are available with developed Nations to recover recyclable material like plastics, ferrous metals, non-ferrous metals and their efficiencies are high and vary material to material. For example magnetic separation achieves a target of ferrous metal recovery is 90% to 95% from e-waste and eddy current separation of non-ferrous metals is more than 90%[MoEF, 2008].

6. Hazards Associated With E-Waste

Informal recycling and recovery processes in the developing Nations like India, China are the vulnerable in the abatement of pollution generated by the e-waste. The presence of heavy metals alone responsible for its hazardousness. They do the recycling and recovery in closed small workshops cause occupational health hazards or dump the leftover after recovery of intended material and let the e-waste burn in open. This open burning of e-waste with heavy metals penetrate in food chain, spoil our aquifers, spoil underground water reserves, decrease the fertility of soil. These are persistent organic pollutants and remain in atmosphere years together and harming the ecology continuously. Even in the controlled and perfect recycling there is possibility of heavy metals leakage. This section will describe the hazards aspects involved for the e-waste treatment and Disposal.

6.1. Hazards Associated while Recycling of E-Waste in Controlled Conditions

In developed Nations, the integrated facilities are in place to do recycling of e-waste and keep the level exposure minimal of heavy metals. However due to stringent Environmental laws in their countries and expensive recycling of e-waste, they are dumping this waste in the developing countries to get it recycled as the labour required for the recycling is much more cheap in these countries. The developing countries without any infrastructure are treating the e-waste generated indigenously as well as dumped by developed Nations and are most effected due to e-waste rudimentary and primitive treatment. However due to international effort as Basel Convention and new technical development like RoHS(Restriction of Hazardous Substances) decreased the use of hazardous substances in e-waste but still there are some hazardous substances remained in the e-waste. Due to their presence, always there is a possibility of hazards. It encompasses hazards during collection and dismantling, mechanical shredding and separation, pyro-metallurgical processing, hydro-metallurgical processing, recycling of plastics, manual dismantling and recovery of valuable materials, acid extraction of metals, melting and extrusion of Plastics, burning of plastics and other materials, dumping of residual materials, Soil and sediment contamination, Water contamination, Air contamination, Human exposures and health effects. Table 05 shows the hazards associated with EOL process, occupational and environmental hazards created by traditional waste handling, controlled recycling and uncontrolled recycling.

Table 05. *Risks associated with end-of-life treatment of electronic waste (e-waste).*

End-of-life process	Occupational risks	Environmental risks
Traditional waste handling.		
Landfilling		Leakage of metals (e.g. Pb, Cu, Ni, Sb, Cd, Zn) and organic compounds (e.g. BFRs, plasticizers).Evaporation of Hg and MeHg.
Incineration		Emission of various metals and organic compounds via exhaust gases (e.g. dioxins, BFRs, PAHs, Cu, Pb, Sb).Leakage of various compounds from ashes (e.g. dioxins, Cu, Pb, Sn)

End-of-life process	Occupational risks	Environmental risks
Controlled recycling.		
Collection and dismantling	Dust containing various compounds during dismantling activities. Dust containing Pb and Ba-oxide from broken CRTs Cuts from CRT glass in case of implosion.Volatile compounds (e.g. Hg) from broken components.	Emissions of volatile compounds (e.g. Hg) from broken components.
Shredding	Dust containing various compounds (e.g.BFRs, TPP, phthalates, Cd, etc.).	
Pyro-metallurgical processes	Dust and fumes of the shredded material andthe melting process, containing various compounds (e.g. Pb, Cd, Hg, Be, BFRs, dioxins, TPP, phthalates).	Emissions of various metals (e.g. Pb, Cd, Hg, Be) and organic compounds from the melting process (e.g.BFRs and dioxins).
Hydrometallurgical process	Acid fumes containing various hazardouscompounds	
Plastic recycling	Dust and fumes of various chlorinated andbrominated compounds (e.g. BFRs anddioxins), and some metal additives (e.g. Cd)	Emissions of various chlorinated and brominated compounds (e.g. dioxins) from the thermal processes used.
Uncontrolled recycling.		
Collection and dismantling	Dust containing various compounds during dismantling activities, e.g. Pb and Ba-oxide from broken CRTs. Cuts from CRT glass in case of implosion. Volatile compounds (incl. Hg) from broken components.	Emission of dust and fumes containing various metals(e.g. Pb, Zn, Cu, Sn, Sb, Cd, Ni, Hg) and organic compounds (e.g. BFRs) to the local environment.
PC-board heating	Exposure to fumes of various compounds from solder and PC-board components (e.g. Pb,Sn, BFRs and dioxins)	Leakage of various compounds (e.g Cu….) from dumped PC-board residues.
Toner sweeping	Exposure to toner dust including carbon black.	Leakage of various compounds from emptied and dumped toner cartridges.
Acid extraction	Exposure to acidic fumes containing various hazardous compounds.	Leakage of various metals (e.g. Pb, Sn, Cu, Sb, Ni, Hg, Ba, Cd) and organic compounds (BFRs, phthalates, TPP, dioxins) from dumped residues of the extraction process.
Shredding	Dust and fumes of various metals and organic compounds present in the plastics (e.g. BFRs, phthalates, TPP, Cd, etc.)	Emissions of dust containing various plastics Components to the local environment.
Plastics and waste burning	Exposure to a wide range of metals (incl. Cd, Cu, Pb, Zn, Sb) and organic compounds (incl. PBDEs, PAHs, PCBs, dioxins) via the smoke.	Emissions of a wide range of metals (incl. Cd, Cu, Pb, Zn, Sb) and organic compounds (incl. PBDEs, PAHs, PCBs, dioxins) to the local, regional and global environment.
Dumping ofresidual materials	Exposure to dust and fumes, containing various compounds, from dumped materials. Secondary exposure via contaminated drinking water and food.	Leakage of various metals and organic compounds to the ground and water reservoirs in the surroundings

Ref:- SWEDISH ENVIRONMENTAL PROTECTION AGENCY REPORT 6417, Recycling and disposal of electronic waste

The exposure to hazardous compounds takes place more while inhalation of fumes and dust. In the ambience of treatment facility, these POPs are affecting the residents continuously and it is observed in Guiyu China that children are suffering from respiratory diseases, skin infections, and stomach problem[Leung et al. 2006, Sepúlvedaetal. 2009]. The table 06 shows the individual effects of these hazardous compounds present in e-waste.

Table 06. *Hazards Associated with Metal/Acid/Compound and Sources*

Metal/Acid /Compound	Source and Associated Hazards.
Lead	Mechanical breaking of CRTs, removal of solder from microchips. Being a neurotoxin affects the kidneys and the reproductive system, mental development in children.
Mercury	Breaking and burning of circuit boards and switches, microbial activity. It affects the central nervous system, kidneys and immune system, impairs foetus growth and harms infants through mother's milk and can enter the human food chain through aquatic.
Cadmium	Crushing and milling of plastics, CRTs and circuit boards. Being a carcinogen causes *Itai-itai* disease, affects the kidneys and softens bones.
Plastics	It is found in circuit boards, cabinets and cables all contain carcinogens. BFRs or brominated flame retardants give out carcinogenic brominated dioxins and furans. Dioxins can harm reproductive and immune systems.
Chromium	It is used to protect metal housings and plates in a computer from corrosion. The Chromium 6 can damage liver and kidneys and cause bronchial maladies including asthmatic bronchitis and lung cancer.
Beryllium	It is found in switch boards and printed circuit boards. It is carcinogenic and causes lung diseases.
Acid	The Sulphuric and hydrochloric acids are used to separate metals from circuit boards. Fumes contain chlorine and sulphur dioxide, which cause respiratory problems. They are corrosive to the eye and skin.
Beryllium oxide(Beryllia)	They are very toxic and may cause cancer by inhalation.
Beryllium metal.	It is very toxic may cause cancer by inhalation. However, Beryllium component scrap is classified as non-hazardous in the OECD, Basel and EU regime.
Selenium	It exposure of high concentrations can cause selenosis.
Polychlorinated biphenyls (PCBs)	It is used as dielectric fluids, heat transfer fluids, additives in adhesives and plastics. It causes cancer in animals. Also effects on the immune system, reproductive system, nervous system, endocrine system.

Metal/Acid /Compound	Source and Associated Hazards.
Dioxin and Furan	These are the by-products in the manufacture of substances like some pesticides as well as during combustion. Dioxins bio-accumulate in the body and can lead to malformations of the foetus, decreased reproduction and growth rates and cause impairment of the immune system among other things .
Brominated flame retardants (BFRs)	The flame retardants make materials, especially plastics and textiles, more flame resistant. It releases while combustion of halogenated case material and printed wiring boards at lower temperatures and cause severe hormonal disorders.
Arsenic	It is a poisonous metallic element and its chronic exposure can lead to various skin disease, decrease nerve conduction velocity, cause lung cancer.
Barium	It is used in sparkplugs, fluorescent lamps and "getters" in vacuum tubes. It is highly unstable in the pure form and forms poisonous oxides when in contact with air. Its short-term exposure can lead to brain swelling, muscle weakness, damage to the heart, liver and spleen.

6.2. Pathways of Hazardous Compounds on Mammalians

The pollutants so produced from e-waste mishandling, effects mammalians through a series of pathways like exposure, uptake, metabolism etc. The whole network is represented in fig. The pollutants with intrinsic toxicity activate metabolisms system. It interacts with other parts of the body and initiates toxic effects anywhere in the body. The physiological changes in the body takes place may be in CNS (Central Nervous System), injury to the reproductive system, interaction with nucleic acids leading to carcinogenesis. The damage or changes depends upon the concentration of pollutants. The action of toxicants may cease storage, biotransformation or excretion.

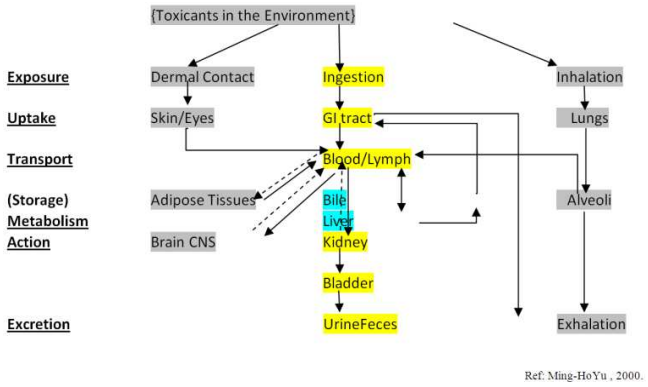


Fig. 11. *The poisoning process in animals and humans by Toxicants.*

The concept soil-plant barrier was introduced in 1980, explaining how metal addition, soil chemistry and plant chemistry affect human being when the soil is full of metals (Chaney, 1980). The plants absorbed metals via pore water. The plants have both active and passive to take up and exclude metals depending upon the internal concentration [US EPA, 2003]. The metals (e.g. copper, selenium, and zinc) are nutritionally essentially required elements at low levels but toxic at higher levels, and others (e.g. lead, arsenic, and mercury) have no known biological functions as metals are naturally occurring having organisms and accumulated in essential metals (Fairbrother et al., 2007).

The pollutants emitted from the e-waste treating site contaminated the water resources in plenty, as the processes pertaining to treatment are both wet and dry and consumes a lot of water and air. For example, in China, the WEEE residue and leftover either dumped in fields or in rivers and irrigation ditches. The samples collected by BAN from the Lijiang River shows heavy contamination of cadmium (0.01–0.033 mg/L against 0.003 mg/L (WHO guidelines)), lead (1.9 to 24 mg/L against 0.01 mg/L (WHO guideline). In view of that people in Guiyu are bound to fetch water from nearby town only after the one year existence of WEEE industry there [BAN et al., 2002].

The e-waste concerns are much more in terms of health and valuable resource. The people engaged in the recovery, recycling and other activities are made aware and serious about the ill and long term effects of e-waste when they handle it. The precautions should be forwarded along with the materials and a due care should be ensured so that the incidents due to mishandling may be obviated or reduced to a minimum scale. The Identification and isolation of hazardous materials is very essential before taking up any kind of e-waste treatment and treat them as per their hazardousness.

In India, E-Waste (Management & Handling) Rules, 2011 call for reduction the use of hazardous substances in electrical and electronic equipments. The threshold value for cadmium 0.01% by weight in homogeneous material and for lead, mercury, hexavalent chromium, poly-brominated-biphenyls and polybrominated di-phenyl ether is 0.1% by weight of the equipment. This reduction will be achieved by 01 May 2014. The equipments are exempted placed six years before the commencement of these rules.[MoEF, Implementation of e-waste rules 2011, CPCB Delhi 32].

7. Conclusion

E-waste management has become one of the emerging problem to the developed and developing countries both as it is a fast growing waste contains very hazardous and toxic substances in their e-wasted components. It is generated more in developed countries than developing countries. The developed countries either dumped it land filling or dispatched it to the developing countries like china and India. The environmental laws for the recovery and recycling from e-waste are very stringent and money intensive in the developed countries. In spite of Basel convention, they dispatch the e-waste to the developing countries in the name of charity, recycling. The developing countries are facing problems as they do not have know how to handle this waste. They are treating it to recover and recycle the material in the equipment with bare hands with rudimentary and primitive methods like open burning, acid leaching and recover in minimum the targeted material like copper, steel

and aluminium from e-waste. Due to these hazardous methods people engaged in this profession are physiologically effected and in the ambience also. The generating quantity of e-waste is very huge and due to these activities, in the developing countries a huge quantity of persistent organic pollutants is emitted in and around workplace of WEEE treating facility. Due to these rudimentary methods they not only enhance the pollutants environmental loading but also lose a good amount of valuable and metals and recyclable materials. In the composition of EEEs the precious metals like Au, Ag, Pd and Pt are used. The e-waste is a treasurer of these materials when it is recovered from e-waste. This possibility of recycling can be enhanced by strengthening the collection of e-waste and promote the formal recycling. Now, we are in 21st century and enjoying the update technology and generating a huge quantity of waste. In view of that it is desirable to dispose the e-waste only through registered recyclers and say no to informal recyclers for the e-waste treatment. The formal/registered recyclers not only recover valuable resources but reduce the e-waste manifolds also by treating the e-waste by environmentally sustainable treatment processes and reduce the burden of natural resources to recover this amount of material through mining and reduce the cancer patients and improve the health condition in the ambience.

References

[1] AEA (2004) AEA Technology: *WEEE & hazardous waste*. A report produced by DEFRA.

[2] Allsopp M., Santillo D., Johnston P. (2006) *Environmental and Human Health Concerns in the Processing of Electrical and Electronic Waste*. Greenpeace Research Laboratories, Technical Note: 04/2006.

[3] Antrekowitsch H., Potesser M., Spruzina W., Prior F. (2006) *Metallurgical recycling of electronic scrap*. Proceedings of the EPDCongress 2006, 12-16 March 2006, San Antonio, Texas, 899-908.

[4] Arensman R. (2000) "*Ready for Recycling*?" Electronic Business. The Management Magazine for the Electronic Industry, November 2000.

[5] BAN & SVTC (2002) Exporting Harm: *The High-Tech Trashing of Asia. Basel Action Network and Silicon Valley Toxics Coalition*. February 25, 2002.

[6] The Basel Action Network (BAN), the Silicon Valley Toxics Coalition (SVTC), Toxics Link India, SCOPE (Pakistan), Greenpeace China. *Exporting harm: the high-tech trashing of Asia*. Seattle, WA, and San Jose, CA; February 25th, 2002.

[7] *Basel Convention on the Control of the Trans-boundary Movement of Hazardous Waste and Their Disposal*. http://www.basel.int, Retrived 2009-10-23.

[8] Boliden (2010) Rönnskär smelter. Fact sheet downloaded from www.boliden.see 2010-01-14.

[9] Babu BR, Parande AK, Basha CA (2007). *Electrical and electronic waste: a global environmental problem.* Waste Manage. Res. 25:307-318.

[10] Chaney, R.L., 1980. *Health risks associated with toxic metals in municipal sludge*. In: Bitton, G., Damron, B.L., Edds, G.T., Davidson, J.M. (Eds.), *Sludge–health risks of land application.* Ann Arbor Science Publishers, Ann Arbor, MI.

[11] Cui J, Forssberg E, (2003) *Mechanical recycling of waste electrical and electronic equipment*: a review. Journal of Hazardous Materials B99: 243-263.

[12] EPA data from "*Municipal Solid Waste in the United States, 2011 Facts and Figures*," May 2013;

[13] EPS Canada (2006) *environmentally sound recycling of electronics*. Guidance document from Electronics Product Stewardship Canada.

[14] European Commission (2003a), *EU Directive 2002/96/EC of the European Parliament and of the Council on Waste Electrical and Electronic Equipment (WEEE).* Brussels, Belgium 2003.

[15] European Commission (2003b), *EU Directive 2002/95/EC of the European Parliament and of the Council on the Restriction of the use of certain Hazardous Substances in Electrical and Electronic Equipment (RoHS)*. Brussels, Belgium 2003.

[16] European Commission (2006), *Commission Regulation (EC) No 1881/2006 of 19 December 2006 setting maximum levels for certain contaminants in foodstuffs*. Retrieved 2010-06-14 from: http://ec.europa.eu/food/food/chemicalsafety/contaminants/dioxins_en.htm.

[17] ETC/SCP, *European Topic Centre on Sustainable Consumption and Production*, http://scp.eionet.europa.eu/themes/waste, Retrived 2009-10-23.

[18] Fairbrother, A., Randall, W., Sappington, K., Wood, W., 2007. *Framework for metals risk assessment*. Ecotox. Environ. Saf. 68,145-227].

[19] Geibig J.R., Socolof M.L (2005) *Solders in electronics:* A life cycle assessment.US EPA 744-R-05-001.

[20] He W., Li G., Ma X., Wang H., Huang J., Xu M., Huang C. (2006) *WEEE recovery strategies and the WEEE treatment status in China.* Journal of Hazardous Materials B 136: 502-512.

[21] Huismann J. et al. (2007) 2008 *Review of Directive 2002/96 on Waste Electrical and Electronic Equipment (WEEE), Final report, United Nations University, for the European Commission*, Contract No. 07010401/2006/442493/ETU/G4, August 2007.

[22] IGES (2009) *Environmental and Human Health Risks associated with the end-of life treatment of electrical and electronic equipment. Institute for Global Environmental Strategies* (IGES), Hayama, Kanagawa, Japan.

[23] Kang HY, Schoenung JM (2004). *Used consumer electronics: a comparative analysis of material recycling technologies*, in: 2004 IEEE International Symposium on Electronics and the Environment. Phoenix, AZ, May 10-13, 2004.

[24] Kang H.Y., Schoenung J.M. (2005) *Electronics waste recycling: A review of U.S.infrastructure and technology options. Resources, Conservation and Recycling* 45: 368-400.

[25] Leung A., Cai Z.W., Wong M.H. (2006) *Environmental contamination from electronic waste recycling at Guiyu, southeast China*. Journal of Material Cycles and Waste Management 8: 21-33.

[26] MoEF.**"***Guidelines for environmentally sound management of e-waste in India"* March 2008.

[27] MoEF "*Implementation of e-waste rules in India*"2011, CPCB Delhi 32.

[28] OECD (2003) *Technical guidance for the environmentally sound management of specific waste streams: used and scrap personal computers*. No. 304. Organisation for Economic Co-operation and Development (OECD) Working Group on Waste Prevention and Recycling. Document: ENV/EPOC/WGWPR (2001)3/FINAL.

[29] Schlummer M., Gruber L., Mäurer A., Wolz G., van Eldrik R. (2007) *Characterization of polymer fractions from waste electrical and electronic equipment (WEEE) and implications for waste management*. Chemosphere 67, 1866-1876.

[30] Sepúlveda A., Schluep M., Renaud F.G., Streicher M., Kuehr R., Hagenlüken C.,Gerecke A.C. (2009) *A review of the environmental fate and effects of hazardous substances released from electrical and electronic equipments during recycling*: *Examples from China and India. Environmental Impact Assessment Review* 30: 28-41.

[31] US EPA (2007) US EPA 2007: *Management of Electronic Waste in the United States*, Draft April 2007, Epa530-D-07-002. United States Environmental Protection Agency, Washington, DC, USA.

[32] UNEP (2005) *E-waste the hidden side of IT equipment's manufacturing and use*. Environment Alert Bulletin 5, January 2005, United Nation Environmental Program, Nairobi, Kenya.

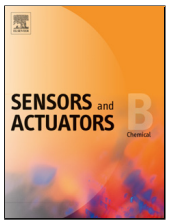
[33] US EPA, 2003. *Multimedia, Multipathway, and Multireceptor Risk Assessment (3MRA) Modeling System.* Environmental Protection Agency, Office of Research and Development, Washington DC. ; Fairbrother et al., 2007).

[34] SWEDISH EPA ISBN 978-91-620-6417-4, ISSN 0282-7298.

[35] Survey "Survey *conducted in Delhi based schools*" 2013.

[36] Zhang and Forssberg, 1997; luga et al., 1998; Li et al, 2004, Hamos GmbH; Kang and Schoenung, 2005.

Accepted Manuscript



Title: Facile Synthesis of 2-Dimensional Transparent Graphene Flakes for Nucleic Acid Detection

Author: Maumita Das Mukherjee Chetna Dhand Neeraj Dwivedi Baijnath P. Singh Gajjala Sumana Ved V. Agarwal Jai S. Tawale Bansi D. Malhotra

PII: S0925-4005(14)01599-8
DOI: http://dx.doi.org/doi:10.1016/j.snb.2014.12.054
Reference: SNB 17844

To appear in: *Sensors and Actuators B*

Received date: 13-9-2014
Revised date: 10-12-2014
Accepted date: 11-12-2014

Please cite this article as: M.D. Mukherjee, C. Dhand, N. Dwivedi, B.P. Singh, G. Sumana, V.V. Agarwal, J.S. Tawale, B.D. Malhotra, Facile Synthesis of 2-Dimensional Transparent Graphene Flakes for Nucleic Acid Detection, *Sensors and Actuators B: Chemical* (2015), http://dx.doi.org/10.1016/j.snb.2014.12.054

This is a PDF file of an unedited manuscript that has been accepted for publication. As a service to our customers we are providing this early version of the manuscript. The manuscript will undergo copyediting, typesetting, and review of the resulting proof before it is published in its final form. Please note that during the production process errors may be discovered which could affect the content, and all legal disclaimers that apply to the journal pertain.

ACCEPTED MANUSCRIPT

Facile Synthesis of 2-Dimensional Transparent Graphene Flakes for Nucleic Acid Detection

Maumita Das Mukherjee,[a] Chetna Dhand,[b] Neeraj Dwivedi,[c] Baijnath P. Singh,[d] Gajjala Sumana,[d] Ved V. Agarwal,[d] Jai S. Tawale,[d] Bansi D. Malhotra[e*]

[a] Amity Institute of Applied Sciences, Amity University, Noida, India
[b]Anti-Infectives Research Group, Singapore Eye Research Institute, Singapore- 168751
[c]Department of Electrical and Computer Engineering, National University of Singapore, Singapore
[d]DST Centre on Biomolecular Electronics, Biomedical Instrumentation Section, Materials Physics & Engineering Division, National Physical Laboratory (CSIR), New Delhi-110012, India
[e] Department of Biotechnology, Delhi Technological University, Delhi-110042, India
*Bansi D. Malhotra, Department of Biotechnology, Delhi Technological University, Delhi-10042, India, **E-mail:** bansi.malhotra@gmail.com; **Contact Number:** +911127294668, +91-11-27871043 or +91-11-27871022, Extension:1609; **Fax:** 91 11 27871023

ABSTRACT

We report on the synthesis of 2-dimensional transparent graphene flakes (GF; 2.2 μm × 50 μm), onto indium-tin-oxide (ITO) coated glass plates, by electrochemical exfoliation of graphite rods using *in-situ* intercalation of potassium ions. Raman spectroscopy, Fourier transform infra-red (FT-IR) spectroscopy, scanning electron microscopy and transmission electron microscopy, are used to probe the formation of graphene structures, revealing the generation of GF. Synthesized GF are employed as DNA immobilization platform for genosensor design for *M.tuberculosis* detection. This GF based biosensing electrode exhibits high sensitivity, fast response and wide detection range etc. These findings are important for cost-effective strategy for the production of GF for application to advanced biosensors, and to understand graphene-based biosensing mechanism specifically for nucleic acid detection.

ACCEPTED MANUSCRIPT

1. Introduction

Tuberculosis (TB) is a worldwide health problem with a massive global burden.[1] *Mycobacterium tuberculosis* is the world's greatest infections that mainly affect the women of reproductive age and is the leading cause of death among people with HIV/AIDS. WHO records estimated about 8.6 million new cases of TB in 2012, among which 1.3 million people are approximated to have died of TB. Research in new diagnostics, drugs and vaccines for TB is happening at an unprecedented rate to achieve the desired target of *tuberculosis*-free world. Tuberculin skin test, sputum smear microscopy, commercial broth based culture systems, LED fluorescence microscopy, nitrate reductase Assay, Xpert MTB/RIF test are among the most explored diagnostic tools for TB detection [3]. However, current diagnostic tools for tuberculosis are highly expensive, often lack sensitivity and can be time consuming. Hence, an efficient diagnosis device is urgently required for timely and effective diagnosis of this disease.

Graphene, a monolayer thick 2-dimensional sp^2 carbon material, has recently gained enormous scientific interest owing to its promising electrical, optical, and mechanical properties [4,5]. Graphene is the most fundamental form of all sp^2-hybridized carbon materials viz. 3-dimensional graphite, 1-dimensional carbon nanotube and 0-dimensional fullerene. Bloch wave-function analysis and tight bonding model have shown that in graphene, the valence and conduction bands intersect at single point of zero states, called as Dirac point (K-point). This junction at the intrinsic Fermi level leads to its zero band gap semiconducting nature and semi-metallic properties [4]. Electrons in graphene behave as massless Dirac fermions, which lead to extremely high carrier mobility (10^6 $cm^2V^{-1}s^{-1}$), responsible for its application towards high-speed electronics [4,6]. Room temperature ballistic transport and high Fermi velocity of electrons

ACCEPTED MANUSCRIPT

(10^6 m/s, $1/300^{th}$ the speed of light) in graphene are some of the additional outstanding properties. This suggests that graphene is an excellent material for electronics [7].

Owing to such exceptional electrical properties, graphene based devices can perhaps be an alternative for fast bimolecular electronic devices including biosensors [8]. However, for the biosensing devices, the applicant material must also contain chemical functionalities viz., hydroxyl, epoxides, carbonyl carboxyl groups, on its surface for biomolecule immobilization. That is why graphene oxide (GO), that contains many oxygen rich functionalities, is a rapidly rising star on the horizon of all aspects of materials science including next generation bimolecular electronics devices [9- 12].

Current approaches to synthesize graphene including chemical vapor deposition and thermal decomposition of silicon carbide wafer offer graphene without such functional groups and have many issues such as process complexity, high temperature processing, low yield, cost and quality [13,14]. Besides this, graphene sheets, due to their high specific surface area, tend to form irreversible agglomerates or even restrict to form graphite by *van der Waals* interactions. Thus, the synthesis and processing of graphene sheets with minimum aggregation continue to be a challenge. Graphite exfoliation in liquids via covalent and non-covalent interactions provides an alternative method for preparing reproducible and scalable single and a few layer graphene films [15]. Recently, Parvez et al. have demonstrated the fabrication of graphene by electrochemical exfoliation of graphite for its application to organic electronics [16]. They realized that the graphene produced by this method contains certain amount of oxygen functionalities on its surface. In view of these, interesting developments, the electrochemical exfoliation of graphite can perhaps be the most simple and best method to produce low cost

ACCEPTED MANUSCRIPT

graphene and at the same time offer an opportunity to modify surface with desired biomolecules for sensing application.

In the present work, we demonstrate a facile and cost effective approach for the synthesis of GF on indium-tin-oxide (ITO) coated glass plate using electrochemical exfoliation process to explore its application for nucleic acid detection. Our efforts are especially dedicated to develop highly sensitive and cost effective diagnosis strategy for *M.tuberculosis* detection.

2. Materials and Methods

2.1. Reagents

Sodium dodecyl sulphate (SDS), Triethanolamine (TEA), potassium iodide (KI), N-hydroxysuccinimide (NHS), N-ethyl-N-(3-dimethylaminopropyl carbodiimide) (EDC), oligonucleotide probe sequence specific to *M. tuberculosis*, complementary target, one-base mismatch, and noncomplementary DNA have been procured from Sigma-Aldrich, Milwaukee, WI. All solutions and glassware have been autoclaved prior to being used, and desired reagents (molecular biology grade) are prepared in deionized water (Milli Q 10 TS). Oligonucleotide sequences used in this work are:

Biotinylated Probe: biotin-5'-GGTCTTCGTGGCCGGCGTTCA-3'

Complementary: 5'-TGAACGCCGGCCACGAAGACC-3'

One-Base Mismatch: 5'-TGAACGCCGACCACGAAGACC-3'

Noncomplementary: 5'-ATGTCTCAAGCCAGCTGCTG-3'

2.2. Synthesis of Graphene Flakes

GF have been synthesized/deposited on ITO coated glass substrates by electrochemical exfoliation of graphite rod using a three electrode system with graphite rod as counter electrode, and Ag/AgCl as the reference electrode. Chronoamperometric exfoliation of graphite has been

Accepted Manuscript

ACCEPTED MANUSCRIPT

carried out at a potential of +1.5V for 60s in aqueous solution containing KI (intercalating agent), SDS (stabilizing agent) and TEA (complexing agent) in varying molar concentration ratios. Such electrochemical synthesis strategy can offer the presence of functional groups on the surface of graphene based nanostructures as predicted by Parvez et al. earlier and corroborated by us in this work by Fourier transform infrared (FT-IR) spectroscopy [16].

2.3. Immobilization of DNA specific to *M. tuberculosis* onto GF/ITO electrode

Probe DNA (ssDNA) specific to *M. tuberculosis* (15µL) has been covalently immobilized onto GF/ITO electrode via amide bond formation between -COOH group of GF and -NH_2 group of DNA using EDC (0.4 M) as the coupling agent and NHS (0.1 M) as activator [17]. The bioelectrode (DNA/GF/ITO) thus fabricated is washed thoroughly with autoclaved phosphate buffer (50mM, pH 7.0) and is stored at 4°C when not in use.

2.4. Instrumentation

Raman spectrum has been recorded at room temperature by exciting the sample with wavelength 514.5 nm using argon laser, Model Innova 70, Coherent, USA. A notch filter has been used to eliminate the Rayleigh line from the scattered radiation. The scattered light has been detected by a single stage Jobin Yvon-Spex HR 640 Czemy-Turner monochromator along with a cooled photomultiplier tube (PMT) operated at voltage of 1600V. FT-IR spectroscopic investigations have been recorded using Perkin–Elmer FT-IR model ‘‘Spectrum BX’’ equipped with the specular reflectance accessory. Morphology of the deposited samples has been examined using high resolution transmission electron microscopy (HR-TEM), model JEM-2100F (JEOL, Japan), and scanning electron microscopy (SEM), Model LEO 40, respectively. Electrochemical response studies of DNA-GF/ITO bioelectrode have been carried out using Autolab Potentiostat/Galvanostat (Eco Chemie, Netherlands), in a conventional three-electrode

Accepted Manuscript

ACCEPTED MANUSCRIPT

electrochemical cell consisting of Ag/AgCl as reference electrode and platinum foil as the counter electrode, in phosphate buffer saline (PBS) solution (0.05 M, pH 7.0, 0.9% NaCl) containing MB as a redox indicator.

3. Results and Discussion

3.1. Electrochemical Exfoliation of Graphene Flakes

Graphene flakes rich in oxygen containing functionalities on its surface have been obtained by chronoamperometric exfoliation of graphite rod at +1.5V at the optimized molar ratio of KI, SDS and TFE as 10:1:2 with pH of the electrolytic aqueous solution maintained at 9. The overall exfoliation strategy towards 2-dimensional graphene flakes is outlined in Fig. 1. Exfoliation of GO sheets has been initialized and facilitated with intercalation of the potassium ions (K^+) within the layers of graphite rods due to the smaller size of the K^+ ions. K^+ ions emerging from potassium iodide get intercalated between the outer and penultimate planes and weaken the *van der Waals* attractive forces between the graphitic planes. Once the penultimate and outer graphite planes get loosened up from each other, the outer plane can be easily leached out in the solution as GO flakes under the influence of applied external electric field. Being part of the electrolytic solution, SDS molecules help in stabilizing the GO flakes and prevent its aggregation (Fig. 1). TEA has been employed to assist K^+ ion to penetrate in graphitic plane by complex formation. Surfactant, moisture and other chemical impurities have been removed from the deposited GO flakes by sonicating the electrodes for about 15 min followed by the heat treatment at 100°C for 20 min. GO flakes are reduced to GF by hydrazine (NH_2NH_2) treatment for 4h at 80°C.

Accepted Manuscript

ACCEPTED MANUSCRIPT

3.2. SEM and TEM Analysis

SEM and TEM investigations have been carried out to analyze structural and textural behavior of electrochemically fabricated films of graphene deposited on ITO. In order to find the optimal conditions for the formation of transparent graphene flakes, the SEM analysis has been done at varying molar concentrations of KI, SDS and TEA during the film deposition process. It has been found that the morphology and the formation probability of graphene flakes are strongly affected by the molar concentrations ratio of KI: SDS: TEA. The different molar concentration of KI, SDS and TEA and their corresponding SEM micrographs have been presented in Fig. 2. It is clear from Fig. 2a-2c, the reduction in SDS concentration from 0.05 to 0.001 M concentration results in granular and uneven morphology of film, which has been approaching to attain the sheet like appearance. The decrease in concentration of KI from 0.1 to 0.01 M (Fig. 2d-2f) further promotes the formation of sheet like structure and also helps in the unification of separate carbon structures leading to the ribbon like skeleton. Furthermore, the reduction in TEA concentration from 0.02 to 0.002 M (Fig. 2g-2h) leads to the construction of long, thin, uniform and transparent flake-like morphology. Hence, at the optimized molar ratio of 0.01:0.001:0.002 or 10:1:2, SEM image of deposited film (Fig. 2g and 2h) shows the fabrication of thin elongated flake-like structures with dimensions of ~2.2 μm width and ~50 μm length. We predict the obtained flakes as graphene flakes, which are so transparent that the surface beneath is noticeably clear (Inset of Fig. 2h), demonstrating its single or double layered skeletal configuration which is also corroborated with the Raman results as discussed later.

To further confirm the formation of transparent flake-like morphology in deposited film at optimal molar concentrations, the HRTEM analysis has been performed. The TEM image shown in Fig. 3a demonstrates a clean GF carrying plenty of ripples, owing to its thin sheet

Accepted Manuscript

ACCEPTED MANUSCRIPT

structure. The long wrinkles are observed and edges of the sheet are folded, creating a crumpled paper veil waves (Fig. 3b) indicating appearance of the flakes, which is in agreement with the SEM images**.**

3.3. Raman and FT-IR Spectroscopic Analyses

Raman spectroscopy is known to be an interesting tool to characterize the carbon materials of all dimensionalities. Especially, Raman spectroscopy is the most reliable way to probe graphene and graphene related materials. We have also employed this tool to confirm the formation of graphene flakes in our sample. Fig. 4a shows the Raman spectrum recorded for GF. The Raman spectrum of sample shows two prominent peaks; one at ~ 1598 cm^{-1} and the other at ~ 2735 cm^{-1}.The peak at ~ 1598 cm^{-1} corresponds to G peak and occurs as a consequence of first order process, which involves doubly degenerate [in-plane transverse optical (ipTO) and longitudinal optical (LO)] phonons of E_{2g} symmetry at the zone center [18]. The peak at ~ 2735 cm^{-1} is assigned to 2D peak and is attributed to second order process, which involves two ipTO phonons near the K point of the Brillouin zone. The observation of intense 2D peak is interesting as this peak is the main characteristic peak of graphene and graphene related materials. Since TEM and SEM analyses predict the formation of transparent GF, the Raman spectroscopy confirms that the flakes are of graphene. Compared with the virgin graphene, which shows a G peak in the range of ~ 1581-1590 cm^{-1} and 2D peak in the range of ~ 2700-2720 cm^{-1}, the G and 2D peak positions are slightly shifted towards higher wavenumber in the synthesized sample. This may be due to the presence of carboxyl functionalities in the graphene flakes, which is further supported by the Fourier transform-infrared (FT-IR) spectroscopic investigations.

In addition, the Raman spectrum of GF exhibits a peak towards the shoulder of G peak. This shoulder peak, which is observed at ~ 1625 cm^{-1}, corresponds to D' peak and arises due to

Accepted Manuscript

ACCEPTED MANUSCRIPT

double resonance intravalley process [15]. Another important feature of Raman spectroscopy is to identify the number of atomic graphene layers by measuring the intensity of 2D peak with respect to G peak i. e. intensity ratio of 2D peak with G peak [I (2D) /I(G)]. The estimation of I(2D)/I(G) ratio in our case shows a value of ~1.6, suggesting the presence of single or double layered GF [18, 19].

FT-IR measurements have been performed to examine the bonding environment of the fabricated GF and the immobilization of DNA onto GF/TO surface. In the FT-IR spectrum of GF deposited on ITO (Fig. 4b), the observed transmission bands centered at 1451 cm^{-1} and 1046 cm^{-1} are assigned to O–H deformation and C–O stretching vibrations, respectively. The peak at 1730 cm^{-1} is attributed to –C=O stretching vibration in the carboxyl group, indicating –COOH functionalization of graphene which is in agreement with results of the Raman spectroscopic studies. Further, FT-IR spectral analysis reveals peak around 1645 cm^{-1}, corresponding to –C=C– stretching mode, which is a characteristic peak of GF. In addition, a peak found at ~ 675 cm^{-1} is attributed to out-of-plane bending of C–H bond. Thus, FT-IR studied indicate that fabricated GF contains oxygen rich functional groups on its surface. Fig 4 (c) corroborates, immobilization of DNA onto GF surface. Peaks seen at 1260, 1604 and 1770 cm^{-1} for ssDNA-GF/ITO bioelectrode are due to P – O stretching of phosphate backbone and C – O stretching vibrations of purines and pyrimidine rings of DNA, respectively. The broad peak seen at 3440 cm^{-1} is due to N – H stretching vibrations indicating immobilization of DNA onto GF/ITO surface.

3.4. Electrochemical and Biosensing response studies of ssDNA-GF/ITO bioelectrode using Differential Pulse Voltammetry (DPV)

Fig. 5a shows the comparative electrochemical response of GF/ITO and ssDNA-GF/ITO electrodes via cyclic voltammetry in PBS (50mM, pH 7.0, 0.9% NaCl) containing 5 mM

ACCEPTED MANUSCRIPT

$[Fe(CN)_6]^{3-/4-}$ as the redox probe/mediator at constant scan rate of 50 mV. The anodic and cathodic peaks seen in the cyclic voltammograms indicate the following redox reactions, respectively:

$$Fe(CN)_6^{-4} \rightarrow Fe(CN)_6^{-3} + e^- \quad \text{(Oxidation Process)} \quad \text{Eq. 1}$$

$$Fe(CN)_6^{-3} + e^- \rightarrow Fe(CN)_6^{-4} \quad \text{(Reduction Process)} \quad \text{Eq. 2}$$

During the cyclic voltammetry measurements, as the scan progress in the forward direction and the potential is sufficiently positive to oxidize $[Fe(CN)_6]^{4-}$ ions, the anodic current start to increase due the oxidation process shown in Eq. 1. The electrode will act as an oxidant for this process. With increased scan rate, the concentration of $[Fe(CN)_6]^{4-}$ ions starts depleting and thus the current also start decaying. On the contrary, as the scan progress in the backward direction, the electrode perhaps acts as reductant and promotes the reduction process (Eq. 2).

On comparing the electrochemical behavior of both the electrodes, reduction in both cathodic peak current (I_{pc}) as well as anodic peak current (I_{pa}) is observed for the DNA immobilized ssDNA-GF/ITO genoelectrode (I_{pa} = 1.86×10^{-5}A; I_{pc} =-1.47×10^{-5}A) with respect to GF/ITO electrode (I_{pa} = 2.286×10^{-5}A; I_{pc} =-1.78×10^{-5}A). This reduction in current clearly indicates that electrode surface modification with the negatively charged DNA moieties plays role in restricting the redox reactions of $[Fe(CN)_6]^{3-/4-}$ at the electrode surface. This may be due to the repulsive interactions between negatively charged $[Fe(CN)6]^{3-/4-}$ ions with the similarly charged phosphate backbone of DNA that hinders the electron transfer process resulting in reduction in the peak currents. Further, the observed widening of difference in the peak potentials (E_{pa}-E_{pc}) in case of ssDNA-GF/ITO bioelectrode (107 mV) compared to GF-ITO electrode (98 mV) indicates slower electron transfer with DNA binding

ACCEPTED MANUSCRIPT

Fig. 5b shows the cyclic voltammograms of ssDNA-GF/ITO electrode with varying the scan rate from 60-300 mVs^{-1}. Both I_{pa} and I_{pc} shows continuous enhancement with increasing scan rate (ν). According to the Randles-Sevcik equation (Eq. 3), the peak current on the forward potential scan should increase linearly with the square root of the scan rate for an electrochemically reversible redox system [17]. Fig. 5c shows the curve between the I_{pa} vs $\nu^{1/2}$ for the ssDNA-GF/ITO electrode revealing linear behavior with the regression coefficient of 0.995 (Eq. 4). Current coefficient ($I_{pa}/\nu^{1/2}$), another indicator for the reversible electron transfer, has also been estimated for different scan rates. Constant value of current coefficient (2.47 $\mu AmV^{-1}s \pm 0.053$ μA) for all the scan rate values clearly reveals that electron transfer at the electrode is fast enough to maintain the equilibrium ratio between the reduced and oxidized forms of the redox couple.

$$I_p = (2.69 \times 10^5) n^{3/2} A D^{1/2} C_i \nu^{1/2} \qquad \text{Eq. 3}$$

$$I_{pa}(A) = 2.386 \times 10^{-6} (AmV^{-1/2}s^{1/2}) \times \nu^{1/2} (mV^{1/2}s^{-1/2}) + 9.27 \times 10^{-7} (A)\,;\ \mathrm{R} = 0.995 \qquad \text{Eq. 4}$$

To demonstrate the application of the graphene flakes based ssDNA-GF/ITO electrode, biosensing studies have been conducted for nucleic acid detection using *M. tuberculosis* as the model system. All the biosensing studies have been conducted in PBS (0.05 M, pH 7.0, 0.9% NaCl) with MB as a redox electroactive hybridization indicator. Fig. 6a shows the results of the hybridization studies carried out on the ssDNA-GF/ITO bioelectrode using MB with varying complementary target concentrations (2.872×10^{-3}-2.872×10^{5} $ng\mu L^{-1}$) by differential pulse voltammetry. MB is known to associate with the unpaired nitrogenous bases of single-stranded DNA as compared to the double-stranded DNA. It shows the maximum peak current for MB at about -2.5 V for ssDNA-GF/ITO bioelectrode carrying only single standard probe DNA with no duplex formation [18]. With increasing concentration of complementary target DNA (specific to *M. tuberculosis*), there is increased formation of double-standard DNA duplex on the

ACCEPTED MANUSCRIPT

bioelectrode surface resulting in continuous decrease in free nitrogenous bases available for MB interactions. This results in consistently reducing current value up to 2.872×10^{5} ngμL^{-1} and remains constant afterwards, indicating that all the immobilized probe molecules on bioelectrode surface are now involved in hybridization at this threshold concentration [20-22]. Fig. 6b shows the plot between the change in peak current ($I_0 - I_{conc}$) with increasing target DNA concentration and it follows the logarithmic equation (Eq. 5).

$$\Delta I\ (I_0\text{-}I_{conc}) = 15.22 + 2.687 \times ln\ (\text{Target DNA Concentration} + 0.00464);\ R=0.976 \qquad \text{Eq. 5}$$

Where I_0 is the peak current at zero concentration of target DNA concentration and I_{conc} is the peak current at particular concentration.

This biosensing analysis clearly reveals that the fabricated DNA-GF/ITO bioelectrode can detect complementary DNA specific to *M. tuberculosis* in the wide range of target nucleic acid concentration from 2.872×10^{-3} to 2.872×10^{5} ngμL^{-1} with enhanced sensitivity (2.27×10^{-6} Ang^{-1}μL), reusability (>12 times) and stability (~6 months).

The selectivity of the probe ssDNA-GF/ITO bioelectrode has been investigated by monitoring redox activity of MB by incubating it with equal concentration (2.8×10^{5} ngμL^{-1}) of complementary, non-complementary and one-base mismatch oligonucleotide sequences, respectively, as shown in Fig. 6c. The highest peak current (78 μA) is obtained for probe DNA-GF/ITO electrode since MB has a strong affinity for the free guanine bases resulting in maximum accumulation of MB at bioelectrode surface. After incubation with the complementary DNA sequence, the peak current decreases drastically by ~50% indicating duplex formation at bioelectrode surface and due to steric and conformational changes induced during the hybridization process. And with the non-complementary DNA, this bioelectrode exhibits insignificant change in the peak current (~10-12%), revealing its high specificity. However,

Accepted Manuscript

ACCEPTED MANUSCRIPT

binding with one-base mismatch sequence results in 25% reduction in the peak current indicating its non-specific binding.

To attest the specificity of this genoelectrode, heat-denatured genomic DNA (*M. tuberculosis*) samples have been used for the DNA hybridization response studies in the presence of MB. Significant decrease in the peak current with respect to that of bioelectrode is observed after incubation with genomic DNA sample revealing its specificity for *M. tuberculosis* detection (Fig. 6d). Further, DNA hybridization response studies carried out as a function of genomic DNA concentration reveal the detection range as 0.015 ngμL^{-1} – 150 ngμL^{-1}, with detection limit of 0.015 ngμL^{-1} for ssDNA–GF/ITO electrode. The comparison of the present system with the other electrodes is given in Table-I.

Table 1: Comparison of ssDNA-GF/ITO electrode along with those reported in literature for DNA biosensors:

Matrix	**Method of immobilization**	**Stability**	**Re-usability**	**Detection limit**	**Ref.**
Nano ZrO_2	Physisorption	----	----	2 2×10^{-10} M	23
Nano ZnO	Physisorption	4 months	10 times	1×10^{-12} M	24
Nano ZrO_2-CNT-CHIT	Physisorption	----	----	7.5×10^{-11} molL^{-1}	25
Nano Fe_2O_3-GOPS/ITO [GOPS=3-glycidoxypropyltrimethoxysilane]	Covalent binding via avidin-biotin coupling	4 months	15 times	0.1×10^{-15} M	26

ACCEPTED MANUSCRIPT

Nano Fe_2O_3-CHIT/ITO	Covalent binding via avidin-biotin coupling	6 months	----	1×10^{-16} M	27
GF/ITO	Covalent immobilization via amide bond formation	6 months	>12 times	2.872×10^{-3} ngμL^{-1} 0.015 ngμL^{-1} (with genomic DNA)	Present work

4. Conclusions

We have developed a simple, fast, and generic method for easy electrochemical fabrication of GF on ITO coated glass substrates and explored its application towards the development of improved nucleic acid sensor for *M. tuberculosis* detection. The detailed morphological and structural investigations of GF/ITO using SEM and TEM studies reveal the formation of the highly transparent graphene having a few layers with flake-like appearance. Further, this biosensor exhibits low detection limit (2.872×10^{-3} ngμL^{-1}), high sensitivity (2.27×10^{-6} Ang^{-1}μL), reusability (>12 times) and stability (~6 months) that are attributed to the enrichment of biomolecules on this novel platform with implications in the emerging field of bioelectronics.

Acknowledgements

MDM acknowledges the financial support received from Department of Science and Technology (SERC/ET-0242/2012). Authors thank Dr. N. Dilawar (NPL, India) for Raman measurements.

Accepted Manuscript

ACCEPTED MANUSCRIPT

References

[1] K. Zaman, Tuberculosis: A global health problem, J. Health Popul. Nutr. 28 (2010) 111-113.

[2] A. I. De Backer, K. J. Mortele, B. L. De Keulenaer, P. M. Parizel, Tuberculosis: Epidemiology, manifestations, and the value of medical imaging in diagnosis, JBR–BTR 89 (2006) 243-250.

[3] C. Hanson, G. Roscigno, New laboratory diagnostic tools for tuberculosis control, WHO Publishers, 2008, ISBN: 9789241597487. [http://www.stoptb.org/assets/documents/global/retooling/Diagnostic_Brochure_Print_2009_Jan_29.pdf].

[4] A. K. Geim, K. S. Novoselov, The rise of graphene, Nat. Mater. 6 (2007) 183-191.

[5] C. N. R. Rao, A. K. Sood, K. S. Subrahmanyam, A. Govindaraj, Graphene: the new two-dimensional nanomaterials, Angew. Chem. Int. Ed. 48 (2009) 7752-7757.

[6] H. Zhou, L. Liao, Y. Liu, S. Jiang, Y. Huang, X. Duan, Graphene: an emerging electronic material, Adv. Mater. 24 (2012) 5782-5825.

[7] Nathan O. Weiss, Hailong Zhou, Lei Liao, Yuan Liu, Shan Jiang, Yu Huang, Xiangfeng Duan, Graphene: An Emerging Electronic Material, Advanced Material 24 (2012) 5782-5825.

[8] T. Kuila, S. Bose, P. Khanra, A. K. Mishra, N. H. Kim, J. H. Lee, Recent advances in graphene-based biosensors, Biosens. Bioelectron. 26 (2011) 4637-4648.

[9] A. Singh, G. Sinsinbar, M. Choudhary, V. Kumar, R. Pasricha, H. N. Verma, S. P. Singh, K. Arora, Graphene oxide-chitosan nanocomposite based electrochemical DNA biosensor for detection of typhoid, Sens. Actuator B-Chem. 185 (2014) 675-684.

Accepted Manuscript

ACCEPTED MANUSCRIPT

[10] K. Ariga, Q. Ji, T. Mori, M. Naito, Y. Yamauchi, H. Abe, J. P. Hill, Enzyme nanoarchitectonics: organization and device application, Chem. Soc. Rev., 42 (2013) 6322 – 6345.

[11] Y. Huang, J. F. Kong, S. S. Venkatraman, Biomaterials and design in occlusion devices for cardiac defects: A review, Acta Biomaterialia 10 (2014) 1088–1101

[12] K. Ariga, Y. Yamauchi, G. Rydzek, Q. Ji, Y. Yonamine, K. C.-W. Wu, J. P. Hill, Layer-by-layer Nanoarchitectonics: Invention, Innovation, and Evolution, Chem. Lett., 43 (2014) 36–68.

[13] S. Park, R. S. Ruoff, Chemical methods for the production of graphenes, Nat. Nanotechnol. 4 (2009) 217-724.

[14] A. K. Geim, Graphene: status and prospects, Science 324 (2009) 1530-1534.

[15] Y. Hernandez, V. Nicolosi, M. Lotya, F. M. Blighe, Z. Sun, S. De, I. T. McGovern, B. Holland, M. Byrne, Y. K. Gun'Ko, J. J. Boland, P. Niraj, G. Duesberg, S. Krishnamurthy, R. Goodhue, J. Hutchison, V. Scardaci, A. C. Ferrari and J. N. Coleman, High-yield production of graphene by liquid-phase exfoliation of graphite, Nat. Nanotechnol. 3 (2008) 563–568.

[16] K. Parvez, R. Li, S. R. Puniredd, Y. Hernandez, F. Hinkel, S. Wang, X. Feng, K. Mullen, Electrochemically exfoliated graphene as solution-processable, highly conductive electrodes for organic electronics, ACS Nano 7 (2013) 3598-3606.

[17] M. Das, C. Dhand, G. Sumana, R. Nagarajan, M. Iwamoto, T. Manaka, B. D. Malhotra, Zirconium oxide-Chitosan Nanobiocomposite for Mycobacterium tuberculosis detection, Biomacromolecules 12 (2011) 540-547.

Accepted Manuscript

ACCEPTED MANUSCRIPT

[18] A. C. Ferrari, D. M. Basko, Raman spectroscopy as a versatile tool for studying the properties of graphene, Nat. Mater. 8 (2013) 235-246.

[19] A. C. Ferrari, Raman spectroscopy of graphene and graphite: Disorder, electron–phonon coupling, doping and nonadiabatic effects, Solid State Commun. 143 (2007) 47-57.

[20] C. Dhand, P. R. Solanki, M. Datta, B. D. Malhotra, Polyaniline/Single-Walled Carbon Nanotubes Composite Based Triglyceride Biosensor, Electroanalysis 22 (2010) 2683-2693.

[21] Kavita Arora, Nirmal Prabhakar, Subhash Chand, B.D. Malhotra, Ultrasensitive DNA hybridization biosensor based on Polyaniline, Biosensors and Bioelectronics 23 (2007) 613–620.

[22] M. Das, G. Sumana, R. Nagarajan, B. D. Malhotra, Zirconia based nucleic acid sensor for Mycobacterium tuberculosis detection, Appl. Phys. Lett. 96 (2010) 133703.

[23] S. H. Zuo, L. F. Zhang ,H. H. Yuan, M. B. Lan, G. A. Lawrance, G. Wei, Electrochemical detection of DNA hybridization by using a zirconia modified renewable carbon paste electrode, Bioelectrochemistry, 74 (2009) 223-226.

[24] M. Das, G. Sumana, R. Nagarajan, B. D. Malhotra, Application of nanostructured ZnO films for electrochemical DNA biosensor, Thin Solid Films 519 (2010) 1196-1201.

[25] Y. Yang, Z. Wang, M. Yang, J. Li, F. Zheng, G. Shen, R. Yu, Electrical detection of deoxyribonucleic acid hybridization based on carbon-nanotubes/nano zirconium dioxide/chitosan-modified electrodes, Anal. Chim. Acta., 584 (2007) 268-274.

[26] N. Prabhakar, P. R. Solanki, A. Kaushik, M. K. Pandey, B. D. Malhotra, Peptide Nucleic Acid Immobilized Biocompatible Silane Nanocomposite Platform for *Mycobacterium tuberculosis* Detection, Electroanalysis, 22 (2010) 2672-2682.

Accepted Manuscript

ACCEPTED MANUSCRIPT

[27] R. Singh, R. Verma, A. Kaushik, G. Sumana, S. Sood, R. K. Gupta, B. D.Malhotra, Chitosan–iron oxide nano-composite platform for mismatch-discriminating DNA hybridization for Neisseria gonorrhoeaedetection causing sexually transmitted disease, Biosensors. Bioelectron., 26 (2011) 2967-2974.

Accepted Manuscript

ACCEPTED MANUSCRIPT

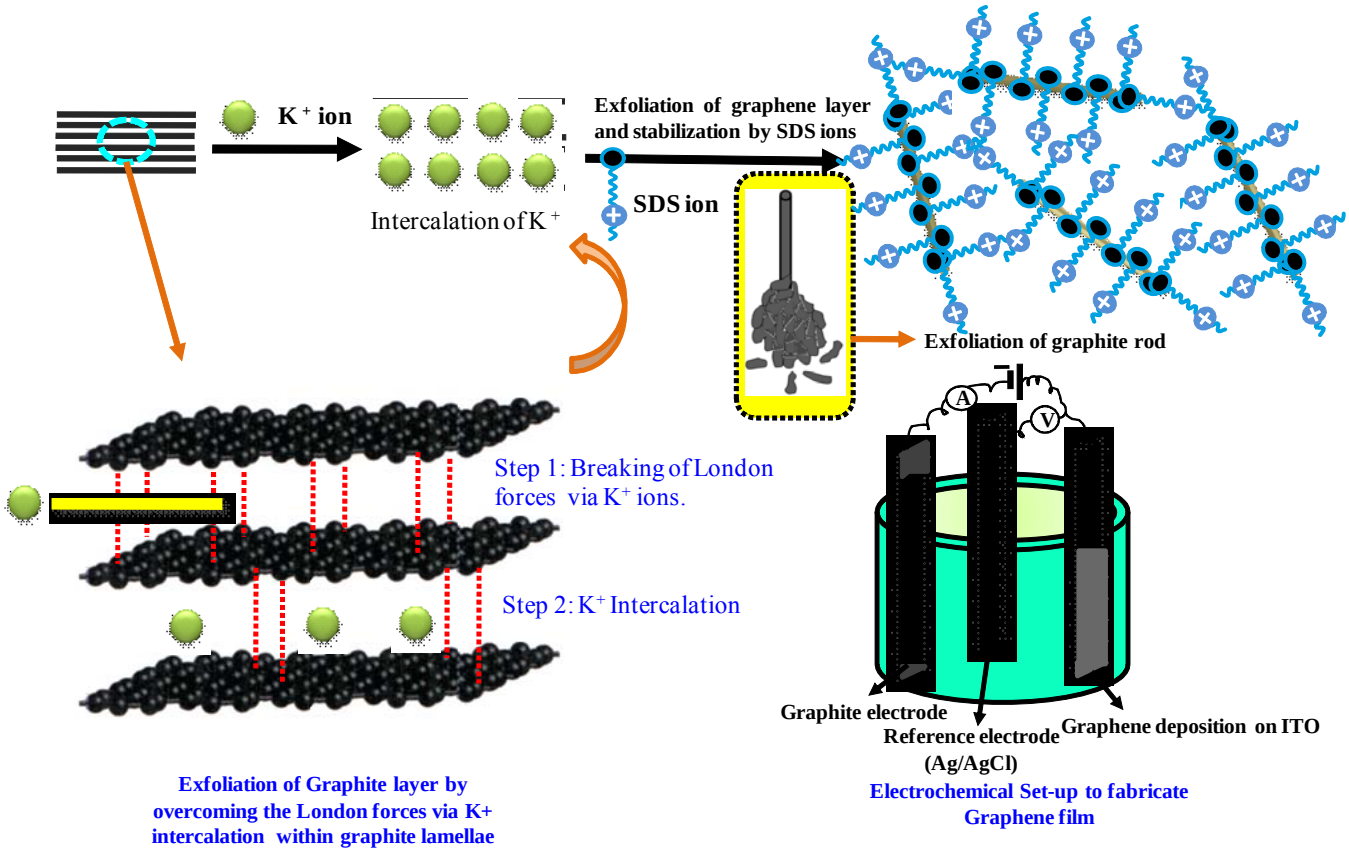


Fig. 1 Schematic showing the fabrication of graphene flakes on ITO substrates by electrochemical exfoliation of graphite sheet via K^+ ion intercalation and SDS stabilization.

Accepted

ACCEPTED MANUSCRIPT

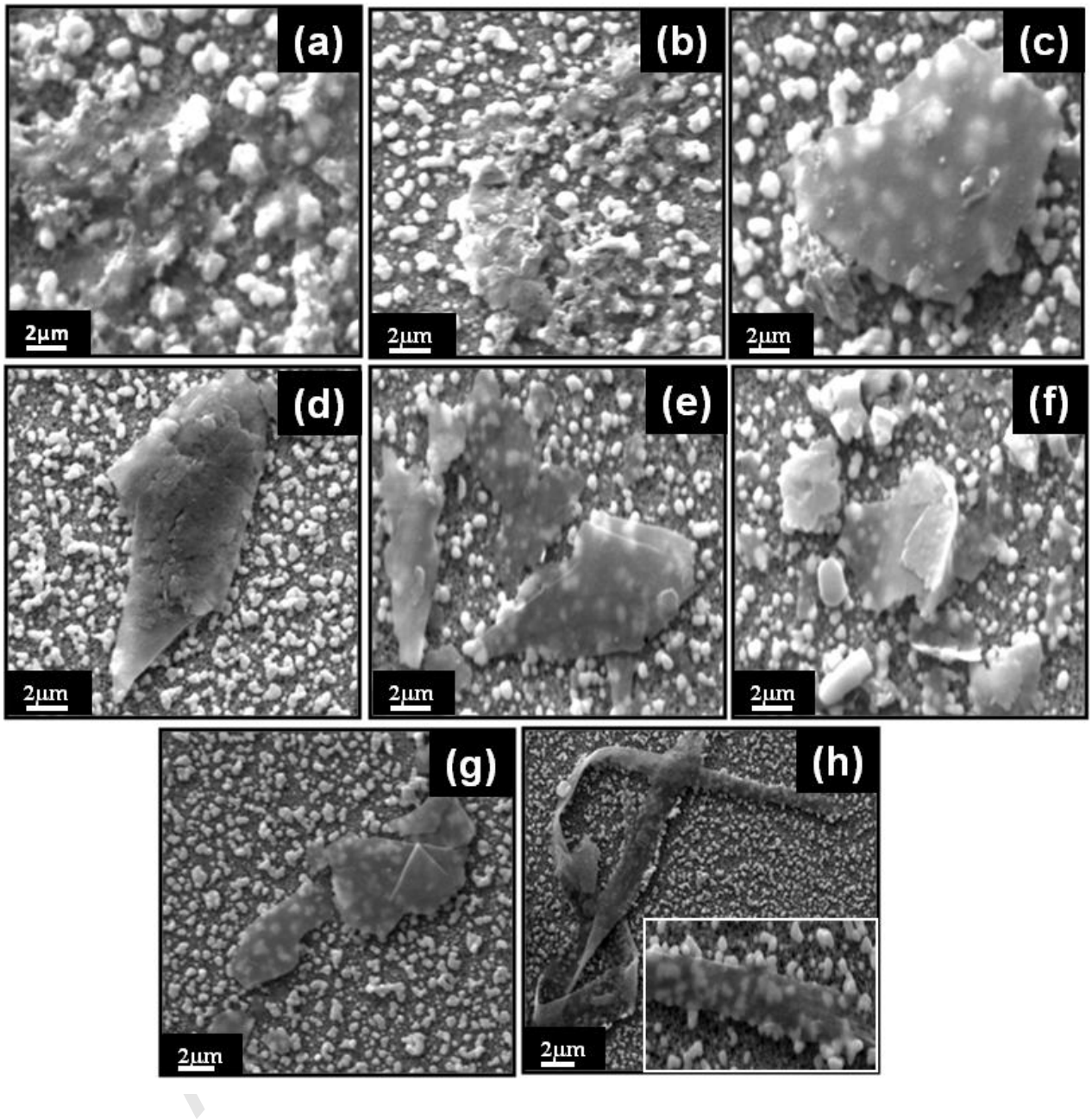


Fig. 2 Optimization of concentrations of KI, SDS and TEA for the fabrication of graphene flakes by SEM analysis. SEM micrographs captured for KI: SDS: TEA molar concentrations of **a)** 1: 0.05: 0.2, **b)** 1: 0.01: 0.2, **c)** 1: 0.001: 0.2, **d)** 0.5: 0.001: 0.2, **e)** 0.1: 0.001: 0.2, **f)** 0.01: 0.001: 0.2, **g)** 0.01: 0.001: 0.02, **h)** 0.01: 0.001: 0.002.

ACCEPTED MANUSCRIPT

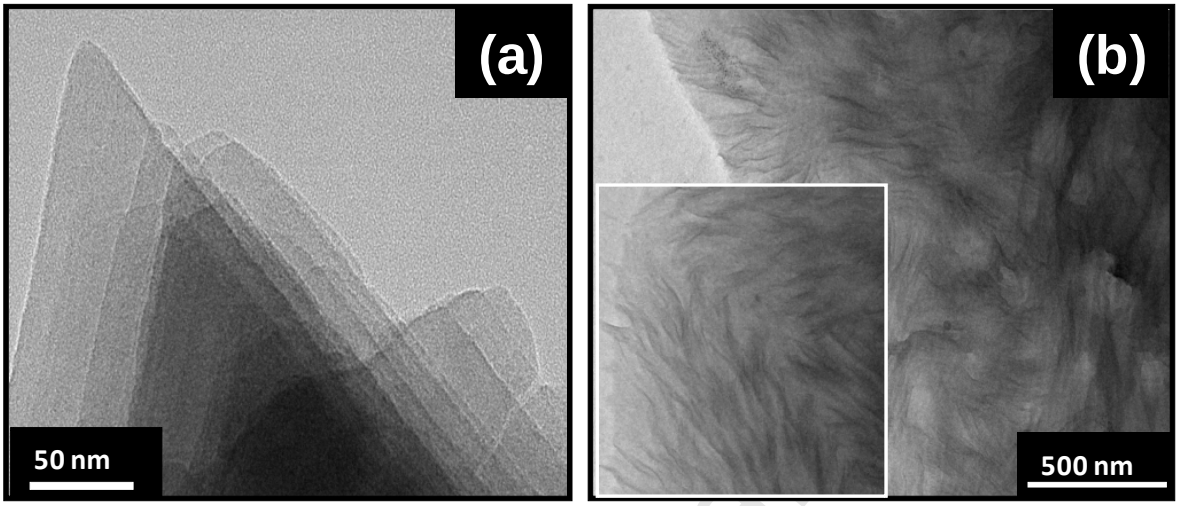


Fig. 3 TEM analysis of graphene Flakes: **(a)** showing its layered morphology and **(b)** revealing plenty of ripples owing to its thin sheet structure.

Accepted Manuscript

ACCEPTED MANUSCRIPT

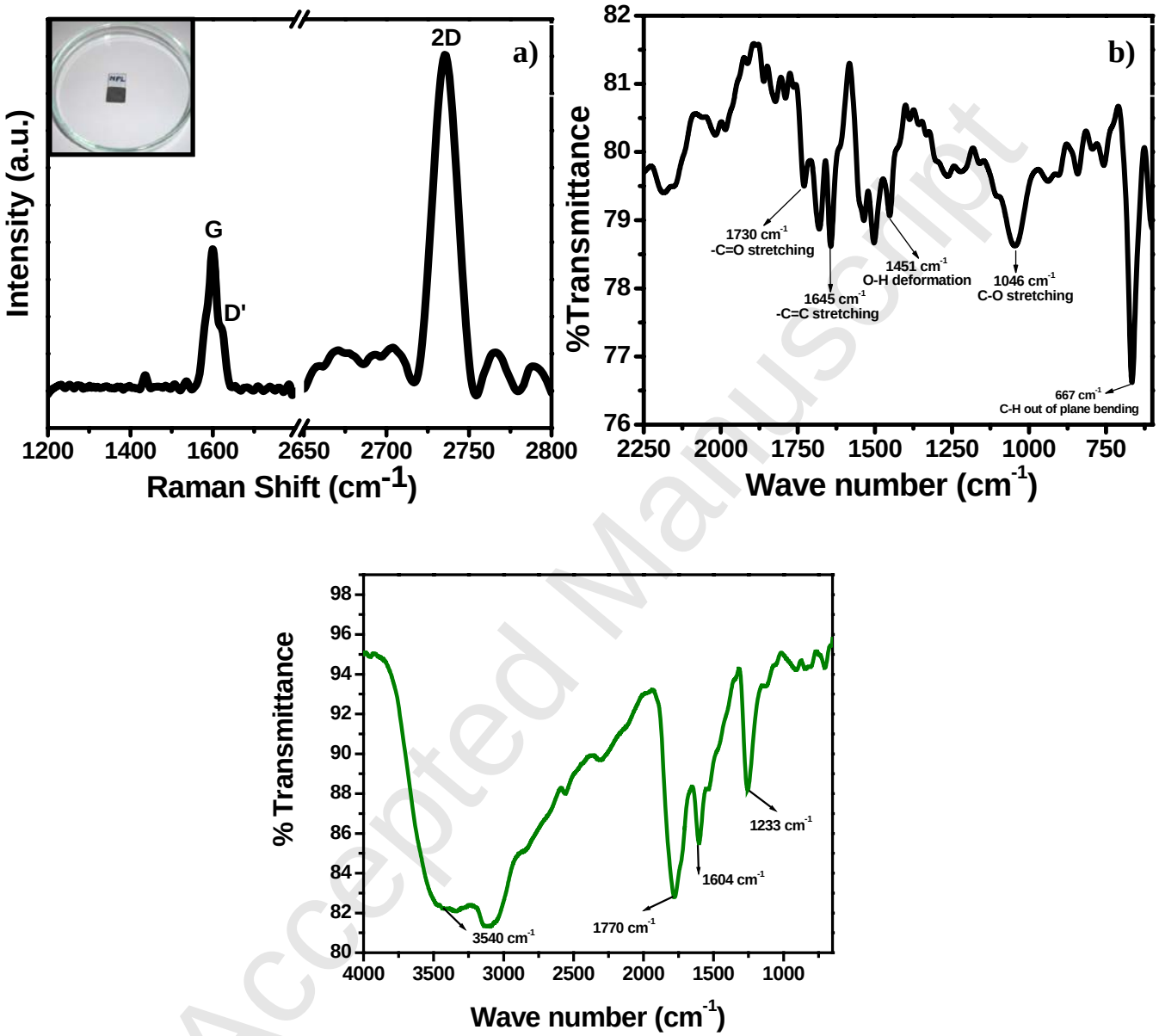


Fig. 4 Spectroscopic Characterization of electrochemically exfoliated Graphene Flakes: **(a)** Micro-Raman spectrum, FT-IR spectrum of **(b)** GF/ITO and **(c)** ssDNA/GF/ITO

Accepted Manuscript

ACCEPTED MANUSCRIPT

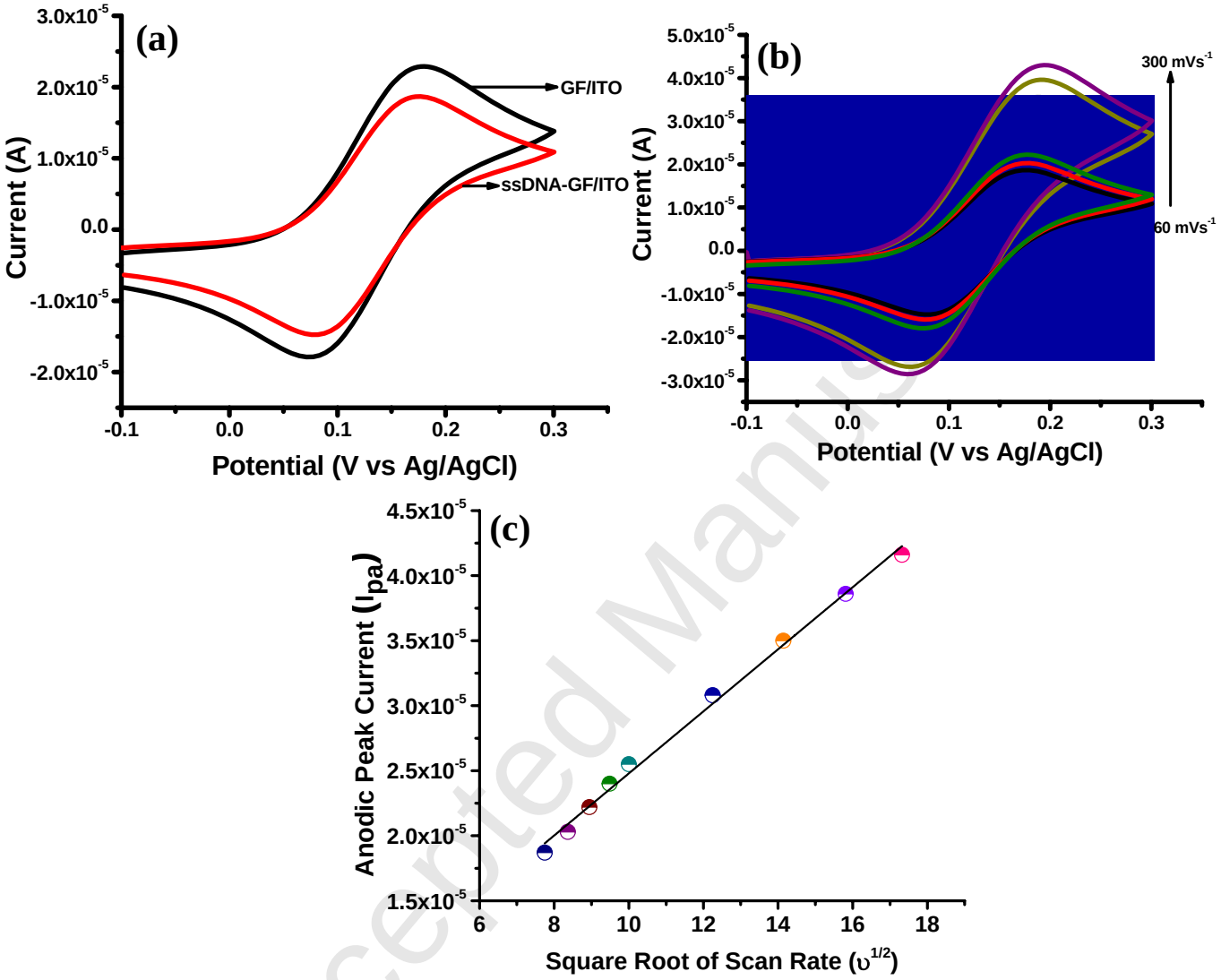


Fig. 5 (a) Cyclic voltammograms of GF/ITO and ssDNA-GF/ITO electrodes in PBS (50mM, pH 7.0, 0.9% NaCl) containing 5 mM $[Fe(CN)_6]^{3-/4}$ at the scan rate of 50 mVs^{-1}, **(b)** cyclic voltammetry curves for ssDNA-GF/ITO genoelectrodes as a function of scan rate from 60 to 300 mVs^{-1}, **(c)** Linearity curve between the anodic peak current (I_{ap}) vs square root of the scan rate for ssDNA-GF/ITO electrode.

ACCEPTED MANUSCRIPT

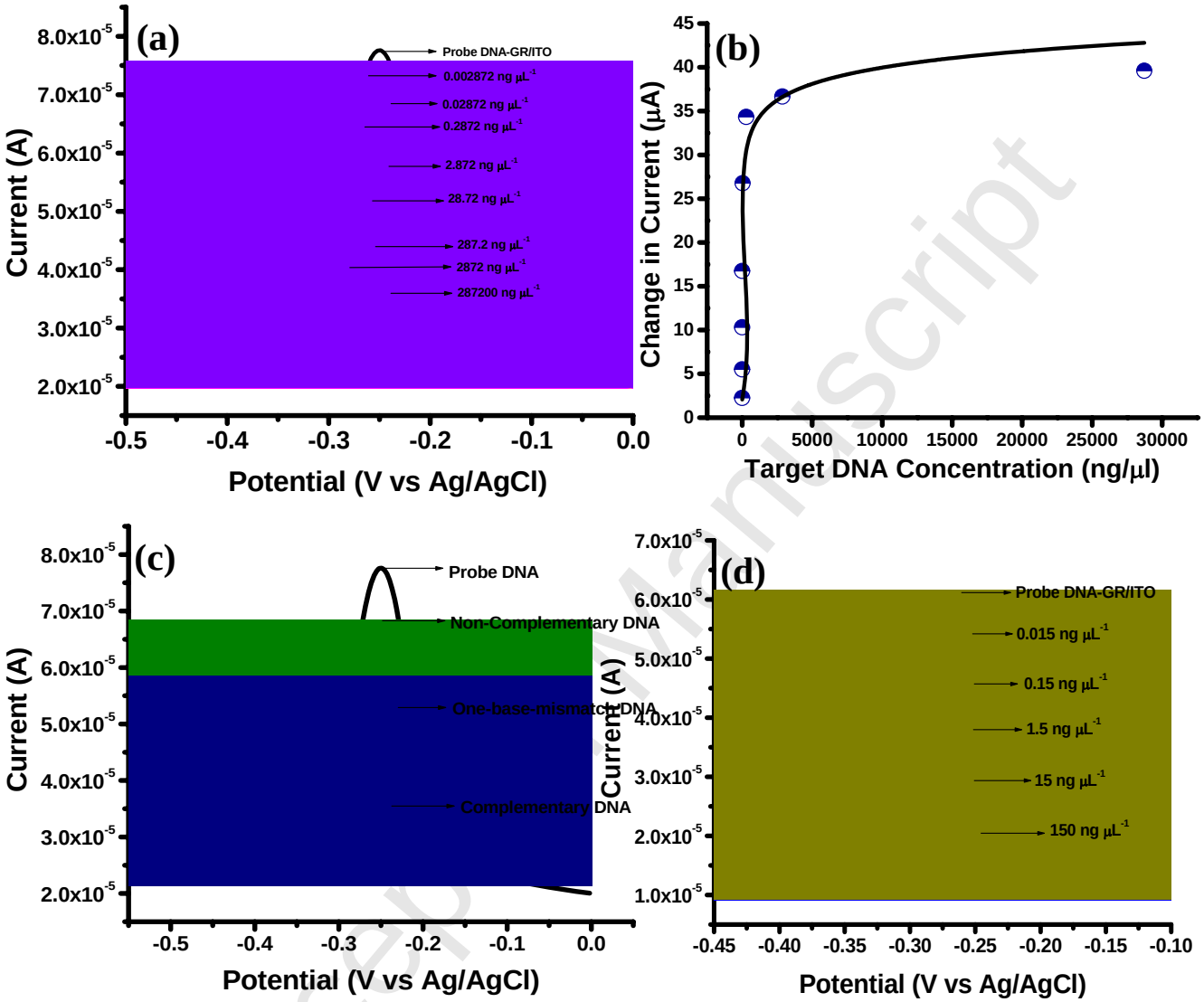


Fig. 6 Differential pulse voltammetry (DPV) studies for ssDNA–GF/ITO bioelectrode: **(a)** after incubating different concentrations of complementary target DNA, **(b)** Plot showing the variation in the change in the peak current (with respect to probe DNA) with increase in target DNA concentration, **(c)** specificity studies by treating the bioelectrode with non-complementary, one-base-mismatch, complementary target DNA, **(d)** by incubating with heat-denatured genomic DNA samples. All these studies have been carried out in phosphate buffer saline (0.05M, pH 7.0, 0.9% NaCl) containing methylene blue as redox indicator.

ACCEPTED MANUSCRIPT

Authors Biography



Dr. Maumita Das Mukherjee received her Ph.D degree (2012), in Chemistry, from University of Delhi, New Delhi, India. She is currently working as Assistant Professor at Amity Institute of Applied Sciences, Amity University, Noida, Uttar Pradesh, India. She has research Experience of 8 years in the area of development of biosensors based on nanomaterials, nanobiocomposites, conducting polymers for health care and glass and glass-ceramic materials.



Chetna Dhand has completed her PhD in Chemistry from University of Delhi in collaboration with National Physical Laboratory, New Delhi, India. Currently, she is working as a Postdoctoral Research Fellow at Singapore Eye Research Institute, Singapore. Her major research interests include nanomaterials for biomedical applications, targeted drug delivery and biosensors.



Neeraj Dwivedi obtained his PhD in Physics from the Indian Institute of Technology Delhi, India. Currently, he is working as a Postdoctoral Research Fellow in the Department of Electrical and Computer Engineering, National University of Singapore, Singapore. His major interests include material science, thin films and coatings, MEMS, nanomaterials for biomedical applications.



Baijanath Pratap Singh achieved his Master degree (M.E.) in Polymer Technology, from the Delhi Technological University (formerly Delhi College of Engineering) in 2010 and gained research experience from NPL, New Delhi. He is working as Assistant Manager (Research and Development Lab) in UFLEX LIMITED.

Accepted Manuscript

ACCEPTED MANUSCRIPT



Dr. G. Sumana received her Ph.D. (1998) from Jiwji University in chemistry. She is currently working as scientist in biomolecular electronics and conducting polymer research group, National Physical Laboratory, New Delhi. She has a research experience of 10 years in controlled drug delivery, liquid crystal polymers, polymer dispersed liquid crystals and biosensors.



Ved Varun Agrawal earned his PhD degree from the Jawaharlal Nehru Center for Advanced Scientific Research in 2008. He now works as a Scientist in the Department of Science & Technology of Biomolecular Electronics, Biomedical Instrumentation Section at National Physical Laboratory (CSIR), New Delhi, India. His current research focuses on utilizing the properties of nanomaterials to improve biosensing characteristics.



Jai S. Tawale earned his M.Sc. in 2006 from Nagpur University in Physics. He now works as a technical assistant at National Physical Laboratory (CSIR), New Delhi. His current research interests are nanostructure materials and characterization.



Dr. B.D.Malhotra received his Ph.D degree in physics from University of Delhi, Delhi, India in 1980. He has published 212 papers, has obtained 9 patents, has edited/co-edited books on biosensors and polymer electronics, and is currently the Scientist G and Head of the Biomolecular Electronics & Conducting Polymer Research Group at the National Physical Laboratory, India. He has research experience of about 25 years in the field of biomolecular electronics and has guided 17 PhD students till date. His current research activities including biosensors, conducting polymers, Langmuir–Blodgett films, self-assembled monolayers nanomaterials and nano bioelectronics, etc.

Accepted Manuscript

Available online at www.pelagiaresearchlibrary.com

Pelagia Research Library

European Journal of Experimental Biology, 2014, 4(6):90-94

ISSN: 2248 –9215
CODEN (USA): EJEBAU

FemA gene in Indian isolates of methicillin resistant *Staphylococcus aureus* – isolation and amplification through real time PCR

Shashank Kr. Singh*[1], Saleha Anwar[2], Hemant Kr. Sharma[2], Upendra Chaudhary[3] and Sunil Kr. Verma*[3]

[1]*Deptt. of Biotechnology, Delhi Technological University, New Delhi, India*
[2]*Dept. of Biosciences, Faculty of Applied Science, Integral University, Lucknow, India*
[3]*Student, Amity Institute of Biotechnology, Amity University, U.P., Lucknow Campus, India*

ABSTRACT

Statphylococcus aureus is a Gram positive bacterium, which is naturally present in nasopharyngeal region of human beings and animals. S. aureus had developed drug resistant capacity to against all penicillin class antibiotics after severe administration since 1941. Firstly, in 1961, Methicillin Resistant Staphylococcus aureus (MRSA) were isolated. In this research, Methicillin Resistant S. aureus (MRSA) were isolated from clinical pus samples. Isolates were grown on Luria Bertani (LB) Agar containing Oxacillin antibiotic by traditional methodologies. Genomic DNA was isolated from the isolates and electrophoresis was performed by using standard criteria. Fem A gene amplification was performed with Real Time PCR and with suitable primers. The amplified gene was produced 510 bp at Agarose Gel Electrophoresis.

Key words: Methicillin Resistant *Staphylococcus aureus (MRSA)* , LB Agar, Real Time PCR, *FemA* gene, Agarose Gel Electrophoresis.

INTRODUCTION

Staphylococcus aureus is one of the most commonly found pathogenic bacteria and is hard to eliminate from the human and animals environment. It is responsible for many nosocomial infections, besides being the main causative agent of food intoxication by virtue of its variety of enterotoxins [**1**]. The toxic shock syndrome of humans and animals is caused by the presence of *S. aureus* **[2]**. It is the commonest of all clinical isolates and responsible for several suppurative types of infections. *S. aureus* is causing a wide variety of diseases including septicemia, pneumonia, wound sepsis, septic arthritis, osteomyelitis and toxic shock syndrome [**3][4]**,carbuncles more serious device and wound related infections, to life threatening conditions, such as bacteremia, necrotizing pneumonia, and endocarditis. *S. aureus* produces different types of virulence factors that facilitate attachment, colonization, cell-cell interactions, immune invasion, and tissue damage [**5**]. They have a differential ability to spread and cause outbreaks in hospitals. However, treatment of these infections has become problematic due to development of methicillin resistance in *S. aureus* isolates. Methicillin resistance first appeared among nosocomial isolates of *S. aureus* in 1961 [**6**]. Worldwide, an estimated 2 billion people carry some form of *S. aureus*, of these up to 53 million (2.7% of carriers) are thought to carry MRSA. As of early 2005, the number of deaths in United Kingdom attributed to

MRSA has been estimated by various sources to lie in the area of 3000 peryear [**7]**. The incidence of methicillin resistant *S. aureus* (MRSA) in India ranges from 30 to70% [**8]**. *S. aureus* is often found passively colonizing human skin and nasal passages. As an opportunistic pathogen, the bacterium can also cause infections that vary widely in their severity and in their susceptibility to antibiotic treatment. This variability is caused by differences in gene content among strains. One source of exposure to novel, potentially more virulent strains of *S. aureus* is recreational swimming areas, since *S. aureus* is readily shed from humans into water [**9]**. Most people are passive carriers of *S. aureus*, which is often found colonizing the nasal passages [**10]**, and in some cases, an infection may arise from self-inoculation of a wound. *S. aureus* infections have been a major problem in hospitals for decades, but the incidence of community-acquired infections has also been increasing [**11][12]**. The type as well as severity often *S. aureus* infection and its response to antibiotic treatment is dictated by the specific suite of virulence and antibiotic resistance associated genes carried by the strain of *S. aureus* causing the infection . There are over 40 virulence-associated genes identified among

various strains of *S. aureus*, many of which are encoded by mobile genetic elements. Over the last few decades, there has been an enormous increase and emergence of *S. aureus* strains **[13]**. The intrinsic resistance to these antibiotics is attributed to the presence of *mecA*, whose product is a 78kDa protein called penicillin binding protein2a [**14]**. Identification of *mec A* in such MRSA strains has led to some knowledge regarding the use of the antibiotic vancomycin [**15]**. The *femA* gene encodes a factor which is essential for methicillin resistance and is universally present in all MRSA isolates. The *femA* gene product, a 48 kDa protein, has been implicated in cell wall metabolism and is found in large amounts in actively growing cultures. Phenotypic methods for detection of methicillin resistant *S. aureus* (MRSA) have been compared with the gold standard which, as of now, is by the detection of *mecA* gene and *femA* gene by polymerase chain reaction (PCR) [**16]**.

MATERIALS AND METHODS

Bacterial strains and culture media: A total of Nine MRSA strains were used in this study. These strains were isolated from pus samples. All strains were stored on 1% Oxacillin containing LB medium. Strains are grown with Brain heart infusion broth and incubated for 12 hrs.

DNA isolation: Total DNA was isolated from 0.5 ml of brain heart infusion broth culture grown 12 hrs for all the MRSA strains used in this study. An aliquot (0.5ml) broth culture was pelleted by centrifugation (5,000 rpm for 5 minutes). The bacterial pellet, resuspended in 300ml of lysis buffer (50mM) Tris Hcl [pH8.0], 100 mM EDTA, 150 mM NaCl, 1% [V/V] (Sodium Dodecyl Sulfate) containing 100 mg of lysostaphin (Sigma Chemical Co., St. Louis, Mo.) and 100 mg of RNase, was incubated at 37.80 C for 30 min. Lysis was achieved by incubation at 37.80 C for 30 min in the presence of 200 mg of Proteinase K. Samples were treated with 1 volume of Phenol – Chloroform - Isoamyl alcohol (25:24:1) and then with 1 volume of Chloroform - Isoamyl alcohol (24:1) prior to precipitation of the aqueous phase in 2 volumes of 95% ethanol – 0.2 M NaCl for 1 h at 2208C. DNA was pelleted by centrifugation (12,500 rpm for 10 min), washed with 80% ethanol, air dried. DNA samples were dissolved in Tris - EDTA buffer (10 mM Tris chloride, 1 mM EDTA [pH 8.0]), and the concentration was determined as micrograms per milliliter according to A260 values. Template DNA in amounts ranging from 10 to 1,000 ng was used in this study.

Polymerase Chain Reaction :The polymerase chain reaction (PCR)is an *in vitro* DNA amplification of target DNA with a pair of primers and a DNA polymerase, resulting in several million fold amplification of the target sequence within few hours. 50µl of DNA sample was taken for the amplification. Then the reaction mixture prepared, which contained 5µl of 10x reaction buffer (500 mM KCl, 15 mM $MgCl_2$, 100 mM Tris HCl pH 8.3,0.1%w/v gelatin). Template DNA was added at a concentration of 200ng/µl. Added 1µl of each primer (Forward Primer **5'**AAAAAAGCACATAACAAGCG**3'** , Reverse primer **5'**GATAAAGAAGAAACGAGCAG**3'**).The primers were used at a final concentration of 100 M. Add 3 µl of 10 mM dNTP mixture. The four deoxyribonucleotide triphosphate (dNTP, dTTP, dGTP, dCTP) were used at a concentration of 100 µl each. To each sample, 1 µl of Taq polymerase (3U/l) was added. The remaining volume made up to with sterile water. Amplification was carried out in a Thermal cycler. Initial denaturation at 94 ^{o}Cfor1 minute followed by 30 cycles, each cycle consisted of denaturation of DNA for 30 seconds at 94 ^{o}C, annealing of the primers for30 seconds at 50 ^{o}C and elongation at 72 ^{o}C. The PCR products were analyzed by gel electrophoresis in a 1% agarose in Tris Acetate buffer (pH 8.3).

Agarose gel electrophoresis: Agarose gel electrophoresis is employed to quickly determine the yield and purity of DNA isolated, or check product of PCR reaction, check progression of restriction enzyme digestion and to size fractionate DNA molecules which then could be eluted from the gel. Cleaned the gel casting apparatus and sealed

both ends of the gel casting tray with an adhesive tape. Prepare 1% agarose gel. Agarose dissolved in 1X TAE buffer. Boil till agarose dissolved completely. Pour the agarose gel solution to the tank when the temperature reaches approximately 55°C. Avoid air bubbles formation. The thickness of the gel should be around 0.5 to 0.9 cm. Keep the gel at room temperature for the agarose to solidify. Remove the comb carefully, ensuring the wells remains intact and peels of the tape from the gel casting tray. Placed the gel in horizontal electrophoresis apparatus containing 1X TAE electrophoresis buffer in the reservoirs. The buffer level should be such that is just covers the agarose gel. 10µl of DNA sample taken and mixed with 3µ l of gel loading dye and loaded into the gel. Then connected the electrophoresis apparatus with 100 V DC current and allowed it to run for 30minutes. Stained the gel with Ethidium Bromide (EtBr) solution of 0.5 µg/ml concentration for 10 minutes. Transfer the gel onto U V transilluminator. Observe the results and note it carefully.

RESULTS AND DISCUSSION

The present study successfully isolated genomic DNA molecules from MRSA isolated strains. Clear bands were seen in gel kept on U V transilluminator. The present study, *femA* gene band showed at 510 b p region. All MRSA isolated strains were produced 510 b p band **(Fig 1).**

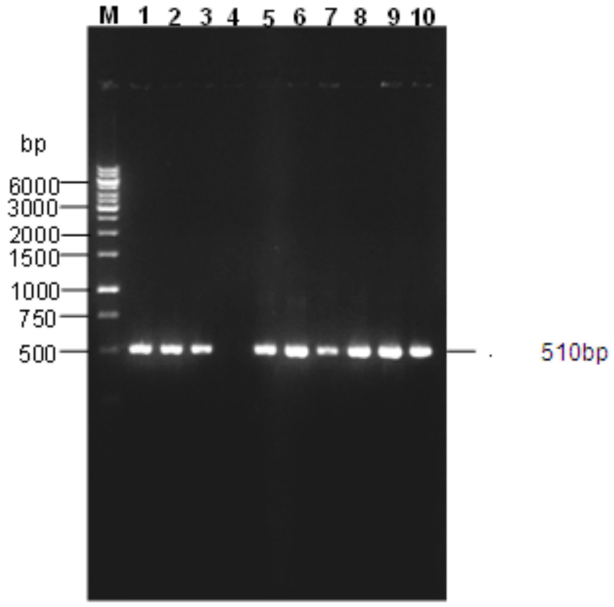


Fig 1 ***Agarose (1%) Gel Electrophoresis showing the PCR amplification of femA gene of MRSA isolates***
(M – Marker; 1, 2, 3, 5, 6, 7, 8, 9 and 10 – MRSA isolates; 4 –Blank)

MRSA now accounts for an important cause of nosocomial infections. MRSA and MSSA are equally pathogenic and capable of causing the same spectrum of nosocomial infections. Initially, there were sporadic reports of methicillin resistance amongst nosocomial *S. aureus* isolates, but later MRSA became a well established hospital acquired pathogen with few reports on increased prevalence of community acquired MRSA with different factors compared to the earlier investigations from Detroit which first reported the community acquired MRSA. The epidemiology of MRSA is also changing over the past few decades. Nearly 51.6% of *S .aureus* isolates were found to be resistant to methicillin in the present study while in the previous studies the incidence was found to be 32.8% in 1994, 24 % in 1996 , 32 % in 1997 . This implies that the incidence of infection by MRSA isolates keeps changing every year and it is on the rise when compared to last few years. Worldwide, an estimated 2 billion people carry some form of *S.*

aureus, of these up to 53 million (2.7% of carriers) are thought to carry MRSA. As of early 2005, the number of deaths in United Kingdom attributed to MRSA has been estimated by various sources to lie in the area of 3000 per year.

The resistance of MRSA to a wide range of anti-bacterial is well documented. This makes the empirical use of antibacterial effective against MRSA imperative. Vancomycin has been clearly shown to be the drug of choice for the treatment of MRSA infections. The virulence genes *mecA* and *femA* were examined because they are believed to be the major contributors to methicillin resistance. Previous studies have assessed the feasibility of the PCR approach either for the identification of *S. aureus* strains or for intrinsic methicillin resistance on the basis of *femA* gene amplification. A probe corresponding to the 39 - end of amplified fragments of the *femA* determinant hybridized to the PCR products of DNAs of *S. aureus* isolates, confirming the *femA* gene origins of these amplified products . Analysis of the *femA* product indicated that this protein is associated with the expression of high levels of methicillin resistance without affecting PBP-2 production. The significance of the *femA* genes in the mechanism of methicillin resistance was supported by the demonstration that an *S. aureus* strain with *femA* gene inactivated lost the methicillin resistance trait, but with the transduction of *femA* genes restored the resistance. Another biochemical analysis suggested that *femA* product may be involved in the metabolism of cell wall synthesis.

CONCLUSION

The present study described in this paper provides detailed information about MRSA and *fem A* gene. *fem A* is one of the toxin producing gene. This gene is very essential to give methicillin resistant nature of MRSA strains. This PCR assay will help to provide the information required for appropriate therapy and infection control during outbreaks of MRSA. It is important to recognize that this technique only can be used to identify strains harboring the toxin genes and is independent of the expression and secretion of the toxin. To verify toxin production by any given isolate, time- and labor-intensive immunological methods may be used to detect the excreted toxins. Considering the low cost and much shorter time required to detect the genes of MRSA by multiplex PCR, this is to be a powerful tool for studying the genotypes of staphylococcal isolates. This procedure was specially developed to fit into the daily work pattern of a routine clinical laboratory, since genotypic detection of drug resistance and the presence of toxin genes is becoming an important component of the diagnostic inventory of such laboratories.

Acknowledgement
We are extremely indebted and thankful for constant support and kind guidance to Ms. Saleha Anwar and Mr. Hemant Kumar Sharma, Department of Biosciences, Faculty of Applied Science, Integral University, Lucknow, U.P., INDIA for their inspiring and innovative thoughts and ideas which helped us a lot in this research and in whole of my academic career. God bless them both.

REFERENCES

[1] Iandolo JJ, *Annu Rev Microbiol,* ***(*1989*)*** 43:375-402.
[2] Schlievert PM, *Journal of Infect Disease,* ***(*1983*)***167:997-1002
[3] Boyd EF and Brussow H, *Trends in Microbiol,* ***(*2002*)***10: 521-529.
[4] Moore PCL and Lindsay JA, *Journal of Clini Microbiol,* ***(*2001*)*** 39: 2760-2767
[5] Matthew TG, Edward HJ, Jodi FA, Sharon LJ, Peacock, Nicholas, Day PJ, Enright MC, Foster TJ, Moore CE, Hurst L, Atkin R, Barron A, Bason N, Bentley SD, Chillingworth C, Chilling worth T, Churcher Cl, Clark L, Corton C, Cronin A, Doggett J , Dowd L, Feltwell T, Hance Z, Harris B, Hauser H, Holroyd S, Jagels K, James KD, Lennard N, Line A, Mayes R, Moule S, Mungall K, Ormond D, Quail M A, Rabbinowitsch E, Rutherford K, Sanders M, Sharp S, Simmonds M, Stevens K, Whitehead S, Barrell BG, Brian G, Sprattand Parkhill J, *Proc of Nat. Acad Sci, U S A,* ***(*2004*)*** 101(26): pp 9786–9791.
[6] Barber M, *Journal of Clin Pathol,****(*1961*)*** 14:385-93.
[7] Johnson AP, Pearson A and Duckworth G, *Journal of Antimicrobial Chemo ther,* ***(*2005*)***, 56(3): 455-462.
[8] Verma S, Joshi S, Chitnis V, Hemwani Nand Chitnis D, *Indian Journal of MedSci,* ***(*2000*)*** 54:535-40.
[9] Charoenca N and Fujioka RS, *Water Sci and Technol,* ***(*1993*)*** 27: 283-289.
[10] Kluytmans J, Belkum VA, and Verbrugh H, Nasal carriage of *Staphylococcus aureus*: epidemiology, underlying mechanisms, and associated risks. *Clin Microbiol Rev,* ***(*1997*)*** 10 (3): 505–520.
[11] Chambers HF, The changing epidemiology of *Staphylococcus aureus*? *Emerg Infect Dise,* ***(*2001*)*** 7: 178-182
[12] Haley RWAW, Hightower RF, Khabbaz C, Thorsberry WJ, Martone JR and HughesAJM, *Ann Intern Med,* ***(*1982*)*** 97:297-308.
[13] Hartman BJ and Tomasz A, *Journal of Bacteriol,* ***(*1984*)*** 158:513-516.
[14] Chambers HF, *Clin Microbiol Rev,* ***(*1997*)*** 10:781-791.
[15] Johnson S, Dominique K and Labischinski H, *FEMS Microbiol Lett,* ***(*1995*)*** 132:221-228.

[16] Mathews AA, Thomas M, Appalaraju Band Jayalakshmi J, *Indian Journal of Pathol Microbiol*, ***(*2010*)*** 53:79-82.

Scientific Online

OPEN JOURNAL OF OCEAN AND COASTAL SCIENCES
In Press

OPEN JOURNAL OF OCEAN AND COASTAL SCIENCES

Hydrodynamic Stability of Complaint Pipe for Normal Complaince

S. Anbukumar*, Munendra Kumar

Department of Civil Engineering, Delhi Technological University, Delhi – 110042, India
***Corresponding author**:

Abstract:
In this paper the hydrodynamic stability of a complaint pipe carrying fluid is analyzed by considering Hagen-Poiseuille flow through a visco-elastic pipe with an outer rigid shroud and an interface intervention. The interface plate used here allows only normal motion to pass through to the solid side. This interface plate is held by light springs at the ends and the springs are so stretched in tension that the plate does not allow mean tangential displacement of the solid side. By the use of the interface plate, the shear stress and the tangential motion from the fluid side are prevented from transmitting to the visco-elastic solid side. The neutral stability curves for different values of the compliance parameter (Γ) and of the solid to fluid viscosity ratio are examined. And it was found that the wall dissipation tends to damp most classes of modes.

Keywords:
Pipe Flow Stability; Normal Compliance; Neutral Curves; Interface Interventions; Visco-elastic Pipe; Static Divergence Modes

1. INTRODUCTION

For a fluid flow in a complaint pipe, by the use of the interface plate, shear stress from the fluid-side and tangential motion from the fluid-side, are not transmitted to the visco-elastic solid-side. Thus, there is only a normal compliance and the system is analogous to a conventional plate spring model which is commonly used in channel flow and boundary layer problems. If there is no intervention as above, there will be finite mean deformation of the visco-elastic medium. In that case, as pointed out by Gkanis and Kumar [1, 2] and Chokshi and Kumaran [3, 4], the equations for the fluctuations of the visco-elastic medium no longer remain linear. This is typically seen by applying the neo-Hookean model for the visco-elastic medium. In our cases with interface interventions, there is no finite mean stress in the visco-elastic medium and the linear visco-elastic model is valid. Therefore, the present problem considers stability of compliant pipe flow in the circumstances where the linear visco-elastic model is valid. The problem with the plate intervention is called herein the "only normal compliance" problem or the N problem. Generally, the fluid flow in a compliant pipe form occurs in natural systems, like flow of blood and other fluids in biological systems. Such flows also occur in industrial applications like flow through hollow fibers, reactors, membranes.

There are two types of pipes which are found in nature, viz. collapsible and non-collapsible pipes. The collapsible pipe is an elastic tube, which, when subjected to a large enough external pressure, has its cross-section deformed significantly in both shape and area; thereby becoming so pliable that flow-induced internal pressure changes can couple strongly with the wall deformation. On the other hand non-collapsible pipes usually have a rigid outer shroud,

or other artifices, and do not undergo any significant flow-induced change in geometry.

The present work considers the non-collapsible pipe flow problem. The interest in this problem of stability of laminar flow over a compliant surface was created following Kramer's [5–8] extensive studies on dolphins and his reported experiments on drag reduction on a body of revolution covered with a designed compliant coating. Kramer called this technique "stabilization by distributed damping", his basic hypothesis being that the viscosity of the substrate fluid, within the compliant coating, would damp out any possible laminar instabilities in the flow. This in turn would lead to delay in transition, and thus cause reduction in drag.

Based on the post Kramer works of Carpenter [9, 10], Carpenter, Davies and Lucey [11] and Carpenter, Lucey and Davies [12], one can say that compliant surfaces could play an important role in controlling laminar to turbulent transition in plane and axisymmetric boundary layer flows. In fact, the challenge here is to find a coating, with optimum physical properties, to achieve the desired goal. The salient results, from an engineering viewpoint, are given by Carpenter and Garrad [13, 14].

The stability of Poiseuille flow in a rigid pipe of circular cross-section has been of continuing interest since the classical experiment of Reynolds [15]. The first fully convincing numerical work on the stability of pipe flow to infinitesimal axisymmetric disturbances in fully developed pipe flow was by Davey and Drazin [16]. They have shown that the flow is stable to infinitesimal axisymmetric disturbances at all Reynolds numbers R and all axial wave numbers α. Their result was confirmed by the important numerical studies of Garg and Rouleau [17] and Salwen and Grosch [18]. Also the results obtained by Gill [19] by asymptotic methods, compare satisfactorily with the numerical studies. Similarly the works of Salwen and Grosch [18] and Garg and Rouleau [17] shown that, the least stable mode for the axisymmetric and the non-axisymmetric disturbances are the centerline modes (*i.e.* with phase speed close to the centerline mean velocity). Despite the stability predicted based on linear theory, Sen, Venkateswarlu and Maji [20] have shown that non-linearity could destabilize pipe flow.

The stability of flow in a non-collapsible / flexible tube was analyzed in a series of papers by Kumaran [21–27], Kumaran and coworkers [25, 26] and Shankar and Kumaran [28] using linear stability analysis. Discussions from here on confined only to non-collapsible pipes and it was found that compliant pipe flow is generally *unstable*. In fact Kumaran found different types of instabilities, for different parametric limits; like, viscous or low Reynolds number instability, low wave number instability, inviscid or high Reynolds number instability, and, wall-mode instability at intermediate Reynolds numbers.

Hamadiche and Gad-el-Hak [29] also studied axisymmetric and non-axisymmetric instabilities in a flexible tube and found instabilities both at low R and at high R. It needs to be mentioned that Kumaran and coworkers, and Hamadiche and Gad-el-Hak, all studied the N +T problem. Only Gajjar, Gibson and Sen [30], and particularly Gibson [31]), studied the N problem, using the Sen and Arora [32] method. The present work looks N problems in compliant pipe flow for the axisymmetric disturbances.

2. FORMULATION

In this study, flow though an incompressible visco-elastic pipe flow is considered for linear stability as shown in the Fig-1. Here a system where a visco-elastic pipe is coupled with Hagen-Poiseuille flow was considered. Infinitesimal disturbances of the combined fluid-solid system are studied for the non-axisymmetric, n = 1, 2, 3, 4 modes. The general non-axisymmetric, and the axisymmetric, problems are respectively mathematically three-dimensional (3-D), and mathematically two-dimensional (2-D) problems.

For the fluid-side,$\hat{v}$, $\hat{w}$ and $\hat{u}$ are the disturbance velocity components in the radial, r, azimuthal, θ, and axial, x, directions respectively, and $\hat{p}$ is the disturbance pressure. Also $\bar{u}$ is the laminar mean velocity given by $\bar{u} = 1 - r^2$.

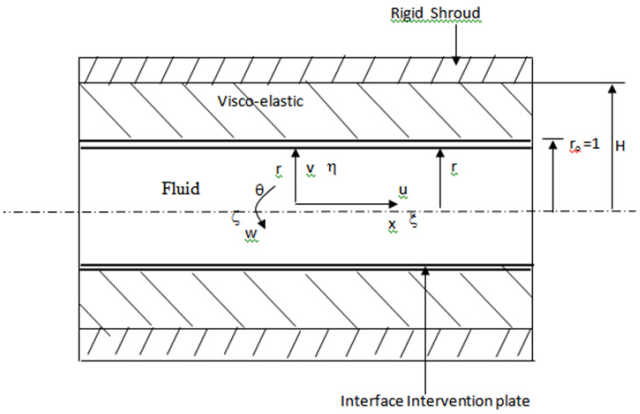


Figure 1. Model of the only normal N compliance problem.

The length and velocity scales in the problem are the radius of the pipe r_o^* and the centerline maximum mean velocity V, and all quantities are normalized using r_o^* and V. The Reynolds number in the problem is$R = V r_o^*/\nu$, where, ν is the kinematic fluid viscosity.

For the solid-side, the disturbance displacements are$\hat{\eta}$, $\hat{\zeta}$ and $\hat{\xi}$ respectively in the r, θ and x directions and $\hat{p}_s$ is the pressure in the solid-side. Also, $H = r_s^*/r_o^*$, where r_s^* is the dimensional outer radius of the visco-elastic wall surrounding the fluid. Thus, the centerline of the pipe is at $r = 0$, the solid-fluid interface (sometimes also called "wall" with subscript 'w' as a carryover from past literature) is at $r = 1$, and, the outer rigid shroud covering the visco-elastic layer is at $r = H$.

2.1 The disturbance equations for the fluid-side

For linear stability analysis, the disturbances in the form of Fourier modes are introduced in the fluid velocity field in the linearised Navier-Stokes and continuity equations, as follows:

$$(\hat{u}, \hat{v}, \hat{w}, \hat{p}) = [u(r), v(r), w(r), p(r)]\ \exp[i\{n\theta + \alpha(x - ct)\}] \tag{1}$$

where, u, v, w and p are the respective amplitude functions, and are functions of r only, corresponding respectively to $\hat{u}$, $\hat{v}$, $\hat{w}$ and $\hat{p}$. Also α and n are respectively the axial and azimuthal wave numbers, with n being an integer with values n = 0, 1, 2, 3, 4 ..... Also, n = 0 corresponds to the 2-D axisymmetric case and n = 1, 2, 3, 4 ..... correspond to the 3-D non-axisymmetric cases. The $c = c_r + \alpha.c_i$ is the complex phase speed with c_r as the real phase speed and αc_i as the amplification factor of disturbances. And, $\omega = \alpha c$ is the complex circular frequency in time. The imaginary part of the wave speed c_i is positive for unstable disturbances, negative for stable disturbances and zero for neutral disturbances.

The linearised Navier-Stokes and continuity equations are given as follows:

u-momentum:

$$i\alpha(\bar{u} - c)u + \bar{u}'v = -i\alpha p + \frac{1}{R}\left[u'' + \frac{u'}{r} - \left(\alpha^2 + \frac{n^2}{r^2}\right)u\right] \tag{2}$$

v-momentum:

$$i\alpha(\bar{u}-c)v = -p' + \frac{1}{R}\left[v'' + \frac{v'}{r} - \left(\alpha^2 + \frac{n^2+1}{r^2}\right)v - \frac{2niw}{r^2}\right] \tag{3}$$

w-momentum:

$$i\alpha(\bar{u}-c)w = -\frac{inp}{r} + \frac{1}{R}\left[w'' + \frac{w'}{r} - \left(\alpha^2 + \frac{n^2+1}{r^2}\right)w + \frac{2niv}{r^2}\right] \tag{4}$$

continuity:

$$i\alpha u + v' + \frac{v}{r} + i\frac{nw}{r} = 0 \tag{5}$$

In the above (2) to (5), and subsequently hereinafter, primes ($'$) will denote differentiation with respect to r.

2.2 The disturbance equations for the visco-elastic material (solid-side)

The Navier equations and continuity equation for the disturbance displacements, in the incompressible visco-elastic medium, *i.e.* with Poisson's ratio 0.5, are given as follows:

ξ - *displacement:*

$$\frac{\partial^2\hat{\xi}}{\partial t^2} = -\frac{\partial\hat{p}_s}{\partial x} + \frac{\hat{K}}{R}\left[\frac{\partial^2\hat{\xi}}{\partial x^2} + \frac{\partial^2\hat{\xi}}{\partial r^2} + \frac{1}{r}\frac{\partial\hat{\xi}}{\partial r} + \frac{1}{r^2}\frac{\partial^2\hat{\xi}}{\partial\theta^2}\right] \tag{6}$$

η - *displacement*:

$$\frac{\partial^2\hat{\eta}}{\partial t^2} = -\frac{\partial\hat{p}_s}{\partial r} + \frac{\hat{K}}{R}\left[\frac{\partial^2\hat{\eta}}{\partial x^2} + \frac{\partial^2\hat{\eta}}{\partial r^2} + \frac{1}{r}\frac{\partial\hat{\eta}}{\partial r} + \frac{1}{r^2}\frac{\partial^2\hat{\eta}}{\partial\theta^2} - \frac{\hat{\eta}}{r^2} - \frac{2}{r^2}\frac{\partial\hat{\zeta}}{\partial\theta}\right] \tag{7}$$

ζ - *displacement*:

$$\frac{\partial^2\hat{\zeta}}{\partial t^2} = -\frac{1}{r}\frac{\partial\hat{p}_s}{\partial\theta} + \frac{\hat{K}}{R}\left[\frac{\partial^2\hat{\zeta}}{\partial x^2} + \frac{\partial^2\hat{\zeta}}{\partial r^2} + \frac{1}{r}\frac{\partial\hat{\zeta}}{\partial r} + \frac{1}{r^2}\frac{\partial^2\hat{\zeta}}{\partial\theta^2} - \frac{\hat{\zeta}}{r^2} + \frac{2}{r^2}\frac{\partial\hat{\eta}}{\partial\theta}\right] \tag{8}$$

continuity:

$$\frac{\partial\hat{\xi}}{\partial x} + \frac{\partial\hat{\eta}}{\partial r} + \frac{\hat{\eta}}{r} + \frac{1}{r}\frac{\partial\zeta}{\partial\theta} = 0 \tag{9}$$

In the above equations (6) to (9), $\hat{K}$ is the visco-elastic parameter which can be written as $\hat{K} = \hat{K}_r + i\hat{K}_i$, that is:

$$\hat{K} = \tilde{K} + \mu_r\frac{\partial}{\partial t} \quad or \quad \frac{\hat{K}}{R} = \frac{\tilde{K}}{R} + \frac{\mu_r}{R}\frac{\partial}{\partial t} \tag{10a, b}$$

Kumaran (1995) defined a compliance parameter Γ as $\Gamma = \sqrt{\rho V^2/G}$, where V is the centerline mean velocity of the fluid, ρ is the density of the visco-elastic material and G is the shear modulus of the visco-elastic material. Γ is an inverse measure of the relative stiffness of the wall coating.

If we compare $\hat{K}$ with the parameter Γ introduced by Kumaran:

$$\frac{\hat{K}}{R} = \frac{1}{\Gamma^2} + \frac{\mu_r}{R}\frac{\partial}{\partial t} \text{ and } \frac{\tilde{K}}{R} = \frac{1}{\Gamma^2} \tag{11}$$

Here$\mu_r = \mu_s/\mu_f$, where μ_r is the viscosity ratio, and, μ_s and μ_f are respectively the viscosities for the solid and fluid sides.

By introducing$\frac{\partial}{\partial t} \rightarrow -i\alpha c$, and taking$\hat{K} \rightarrow K$, with $K = K_r + iK_i$:

$$K_r = \frac{R}{\Gamma^2} + \alpha\mu_r c_i = \tilde{K} + \alpha\mu_r c_i \;;\; K_i = -\alpha\mu_r c_r \tag{12a, b}$$

Similarly, as in the case of the fluid-side, the disturbances in the form of Fourier modes are introduced for the wall displacement field for the solid-side as:

$$(\hat{\xi},\ \hat{\eta}, \hat{\zeta}, \hat{p}_s) = [\xi(r),\ \eta(r), \zeta(r), p_s(r)]\ \exp[i\{n\theta + \alpha(x - ct)\}], \tag{13}$$

where, ξ, η, ζ and p_s are the respective amplitude functions for $\hat{\xi}$, $\hat{\eta}$, $\hat{\zeta}$ and $\hat{p}_s$.

Inserting the equation for the solid displacement eq. (13) into eqs. (6)-(9), one gets the following equations:

ξ- displacement:

$$-\alpha^2 c^2 \xi = -i\alpha p_s + \frac{K}{R}\left[\xi'' + \frac{\xi'}{r} - (\alpha^2 + \frac{n^2}{r^2})\,\xi\right] \tag{14}$$

η- displacement:

$$-\alpha^2 c^2 \eta = -p_s' + \frac{K}{R}\left[\eta'' + \frac{\eta'}{r} - (\alpha^2 + \frac{n^2+1}{r^2})\,\eta - \frac{2ni\zeta}{r^2}\right] \tag{15}$$

ζ- displacement:

$$-\alpha^2 c^2 \zeta = -\frac{inp_s}{r} + \frac{K}{R}\left[\zeta'' + \frac{\zeta'}{r} - (\alpha^2 + \frac{n^2+1}{r^2})\,\zeta - \frac{2ni\eta}{r^2}\right] \tag{16}$$

continuity:

$$i\alpha\xi + \eta' + \frac{\eta}{r} + \frac{in\zeta}{r} = 0. \tag{17}$$

2.3 Boundary conditions for the normal compliance problem

The boundary conditions for the normal compliance problem, for different azimuthal wave numbers n, are given below. Also we know that for the axisymmetric case, $n = 0$; $w(r) \equiv 0$ and $\zeta(r) \equiv 0$.

a. At the Centerline of the pipe, (ie., at $r = 0$):

for $n = 0$:

$$u'(0) = 0, \quad v(0) = 0\,. \tag{18}$$

for $n = 1$:

$$u(0) = 0,\ \ v + iw = 0,\ \ v'(0) = 0\ \ (or)\ \ w'(0) = 0) \tag{19}$$

for $n > 1$:

$$u(0) = 0, \quad v(0) = 0, \quad w(0) = 0 \tag{20}$$

b. At the Outer rigid shroud of the pipe (ie., at r =H):

At the outer surface of the visco-elastic pipe, there is a rigid shroud. Hence at $r = H$ the boundary conditions will be:

$$\xi(H) = 0, \quad \eta(H) = 0, \quad \zeta(H) = 0 \tag{21}$$

c. At the Fluid-solid interface:

At the interface, again linearised with respect to $r = 1$, the boundary conditions are given by the continuity of velocities and stresses. Since the plate has no in-plane motion, therefore no in-pane motion is transmitted to the solid-side. This, along with the no-slip condition, and also continuity of normal velocity in the fluid and the solid side, give the following:

$$u_w + \eta_w \bar{u}_w' = 0 \ , \ v_w = -i\alpha c \eta_w \ , \ w_w = 0 \tag{22}$$

As far as the transmitted stresses at the interface are concerned, due to the intervention of the plate, no in-plane stresses, viz. τ_{rx}, $\tau_{r\theta}$ are transmitted to the solid-side. Thus only the normal stress is transmitted. This gives:

$$\sigma_{rr} = \tau_{rr} \ , \ (orverynearly) \ p_{wf} = p_{ws} \ , \ \sigma_{rx} = 0 \ , \ \sigma_{r\theta} = 0 \tag{23}$$

Here, p_{wf} and p_{ws} are respectively the interfacial pressure for the fluid-side and the solid-side.

3. NUMERICAL METHODS

In the present work, the differential equations are manipulated to get two coupled equations in u, v for the fluid-side, and two coupled equations inξ, η for the solid-side for the non-axisymmetric cases. For the 2-D axisymmetric case corresponding to $n = 0$, the equations can be manipulated to get a fourth-order ordinary differential equation for $v = v(r)$ for the fluid-side, and a fourth-order ordinary differential equation for $\eta = \eta(r)$ for the solid-side.

Therefore, the basic set of differential equations for the disturbances are discretised to matrix form as follows:

$$[A_{IJ}]\,[\Gamma_J] = [P_I], I, J = 1, 2, 3, 4, ..(2N+2), \tag{24}$$

where, 'N' is the number of intervals in the finite-difference solution and $[A_{IJ}]$ is a coefficient matrix of size (2N+2) (2N+2) for the non-axisymmteric case. Also the vector Γ_J consists of u_j, v_j each of size 1 × (N+1), for the fluid-side, and similarly it consists of ξ_j, $\eta_j$each of size 1 × (N+1) for the solid-side. For the 2-D axisymmetric case, the size of $[A_{IJ}]$ is (N+1) (N+1). Again there are two sets of $[A_{IJ}]$ one each respectively for the fluid-side and the solid-side. And the vector Γ_J respectively consists of $v_j$for the fluid-side and η_j for the solid-side, each of size 1 (N+1). The eigenvalue problem is solved by matching the interface boundary conditions.

4. RESULTS AND DISCUSSIONS

The force-momentum balance method is the classical method of solving a combined fluid-solid stability problem. In this section, the neutral stability curves are drawn for the N problem, for the axisymmetric (n=0) and non axisymmetric (n=1,2,3,4...) modes.

4.1 The N problem for the visco-elastic wall

This problem has not been studied before by other workers, except for Gibson[31]. Gibson studied the normal compliance problem by using the Sen and Arora[32] method. Gibson's work does not describe neutral curves, and is based on a kinematic compliance parameter.

a. Axisymmetric modes (n=0)

The effect of wall compliance Γ and the effect of wall damping $\mu_r$for axisymmetric modes for normal compliance problem are discussed below:

(i) Effect o wall compliance Γ

Figure 2 shows the neutral curves for different value of compliance parameter for $n = 0$ modes. In this case, $\mu_r = 0, H = 2$ are taken. It is observed from **Figure 2** that area of neutral curves increases as the value of compliance parameter Γ is increased *i.e.* the instability of normal modes are increased for increasing the value of Γ. It is also found that the normal instability is higher for lower values of Reynolds number R. So, compliant pipe flow is more unstable as compared to rigid pipe flow. The instability of compliant pipe flow is reducing for higher values of Reynolds number R as seen in the **Figure 2**. From the Reynolds experiment, it is found that the rigid pipe flow is more stable for lower R and is unstable for higher values of R.

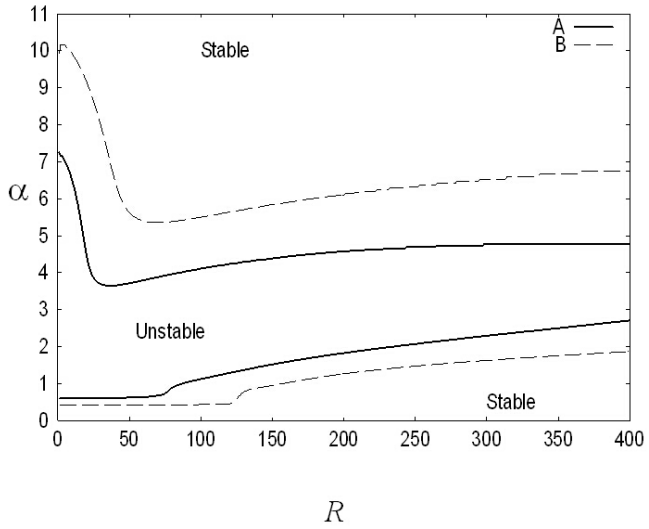


Figure 2. Neutral stability curves for different Γ for the N, n = 0 modes, $\mu_r = 0$. 'A' is for Γ = 6, 'B' is for Γ = 8.

(ii) Effect of wall damping μ_r

Next we look at the effect of $\mu_r$for the $n = 0$ modes (with $H = 2$) for Γ =6. **Figure 3** shows the influence of μ_r in

the (α, R)-plane and it is seen that μ_r has very small influence in the lower values of R. So, a class C mode exists in this region. This is further confirmed in **Figure 4** where the same neutral curves are plotted in the (c_r, R)-plane. Here, the upper and lower limbs do a flip flap between **Figure 3** and **Figure 4**, and also static divergence (SD) modes are seen to exist. It is also observed from **Figure 3** that the instability of normal modes are decreased for the higher values of $\mu_r$for intermediate to higher value of Reynolds number R.

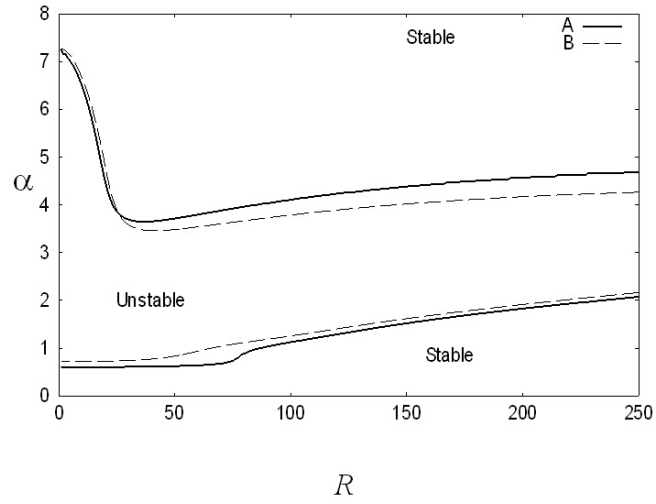


Figure 3. Neutral stability curves for different μ_r for the N, n = 0 modes. 'A' is for $\Gamma = 6$, $\mu_r = 0$, 'B' is for $\Gamma = 6$, $\mu_r = 0.1$.

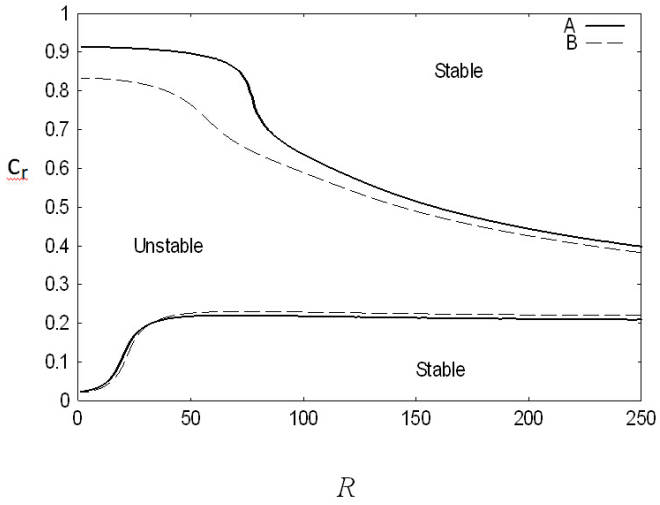


Figure 4. Neutral curves c_r versus R for different μ_r for the N, n = 0 modes. 'A' is for $\Gamma = 6$, $\mu_r = 0$, 'B' is for $\Gamma = 6$, $\mu_r = 0.1$.

b. Non-axisymmetric modes (n= 1,2,3,4)

The effect of wall compliance Γ and the effect of wall damping $\mu_r$for non-axisymmetric modes n= 1,2,3,4 for normal compliance problem are discussed below:

(i) Effect of wall compliance Γ

Figure 5 to **Figure 8** show the neutral curves for different value of compliance parameter Γ for n = 1,2,3,4 modes.

In these cases, $\mu_r = 0$, $H = 2$ are taken. It is observed from these figures that the instability of normal compliance modes have marginal effect of Γ.

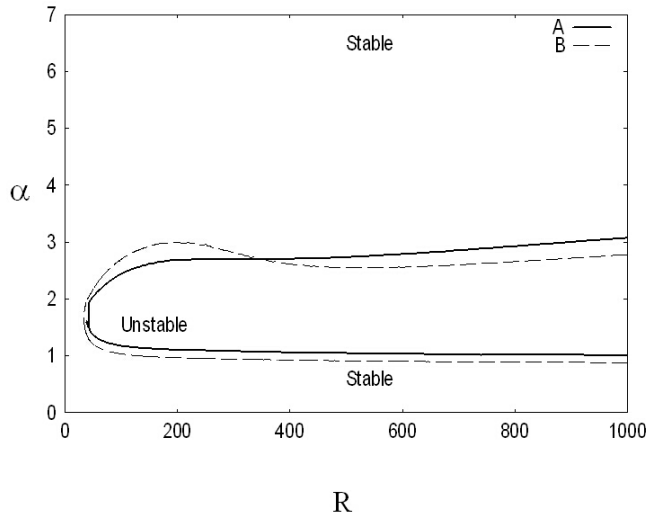


Figure 5. Neutral stability curves for different Γ for the N, n = 1 modes. 'A' is for Γ = 6, 'B' is for Γ = 7.

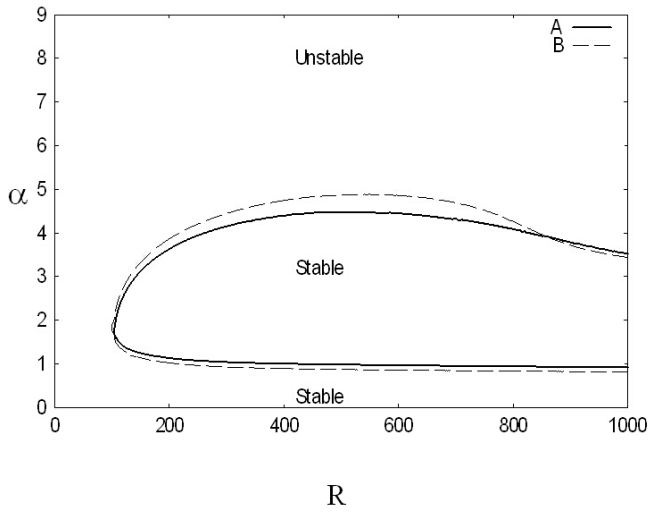


Figure 6. Neutral stability curves for different Γ for the N, n = 2 modes. 'A' is for Γ = 7, 'B' is for Γ = 8.

(ii) Effect of wall damping μ_r

Figure 9 to **Figure 11** show the effect of μ_r in the (α, R)-plane for n = 1,2,3 modes. **Figure 9** shows the effect of $\mu_r$for n=1 modes and Γ=7. It is found that the instability of normal modes are decreased for increasing the value of μ_r *i.e.* higher values of $\mu_r$increases the rigidity. It means that the rigid pipe flow is more stable than the compliant pipe flow. **Figure 10** shows the neutral curve for n=2 modes and Γ=7. It is seen that effect of μ_r is very less in lower limb of the neutral curve and effect of μ_r is very higher for upper limb of neutral curve for lower value of R. Again, it is found that the instability of compliant pipe flow is decreased for increasing the value of μ_r. **Figure 11** shows the neutral curve in (α, R)-plane for n=3 modes and Γ=8. It is found that the effect of μ_r is higher for lower value of R

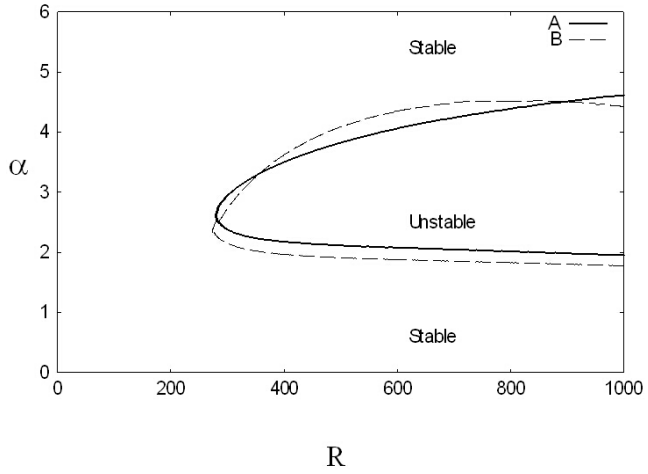


Figure 7. Neutral stability curves for different Γ for the N, n = 3 modes. 'A' is for Γ = 8, 'B' is for Γ = 9.

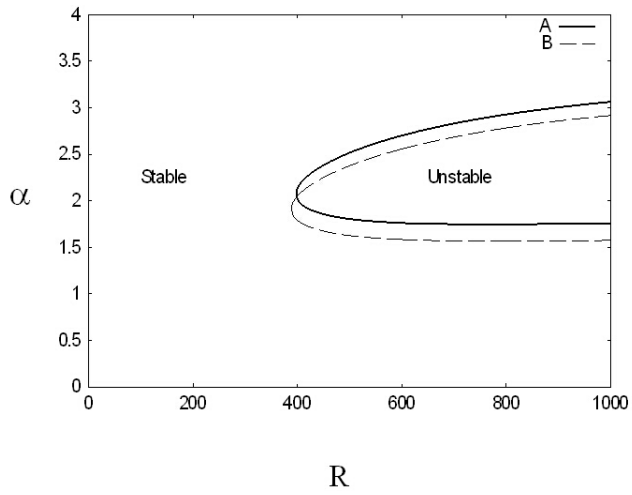


Figure 8. Neutral stability curves for different Γ for the N, n = 4 modes. 'A' is for Γ= 8, 'B' is for Γ = 9.

and is less for higher value of μ_r. It is also concluded that the higher value of μ_r increases the stability of compliant pipe flow.

5. CONCLUSIONS

From the above discussions based on N problems, the following conclusions can be drawn both for the axisymmteric and the non-axisymmteric disturbances.

After looking through all the results discussed above, the one conclusion that emerges most prominently is that compliant pipe flow is very unstable at all ranges of the Reynolds number R due to one or other mechanism. It is unstable as low R, intermediate R, high R, low α, intermediate α and high α. Further, it exhibits static divergence, SD, instability at low R and intermediate α Most of the instabilities are class B except for the SD instability which is

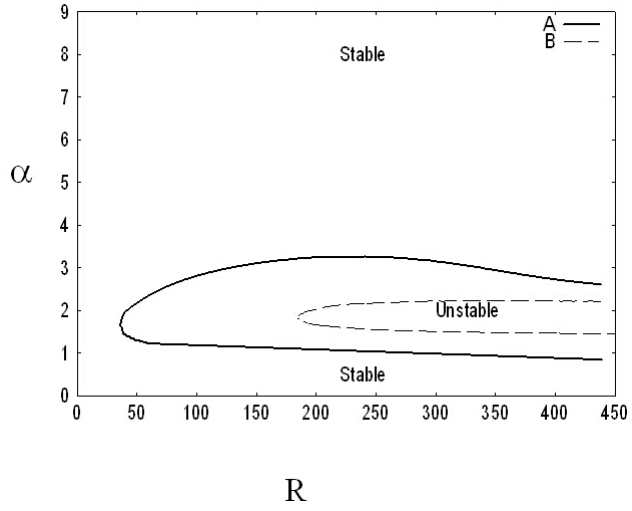


Figure 9. Neutral stability curves for different μ_r for the N, n = 1 modes. 'A' is for $\Gamma = 7$, $\mu_r = 0$ 'B' is for $\Gamma = 7$, $\mu_r = 0.1$.

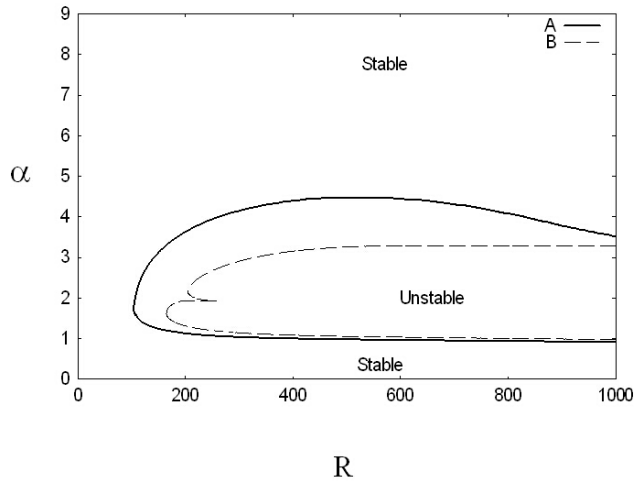


Figure 10. Neutral stability curves for different μ_r for the N, n = 2 modes. 'A' is for $\Gamma = 7$, $\mu_r = 0$, 'B' is for $\Gamma = 7$, $\mu_r = 0.2$.

class C.

It is also concluded that the higher value of compliance parameter Γ increases the instability of compliant pipe flow. *i.e.* higher the Γ more the flexibility of surface. The higher value of $\mu_r$decreases the instability of the compliant pipe flow *i.e.* higher the value of μ_r more the rigidity of surface.

References

[1] V. Gkanis and S. Kumar, "Instability of creepting Couette flow past a neo-Hookean solid," *Physics of Fluids (1994-present)*, vol. 15, no. 10, pp. 2864–2871, 2003.

[2] V. Gkanis and S. Kumar, "Stability of pressure-driven creeping flows in channels lined with a nonlinear elastic

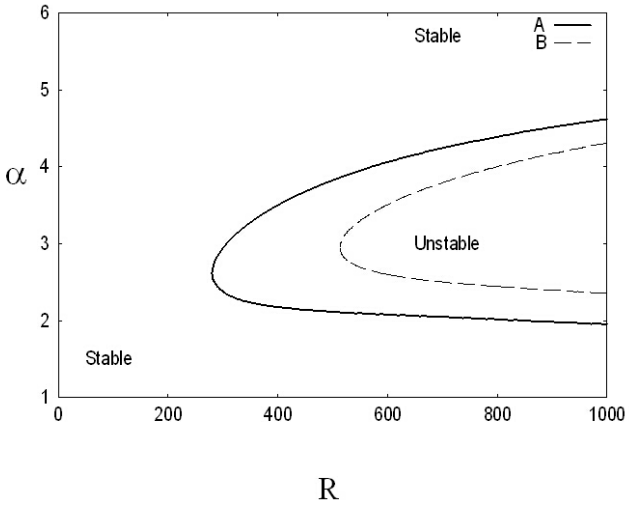


Figure 11. Neutral stability curves for different μ_r for the N, n = 3 modes. 'A' is for $\Gamma = 8$, $\mu_r = 0$ 'B' is for $\Gamma = 8$, $\mu_r = 0.3$.

solid," *Journal of Fluid Mechanics*, vol. 524, pp. 357–375, 2005.

[3] P. Chokshi and V. Kumaran, "Stability of the flow of a viscoelastic fluid past a deformable surface in the low Reynolds number limit," *Physics of Fluids*, vol. 19, no. 10, p. 104103, 2007.

[4] P. Chokshi and V. Kumaran, "Weakly nonlinear analysis of viscous instability in flow past a neo-Hookean surface," *Physical Review E*, vol. 77, no. 5, p. 056303, 2008.

[5] M. O. Kramer, "Boundary-layer stabilization by distributed damping," *Journal of the Aeronautical Sciences*, vol. 24, no. 6, pp. 459–460, 1957.

[6] M. O. Kramer, "Boundary layer stabilization by distributed damping," *Journal of Aero/Space*, vol. 27, p. 69, 1960.

[7] M. O. Kramer, "Boundary layer stabilization by distributed damping," *Journal of the American Society for Naval Engineers*, vol. 74, pp. 341–348, 1960.

[8] M. O. Kramer, "Hydrodynamics of dolphin, in advance Hydro-science," vol. 2, pp. 110–130, 1965.

[9] P. W. Carpenter, "Status of transition delay using compliant walls," *Viscous Drag Reduction in Boundary Layers*, vol. 123, pp. 79–113, 1990.

[10] P. W. Carpenter, "Current status of the wall compliance for Laminar flow control," *Experimental Thermal and Fluid science*, vol. 16, no. 1, pp. 133–140, 1998.

[11] P. W. Carpenter, C. Davies, and A. D. Lucey, "Hydrodynamics and compliant walls: Does the Dolphin have a secret?," *Current Science*, vol. 79, no. 6, pp. 758–765, 2000.

[12] P. W. Carpenter, A. D. Lucey, and C. Davies, "Progress on the use of compliant walls for Laminar flow control," *Journal of Aircraft*, vol. 38, no. 3, pp. 504–512, 2001.

[13] P. Carpenter and A. Garrad, "Hydrodynamic stability of flow over Kramer type compliant surfaces, Part 1, Tollmien Schlichting instabilities," *Journal of Fluid Mechanics*, vol. 150, pp. 465–510, 1985.

[14] P. Carpenter and A. Garrad, "Hydrodynamic stability of flow over Kramer type compliant surfaces, Part 2, Tollmien Schlichting instabilities," *Journal of Fluid Mechanics*, pp. 199–232, 1985.

[15] O. Reynolds, "An experimental investigation of the circumstances which determine whether the motion of water shall be direct or sinuous, and of the law of resistance in parallel channels," *Phill. Trans. Roy. Soc.*, vol. 174, pp. 953–982, 1883.

[16] A. Davey and P. Drazin, "Stability of Poiseuille flow in a pipe," *Journal of Fluid Mechanics*, vol. 36, no. 02, pp. 209–218, 1969.

[17] V. Garg and W. Rouleau, "Linear spatial problem of the pipe-Poiseuille flow," *Journal of Fluid Mechanics*, vol. 54, no. 1, pp. 113–127, 1972.

[18] H. Salwen and C. E. Grosch, "The stability of Poiseuille flow in a pipe of circular -section," *Journal of Fluid Mechanics*, vol. 54, pp. 93–112, 1972.

[19] A. Gill, "On the behaviour of small disturbances to Poiseuille flow in a circular pipe," *Journal of Fluid Mechanics*, vol. 21, no. 01, pp. 145–172, 1965.

[20] P. Sen and D. Venkateswarlu, "On stability of pipe-Poiseuille flow to finite-amplitude axisymmetric and non-axisymmetric disturbances," *Journal of Fluid Mechanics*, vol. 158, pp. 289–316, 1985.

[21] V. Kumaran, "Stability of the Viscous flow of a fluid through a compliant tube," *Journal of Fluid Mechanics*, vol. 294, pp. 259–281, 1995.

[22] V. Kumaran, "Stability of the Viscous flow of a fluid through a compliant tube at high Reynolds number," *Journal of Fluid Mechanics*, vol. 302, pp. 117–139, 1995.

[23] V. Kumaran, "Stability of an inviscid flow through a compliant tube," *Journal of Fluid Mechanics*, vol. 320, pp. 1–17, 1996.

[24] V. Kumaran, "Stability of the fluid flow through a compliant tube at intermediate Reynolds number," *Journal of Fluid Mechanics*, vol. 357, pp. 123–140, 1998.

[25] V. Kumaran, "Stability of the wall modes in a compliant tube," *Journal of Fluid Mechanics*, vol. 362, pp. 1–15, 1998.

[26] V. Kumaran, "Classification of instabilities in the flow past compliant surfaces," *Current Science*, vol. 79, pp. 766–773, 2000.

[27] V. Kumaran, "Stability of flow through compliant tubes," *IUTAM Symp. on Flow Past Highly Compliant Boundaries and in Collapsible Tubes*, pp. 95–118, 2001.

[28] V. Shankar and V. Kumaran, "Stability of fluid flow in a flexible tube to non-axisymmetric disturbances," *Journal of Fluid Mechanics*, vol. 407, pp. 291–314, 2000.

[29] M. Hamadiche and M. Gad-el Hak, "Temporal stability of flow through a visco-elastic tubes," *Journal of Fluids and Structures*, vol. 16, no. 3, pp. 331–359, 2002.

[30] J. Gajjar, A. Gibson, and P. Sen, "Instability in compliant pipe and related flows," *IUTAM Sympo. on Flow in Collapsible Tubes and Past other Highly Compliant Boundaries*, 2001.

[31] A. Gibson, "Stability of internal flows bounded by compliant walls: A Kinematic approach," 2001.

[32] P. Sen and D. Arora, "On the stability of laminar boundary-layer flow over a flat plate with a compliant surface," *Journal of Fluid Mechanics*, vol. 197, pp. 201–240, 1988.

frontiers in
CELL AND DEVELOPMENTAL BIOLOGY

Stem Cell Research

Induced Pluripotent Stem Cells: Applications in regenerative medicine, disease modelling and drug discovery

Vimal kishor Singh

Journal Name:	Frontiers in Cell and Developmental Biology
ISSN:	2296-634X
Article type:	Review Article
Received on:	05 Nov 2014
Accepted on:	06 Jan 2015
Provisional PDF published on:	06 Jan 2015
Frontiers website link:	www.frontiersin.org
Citation:	Singh VK(2015) Induced Pluripotent Stem Cells: Applications in regenerative medicine, disease modelling and drug discovery. *Front. Cell Dev. Biol.* 3:2. doi:10.3389/fcell.2015.00002
Copyright statement:	© 2015 Singh. This is an open-access article distributed under the terms of the Creative Commons Attribution License (CC BY). The use, distribution and reproduction in other forums is permitted, provided the original author(s) or licensor are credited and that the original publication in this journal is cited, in accordance with accepted academic practice. No use, distribution or reproduction is permitted which does not comply with these terms.

This Provisional PDF corresponds to the article as it appeared upon acceptance, after rigorous peer-review. Fully formatted PDF and full text (HTML) versions will be made available soon.

Title:

Induced Pluripotent Stem Cells: Applications in regenerative medicine, disease modelling and drug discovery.

Running Title:

IPSc based disease modelling and their potential uses in clinics.

Author:

Vimal Kishor Singh[1*], Manisha Kalsan[2], Neeraj Kumar[2], Abhishek Saini[2], Ramesh Chandra[3]

Author affiliations:

1- Associate Professor (INSPIRE faculty), Stem cell research laboratory, Dept. of Biotechnology, Delhi Technological University, Delhi-110042.
2- Stem Cell Research Laboratory, Dept. of Biotechnology, Delhi Technological University, Delhi-110042.
3- Dr. B. R. Ambedkar Centre for Biomedical Research, University of Delhi, Delhi-110007, India.

***Correspondance:**

Dr. Vimal Kishor Singh: Stem Cell Research Laboratory, Department of Biotechnology, Delhi Technological University, Shahbad Daulatpur, Bawana Road, Delhi-110042 vim_kissor@yahoo.co.in; vimalkishorsingh@gmail.com, vimalksingh@dce.ac.in

Keywords – iPSC, reprogramming, pluripotency, differentiation, disease modelling, drug discovery, gene therapy.

ABSTRACT

Recent progresses in the field of Induced Pluripotent Stem Cells (iPSCs) have opened up many gateways for the research in therapeutics. iPSCs are the cells which are reprogrammed from somatic cells using different transcription factors. IPSCs possess unique properties of self renewal and differentiation to many types of cell lineage. Hence could replace the use of embryonic stem cells, and may overcome the various ethical issues regarding the use of embryos in research and clinics. Overwhelming responses prompted worldwide by a large number of researchers about the use of iPSCs evoked a large number of peple to establish more authentic methods for iPSC generation. This would require understanding the underlying mechanism in a detailed manner. There have been a large number of reports showing potential role of different molecules as putative regulators of iPSC generating methods. The molecular mechanisms that play role in reprogramming to generate iPSCs from different types of somatic cell sources involves a plethora of molecules including miRNAs, DNA modifying agents (viz. DNA methyl transferases), NANOG, etc. While promising a number of important roles in various clinical/research studies, iPSCs could also be of great use in studying molecular mechanism of many diseases. There are various diseases that have been modelled by uing iPSCs for better understanding of their etiology which maybe further utilized for developing putative treatments for these diseases. In addition, iPSCs are used for the production of patient-specific cells which can be transplanted to the site of injury or the site of tissue degeneration due to various disease conditions. The use of iPSCs may eliminate the chances of immune rejection as patient specific cells may be used for transplantation in various engraftment processes. Moreover, iPSC technology has been employed in various diseases for disease modelling and gene therapy. The technique offers benefits over other similar techniques such as animal models. Many toxic compounds (different chemical compounds, pharmaceutical drugs, other hazardous chemicals, or environmental conditions) which are encountered by humans and newly designed drugs may be evaluated for toxicity and effects by using iPSCs. Thus, the applications of iPSCs in regenerative medicine, disease modelling, and drug discovery are enormous and should be explored in a more comprehensive manner.

INTRODUCTION

Discovery of self-renewal by any living cell was one of the major breakthrough reported by Ernest A. McCulloch and James E. Till (1961) who while subjecting the mice with lethal doses of radiation followed by injection of bone marrow cells found that these cells formed clumps due to cells cloned from them which was the main reason of survival of the mice **(Till et al, 1961).** Later studies defined their potential for differentiation into different cell types and self-renewal without senescence, and termed as Stem Cells. Stem cells can be defined on the basis of their origin and potency into Adult Stem Cells and Embryonic Stem Cells (ESC), similarly, considering their potency as the base of classification, stem cells can be classified into unipotent, multipotent, oligopotent, pluripotent and totipotent **(Lan et. al, 2012).** Totipotent are those which can differentiate into embryonic as well as extra-embryonic tissues such as the placenta. Pluripotent stem cells are those which can differentiate into other cells of the adult body. This property exists for only a specific time period of pre-implantation development in the cells forming Inner Cell Mass (ICM). As the cells differentiate into other cell lineages, their self renewing potential decreases due to various epigenetic changes which leads to the loss of pluripotency. Further research conducted on human stem cells made burgeoning use of human ESCs for which embryo needed to be isolated on regular basis that evoked several ethical issues among socio-research communities. There have been efforts by different research groups to bypass these ethical/ technical problems. Subsequent studies demonstrated many advancements in the related techniques such as cloning in frog **(Gurdon et al 1962),** generation of mouse Stem Cells (SCs) **(Evans & Kaufman 1981)**, cloning in sheep **(Wilmut et al 1997),** generation of Human Stem Cells (HSCs) **(Thomson et al 1998),** and development of Embryonic stem cell fusion technique **(Tada et al, 2001).** These findings contributed greatly to the development of cells that could eliminate ethical issues **(figure 1).** However, the major breakthrough came in 2006 when Takahashi and Yamanaka introduced the concept of induced pluripotent stem cells (iPSCs) by generating stem cells that were having properties relating to ESCs. iPSCs were generated by using a combination of 4 reprogramming factors, including Oct4 (Octamer binding transcription factor-4), Sox2 (Sex determining region Y)-box 2, Klf4 (Kruppel Like Factor-4) and c-Myc and were demonstrated both self-renewing and differentiating like ESCs, and thus, could be used as an alternative for hESCs in various clinics/research.Since then, a number of different reprogramming factors/methods have been established. iPSCs generation may employ combination of different reprogramming factors, viz., a cocktail of various reprogramming

factors, direct use of proteins, miRNA, peptide etc. Factors (LIN28 + Nanog,Esrrb, Pax5 shRNA, C/EBPa, p53 siRNA, UTF1, DNMT shRNA, Wnt3a, SV40 LT(T), hTERT) or chemicals (BIX-01294, BayK8644, RG108, AZA, dexamethasone, VPA, TSA, SAHA, PD025901 + CHIR99021(2i), A-83-01) have been found which are able to replace one or the other reprogramming factors from basal reprogramming factors or to enhance the efficiency of reprogramming **(Yu et al 2007, Feng et al 2009, Hanna et al 2008, Zhao et al 2008, Mikkelson et al 2008, Marson et al 2008, Mali et al 2008, Park et al 2008a, Shi et al 2008a, b, Huangfu et al 2008 a, b, Silva et al 2008, Li et al 2009).**

Similarly, there have been significant advancements in methods/ techniques employed to deliver these factors such as Nuclear Transfer, Transcription Factors (Oct4, Sox2, Klf4 and c-Myc) and different reprogramming technologies, including Integration viral vectors and Integration free vectors (Plasmid DNA & transferase, Viral vectors, and Excision of integrated transgenes) **(Hochedlinger et al 2002, Takahashi et al 2006a, Takahashi et al 2006 b, Stadtfeld 2008a, Stadtfeld et al 2008b, Fusaki et al 2009, Gonzalez et al 2009, Yu et al 2007, Yusa et al 2009) (Table 2).** The various sources, delivery methods and their cognate approaches with different combinations of transcription factors differ significantly in their efficiency **(Table 1 and Table 2).**

Since their discovery, iPSCs have been used in many research & clinical studies including *disease modelling, regenerative medicine, and drug discovery/ drug cytotoxicity studies*. For disease modelling, somatic cells possessing the characteristics of diseased cells from patient are used for the generation of iPSCs and are further utilized for studying the diseases. Similarly, iPSCs are widely utilized for the regeneration of tissue-specific cells for the transplantation to patients of various injuries or degenerative diseases. Studies like drug discovery which implies screening of small molecules, testing of toxicity for assessment of safety, have successfully exploited iPSCs based technique. A large number of reports have accumulated indicating a need for discussing various apects of these techniques and their future perspectives in clinical/research studies. This article focuses the importance of these cells for therapeutics and research benefits in different biological sciences.

Regulatory factors of iPSCs generation: An overview

1. Generation of iPSCs

Theoretically, iPSCs can be generated by using any somatic cell by employing appropriate reprogramming factors and most convenient method for their introduction to somatic cells. iPSC generation is reported by using cells from different sources such as fibroblasts, cord blood, peripheral blood **(Table1).** There are large numbers of reports showing the whole process in a detailed manner that can be summarized in three major steps- i) establishment of initial cell culture, ii) induction of iPSCs and, iii) characterization & expansion of iPSCs **(Figure 2)**. Firstly, the source cells are isolated and cultured. The reprogramming factors are then introduced into those cultured cells. There are two types of methods for the introduction of reprogramming factors- Integrating Systems (retroviral, lentiviral, inducible lentiviral) and Non-Integrating Methods (non intergrating viral vectors (sendai virus, adeno virus), plasmid DNA transfer, transgenes, recombinant proteins, synthetic mRNA) **(Table2).** These transfected cells are incubated on feeder layers (a number of cells have been demonstrated as feeder cells, example., fibroblasts, keratinocytes) under appropriate media conditions and after the expression of these reprogramming factors, generation of iPSCs occurs. The cultured iPSC colonies can be characterised by different morphological and physiochemical methods. The morphological examination of iPSCs can be done on the basis of round shape, large nucleolus, and scant cytoplasm of iPSCs as similar to ESCs **(Thomson et al 1998)**. Reprogrammed colonies are tightly packed, sharp edged, flat, mitotically very active due to the possession of property of self renewal. Though it is hard to define iPSCs solely on the basis of their morphology, these characteristics give a quick idea about their states. Further, iPSCs may be defined on the basis of expression of different cell surface proteins (SSEA-4, alkaline phosphatase) and transcription factors Oct4, Sox2, Nanog which can also be used for the characterization **(Adewumi et al 2007). Figure 3** describes the necessary requirements (Yamanaka's cocktail, alternative factors or chemicals for the replacement of one or more basal reprogramming factors enhancement of efficiency of generation) for the generation of iPSCs.

2. Different factors that play role in the generation of iPSCs.

As discussed above, the generation of iPSCs from somatic cells requires the introduction of reprogramming factors into the somatic cells. This can be done by two types of methods- Integrating Viral Vector Systems and Non-Integrating Systems. Integrating methods are those in

which the viral vector gets integrated into the host cell genome. The use of retrovirus and lentivirus comes under this category **(Brambrink et al 2008, Stadtfeld et al 2008a, b, Takahashi et al 2006b)**. This method has a high efficiency but it poses the risks of cancer formation and hence, different approaches have also been worked on. Non-Integrating methods are those in which no integration in host cell genome occurs. Different approaches such as viral vectors (Adeno virus and Sendai virus), Plasmid DNA, and the use of RNA and proteins come under this category. Adeno virus (dsDNA) and Sendai virus (RNA) are non-integrating viral vectors which have been used in iPSC generation **(Fusaki et al 2009, Stadtfeld et al 2008a, Takahashi et al 2006b)**. Plasmids such as oriP/EBNA1 (derived from Epstein-bar virus), containing reprogramming factors has been used for reprogramming, but the efficiency was found to be low **(Yu et al 2009)**. Direct delivery of reprogramming proteins has also been carried out by fusing them with a cell penetrating peptide **(Kim et al 2009b)**. Yashioka et al used a different approach using a single self replicating RNA replicon which expressed high levels of Yamanaka's factors for transfection into fibroblasts to be reprogrammed into iPSCs and found the iPSCs to be having all properties of pluripotent stem cells **(Yashioka et al 2013)**.

Once the reprogramming factors are delivered to the somatic cells, they come into play for transforming those somatic cells into iPSCs. Not only they have their individual roles, but they interact with each other complementarily.

APPLICATIONS OF iPSCs

The treatment of many diseases is difficult because of the lack of information about the mechanisms that play a role in the disease progression. For this reason, diseases need to be modelled so that treatment could be developed aiming the main cause of the disease. There are a large number of disease testing models which have developed during previous era. Some of them are capable of mimicking human cellular microenvironment and metabolism to some extent. Many animal models such as rat, mice, dogs monkey, dog, and primates have been used for disease modelling. However, the use of animals as disease models is limited due to existing variability in the genetic make-up of them that is highly responsible for the biological functions and hence differences are exhibited while compared with human individuals. Secondly, the problem further gets complicated when the individuals are of two different species. Different species have different genetic makeup and hence different proteins. And thus, none of the animal model is able to fully mimick the human cell microenvironment. So, a different approach which can provide the same environment as in human cells is required and iPSCs pose to be a good alternative with some advantages as well. In case of iPSCs, there is no need of proliferation again and again, and, their derivatives are functional in-vitro as well as in-vivo after transplantation. Induced pluripotent stem cells (iPSCs) are widely used in therapeutics for disease modelling, regenerative medicine, and drug discovery **(Figure 4)**.

1) Disease Modelling

The use of iPSCs for disease modelling is based on the fact that these cells are capable of self renewing and that these cells can differentiate into all types of cells of the human body which can be utilized for the preparation of different disease models to study those diseases. Moreover, a patient specific iPSC could be of enormous use as far as development of specific therapeutics regimen/drug is concerned. By combining 3D culture with extracellular matrix proteins, in-vivo microenvironment can be mimicked. Lee et al used iPSCs for the modelling of pathogenesis in Familial Dysautonomia **(Lee et al 2009)**. Since then, there have been many cases in which iPSCs have helped out in studying various mechanisms that play role in different diseases, a few have been described below.

Moad et al used human prostate and urinary tract cells for the formation of iPSCs and further for studying the mechanisms that regulate the differentiation of prostate and urinary tract cells. With their study, they reported the first successful reprogramming of bladder, prostate and ureter

stromal fibroblasts into a pluripotent state and concluded that iPSCs generated from prostate and urinary tract had better efficiency of differentiation to cells of prostate and urinary tract as compared to iPSCs derived from skin fibroblasts which showed that organ of origin plays an important role in terms of efficiency of differentiation **(Moad et al 2013**).

Various types of diseases which are caused by some deficiency have been studied by using iPSCs. Park et al used iPSCs from patients of various diseases like *Adenosine Deaminase Deficiency-related Severe Combined ImmunoDeficiency (ADA-SCID), Shwachman-Bodian-Diamond syndrome (SBDS), Gaucher disease (GD) type III* for the study of disease models and drug discovery. They used dermal fibroblasts or bone-marrow derived mesenchymal stem cells for the generation of human iPSCs by the transduction of all four or three (excluding c-Myc) transcription factors. It was found from their study that ADA-SCID, SBDS, and Gaucher's disease type III are inherited in a classical Mendelian Inheritance manner like congenital disorders which are autosomal recessive. These diseases were shown to be caused by point mutations in those genes which were vital for normal hematopoiesis and immunological function. They also reported the point mutations in ADA-SCID, SBDS, and GD type III. They also studied *Duchenne (DMD) and Becker muscular dystrophy (BMD), Parkinson disease (PD), Huntington disease (HD), juvenile-onset, type 1 diabetes mellitus (JDM), Down syndrome (DS) /trisomy 21 and the carrier state of Lesch-Nyhan syndrome* (**Park et al 2008b**).

There are many syndromes which are caused by the existence of one or more extra copies of a chromosome. Downs syndrome is one such example. Briggs et al used iPSCs for the identification of molecular networks that drive the different aspects related to pathogenesis in Down's Syndrome. iPSCs in combination with microarray and RNA sequencing technology, can be used to generate phenotype-genotype maps of complex diseases by linking various defects with phenotypes, like in Down's Syndrome using Chromosome engineering of Down Syndrome-iPSCs **(Briggs et al 2013).**

Neurogenerative diseases have also been studied using iPSCs as disease models. Parkinson's Disease (PD) is a very common neurodegenerative disease, in which, dopaminergic neurons of substantia nigra (a structure in mid brain) get lost and formation of Lewy's bodies (inclusions in the cytoplasm of neurons all over the body) occurs. Treatment of this disease had not been possible due to the reason that by the time, PD gets clinically manifested, the neurons have already lost, which makes it very difficult to be able to study the underlying mechanisms of PD

so as to develop a treatment of it. In such a situation, iPSCs can be used and experiments have also been carried out in this aspect. Nguyen et al studied G2019S mutation in LRRK2 (Leucine Rich Repeat Kinase2) gene. This mutation has been reported in cases of sporadic and familial PD. Fibroblasts from a 60-year old female homologous for G2019S mutation were used as a source for the generation of iPSCs. Retrovirus was used for the transduction of Oct4, Sox2, and Klf4 into the fibroblasts, which after 2 months of transfection developed 3 colonies of human embryonic stem cells, which were analysed and found out to be similar to hESCs and wild type iPSCs. For differentiation of G2019S iPSCs to dopaminergic neurons, a combination of mib-brain selective patterning factors, sonic hedgehog (SHH) (induces the differentiation of dopaminergic neurons in substantia nigra), & Fibroblast growth factor 8 beta (FGF8b) (induces the development of cerebellum by the activation of Ras-extracellular signal- regulated kinase (ERK) pathway) and small molecules was used. The neurons generated by this method were functionally active and were found to be able to form active neural networks. The findings suggested LRRK2 to be having an important role in survival of neurons and disruption of which can cause PD. **(Nguyen et al 2011, Hurtado-Lorenzo et al 2004, Sato et al 2004).** Similarly, a different group has also worked for the generation of iPSCs in PD. Devine et al developed iPSCs from fibroblasts taken from a PD affected person possessing triplication of Synuclein gene by the transduction of four basic transcription factors. These iPSCs were then directed to differentiate into dopaminergic neurons in vitro for the study of PD **(Devine et al 2011).**

These findings from modelling different diseases (mutations which are causing them, the pathological phenotypes caused by defects in various networks, genes playing an important role) help out in knowing the molecular mechanisms underlying the disease better, which ultimately carries the work forward to knowing the disease better for the development of a treatment. This is evident from burgeoning reports on use of IPSc for the the purpose of disease modelling **(Table 4)**. However, the technique suffers from various inherited risks and limitations as discussed ahead.

2) Regenerative medicine

In regenerative medicine the injured or degenerated tissues are repaired by the generation of those tissues with the help of iPSCs in labs and then transplanting them to the site of injury or degeneration. Important issues associated with gene therapy are availability of tissue or organ and immunorejection. It is quite often that patients die because of the non-availability of donors

which is a result of the fact that the population is non aware of the scarcity of donors and the ever inceasing need of organs due to accidents and degenerative diseases. Also, a patient can only be transplated with the cells, tissues, or organs from the person who does not have any disease and whose physiological profile matches with the patient. Keeping these risks in mind, various tests are conducted before transplating tissues or organs into the patient's body. The use of iPSCs offers a good approach for these treatments as the cells that will be transplanted to patient's body will be differentiated from the repaired iPSCs generated from the somatic cells from patient's own body. iPSCs have been used in treating a number of injuries and degenerative diseases. A comprehensive detail of all those would be beyond the scope of this article, however, major arguments are discussed below. Different injuries as a result of human activities, accidents or natural calamities can also be treated by the gene therapy utilizing iPSCs. The various conditions that can be treated are Hematopoietic disorders, Musculoskeletal injury, Spinal cord injury, liver damage by the generation of specific cells with the help of iPSCs **(Suzuki et al 2013, Tan et al 2012, Nori et al 2011, Liu et al 2011b).**

Other than accidental injuries, diseases can also be treated with the help of iPSCs. Kazuki et al corrected the genetic deficiency in iPSCs from a human Duchhene Muscular Dystrophy (DMD) patient. They used Human Artificial Chromosome (HAC) for the expression of complete sequence of Dystrophin (DYS). They used fibroblasts from the DMD patient for the generation of iPSCs. HAC was used for the correction in the deletion or mutation in the Dystrophin gene present in iPSCs by transfer of DYS-HAC (complete genomic sequence of dystrophin in HAC) using Microcell-mediated chromosome transfer (MMCT) **(Kazuki et al 2009)**. MMCT is a technique in which micro cells containing few chromosomes are fused with whole cells **(Doherty et al 2003)**.

iPSCS can also be used in cases of hepatocytes where loss of function of hepatocytes in culture and limited organ availability act as obstacles when fetal or adult progenitors are used for the development of hepatocytes. This lead to making use of iPScs for the generation of hepatocytes for various liver problems.

Recently, there are accumulating data on the use of iPSC for ex-vivo blood expansion of various blood components. They can be used for the generation of Red Blood Cells (RBCs) which could be utilized for the generation of blood that is required over the globe for the purpose of treatment

of various damages or diseases. There are various techniques by which we can use ESCs/iPSCs for the production of RBCs **(Lim et al, 2013).**

iPSCs can also be used for the generation of various cells which can help in the repairmen of many tissues, for example, cardiovascular cells for the repairment of heart valves, vessels and ischemic tissues, but are limitations like safe delivery, post treatment adverse effects and standardization of protocols to generate large amounts of pure good quality cells. These obstacles once overcome, offer great opportunities for the applications of iPSCs for generating cardiovascular cells and studying corresponding diseases **(Levenberg et al 2010, Cao et al 2008, Laflamme et al 2007).**

Various degenerative diseases in which cells death causes many symptoms have been treated by gene therapy using iPSCs. One such case is Retinitis pigmentosa (RP) where eye's retina degeneration causes impaired vision. For the treatment of RP, iPSCs were generated from the patient suffering with the disease which were then showed to differentiate into rod photoreceptor cells (**Yoshida et al 2014**). The differentiation of iPSCs to Retinal pigmented epithelium is proved to be beneficial for patients of Retinal Pigmentosa and Age-related Macular Degeneration (AMD) (**Li et al 2012**).

Gene therapy using iPSCs has also been used to treat various primary immunodeficiencies like *Chronic Granulomatous disorder (CGD)*, an autosomal recessive or X-linked disorder which affects the function of neutrophils, and *Wiskott–Aldrich syndrome (WAS*), X-linked deficiency caused by mutation in WAS gene encoding WAS protein (WASp) which is an actin cytoskeletol regulator in hematopoietic lineage. **(Jiang et al 2012, Klein et al 2003).**

The technology of genome editing or genome engineering, which includes the use of different genome editing technologies like Zinc Finger Nucleases (ZFNs), Transcription Activators like effector nucleases (TALENs), CRISPR/Cas systems, Meganucleases, Adeno-associated viruses, and adenoviruses, offers an opportunity for the efficient introduction of various insertions or deletions that range from single nucleotides to insertion/deletion of whole genes which has a capability of taking disease modelling to new heights **(Hockemeyer et al 2009, Hockmeyer et al 2011, Grizot et al 2009, Khan et al 2010, Suzuki et al 2008).** Choi et al reported the gene correction in alpha 1 anti trypsin (AAT) deficiency by the use of TALENs. A pair of TALEN expression vectors was constructed. This construct recognised the sequences flanking the Z mutation of the AAT gene. After co-nucleofection of targeting vector & TALEN expression

vector was carried out, PCR and Southern blot was done. The results showed a highly efficient & simultaneous targeting of both alleles **(Choi et al 2013)**.

Once the specific cells are formed they can be transplanted to the specific site, in case of degenerative diseases, for the cure of the disease. And, in case where diseased cells which possess some mutation, the mutation is first corrected to form normal iPSCs and then these iPSCs are differentiated into specific cell types by providing the specific conditions required for the development of those cells. These repaired cells can then be transplanted into the body of the organism from which the cells for the generation of iPSCs were isolated.

3) Drug discovery and cytotoxicity studies

Another important role offered by the use of iPSCs based methodology is their complementarity to drug discovery or prediction of toxicity via animal models. Animals or in-vitro animal derived cells are used as testing systems butare limited by their inability to to replicate the "exact" human physiological conditions and related phenotypic attributions. Sometimes, the benefits demonstrated in the animal models do not come out to be beneficial in humans, for example, the SOD (superoxidase dimutase) gene associated with ALS (Amyotrophic Lateral Sclerosis) allowed the identification of Vitamin E and Creatine to be relievers of the diseased phenotype which failed to cause any improvements in humans **(Desnuelle et al 2001, Groeneveld et al 2003, Shefner et al 2004).** And also, animal models are not good testing models for drug toxicity as a chemical may be toxic to an animal but may not be toxic to a different animal. For carcinogenic agents as well, different agents pose different levels of carcinogenicity in different animals, for example, formaldehyde is more carcinogenic to rats as compared to mice **(Kerns et al 1983)**. Finally, a newly discovered drug or therapy must be tested on human cells or human test models itself. These reasons make it more important to be able to use the systems closer to humans. Moreover, these studies need to be done in a system where the results could be directly extrapolated to humans. These studies include steps such as prediction/ identification of a potential drug molecule followed by its synthesis, generation of iPSCs, their differentiation to specific somatic cells, and testing for toxic or non-toxic effects of the synthesized drug on the somatic cells. For toxicity studies, iPSCs from normal and diseased cells are used to generate neurons, hepatocytes, cardiomyocytes etc. Toxicity and potential side-effects are often most common cause to rule out most of the therapeutic molecules.

There is a long pipeline between the time when a hit is identified and the time when it reaches the market. Before using drugs on humans, their toxic effects must be properly evaluated for a safe administration of those drugs which is very costly. Only 10% of the drugs that enter clinical trials are able to reach market approval stage. The cost of developing a drug is increasing with the estimated cost of whole process being US$1.2-1.7 billion per drug compound **(Gunaseeli et al 2010, Kaitin et al 2008, Sollano et al 2008).** The development of 30% of the medicines was abandoned because of lack of efficacy and 30% due to concerns associated with safety (cardiotoxicity, hepatotoxicity) **(Laustriat et al 2010).** The blocking of human ether-a-go-go related gene 1 (*hERG1*) channel by drug is associated with longer duration of ventricular repolarization which causes long QT syndrome. The response of iPSC-derived cardiomyocytes have been reported in response of cardiac and non cardiac drugs in terms of electrophysiological capacity **(Tanaka et al 2009, Yoshida et al 2010, Yokoo et al 2009, Asai et al 2010)**. The generation of functional hepatocytes using iPSCs has also been reported **(Sullivan et al 2010).** Due to lack in early detection of drug toxicity in human tissues, the process becomes more costly and extensively time consuming. Development of toxicity models that predict more accurately before clinical trials may help to reduce costs by demonstrating cardiotoxicity or hepatotoxicity caused by the drugs much before they reach clinical trials; reducing the time taken for clinical trials of the drugs which will fail due to cytotoxicity in the later stages of trials. iPSCs have been explored by many research groups in order to identify compounds which are toxic or pose side-effects. The use of iPSCs offer better alternative to conventional tests of toxicology and drug research and offer better chemical safety assessment as they provide a more similar environment to human physiological conditions than is provided by conventional testing systems which make use of animals. For example, iPSCs have been used to establish test systems for cytotoxicity-cardiotoxicity, hepatotoxicity and embryotoxicity testing **(Kimmel et al 1982, Sieler et al 2004).**

iPSCs have the potential of providing native cells for splicing and post translational modifications that does not come with the small molecule screening systems using purified protein or recombinant cell lines used for the over-expression of the protein of interest which has aided in the process of drug screening. The use of iPSCs in drug screening has also been reported. Stem Cells enable the identification of molecules therapeutically useful and able to modulate the behaviour of tumorigenic and normal stem cells. But as the use of embryonic stem cells is limited because of the concerned ethical issues, iPSCs (normal & tumorigenic) can be used as an alternative.

McNeisch et al used neurons that were expressing a-amino- 3-hydroxyl-5-methyl-4-isoxazoleproprionate (AMPA) subtype glutamate receptors using mouse iPSCs and used them for the identification of small molecule AMPA potentiators (**McNeisch et al 2010**). Choi et al used hepatic cells derived from iPSCs generated from patients with alpha-1 anti-trypsin deficiency for the screening of 3131 compounds of Johns Hopkins Drug Library. After immunofluorescence, total AAT fluorescence intensity was measured for each well. Out of 262 compounds which inhibited the accumulation of AAT by more than 50%, 43 compounds after literature survey were found to be FDA approved, clinically used internationally, and exerting no major side effect. These compounds were further tested by using four different lines of AAT-deficiency iPSCs and final 5 hits, which gave consistent results in all the four iPSC lines were selected (**Choi et al 2013**). iPSCs also help in studying ADME (Absorption, Distribution, Metabolism, Excretion) properties of drugs which has highly speeded up drug discovery and development **(Bahadduri et al 2010).**

Advantages of iPSC technology

iPSCs offer various advantages as compared with gene therapy by the use of nuclear transfer or Embryonic Cell mediated gene therapy **(Kazuki et al 2009).**

1) The ethical issues are elimited by the use of iPSCs.

The use of ESCs in research is laden with ethical issues regarding personhood, justice towards humankind and human dignity that are associated with the use of human life in its earliest form, the embryo. Additional concerns that surround the use of ESCs are informed consent, improper incentives and health and safety concerns of the women donating eggs for the generation of embryos by in-vitro fertilization. iPSCs have solved the controversy over the destruction of embryos associated with the use of ESCs in research.

2) Reduced chances of immunorejection.

iPSCs are generated from the somatic cells of one's own body and hence there is no risk of immunorejection of these autologous cells. Guha et al differentiated mouse iPSCs into embryoid bodies and different tissue specific cells. After the transplantation of these iPSC derived EBs or

tissue specific cells, no evidence of increased Tcell proliferation or an antigen- specific secondary immune response was found (**Guha et al 2013**).

3) Throughput screening for predicting toxicity /therapeutic responses of newly developed drugs.

The concept of using iPSCs to predict toxicology and therapeutic responses of drugs in based on the property of iPSCs to continuously self renew which make it possible to generate libraries and their ability to give rise to all types of body cells make them suitable to be used for prediction of toxicity and possible side effects of newly developed drugs in different body cells (**Wobus et al 2011**).

4) Lowering the overall cost and risk of clinical trials.

For every new drug to reach market, around 5000-10,000 compounds need to be tested during preclinical trials. Therefore, any strategy which standardizes the prediction of toxicity would impact the cost. Many drugs fail after Phase III, for example BMS-094 (hepatitis C drug) failed after death of a patient. The cost used for the clinical trials could be reduced by using iPSCs to provide the toxicity details of the drug by different cytotoxicity assays. Much of the cost for preclinical testing is due to the requirement of animal models for estimation of bioavailability of new drug. As animal models do not mimic the microenvironment of the human cells fully, the use of iPSCs for these tests may cut the cost associated with providing animal models which will ultimately decrease the overall costs of the clinical trials.

5) Development of a personalized approach for administration of drugs.

As, iPSCs are derived from individual patients, these offer scientists an opportunity for modelling diseases on a patient-by-patient basis. This enables screening the genomic differences between individuals that may help in the progression of disease, and the screening of pharmacological agents to find the ideal one for each individual (**Chun et al 2011**).

6) Gene targeting and correction technologies (Gene Therapy)

Reprogramming of somatic cells from any genetic background to iPSCs has allowed the generation of cell lines possessing disease-causing mutations. The ability of modifying the specific sites in a genome for altering the genes of interest becomes highly important here. To realize the full potential of iPScs, methods for efficient genetic modifications are required.

7) For disease modelling, the phenotypes need to be consistent every time, which is a possibility in case of iPSCs

Many research groups have modelled various diseases using iPSCs and the cell lines developed were found to be consistent phenotypically. Fong et al developed Tauopathy derived iPSCs carrying a TAU-A152T mutation. The phenotypes observed in the cells from iPSCs were consistent with those in patients with the mutation (**Fong et al 2013**).

Limitations and/or risks associated with the use of IPSCs ic clinics

There are some limitations/disadvantages associated with iPSCs as well. Generation of iPSCs make use of retroviral or lentiviral systems, so, it needs to be concerned if the viral systems get incorporated with the host genome. The genetic material inserted via retroviral vectors may randomly integrate into the genome of the host which can cause genetic aberration and teratoma formation **(Howe et al 2008)**. The transcription of the transgenes inserted via vector systems may resume in the cells that have been formed by the differentiation of iPSCs **(Okita et al 2007).** The assessment also becomes complex as it depends on number of variables, like small molecules for the enhancement of iPSCs production are used or not, whether the factors used for reprogramming are contained in single vectors or multiple vectors, and which source has been used for the generation of iPSCs, contribute to the differences in the epigenome, genotype and phenotype of the iPSCs produced which make it difficult to determine whether the problems occurred due to the technology or the reprogramming method(s) **(Howe et al 2008, Li et al 2011)**. It is possible to use iPSCs for modelling of the diseases which have a phenotype and are monogenic but in case of complex diseases the role of genetic and epigenetic factors is uncertain which makes modelling of disease a tough job. It is not possible for iPSCs to model every disease successfully, hence, it should be noted if the iPSCs derivatives are getting properly matured to the cells of interest or not in order to know if they are suitable to be used for the purpose of our interest or not. The altered expressions of the basal reprogramming factors has also been reported to cause diseases. The overexpression of Oct4 may lead to epithelial cell dysplasia **(Hochedlinger et al 2005).** The aberrant expression of Sox2 has been reported to cause mucinous colon carcinoma **(Park et al 2008c).** Klf4 has role in the formation of breast tumours **(Ghaleb et al 2005).** c-Myc plays an important role in the formation of around 70% of human cancers **(Kuttler et al 2006).** For this reason, retroviral introduction of c-Myc is also

advised to be avoided for use in clinical applications **(Okita et al 2007).** Zhang et al reported that out of 593 genes that express in iPSCs, 209 genes were found to express in cancer tissues and tumour cells. 5 oncogenes were found to overexpress in iPSCs whereas the oncogene RAB25 was found to express in cells derived from iPSCs **(Zhang et al 2012).** RAB25 (member of RAS protein family) plays an important role in survival of cancer cells **(Cheng et al 2013).** The different pros and cons of the use of iPSCs in different applications has been mentioned in **Table 5**.

Quality control testing of iPSCs

There are many things which need to be considered before using iPSCs clinically for regenerative medicine. The manufacture of clinical grade iPSCs demand quality control at different levels of the manufacturing process. Firstly, it is important to decide whether the therapy would be autologous or allogeneic. Autologous therapy should be such that it is able to manage the differences in the patient in terms of age, health and gender which could affect the quality, consistency and safety of the final product. It requires long term study of the increased risk of tumour formation as the patient would not be expected to have any immune response. The alternative, allogeneic therapy offer well characterized cell banks for therapeutics to be established. Donors need to meet strict eligibility requirements and the donor must be aware of the use & testing of his sample and that the collection of sample would be carried out in an ethical way. After the collection and culture of the source cell, a suitable reprogramming method is to be decided. The use of retroviral vectors has risks of insertional mutagenesis and hence their use is not ideal for clinical applications. Non-viral methods address this question and the method is chosen according to pros & cons associated. Once the iPSCs have generated, proper characterization is vitally required. For the verification that the iPSCs generated are really pluripotent, the expression of different pluripotency markers is assessed. It must be checked if the iPSCs generated can differentiate to all the three germ layers. To further check the ability of the iPSCs to differentiate, the efficiency of generation of the cells which are required for the therapy is determined. The cells generated must be tested to be functional, so the physiological properties of cells generated from iPSCs were compared with that of the cells generated from ESCs. The final product has variability which depends on the quality of starting material used as cell source, difference in other raw materials used for cell culture, and the protocol followed. Identifying and controlling these is important to standardize any manufacturing process to demonstrate reproducibility and consistent production meeting the specifications. Research

based methods that have manual nature may not prove to be ideal for the large production of cells. Quality control testing for final product & preparation procedures must also be designed. For administration of fresh cells, there is need of a rapid method for detection of contamination. Plans must be there in case if the sample fails the sterility test, if the patient has already been administered with the product. Once the quality testing has been done, it should be ensured that the final cell therapeutic is meeting all the required specifications. For allogeneic therapies, a cell bank must be established which would contain the starting cell material and it should be tested to check the consistency of that material. Establishment of a large cell bank is not important for autologous therapeutics; a small bank would serve the purpose of identification & minimization of variability that may result from initial reprogramming. The colonies which meet the specifications of karyotype, marker expression, mycoplasma/bacterial/fungal contaminate and growth characteristics, are expanded to build a bank. Additional knowledge about the post release handling of the cell product is also required. It is important to ensure that the final cell product is representative of therapeutic that will be subjected to human clinical trials. Preclinical animal studies should be able to address the safety of the cell product which includes the affects of the contaminants present in the cell population from donor, chances of teratoma formation and generation of karyotypically unstable cells. It should be ensured that the changes in process associated with change from animal studies to production for clinical use would not cause any significant problems.

Future perspectives

Since the emergence of the field of iPSCs, it has highly developed and successfully expanded to different fields of regenerative medicine. Their application in clinical research will surely benefit the patients in future. At present there are few, but important applications of iPSCs but, if this field keeps on growing at the present pace, it wouldn't take long to expand the applications of iPSCs to more biological fields to aid research & treatments. iPSCs are important in disease modelling as they do not have ethical issues concerned as in case of ESCs and provide with the physiological conditions more close to humans which is not an advantage with the animal disease models. iPSCs also have a possibility of giving consistent phenotypes every time, which is an important issue for disease modelling. More and more types of diseased cells are being tried to be modelled, but, it still has many limitations that are encountered while working with iPSCs, which need to be overcome. Also, it is not possible to be able to model every disease, so, further exploration of modelling diseases with iPSCs is required. As iPSCs eliminate the chances of

immunorejection, they hold great importance in Gene therapy. But the generation of iPSCS itself has many issues associated it like incorporation of vectors into host genomes, and the dependence on the various factors like usage of small molecules, single or multiple vectors, source of cells, which make the generation of iPSCs a risky task and hence, more about iPSCs need to be explored to make it easier to generate them and to be able to apply them to various other important and attractive areas of medical sciences for their proper utilization to achieve the advantages that use of iPSCs can have. And, different advances in the field, including the solution of many limitations mentioned above would prove to be beneficial for increasing therapeutic potential. The present situation of the applications of iPSCs deals with the laboratory scale production and testing assay. A lot has to be done to realize the applications of iPSCs at a higher level, for the use in hospitals, to be beneficial for the patients.

Conclusion

The iPSC therapy is in infancy but a constant progress in reprogramming technologies has occurred; new and improved methods are gathering. As iPSCs can differentiate to different cell types, we can generate the required cells for the study or treatment of numerous diseases and determination of drug toxicity. The therapy using HSCs is being used since a long time. The change from allogeneic to autologous iPSCs has been a major breakthrough. Autologous therapy also offers the advantage of personalized medicine.

Acknowledgement

We thank the Honourable Chairman and the Honourable Vice-Chancellor of Delhi Technological University, Shahbad Daulatpur, Bawana Road, Delhi-42, for the support. Dr. Vimal Kishor Singh particularly thanks the Dept of Science and Technology (DST) and Indian National Science Academy (INSA), India, for the research grant.

REFERENCES

1. Aasen, T., Raya, A., Barrero, M.J., Garreta, E., Consiglio, A., Gonzalez, F., et al. (2008). Efficient and rapid generation of induced pluripotent stem cells from human keratinocytes. *Nat Biotechnol*. 26(11), 1276-1284. doi:10.1038/nbt.1503.
2. Adewumi, O., Aflatoonian, B., Ahrlund-Richter, L., Amit, M., Andrews, P.W., Beighton, G., et al. (2007). Characterization of human embryonic stem cell lines by the International Stem Cell Initiative. *Nat Biotechnol*. 25(7), 803–816. doi:10.1038/nbt1318.
3. Amenduni, M., De Filippis, R., Cheung, A.Y.L., Disciglio, V., Epistolato, M.C., Ariani, F., *et al*. (2011). iPS cells to model CDKL5-related disorders. *European Journal of Human Genetics* 19, 1246–1255. doi: 10.1038/ejhg.2011.131.
4. Asai, Y., Tada, M., Otsuji, T.G. and Nakatsuji, N. (2010) Combination of functional cardiomyocytes derived from human stem cells and a highly-efficient microelectrode array system: an ideal hybrid model assay for drug development. *Curr. Stem Cell Res. Ther.* 5, 227–232.
5. Bahadduri, P.M., Polli, J.E., Swaan, P.W., and Ekins, S. (2010). Targeting drug transporters - combining in silico and in vitro approaches to predict in vivo. *Methods Mol Biol.* 637:65-103. doi: 10.1007/978-1-60761-700-6_4.
6. Batista, L.F., Pech, M.F., Zhong, M.F., Nguyen, H.N., Xie, K.T., Zaug, A.J., *et al.* (2011). Telomere shortening and loss of self-renewal in dyskeratosis congenita induced pluripotent stem cells. *Nature*. 474(7351):399-402. doi: 10.1038/nature10084.
7. Brambrink, T., Foreman, R., Welstead, G.G., Lengner, C.J., Wernig, M., Suh, H., et al. (2008). Sequential expression of pluripotency markers during direct reprogramming of mouse somatic cells. Cell Stem Cell. 2(2):151-9. doi: 10.1016/j.stem.2008.01.004
8. Briggs, J.A., Mason, E.A., Ovchinnikov, D.A., Wells, C.A., Wolvetang, E.J. (2013) Concise Review: New Paradigms for Down Syndrome Research Using Induced Pluripotent Stem Cells: Tackling Complex Human Genetic Disease. *STEM CELLS TRANSLATIONAL MEDICINE.* 2:175–184. doi: 10.5966/sctm.2012-0117
9. Campuzano V, Montermini L, Molto MD, Pianese L, Cossee M, Cavalcanti F, et al. (1996). Friedreich's ataxia: autosomal recessive disease caused by an intronic GAA triplet repeat expansion. *Science*. 271:1423-1427.

10. Cao, F., Wagner, R.A., Wilson, K.D., Xie, X., Fu, J.D., Drukker, M., et al. (2008). Transcriptional and functional profiling of human embryonic stem cell-derived cardiomyocytes. *PLoS One.* 3(10):e3474. doi: 10.1371/journal.pone.0003474.
11. Carvajal-Vergara, X., Sevilla, A., D'Souza, S.L., Ang, Y.S., Schaniel, C., Lee, D.F., *et al.* (2010). Patient-specifi c induced pluripotent stem-cell derived models of LEOPARD syndrome. *Nature*. 465(7299):808-12. doi: 10.1038/nature09005
12. Cheng, K.W., Agarwal, R., Mitra, S., and Mills, G.B. (2013) Rab25 Small GTPase Mediates Secretion of Tumor Necrosis Factor Receptor Superfamily Member 11b (osteoprotegerin) Protecting Cancer Cells from Effects of TRAIL. *J Genet Syndr Gene Ther*. 4:153. doi: 10.4172/2157-7412.1000153
13. Chestkov, I.V., Vasilieva, E.A., Illarioshkin, S.N., Lagarkova, M.A., and Kiselev, S.L. (2014) Patient-Specific Induced Pluripotent Stem Cells for SOD1-Associated Amyotrophic Lateral Sclerosis Pathogenesis Studies. *Acta Naturae*. 6(1): 54–60.
14. Choi, M.S., Kim, Y., Shim, J.S., Park, J.T., Wang, R., Leach, S.D., et al. (2013). Efficient drug screening and gene correction for treating liver disease using patient-specific stem cells. Hepatology. 57(6): 2458–2468. doi:10.1002/hep.26237.
15. Chun, Y.S., Byun, K., and Lee, B. (2011). Induced pluripotent stem cells and personalized medicine: current progress and future perspectives. *Anat Cell Biol.* 44:245-255. Doi: http://dx.doi.org/10.5115/acb.2011.44.4.245
16. Desnuelle, C., Dib, M., Garrel, C. and Favier, A. (2001) A double-blind, placebo-controlled randomized clinical trial of alpha-tocopherol (vitamin E) in the treatment of amyotrophic lateral sclerosis. ALS riluzole-tocopherol Study Group. Amyotroph. Lateral Scler. *Other Motor Neuron Disord.* 2, 9–18.
17. Devine, M.J., Ryten, M., Vodicka, P., Thomson, A.J., Burdon, T., Houlden, H., et al. (2011). Parkinson's disease induced pluripotent stem cells with triplication of the α-synuclein locus Nature communications. 2:440 DOI: 10.1038/ncomms1453
18. Dimos, J.T., Rodolfa, K.T., Niakan, K.K., Weisenthal, L.M., Mitsumoto, H., Chung, W., *et al.* (2008). Induced pluripotent stem cells generated from patients with ALS can be differentiated into motor neurons. *Science.* 321(5893):1218-21. doi: 10.1126/science.1158799.
19. Doherty AM, Fisher EM. (2003). Microcell-mediated chromosome transfer (MMCT): small cells with huge potential. Mamm Genome. 14(9):583-92.

20. Ebert, A.D., Yu, J., Rose, F.F. Jr., Mattis, V.B., Lorson, C.L., Thomson, J.A., *et al.* (2009). Induced pluripotent stem cells from a spinal muscular atrophy patient. *Nature.* 457(7227):277-80. doi: 10.1038/nature07677.
21. Evans, M.J., and Kaufman, M.H. (1981). Establishment in culture of pluripotential cells from mouse embryos. *Nature.* 292:154–156.
22. Farra, N., Zhang, W.B., Pasceri, P., Eubanks, J.H., Salter, M. W., and Ellis, J. (2012). Rett syndrome induced pluripotent stem cell-derived neurons reveal novel neurophysiological alterations. *Molecular Psychiatry*. 17, 1261–1271. doi:10.1038/mp.2011.180.
23. Feng, B., Jiang, J., Kraus, P., Ng, J.H., Heng, J.C., Chan, Y.S., et al. (2009). Reprogramming of fibroblasts into induced pluripotent stem cells with orphan nuclear receptor Esrrb. *Nat. Cell Biol.* 11, 197–203. doi: 10.1038/ncb1827.
24. Filareto, A., Parker, S., Darabi, R., Borges, L., Iacovino, M., Schaaf, T., *et al.* (2013). An *ex vivo* Gene Therapy Approach to Treat Muscular Dystrophy Using inducible Pluripotent Stem Cells. *Nat Commun.* 4: 1549. doi:10.1038/ncomms2550
25. Fong, H., Wang, C., Knoferle, J., Walker, D., Balestra M.E., Tong, L.M. (2013) Genetic Correction of Tauopathy Phenotypes in Neurons Derived from Human Induced Pluripotent Stem Cells. *Stem Cell Reports*. 1(3):226-234. doi: 10.1016/j.stemcr.2013.08.001.
26. Fong, Y.W., Inouye, C., Yamaguchi, T., Cattoglio, C., Grubisic, I., and Tjian R. (2011). A DNA Repair Complex Functions as an Oct4/Sox2 Coactivator in Embryonic Stem Cells. Cell. 147(1): 120–131. doi:10.1016/j.cell.2011.08.038.
27. Fusaki, N., Ban H., Nishiyama A., Saeki K. and Hasegawa, M., et al. (2009). Efficient induction of transgene-free human pluripotent stem cells using a vector based on Sendai virus, an RNA virus that does not integrate into the host genome. *Proc Jpn Acad Ser B Phys Biol Sci.* 85(8), 348–362. doi:10.2183/pjab.85.348.
28. Gangopadhyay, S.B., Sherratt, T.G., Heckmatt, J.Z., Dubowitz, V., Miller, G., Shokeir, M., *et al.* (1992). Dystrophin in Frameshift Deletion Patients with Becker Muscular Dystrophy. *Am. J. Hum. Genet*. 51:562-570
29. Ghaleb, A.M., Nandan, M.O., Chanchevalap, S., Dalton, W.B., Hisamuddin, I.M., and Yang, V.W. (2005) Krüppel-like factors 4 and 5: the yin and yang regulators of cellular proliferation. *Cell Res.* 15(2):92-6.
30. Gonzalez, F., Barragan Monasterio, M., Tiscornia, G., Montserrat Pulido, N., Vassena, R., Batlle Morera, L., et al. (2009). Generation of mouse-induced pluripotent stem cells by

transient expression of a single nonviral polycistronic vector. *Proc Natl Acad Sci U S A.* 106(22):8918-22. doi: 10.1073/pnas.0901471106.

31. Grizot S., Smith J., Daboussi F., Prieto J., Redondo P., Merino N., et al. (2009). Efficient targeting of a SCID gene by an engineered single-chain homing endonuclease. *Nucleic Acids Res.* 37, 5405–5419. doi: 10.1093/nar/gkp548.
32. Groeneveld, G.J., Veldink, J.H., van der Tweel, I., Kalmijn, S., Beijer, C., de Visser, M., *et al.* (2003) A randomized sequential trial of creatine in amyotrophic lateral sclerosis. *Ann. Neurol.* 53, 437–445.
33. Guha, P., Morgan J.W., Mostoslavsky, G., Rodrigues, N.P., and Boyd A.S. (2013) Lack of immune response to differentiated cells derived from syngeneic induced pluripotent stem cells. *Cell Stem Cell*. 12(4):407-12. doi: 10.1016/j.stem.2013.01.006.
34. Gunaseeli, I., Doss, M.X., Antzelevitch, C., Hescheler, J. and Sachinidis, A. (2010) Induced pluripotent stem cells as a model for accelerated patient- and disease-specific drug discovery. *Curr. Med. Chem.* 17, 759–766.
35. Gurdon, J.B. (1962). The developmental capacity of nuclei taken from intestinal epithelium cells of feeding tadpoles. *J. Embryol. Exp. Morphol.* 10:622–640.
36. Haase, A., Olmer, R., Schwanke, K., Wunderlich, S., Merkert, S., Hess, C., et al. (2009). Generation of induced pluripotent stem cells from human cord blood. *Cell Stem Cell*. 5(4), 434-41. doi: http://dx.doi.org/10.1016/j.stem.2009.08.021
37. Hanna, J., Markoulaki, S., Schorderet, P., Carey, B.W., Beard, C., Wernig, M., et al. (2008). Direct reprogramming of terminally differentiated mature B lymphocytes to pluripotency. *Cell*. 133, 250–264. doi: 10.1016/j.cell.2008.03.028
38. Hochedlinger, K., Jaenisch, R. (2002). Nuclear transplantation: lessons from frogs and mice. *Curr Opin Cell Biol.* 14(6):741-8.
39. Hochedlinger, K., Yamada, Y., Beard, C., and Jaenisch, R. (2005) Ectopic expression of Oct-4 blocks progenitor-cell differentiation and causes dysplasia in epithelial tissues. *Cell*. 121(3):465-77.
40. Hockemeyer D., Soldner F., Beard C., Gao Q., Mitalipova M., DeKelver R. C., et al. (2009). Efficient targeting of expressed and silent genes in human ESCs and iPSCs using zinc-finger nucleases. *Nat. Biotechnol.* 27, 851–857. doi: 10.1038/nbt.1562.
41. Hockemeyer D., Wang H., Kiani S., Lai C. S., Gao Q., Cassady J. P., et al. (2011). Genetic engineering of human pluripotent cells using TALE nucleases. *Nat. Biotechnol.* 29, 731–734. doi: 10.1038/nbt.1927.

42. Howe, S.J., Mansour, M.R., Schwarzwaelder, K., Bartholomae, C., Hubank, M., Kempski, H., et al. (2008). Insertional mutagenesis combined with acquired somatic mutations causes leukemogenesis following gene therapy of SCID-X1 patients. *J Clin Invest.* 118(9):3143-50. doi: 10.1172/JCI35798.
43. Huangfu, D., Maehr, R., Guo, W., Eijkelenboom, A., Snitow, M., Chen, A.E., et al. (2008a). Induction of pluripotent stem cells by defined factors is greatly improved by small-molecule compounds. *Nat. Biotechnol.* 26, 795–797. doi: 10.1038/nbt1418.
44. Huangfu, D., Osafune, K., Maehr, R., Guo, W., Eijkelenboom, A., Chen, S., et al. (2008b). Induction of pluripotent stem cells from primary human fibroblasts with only Oct4 and Sox2. *Nat. Biotechnol.* 26, 1269–1275. doi: 10.1038/nbt.1502.
45. Hurtado-Lorenzo, A., Millan, E., Gonzalez-Nicolini, V., Suwelack, D., Castro, M.G., and Lowenstein, P.R. (2004). Differentiation and Transcription Factor Gene Therapy in Experimental Parkinson's Disease: Sonic Hedgehog and Gli-1, but Not Nurr-1, Protect Nigrostriatal Cell Bodies from 6-OHDA-Induced Neurodegeneration. Mol Ther. 10(3): 507–524. doi: 10.1016/j.ymthe.2004.05.021
46. Israel, M.A., Yuan, S.H., Bardy, C., Reyna, SM., Mu, Y., Herrera, C., et al. (2012). Probing sporadic and familial Alzheimer's disease using induced pluripotent stem cells. *Nature.* 482(7384):216- 20. doi: 10.1038/nature10821.
47. Jiang, Y., Cowley, S.A., Siler, U., Melguizo, D., Tilgner, K., Browne, C., et al. (2012). Derivation and Functional Analysis of Patient-Specific Induced Pluripotent Stem Cells as an In Vitro Model of Chronic Granulomatous Disease. *Stem Cells.* 30(4): 599–611. doi: 10.1002/stem.1053
48. Kaitin, K.I. (2008) Obstacles and opportunities in new drug development. *Clin. Pharmacol. Ther.* 83, 210–212. doi: 10.1038/sj.clpt.6100462
49. Kaye, J.A., and Finkbeiner, S. (2013). Modeling Huntington's disease with induced pluripotent stem cells. *Mol Cell Neurosci*. 56:50-64. doi: 10.1016/j.mcn.2013.02.005.
50. Kazuki, Y., Hiratsuka, M., Takiguchi, M., Osaki, M., Kajitani, M., Hoshiya, H., *et al* (2009). Complete Genetic Correction of iPS Cells From Duchenne Muscular Dystrophy. *The American Society of Gene & Cell Therapy*. 18(2):386–393. DOI:10.1038/mt.2009.274.
51. Kerns, W.D., Pavkov, K.L., Donofrio, D.J., Gralla, E.J., Swenberg, J.A. (1983). Carcinogenicity of formaldehyde in rats and mice after long-term inhalation exposure. Cancer Res. 43(9):4382-92.

52. Khan I. F., Hirata R. K., Wang P. R., Li Y., Kho J., Nelson A., et al. (2010). Engineering of human pluripotent stem cells by AAV-mediated gene targeting. *Mol. Ther.* 18, 1192–1199. doi: 10.1038/mt.2010.55.
53. Kim, D., Kim, CH., Moon, JI., Chung, YG., Chang, MY., Han, BS., et al. (2009b). Generation of Human Induced Pluripotent Stem Cells by Direct Delivery of Reprogramming Proteins. *Cell Stem Cell.* 4(6), 472–476. doi:10.1016/j.stem.2009.05.005.
54. Kim, J.B., Greber, B., Araúzo-Bravo, M.J., Meyer, J., Park, K.I., Zaehres, H., et al. (2009a). Direct reprogramming of human neural stem cells by OCT4. *Nature.* 461(7264), 649-3. doi: 10.1038/nature08436.
55. Klein, C., Nguyen, D., Liu, C.H., Mizoguchi, A., Bhan, A.K., Miki, H., et al. (2003). Gene therapy for Wiskott-Aldrich syndrome: rescue of T-cell signaling and amelioration of colitis upon transplantation of retrovirally transduced hematopoietic stem cells in mice. *Blood.* 101(6):2159-66.
56. Ku, S., Soragni, E., Campau, E., Thomas, E.A., Altun, G., Laurent, L.C., *et al*. (2010). Friedreich's Ataxia Induced Pluripotent Stem Cells Model Intergenerational GAA•TTC Triplet Repeat Instability. *Cell Stem Cell.* 7(5): 631–637. doi: 10.1016/j.stem.2010.09.014.
57. Kunisato, A., Wakatsuki, M., Shinba, H., Ota, T., Ishida, I. and Nagao, K., et al (2011).Direct generation of induced pluripotent stem cells from human nonmobilized blood. *Stem Cells Dev.* 20(1), 159-68. doi: 10.1089/scd.2010.0063
58. Kuttler, F., and Mai, S. (2006). c-Myc, Genomic Instability and Disease. *Genome Dyn*.1:171-90. doi: 10.1159/000092507.
59. Laflamme, M.A., Chen, K.Y., Naumova, A.V., Muskheli, V., Fugate, J.A., Dupras, S.K., et al. (2007). Cardiomyocytes derived from human embryonic stem cells in pro-survival factors enhance function of infarcted rat hearts. *Nat Biotechnol.* 25(9):1015-24.
60. Laustriat, D., Gide, J. and Peschanski, M. (2010) Human pluripotent stem cells in drug discovery and predictive toxicology. *Biochem. Soc. Trans.* 38, 1051–1057. doi: 10.1042/BST0381051
61. Lee, G., and Studer, L. (2011). Modelling familial dysautonomia in human induced pluripotent stem cells. *Phil. Trans. R. Soc. B*. 366, 2286–2296. doi:10.1098/rstb.2011.0026.
62. Legius, E., Schrander-Stumpel, C., Schollen, E., Pulles-Heintzberger, C., Gewillig, M., and Fryns, J.P. (2002) PTPN11 mutations in LEOPARD syndrome. *J Med Genet*. 39(8):571-4.

63. Lei, K., Chen, Y., Chen, H., Wong, L.C., Liu, J., McConkie-Rosell, A., *et al.* (1995). Genetic Basis of Glycogen Storage Disease Type 1a: Prevalent Mutations at the Glucose-6-Phosphatase Locus. *Am J Hum Genet.* 57(4): 766–771.
64. Levenberg, S., Ferreira, L.S., Chen-Konak, L., Kraehenbuehl, T.P., and Langer, R. (2010). Isolation, differentiation and characterization of vascular cells derived from human embryonic stem cells. *Nat Protoc.* 5(6):1115-26. doi: 10.1038/nprot.2010.31
65. Li, W., Wei, W., Zhu, S., Zhu, J., Shi, Y., Lin, T., et al. (2009). Generation of rat and human induced pluripotent stem cells by combining genetic reprogramming and chemical inhibitors. *Cell Stem Cell*. 4, 16–19. doi: 10.1016/j.stem.2008.11.014
66. Li, Y., Tsai Y., Hsu, C., Erol, D., Yang, J., Wu, W., et al. (2012). Long-term Safety and Efficacy of Human-Induced Pluripotent Stem Cell (iPS) Grafts in a Preclinical Model of Retinitis Pigmentosa. *MOL MED* 18:1312-1319. doi: 10.2119/molmed.2012.00242
67. Li, Y., Zhang, Q., Yin, X., Yang, W., Du, Y., Hou, P., et al. (2011). Generation of iPSCs from mouse fibroblasts with a single gene, Oct4, and small molecules. *Cell Res.* 21(1):196-204. doi: 10.1038/cr.2010.142.
68. Liu, G.H., Barkho, B.Z., Ruiz, S., Diep, D., Qu, J., Yang, S.L., *et al.* (2011a). Recapitulation of premature ageing with iPSCs from Hutchinson–Gilford progeria syndrome. *Nature*. 472(7342):221-5. doi: 10.1038/nature09879.
69. Liu, H., Kim, Y., Sharkis, S., Marchionni, L., and Jang, Y. (2011b). In Vivo Liver Regeneration Potential of Human Induced Pluripotent Stem Cells from Diverse Origins. *Sci Transl Med*. 3(82): 82ra39. doi: 10.1126/scitranslmed.3002376
70. Liu, H., Ye, Z., Kim, Y.H., Sharkis, S. and Jang, Y.Y. (2010). Generation of Endoderm derived Human iPS cells from Primary Hepatocytes. *Hepatology*. 51(5), 1810-1819. doi: 10.1002/hep.23626
71. Maherali, N., Ahfeldt, T., Rigamonti, A., Utikal, J., Cowan, C. and Hochedlinger, K. (2008). A high-efficiency system for the generation and study of human induced pluripotent stem cells. *Cell Stem Cell*. 3(3), 340-5. doi: 10.1016/j.stem.2008.08.003.
72. Mali, P., Ye, Z., Hommond, H.H., Yu, X., Lin, J., Chen, G., et al. (2008). Improved efficiency and pace of generating induced pluripotent stem cells from human adult and fetal fibroblasts. *Stem Cells.* 26, 1998–2005. doi: 10.1634/stemcells.2008-0346.
73. Marson, A., Foreman, R., Chevalier, B., Bilodeau, S., Kahn, M., Young, R.A., et al. (2008). Wnt signaling promotes reprogramming of somatic cells to pluripotency. *Cell Stem Cell.* 3, 132–135. doi: 10.1016/j.stem.2008.06.019

74. McNeish, J., Roach, M., Hambor, J., Mather, R.J., Weibley, L., Lazzaro, J., Gazard, J., Schwarz, J., *et al.* (2010). High throughput screening in embryonic stem cell derived neurons identifies potentiators of a-amino-3-hydroxyl-5-methyl-4- isoxazolepropionate-type glutamate receptors. *J Biol. Chem.* 285(22):17209-17. doi: 10.1074/jbc.M109.098814.
75. Mikkelsen, T.S., Hanna, J., Zhang, X., Ku, M., Wernig, M., Schorderet, P., et al. (2008). Dissecting direct reprogramming through integrative genomic analysis. *Nature.* 454, 49–55. doi: 10.1038/nature07056.
76. Moad, M., Pal, D., Hepburn, A.C., Williamson, S.C., Wilson, L., Lako, M., *et al.* (2013). A Novel Model of Urinary Tract Differentiation, Tissue Regeneration, and Disease: Reprogramming Human Prostate and Bladder Cells into Induced Pluripotent Stem Cells. *Eur Urol.* 64(5):753–761. doi: 10.1016/j.eururo.2013.03.054
77. Nguyen, H.N., Byers, B., Cord, B., Shcheglovitov, A., Byrne, J., Gujar, P., et al. (2011). LRRK2 Mutant iPSC-Derived DA Neurons Demonstrate Increased Susceptibility to Oxidative Stress Cell Stem Cell. 8(3): 267–280. doi:10.1016/j.stem.2011.01.013.
78. Nori, S., Okada, Y., Yasuda, K., Tsuji, O., Takahashi, Y., Kobayashi, Y., et al. (2011). Human-induced pluripotent stem-cell–derived neurospheres promote motor functional recovery after spinal cord injury in mice. *Proc Natl Acad Sci U S A.* 108(40): 16825–16830. doi: 10.1073/pnas.1108077108
79. Okita, K., Nakagawa, M., Hyenjong, H., Ichisaka, T. and Yamanaka, S. (2008). Generation of mouse induced pluripotent stem cells without viral vectors. *Science.* 322(5903), 949-53. doi: 10.1126/science.1164270
80. Okita, K., Ichisaka, T., and Yamanaka, S. (2007). Generation of germline-competent induced pluripotent stem cells. Nature. 448, 313-317. doi: 10.1038/nature05934
81. Pappas, J.J., and Yang, P.C. (2008). Human ESC vs. iPSC- Pros and Cons. *J. of. Cardiovasc. Trans. Res.* 1:96-99. DOI 10.1007/s12265-008-9032-2.
82. Park, E.T., Gum, J.R., Kakar, S., Kwon, S.W., Deng, G., and Kim, Y.S. (2008c). Aberrant expression of SOX2 upregulates MUC5AC gastric foveolar mucin in mucinous cancers of the colorectum and related lesions. *Int J Cancer*. 122(6):1253-60.
83. Park, I.H., Arora, N., Huo, H., Maherali, N., Ahfeldt, T., Shimamura, A., *et al.* (2008b). Disease-specific induced pluripotent stem cells. *Cell.* 134(5):877-86. doi: 10.1016/j.cell.2008.07.041.

84. Park, I.H., Zhao, R., West, J.A., Yabuuchi, A., Huo, H., Ince, T.A., et al. (2008a). Reprogramming of human somatic cells to pluripotency with defined factors. *Nature*. 451, 141–146.
85. Rashid, S.T., Corbineau, S., Hannan, N., Marciniak, S.J., Miranda, E., Alexander, G., *et al.*. (2010) Modeling inherited metabolic disorders of the liver using human induced pluripotent stem cells. *J Clin Invest.* 120:3127-36. doi: 10.1172/JCI43122.
86. Rosen, D.R., Siddique, T., Patterson, D., Figlewicz, D.A., Sapp, P., Hentati, A., *et al*. (1993). Mutations in Cu/Zn superoxide dismutase gene are associated with familial amyotrophic lateral sclerosis. *Nature*. 362:59-62
87. Ruiz, S., brennand, K., Panopoulos, A.D., Herrerias, A., Gage, F.H. and Izpisua-Belmonte, J.C. (2010). High-Efficient Generation of Induced Pluripotent Stem Cells from Human Astrocytes. *PLoS ONE* 5(12), e15526. DOI: 10.1371/journal.pone.0015526.
88. Sato, T., Joyner, A.L., and Nakamura, H. (2004). How does Fgf signaling from the isthmic organizer induce midbrain and cerebellum development? Dev Growth Differ. 46(6):487-94.
89. Sauer, A.V., Morbach, H., Brigida, I., Ng, Y.S., Aiuti, A., Meffre, E. (2012). Defective B cell tolerance in adenosine deaminase deficiency is corrected by gene therapy. *J Clin Invest*. 122(6):2141–2152. doi: 10.1172/JCI61788.
90. Seiler, A., Visan, A., Buesen, R., Genschow, E., and Spielmann, H. (2004). Improvement of an in vitro stem cell assay for developmental toxicity: the use of molecular endpoints in the embryonic stem cell test. *Reprod Toxicol.* 18(2):231-40.
91. Seki, T., Yuasa, S., Oda, M., Egashira, T., Yae, K., Kusumoto, D., et al. (2010). Generation of induced pluripotent stem cells from human terminally differentiated circulating T cells. Cell Stem Cell. 7(1), 11-4. doi:10.1016/j.stem.2010.06.003.
92. Shefner, J.M., Cudkowicz, M.E., Schoenfeld, D., Conrad, T., Taft, J., Chilton, M., *et al*. (2004) NEALS Consortium. A clinical trial of creatine in ALS. *Neurology* 63, 1656–1661.
93. Shi, Y., Desponts, C., Do, J.T., Hahm, H.S., Scholer, H.R., and Ding, S. (2008a). Induction of pluripotent stem cells from mouse embryonic fibroblasts by Oct4 and Klf4 with small-molecule compounds. *Cell Stem Cell*. 3, 568–574. doi: 10.1016/j.stem.2008.10.004.
94. Shi, Y., Do, J.T., Desponts, C., Hahm, H.S., Scholer, H.R., and Ding, S. (2008b). A combined chemical and genetic approach for the generation of induced pluripotent stem cells. *Cell Stem Cell.* 2, 525–528. doi: 10.1016/j.stem.2008.05.011.

95. Silva, J., Barrandon, O., Nichols, J., Kawaguchi, J., Theunissen, T.W., and Smith, A. (2008). Promotion of reprogramming to ground state pluripotency by signal inhibition. *PLoS Biol.* 6, e253. DOI: 10.1371/journal.pbio.0060253

96. Soejitno, A., and Prayudi, P.K.A. (2011). The prospect of induced pluripotent stem cells for diabetes mellitus treatment. *Ther Adv Endocrinol Metab.* 2(5):197-210. doi: 10.1177/2042018811420198.

97. Soldner, F., Hockemeyer, D., Beard, C., Gao, Q., Bell, G.W., Cook, E.G., *et al*. (2009). Parkinson's disease patient derived induced pluripotent stem cells free of viral reprogramming factors. *Cell*. 136(5):964-977. doi: 10.1016/j.cell.2009.02.013.

98. Sollano, J.A., Kirsch, J.M., Bala, M.V., Chambers, M.G. and Harpole, L.H. (2008) The economics of drug discovery and the ultimate valuation of pharmacotherapies in the marketplace. *Clin. Pharmacol. Ther.* 84, 263–266. doi: 10.1038/clpt.2008.117.

99. Somers, A., Jean, J.C., Sommer, C.A., Omari, A., Ford, C.C., Mills, J.A., et al. (2010). Generation of transgene-free lung disease-specific human induced pluripotent stem cells using a single excisable lentiviral stem cell cassette. *Stem Cells* 28(10), 1728-40. doi: 10.1002/stem.495.

100. Song, B., Niclis, J.V., Alikhan, M.A., Sakkal, S., Sylvain, A., Kerr, P.G., et al. (2011). Generation of Induced Pluripotent Stem Cells from Human Kidney Mesangial Cells. *J Am Soc Nephrol.* 22(7), 1213-1220. doi:10.1681/ASN.2010101022JASN.

101. Stadtfeld, M., Maherali, N., Breault, D.T., and Hochedlinger, K. (2008a). Defining molecular cornerstones during fibroblast to iPS cell reprogramming in mouse. *Cell Stem Cell.* 2(3):230-40. doi: 10.1016/j.stem.2008.02.001.

102. Stadtfeld, M., Nagaya, M., Utikal, J., Weir, G., and Hochedlinger, K. (2008b). Induced pluripotent stem cells generated without viral integration. *Science.* 322(5903):945-9. doi: 10.1126/science.1162494.

103. Sugii, S., Kida, Y., Kawamura, T., Suzuki, J., Vassena, R., Yin, Y.Q., et al. (2010). Human and mouse adipose-derived cells support feeder-independent induction of pluripotent stem cells. *Proc Natl Acad Sci U S A.* 107(8), 3558-63. doi: 10.1073/pnas.0910172106.

104. Sullivan, G.J., Hay, D.C., Park, I.H., Fletcher, J., Hannoun, Z., Payne, C.M., *et al.* (2010) Generation of functional human hepatic endoderm from human induced pluripotent stem cells. *Hepatology* 51, 329–335.

105. Suzuki K., Mitsui K., Aizawa E., Hasegawa K., Kawase E., Yamagishi T., et al. (2008). Highly efficient transient gene expression and gene targeting in primate embryonic stem cells with helper-dependent adenoviral vectors. *Proc. Natl. Acad. Sci. USA* 105, 13781–13786. doi: 10.1073/pnas.0806976105.

106. Suzuki, N., Yamazaki, S., Yamaguchi, T., Okabe, M., Masaki, H., Takaki, S., et al. (2013). Generation of Engraftable Hematopoietic Stem Cells From Induced Pluripotent Stem Cells by Way of Teratoma Formation. *Mol Ther.* 21(7): 1424–1431. doi: 10.1038/mt.2013.71

107. Tada, M., Takahama, Y., Abe, K., Nakatsuji, N., and Tada, T. (2001). Nuclear reprogramming of somatic cells by in vitro hybridization with ES cells. *Curr. Biol.* 11(19):1553–1558.

108. Takahashi, K., and Yamanaka, S. (2006a) Induction of pluripotent stem cells from mouse embryonic and adult fibroblast cultures by defined factors. *Cell.* 126(4):663–676.

109. Takahashi, K., Ichisaka, T., and Yamanaka, S. (2006b). Identification of genes involved in tumor-like properties of embryonic stem cells. *Methods Mol Biol.* 329:449-58.

110. Tan, Q., Lui, P.P.Y., Rui, Y.F., and Wong, Y.M. (2012). Comparison of Potentials of Stem Cells Isolated from Tendon and Bone Marrow for Musculoskeletal Tissue Engineering. *Tissue Eng Part A.* 18(7-8): 840–851. doi: 10.1089/ten.tea.2011.0362

111. Tanaka, T., Tohyama, S., Murata, M., Nomura, F., Kaneko, T., Chen, H., *et al.* (2009) In vitro pharmacologic testing using human induced pluripotent stem cell-derived cardiomyocytes. *Biochem. Biophys. Res. Commun*. 385, 497–502. doi: 10.1016/j.bbrc.2009.05.073.

112. Thomson, J.A., Itskovitz-Eldor, J., Shapiro, S.S., Waknitz, M.A., Swiergiel, J.J., Marshall, V.S., *et al.* (1998). Embryonic stem cell lines derived from human blastocysts. *Science.* 282(5391):1145-7.

113. Till, J. E., and McCulloch, E.A. (1961) A Direct Measurement of the Radiation Sensitivity of Normal Mouse Bone Marrow Cells. *RADIATION RESEARCH*. 14, 213-222.

114. Tulpule, A., Kelley, J.M., Lensch, M.W., McPherson, J., Park, I.H., Hartung, O., *et al.* (2013). Pluripotent stem cell models of Shwachman-Diamond syndrome reveal a common mechanism for pancreatic and hematopoietic dysfunction. *Cell Stem Cell*. 12(6): 727–736. doi: 10.1016/j.stem.2013.04.002.

115. Utikal, J., Maherali, N., Kulalert, W. and Hochedlinger, K. (2009). Sox2 is dispensable for the reprogramming of melanocytes and melanoma cells into induced pluripotent stem cells. *J Cell Sci.* 122(19), 3502–3510. doi:10.1242/jcs.054783

116. Wang, X.M., Yik, W.Y., Zhang, P., Lu, W., Dranchak, P.K., Shibata, D., *et al.* (2012). The gene expression profiles of induced pluripotent stem cells from individuals with childhood cerebral adrenoleukodystrophy are consistent with proposed mechanisms of pathogenesis. *Stem Cell Research & Therapy*. 3(5):39. doi:10.1186/scrt130.

117. Warren, L., Manos, P.D., Ahfeldt, T., Loh, Y.H., Li, H., Lau, F., et al. (2010). Highly Efficient Reprogramming to Pluripotency and Directed Differentiation of Human Cells with Synthetic Modified mRNA. Cell Stem Cell 7(5), 618-630. doi: 10.1016/j.stem.2010.08.012

118. Wilmut, I., Schnieke, A.E., McWhir, J., Kind, A.J., and Campbell, K.H. (1997). Viable offspring derived from fetal and adult mammalian cells. *Nature.* 385: 810–813.

119. Wobus, A.M., and Loser, P. (2011) Present state and future perspectives of using pluripotent stem cells in toxicology research. *Arch Toxicol.* 85:79–117

120. Woltjen, K., Michael, I.P., Mohseni, P., Desai, R., Mileikovsky, M., Hämäläinen, R., et al. (2009), "piggyBac transposition reprograms fibroblasts to induced pluripotent stem cells. *Nature* 458(7239), 766-70. doi: 10.1038/nature07863.

121. Xu, D., Alipio, Z., Fink, L.M., Adcock, D.M., Yang, J., Ward, D.C., I. (2009). Phenotypic correction of murine hemophilia A using an iPS cell-based therapy. *Proc Natl Acad Sci USA.* 106(3):808-13. doi: 10.1073/pnas.0812090106

122. Yazawa, M., Hsueh, B., Jia, X., Pasca, A.M., Bernstein, J.A., Hallmayer, J., *et al.* (2011). Using induced pluripotent stem cells to investigate cardiac phenotypes in Timothy syndrome. *Nature*. 471(7337):230-4. doi: 10.1038/nature09855.

123. Ye, Z., Zhan, H., Mali, P., Dowey, S., Williams, D.M., Jang, Y.Y., et al. (2009). Human-induced pluripotent stem cells from blood cells of healthy donors and patients with acquired blood disorders. *Blood* 114(27), 5473–5480. doi: 10.1182/blood-2009-04-217406.

124. Yokoo, N., Baba, S., Kaichi, S., Niwa, A., Mima, T., Doi, H., *et al*. (2009) The effects of cardioactive drugs on cardiomyocytes derived from human induced pluripotent stem cells. *Biochem. Biophys. Res. Commun*. 387, 482–488. doi: 10.1016/j.bbrc.2009.07.052.

125. Yoshida, T., Ozawa, Y., Suzuki, K., Yuki, K., Ohyama, M., Akamatsu, W., et al. (2014). The use of induced pluripotent stem cells to reveal pathogenic gene mutations and explore treatments for retinitis pigmentosa. *Mol Brain*. 7:45. doi: 10.1186/1756-6606-7-45.

126. Yoshida, Y., and Yamanaka, S. (2010) Recent stem cell advances: induced pluripotent stem cells for disease modeling and stem cell-based regeneration. *Circulation* 122, 80–87. doi: 10.1161/CIRCULATIONAHA.109.881433

127. Yoshioka, N., Gros, E., Li, H., Kumar, S., Deacon, D.C., Maron, C. (2013). Efficient Generation of Human iPSCs by a Synthetic Self-Replicative RNA. Cell Stem Cell. 13(2)246–254. DOI: http://dx.doi.org/10.1016/j.stem.2013.06.001

128. Yu, J., Hu, K., Smuga-Otto, K., Tian, S., Stewart, R., Slukvin, II., et al. (2009). Human induced pluripotent stem cells free of vector and transgene sequences. *Science.* 324(5928):797-801. doi: 10.1126/science.1172482.

129. Yu, J., Vodyanik, M.A., Smuga-Otto, K., Antosiewicz-Bourget, J., Frane, J.L., Tian, S., et al. (2007). Induced pluripotent stem cell lines derived from human somatic cells. *Science* 318(5858), 1917-20. doi: 10.1126/science.1151526.

130. Yusa, K., Rad, R., Takeda, J., and Bradley, A. (2009). Generation of transgene-free induced pluripotent mouse stem cells by the piggyBac transposon. *Nat Methods.* 6(5):363-9. doi: 10.1038/nmeth.1323.

131. Zhang, G., Shang, B., Yang, P., Cao, Z., Pan ,Y., and Zhou, Q. (2012). Induced pluripotent stem cell consensus genes: implication for the risk of tumorigenesis and cancers in induced pluripotent stem cell therapy. *Stem Cells Dev*.21(6):955-64. doi: 10.1089/scd.2011.0649.

132. Zhang, M., Yang, C., Liu, H., and Sun, Y. (2013). Induced Pluripotent Stem Cells Are Sensitive to DNA Damage. *Genomics, Proteomics & Bioinformatics.* 11(5)320–326. doi:10.1016/j.gpb.2013.09.006

133. Zhao, Y., Yin, X., Qin, H., Zhu, F., Liu, H., Yang, W., et al. (2008). Two supporting factors greatly improve the efficiency of human iPSC generation. *Cell Stem Cell*. 3, 475–479. doi: 10.1016/j.stem.2008.10.002.

134. Zhou, Q., Brown, J., Kanarek, A., Rajagopal, J., and Melton, D.A. (2008). In vivo reprogramming of adult pancreatic exocrine cells to β-cells. *Nature.* 455, 627-632 doi:10.1038/nature07314.

135. Zhou, T., Benda, C., Dunzinger, S., Huang, Y., Ho, J.C., Yang, J., et al. (2012). Generation of human induced pluripotent stem cells from urine samples. *Nature Protocols.* 7:2080-2089 doi:10.1038/nprot.2012.115.

LEGENDS OF FIGURES

Figure 1: Historical timeline showing events that led to the development of iPSCs and the recent advances that have occurred in the field.

Figure 2: An overview of the methodology for the generation of iPSCs. 1) establishment of culture: the source cells are cultured for further use as host cells for the delivery of reprogramming proteins. 2) the cultured source cells are then transfected with the four factors from Yamanaka's cocktail and incubated on feeder layers that provide the nourishment to host cells and are responsible for the formation of extra cellular matrix, under suitable conditions of media. Two types of methods for the delivery of reprogramming factors into the somatic cells can be used- Integrating viral vector systems and Non-Integrating methods. 3) after the formation of iPSCs, the are characterized by different morphological and physicochemical analyses, which is followed by the expansion of iPSCs.

Figure 3 : Introduction of the four transcription factors (Oct-4, Sox-2, Klf-4, and c-Myc) leads to reprogramming of a somatic cell to an Induced Pluripotent Stem Cell (iPSC) which can further differentiate into different types of cells. Many factors or chemicals are able to replace one of the factors from the basic 4 factors required for reprogramming, and for the enhancement many other small molecule chemicals or factor are also used.

Figure 4: There are many applications of iPSCs in the fields of gene therapy, disease modelling & drug discovery. Somatic cells from the patient are used for the generation of diseased iPSCs. These diseased iPSCs may be repaired by Gene Therapy and further used for the generation of healthy somatic cells to be transplanted to the patient, or they may be used to produce unrepaired somatic cells for disease modelling or drug screening.

Type of cells	Reprogramming Factors	Reference
Fibroblast	OSKM	**Takahashi et al 2006a**
	OSLN	**Yu et al 2007**
Keratinocytes	OSKM	**Aasen et al 2008**
Cord blood endothelial cells	OSLN	**Haase et al 2009**
Cord blood stem cells	OSKM	**Ye et al 2009**
Neural stem cells	O	**Kim et al 2009a**
Melanocytes	OSKM	**Utikal et al 2009**
Amniotic cells	OSKM	**Li et al 2009**
Adipose derived stem cells	OSKM	**Sugii et al 2010**
Hepatocytes	OSKM	**Liu et al 2010**
Circulating T cells	OSKM	**Seki et al 2010**
Astrocytes	OSKM	**Ruiz et al 2010**
Peripheral blood	OSKM	**Kunisato et al 2011**
Kidney mesangial cells	OSKM	**Song et al 2011**
Urine cells	OS	**Zhou et al 2012**

Table1: Different cell sources and different combinations of reprogramming factors have been used by different groups for reprogramming to IPSCs (O- Oct4; S- Sox2; K- Klf4; M- c-Myc; N- Nanog, L- Lin28).

	Reprogramming	Factors	Cell type	Efficiency	Reference
Integrating methods	Retroviral Transduction	OSKM	Mouse fibroblast	0.001-1%	**Takahashi et al 2006a**
		OSK + VPA	Neonatal	1%	**Huangfu et al 2008a**
	Lentiviral	OSKM	Human fibroblast	0.1-1%	**Yu et al 2007**
		OK + parnate + CHIR99021	Neonatal	0.02%	**Li et al 2009**
	Inducible lentiviral	OSKM	Human fibroblast	0.1-2%	**Maherali et al 2008**
Non Integrating methods	Sendai virus	OSKM	Human fibroblast	~0.1%	**Fusaki et al 2009**
	Adeno viral transduction	OSKM	Mouse fibroblast	~0.001%	**Stadfeld et al 2008a**
	Plasmid DNA transfer	OSK	Fibroblast	0.00%	**Okita et al 2008**
	lox p lentivirus	OSKM	Fibroblast	0.1-1%	**Somers et al 2010**
	PiggyBAC	OSKM	Fibroblast	0.01%	**Woltjen et al 2009**
	Polyarginine tagged polypeptide	OSKM	Neonatal fibroblast	0.00%	**Kim et al 2009b**
	RNA modified synthetic mRNA	OSKM	Human fibroblast	4.40%	**Warren et al 2010**

Table2: Different delivery methods for transfer of different combinations of transcription factors have different efficiencies of reprogramming (O- Oct4; S- Sox2; K- Klf4; M- c-Myc).

Factor/ Chemical	Function	Able to replace	Reference
Nanog	ESC-specific transcription factor	together with Lin28, able of replacing K and M	**Yu et al 2007**
Lin28	ESC-specific RNA-binding protein	together with Nanog, able of replacing K and M	**Yu et al 2007**
Esrrb	Orphan Nuclear Receptor	K	**Feng et al 2009**
SV40 LT (T)	SV40 large T antigen used for cell transformation	K; M* and Lin28, Nanog	**Mali et al 2008**
BIX-01294	inhibitor of G9a histone methyltransferase	S, O	**Shi et al 2008a,b**
VPA	inhibitor of histone deacetylase	K and M	**Huangfu et al 2008a**

Table 3: Many factors and chemicals are able to replace the basal transcriptions factors used for reprogramming (O- Oct4; S- Sox2; K- Klf4; M- c-Myc; M*- N-Myc).

Disease/ Syndrome	Cause(s)	Features	Cells used for iPSC generation	System Used	References
Parkinson's Disease (PD)	Familial forms caused by α-synuclein, ubiquitin carboxy terminal hydroxylase L1, parkin, DJ-1, putative serine threonine kinase 1 and leucine rich repeat kinase 2	Loss in nigrostriated dopaminergic neurons in substantia nigra; presence of Lewy bodies	Dermal fibroblasts of patient with idiopathic PD	Lentiviral	**Soldner et al 2009**
Huntington Disease (HD)	CAG repeats (36 or more) in the first exon of *htt* gene gets expanded abnormally	Degeneration in striatum & cerebral cortex	Fibroblasts	Lentiviral	**Kaye et al 2013, Park et al 2008b**
ALS or Lou Gehrig's disease	Autosomal dominant mutation in superoxide demutase (SOD1)	Death of motor neurons of the motor cortex, brain stem & spinal cord	Fibroblasts	Lentiviral	**Chestkov et al 2014, Rosen et al 1993**

Friedreich's ataxia (FRDA)	GAA trinucleotide repeat in the first exon of the frataxin gene gets expanded	Accumulation of mitochondrial iron, specific enzymes in mitochondria become defective, sensitivity to oxidative stress increases, cell death mediated by free radicals	Fibroblasts	Lentiviral	**Campuzano et al 1996, Ku et al 2010**
Lesch-Nhyan syndrome (carrier state)	Deficiency of hypoxanthine guanine Phospho ribosyl transferase (HPRT)	over-production of uric acid, low or medium level of mental retardation, megaloblastic anemia is frequent	Dermal fibroblasts	Lentiviral	**Park et al 2008b**
Shwachman-Bodian-Diamond syndrome (SBDS)	Mutations in the Shwachman-Bodian-Diamond syndrome (SBDS) gene	Exocrine pancreatic insufficiency, predisposition to leukemia, hematopoietic dysfunction	Fibroblasts	Lentiviral	**Tulpule et al 2013**

Gaucher's type III	Deficiency of acid hydrolase, β-glucocerebrosidase, or glucosylceramidase	myoclonal epilepsy, nerve deafness	Fibroblasts	Lentiviral	**Park et al 2008b**
Becker type Muscular Dystrophy (BMD)	Mutation in Dystrophin gene	Loss of walking ability, but progression slower than DMD	Fibroblasts	Lentiviral	**Park et al 2008b**
Downs syndrome/ Trisomy 21	trisomy of chromosome 21	Cardiac and cognitive defects, premature Alzheimers Disease and ageing, dysmorphic facial features	Fibroblasts	Lentiviral	**Briggs et al 2013, Park et al 2008b**
Familial Dysautonomia (FD) or Riley-Day syndrome	Autosomal recessive disorder caused by a single mutation in exon 20 in I-K-B kinase complex associated protein (IKBKAP) gene	Dysfunction of small fiber sensory neurons	Fibroblasts	Lentiviral	**Lee et al 2011**

Childhood Cerebral Adreno Leuko Dystrophy (CCALD)	Mutation in *ABCD1* gene	Adrenal cortex, nervous system and testes get affected, leading to rapid cerebral demyelination and adrenocortical atrophy.	Skin fibroblasts	retroviral	**Wang et al 2012**
Rett's syndrome	Classic form caused by loss-of-function mutation in Methyl-CpG-binding protein 2 (MECP2) gene on the X - chromosome, variants caused by mutations in FOXG1 or CDKL1 on chromosome 14 and X-chromosome respectively	neurocognitive regression & autistic behavior	Fibroblasts	retroviral	**Farra et al 2012, Amenduni et al 2011**
Duchenne type Muscular Dystrophy (DMD)	Biochemical & genetic defects in Dystrophin-glycoprotein complex	Loss of walking ability	Tail tip fibroblasts (mouse)	retroviral	**Gangopadhyay et al 1992, Filareto et al 2013**
Generation of human prostate and urinary tract cells	NA	NA	Human prostate and urinary tract	Lentiviral	**Moad et al 2013**

			cells		
Adenosine Deaminase deficiency-related Severe Combined Immunodeficiency (ADA-SCID)	Defects in Adenosine deaminase (AD) gene	Impaired development and functioning of T, B, and NK cells; complete absence of humoral and cellular immunity; recurrence of infections.	Bone Marrow derived mesenchymal cells	Lentiviral	**Sauer et al 2012, Park et al 2008b**
Type 1 Diabetes Mellitus (DM)	Progressive β-cell destruction	Long term micro and macro-vascular complications.	Fibroblasts	Lentiviral	**Soejitno et al 2011, Park et al 2008b**
Hemophilia A	Deficiency of factor VIII	Decreased protein production, inefficient clotting of blood	Fibroblasts	retroviral	**Xu et al, 2009**
Glycogen storage disease 1a	Mutation in Glucose-6-Phosphate gene	Increased accumulation of lipids and glycogen	Dermal fibroblasts	retroviral	**Lei et al 1995, Rashid et al 2010**

Familial hypercholestrolaemia	Mutation in Low density Lipoprotein receptor (LDLR) gene	Deficiency of LDL-receptor mediated uptake of cholesterol	Dermal fibroblasts	retroviral	**Rashid et al 2010**
Spinal muscular atrophy	Mutation in Survival of Motor Neuron 1 (SMN1) gene	Paralysis, muscle weakness and often death	Fibroblasts	Lentiviral	**Ebert et al 2009**
Hutchinson-Gilford Progeria Syndrome	Point mutations in Lamin A	Premature atherosclerosis, vascular smooth muscles gets degraded	Fibroblasts	retroviral	**Liu et al 2011a**
Alzheimer disease	Duplication of Amyloid β Precursor Protein (APP)	Presence of neurofibrillary tangles and amyloid plaques in the brain	Fibroblasts	retroviral	**Israel et al 2012**
LEOPARD syndrome	Mutation in Protein Tyrosine Phosphatase Nonreceptor type 11 (PTPN11) gene	Cardiac abnormalities, ocular hypertelorism, & growth retardation.	Fibroblasts	retroviral	**Carvajal-Vergara et al 2010, Leguis et al 2002.**
Timothy's syndrome	CACNA1C	Webbed fingers & toes, autism, immune deficiency	Fibroblasts	retroviral	**Yazawa et al 2011**

Dyskeratosis congentia	Mutation in Dyskerin (DKC1) gene	Increased failure of bone marrow, pulmonary fibrosis & cancer, oral leykoplakia, abnormal skin pigmentation and nail dystrophy	Fibroblasts	retroviral	**Batista et al 2011**
α1-antitrypsin deficiency	Mutation in α1-antitrypsin **(**A1AT) gene	misfolded α1-antitrypsin gets aggregated in the endoplasmic reticulum	Dermal fibroblasts	retroviral	**Rashid et al 2010**

Table 4: List of diseases where iPSCs have been used for gene therapy and disease modelling.

	Pros	Cons
Due to Characteristics of iPSCs	Eliminates ethical issues	Premature ageing
	Reduced chances of immunorejection **(Guha et al 2013)**	high rate of apoptosis
	Reduced risks of clinical trials	Low level DNA damage repair **(Zhang et al 2012)**
	Consistent phenotypes for disease modelling **(Fong et al 2013)**	Sensitive to Ionizing radiation
	Differentiation to any cell type	Low rate of reprogramming
Due to technology of development	Continuous cell supply	Insertional Mutagenesis **(Howe et al 2008, Okita et al 2007)**
	Possible preservation	Tumourogenesis **(Okita et al 2007).**
	Availability and accessability of source cells	Chances of development of diseases due to factors used **(Hochedlinger et al 2005, Park et al 2008c, Ghaleb et al 2005, Kuttler et al 2006)**
	Personalization of treatment **(Chun et al 2011)**	Suboptimal standardization **(Pappas et al 2008)**
Applications	High-throughput screening of drugs and toxicity prediction **(Wobus et al 2011, Choi et al 2013)**	Complex assessment
	Reduced cost	Complex diseases become difficult to be modelled
	Gene correction therapies add to the benefits from iPSCs **(Choi et al 2013)**	Immature cells cause problems during cell line development

Table 5: The pros and cons associated with the use of iPSC.

Figure 1.JPEG

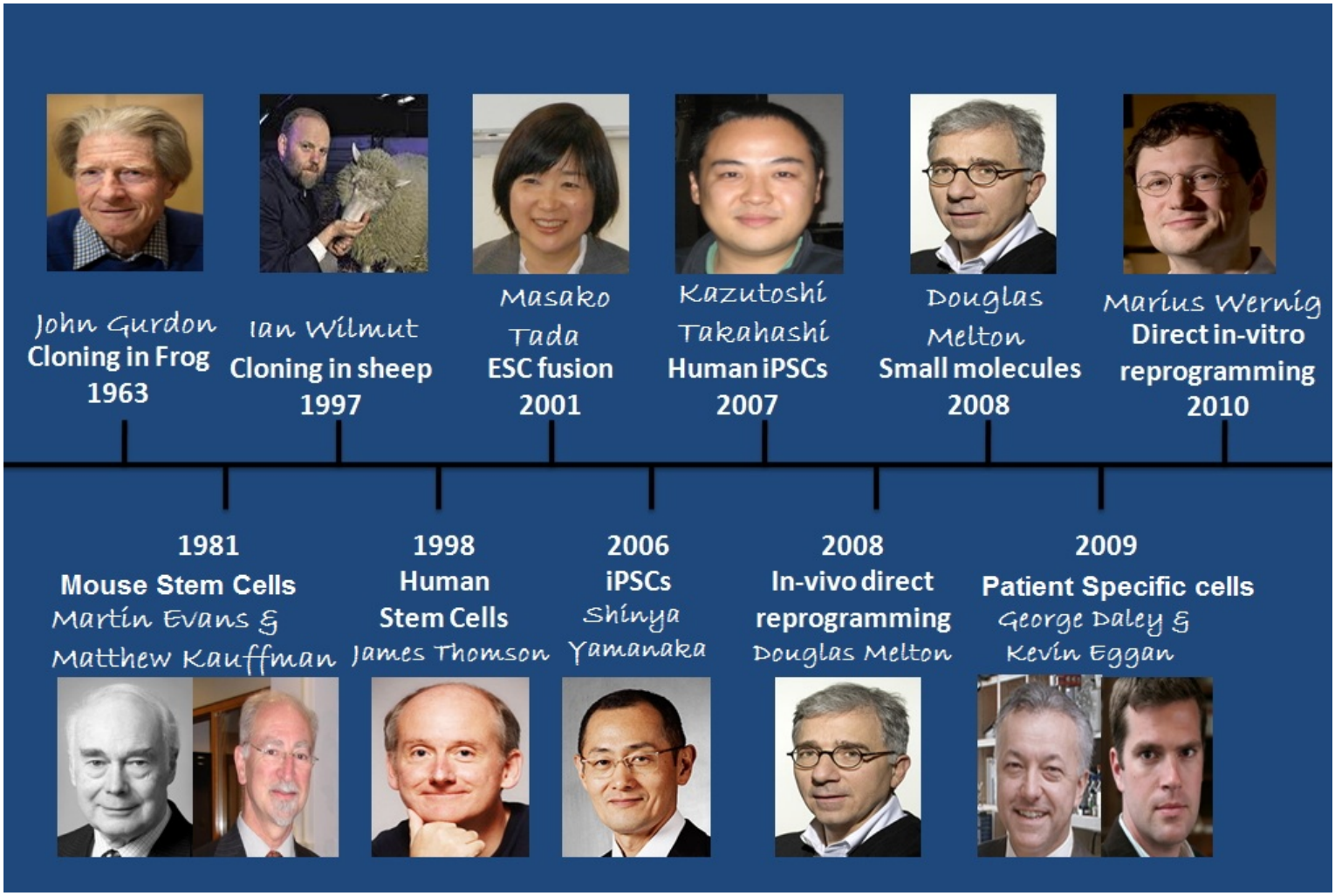


Figure 2.JPEG

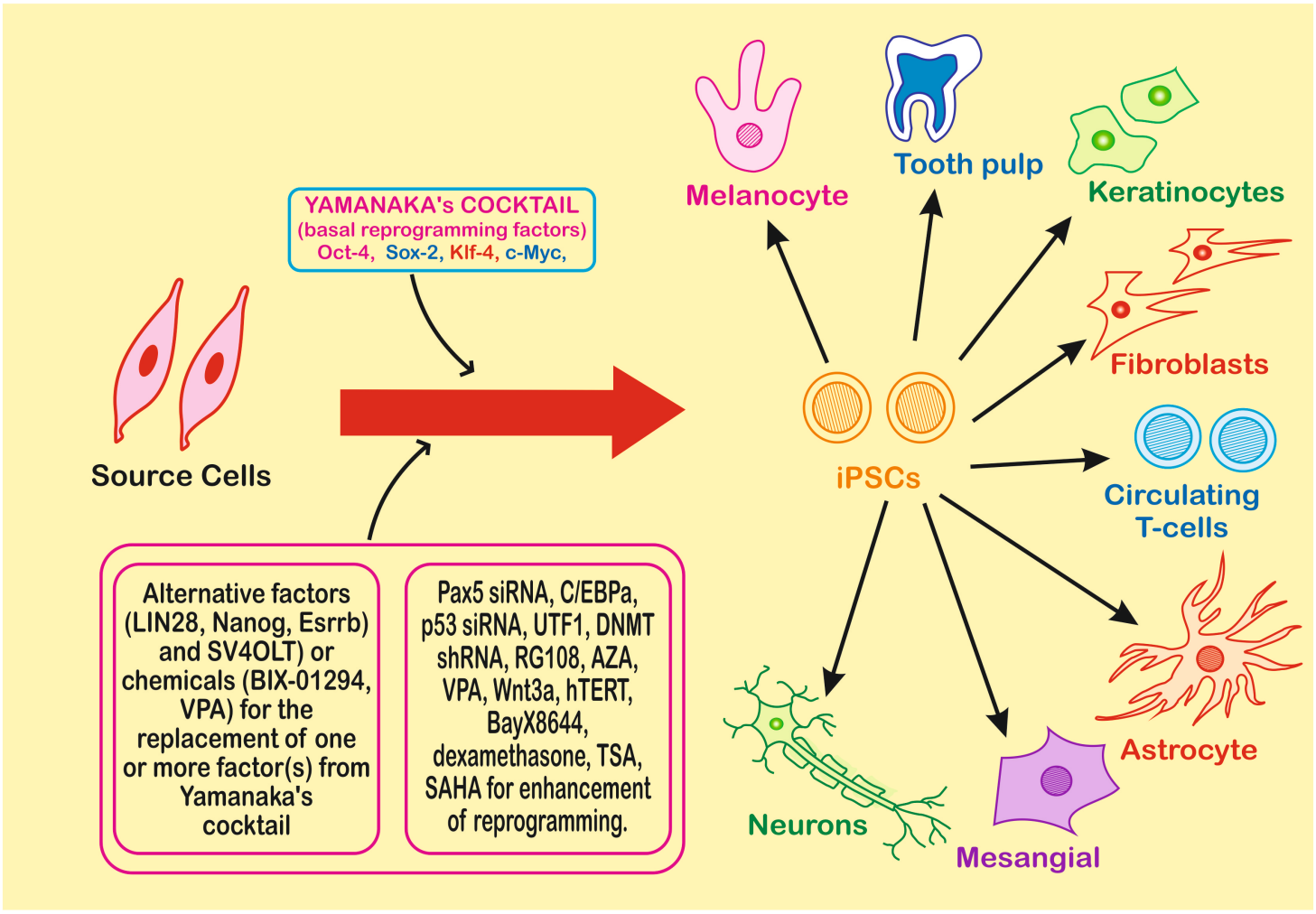


Figure 3.JPEG

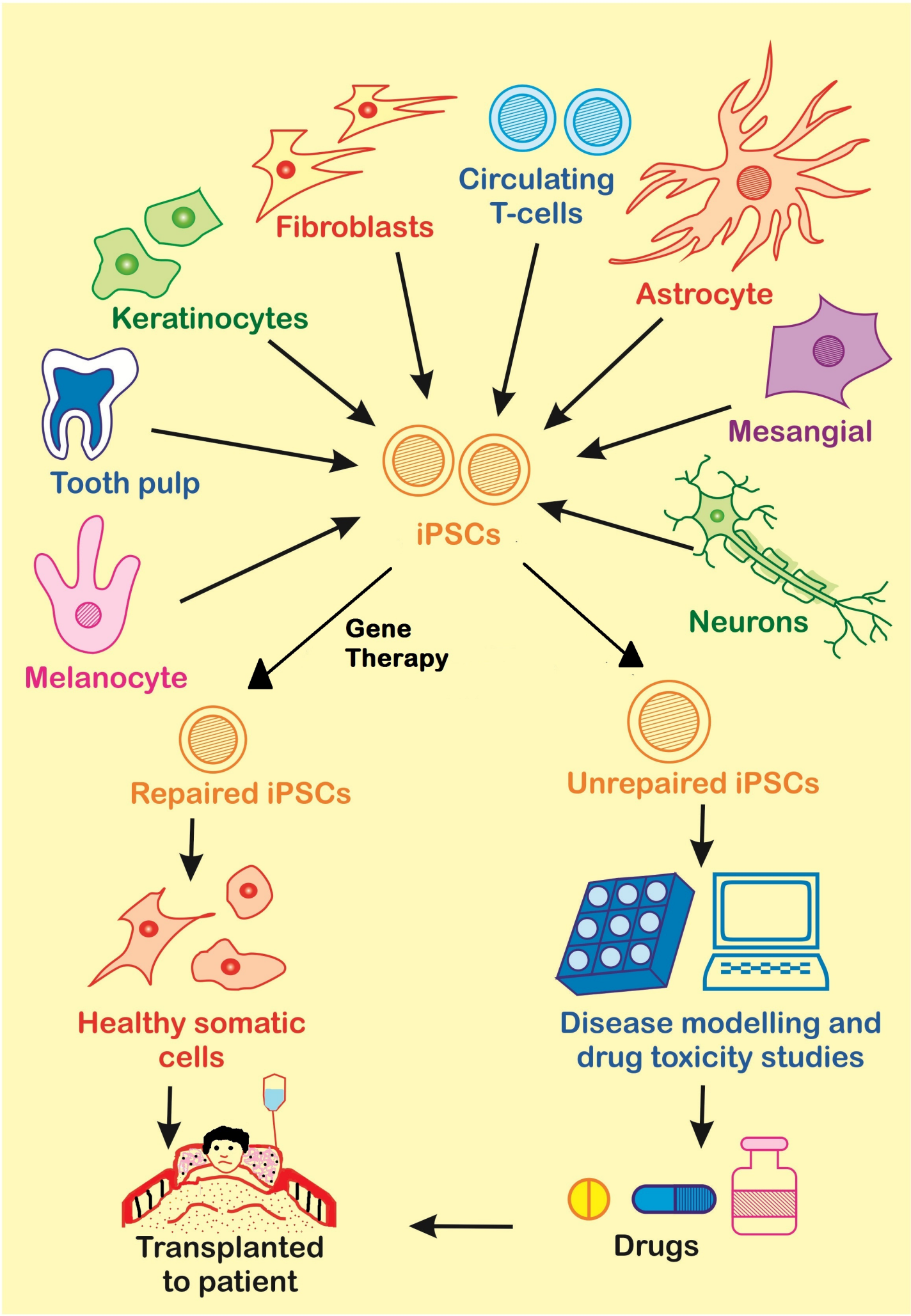
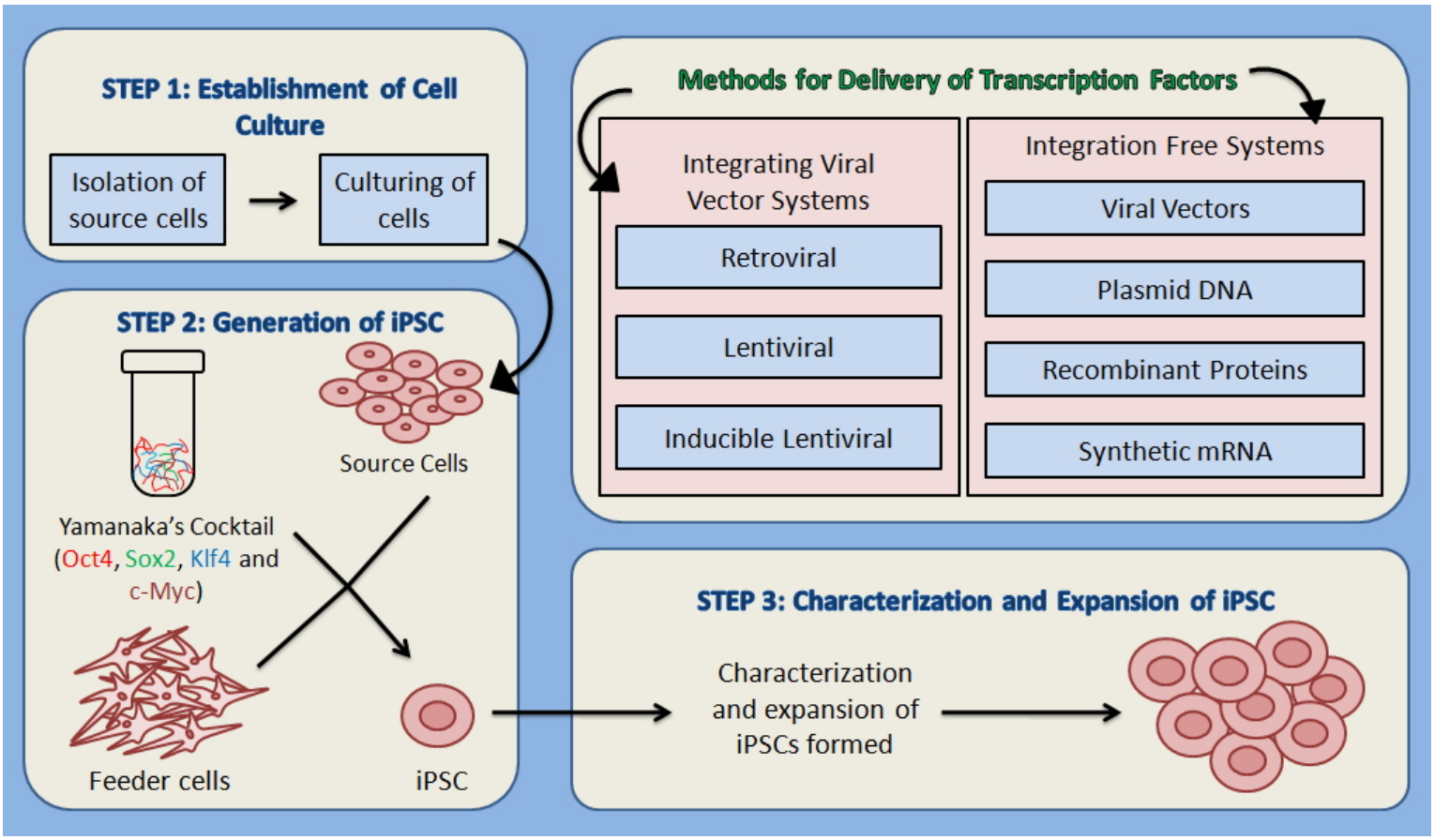


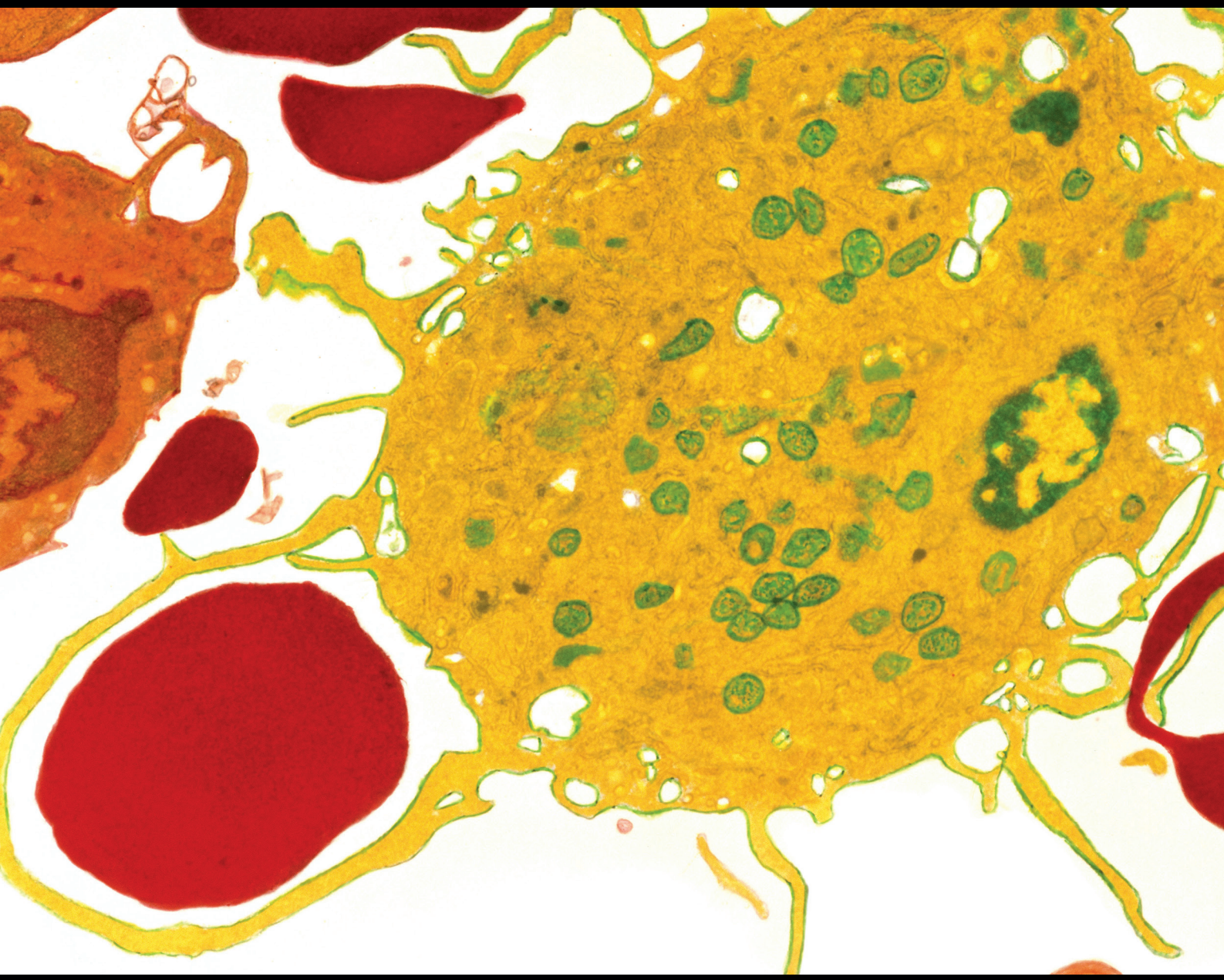
Figure 4.JPEG



Conference Papers in Science

National Conference on Advances in Materials Science for Energy Applications

Guest Editors: S. Anantha Ramakrishna, Ramesh Chandra, G. N. Tiwari, P. Mandal, and R. K. Shivpuri



National Conference on Advances in Material Science for Energy Applications

Conference Papers in Science

National Conference on Advances in Material Science for Energy Applications

Guest Editors: S. Anantha Ramakrishna, Ramesh Chandra, G. N. Tiwari, P. Mandal, and R. K. Shivpuri

Copyright © 2014 Hindawi Publishing Corporation. All rights reserved.

This is a special issue published in "Conference Papers in Science." All articles are open access articles distributed under the Creative Commons Attribution License, which permits unrestricted use, distribution, and reproduction in any medium, provided the original work is properly cited.

Contents

National Conference on Advances in Material Science for Energy Applications, S. Anantha Ramakrishna, Ramesh Chandra, G. N. Tiwari, P. Mandal, and R. K. Shivpuri
Volume 2014, Article ID 539291, 2 pages

Study of Rheological Properties of Industrial Lubricants, Ajay Vasishth, Piyush Kuchhal, and Gagan Anand
Volume 2014, Article ID 324615, 5 pages

Dielectric Properties of SnO^2 Thin Film Using SPR Technique for Gas Sensing Applications, Ayushi Paliwal, Anjali Sharma, Monika Tomar, and Vinay Gupta
Volume 2014, Article ID 656120, 4 pages

Study of Structural and Electronic Behavior of BeH_2 as Hydrogen Storage Compound: An Ab Initio Approach, Vikas Nayak, Suman Banger, and U. P. Verma
Volume 2014, Article ID 807893, 5 pages

Near-Field Hot Spots in Gold Nanoplasmonic Templates and Their Use for Surface Enhanced Raman Scattering Sensing Application, Prasanta Mandal
Volume 2014, Article ID 396826, 5 pages

NO_2 Sensing Properties of WO_3 Thin Films Deposited by Rf-Magnetron Sputtering, Savita Sharma, Monika Tomar, Nitin K. Puri, and Vinay Gupta
Volume 2014, Article ID 683219, 5 pages

Harnessing Solar Energy for Every Home: Energy Saving Applications, Jitisha Aggarwal and M. L. Aggarwal
Volume 2014, Article ID 628294, 3 pages

Study of Magnetic Property of Sn Doped Ni-Zn-Fe Nanoparticles, B. S. Tewari, Archana Dhyani, S. K. Joshi, Santosh Dubey, and Kailash Pandey
Volume 2014, Article ID 816970, 4 pages

On the Issue of Radiation-Induced Instability in Binary Solid Solutions, Santosh Dubey, S. K. Joshi, and B. S. Tewari
Volume 2014, Article ID 849241, 5 pages

Effect of MgO and V_2O_5 Catalyst on the Sensing Behaviour of Tin Oxide Thin Film for SO_2 Gas, Punit Tyagi, Anjali Sharma, Monika Tomar, and Vinay Gupta
Volume 2014, Article ID 812627, 4 pages

Synthesis and Characterisation of Thin Films of Bismuth Triiodide for Semiconductor Radiation Detectors, Alka Garg, Monika Tomar, and Vinay Gupta
Volume 2014, Article ID 370436, 3 pages

Hindawi Publishing Corporation
Conference Papers in Science
Volume 2014, Article ID 539291, 2 pages
http://dx.doi.org/10.1155/2014/539291

Editorial

National Conference on Advances in Material Science for Energy Applications

S. Anantha Ramakrishna,[1] Ramesh Chandra,[2] G. N. Tiwari,[3] P. Mandal,[4] and R. K. Shivpuri[5]

[1]*Department of Physics, Indian Institute of Technology Kanpur, Kanpur 208016, India*
[2]*Institute Instrumentation Centre, Indian Institute of Technology Roorkee, Roorkee 247667, India*
[3]*Centre for Energy Studies, Indian Institute of Technology Delhi, Delhi 110016, India*
[4]*Department of Physics, University of Petroleum and Energy Studies, Dehradun 248007, India*
[5]*Department of Nuclear Science and Technology, University of Petroleum and Energy Studies, Dehradun 248007, India*

Correspondence should be addressed to S. Anantha Ramakrishna; sar@iitk.ac.in

Received 7 October 2014; Accepted 7 October 2014; Published 22 December 2014

Copyright © 2014 S. Anantha Ramakrishna et al. This is an open access article distributed under the Creative Commons Attribution License, which permits unrestricted use, distribution, and reproduction in any medium, provided the original work is properly cited.

Aims and Scope. The National Conference on "Advances in Material Science for Energy Applications" (AMSEA) was organized by University of Petroleum and Energy Studies, Dehradun, India, for the first time. The aim of the conference was to bring experts from all over the country to showcase their contributions towards the advances in the science of materials for energy applications. In addition, the conference intended to educate the people about the usefulness of solar energy and nuclear energy in filling the gigantic gap between the energy production and consumption. The conference was a good platform for young scientists, engineers, research scholars, and students to exchange their thoughts and ideas and to encourage further development of the existing knowledge on energy harvesting.

During the two-day conference (9-10 January 2014), several important topics related to fabrication and characterization of materials for energy applications such as "Materials/techniques for solar energy applications," "Advances in thin film technology," "Optically-active nano-structured materials," "Advances in nanofluids," "Advanced materials for nuclear energy applications," and "Advances in synthesis and characterization technique" were covered in lectures and poster sessions. The conference started with distinguished and plenary lectures delivered by leading experts in Material Science from reputed institutes like IITs and universities in the country. In addition, each individual session began with invited talks of well-known researchers in the respective fields. The conference was a great success, having a significant number of participants contributing their papers to the sessions.

The published proceeding papers cover topics on energy storage, solar cell, radiation detector, and materials for sensor applications, industrial lubricants, and so forth. Authors of these papers have shown the significance of the materials and methods or technology developed. For example, V. Nayak et al. have studied BeH_2 as hydrogen storage material. M. Tomar et al. have investigated various materials for NO_2 and SO_2 gas sensors. J. Aggarwal et al. have proposed a prototype device for solar harnessing. There is also a report on materials for semiconductor radiation detector by A. Garg et al. Other research groups have developed and characterized various materials having direct or indirect impact on energy applications.

Acknowledgments

The conference was well supported financially by the Department of Science and Technology (SERB division) of Government of India, Sinsil International, Aimil Ltd. (Instruments and Technologies), India, Allahabad Bank, India. We owe special thanks to Dr. Parag Diwan, Vice Chancellor, and Dr. Utpal Ghosh, Pro-Vice Chancellor of UPES, for their support and encouragement in conducting such conference of national importance. We thank Mr. Dinesh Agarwal, Hon'ble

Cabinet Minister, Government of Uttarakhand, India, for inaugurating the conference.

S. Anantha Ramakrishna
Ramesh Chandra
G. N. Tiwari
P. Mandal
R. K. Shivpuri

Hindawi Publishing Corporation
Conference Papers in Science
Volume 2014, Article ID 324615, 5 pages
http://dx.doi.org/10.1155/2014/324615

Conference Paper

Study of Rheological Properties of Industrial Lubricants

Ajay Vasishth,[1] Piyush Kuchhal,[2] and Gagan Anand[2]

[1] *Department of Physics, Chandigarh University, Chandigarh, Punjab 160017, India*
[2] *Department of Physics, University of Petroleum and Energy Studies, Dehradun 248007, India*

Correspondence should be addressed to Gagan Anand; gagan4567@rediffmail.com

Received 11 February 2014; Accepted 11 March 2014; Published 14 May 2014

Academic Editors: R. K. Shivpuri and G. N. Tiwari

This Conference Paper is based on a presentation given by Gagan Anand at "National Conference on Advances in Materials Science for Energy Applications" held from 9 January 2014 to 10 January 2014 in Dehradun, India.

Copyright © 2014 Ajay Vasishth et al. This is an open access article distributed under the Creative Commons Attribution License, which permits unrestricted use, distribution, and reproduction in any medium, provided the original work is properly cited.

The most important rheological parameter for lubricants is viscosity as it also affects the tribological properties like friction between interacting surfaces and wear. This research intends to study the relationship between viscosity and temperature at different shear rates for multiple grades of three different categories of lubricants used for different applications viz. L1: MG20W50 (engine oil), L2: SAE20W50 (engine oil), L3: MC20W50 (mineral engine oil), L4: EP90 (gear oil), and L5: DXTIII (steering fluid). Constant high dynamic viscosity, shear stress, and low compressibility at different temperatures in multigrade as well as single grade industrial oil will help to maintain the surface film over the period of time and hence the reduction in wear. The dynamic viscosity of these chosen samples has been measured experimentally in temperature range of 20 to 50°C. The measurements have been extended to observe the dependence of shear rate, time, and temperature on the dynamic viscosity. All the samples are observed to behave like Newtonian fluids in the entire temperature range of study. Further, all samples seem to obey the Arrhenius relationship with temperature. Shear stress shows linear variation with shear rate exhibiting uniform viscosity which is substantiated by almost no variation in dynamic viscosity with shear rate for value above 5 per second.

1. Introduction

The role of lubrication is an important part in the field of tribology. Lubrication is to smoothen the movement of one surface over another and to maintain the viscoelastic behavior [1].

Lubricants are commonly used for lubrication to reduce the friction and wear of surfaces in contact [2] and effective heat transfer due to good thermal conductivity. Most lubricants are liquids (such as mineral oils, synthetic oil, silicon fluids, water, etc.). Selection of lubricant is very important for providing machine tools a longer life. To select an appropriate lubricant, it is necessary to know its properties, lubrication system of applied machinery, conditions of machinery, cost of lubricant [3]. Common properties of lubricating oil are: viscosity, viscosity index, density, compressibility, surface tension, cloud point, pour point or low temperature property, flash point, friction coefficient, high boiling point, low freezing point, thermal stability, corrosion prevention, high resistance to oxidation, and so forth. The most important property is its viscosity. Viscosity is a function of temperature and pressure. The relationship between the viscosity and temperature and the relationship between viscosities and pressure are also important in lubricant rheology as well as for the life of machine elements. Just as temperature rise reduces the viscosity of lubricating oil, also an increase in pressure produces a rise in its viscosity. Barus expressed a relation between viscosity and pressure introducing a constant α named pressure-viscosity coefficient [4]. In recent years, pressure viscosity relationship became an important parameter of lubricating oil to understand its performance, especially in high-temperature applications, so viscosity measurement becomes an important tool for doing so. Rheology is the study of the flow of matter: mainly liquids but also soft solids or solids under conditions in which they flow rather than deform elastically. It would be difficult to imagine any

Table 1: Shear stress, dynamic viscosity and torque versus temperature measurements for the samples L1, L2, L3, L4, L5 at shear rate 10.

Temp (°C)	Viscocity (Pa·s)					Shear stress (Pa)					Torque (mNm)				
	L1	L2	L3	L4	L5	L1	L2	L3	L4	L5	L1	L2	L3	L4	L5
20	0.45	0.61	0.46	0.51	0.24	4.51	6.07	4.58	5.09	2.43	0.06	0.08	0.06	0.07	0.03
25	0.38	0.49	0.36	0.44	0.19	3.84	4.91	3.64	4.44	1.93	0.05	0.06	0.05	0.06	0.03
30	0.29	0.40	0.34	0.37	0.15	2.87	4.04	3.40	3.69	1.46	0.04	0.05	0.04	0.05	0.02
35	0.26	0.34	0.27	0.30	0.12	2.64	3.40	2.68	3.03	1.17	0.03	0.04	0.03	0.04	0.02
40	0.24	0.29	0.17	0.27	0.12	2.37	2.90	1.68	2.69	1.19	0.03	0.04	0.02	0.04	0.02
45	0.24	0.25	0.16	0.24	0.07	2.37	2.49	1.59	2.39	0.71	0.03	0.03	0.02	0.03	0.01
50	0.22	0.20	0.15	0.23	0.06	2.22	1.95	1.52	2.26	0.59	0.03	0.03	0.02	0.03	0.01

Table 2: Shear stress, viscosity and torque measurements for the samples L1, L2, L3, L4 and L5 at room temperature.

Shear rate	Viscocity					Stress					Torque				
	L1	L2	L3	L4	L5	L1	L2	L3	L4	L5	L1	L2	L3	L4	L5
(1/s]			(Pa·s)					(Pa)					(mNm)		
10	0.41	0.53	0.56	0.47	0.20	4.06	5.33	5.60	4.67	1.98	0.05	0.07	0.07	0.06	0.02
20	0.37	0.50	0.42	0.43	0.18	7.41	10.10	8.47	8.51	1.78	0.10	0.13	0.11	0.11	0.03
30	0.35	0.48	0.40	0.41	0.13	10.40	14.50	11.90	12.20	1.27	0.14	0.19	0.15	0.16	0.04
40	0.34	0.47	0.39	0.40	0.11	13.60	18.70	15.70	15.80	1.12	0.18	0.24	0.21	0.21	0.05
50	0.33	0.46	0.39	0.39	0.11	16.70	22.90	19.40	19.40	1.05	0.22	0.30	0.25	0.25	0.06
60	0.33	0.45	0.39	0.38	0.10	19.80	27.30	23.20	22.90	1.02	0.26	0.35	0.30	0.30	0.07
70	0.33	0.45	0.39	0.38	0.10	23.00	31.70	27.00	26.50	1.00	0.30	0.41	0.35	0.34	0.09
80	0.33	0.45	0.39	0.38	0.10	26.50	36.00	30.80	30.30	1.01	0.34	0.47	0.40	0.39	0.10
90	0.33	0.45	0.39	0.38	0.10	29.40	40.40	34.70	34.00	0.99	0.38	0.53	0.45	0.44	0.12
100	0.33	0.45	0.39	0.38	0.10	32.70	44.80	38.70	37.90	0.98	0.42	0.58	0.50	0.49	0.13

type of machinery without lubrication. One of the single largest applications for lubricants, in the form of motor oil, is protecting the internal combustion engines in motor vehicles and powered equipment. Typically lubricants contain 90% base oil (most often petroleum fractions, called mineral oils) and less than 10% additives. Vegetable oils or synthetic liquids such as hydrogenated polyolefin, esters, silicones, fluorocarbons, and many others are sometimes used as base oils. Additives deliver reduced friction and wear, increased viscosity, improved viscosity index, resistance to corrosion and oxidation, aging or contamination, and so forth. Lubricants such as 2-cycle oil are added to fuels like gasoline which has low lubricity [5]. Motor oils are derived from petroleum-based and non-petroleum-synthesized chemical compounds. Motor oils are mainly blended by using base oils composed of hydrocarbons, polyalphaolefins (PAO), and polyinternal olefins (PIO) [6, 7], which are organic compounds consisting entirely of carbon and hydrogen. The base oils of some high-performance motor oils however contain up to 20% by weight of esters. Lubricating oil creates a separating film between surfaces of adjacent moving parts to minimize direct contact between them, decreasing heat caused by friction and reducing wear, thus protecting the engine [8, 9]. Maintenance of high pressure viscosity index at different temperatures in multigrade as well as single grade engine oil is key to its sustained performance. It is also a deciding factor of wear of machine parts. Better rheological behavior with temperature will lead to better tribology [10]. Mia and Ohno [11] measured adiabatic bulk modulus K using Sing around technique [12]. Ohno and Hirano [13] calculated tangent bulk modulus K_T using high-pressure densitometer. Tsubouchi and Shinoda used tangential bulk modulus to characterize oily high bulk modulus fluid [14]. Prashant Thapliyal et al. [15] calculated adiabatic bulk modulus of piezoviscous elastic engine oils by measuring ultrasonic velocity using Nanofluid Interferometer.

2. Experimental

Industrial lubricating oils L1, L2, L3, L4, and L5 are considered as sample oils as shown in Figure 1. Viscosity with rise in temperature was measured using Rheometer MCR302 (Figure 2), SN000000, ID 80963516 from Anton Paar Gurgaon. Measuring system PP25/PE-SN25125 (d = 0.4 mm) with accessory TUI = P-PTD200-SN 81183777 was used.

2.1. Measurement of Viscosity, Shear Stress, and Torque with Temperature. The setup shown in Figure 2 is used to measure the shear stress (σ), viscosity (η), and torque (τ) for all five samples as a function of temperature in a range from 20°C to 50°C at constant shear rate (γ) of 10 $\sec^{-1}$. 31 data points were selected with measuring duration of 2 min. Shear stress, viscosity, and shear rate are related to the following relation



Figure 1: Samples L1, L2, L3, L4, and L5.



Figure 2: Anton Paar MCR302.

$\sigma = \eta\gamma$. The measured values of shear stress, viscosity, and torque with temperature are reported in Table 1.

2.2. Measurement of Viscosity, Shear Stress, Speed, and Torque with Shear Rate. The experimental set up mentioned in 2.0 was used for this purpose. 100 measure points were selected with duration of 2 s and shear rate varied from 1 to 100/s. All the measurements were done at room temperature with variation in speed while the duration of measurement was fixed at 2 s. The results are reported in Table 2.

3. Results and Discussion

Figure 3 shows the exponential variation between dynamic viscosity with temperature for the samples L1, L2, L3, and L5, having trend for L1 as $\eta = 1.34e^{0.694T}$, for L2 $\eta = 1.43e^{0.549T}$, for L3 $\eta = 1.78e^{0.0835T}$, for L4 $\eta = 0.0991e^{0.041T}$, and for L5 $\eta = 0.649e^{0.0496T}$. Here η denotes dynamic viscosity while T denotes temperature. All the samples are found to obey Reynolds' equation [16] as follows:

$$\mu_0 = be^{-aT_A} \quad (1)$$

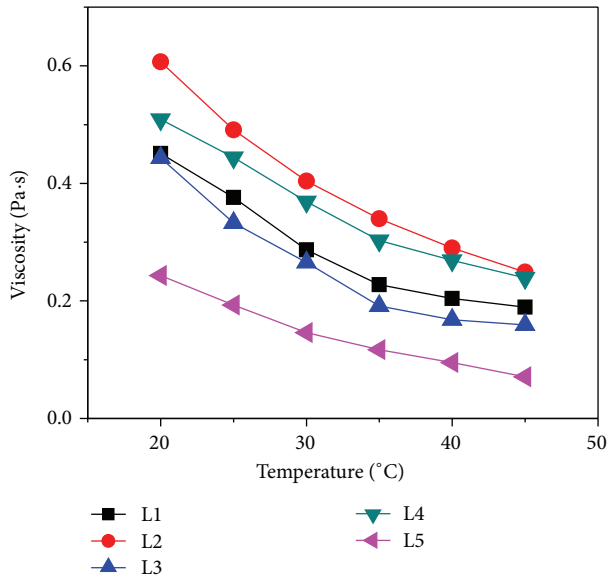


Figure 3: Dynamic viscosity versus temperature for L1, L2, L3, L4, and L5.

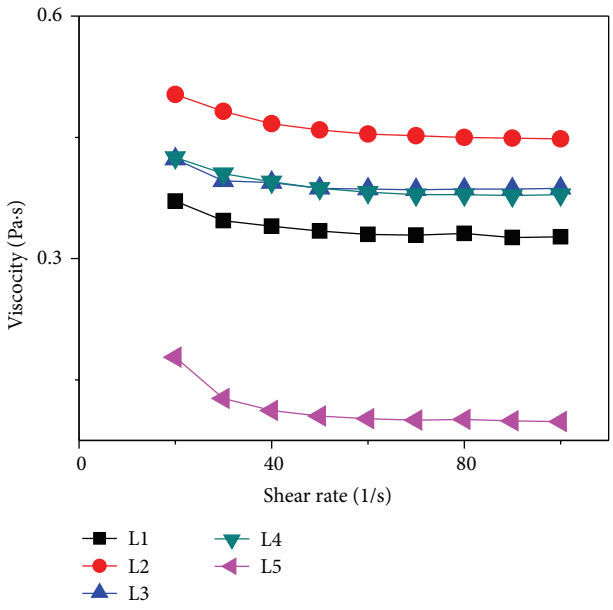


Figure 4: Dynamic viscosity versus shear rate for L1, L2, L3, L4, and L5.

where μ_0 is dynamic viscosity at atmospheric pressure and T_A is absolute temperature. Figure 4 shows the variation of viscosity with shear rate for L1, L2, L3, L4, and L5 samples. Figure 5 shows the stress versus shear rate variation which is found to be liner for all samples with L5 depicting lowest slope. Straight line graphs of stress versus shear rate depict trends for L1 as $\sigma = 0.317\gamma + 0.919$, for L2 as $\sigma = 0.433\gamma + 1.38$, for L3 as $\sigma = 0.378\gamma + 0.606$, for L4 as $\sigma = 0.365\gamma + 1.15$, and for L5 as $\sigma = 0.099\gamma - 0.183$. Dynamic viscosity initially decreases with shear rate denoting piezoviscous behavior while for range above 10 per second it is almost constantly showing

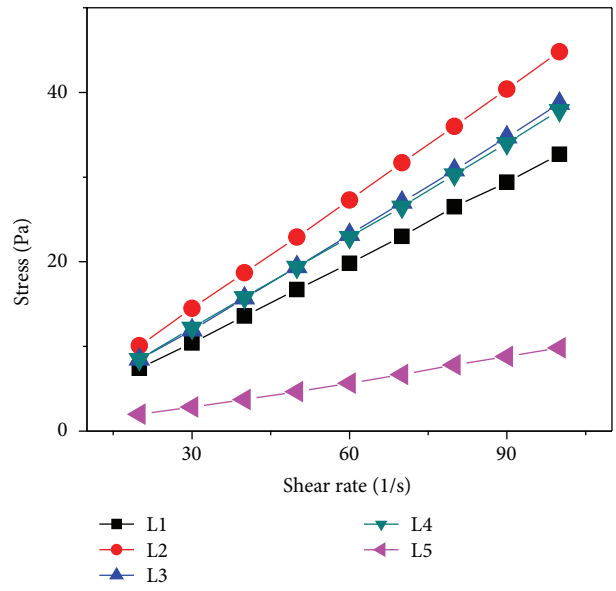


FIGURE 5: Shear stress versus shear rate for L1, L2, L3, L4, and L5.

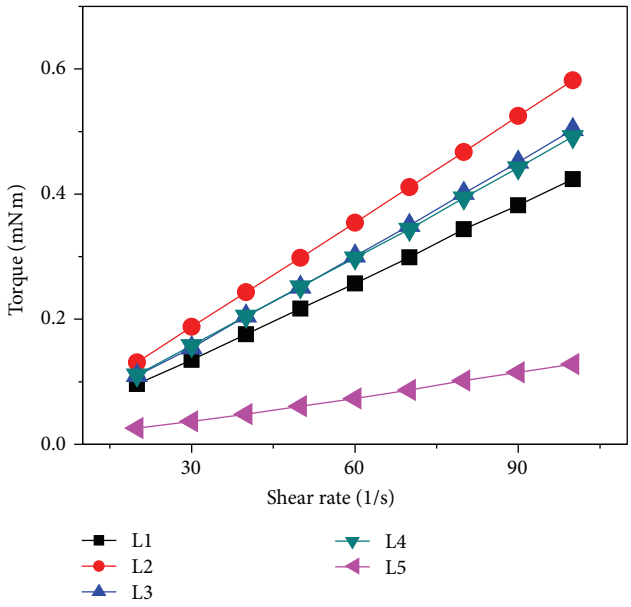


FIGURE 6: Torque versus shear rate for L1, L2, L3, L4, and L5.

Newtonian behavior. Figure 6 shows torque versus shear rate for all samples with almost linear dependence. The observed trends for L1 as $\tau = 0.004\gamma + 0.011$, for L2 as $\tau = 0.005\gamma + 0.017$, for L3 as $\tau = 0.007\gamma + 0.004$, for L4 as $\tau = 0.44\gamma + 0.014$, and for L5 as $\tau = 0.0013\gamma - 0.002$, respectively.

4. Conclusions

The conclusions can be drawn as follows.

(a) L2 and L3 show relatively lower variation of dynamic viscosity with temperature, thus depicting consistent behavior with temperature variations.

(b) Lowest slope of stress versus shear rate curve for L5 suggests more fluidity which is verified by its comparatively lower dynamic viscosity.

(c) Dynamic viscosity decreases with temperature for all the samples showing second degree polynomial variation.

(d) Shear stress shows linear variation with shear rate showing uniformity in viscosity which is substantiated by almost no variation in dynamic viscosity with shear rate for value above 5 per second. It shows that the given lubricants depict Newtonian behavior in hydrostatic regime.

(e) Lubricants L1, L2, L3, and L5 obey Reynolds' equation $\mu_0 = be^{-aT_A}$.

Conflict of Interests

The authors declare that there is no conflict of interests regarding the publication of this paper.

References

[1] B. Bhushan, *Principles and Applications of Tribology*, John Wiley & Sons, New York, NY, USA, 1999.

[2] A. R. Lansdown, *Lubrication: A Practical Guide to Lubricant Selection*, Pergamon Press, Oxford, UK, 1982.

[3] W. R. Schowalter, *Mechanics of Non-Newtonian Fluids*, Pergamon Press, Oxford, UK, 1978.

[4] C. Barus, "Isothermal, isopiestics and isometrics relative to viscosity," *The American Journal of Science*, vol. 45, pp. 87–96, 1893.

[5] *Engine Oil Licensing and Certification System*, API 1509, 15th edition, 2002, Appendix E: API Base Oil Interchangeability Guidelines for Passenger Car Motor Oils and Diesel Engine Oils (revised).

[6] R. H. Schlosberg, J. W. Chu, G. A. Knudsen, E. N. Suciu, and H. S. Aldrich, "High stability esters for synthetic lubricant applications," *Lubrication Engineering*, vol. 57, no. 2, pp. 21–26, 2001.

[7] M. Woydt, "No/Low SAP and alternative engine oil development and testing," *Journal of ASTM International*, vol. 4, no. 10, 2007.

[8] K. Dieter, *Lubricants and Related Products*, Chemie, Hoboken, NJ, USA, 1984.

[9] N. Ohno, N. Kuwano, and F. Hirano, "Observation of mechanical behaviour of solidified oils by using photoelastic method," *Journal of Japan Society of Lubrication Engineers*, vol. 33, no. 9, pp. 693–699, 1988.

[10] S. Mia and N. Ohno, "Relation between low temperature fluidity and sound velocity of lubricating oil," *Tribology International*, vol. 43, no. 5-6, pp. 1043–1047, 2010.

[11] S. Mia and N. Ohno, "Prediction of pressure-viscosity coeffi cient of lubricating oils based on sound velocity," *Lubrication Science*, vol. 21, no. 9, pp. 343–354, 2009.

[12] S. Mia and N. Ohno, "Effect of high adiabatic bulk modulus on the rheological behavior of hydraulic fluid," in *Proceedings of the 13th Asian Congress of Fluid Mechanics*, pp. 17–21, Dhaka, Bangladesh, December 2010.

[13] N. Ohno and F. Hirano, "High pressure rheology analysis of traction oils based on free volume measurements," *Lubrication Engineering*, vol. 57, no. 7, pp. 16–22, 2001.

[14] T. Tsubouchi and J. Shinoda, "Characterization of oily high bulk modulus fluid," in *Proceedings of the World Tribology Congress*, p. 532, Kyoto, Japan, September 2009.

[15] P. Thapliyal, R. Sethi, A. Vasishth, and G. Anand, "Study of elastic and rheological properties of piezoviscous elastic engine oils," in *Proceedings of the International Conference on Nanotechnology in Conventional and Alternative Energy Systems: A Global Status and Pathways*, University of Petroleum and Energy Studies, Dehradun, India, August 2013.

[16] D. Knezevic and V. Savic, "Mathematical modelling of changing of dynamic viscosity, as a function of temperature and pressure, of mineral oils for hydraulic systems," *Facta Universitatis, Series: Mechanical Engineering*, vol. 4, no. 1, pp. 27–34, 2006.

Hindawi Publishing Corporation
Conference Papers in Science
Volume 2014, Article ID 656120, 4 pages
http://dx.doi.org/10.1155/2014/656120

Conference Paper

Dielectric Properties of SnO_2 Thin Film Using SPR Technique for Gas Sensing Applications

Ayushi Paliwal,[1] Anjali Sharma,[1] Monika Tomar,[2] and Vinay Gupta[1]

[1] *Department of Physics and Astrophysics, University of Delhi, Delhi 110007, India*
[2] *Department of Physics, Miranda House, University of Delhi, Delhi 110007, India*

Correspondence should be addressed to Vinay Gupta; drguptavinay@gmail.com

Received 8 February 2014; Accepted 11 March 2014; Published 6 May 2014

Academic Editors: P. Mandal, R. K. Shivpuri, and G. N. Tiwari

This Conference Paper is based on a presentation given by Ayushi Paliwal at "National Conference on Advances in Materials Science for Energy Applications" held from 9 January 2014 to 10 January 2014 in Dehradun, India.

Copyright © 2014 Ayushi Paliwal et al. This is an open access article distributed under the Creative Commons Attribution License, which permits unrestricted use, distribution, and reproduction in any medium, provided the original work is properly cited.

Focus has been made on the determination of dielectric constant of thin dielectric layer (SnO_2 thin film) using surface plasmon resonance (SPR) technique and exploiting it for the detection of NH_3 gas. SnO_2 thin film has been deposited by rf-sputtering technique on gold coated glass prism (BK-7) and its SPR response was measured in the Kretschmann configuration of attenuated total reflection using a p-polarised light beam at 633 nm wavelength. The SPR response of bilayer film was fitted with Fresnel's equations in order to calculate the dielectric constant of SnO_2 thin film. The air/SnO_2/Au/prim system has been utilized for detecting varying concentration (500 ppm to 2000 ppm) of NH_3 gas at room temperature using SPR technique. SPR curve shows significant shift in resonance angle from 44.8° to 56.7° on exposure of fixed concentration of NH_3 gas (500 ppm to 2000 ppm) with very fast response and recovery speeds.

1. Introduction

Surface Plasmon Resonance (SPR) is a powerful and sensitive technique to study the dielectric and optical properties of metal-dielectric interface, thus it can be exploited for the detection of harmful and toxic gases [1]. There are two configurations for exciting surface plasmon (SP) wave at the metal-dielectric interface: one is Otto configuration [2] and the other is Kretschmann [3] configuration. Kretschmann configuration is the most commonly used, where a light wave is totally reflected at the interface between the prism coupler and the thin metal layer (deposited on the prism surface) and excites a SP wave at the outer boundary of the metal by evanescently tunnelling through the thin metal layer [3]. The changes in the plasmon dispersion relations due to variation in refractive index of the sensing film will cause changes in the SPR reflectance curve [4]. The changes in the SPR curve are used to systematically calibrate the physical factors and hence the system can be exploited as a sensor.

Transparent conducting (metal) oxide thin films have been the subject of research interest over a number of decades specially for gas detection. SnO_2 based systems, in particular, have been the focus of many of these investigations worldwide because it is a naturally nonstoichiometric prototypical transparent semiconducting oxide having rutile structure [5]. It has a high band gap of ~4 eV and when suitably doped, can be used both as a p-type and n-type semiconductor [6]. Although a lot of work has been carried out on SnO_2 based semiconductor gas sensors based conductometric detection technique. However, integration of SPR technique is yet to be carried out with detection of toxic gases at room temperature.

In this work, SnO_2 thin film was deposited by the rf sputtering technique on Au coated BK7 glass prism, and its SPR response in the Kretschmann geometry was measured. The SPR response of SnO_2/Au bi-layer film was fitted with Fresnel's equations by using a MATLAB program. The air/SnO_2/Au/prism system is further exploited for the detection of NH_3 gas at varying concentration from 500 ppm to 2000 ppm.

2. Experimental Details

In the present work, efforts have been made towards studying the dielectric properties of tin oxide thin film especially at optical frequency (λ = 633 nm), the surface plasmon modes have been excited at the SnO_2/gold interface in Kretschmann configuration using a right angled BK7 glass prism (n_p = 1.517) with the help of a laboratory assembled system. The optimised 40 nm thin film of gold was deposited on the hypotenuse face of glass prism (BK-7) by thermal evaporation technique where gold (Au) wire (99.999% pure) was evaporated. The thickness and deposition rate of the Au thin film were precisely controlled in situ using a quartz crystal, thickness monitor and deposition was carried out at a rate of 5 Å/s. Then the gold plated prisms were annealed at 300°C in air for 1 hour to get the stabilised SPR mode. SnO_2 thin film was deposited on gold plated glass prisms by rf-diode sputtering technique using a 4″ diameter metal Sn target (99.999% pure). 110 nm thin SnO_2 film was deposited at a sputtering pressure of 10 mTorr for 1 hr in gas ambient of 60% Ar and 40% O_2 in the sputtering chamber.

Crystallographic studies of SnO_2 thin film have been carried out using a Bruker D 8 X Ray diffractometer. The X-ray diffraction is carried out for SnO_2 thin film after a post deposition annealing treatment at 300°C in air for 3 hours. The band gap of SnO_2 thin film has been estimated from the UV-visible spectra, within the wavelength range of 190–1100 nm using a computer interfaced Perkin Elmer (lambda 35) UV-visible dual beam spectrophotometer.

For gas sensing applications, a special sample cell was indigenously designed having an opening window for attaching the prism such that the sensing thin film (SnO_2) is in contact with the environment inside the cell. Initially, the vacuum was created inside the gas cell using a mechanical pump which ensures the removal of other foreign molecules that could otherwise interfere with the sensing film. NH_3 gas of a particular concentration was inserted into the sample cell using a microsyringe. The SPR reflectance curve was recorded while target gas was inserted inside the gas cell for the entire range of incident angle using an optical power meter and a rotation stage (Make: Optiregion).

3. Results and Discussions

The XRD pattern of the SnO_2 thin film is shown in Figure 1. Reflection peaks at 2θ = 26.5°, 33.9°, and 51.8° corresponding to planes (110), (101), and (211) planes of SnO_2, respectively are in good agreement to the reported values for rutile structure [7], confirming the formation of polycrystalline SnO_2 thin film.

The optical transmission spectra of the SnO_2 thin film, deposited on quartz substrate, are shown in Figure 2. SnO_2 thin film shows the good optical transparency of about more than 80% in the visible region. A sharp absorption edge at ~310 nm is obtained for the SnO_2 thin film. Optical band gap of the SnO_2 thin films was calculated from the intercept on energy axis obtained by extrapolating the linear portion of the Taue plot of $(\alpha h\nu)^2$ versus photon energy ($h\nu$) as shown in the inset of Figure 2. Estimated value of bandgap for annealed

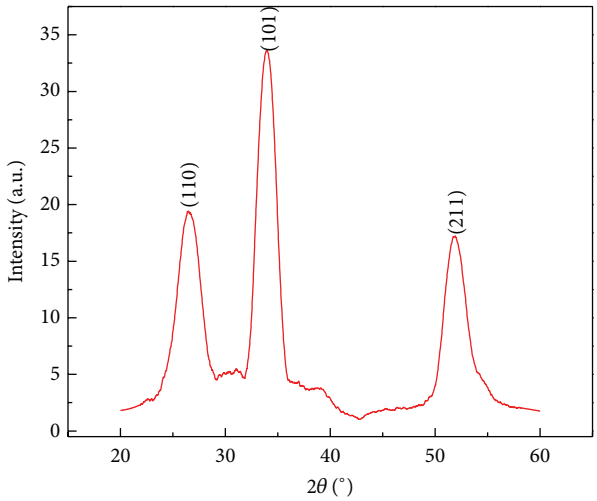


Figure 1: XRD spectra of SnO_2 thin film.

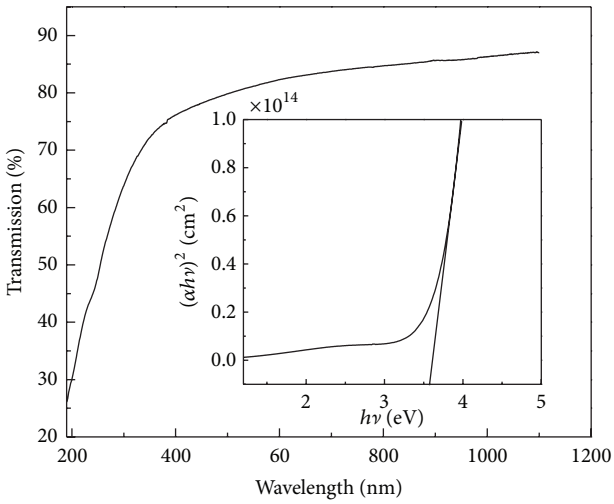


Figure 2: Transmission spectra of SnO_2 thin film.

SnO_2 thin films is found to be 3.58 eV which is close to the values reported by other workers for SnO_2 thin films [8].

Figure 3 shows the SPR reflectance curves obtained for the prepared air/Au/prism and air/SnO_2/Au/prism systems. A well-defined and sharp SPR reflectance curve is obtained for the air/Au/prism system (Figure 3). The reflectance was found to decrease rapidly with increase in incident angle, attained a dip (reflectance minima) at a resonance angle (θ_{SPR}) of 43.8° (Figure 3), and thereafter started increasing sharply with further increase in the incident angle. When SnO_2 thin film is deposited on Au coated prism (Au/prism), the SPR curve shifts to higher resonance angle (Figure 3). The observed shift in SPR curve is related to the change in dielectric media from air for the air/Au/prism structure to SnO_2 film for air/SnO_2/Au/prism structure. It may be noted from Figure 3 that the minimum value of reflectance at resonance angle (θ_{SPR}) increases significantly from 0.26 to 0.32 on depositing a SnO_2 thin film on Au/prism system.

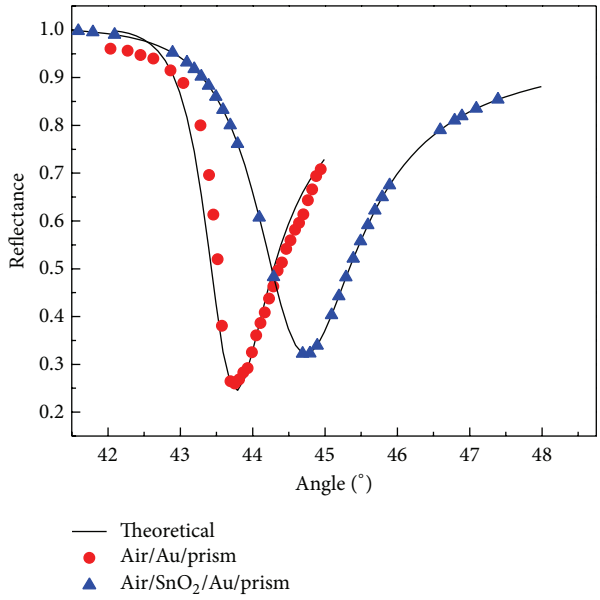


FIGURE 3: Variation of SPR response with incident angle for air/Au/prism and air/SnO_2/Au/prism systems.

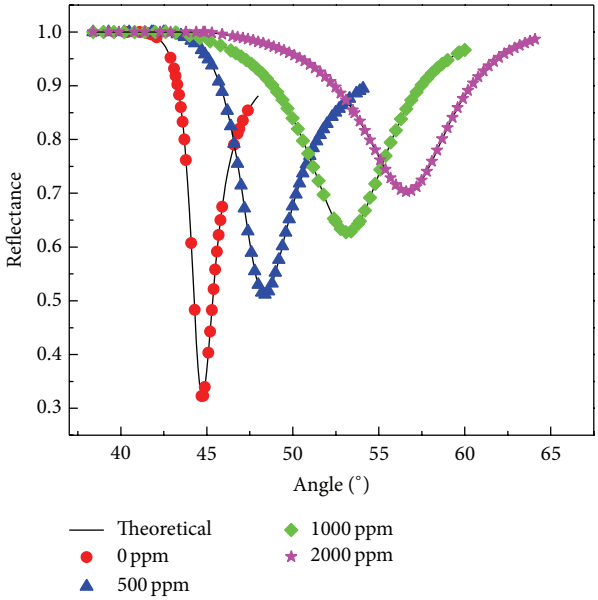


FIGURE 4: SPR reflectance curves for air/SnO_2/Au/prism system for varying concentrations of NH_3 gas.

This is attributed to the fact that the backscattered field which is in antiphase with that of the incoming light interferes destructively with the incoming light and hence, maximum light is not able to couple with the SPR mode and the value of reflectance increases on depositing SnO_2 thin film [4, 9]. In order to obtain the complex dielectric constant, the experimentally obtained SPR reflectance curves were fitted with the theoretical SPR curves simulated using Fresnel's equations for one layer system (air/Au/prism) [10]. The best fitted SPR curve (solid curve) for Au/prism system is also shown in Figure 3. The estimated value of dielectric constant of Au film was about $-11.9 + 0.7i$, which is close to the corresponding value reported in literature [3]. The known values of dielectric constant of prism, $\varepsilon_0 = (1.517)^2$ and the dielectric constant of air $\varepsilon_3 = 1.0$ along with estimated value of dielectric constant of Au are used to find out the complex dielectric constant of SnO_2 thin films using Fresnel's equations for two layer system (air/SnO_2/Au/prism) [10]. Furthermore, to find out the value of complex refractive index $(n_i + ik_i)$ of SnO_2 thin film, the estimated value of complex dielectric constant $(\varepsilon_i = \varepsilon_i' + i\varepsilon_i'')$ was utilized [3]. The value of complex dielectric constant estimated at $\lambda = 633$ nm for SnO_2 thin film was about $2.07 + 0.001i$. The room temperature value of complex refractive index $(n_i + ik_i)$ for SnO_2 thin film was estimated to be $1.439 + 0.032i$ which is in agreement with the reported results [11].

Since surface plasmon resonance (SPR) is very sensitive to any change occurring at the surface of the metal oxide (dielectric) layer, presence of extremely thin gas sensing coatings on the surface of the noble metal layer (Au) can be used to detect gas molecules based on the change in Plasmon resonance conditions. As reported in literature, SnO_2 is most utilized metal oxide thin film for gas sensing purposes though there are few issues that need the urgent need of research community. Hence, gas sensing applications of SnO_2 thin film have been explored to detect NH_3 gas using surface plasmon resonance technique. Figure 4 shows the SPR reflectance curves obtained for the air/SnO_2/Au/prism system at $\lambda = 633$ nm, when the system is exposed to different concentration of NH_3 gas. The SPR dip angle and minimum reflectance increases with increase in the concentrations of NH_3 gas as shown in Figure 4 which is due to increase in the refractive index of SnO_2 thin film in the presence of reducing gas (NH_3). The change in the refractive index of the sensing film introduces the change in the surface plasmon dispersion relations and hence changes the SPR reflectance curve [12]. This may be attributed to the fact that when NH_3 gas interacts with the surface of SnO_2 thin film. It releases free electrons to SnO_2 surface which causes change in SPR conditions leading to shift in SPR reflectance curve.

4. Conclusions

SnO_2 thin film was deposited by the rf-diode sputtering technique on Au coated BK7 glass prisms and its SPR response was measured in the Kretschmann geometry of attenuated total reflection using a p-polarized He-Ne laser beam at 633 nm wavelength. The SPR response of Au/SnO_2 bi-layer film was also simulated with Fresnel's equations in order to compare with experimental data and also to find the complex dielectric constant and refractive index of SnO_2 thin film. The complex dielectric constant and refractive index of SnO_2 thin film were determined to be $2.07+0.001i$ and $1.439+0.032i$ which are close to the reported values. The SnO_2 thin film is further used for NH_3 gas sensing at room temperature and the initial results demonstrated that NH_3 gas sensing of SnO_2/Au bi-layer films using SPR is feasible.

Conflict of Interests

The authors declare that there is no conflict of interests regarding the publication of this paper.

Acknowledgments

The authors are thankful to the Department of Science and Technology (DST), India, for financial support. One of the authors Ayushi Paliwal is also thankful to the CSIR and University of Delhi for the research fellowship and teaching assistantship, respectively.

References

[1] R. Tabassum, S. K. Mishra, and B. D. Gupta, "Surface plasmon resonance-based fiber optic hydrogen sulphide gas sensor utilizing Cu–ZnO thin films," *Physical Chemistry Chemical Physics*, vol. 15, no. 25, pp. 11868–11874, 2013.

[2] A. Otto, "Excitation of nonradiative surface plasma waves in silver by the method of frustrated total reflection," *Zeitschrift für Physik*, vol. 216, no. 4, pp. 398–410, 1968.

[3] S. Saha, N. Mehan, K. Sreenivas, and V. Gupta, "Temperature dependent optical properties of (002) oriented ZnO thin film using surface plasmon resonance," *Applied Physics Letters*, vol. 95, no. 7, Article ID 071106, 2009.

[4] Z. Bao, G. L. D. Jiang, W. Cheng, and X. Ma, "ZnO sensing film thickness effects on the sensitivity of surface plasmon resonance sensors with angular interrogation," *Materials Science and Engineering B*, vol. 171, no. 1–3, pp. 155–158, 2010.

[5] R. Brahma, M. G. Krishna, and A. K. Bhatnagar, "Optical, structural and electrical properties of Mn doped tin oxide thin films," *Bulletin of Materials Science*, vol. 29, no. 3, pp. 317–322, 2006.

[6] C. Luan, Z. Zhu, W. Mi, and J. Ma, "Effect of Sb doping on structural, electrical and optical properties of epitaxial SnO_2 films grown on r-cut sapphire," *Journal of Alloys and Compounds*, vol. 586, pp. 426–430, 2014.

[7] K. Ihokura and J. Watson, *The Stannic Oxide Gas Sensor Principles and Applications*, CRC Press, Boca Raton, Fla, USA, 1994.

[8] A. Sharma, M. Tomar, and V. Gupta, "SnO_2 thin film sensor with enhanced response for NO_2 gas at lower temperatures," *Sensors and Actuators B*, vol. 156, no. 2, pp. 743–752, 2011.

[9] H. Raether, *Surface Plasmons on Smooth and Rough Surfaces and on Gratings*, Springer, Berlin, Germany, 1986.

[10] S. K. Özdemir and G. Turhan-Sayan, "Temperature effects on surface plasmon resonance: design considerations for an optical temperature sensor," *Journal of Lightwave Technology*, vol. 21, no. 3, pp. 805–814, 2003.

[11] Y. S. Hsu and S. K. Ghandi II, "The effect of phosphorus doping on tin oxide films made by the oxidation of phosphine and tetramethyltin I. Growth and etching properties," *Journal of The Electrochemical Society*, vol. 127, no. 7, pp. 1592–1595, 1980.

[12] E. Maciak, Z. Opilski, and T. Pustelny, " Effect of humidity on NH_3 gas sensitivity of Nafion/WO_3 sensing structure of SPR sensor," *Molecular and Quantum Acoustics*, vol. 26, pp. 205–215, 2005.

Hindawi Publishing Corporation
Conference Papers in Science
Volume 2014, Article ID 807893, 5 pages
http://dx.doi.org/10.1155/2014/807893

Conference Paper

Study of Structural and Electronic Behavior of BeH_2 as Hydrogen Storage Compound: An Ab Initio Approach

Vikas Nayak, Suman Banger, and U. P. Verma

School of Studies in Physics, Jiwaji University, Gwalior 474 011, India

Correspondence should be addressed to Vikas Nayak; vikas.nayak88@gmail.com

Received 28 January 2014; Accepted 3 March 2014; Published 27 April 2014

Academic Editors: P. Mandal, R. K. Shivpuri, and G. N. Tiwari

This Conference Paper is based on a presentation given by Vikas Nayak at "National Conference on Advances in Materials Science for Energy Applications" held from 9 January 2014 to 10 January 2014 in Dehradun, India.

Copyright © 2014 Vikas Nayak et al. This is an open access article distributed under the Creative Commons Attribution License, which permits unrestricted use, distribution, and reproduction in any medium, provided the original work is properly cited.

The quantum mechanical calculations based on density functional theory (DFT) have been performed to study ground state structural and electronic properties of BeH_2 and along with doping of two (BeH_2 + 2H) and four (BeH_2 + 4H) hydrogen atoms. The generalized gradient approximation (GGA) has been employed for the exchange correlation energy. The most stable space group of BeH_2 is *Ibam*. Its optimized equilibrium unit cell volume, bulk modulus and its first-order pressure derivative, and electronic properties have been obtained. Our predicted unit cell parameters for BeH_2 $a = 9.2463$ Å, $b = 4.2352$ Å, and $c = 7.8464$ Å are in very good agreement with the earlier reported experimental and theoretical results. The electronic band structure of BeH_2 shows its behavior as an insulator. The stability of BeH_2 along with doped hydrogen atoms increases, while the energy band gap decreases with the increase in number of doped hydrogen atoms. On these bases, we predict that BeH_2 is a promising material for hydrogen storage.

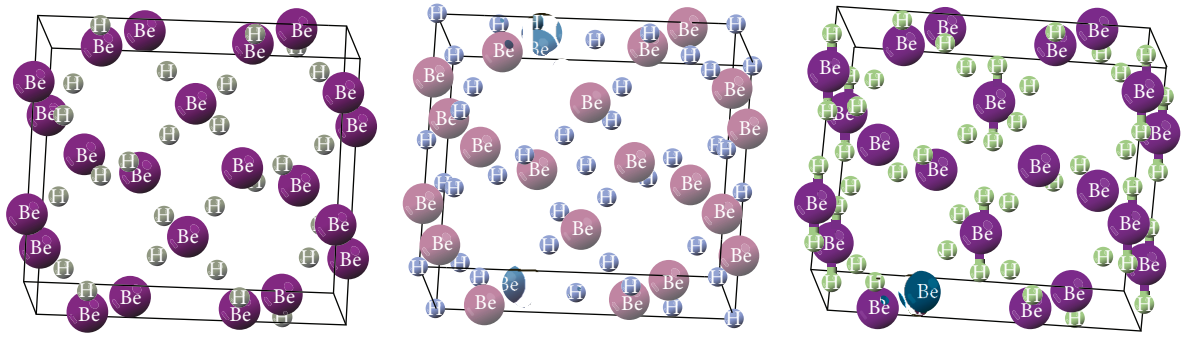
1. Introduction

Energy storage for the future is a great concern for the researchers and scientists. We need materials like metal hydrides for various potential applications, that is, for hydrogen storage, in fuel cells and internal combustion engines, as electrodes for rechargeable batteries, and in energy conversion devices. The metal hydrides for hydrogen storage need to be able to form hydrides with a high hydrogen-to-metal mass ratio, but they should not be too stable, so that the hydrogen can easily be released without excessive heating. Beryllium and magnesium and beryllium-magnesium-based hydrides contain a relatively high fraction of hydrogen by weight but need to be heated ~250 to 300°C in order to release the hydrogen. The alkali-metal and alkaline-earth-metal hydrides represent series with largely ionic bonding. The high pressure behavior of the alkali-metal monohydrides is expected to parallel of the alkali-metal halides [1]. However, there is no systematic high-pressure study on the alkaline-earth-metal hydrides. If BeH_2 becomes metallic when subjected to high pressures, one can entertain the possibility that its properties could resemble those of metallic hydrogen. BeH_2 is commonly considered as a covalent hydride with a postulated polymeric crystal structure made up of H-bridged chains. However, mainly owing to experimental difficulties in the synthesis of the material, the structure has long remained unknown [2]. Crystalline BeH_2 has been synthesized and the structure has been established as body centered orthorhombic by synchrotron-radiation-based powder X-ray diffraction [3]. First-principles total-energy calculations were performed for various types of structural variants, among which it was confirmed that the experimentally observed body centered orthorhombic (*Ibam*) structure of BeH_2 has the lowest total energy.

In this paper, we have carried out the first-principles calculations of the ground-state behavior of BeH_2 in *Ibam*

Table 1: Calculated structural parameters, bulk modulus B and its pressure derivative B_0', and energy for orthorhombic BeH_2 are listed with available references.

Compound	Lattice parameter (in Å)			B (in Gpa)	B_0'	E (in Ry)	Reference
	a	b	c				
BeH_2	9.246	4.235	7.846	53.24	5.0	−191.285	
	9.082	4.160	7.707				[3, 4]
	8.982	4.156	7.645	23.79			[5, 6]
BeH_2 + 2H	9.475	4.341	8.091	50.42	3.2	−193.202	
BeH_2 + 4H	10.078	4.616	8.553	40.04	2.9	−194.901	



(a) (b) (c)

Figure 1: Crystal structures of (a) BeH_2, (b) BeH_2 + 2H, and (c) BeH_2 + 4H in *Ibam* phase.

phase. Results for the structural and electronic properties are systematically presented. The calculations have also been extended for extra hydrogen added structures (BeH_2 + 2H and BeH_2 + 4H) in the same phase. The obtained results are discussed in this paper.

2. Computational Details

The structural and electronic properties of the BeH_2 are obtained using density functional theory (DFT) [7, 8]. The full potential-linearized augmented plane wave (FP-LAPW) method has been employed for the calculation as implemented in the Wien2k code [9]. Generalized gradient approximation (GGA) is used to calculate the exchange-correlation functional. We expand the basis function up to $R_{MT} * k_{max} = 7$, where R_{MT} is the smallest radius of the muffin-tin (MT) spheres and k_{max} is the maximum value of the reciprocal lattice vectors. The maximum l value for the wave function expansion inside the atomic spheres was confined to $l_{max} = 10$. The k-points used in the calculations were based on $5 \times 5 \times 5$ Monkhorst-Pack scheme [10]. The iteration process was repeated until the calculated total energy and charge of the crystal converge to less than 0.0001 Ry and 0.001 e^-, respectively. In order to avoid ambiguities regarding the calculated results, we have used the same value of the energy cutoff as well as k-grid density for convergence for all the structural variants studied. The present theoretical approach has been successfully applied to study ambient- and high-pressure phases computationally.

The bulk BeH_2 exhibits *Ibam* structure in ground state. The obtained unit cell parameters for this structure of BeH_2 are listed in Table 1. In order to obtain the equilibrium structural parameters, we carried out optimization of the total energy as a function of unit cell volume. Obtained sets of the unit cell volume and corresponding total energy have been fitted to the Murnaghan's equation of state [11]. The bulk BeH_2 has also been studied with added number of hydrogen for the purpose of comparison between the ground state electronic properties of BeH_2 and with the doped hydrogen BeH_2. The studied variants are BeH_2 + 2H and BeH_2 + 4H. The obtained structural parameters for all the variants have been listed in Table 1.

3. Results and Discussion

3.1. Structural Properties. The ground state of BeH_2 has been synthesized experimentally [3] and studied theoretically [5]. Its orthorhombic unit cell (space group *Ibam*) is composed of twelve BeH_2 formula units as shown in Figure 1(a).

The primitive cell contains six formula units. The Wyckoff positions of different atoms are two Be1 (4a), four Be2 (8j), eight H1 (16k), and four H2 (8j). Each Be1 is surrounded by four H1 atoms to build the tetrahedral structure and each Be2 connects with two H1 atoms and two H2 atoms. Calculated atomic structural parameters for orthorhombic BeH_2 are included in Table 1. The obtained results of BeH_2 are in excellent agreement with the previous theoretical results [5, 6] and available experimental data [3, 4].

BeH_2 also studied with two and four extra added hydrogen atoms. Optimized values for unit cell volume and corresponding energy are fitted to Murnaghan's equation of state [11]. The optimization curve is shown in Figure 2. From

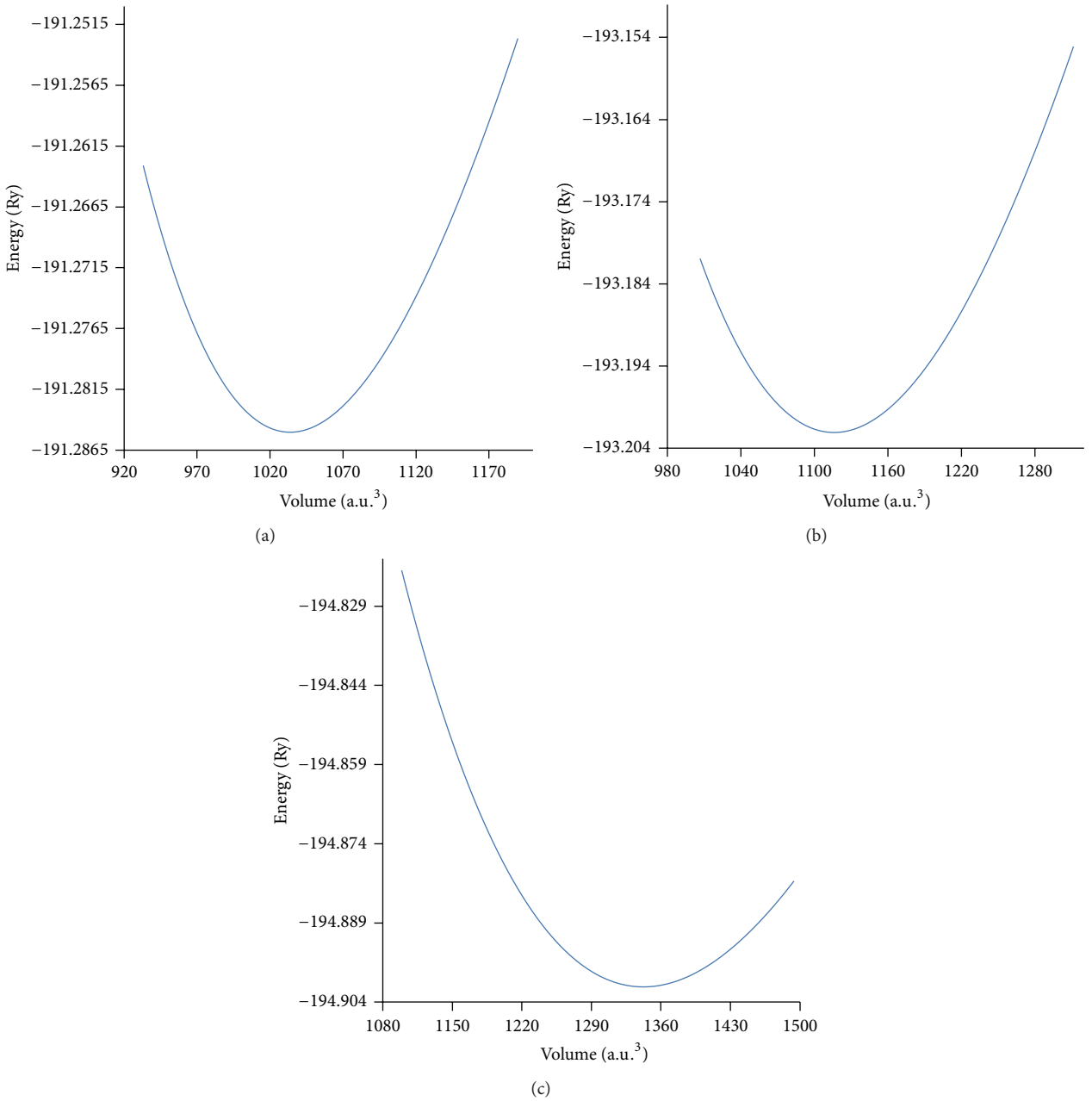


FIGURE 2: Optimization curves for (a) BeH_2 (b) BeH_2 + 2H, and (c) BeH_2 + 4H.

the optimized unit cell volume, we have calculated the lattice parameters of BeH_2 + 2H and BeH_2 + 4H. The obtained unit cell parameters and other constants are listed in Table 1.

It is evident from Table 1 and plots in Figure 2 that the optimized energy of BeH_2 is less than that of BeH_2 + 2H and the energy of BeH_2 + 2H is less than that of BeH_2 + 4H. This indicates clearly that the stability of structures increases with the increase in the number of hydrogen atoms. A plot of total energy as a function of the doped hydrogen atoms is shown in Figure 3(a) and plot of unit cell volume versus number of doped hydrogen atoms is shown in Figure 3(b). The plot in Figure 3(a) shows linear behavior, while plot in Figure 3(b) is nonlinear.

The band structure of BeH_2 shows insulator behavior as in this case direct energy band gap is ~5.8 eV, while band structure plots for BeH_2 + 2H and BeH_2 + 4H show semiconducting behavior because in these cases indirect energy band gaps are, respectively, ~2.2 eV and ~2.5 eV (Figure 4). It is very interesting to note that below Fermi energy level width of a group of valence-band is ~6.5 eV which is in excellent agreement with earlier reported data [5]. The width of the group of valence-bands increases with

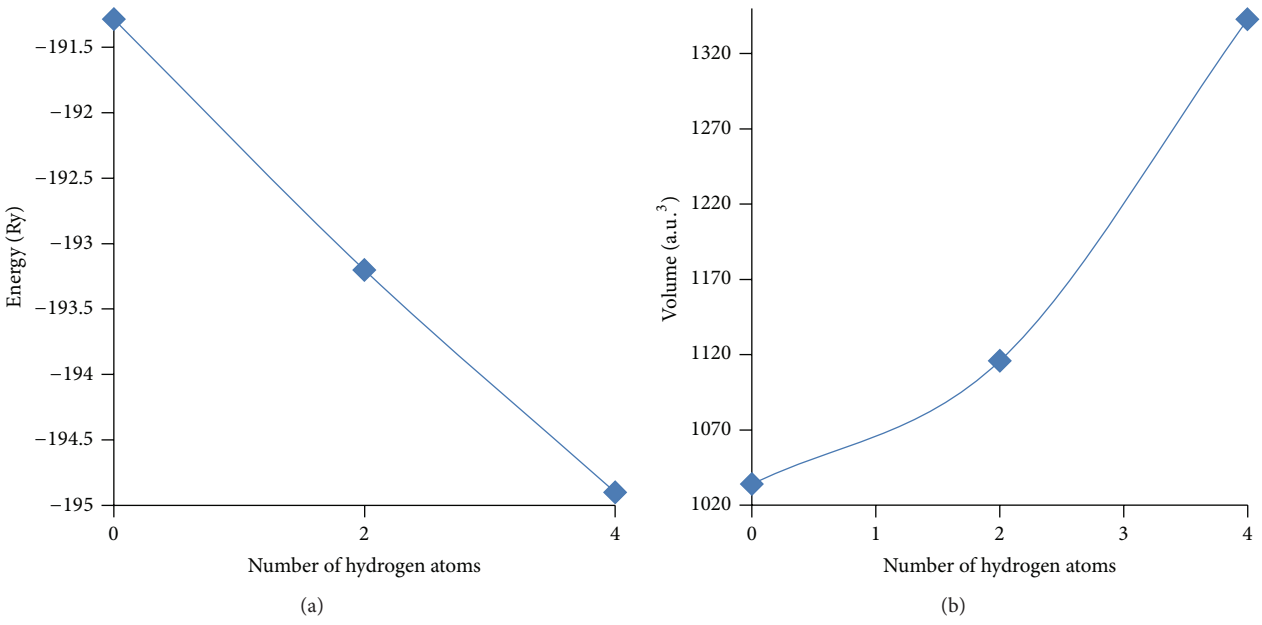


Figure 3: A plot between optimized energy and added extra number of hydrogen.

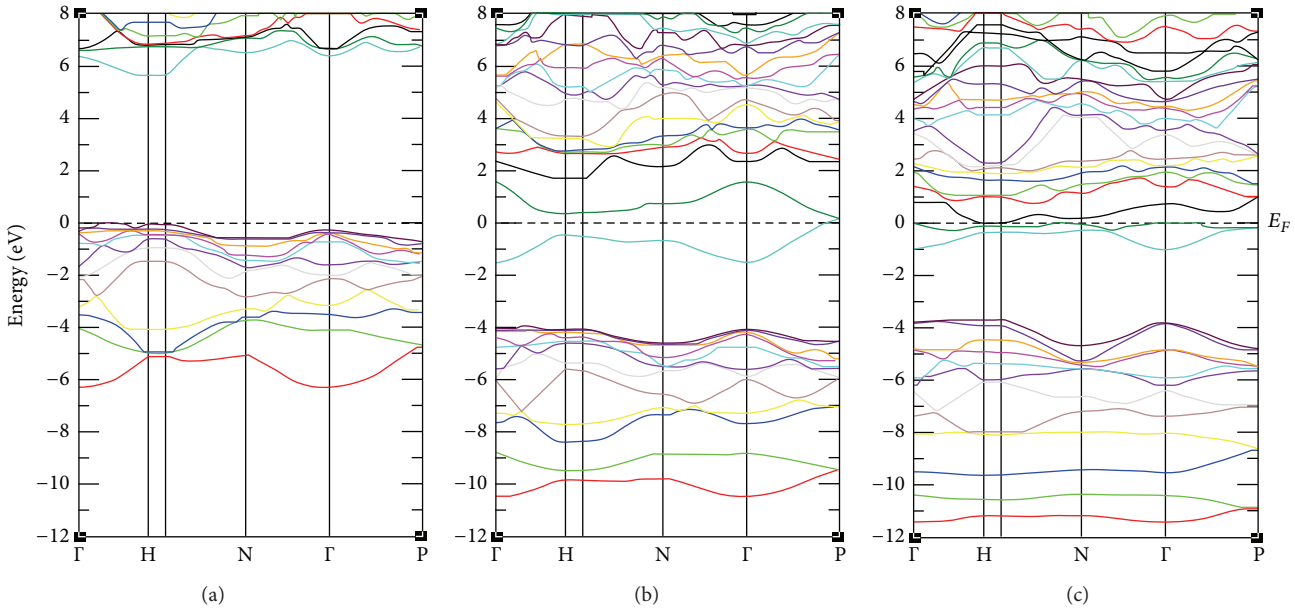


Figure 4: Electronic band structures for (a) BeH_2, (b) BeH_2 + 2H, and (c) BeH_2 + 4H.

the increase in number of doped hydrogen atoms. For BeH_2 + 2H, this width is ~6.5 eV and for BeH_2 + 4H it is ~7.5 eV. The behavior of conduction bands is somewhat different. Corresponding to two doped hydrogen atoms conduction bands near Fermi level are separated, while for 6 doped hydrogen atoms they are further compressed. This shows that number of added hydrogen atoms has significant effect on energy levels.

4. Conclusions

In this work, the structural stability of the Beryllium Hydride, BeH_2, and doped hydrogen compounds BeH_2 + 2H and BeH_2 + 4H have been studied by the first-principles calculations. The equilibrium structures of these compounds are obtained from DFT/GGA total energy minimization. The obtained results for BeH_2 are in excellent agreement with

the reported experimental and theoretical results. BeH_2 is an insulator and BeH_2 + 2H and BeH_2 + 4H are semiconductor. The effect of added hydrogen atoms is very clear. The stability of BeH_2 + 4H > BeH_2 + 2H > BeH_2. Lower value of total energy in BeH_2 + 4H shows that hydrogen storage in BeH_2 is one of very good option (Figure 2).

Conflict of Interests

The authors declare that there is no conflict of interests regarding the publication of this paper.

References

[1] St. J. Duclos, Y. K. Vohra, A. L. Ruoff, S. Filipek, and B. Baranowski, "High-pressure studies of NaH to 54 GPa," *Physical Review B*, vol. 36, no. 14, pp. 7664–7667, 1987.

[2] D. R. Armstrong, J. Jamieson, and P. G. Perkins, "The electronic structures of polymeric beryllium hydride and polymeric boron hydride," *Theoretica Chimica Acta*, vol. 51, no. 2, pp. 163–172, 1979.

[3] G. S. Smith, Q. C. Johnson, D. K. Smith et al., "The crystal and molecular structure of beryllium hydride," *Solid State Communications*, vol. 67, no. 5, pp. 491–494, 1988.

[4] M. Ahart, J. L. Yarger, K. M. Lantzky, S. Nakano, H.-K. Mao, and R. J. Hemley, "High-pressure Brillouin scattering of amorphous BeH_2," *The Journal of Chemical Physics*, vol. 124, no. 1, Article ID 014502, 2006.

[5] P. Vajeeston, P. Ravindran, A. Kjekshus, and H. Fjellvåg, "Structural stability of BeH_2 at high pressures," *Applied Physics Letters*, vol. 84, no. 1, pp. 34–36, 2004.

[6] U. Hantsch, B. Winkler, and V. Milman, "The isotypism of BeH_2 and SiO_2: an ab initio study," *Chemical Physics Letters*, vol. 378, no. 3-4, pp. 343–348, 2003.

[7] P. Hohenberg and W. Kohn, "Inhomogeneous electron gas," *Physical Review*, vol. 136, no. 3, pp. B864–B871, 1964.

[8] W. Kohn and L. J. Sham, "Self-consistent equations including exchange and correlation effects," *Physical Review*, vol. 140, no. 4, pp. A1133–A1138, 1965.

[9] P. Blaha, K. Schwarz, P. Sorantin, and B. Rckey, "Full-potential, linearized augmented plane wave programs for crystalline systems," *Computer Physics Communications*, vol. 59, no. 2, pp. 399–415, 1990.

[10] H. J. Monkhorst and J. D. Pack, "Special points for Brillouin-zone integrations," *Physical Review B*, vol. 13, Article ID 5188, 1976.

[11] F. Murnaghan, "The compressibility of media under extreme pressures," *Proceedings of the National Academy of Sciences of the United States of America*, vol. 30, no. 9, pp. 244–247, 1944.

Hindawi Publishing Corporation
Conference Papers in Science
Volume 2014, Article ID 396826, 5 pages
http://dx.doi.org/10.1155/2014/396826

Conference Paper

Near-Field Hot Spots in Gold Nanoplasmonic Templates and Their Use for Surface Enhanced Raman Scattering Sensing Application

Prasanta Mandal

Department of Physics, University of Petroleum and Energy Studies, Dehradun 248007, India

Correspondence should be addressed to Prasanta Mandal; pmandal@ddn.upes.ac.in

Received 19 January 2014; Accepted 2 April 2014; Published 14 April 2014

Academic Editors: R. Chandra and R. K. Shivpuri

This Conference Paper is based on a presentation given by Prasanta Mandal at "National Conference on Advances in Materials Science for Energy Applications" held from 9 January 2014 to 10 January 2014 in Dehradun, India.

Copyright © 2014 Prasanta Mandal. This is an open access article distributed under the Creative Commons Attribution License, which permits unrestricted use, distribution, and reproduction in any medium, provided the original work is properly cited.

Finite difference time domain (FDTD) method is adapted to investigate near-field enhancement effects on plasmonic structures (patterned in gold film) such as concentric rings with small separation, square, and rectangle. The near-fields effect on surface enhanced Raman scattering (SERS) is typically studied on square and rectangular structures. These metal structures are fabricated by laser interference lithography. Raman active molecules (Rhodamine 6G in PMMA (polymethyl methacrylate)) are spread onto patterned structure by spin coating, and Renishaw inVia Raman spectrometer was used to study SERS. Typical SERS enhancement of the order of 10^5 is seen for square and rectangular structures. It is observed that the corner points and edges of square and rectangular structures are most sensitive to concentrate near fields. In the case of concentric rings, huge near fields are seen to exist at the gap between the metal rings. Concentric rings are proposed to be very effective structure for SERS sensing applications such as molecular identification and biological mapping.

1. Introduction

Near-field assisted surface enhanced Raman scattering (SERS) is an efficient light scattering process which can be used for molecular sensing purpose. In SERS process, huge plasmonic near fields existing due to the localized and propagating surface plasmon resonances around the metal nanostructures have been the most important factors [1–5]. It can assist in achieving even 10^8–10^{10} times enhancement of the scattered signal. Thus, engineering the plasmonic structures to achieve densely packed near-field spots or hot spots is a prior must. This optimized structure can be used to explore trace molecular detection, biological sensing, and molecular vibrational studies [1–10].

Near-field localization and studies of SERS on a variety of plasmonic structures have been reported previously by various researchers [11–15]. It is also reported that two-dimensional (2D) structures are superior compared to one-dimensional (1D) structure. It is preferable if the plasmonic structures are insensitive to the input excitation beam. In this work we propose a novel concentric ring structure (Figure 1) for the efficient near-field localization. Here concentric rings will be highly insensitive to the polarization state of the input light beam (unpolarized or transverse magnetic (TM) and transverse electric (TE)); thus SERS templates consisting of concentric rings will be very easy to perform SERS without prior information of the polarization of the input beam. Near-field localization is compared with square and rectangular geometries.

2. Designing of Plasmonic Structures for Simulation

The following designing parameters are considered for the computer simulation (3D). The finite difference time domain method (Optiwave) is utilized for the analysis of the near fields. The enhanced near field around the edges and corners

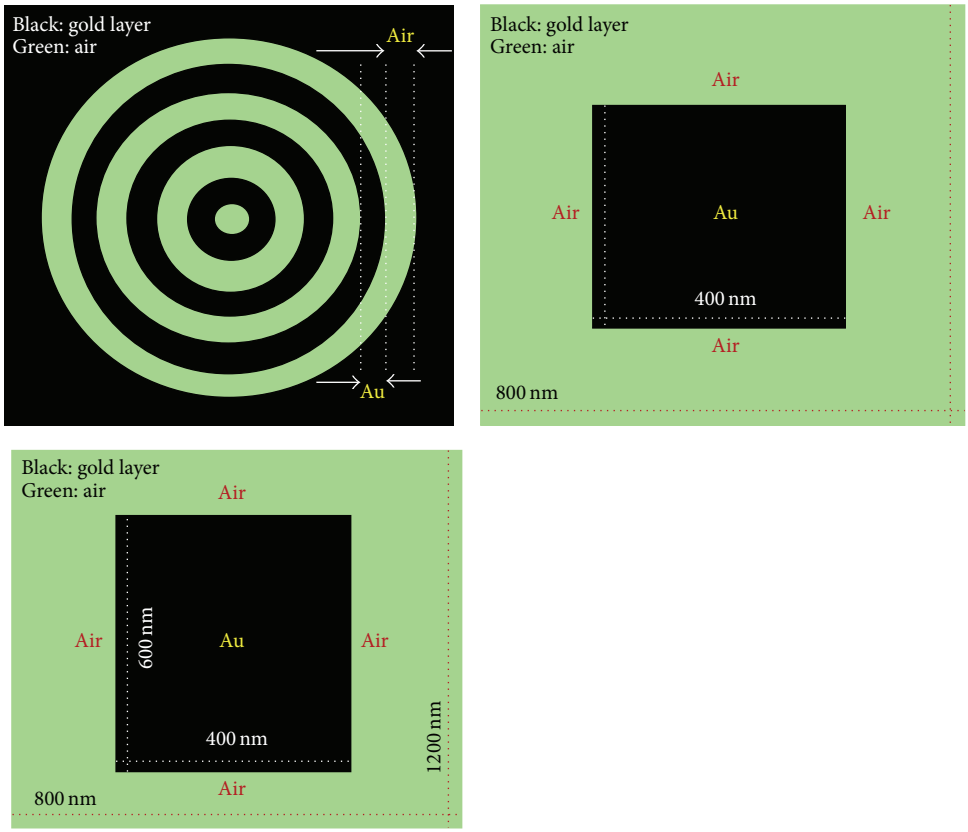


FIGURE 1: Design parameters for the structures under investigation. Concentric rings (top-left), unit cell of the square array of gold (top-right), and unit cell of rectangular array of gold (bottom-left).

of plasmonic metal nanostructures is caused by propagating or localized plasmon resonances or coupled modes of both of them [2, 3]. To understand the effect of near-fields localization and the interaction with Raman active probe molecules plasmonic structures, that is, concentric rings, square array and rectangular array are modeled as free standing templates. The structures are very similar to the structures shown in Figure 1. All the structures are designed to have a depth of 100 nm. For square and rectangular structures the duty cycle is assumed to be 50 : 50. Concentric rings have width of 50 nm. Periodic boundary conditions are applied along x- and y-axes, and in the z-direction, anisotropic perfectly matched layers are applied. A normally incident plane wave having wavelength of 785 nm is used for the excitation. Polarization of incident pump is set to x-pol. The periodicity of the lattice is fixed at 800 nm for square and 800 nm and 1200 nm for rectangular lattice.

3. Experimental Details

Square and rectangular plasmonic structures are fabricated by using laser interference lithography. The details of the fabrication procedure have been reported previously [2, 3]. As the dimensions of the concentric rings structure are very small and the fabrication is only possible through either electron beam lithography or focused ion beam approach, the testing of SERS at this moment is not feasible. For SERS measurement typical square and rectangular plasmonic structure are considered. Rhodamine 6G (R6G) probe molecules (50 micromolar) in PMMA (PMMA in chlorobenzene: MICROCHEM, Germany) were spin coated (resulted in ~50 nm thick film) onto the plasmonic structures. Renishaw inVia Raman spectrometer typically with 785 nm laser at 3 mW input power was employed to conduct the SERS experiments. The laser was focused through 50x objective (0.75 NA, spot size ~ 5 μm) and the back scattered signal was collected through the same objective. The signal was integrated for 20 s and 2 accumulations.

4. Analysis of Simulation Results

The (E_z, E_x, E_y) field distribution for concentric ring structure is shown in Figure 2. The polarization of input field was set to x-polarization (parallel to x-direction). The distribution of E_x field in Figure 2(a) shows concentrated near fields around the metal ring edges. The strength of the concentrated field is much higher, about 100 times compared to that from flat portion. The field is enhanced throughout the structure in a modulated fashion (field is stronger at about x = 200 nm and 600 nm). This trend is also observed in the case of E_y

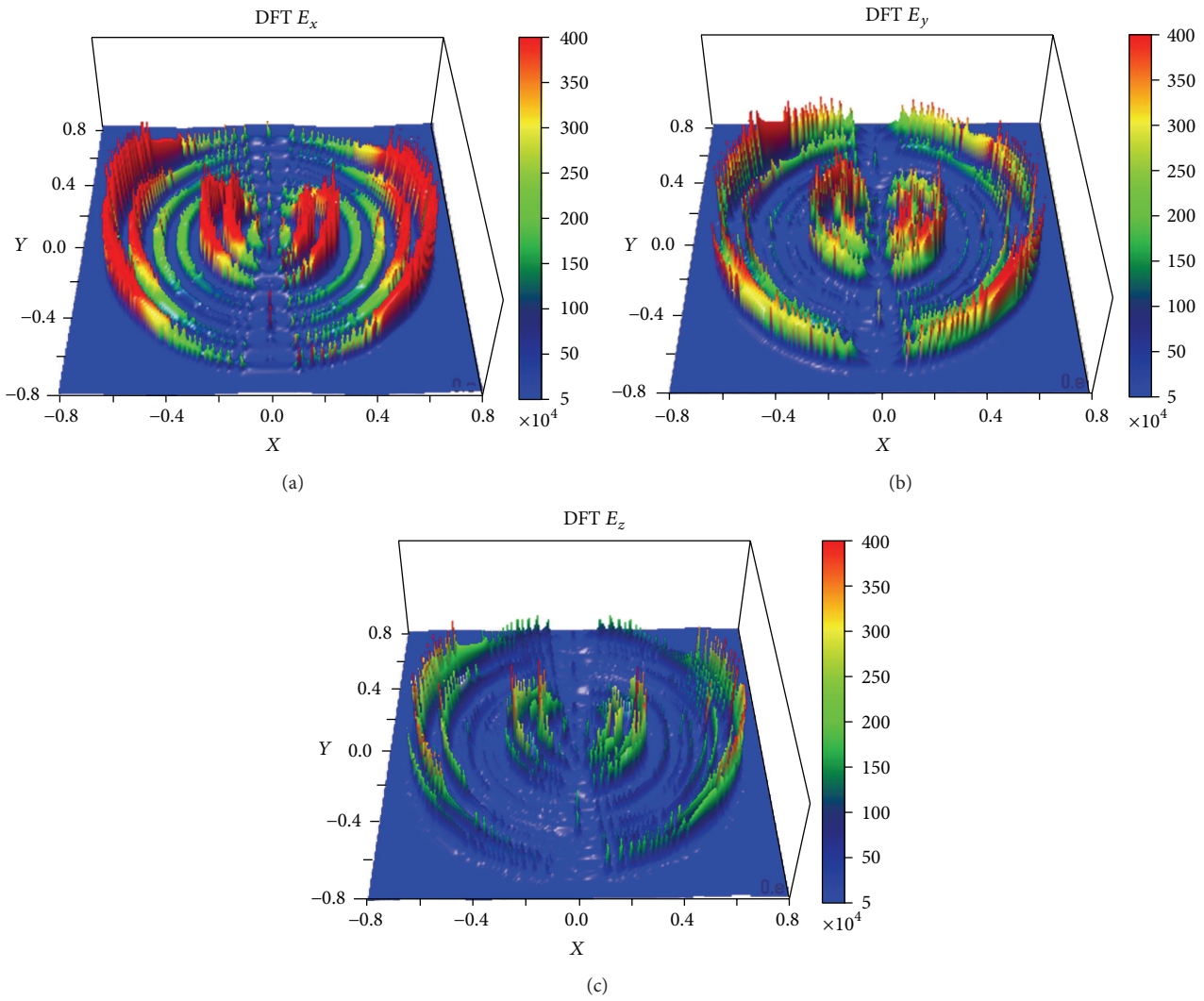


FIGURE 2: Distribution of near fields for the gold concentric rings with the electric field components as E_x (a), E_y (b), and E_z (c). The coloured scale bar represents the field strength throughout the structure.

field distribution as well as E_z. The strength of the near field confined along the vertical direction (E_z) is weaker compared to in-plane confinement (E_x and E_y). The field distribution and large enhancements suggest the effectiveness of the structure for SERS as the scattering process varies with E^4 [16]. The modulated enhancement is the result of combined effect of localized and propagating plasmon resonances.

Electric field distribution for square array of gold lattice is shown in Figure 3. Near field is concentrated at the corners and edges. Field enhancement is clearly observed from E_x and E_y field distributions, whereas field confinement along the vertical direction is not significant. Similar field distribution is observed for rectangular structure (not shown here). Comparing with the field confinement in ring structure it is observed that the overall field strength is higher compared to square and rectangular structures.

5. SERS Results

Raman spectra of R6G-PMMA molecules spin coated onto 2D square and rectangular patterned templates are shown in Figure 4. Raman spectrum from flat (unpatterned gold film) gold is plotted as inset of the figure. The spectra for square and rectangle samples show strong characteristic peaks at 613, 775, 1190, 1312, 1363, 1507, 1602, and 1650 cm^{-1} of R6G and PMMA probe molecules as reported earlier [2, 3].

6. Discussions and Conclusions

Concentric ring structure is proposed to be highly effective for near-field confinement and surface enhanced Raman scattering. The proposed structure is insensitive to incident beam polarization and thus easy to perform SERS experiment. The field confinement is observed to be modulated

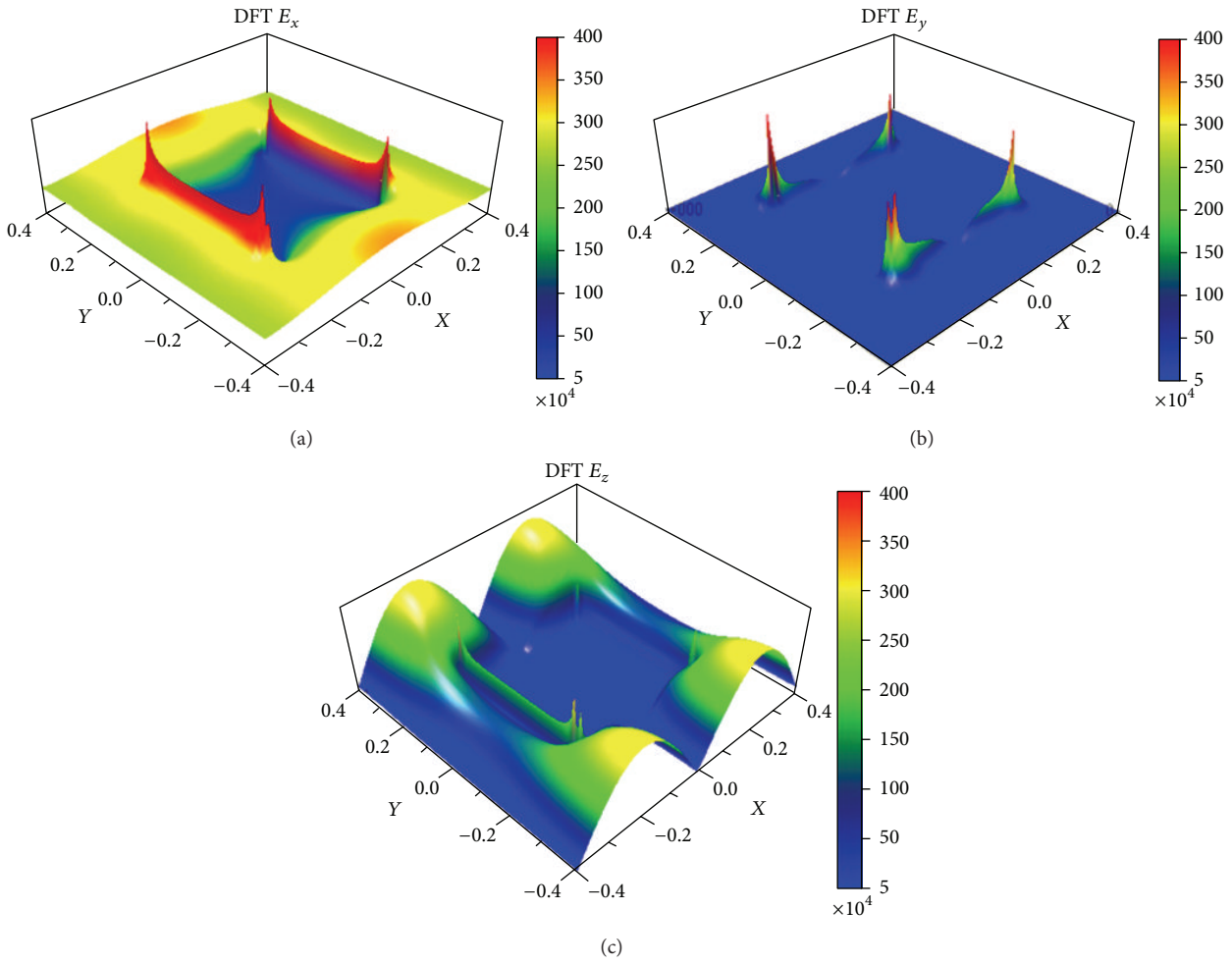


FIGURE 3: Distribution of near fields for the square array of gold as described in Figure 1. Electric field components are E_x (a), E_y (b), and E_z (c). The coloured scale bar represents the field strength throughout the structure and is kept as in Figure 2 for easy comparison.

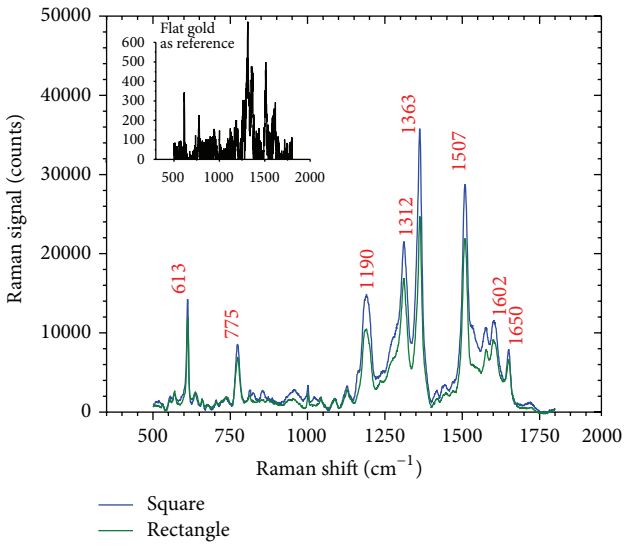


FIGURE 4: Raman spectra obtained from R6G-PMMA probe molecules deposited on 2D square and rectangle plasmonic templates. Inset shows the spectrum obtained from flat gold film keeping all other parameters identical.

in nature which is indicative of near-field contribution from propagating plasmon resonance. The total field enhancement for unit area is very high compared to that for other plasmonic structures.

It is much challenging to further enhance near field in the proposed ring structure to make it densely packed.

Conflict of Interests

The author declares that there is no conflict of interests regarding the publication of this paper.

Acknowledgment

The author thanks Dr. S. Mukhopadhyay at IISER Mohali, India, for Raman facility to collect SERS data.

References

[1] M. Kahl and E. Voges, "Analysis of plasmon resonance and surface-enhanced Raman scattering on periodic silver

structures," *Physical Review B—Condensed Matter and Materials Physics*, vol. 61, no. 20, pp. 14078–14088, 2000.

[2] P. Mandal and S. A. Ramakrishna, "Dependence of surface enhanced raman scattering on the plasmonic template periodicity," *Optics Letters*, vol. 36, no. 18, pp. 3705–3707, 2011.

[3] P. Mandal, A. Nandi, and S. Anantha Ramakrishna, "Propagating surface plasmon resonances in two-dimensional patterned gold-grating templates and surface enhanced Raman scattering," *Journal of Applied Physics*, vol. 112, Article ID 044314, 2012.

[4] M. D. Doherty, A. Murphy, J. McPhillips, R. J. Pollard, and P. Dawson, "Wavelength dependence of raman enhancement from gold nanorod arrays: quantitative experiment and modeling of a hot spot dominated system," *Journal of Physical Chemistry C*, vol. 114, no. 47, pp. 19913–19919, 2010.

[5] C. M. Aikens and G. C. Schatz, "TDDFT studies of absorption and SERS spectra of pyridine interacting with Au_{20}," *Journal of Physical Chemistry A*, vol. 110, no. 49, pp. 13317–13324, 2006.

[6] J. Beermann, S. M. Novikov, K. Leosson, and S. I. Bozhevolnyi, "Surface enhanced Raman imaging: periodic arrays and individual metal nanoparticles," *Optics Express*, vol. 17, no. 15, pp. 12698–12705, 2009.

[7] Q. Zhou, Y. Liu, Y. He, Z. Zhang, and Y. Zhao, "The effect of underlayer thin films on the surface-enhanced Raman scattering response of Ag nanorod substrates," *Applied Physics Letters*, vol. 97, Article ID 121902, 2010.

[8] Y. Hou, J. Xu, P. Wang, and D. Yu, "Surface-enhanced Raman spectroscopy on coupled two-layer nanorings," *Applied Physics Letters*, vol. 96, Article ID 203107, 2010.

[9] Y. Jiao, J. D. Ryckman, P. N. Ciesielski, C. A. Escobar, G. K. Jennings, and S. M. Weiss, "Patterned nanoporous gold as an effective SERS template," *Nanotechnology*, vol. 22, no. 29, Article ID 295302, 2011.

[10] X. Deng, G. B. Braun, S. Liu et al., "Single-order, subwavelength resonant nanograting as a uniformly hot substrate for surface-enhanced Raman spectroscopy," *Nano Letters*, vol. 10, no. 5, pp. 1780–1786, 2010.

[11] S.-H. Ciou, Y.-W. Cao, H.-C. Huang, D.-Y. Su, and C.-L. Huang, "SERS enhancement factors studies of silver nanoprism and spherical nanoparticle colloids in the presence of bromide ions," *Journal of Physical Chemistry C*, vol. 113, no. 22, pp. 9520–9525, 2009.

[12] X. Deng, G. B. Braun, S. Liu et al., "Single-order, subwavelength resonant nanograting as a uniformly hot substrate for surface-enhanced Raman spectroscopy," *Nano Letters*, vol. 10, no. 5, pp. 1780–1786, 2010.

[13] B. Cui, L. Clime, K. Li, and T. Veres, "Fabrication of large area nanoprism arrays and their application for surface enhanced Raman spectroscopy," *Nanotechnology*, vol. 19, no. 14, Article ID 145302, 2008.

[14] L. Gunnarsson, E. J. Bjerneld, H. Xu, S. Petronis, B. Kasemo, and M. Käll, "Interparticle coupling effects in nanofabricated substrates for surface-enhanced Raman scattering," *Applied Physics Letters*, vol. 78, no. 6, pp. 802–804, 2001.

[15] K. D. Alexander, K. Skinner, S. Zhang, H. Wei, and R. Lopez, "Tunable SERS in gold nanorod dimers through strain control on an elastomeric substrate," *Nano Letters*, vol. 10, no. 11, pp. 4488–4493, 2010.

[16] A. M. Michaels, M. Nirmal, and L. E. Brus, "Surface enhanced Raman spectroscopy of individual rhodamine 6G molecules on large Ag nanocrystals," *Journal of the American Chemical Society*, vol. 121, no. 43, pp. 9932–9939, 1999.

Hindawi Publishing Corporation
Conference Papers in Science
Volume 2014, Article ID 683219, 5 pages
http://dx.doi.org/10.1155/2014/683219

Conference Paper

NO_2 Sensing Properties of WO_3 Thin Films Deposited by Rf-Magnetron Sputtering

Savita Sharma,[1,2] Monika Tomar,[3] Nitin K. Puri,[2] and Vinay Gupta[1]

[1] *Department of Physics and Astrophysics, University of Delhi, Delhi 110007, India*
[2] *Department of Applied Physics, Delhi Technological University, Delhi 110042, India*
[3] *Physics Department, Miranda House, University of Delhi, Delhi 110007, India*

Correspondence should be addressed to Vinay Gupta; drguptavinay@gmail.com

Received 8 February 2014; Accepted 11 March 2014; Published 10 April 2014

Academic Editors: P. Mandal, R. K. Shivpuri, and G. N. Tiwari

This Conference Paper is based on a presentation given by Savita Sharma at "National Conference on Advances in Materials Science for Energy Applications" held from 9 January 2014 to 10 January 2014 in Dehradun, India.

Copyright © 2014 Savita Sharma et al. This is an open access article distributed under the Creative Commons Attribution License, which permits unrestricted use, distribution, and reproduction in any medium, provided the original work is properly cited.

Tungsten trioxide (WO_3) thin films were deposited by Rf-magnetron sputtering onto Pt interdigital electrodes fabricated on corning glass substrates. NO_2 gas sensing properties of the prepared WO_3 thin films were investigated by incorporation of catalysts (Sn, Zn, and Pt) in the form of nanoclusters. The structural and optical properties of the deposited WO_3 thin films have been studied by X-ray diffraction (XRD) and UV-Visible spectroscopy, respectively. The gas sensing characteristics of all the prepared sensor structures were studied towards 5 ppm of NO_2 gas. The maximum sensing response of about 238 was observed for WO_3 film having Sn catalyst at a comparatively lower operating temperature of 200°C. The possible sensing mechanism has been highlighted to support the obtained results.

1. Introduction

Nitrogen dioxide (NO_2) is one of the most harmful gases to the ecosystem and provides a major contribution to air pollution [1]. The detection of NO_2 is crucial for monitoring environmental pollution resulting from combustion processes, particularly industrial emissions or vehicle exhaust [2]. Occupational Safety and Health Administration (OSHA, United States Department of Labour) declares the Permissible Exposure Limit (PEL) of NO_2 gas as 5 ppm for general industries and 20 ppm as Immediately Dangerous to Life or Health Concentrations (IDLHs) [3]. NO_2 gas is the main precursor for ozone layer depletion in lower atmosphere and also produces acid rain which is slowly damaging the ecosystem. Commercially, many NO_2 gas sensors are available in the market but they have poor sensitivity, high operating temperature, bulky size and are very costly. Thus, there is an urgent requirement of cheap, highly sensitive and selective NO_2 gas sensors which could be operated at lower operating temperature.

Gas sensors based on metal oxide semiconductors are used in a wide variety of applications including gas monitoring and detection applications [4–6]. Considerable research has been carried out on the development of chemical sensors based on semiconductor metal oxides such as SnO_2, ZnO, and TiO_2 because of their high sensitivity towards many reducing as well as oxidizing gases [7–9]. Tungsten trioxide has attractive electrical properties and reactivity to oxidizing gases making it one of the best candidates for gas sensing applications [10–12]. The tungsten trioxide (WO_3) thin films and nanostructures are seen to be an excellent candidate for NO_2 gas detection [13, 14] because the W transition metal is found to be with different oxidation states (W^{5+}, W^{6+}) enhancing the oxidizing power of NO_2 gas molecules onto the surface of WO_3 metal oxide. Thus, in the present work, WO_3 thin film based gas sensors have been exploited for the trace level (5 ppm) detection of NO_2 gas. Effect of different catalysts (Sn, Zn, and Pt) incorporated on the surface of SnO_2 thin film in the form of nanoclusters has also been studied for NO_2 gas detection.

Table 1: Deposition parameters for WO_3 thin film using Rf magnetron sputtering.

Target	W metal target (99.999% pure)
Substrate	IDE/corning glass; corning glass
Target to substrate distance	6 cm
Sputtering pressure	10 mT
RF power	50 Watt
Gas composition ($Ar : O_2$)	60 : 40

2. Experimental Details

WO_3 thin film has been deposited by Rf-magnetron sputtering technique using a 2-inch W metal target (99.999% pure) in a reactive gas ambient of Ar and O_2 gas mixture. WO_3 thin films were fabricated onto the corning glass substrates patterned with Pt interdigital electrodes (IDEs). The description of fabrication of Pt IDEs has been mentioned elsewhere [9]. The typical growth conditions used for the deposition of WO_3 thin film are summarized in Table 1. WO_3 thin films were deposited under the growth pressure of 10 mTorr with argon to oxygen ratio of 60 : 40 by applying a Rf power of 50 W.

For the formation of nanocrystalline WO_3 thin film, in situ annealing was carried out at a substrate temperature of 400°C for 1 hour in 60% Ar: 40% O_2 environment. In order to get the enhanced sensing response characteristics, Sn, Zn, and Pt metal catalysts were incorporated onto the surface of WO_3 thin film in the form of nanoclusters on separate sensors. Sn, Zn, and Pt were also deposited using sputtering technique using their respective metal targets under the sputtering pressure of 10 mT and in 100% argon gas ambient. Nanoclusters of metal catalysts were deposited using a shadow mask of uniformly distributed pores of 600 μm diameter onto the surface of WO_3 thin film. X-ray diffraction (XRD) study was carried out using Bruker D-8 X-ray diffractometer. Optical properties have been studied via UV-visible spectrophotometer (Lambda 35). WO_3 film thickness was measured using surface thickness profiler (DEKTAK 150). Gas sensing characteristics of the prepared WO_3 thin film based sensors were studied in a specially designed "Gas Sensor Measurement and Calibration System (GSMCS)." Changes in the sensor resistance were recorded after every second using a digital multimeter (Keithley 2700) interfaced with computer. The sensing response of prepared WO_3 thin film based structures was calculated using the relation: $S = R_g/R_a$, where R_g is the resistance of sensor in the presence of target NO_2 gas and R_a is the resistance of the sensor in the absence of target NO_2 gas.

3. Results and Discussion

Figure 1 shows the X-ray diffraction (XRD) spectra of WO_3 thin films deposited on corning glass substrate at a substrate temperature of 400°C. The XRD spectra show the formation of orthorhombic structure (JCPDS Card no. 35-0270) of WO_3 and do not show the presence of any other secondary phase indicating the growth of single phase and polycrystalline

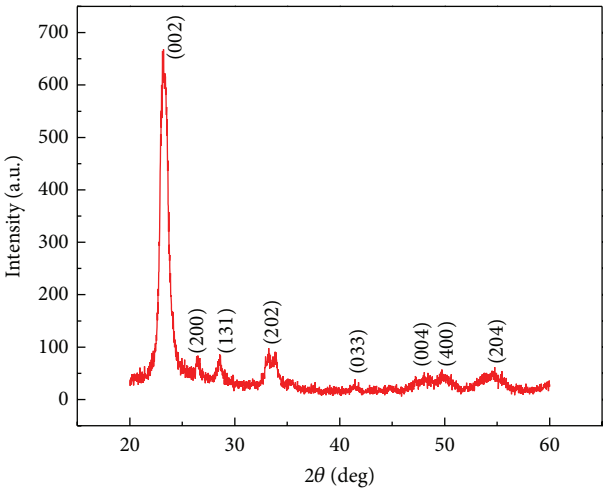


Figure 1: XRD patterns of the WO_3 thin film.

WO_3 thin films. It is observed from Figure 1 that reflection corresponding to (002) plane is dominant and is relatively intense indicating preferential orientation of the deposited WO_3 thin film. The crystallite size calculated from the Debye Scherrer formula is found to be 17.73 nm which is relatively small leading to increase in grain boundaries suitable for gas sensing applications.

UV-visible transmission spectra of annealed WO_3 thin film deposited over corning glass substrate were measured in the wavelength range of 190 to 1100 nm and are shown in Figure 2(a). It can be seen that the film is highly transparent (88%) in the visible region showing good optical quality and low absorption losses. The presence of fringes at higher wavelength confirms that the prepared WO_3 thin film is free from any inhomogeneity. The onset of sharp fundamental absorption edge at about 310 nm was observed in the deposited WO_3 thin films (Figure 2(a)).

The Tauc plot of $(\alpha h\nu)^2$ versus photon energy ($h\nu$) (where α is absorption coefficient, h is planks constant, and ν is frequency of the incident radiation) of the WO_3 thin film deposited at 10 mT sputtering pressure is shown in Figure 2(b). Optical bandgap of the WO_3 thin film was calculated from the linear portion of the Tauc plot. Linear region is clearly seen in Figure 2(b) at $h\nu > 3.5$ eV for WO_3 thin film which is in accordance with the well-known absorption law $\alpha h\nu \sim (h\nu - E_g)^{1/2}$ being characteristic for direct optical transitions. Estimated value of bandgap of the WO_3 thin film is found to be 3.90 eV and is close to the reported value [15].

Figure 3 shows the variation of sensing response of all the prepared WO_3 thin film based sensor structures (WO_3, WO_3/Sn, WO_3/Zn, and WO_3/Pt) as a function of temperature towards 5 ppm of NO_2 gas. It is observed that the value of resistance of the sensors in the presence of air (R_a) increases to a higher stable value (R_g) when target NO_2 gas is inserted into chamber due to the oxidising nature of NO_2. When the NO_2 gas is flushed out of the chamber, all the fabricated sensors retain their original high resistance value (R_a).

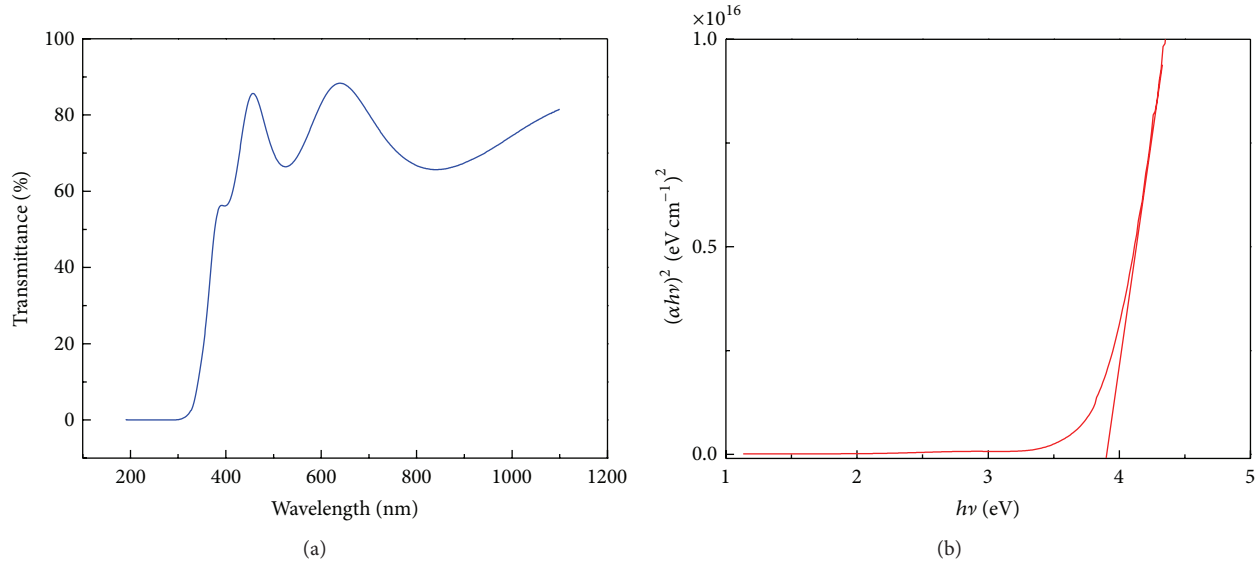


FIGURE 2: (a) UV-visible transmittance spectra of the WO_3 thin film prepared on corning glass substrate. (b) Tauc Plot of WO_3 thin film.

TABLE 2: Sensor response, response time, and recovery time at their respective operating temperatures for the fabricated sensor structures.

Sensor	Sensor response	Operating temperature (°C)	Response time	Recovery time
WO_3/Sn	238	200	32 sec	15.3 min
WO_3/Zn	173	250	5.2 min	18 min
WO_3/Pt	118	270	4.6 min	17 min

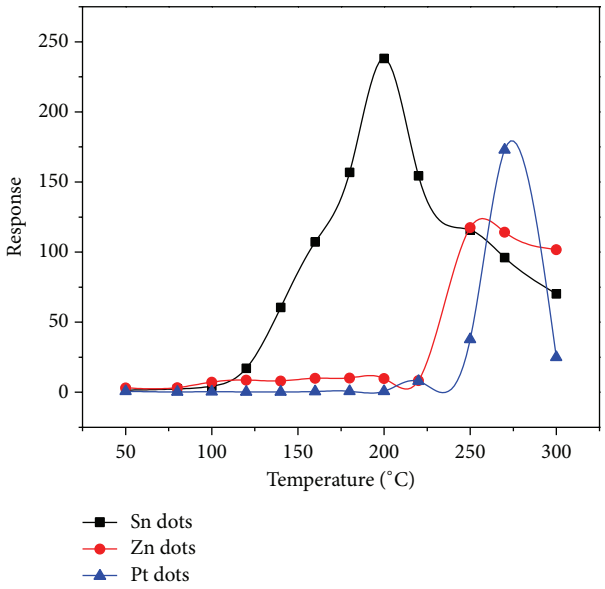


FIGURE 3: Variation of sensor response with temperature for the sensor structures: WO_3/Sn, WO_3/Zn, and WO_3/Pt towards 5 ppm of NO_2 gas.

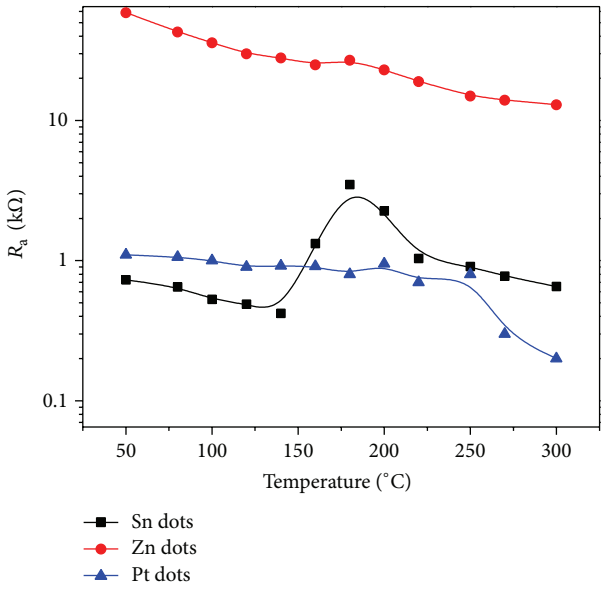


FIGURE 4: Variation of sensor resistance in air (R_a) with temperature for the sensor structures: WO_3/Sn, WO_3/Zn, and WO_3/Pt.

Figures 4 and 5 show the variation of sensor resistance in the presence of air (R_a) and in the presence of NO_2 gas (R_g), respectively, with temperature for all the prepared sensors (WO_3/Pt, WO_3/Sn, and WO_3/Zn nanoclusters). It can be observed from Figures 4 and 5 that the value of R_a and R_g decreases with increase in temperature. When NO_2 gas interacts with the sensor surface at a particular

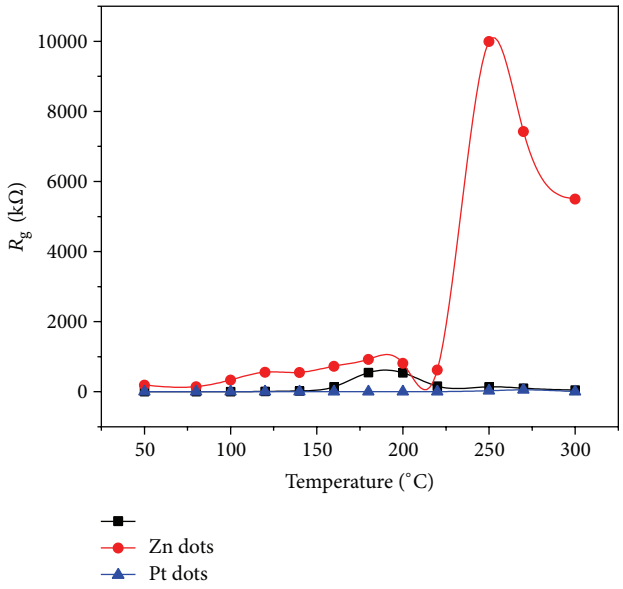


FIGURE 5: Variation of sensor resistance in the presence of 5 ppm NO_2 gas with temperature for sensor structures: WO_3/Sn, WO_3/Zn, and WO_3/Pt.

temperature, the value of resistance increases from R_a to R_g. The maximum increase in the value of R_g is observed for WO_3/Zn nanoclusters sensor structure; however, the higher value of R_a as compared to other sensor structures restricts the further enhancement in sensing response. Moreover, the maximum sensor response has been observed for WO_3/Sn sensor structure which may be attributed to the possible spillover of NO and O^- species onto the uncovered surface of WO_3 thin film. It can be observed from Figure 3 that the maximum sensing response of ~238 has been obtained for the WO_3/Sn sensor at a low operating temperature of 200°C. The obtained sensor response for all the sensors with response and recovery speeds at their respective operating temperatures is summarized in Table 2. It may be seen that the WO_3/Sn sensor exhibits comparatively high sensing response with fast response and recovery speeds at low operating temperature of 200°C. WO_3/Pt and WO_3/Zn sensors show a moderate response of 118 and 173, respectively, at high operating temperatures of 270°C and 250°C, respectively. For WO_3/Sn sensors, NO_2 gas reacts with free Sn sites as well in the similar way as with W sites and captures electrons thus giving a high sensor response [14]. NO_2 gas on interaction with Sn nanoclusters gets converted into NO and O^- species which spill over the WO_3 surface and captured electrons from WO_3 thin film thereby increasing sensing response.

4. Conclusion

The enhanced sensing response of 238 towards 5 ppm of NO_2 was obtained for WO_3/Sn sensor structure at a low operating temperature of 200°C as compared to other fabricated sensors, namely, WO_3/Zn, WO_3/Pt, and WO_3. Enhanced sensing response for WO_3/Sn sensor structure is attributed to the spillover of NO_2 species over WO_3 surface thus enhancing the adsorption of NO_2 gas on the sensor surface that leads to an increased sensor response.

Conflict of Interests

The authors declare that there is no conflict of interests regarding the publication of this paper.

Acknowledgments

The authors are thankful to the Department of Science and Technology (DST) and GAIL India Ltd. for the financial support to carry out this work. One of the authors (Savita Sharma) is thankful to the Delhi Technological University (DTU) for the teaching assistantship.

References

[1] B. T. Marquis and J. F. Vetelino, "A semiconducting metal oxide sensor array for the detection of NO_x and NH_3," *Sensors and Actuators B: Chemical*, vol. 77, no. 1-2, pp. 100–110, 2001.

[2] L. Shi, Y. Hasegawa, T. Katsube, K. Onoue, and K. Nakamura, "Highly sensitive NO_2 gas sensor fabricated with RF induction plasma deposition method," *Sensors and Actuators B: Chemical*, vol. 99, no. 2-3, pp. 361–366, 2004.

[3] http://www.osha.gov/.

[4] K. Potje-Kamloth, "Semiconductor junction gas sensors," *Chemical Reviews*, vol. 108, no. 2, pp. 367–399, 2008.

[5] D. E. Williams, "Semiconducting oxides as gas-sensitive resistors," *Sensors and Actuators B: Chemical*, vol. 57, no. 1–3, pp. 1–16, 1999.

[6] W. Göpel and K. D. Schierbaum, "SnO_2 sensors: current status and future prospects," *Sensors and Actuators B: Chemical*, vol. 26, no. 1–3, pp. 1–12, 1995.

[7] L. Liu, T. Zhang, L. Wang, and S. Li, "Improved ethanol sensing properties of Cu-doped SnO_2 nanofibers," *Materials Letters*, vol. 63, no. 23, pp. 2041–2043, 2009.

[8] Y. Wang, W. Jia, T. Strout et al., "Ammonia gas sensor using polypyrrole-coated TiO_2/ZnO nanofibers," *Electroanalysis*, vol. 21, no. 12, pp. 1432–1438, 2009.

[9] A. Sharma, M. Tomar, and V. Gupta, "SnO_2 thin film sensor with enhanced response for NO_2 gas at lower temperatures," *Sensors and Actuators B: Chemical*, vol. 156, no. 2, pp. 743–752, 2011.

[10] C. Zhang, M. Debliquy, A. Boudiba, H. Liao, and C. Coddet, "Sensing properties of atmospheric plasma-sprayed WO_3 coating for sub-ppm NO_2 detection," *Sensors and Actuators B: Chemical*, vol. 144, no. 1, pp. 280–288, 2010.

[11] C. Zhang, A. Boudiba, C. Navio et al., "Highly sensitive hydrogen sensors based on co-sputtered platinum-activated tungsten oxide films," *International Journal of Hydrogen Energy*, vol. 36, no. 1, pp. 1107–1114, 2011.

[12] A. Boudiba, C. Zhang, C. Navio, C. Bittencourt, R. Snyders, and M. Debliquy, "Preparation of highly selective, sensitive and stable hydrogen sensors based on Pd-doped tungsten trioxide," *Procedia Engineering*, vol. 5, pp. 180–183, 2010.

[13] P. V. Tong, N. D. Hoa, V. V. Quang, N. V. Duy, and N. V. Hieu, "Diameter controlled synthesis of tungsten oxide nanorod bundles for highly sensitive NO_2 gas sensors," *Sensors and Actuators B*, vol. 183, pp. 372–380, 2013.

[14] A. Sharma, M. Tomar, and V. Gupta, "Low temperature operating SnO_2 thin film sensor loaded with WO_3 micro-discs with enhanced response for NO_2 gas," *Sensors and Actuators B: Chemical*, vol. 161, no. 1, pp. 1114–1118, 2012.

[15] A. Paliwal, A. Sharma, M. Tomar, and V. Gupta, "Optical properties of WO_3 thin films using surface plasmon resonance technique," *Journal of Applied Physics*, vol. 115, no. 4, Article ID 043104, 2014.

Hindawi Publishing Corporation
Conference Papers in Science
Volume 2014, Article ID 628294, 3 pages
http://dx.doi.org/10.1155/2014/628294

Conference Paper

Harnessing Solar Energy for Every Home: Energy Saving Applications

Jitisha Aggarwal[1] and M. L. Aggarwal[2]

[1] *Electronics Engineering Department, YMCA University of Science & Technology (State Government University), Faridabad, Haryana 121 006, India*
[2] *Mechanical Engineering Department, YMCA University of Science & Technology (State Government University), Faridabad, Haryana 121 006, India*

Correspondence should be addressed to Jitisha Aggarwal; jitisha27@gmail.com

Received 19 December 2013; Accepted 19 February 2014; Published 10 April 2014

Academic Editors: R. K. Shivpuri and G. N. Tiwari

This Conference Paper is based on a presentation given by Jitisha Aggarwal at "National Conference on Advances in Materials Science for Energy Applications" held from 9 January 2014 to 10 January 2014 in Dehradun, India.

Copyright © 2014 J. Aggarwal and M. L. Aggarwal. This is an open access article distributed under the Creative Commons Attribution License, which permits unrestricted use, distribution, and reproduction in any medium, provided the original work is properly cited.

Most of the present day resources of energy are limited and irreplaceable. The next generation will face acute energy crisis if alternate resources of energy are not developed concurrently. Increasing cost and import of conventional resources have bad effect on the economy of a country, and the only cheaper solution is "unlimited power" from the sun. The use of solar energy is so far limited in household applications. In fact, if we harness only 0.0034 percent of the solar energy reaching the Earth's surface, the energy need of the whole world will be met. In the present work, a substitute of 10-watt conventional night lamp has been proposed by a solar night lamp of the same light intensity through an experimental setup. The developed solar system is cheaper, portable, user friendly, and free from maintenance. The paper stresses on the need of replacement of conventional night lamp by solar night lamp in every home for reducing the energy crisis at present.

1. Introduction

Scarcity and cost of fossil fuels combined with their greenhouse gas emissions make the development of nonfossil fuel based methods of transportation a high-priority task. This interest was further fueled by world apprehensions concerned with nuclear wastes and nuclear safety on one hand and global warming on the other hand [1, 2]. These considerations make solar energy the ultimate strategic choice as a source of world energy. As a result of current day satellite technology, designers now have a more or less clear picture about solar energy intensity distribution worldwide. Solar energy research emphasis over the past three decades was concentrated on two main aspects of this subject. The first is concerned with solar energy direct heat production and the second is involved with solar energy electricity production. Recent technological developments in thin-film photovoltaics, such as amorphous silicon [1, 2] and hybrid dye-sensitized/photovoltaic (PV) cells, are leading to new generations of consumer portable solar arrays. These new arrays are lightweight, durable, and flexible and have been reported to achieve power efficiencies of up to 10% [3].

There are many types of solar power lights that can be used to illuminate your home and surrounding and at the same time save the natural resources. These lighting systems will not only save electricity but also cause less pollution, by emitting less amounts of heat when compared to conventional lighting sources like bulbs. Solar lantern lights are extensively used for indoor lighting. All of the solar lighting devices used for indoor lighting need to be charged when sunlight is available and used during night time.

Home lighting systems are powered by solar energy using solar cells that convert solar energy (sunlight) directly to electricity. The electricity is stored in batteries and used for

Table 1: Details of parts of night solar lamp.

Serial number	Part name	Specification	Size	Cost
1	Rechargeable battery	3 V, general	5 cm × 2 cm	Rs. 30
2	Solar panel (collector)	Photovoltaic (PV) cells	5 cm × 4 cm	Rs. 35
3	LED	20 mA and 3 V (2 numbers)	1.5 cm × 0.5 cm	Rs. 5
4	Switch	Plastic, 12 V, O.5 A	1.5 cm × 0.5 cm	Rs. 5
5	Glass on LED to form lamp	General thin glass	9 cm × 6 cm	Rs. 10
6	Bottom plastic box	Light flexible thermoplastic material	9 cm × 5 cm	Rs. 10
7	Others: diode and connecting wires	—	Negligible	Rs. 10

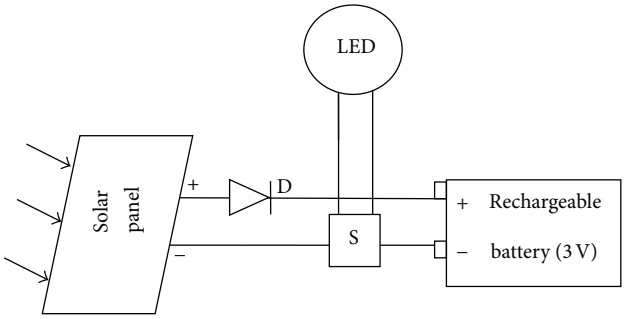


Figure 1: Circuit diagram for solar power light.



Figure 2: Solar night lamp for commercial applications.

the purpose of lighting whenever required. These systems are useful in nonelectrified rural areas and as reliable emergency lighting systems for important domestic, commercial, and industrial applications. Though a lot of work has been done on solar energy, its commercial utility of small size, portable, and cheaper solar devices for every home has not been in use so far. The present work demonstrates experimentally tested portable solar energy system for every home for saving the energy of the country.

2. Materials and Method

The system comprises solar panel, rechargeable battery, LED, glass, switch, resistance, and diode (Figure 1). The overall size of portable solar night lamp is 12 cm × 9 cm, the total weight is 100 gm, and the total manufacturing cost is Rs. 105. LED, glass cover on LED, and solar panel are kept outside, while all other components are enclosed in a plastic box. The cost, specification, and size of various equipment are shown in Table 1.

The system in Figure 1 was designed to give a daily working time of 6-7 hours with the fully charged battery. The system provided for buffer storage for 4-5 nonsunny/cloudy days. The solar night lamp (Figure 2) had been working for the last six months and is still working without any maintenance.

Electricity generated from thermal power station is an expensive source of electricity; solar energy has turned it into an economical power source in the long-run. The amount of electricity generated from solar energy depends upon the available sunlight.

3. Results and Discussion

Conventional Electric Energy Consumption of Night Electric Lamp in a City (Energy Provided by Thermal Power Station). The energy consumption during night for two electric lamps of 10 W each in a house is 2 × 10 = 20 W. Let us assume that the number of houses in a city is 50000, the energy consumed by one house in a year is (20 × 8 × 365)/1000 = 58.4 KWh/Yr, the yearly electricity bill of one house is 58.4 × 6 = Rs. 350.4, the energy consumed by 50000 houses in the city in a year is 58.4×50000 = 2920000 KWh/Yr, and the yearly electricity bill of 50000 houses is 2920000 × 6 = Rs. 17520000 = 1.752 crore.

Solar Energy Consumption of Night Solar Lamp in a City with the Same Light Intensity. The initial cost of one solar lamp is Rs. 105; the commercial price of the solar equipment (including taxes, sales, and marketing cost) is Rs. 150. Assuming that the life of solar equipment is one year (it is expected to be more), the cost of 50000 solar night lamps (2 in each house) is 150 × 2 × 50000 = Rs. 15000000 = 1.50 crore. The operational unit cost of the electricity is nil.

Comparison. Saving in the energy consumed from conventional thermal power station, hence, by 50000 houses in

the city in a year is equal to 2920000 KWh/Yr, because these houses are getting energy from solar night lamps; the yearly saving of cost using solar night bulbs for 50000 houses is 1.752 − 1.50 = Rs. 0.252 cr; the yearly saving of cost using solar night bulb for one house is 350.4 − 150 × 2 = Rs. 50.4.

Other Benefits of Solar Power Lights. The biggest advantage of using solar power is that it is an inexhaustible source of energy. Once you have installed the system, you do not have to worry that you would ever be without electricity, because the sun is always going to be there. The next advantage of using solar energy is that it does not emit any pollution into the environment. Solar panels do not release any emissions into the atmosphere while generating electricity. In the most remote locations, solar energy is the ideal source of electricity. A big advantage of solar energy systems is that a properly installed system does not require much maintenance.

4. Conclusions

It was established by testing the system during the last six months that if charged for 6-7 hrs in summer sunlight, the battery is capable of supplying stored energy to solar night lamp for 4-5 nights. The developed solar system is costing Rs. 150 only, portable, user friendly, and free from maintenance. It is established that there is need for replacement of conventional night lamp by solar night lamp in every home for the cheaper unit cost as well as solution of energy crisis at present.

Conflict of Interests

The authors declare that there is no conflict of interests regarding the publication of this paper.

References

[1] G. Danese, F. Leporati, R. Lombardi, M. Nucita, G. Pedrazzini, and G. Ricotti, "A profile in NiCd and NiMH batteries instrument for the characterization of voltage and temperature," in *Proceedings of the 23rd Euromicro Conference*, pp. 178–183, September 1997.

[2] M. Gonzalez, F. J. Ferrero, J. C. Anton, and M. A. Perez, "Considerations to improve the practical design of universal and full-effective NiCd/NiMH battery fast-chargers," in *Proceedings of the 14th annual Applied Power Electronics Conference and Exposition (APEC '99)*, vol. 1, pp. 167–173, March 1999.

[3] M. Gonzalez, M. A. Perez, J. C. Campo, and F. J. Ferrero, "Accurate detection algorithm of battery full-capacity under fast-charge," in *Proceedings of the IEEE Instrumentation and Measurement Technology Conference (IMTC '98)*, vol. 2, pp. 755–759, May 1998.

Hindawi Publishing Corporation
Conference Papers in Science
Volume 2014, Article ID 816970, 4 pages
http://dx.doi.org/10.1155/2014/816970

Conference Paper

Study of Magnetic Property of Sn Doped Ni-Zn-Fe Nanoparticles

B. S. Tewari, Archana Dhyani, S. K. Joshi, Santosh Dubey, and Kailash Pandey

Department of Physics, University of Petroleum and Energy Studies, Dehradun 248007, India

Correspondence should be addressed to B. S. Tewari; bstewari@ddn.upes.ac.in

Received 5 February 2014; Accepted 11 March 2014; Published 9 April 2014

Academic Editors: R. Chandra, P. Mandal, R. K. Shivpuri, and G. N. Tiwari

This Conference Paper is based on a presentation given by B. S. Tewari at "National Conference on Advances in Materials Science for Energy Applications" held from 9 January 2014 to 10 January 2014 in Dehradun, India.

Copyright © 2014 B. S. Tewari et al. This is an open access article distributed under the Creative Commons Attribution License, which permits unrestricted use, distribution, and reproduction in any medium, provided the original work is properly cited.

The $Ni_{0.6+x}Zn_{0.4}Sn_xFe_{2-2x}O_4$ (x = 0.00 to 0.04) samples were prepared by solution route technique. These samples were characterized by XRD and EPR spectra at X-band frequency (~9.2 GHz). The XRD spectra of these ferrites confirm the formation of spinel structure. The average particle size calculated by using Scherrer's formula was found to be of the order of 24.7 nm. The EPR spectra of these ferrites are mainly due to Fe^{3+} ions. Fe^{2+} ions have very short spin-lattice relaxation time and therefore EPR spectra of Fe^{2+} could be observed only at very low temperature. This fact is also supported by the isomer shift values of these ferrites obtained from Mössbauer spectroscopy. The variation of g_{eff} and ΔH_{PP} with Sn^{4+} concentration is attributed to the variation of superexchange interaction. Moreover in this system the dominant process of relaxation is the spin lattice relaxation rather than the spin-spin interaction.

1. Introduction

Ferrites are certain double oxides of iron and another metal taken as the most important ferromagnetic substances. The magnetic ferrites fall mainly into two groups with different crystal structures. One is cubic ferrites having the general formula $MO{\cdot}Fe_2O_3$ where M is a divalent metal ion, like Mn, Ni, Fe, Co, and Mg. Second one is hexagonal ferrites. The most important member in this group is barium-ferrites $BaO{\cdot}6Fe_2O_3$. The ferrites are ionic compounds, and their magnetic properties are due to the magnetic ions they contain. The commercial value lies in the fact that they have higher values of saturation magnetization and Curie temperature, which are imperative for use as core materials. They are more suitable for high power application in addition to the applications, such as multilayer chip inductor and electromagnetic interference (EMI) suppression; recent studies suggest their applications in biomedical applications such as molecular imaging and drug delivery [1–4].

There are two main classes of materials containing zinc ferrites, that is, Mn-Zn ferrites and Ni-Zn ferrites. Out of them Ni-Zn ferrites are designed for very high frequency operation, to more than 100 MHz as well as very high resistivity, about 10^5 ohm cm. The effect of TiO_2 addition on saturation magnetization and magnetic spectrum of $Ni_{0.3}Zn_{0.7}Fe_2O_4$ has been studied [4]. An unexpected dip was reported in the saturation magnetization curve at a particular Ti^{4+} concentration in Ti^{4+}-substituted Ni-Zn ferrite [5]. It has also been concluded that lattice parameter decreased with the increase of Ti^{4+} up to a certain concentration and subsequently it increased monotonically.

The variation of lattice parameter with high valent substitution is a combined effect of cation size on [6]:

(i) "b"-the repulsion parameter for A site and

(ii) "M"-Madelung Constant. He also observed a similar type of anomalous behavior in saturation curve for a wide range of Ti-substituted Ni-Zn ferrites.

The present work is done to record and analyse the electronic paramagnetic resonance (EPR) spectra of Sn-substituted Ni-Zn ferrite for various Sn concentrations at room temperature and liquid nitrogen temperature. The characterization of the prepared samples was done by XRD analysis. This work is a step towards studying the physical processes leading to anomalous behavior of magnetization in the Sn-substituted Ni-Zn ferrites [7, 8].

2. Experimental Technique

In the present work the EPR spectroscopy technique is employed. EPR spectroscopy studies the interaction of electron magnetic moment with a magnetic field and thus is applicable only to the systems having unpaired electrons (paramagnetic substances) or net angular momentum. EPR spectrum can be used to identify an unknown transition metal ion or lattice defect; it may be used to distinguish between the several valence states of the same ion. EPR spectrum frequently identifies the lattice site and symmetry of the paramagnetic species, particularly if single crystal data are available. Considerable information can be obtained about the nuclei in the immediate neighborhood of the absorbing spin and sometimes relaxation time data detects long range effects. The concentration of paramagnetic species may also be determined.

The important parameters from the EPR signal to be calculated are

(i) g-factor . It is calculated as

$$g = 2.00367 \frac{H_{\mathrm{DPPH}}}{H_r}, \tag{1}$$

where H_r in the original absorption curve is the field corresponding to absorption (i.e., resonance field) for the given sample. In derivative curve it is measured.

(ii) Line width. It is defined as full width at half maximum (FWHM) for original absorption curve. For first derivative curve it is given by the peak-to-peak distance along magnetic field axis; that is,

$$\Delta H_{\mathrm{pp}} = \left[H\left(\text{peak } 2\right) - H\left(\text{peak } 1\right)\right]. \tag{2}$$

(iii) Spin-spin relaxation. It is calculated using the formula $1/T_2 = \pi g \mu_B \Delta H/h$, where ΔH is the FWHM (full width at half maximum) of the absorption peak or peak-to-peak line width of the first derivative curve.

3. Results

The EPR spectra of all the samples have an intense broad asymmetric peak having peak-to-peak line width $\Delta H_{\mathrm{pp}} \sim 2$ KGauss at room temperature. The spectra also have a very weak shoulder near zero field. The appearance of this weak shoulder near zero may be due to anisotropy effect. Here we are not interested in this particular investigation. Our discussion will be confined only for the peak corresponding to $g_{\mathrm{eff}} \sim 4$ for ferrites.

The graph plotted between g_{eff} and the Sn concentration x at room temperature is shown in Figure 1. The g_{eff} for base ferrite (i.e., $x = 0.00$) is found to be 4.49 and it decreases to 2.98 up to $x = 0.008$. It again increases to 3.21 at $x = 0.012$ and then decreases to 2.95 up to $x = 0.04$.

The variation of peak-to-peak line width ΔH_{pp} as a function of "x" in the $Ni_{0.6+x}Zn_{0.4}Sn_xFe_{2-2x}O_4$ ($x = 0.00$ to 0.04) ferrite system at room temperature is shown in Figure 2. The value of ΔH_{pp} for $x = 0.00$ comes out to be 1.92 KGauss.

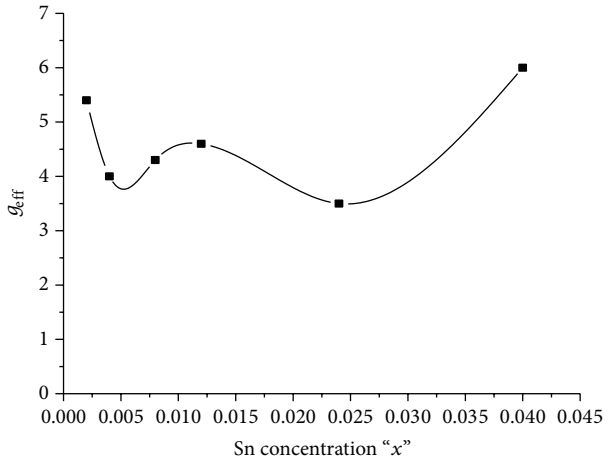


Figure 1: g_{eff} versus Sn concentration "x" in $Ni_{0.6+x}Zn_{0.4}Sn_xFe_{2-2x}O_4$ at RT.

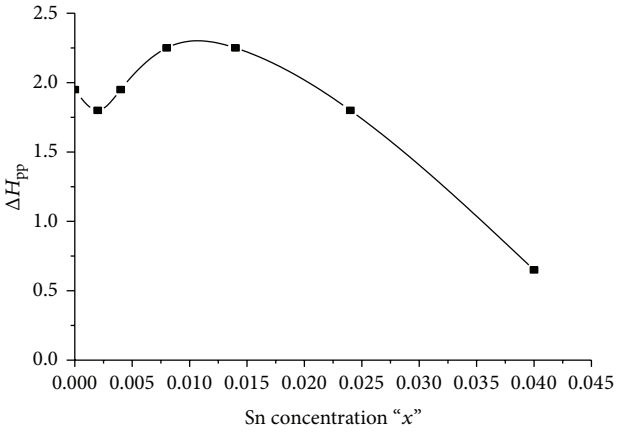


Figure 2: ΔH_{pp} versus Sn concentration "x" in $Ni_{0.6+x}Zn_{0.4}Sn_xFe_{2-2x}O_4$ at RT.

It attains a maximum value of 2.225 KGauss at $x = 0.008$ and at $x = 0.012$. It then decreases monotonically to a value of 0.72 KGauss up to $x = 0.04$. The variation of relaxation time T_2 with Sn concentration x at room temperature is plotted in Figure 3. For the base ferrite, $Ni_{0.6}Zn_{0.4}Fe_2O_4$, the value of relaxation time comes out to be of the order of 2.63×10^{-11} seconds at room temperature. Here we do not observe any systematic behaviour of relaxation time with Sn concentration. Previous workers [9–11] have also reported such smaller values of relaxation time for Fe^{3+} ions.

The magnetic interaction causes broadening of the resonance lines as the temperature is increased, if the interacting spins are alike, whereas it causes narrowing of resonance lines when unlike spins are involved. Since in $Ni_{0.6+x}Zn_{0.4}Sn_xFe_{2-2x}O_4$ ferrite two different kinds of paramagnetic spins, namely, Ni^{2+} and Fe^{3+}, are involved, the exchange interaction might be responsible for narrowing of the resonance peaks with increase of temperature.

The observed EPR spectra of the ferrite studied here is due to Fe^{3+} ions and not due to Fe^{2+} ions. The reason is that Fe^{2+}

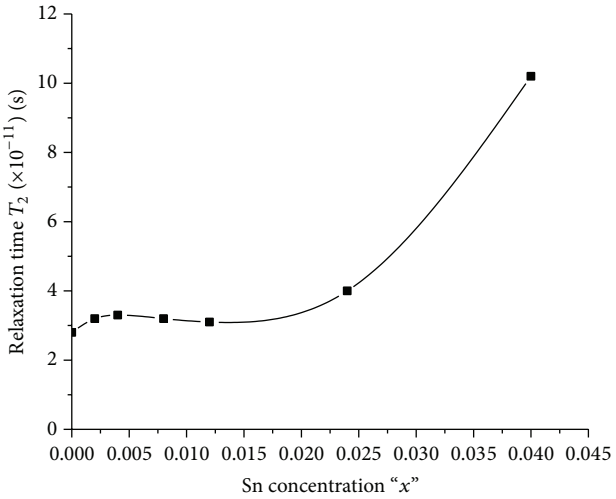


FIGURE 3: Relaxation time T_2 versus Sn concentration "x" in $Ni_{0.6+x}Zn_{0.4}Sn_xFe_{2-2x}O_4$ at RT.

ions have very short spin lattice relaxation time and EPR can be observed at very low temperature (close to liquid Helium). Determination of isomer shift in this system of ferrite by ^{57}Fe Mössbauer spectroscopy confirmed the fact that iron is in Fe^{3+} state [12].

The value of g_{eff} for bound unpaired electron is different than the value of g_{eff} for a free electron. g_{eff} for a bound electron depends on the magnetic interaction involving the orbital angular momentum of the unpaired electrons. Since the chemical environment of the unpaired electron changes the orbital angular momentum of the unpaired electron, therefore, one can say that g_{eff} value likewise depends upon the chemical environment of the paramagnetic ions under consideration. The orbital angular momentum involves two types of magnetic interactions. One is the interaction of the orbital angular momentum with the electron spin, that is, the spin orbit coupling. The other interaction is that of the orbital angular momentum with the external magnetic field. The strength of these interactions affects the position and the width of the absorption peak in EPR spectra.

The occurrence of the finite line width in EPR spectrum is due to the fact that the electrons interact with externally applied magnetic field but they also interact magnetically with the surrounding of the samples. Thus the resultant magnetic field seen by a population of electron spins is not quite the same throughout the population even when they are subjected to the same applied field. Consequently resonance absorption line obtained for a given value of the resultant field will be obtained over a range of values of the applied field.

In many magnetic materials the EPR study has revealed that the variation of the resonance line width ΔH_{pp} is caused by the microscopic magnetic interactions inside the material, mainly the interparticle magnetic dipole interaction and the superexchange interaction. In the case of ferromagnetic particles, the intrinsic molecular magnetic moments are large; therefore magnetic dipole interaction among these particles is very strong. Magnitude of this interaction is inversely proportional to the cube of average interparticle distance [13–15]. On other hand, superexchange interaction between magnetic ions through oxygen anions can reduce the value of ΔH_{pp}. The temperature dependence of relaxation time shows that, if line width is determined by spin lattice relaxation, it will decrease rapidly as temperature decreases. Further the elastic properties of these nanoparticles are currently being studied for their specific applications of high frequency devices [16].

Conflict of Interests

The authors declare that there is no conflict of interests regarding the publication of this paper.

References

[1] F. G. Brockman, V. D. Heide, and M. W. Louwerce, "Ferroxcube for proton synchrotrons," *Phillips Technical Review*, vol. 30, pp. 312–329, 1969.

[2] T. Nomura, "New evolution of ferrite for multilayer chip components," in *Proceedings of 6th International Conference on Ferrites*, vol. 6, p. 1198, Tokyo, Japan, 1992.

[3] T. Nakamura, "Snoek's limit in high-frequency permeability of polycrystalline Ni-Zn, Mg-Zn, and Ni-Zn-Cu spinel ferrites," *Journal of Applied Physics*, vol. 88, no. 1, pp. 348–353, 2000.

[4] Z. Liu, F. Kiessling, and J. Gatjens, "Another journal on nanomaterials?" *Nanomaterials*, vol. 1, pp. 1–2, 2010.

[5] D. C. Khan and M. Misra, "Magnetic, Mössbauer and electrical properties of Ti-substituted $Ni_{0.3}Zn_{0.7}Fe_2O_4$," *Bulletin of Materials Science*, vol. 7, no. 3-4, pp. 253–270, 1985.

[6] V. S. Ananthan, *Effect of titatanium zirconium and tin on the variation of saturation magnetisation curie temperature and lattice parameter [M.S. thesis]*, Indian Institute of Technology, Kanpur, India, 1983.

[7] A. R. Das, V. S. Ananthan, and D. C. Khan, "Lattice parameter variation and magnetization studies on titanium-, zirconium-, and tin-substituted nickel-zinc ferrites," *Journal of Applied Physics*, vol. 57, no. 8, pp. 4189–4191, 1985.

[8] R. C. Srivastava, D. C. Khan, and A. R. Das, "Mössbauer and magnetic studies of Ti^{4+}-substituted Ni-Zn ferrites," *Physical Review B*, vol. 41, no. 18, pp. 12514–12521, 1990.

[9] R. C. Srivastava, D. C. Khan, A. R. Das, and T. M. Srinivasan, "Mössbauer and magnetic studies of titanium doped nickel ferrite," in *Proceedings of the 5th International Conference on Ferrites*, vol. 359, 1989.

[10] N. Bloembergen and S. Wang, "Relaxation effects in para- and ferromagnetic resonance," *Physical Review*, vol. 93, no. 1, pp. 72–83, 1954.

[11] A. Upadhyay, *Electron paramagnetic resonance study of Ti substituted $NiFe_2O_4$ [M.S. thesis]*, G. B. Pant University of Ag. & Technology, Pantnagar, India, 2001.

[12] K. Pandey, *Electron paramagnetic resonance study of Ti substituted Ni-Zn ferrite [M.S. thesis]*, G. B. Pant University of Ag. & Technology, Pantnagar, India, 2003.

[13] D. C. Khan, R. C. Srivastava, and A. R. Das, "Mossbauer and magnetic studies of Sn^{4+}-substituted Ni-Zn ferrites," *Journal of Physics: Condensed Matter*, vol. 4, no. 5, article 018, pp. 1379–1385, 1992.

[14] T. Komatso, N. Soga, and N. Konagi, "ESR study of $NiFe_2O_4$ precipitation process from silicate glasses," *Journal of Applied Physics*, vol. 50, p. 6469, 1979.

[15] T. Komatso, N. Soga, and N. Konagi, "Superparamagnetic effects in the ferromagnetic resonance of silica supported nickel particles," *The Journal of Chemical Physics*, vol. 75, p. 5596, 1981.

[16] K. Praveena, K. Sadhana, and S. R. Murthy, "Elastic behaviour of Sn doped Ni-Zn ferrites," *International Journal of Scientific and Research Publications*, vol. 3, no. 2, 2013.

Hindawi Publishing Corporation
Conference Papers in Science
Volume 2014, Article ID 849241, 5 pages
http://dx.doi.org/10.1155/2014/849241

Conference Paper

On the Issue of Radiation-Induced Instability in Binary Solid Solutions

Santosh Dubey, S. K. Joshi, and B. S. Tewari

Department of Physics, University of Petroleum and Energy Studies, Dehradun 248007, India

Correspondence should be addressed to Santosh Dubey; santosh.dubey@ddn.upes.ac.in

Received 4 February 2014; Accepted 18 March 2014; Published 3 April 2014

Academic Editors: R. K. Shivpuri and G. N. Tiwari

This Conference Paper is based on a presentation given by Santosh Dubey at "National Conference on Advances in Materials Science for Energy Applications" held from 9 January 2014 to 10 January 2014 in Dehradun, India.

Copyright © 2014 Santosh Dubey et al. This is an open access article distributed under the Creative Commons Attribution License, which permits unrestricted use, distribution, and reproduction in any medium, provided the original work is properly cited.

The stability of a binary solid solution under irradiation has been studied. This has been done by performing linear stability analysis of a set of nonlinear reaction-diffusion equations under uniform irradiation. Owing to the complexity of the resulting system of eigenvalue equations, a numerical solution has been attempted to calculate the dispersion relations. The set of reaction-diffusion equations represent the coupled dynamics of vacancies, dumbbell-type interstitials, and lattice atoms. For a miscible system (Cu-Au) under uniform irradiation, the initiation and growth of the instability have been studied as a function of various control parameters.

1. Introduction

Materials under irradiation are a class of dissipative systems driven far away from the equilibrium state due to production of high densities of defects. These systems decay to lower energy metastable states by the process of phase transformation, microstructure evolution, spatial organization of compositional fluctuations and microstructural elements, and so forth [1]. The spatial organization of compositional fluctuations and microstructural elements happens when the material becomes unstable to infinitesimal perturbations in the order parameter characterizing the pattern: for example, in the case of compositional fluctuations, the order parameter is the composition, whereas, in the case of microstructural elements, the order parameter is the density of these elements. Well known examples of spatial organization of microstructural elements are voids [2–4] and bubble lattices [5, 6], precipitate ordering [7], and ordering of vacancy dislocation loops [8]. On the other hand, spatial organization of compositional fluctuations has been observed in two types of material systems. In thermodynamically unstable systems (e.g., Fe-35%Ni-Cr), the spatial organization of compositional fluctuations takes place when a sluggish long wavelength spinodal-type instability in the composition is accelerated under irradiation, which lead to decomposition of the solid solution; long-term thermal annealing of the irradiated specimen has no effect on the state of the material [9]. On the other hand, in thermodynamically stable systems (e.g., Fe-15%Ni-Cr), the origin of compositional fluctuations is solely due to irradiation. When irradiation is turned off and irradiated sample is annealed for long time, the material attains its homogeneous state [10]. The presence of spatial structures with definite characteristics has strong influence on the physical and mechanical properties of the materials. Therefore, it is important to understand the origin of these structures; the first step towards that goal is to figure out under what conditions the material may become unstable to infinitesimal perturbations with respect to its uniform state.

The issue of solid solution instability under irradiation has been addressed by several researchers in the past. These investigations may be broadly categorized into two major themes. In one class of investigation, the state of the material under irradiation is represented by a coupled system of reaction-diffusion equations in defect and material component fields. In these formulations, the origin and subsequent growth of the instability have been attributed to the presence of vacancy-interstitial recombination reactions, assisted by off-diagonal terms of the diffusion matrix [11–15]. In the other

class of investigations, first proposed by Martin [16], the state of a material is described by the evolution of one conserved order parameter in the Cahn-Hilliard type framework. In this formulation, the evolution of the order parameter is governed by two competing dynamics: fixed length athermal ballistic exchanges and thermal diffusion. Martin's approach was extended by Enrique and Bellon for arbitrary length ballistic exchanges, in order to construct a phase diagram identifying three possible regimes of material response as a function of forcing parameters: these regions have been identified as solid solution, patterning, and macroscopic phase separation [17, 18]. The applicability of this model in solid solutions under high temperature irradiation is questionable, because, under high temperature irradiation, the defects are present in nonequilibrium proportions and are sufficiently mobile. Therefore, the response of the material should be governed by a coupled defect (nonconserved) and conserved dynamics, instead of conserved dynamics only.

In the present study, the instability of a solid solution under irradiation has been investigated. For a binary system under irradiation, there are six species in the model: three off-lattice dumbbell interstitials, vacancy, and two material components. All the defect species diffuse either by vacancy mechanism or by interstitialcy mechanism. The diffusion of material components is coupled to the diffusion of the defects. The defects participate in two types of reactions: vacancy-interstitial recombination and change in dumbbell type when a dumbbell interstitial encounters a lattice atom of different type. The defect production has been considered uniform in space and time. The model consists of a set of six coupled nonlinear reaction-diffusion equations with uniform source. For a miscible system (Cu-Au) under irradiation, the linear stability analysis of the reaction-diffusion equations shows that the solid solution indeed becomes unstable when a set of control parameters (temperature, defect production rate, and initial alloy composition) is varied in a certain way.

Section 2 briefly outlines the summary of the model presented elsewhere [19], followed by the linear stability analysis of the model equations under uniform irradiation in Section 3. The results of the linear stability analysis have been presented in Section 4. Section 5 presents the conclusion of the present work.

2. Model Summary

We consider an ideal, concentrated binary solid solution, AB, under irradiation. There are six species in the model: three types of dumbbell interstitials (AA, BB, and AB), vacancy, and A and B lattice atoms. Under operating temperatures of nuclear reactors, the defects are sufficiently mobile. All the defect species diffuse either via vacancy mechanism or via interstitialcy mechanism. The diffusion of the material components is mediated by the defects. In addition to diffusion, defects also participate in two types of reactions: vacancy-interstitial recombination and change in the dumbbell-type reactions. Change in the dumbbell type happens when a dumbbell encounters a lattice atom of different type than its constituents. In this formulation, A is a faster diffusing species both by vacancy and interstitialcy mechanism, whereas B is the slower diffusing species. Evolution of all the species is governed by reaction-diffusion type dynamics with uniform defect generation term,

$$\frac{\partial C_i}{\partial t} = -\nabla \cdot J_i + R_i + S_i, \tag{1}$$

where $J_i = \sum D_{ik} \nabla C_k$, R_i , and S_i are the flux, reaction, and source terms of ith species (i = AA, BB, AB, V, A, B), respectively; D_{ik} is an $n \times n$ matrix of concentration-dependent diffusion coefficients, where n is the number of species in the model; C_k is the fractional concentration of kth species. Derivation of the defect fluxes has been carried out in the Fickian way. For simplicity in the derivation, the solid solution is considered isotropic and the correlation effects between successive defect jumps have also been ignored. These assumptions led us to derive the flux expressions in 1D and generalize into higher dimensions in a straightforward manner. Although these assumptions may introduce a certain degree of uncertainty in quantitative estimations, they will not affect the nature of the solution we are aiming at. The details of the derivation for J_i and R_i have been presented somewhere else [19]. For source terms, S_i, we have used the following expressions:

$$\begin{aligned} S_{\mathrm{AA}} &= K_0 C_{\mathrm{A}}^2, \\ S_{\mathrm{BB}} &= K_0 C_{\mathrm{B}}^2, \\ S_{\mathrm{AB}} &= 2K_0 C_{\mathrm{A}} C_{\mathrm{B}}, \\ S_v &= S_{\mathrm{AA}} + S_{\mathrm{BB}} + S_{\mathrm{AB}}, \\ S_{\mathrm{A}} &= -2S_{\mathrm{AA}} - S_{\mathrm{AB}}, \\ S_{\mathrm{B}} &= -2S_{\mathrm{BB}} - S_{\mathrm{AB}}, \end{aligned} \tag{2}$$

such that

$$S_{\mathrm{AA}} + S_{\mathrm{BB}} + S_{\mathrm{AB}} + S_v + S_{\mathrm{A}} + S_{\mathrm{B}} = 0, \tag{3}$$

where K_0 is defect production rate.

Before performing linear stability analysis, the system of reaction-diffusion equations has been nondimensionalized with respect to the intrinsic length and time scales of the system. This has been achieved by the following transformations:

$$\begin{aligned} (x, y, z) \longrightarrow l\,(\tilde{x}, \tilde{y}, \tilde{z}) \Longrightarrow \nabla \longrightarrow l^{-d}\tilde{\nabla}, \\ t \longrightarrow \tau \tilde{t}, \end{aligned} \tag{4}$$

where d represents the dimension. In the present study, we have taken $d = 2$. The time scale (τ) has been defined as the inverse of the fastest reaction rate, $K_{\max}$, whereas length scale (l) depends upon the fastest diffusing rate, $D_{\max}$,

$$\tau = \frac{1}{K_{\max}}, \qquad l = \sqrt{\frac{D_{\max}}{K_{\max}}}. \tag{5}$$

The nondimensionalized system of equations may be expressed as

$$\frac{\partial Ci}{\partial \tilde{t}} = -\tilde{\nabla} \cdot \tilde{J}i + \tilde{R}i + \tilde{S}i. \tag{6}$$

3. Linear Stability Analysis

The concentrations C_i in the nondimensionalized system of (6) have been perturbed by an infinitesimal amount, δC_i, about its uniform value $\widehat{C}_i$,

$$\delta C_i = C_i - \widehat{C}_i. \tag{7}$$

Plugging (7) in (6) and considering quasi-static approximation, that is, when the stability of the uniform state is calculated by considering them stationary at each moment, we get a linearized system of equations in terms of perturbations in the concentrations,

$$\frac{\partial \delta Ci}{\partial t} = -\widetilde{\nabla} \cdot \widetilde{J}i\,(\delta \mathbf{C}) + \widetilde{R}i\,(\delta \mathbf{C}) + \widetilde{S}i\,(\delta \mathbf{C}), \tag{8}$$

where $\delta\mathbf{C}$ represents a vector of perturbations in the concentration of other species. As according to [20, 21], although quasi-static approximation may not be able to capture the growth rate of the perturbations correctly, it is able to predict the instability threshold quite accurately. In this regard, one will expect instability when at least one of the eigenvalues of the evolution matrix has a positive real part.

The perturbations grow in space and time as follows:

$$\delta C_i = \eta_i e^{\omega t + ikx}, \tag{9}$$

where η_i is the amplitude of the perturbation in the ith species concentration, ω is the growth factor, and k is the wavevector of the sinusoidal perturbations. Plugging (9) in the linearized system of (8), we get six eigenvalue equations,

$$\begin{aligned}
\omega\eta_{\mathrm{AA}} &= \xi_{\mathrm{AA}}^{(\mathrm{AA})}\eta_{\mathrm{AA}} + \xi_{\mathrm{AB}}^{(\mathrm{AA})}\eta_{\mathrm{AB}} + \xi_{v}^{(\mathrm{AA})}\eta_{v} \\
&\quad + \xi_{\mathrm{A}}^{(\mathrm{AA})}\eta_{\mathrm{A}} + \xi_{\mathrm{B}}^{(\mathrm{AA})}\eta_{\mathrm{B}}, \\
\omega\eta_{\mathrm{BB}} &= \xi_{\mathrm{BB}}^{(\mathrm{BB})}\eta_{\mathrm{BB}} + \xi_{\mathrm{AB}}^{(\mathrm{BB})}\eta_{\mathrm{AB}} + \xi_{v}^{(\mathrm{BB})}\eta_{v} \\
&\quad + \xi_{\mathrm{A}}^{(\mathrm{BB})}\eta_{\mathrm{A}} + \xi_{\mathrm{B}}^{(\mathrm{BB})}\eta_{\mathrm{B}}, \\
\omega\eta_{\mathrm{AB}} &= \xi_{\mathrm{AA}}^{(\mathrm{AB})}\eta_{\mathrm{AA}} + \xi_{\mathrm{BB}}^{(\mathrm{AB})}\eta_{\mathrm{BB}} + \xi_{\mathrm{AB}}^{(\mathrm{AB})}\eta_{\mathrm{AB}} \\
&\quad + \xi_{v}^{(\mathrm{AB})}\eta_{v} + \xi_{\mathrm{A}}^{(\mathrm{AB})}\eta_{\mathrm{A}} + \xi_{\mathrm{B}}^{(\mathrm{AB})}\eta_{\mathrm{B}}, \\
\omega\eta_{v} &= \xi_{\mathrm{AA}}^{(v)}\eta_{\mathrm{AA}} + \xi_{\mathrm{BB}}^{(v)}\eta_{\mathrm{BB}} + \xi_{\mathrm{AB}}^{(v)}\eta_{\mathrm{AB}} \\
&\quad + \xi_{v}^{(v)}\eta_{v} + \xi_{\mathrm{A}}^{(v)}\eta_{\mathrm{A}} + \xi_{\mathrm{B}}^{(v)}\eta_{\mathrm{B}}, \\
\omega\eta_{\mathrm{A}} &= \xi_{\mathrm{AA}}^{(\mathrm{A})}\eta_{\mathrm{AA}} + \xi_{\mathrm{BB}}^{(\mathrm{A})}\eta_{\mathrm{BB}} + \xi_{\mathrm{AB}}^{(\mathrm{A})}\eta_{\mathrm{AB}} \\
&\quad + \xi_{v}^{(\mathrm{A})}\eta_{v} + \xi_{\mathrm{A}}^{(\mathrm{A})}\eta_{\mathrm{A}} + \xi_{\mathrm{B}}^{(\mathrm{A})}\eta_{\mathrm{B}}, \\
\omega\eta_{\mathrm{B}} &= \xi_{\mathrm{AA}}^{(\mathrm{B})}\eta_{\mathrm{AA}} + \xi_{\mathrm{BB}}^{(\mathrm{B})}\eta_{\mathrm{BB}} + \xi_{\mathrm{AB}}^{(\mathrm{B})}\eta_{\mathrm{AB}} \\
&\quad + \xi_{v}^{(\mathrm{B})}\eta_{v} + \xi_{\mathrm{A}}^{(\mathrm{B})}\eta_{\mathrm{A}} + \xi_{\mathrm{B}}^{(\mathrm{B})}\eta_{\mathrm{B}},
\end{aligned} \tag{10}$$

where ξ_i^j (i, j = AA, BB, AB, v, A, B) are complicated functions of k, concentrations, and diffusion and reaction coefficients. Equations (10) may also be expressed in a condense form as

$$\mathbf{A}\eta = \omega\eta. \tag{11}$$

Owing to complexity of the analytical estimation of the eigenvalues of the evolution matrix $\mathbf{A}$ (matrix of ξ coefficients) and hence the dispersion relations, a numerical estimation of the eigenvalues has been made using *eig* function of Matlab.

4. Results and Discussions

Considering Cu-Au as the system of interest [22], the system of (11) has been solved as an eigenvalue problem to get six eigenvalues $(\omega_1, \ldots, \omega_6)$. In this alloy, Cu is a faster and Au is a slower diffusing species. Imaginary part of all the eigenvalues is zero, which means that the system's response is nonoscillatory. Also, only one out of six eigenvalues (ω_6) has been found to change sign from a negative to a positive value under a specific set of control parameters. Other eigenvalues remain always negative. Figure 1 shows the behavior of all the eigenvalues with respect to the wavevector k. In this figure, all the stable and unstable eigenvalues have been displayed. We see that, out of six eigenvalues, only one (ω_6) becomes unstable under the prevailing irradiation conditions and temperature. Other eigenvalues are stable for all k values. This shows that the material under irradiation indeed becomes unstable under a certain set of irradiation conditions and remains stable otherwise.

5. Conclusion

Stability of a binary solid solution under irradiation has been studied. There are six species in the model: three dumbbells as off-lattice species, vacancies, and two material components as on-lattice species. The temporal evolution of the solid solution is described by a set of coupled nonlinear reaction-diffusion equations in all the species concentration. Defects diffuse either by vacancy mechanism (vacancies) or by interstitialcy mechanism (dumbbells). The diffusive flux of the defects has been derived in the Fickian framework by considering the solid solution to be isotropic and ideal. The correlation effects in the defect jumps have also been neglected. The flux of the atomic species is coupled to the defect fluxes. Defects also participate in two types of reactions: recombination and change in the dumbbell type. Stability of the solid solution has been investigated by performing linear stability analysis of the set of six reaction-diffusion equations with respect to the uniform state of the binary solid solution under quasi-static approximation [20, 21]. For a miscible Cu-Au solid solution, the resulting system of eigenvalue equations has been solved numerically to calculate the dispersion relations showing a relation between the growth factors (eigenvalues) and wavevectors of the sinusoidal perturbations. Real part of one of the growth factors changes sign from a negative to a positive value, signifying the presence of unstable eigenmodes under specific simulation conditions. When simulation conditions are varied beyond the instability threshold values, the growth factor and the window of unstable eigenmodes change. The results obtained in this investigation indicate that, under specific simulation conditions, the binary solid solution indeed becomes unstable to infinitesimal sinusoidal perturbations, which might

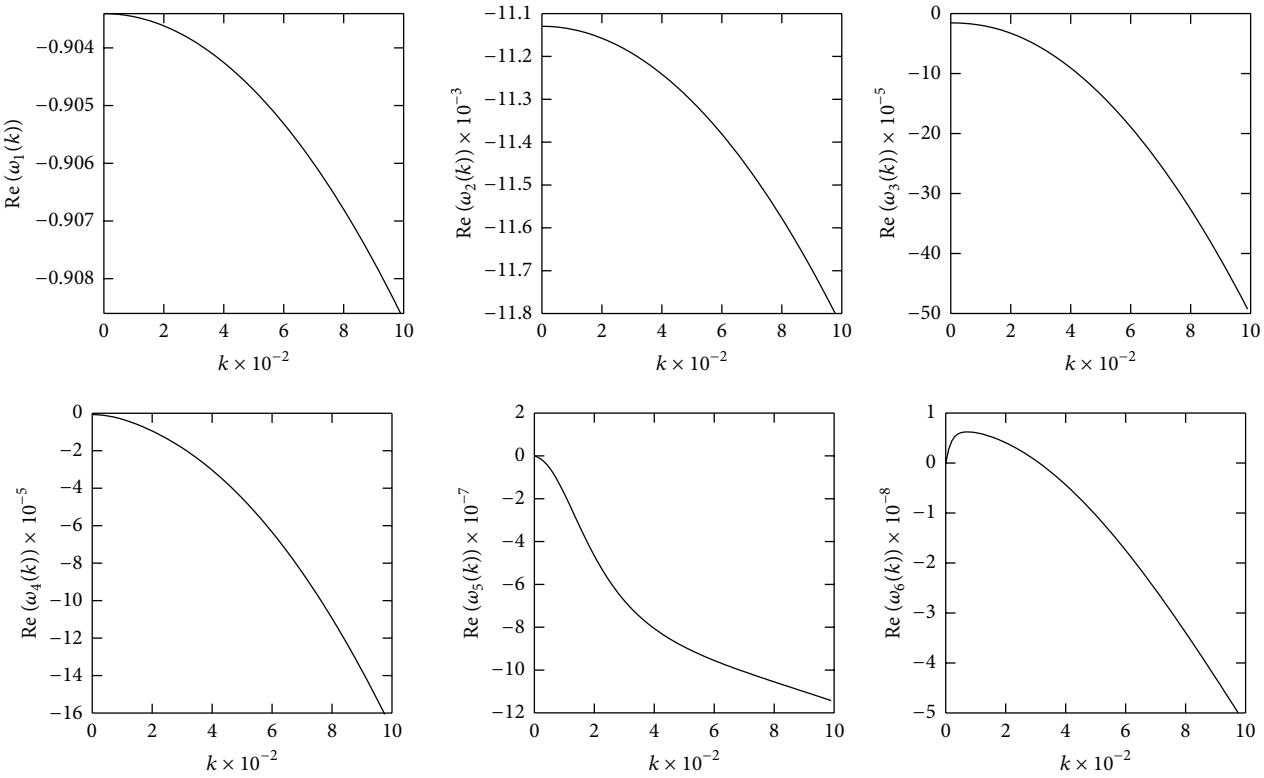


FIGURE 1: Stable ($\omega_1 \ldots \omega_5$) and unstable (ω_6) growth factors (eigenvalues) of the system calculated at temperature 850 K and a dpa rate of 2×10^{-6} dpa/$\widetilde{t}$. The fractional alloy concentration is $C_{Cu} = 0.1$ and $C_{Au} = 0.9$.

result in the formation of stationary self-organized dissipative structures or composition patterns.

Conflict of Interests

The authors declare that there is no conflict of interests regarding the publication of this paper.

References

[1] M. C. Cross and P. C. Hohenberg, "Pattern formation outside of equilibrium," *Reviews of Modern Physics*, vol. 65, no. 3, pp. 851–1112, 1993.

[2] J. H. Evans, "Observations of aregular void array in high purity molybdenum irradiated with 2 MeV nitrogen ions," *Nature*, vol. 229, no. 5284, pp. 403–404, 1971.

[3] J. Evans, "Observations of a regular void array in high purity molybdenum and T.Z.M. irradiated at high temperatures with 2MeV nitrogen ions," *Radiation Effects*, vol. 10, no. 1-2, pp. 55–60, 1971.

[4] K. Krishan, "Kinetics of void-lattice formation in metals," *Nature*, vol. 287, no. 5781, pp. 420–421, 1980.

[5] S. L. Sass and B. L. Eyre, "Diffraction from void and bubble arrays in irradiated molybdenum," *Philosophical Magazine*, vol. 27, no. 6, pp. 1447–1453, 1973.

[6] P. B. Johnson, D. J. Mazey, and J. H. Evans, "Bubble structures in He^+ irradiated metals," *Radiation Effects*, vol. 78, no. 1–4, pp. 147–156, 1982.

[7] J. H. Evans and D. J. Mazey, "Evidence for solid krypton bubbles in copper, nickel and gold at 293K," *Journal of Physics F: Metal Physics*, vol. 15, no. 1, article 001, pp. L1–L6, 1985.

[8] W. Jager, P. Ehrhart, and W. Schilling, "Dislocation patterning under irradiation," in *Nonlinear Phenomena in Materials Science*, G. Martin and L. Kubin, Eds., chapter 2, p. 279, Transtech, Aedermannsdorf, Switzerland, 1988.

[9] F. A. Garner, J. M. McCarthy, K. C. Russell, and J. J. Hoyt, "Spinodal-like decomposition of Fe-35Ni and Fe-Cr-35Ni alloys during irradiation or thermal aging," *Journal of Nuclear Materials*, vol. 205, pp. 411–425, 1993.

[10] C. M. Shepherd and T. M. Williams, "Intragranular compositional oscillations in neutron-irradiated austenitic steels," *Journal of Nuclear Materials*, vol. 168, no. 3, pp. 337–339, 1989.

[11] G. Martin, "Contribution of dissipative processes to radiation-induced solid-solution instability," *Physical Review B*, vol. 21, no. 6, pp. 2122–2130, 1980.

[12] G. Martin, "Long-range periodic decomposition of irradiated solid solutions," *Physical Review Letters*, vol. 50, no. 4, pp. 250–252, 1983.

[13] K. Krishan and C. Abromeit, "Calculation of radiation-induced instability in concentrated alloys," *Journal of Physics F: Metal Physics*, vol. 14, no. 5, article 008, pp. 1103–1116, 1984.

[14] S. M. Murphy, "Instabilities in concentrated alloys under irradiation," *Philosophical Magazine*, vol. 58, no. 2, pp. 417–433, 1988.

[15] C. Abromeit and G. Martin, "Dynamical phase changes induced by point defect fluxes under irradiation," *Journal of Nuclear Materials*, vol. 271-272, pp. 251–255, 1999.

[16] G. Martin, "Phase stability under irradiation: ballistic effects," *Physical Review B*, vol. 30, no. 3, pp. 1424–1436, 1984.

[17] R. A. Enrique and P. Bellon, "Compositional patterning in systems driven by competing dynamics of different length scale," *Physical Review Letters*, vol. 84, no. 13, article 2885, 2000.

[18] R. A. Enrique and P. Bellon, "Compositional patterning in immiscible alloys driven by irradiation," *Physical Review B*, vol. 64, no. 13, Article ID 134111, 2001.

[19] S. Dubey and A. El-Azab, "Irradiation-induced composition patterns in binary solid solutions," *Journal of Applied Physics*, vol. 114, no. 12, Article ID 124901, 2013.

[20] N. M. Ghoniem and D. Walgraef, "Evolution dynamics of 3D periodic microstructures in irradiated materials," *Modelling and Simulation in Materials Science and Engineering*, vol. 1, no. 5, article 001, pp. 569–590, 1993.

[21] B. S. Jhaveri and G. M. Homsy, "The onset of convection in fluid layers heated rapidly in a time-dependent manner," *Journal of Fluid Mechanics*, vol. 114, pp. 251–260, 1982.

[22] T. Hashimoto, Y. Isobe, and N. Shigenaka, "A model for radiation-induced segregation in fcc binary alloys," *Journal of Nuclear Materials*, vol. 225, pp. 108–116, 1995.

Hindawi Publishing Corporation
Conference Papers in Science
Volume 2014, Article ID 812627, 4 pages
http://dx.doi.org/10.1155/2014/812627

Conference Paper

Effect of MgO and V_2O_5 Catalyst on the Sensing Behaviour of Tin Oxide Thin Film for SO_2 Gas

Punit Tyagi,[1] Anjali Sharma,[1] Monika Tomar,[2] and Vinay Gupta[1]

[1] *Department of Physics and Astrophysics, University of Delhi, Delhi 110007, India*
[2] *Physics Department, Miranda House, University of Delhi, Delhi 110007, India*

Correspondence should be addressed to Vinay Gupta; drguptavinay@gmail.com

Received 8 February 2014; Accepted 10 March 2014; Published 2 April 2014

Academic Editors: P. Mandal, R. K. Shivpuri, and G. N. Tiwari

This Conference Paper is based on a presentation given by Punit Tyagi at "National Conference on Advances in Materials Science for Energy Applications" held from 9 January 2014 to 10 January 2014 in Dehradun, India.

Copyright © 2014 Punit Tyagi et al. This is an open access article distributed under the Creative Commons Attribution License, which permits unrestricted use, distribution, and reproduction in any medium, provided the original work is properly cited.

The present work shows the SO_2 gas sensing property of SnO_2 thin film based sensor prepared by using RF sputtering technique. Different catalysts (MgO and V_2O_5) in form of nanoclusters having diameter of 600 μm have been loaded on SnO_2 surface to detect SO_2 gas. The sensing response of all these films towards SO_2 is monitored. Microstructural studies have been carried out using XRD and UV-Visible Spectrophotometer and a good correlation has been found between the microstructural and gas sensing properties of these deposited samples. Both catalysts when incorporated with SnO_2 film show high selectivity towards SO_2 gas at lower operating temperature. MgO gives a sensitivity of 317% at an operating temperature of 280°C towards 500 ppm of SO_2 gas whereas V_2O_5 catalyst gives a sensitivity of 166% at 280°C for the same amount of gas.

1. Introduction

Recently, substantial interest has arisen in terms of protecting the environment from various air pollutants generated by combustion exhausts. SO_2 is one of the most hazardous atmospheric pollutants because it directly contributes to acid rain. Several studies have shown that repeated exposure to low levels of SO_2 (<5 ppm) can cause permanent pulmonary impairment [1]. The long-term and short-term exposure limits for SO_2 gas are 2 ppm and 5 ppm, respectively. Therefore, the development of an efficient SO_2 gas sensor for environmental monitoring has become a necessary task.

There are various techniques for determining the SO_2 gas concentration in the atmosphere such as ion chromatography [2], Fourier transform infrared spectrometry [3], optical fiber sensors [4], SAW gas sensors [5], conductometry [6], and electrochemical methods [7]. Amongst all the techniques, conductometric sensors are fast, highly sensitive, reproducible, of low cost, and convenient.

Semiconducting tin oxide (SnO_2) based conductometric gas sensors have received much attention for more than four decades due to their suitable physical-chemical properties and possibility to detect wide variety of gases with high response [8–11]. SnO_2 is naturally nonstoichiometric having a rutile phase that eases the adsorption of oxygen on its surface and thus it is highly sensitive towards many toxic and harmful gases [10, 11]. The main problem with the pure SnO_2 thin film based gas sensors is their poor selectivity and high operating temperatures that can be improved to a great extent by using specific catalysts [12, 13].

The aim of this study is to develop a SnO_2 thin film based SO_2 gas sensor with MgO and V_2O_5 catalysts having efficient response characteristics.

2. Experimental

SnO_2 thin films of 90 nm thickness were deposited using RF diode sputtering technique using a metal Sn target (99.999% pure) in a reactive ambient of Ar and O_2 gas mixture as optimized in our previous work [14]. The sensing response characteristics of SnO_2 thin films were studied using Interdigital Electrodes (IDEs) of platinum (Pt) as shown in Figure 1.

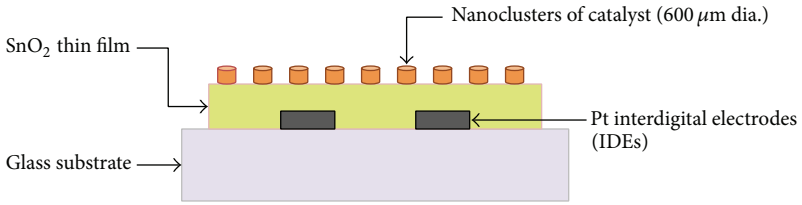


Figure 1: Cross-sectional view of the SnO_2 thin film sensor with nanoclusters of catalysts on Pt IDEs.

The sensor fabrication details are given in our previous report [14]. For the enhanced and selective gas sensing response characteristics, nanoclusters of MgO and V_2O_5 of 10 nm thickness and 600 μm diameter were dispersed uniformly over the surface of SnO_2 thin film by pulsed laser deposition technique (PLD) using a fourth harmonic (λ = 266 nm) of Nd:YAG laser with fluence $\approx$ 1.5 J/cm^2 using a shadow mask. Ceramic targets of MgO and V_2O_5 of 1$''$ diameter were used for deposition using PLD. The as-grown sensing elements (MgO/SnO_2 and V_2O_5/SnO_2) were annealed at 300°C in air for 3 h to stabilize the sensor.

Thickness and surface roughness of deposited thin films were measured using a (Veeco Dektak 150) surface profiler. Crystalline structure of SnO_2 thin films was studied using Bragg-Brentano (θ-2θ) scan of an X-ray diffractometer (Bruker D8 Discover) using the CuKα_1 source (λ = 0.154 nm). A double beam UV-Visible Spectrophotometer (Perkin Elmer, Lambda 35) was used to study the optical properties of SnO_2 thin films.

A specially designed gas sensor test rig (GSTR) has been used to study the gas sensing response characteristics of the sensing layer for SO_2 gas. The sensor was placed on a temperature controlled heating block inside the glass test chamber to measure the sensor response as a function of temperature (100 to 300°C). At each temperature, the sensor was first stabilized in air to obtain a stable resistance value. Target gas (SO_2) of specific concentration (500 ppm) was introduced into the test chamber and changes in the sensor resistance were recorded after every second using a data acquisition system consisting of a digital multimeter (model: Keithley 2700) interfaced with a computer. SO_2 is a reducing gas and the sensor response is defined as

$$S = \frac{R_a - R_g}{R_g}, \quad (1)$$

where R_a and R_g are the resistance of the sensor element in the presence of atmospheric air and resistance of target SO_2 gas, respectively.

3. Results and Discussions

Figure 2 shows the X-ray diffraction (XRD) pattern of the SnO_2 sensor structure. The diffraction peaks observed at 2θ = 26.6°, 33.8°, and 51.8° can be assigned to (110), (101), and (211) planes of the rutile structure of SnO_2, respectively [15]. The observed XRD peaks are found to be broad indicating that the particles are of small size. No peaks corresponding to any

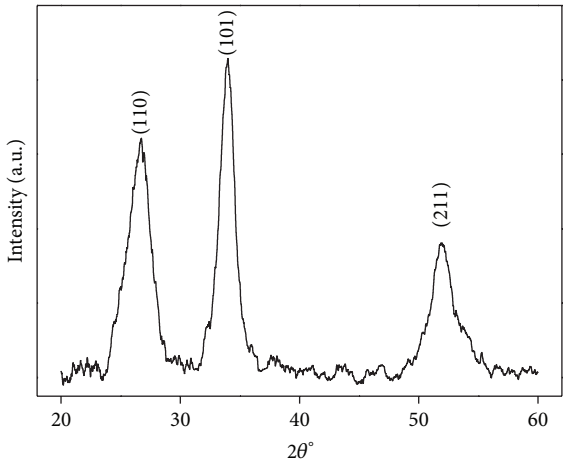


Figure 2: X-ray diffraction pattern of SnO_2 sensor structure.

secondary phase due to MgO and V_2O_5 have been observed in the XRD spectra which may be attributed to the small thickness of the nanoclusters of the catalysts. The crystallite size was estimated by fitting the width of dominant (101) diffraction peak using Scherrer's formula and is found to be ~8 nm.

Figure 3 shows the transmittance spectra of the SnO_2 thin film. The films exhibit a high transmission (>80%) in the visible region and show a sharp fundamental absorption edge at around 340 nm. The value of optical band gap was estimated from the Tauc plot and is found to be 3.9 eV which matches very well the reported value [16].

Figure 4 shows the sensing response of bare SnO_2 film and SnO_2 film having MgO and V_2O_5 as catalysts. Bare SnO_2 thin film based sensor showed no response whereas sensors having MgO and V_2O_5 catalysts are showing a response of 3.17 and 1.66, respectively. Table 1 shows the sensor response (%), response time, and recovery time of the prepared samples at their operating temperature (280°C). It can be seen from Table 1 that the sensor response (%) is low for SnO_2 thin film and gets improved with V_2O_5 as a catalyst and the maximum value of response (%) is found for the SnO_2 with MgO thin film as catalyst with a response time and recovery time of 59 s and 52 s, respectively. MgO and V_2O_5 doped SnO_2 sensors for sensing SO_2 gas have already been reported by Lee et al. [13]. However, the sensing response is reported to be poor (44%) at a high operating temperature (400°C) towards 1 ppm of SO_2 gas. Since gas sensing is a surface phenomenon, the incorporation of catalyst/modifier

Table 1: Sensing response characteristics of the prepared sensors at an operating temperature of 280°C.

Serial number	Sample	Response (%)	Response time (s)	Recovery time (s)
1	SnO_2	107	—	—
2	$SnO_2 + V_2O_5$	166	90	43
3	SnO_2 + MgO	317	59	52

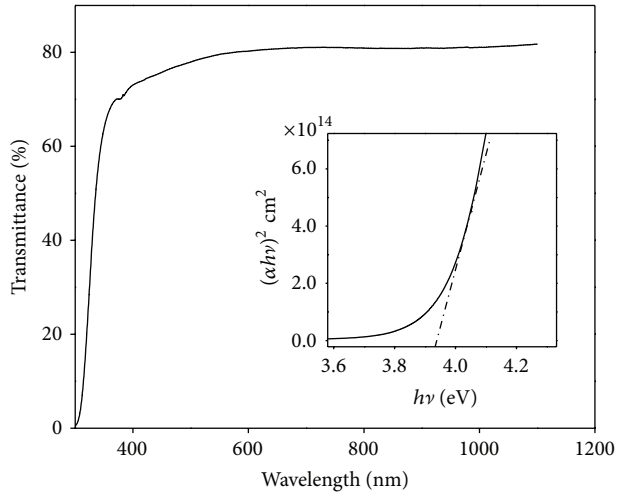


Figure 3: Transmittance spectra of SnO_2 film deposited on glass substrate. Inset: Tauc plot for the SnO_2 thin film.

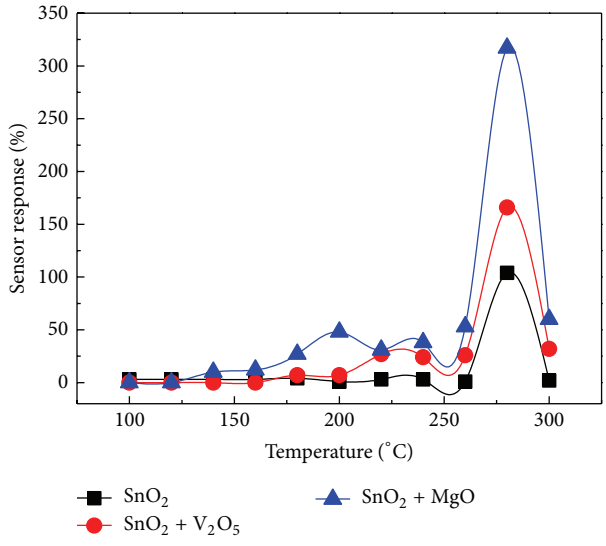


Figure 4: Sensing response of SnO_2 thin film, SnO_2 thin film having V_2O_5 catalyst, and SnO_2 thin film having MgO catalyst as a function of temperature.

in the form of nanoclusters onto the surface of SnO_2 thin film is proved to give enhanced sensing response of 317% and 166% at 280°C towards 500 ppm SO_2 gas.

4. Conclusion

SnO_2 thin films of desired morphology and higher electrical resistance have been deposited by RF sputtering for efficient detection of SO_2 gas. SnO_2 film with MgO catalyst exhibits enhanced sensor response of 317% with moderate response time of 59 s and recovery time of 52 s at an operating temperature of 280°C. The sensor response and recovery time are governed by the adsorption and desorption of SO_2 gas molecules at the sensor surface. The formation of SnO_2 thin film with desired surface morphology having moderate porosity and appropriate catalysts results in an enhanced sensing response towards SO_2 gas (500 ppm) at a low operating temperature of 280°C.

Conflict of Interests

The authors declare that there is no conflict of interests regarding the publication of this paper.

Acknowledgments

Authors are thankful for the Department of Science and Technology (DST), GAIL India Ltd. and National Program on Micro and Smart Systems (NPMASS) for the financial support to carry out this work.

References

[1] http://avogadro.chem.iastate.edu/MSDS/sulfur_dioxide.pdf.

[2] M. Nonomuraac and T. Hobob, "Simultaneous determination of sulphur oxides, nitrogen oxides and hydrogen chloride in flue gas by means of an automated ion chromatographic system," *Journal of Chromatography A*, vol. 804, pp. 151–155, 1998.

[3] F. W. Koehler, G. W. Small, R. J. Combs, R. B. Knapp, and R. T. Kroutil, "Automated detection of sulfur dioxide in stack emissions by passive Fourier transform infrared spectrometry," *Vibrational Spectroscopy*, vol. 27, no. 2, pp. 97–107, 2001.

[4] H. Y. Xu, K. M. Wang, D. N. Wang, and Q. C. Li, "Studies on a fiber optical sensor for sulfur dioxide with a high sensitivity," *Chemical Journal of Chinese Universities*, vol. 19, no. 9, pp. 1401–1404, 1998.

[5] S. Qin, Z. Wu, Z. Tang, Y. Song, F. Zeng, and D. Zhao, "Sensitivity to SO2 of the SAW gas sensor with triethanolamine modified with boric acid," *Sensors and Actuators, B: Chemical*, vol. 66, no. 1, pp. 240–242, 2000.

[6] P. K. Dasgupta and S. Kar, "Measurement of gases by a suppressed conductometric capillary electrophoresis separation system," *Analytical Chemistry*, vol. 67, no. 21, pp. 3853–3860, 1995.

[7] J. F. Currie, A. Essalik, and J.-C. Marusic, "Micromachined thin film solid state electrochemical CO_2, NO_2 and SO_2 gas sensors," *Sensors and Actuators B*, vol. 59, no. 2, pp. 235–241, 1999.

[8] A. Chowdhuri, V. Gupta, and K. Sreenivas, "Fast response H_2S gas sensing characteristics with ultra-thin CuO islands on

sputtered SnO_2," *Sensors and Actuators B*, vol. 93, no. 1-3, pp. 572–579, 2003.

[9] D. Haridas, K. Sreenivas, and V. Gupta, "Improved response characteristics of SnO_2 thin film loaded with nanoscale catalysts for LPG detection," *Sensors and Actuators B*, vol. 133, no. 1, pp. 270–275, 2008.

[10] Md. Shahabuddin, A. Sharma, J. Kumar, M. Tomar, A. Umar, and V. Gupta, "Metal clusters activated SnO_2 thin film for low level detection of NH_3 gas," *Sensors and Actuators B*, vol. 194, pp. 410–418, 2014.

[11] T. Zhanga, L. Liua, Q. Qia, S. Li, and G. Lua, "Development of microstructure In/Pd-doped SnO_2 sensor for low-level CO detection," *Sensors and Actuators B*, vol. 139, no. 2, pp. 287–291, 2009.

[12] X. Liang, T. Zhong, B. Quan, B. Wang, and H. Guan, "Solid-state potentiometric SO_2 sensor combining NASICON with V_2O_5-doped TiO_2 electrode," *Sensors and Actuators B*, vol. 134, no. 1, pp. 25–30, 2008.

[13] S. C. Lee, B. W. Hwang, S. J. Lee et al., "A novel tin oxide-based recoverable thick film SO_2 gas sensor promoted with magnesium and vanadium oxides," *Sensors and Actuators B*, vol. 160, no. 1, pp. 1328–1334, 2011.

[14] P. Tyagi, A. Sharma, M. Tomar, and V. Gupta, "Pd nanoclusters integrated SnO_2 thin film sensor for low temperature detection of SO_2 gas with enhanced response," *Chemical Sensors*, vol. 4, article 18, 2014.

[15] M. Verma and V. Gupta, "A highly sensitive SnO_2-CuO multi-layered sensor structure for detection of H_2S gas," *Sensors and Actuators B*, vol. 166-167, pp. 378–385, 2012.

[16] T. J. Stanimirova, P. A. Atanasov, I. G. Dimitrov, and A. O. Dikovska, "Investigation on the structural and optical properties of tin oxide films grown by pulsed laser deposition," *Journal of Optoelectronics and Advanced Materials*, vol. 7, no. 3, pp. 1335–1340, 2005.

Hindawi Publishing Corporation
Conference Papers in Science
Volume 2014, Article ID 370436, 3 pages
http://dx.doi.org/10.1155/2014/370436

Conference Paper

Synthesis and Characterisation of Thin Films of Bismuth Triiodide for Semiconductor Radiation Detectors

Alka Garg,[1] Monika Tomar,[2] and Vinay Gupta[3]

[1] *Gargi College, University of Delhi, Siri Fort Road, New Delhi 110049, India*
[2] *Miranda House, University of Delhi, Delhi 110007, India*
[3] *Department of Physics and Astrophysics, University of Delhi, Delhi 110007, India*

Correspondence should be addressed to Alka Garg; alkagargi67@yahoo.com

Received 7 February 2014; Accepted 18 March 2014; Published 2 April 2014

Academic Editors: P. Mandal, R. K. Shivpuri, and G. N. Tiwari

This Conference Paper is based on a presentation given by Alka Garg at "National Conference on Advances in Materials Science for Energy Applications" held from 9 January 2014 to 10 January 2014 in Dehradun, India.

Copyright © 2014 Alka Garg et al. This is an open access article distributed under the Creative Commons Attribution License, which permits unrestricted use, distribution, and reproduction in any medium, provided the original work is properly cited.

Bismuth iodide is a potentially active material for room temperature radiation detector, as it is well reported in the literature that it has both wide energy band gap and high atomic absorption coefficient. Crystalline films of high atomic number and high radiation absorption coefficient can absorb the X-rays and convert them directly into electrical charges which can be read by imaging devices. Therefore, it was proposed to grow thin films of Bismuth iodide on glass substrate using thermal evaporation technique in vacuum to avoid the inclusion of impurities in the films. The structural studies of the films were carried out using XRD and optical absorption measurement was carried out in the UV/VIS region using spectrophotometer. All Bismuth iodide films grown at room temperature are polycrystalline and show X-ray diffraction peaks at angles reported in research papers. The optical transmission spectra of BiI_3 films show a high transmission of about 80% in visible region with a sharp fall near the fundamental absorption at 650 nm. Resistivity of the as-grown film was found to be around 10^{12} ohm-cm suitable value for X-ray detection application. Films were subjected to scanning electron microscopy to study the growth features of both as-grown and annealed films.

1. Introduction

Gamma ray detectors have become increasingly important for the application of medical imaging and environmental safety. Photographic films, Phosphor screens, and Silicon array have been used as imaging detectors for many years but all these devices are indirect detectors with low efficiency and poor spatial resolution. Compound semiconductors are the most promising radiation detector compared to high purity Ge and Si because of their moderate band gap and ability to operate at room temperature [1]. Bismuth iodide is one such compound semiconductor with potential for room temperature gamma and X-ray detection applications [2]. Bismuth Triiodide is having both high atomic number and high absorption coefficient, important parameters for material to detect X-rays and Gamma rays [3]. Bismuth Triiodide is a layered compound having low melting point of 408°C. BiI_3 is stable within the range from melting point to room temperature [4]. BiI_3 is reported to have vapor pressure of around 90 mbar at temperatures 250°C to 300°C [5, 6]. Therefore, BiI_3 films can be grown from both liquid and vapour phases. BiI_3 has been reported with different band gap characteristics and values. Experimentally and computationally, band gap value is ranging from 1.5 eV to 2.2 eV [7]. It is reported that BiI_3 has both direct and indirect band gaps.

The aim of the present work is to prepare polycrystalline thin films of Bismuth Triiodide by thermal evaporation method and study the optical and structural properties of the material to present preliminary results which would be in future help in developing Bismuth iodide as room temperature radiation detector.

2. Experimental

Bismuth Triiodide films were grown on glass substrate (2 cm × 6 cm) at room temperature by conventional thermal evaporation technique using molybdenum boat at a pressure approximately 10^{-6} Torr. Starting material (99.99% purity) procured from Aldrich chemicals was used for growing films. Uniformity and thickness of the films were found out using DEKTAK 150 surface profiler. The deposition rate was maintained to be slow around 5-6 nm/s as the higher deposition rate led to nonuniform film growth and low sticking adherence to the glass substrate.

Structural analysis of the as-grown and annealed films was carried out using X-ray diffraction using Bruker D8 XRD. Optical transmission spectra of the annealed and as-grown Bismuth Triiodide films deposited on the glass substrate were recorded as a function of wavelength in the range (200–1100) nm at room temperature using Perkin Elemer, lamda 35 UV/VIS spectrometer. Surface morphology of the films has been studied through scanning electron microscope (SEM MIRA3TESCAN)) to ascertain the uniformity of as-grown and annealed films. The resistivity of films was measured using Keitheley semiconductor analyser (SCS 4200).

3. Result and Discussion

The as deposited BiI_3 films were found to be smooth and strongly adhered to the substrate surface. The as-grown films were polycrystalline and stoichiometric (as per X-ray diffraction). Figure 1 shows the XRD pattern of as grown Bismuth Triiodide films. Sharp and well-defined reflections corresponding to (003), (006), (008), (009), (300), (0010), and (0012) planes of BiI_3 were observed at around 2θ = 12.79°, 25.78°, 26.99°, 35.27°, 39.09°, 41.59°, 43° and 52.99°, respectively, which are in good agreement to the corresponding reflections reported in the PCPDF card number 76–1742. The XRD analysis shows a high degree of orientation with basal plane parallel to substrate and c-axis normal to the substrate. On annealing, the intensity of certain peaks are increasing along with appearance of planes. The crystalline size of the as-grown and annealed film was estimated by fitting the FWHM of dominant (003) plane using Scherrer's formula:

$$d = \frac{K\lambda}{\beta \operatorname{Cos}\theta}, \tag{1}$$

where K is 0.94, λ is X-ray wavelength, β is FWHM, and θ is diffraction peak position. The estimated value of crystallite size is about 32 nm. On annealing the films, decrease in FWHM from approximately from 0.2470 to 0.2006 manifests an improvement in the crystalline quality and enlargement of grain size from around 32 nm to 40 nm.

Figure 2 shows the optical transmittance spectrum of the BiI_3 films deposited on the glass substrate. Films exhibit a high optical transmission (80%) in the visible range and show a sharp fundamental absorption edge at around 650 nm. The presence of well-defined interference pattern in the optical transmittance spectra indicates the growth of uniform good quality BiI_3 film free from any inhomogeneity which is also well explained by sharp reflections in the XRD pattern. The value of optical band gap (E_g) was estimated from the linear portion of the Tauc plot (Figure 3) between $(\alpha h\nu)^2$ with photon energy ($h\nu$), where α is the absorption coefficient and ν is the optical frequency. The value of E_g was found to be about 1.82 eV which is close to the corresponding reported value for BiI_3 thin film by other workers.

Scanning electron microscope (SEM) micrographs are shown in Figures 4 and 5. The surface morphology of BiI_3 is of uniform nature having nanocrystalline size grains whose sizes are close to the grain size reported from XRD. Films on annealing appear to be highly oriented suggesting micrograins aligned themselves to grow parallel to the substrate [8]. Also, it appears that film is grown by layer growth mechanism

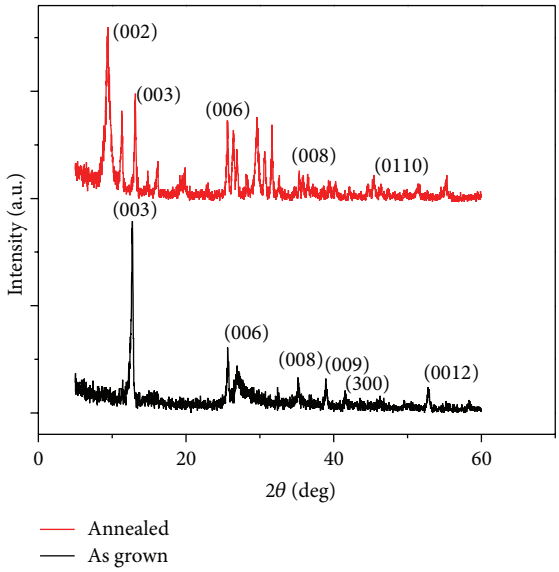


Figure 1: XRD of as-grown and annealed films of Bismuth TriIodide.

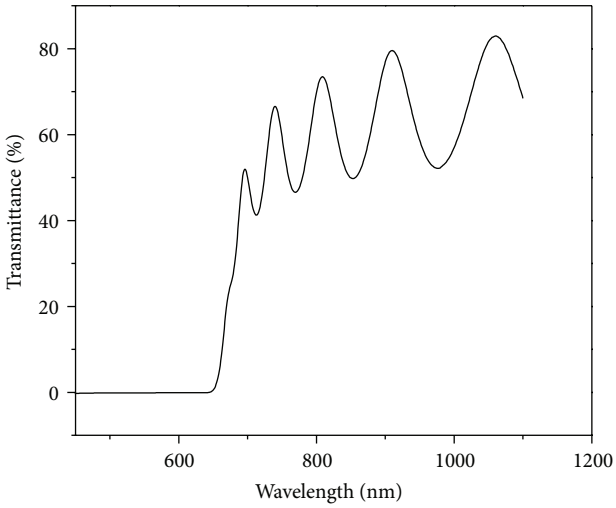


Figure 2: Optical transmission spectra of as-grown BiI_3 thin film.

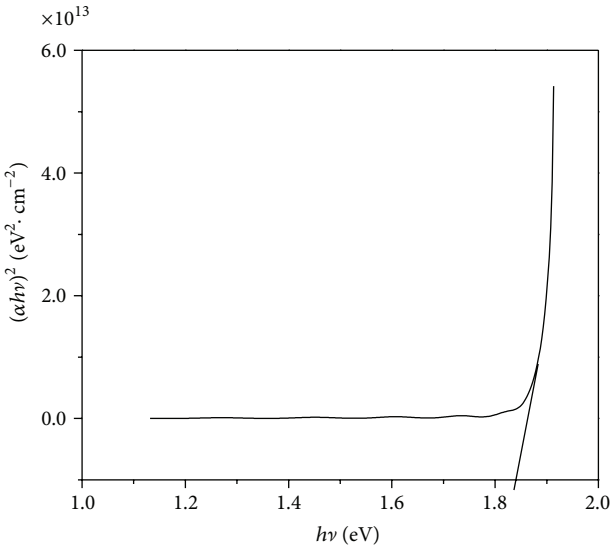


Figure 3: Tauc plot of BiI3 thin film.

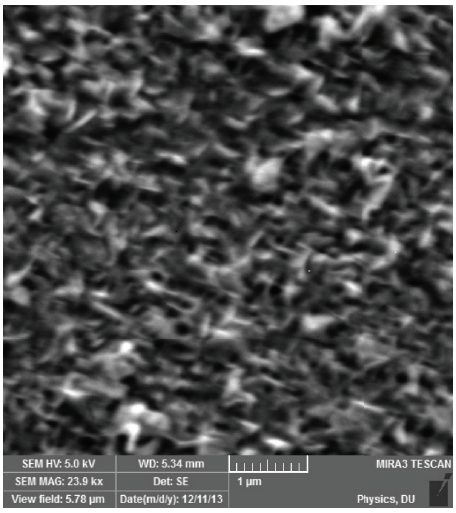


Figure 4: SEM micrograph of as-grown film of Bismuth Triiodide.

which is a characteristic property of layered compounds like Bismuth Triiodide.

4. Conclusion

BiI_3 thin films were grown by thermal evaporation technique. Structural, morphological, and optical properties of thin films were studied by XRD, SEM, and UV-visible spectroscopy, respectively. It was observed that the films were polycrystalline with hexagonal nature and grain size increased upon annealing the films at 100°C. Also, on annealing microcrystalline grains arranged themselves periodically indicating improvement in the crystalline quality of the film.

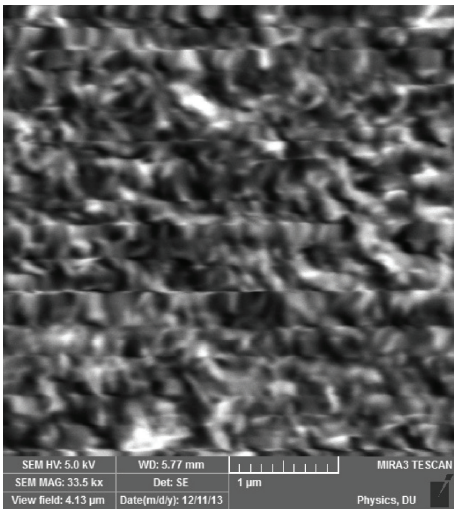


Figure 5: SEM micrograph of annealed film of Bismuth Triiodide.

Conflict of Interests

The authors declare that there is no conflict of interests regarding the publication of this paper.

References

[1] P. J. van Heerden, *The crystal counter [Ph.D. thesis]*, Utrecht University, 1945.

[2] M. Matsumoto, K. Hitomi, T. Shoji, and Y. Hiratate, "Bismuth tri-iodide crystal for nuclear radiation detectors," *IEEE Transactions on Nuclear Science*, vol. 49, no. 5, pp. 2517–2520, 2002.

[3] P. R. Bennet, K. S. Shah, L. J. Cirignano, M. B. Klugerman, L. P. Moy, and M. R. Squillante, "Characterization of polycrystalline TlBr films for radiographic detectors," *IEEE Transactions on Nuclear Science*, vol. 46, no. 3, pp. 266–272, 1999.

[4] F. E. Rosztoczy and D. Cubicciotti, "The bismuth iodide-iodine phase diagram," *The Journal of Physical Chemistry*, vol. 69, no. 1, pp. 124–127, 1965.

[5] D. Cubicciotti and F. J. Keneshea Jr., "The vapor pressures of BiIs over liquid bi-BiI_3 solutions," *The Journal of Physical Chemistry*, vol. 63, no. 2, pp. 295–297, 1959.

[6] J. H. Kim and S. Blairs, "Sublimation study of BiI_3," *The Journal of Chemical Thermodynamics*, vol. 22, no. 8, pp. 803–814, 1990.

[7] D. Nason and L. Keller, "The growth and crystallography of bismuth tri-iodide crystals grown by vapor transport," *Journal of Crystal Growth*, vol. 156, no. 3, pp. 221–226, 1995.

[8] L. Fornaro, E. Saucedo, L. Mussio, A. Gancharov, and A. Cuña, "Bismuth tri-iodide polycrystalline films for digital X-ray radiography applications," *IEEE Transactions on Nuclear Science*, vol. 51, no. 1, pp. 96–100, 2004.

Available online at www.sciencedirect.com

ScienceDirect

Procedia Engineering 87 (2014) 1067 – 1070

Procedia Engineering

www.elsevier.com/locate/procedia

EUROSENSORS 2014, the XXVIII edition of the conference series

NO_x Sensing properties of Barium Titanate thin films

S. Sharma[1,3], A. Sharma[1], M. Tomar[2], N. K. Puri[3] and V. Gupta[1]*

1Department of Physics and Astrophysics, University of Delhi, Delhi 110007, India
2Physics Department, Miranda House, University of Delhi, Delhi 110007, India
3Department of Applied Physics, Delhi Technological University, Delhi 110042 , India

Abstract

In the present work, Barium titanate $BaTiO_3$ (BTO) thin films were prepared by sol - gel spin coating method. High resolution X-ray diffraction study reveals the formation of single phase polycrystalline structure of barium titanate thin films. The films were found to be highly transparent in the visible region and a rough and porous surface morphology which is beneficial for gas sensing applications. Gas-sensing performance of BTO thin film based sensor was studied for varying concentration of NO_x gas at room temperature. The sensor showed enhanced response (17.6% to 33.3%) with increase in concentration of NO_x gas (50 to 500 ppm). Results highlight the fact that multifunctional BTO films can be exploited for efficient NO_x gas even at room temperature.

© 2014 Published by Elsevier Ltd. This is an open access article under the CC BY-NC-ND license
(http://creativecommons.org/licenses/by-nc-nd/3.0/).

Peer-review under responsibility of the scientific committee of Eurosensors 2014

Keywords: Gas sensing; Sol-gel; Polycrystalline; Multifunctional; Thin film

1. Introduction

Metal oxide gas sensors are extensively studied due to their improved sensing characteristics, i.e. sensitivity, selectivity, stability, and response rate towards various gases to meet the increasing need of sensors in complicated systems [1]. The first semiconductor oxide (ZnO) based gas sensor was reported by Seiyama et al. in 1962. Since then, there have been numerous studies on other oxide semiconductors such as SnO_2, ZnO, In_2O_3, TiO_2, a-Fe_2O_3, HfO_2, WO_3, $BaSnO_3$ etc. for detecting a number of toxic and harmful gases. Now a days, air pollution by nitrogen oxides (NO_x), mainly NO and NO_2, is becoming an important environmental issue. As a matter of fact, NO_x associated with other pollutants like volatile organic compounds (VOC) is responsible for the formation of ozone in

* Corresponding author. Tel.: +919811563101; fax: +91-11-27667036.
E-mail address: drguptavinay@gmail.com

1877-7058 © 2014 Published by Elsevier Ltd. This is an open access article under the CC BY-NC-ND license
(http://creativecommons.org/licenses/by-nc-nd/3.0/).
Peer-review under responsibility of the scientific committee of Eurosensors 2014
doi:10.1016/j.proeng.2014.11.347

lower atmosphere, smog in urban areas and also chemical reaction of NO_2 gas with water vapor causes acid rain [2-3]. Therefore, the development of a NO_x gas sensor for environmental monitoring has become a necessary task. Barium Titanate, $BaTiO_3$ (BTO) thin film is the most attractive ferroelectric material with high dielectric constant and is used for various applications including UV sensing, capacitors, memories etc. [4-6]. So far only ferroelectric and electrical properties of BTO have been widely studied and very few reports available on its gas sensing properties. Sol-gel spin coating method is a desirable low cost option for deposition of sensing layer and ease of integration with the existing semiconductor technology. Additional advantages of the sol-gel method are low-temperature processing, good chemical homogeneity, easy control of films composition, and uniform deposition on large size substrates [7]. So, the main objective of the present work is to study the gas sensing properties of BTO thin films prepared by sol-gel spin coating method to make it multifunctional.

2. Experimental Details

Barium acetate [$Ba(CH_3COO)_2$] and titanium (IV) isopropoxide [$Ti(CH_3CH_3CHO)_4$] were used as the precursors for the fabrication of barium titanate thin films. Barium acetate was first dissolved in acetic acid [CH_3COOH] and then diluted with 2-methoxy ethanol [$CH_3OCH_2CH_2OH$]. An equimolar amount of $Ti((CH_3)_2CHO)_4$ was added drop wise to the above solution, keeping it constantly stirred and filtered using microfiber glass filter paper. Thin films were prepared on quartz glass substrate by spin coating technique. Following the deposition, the films were pyrolysed for 5 minutes at 300°C in air. Thicker films were prepared by repeating the deposition cycle (the thickness of each coating was being 70 nm. The deposited films of required thickness (350 nm) were then annealed at 700°C in air for three hours by using a conventional temperature controlled tube furnace. For gas sensing measurements, BTO film was also deposited over the inter digital electrode (IDE) patterned corning glass substrates under the similar conditions. Fabrication of IDEs has been reported elsewhere [8].

High resolution X-Ray diffraction (XRD) study was performed to get the perovskite structure and phase formation of the prepared thin films using Bruker D-8 diffractometer. XRD spectra of the sample have been recorded in the range 20°–60°. Optical properties of barium titanate thin films has been studied like UV-visible spectrophotometer (Perkin Elmer; model : Lambda 35). The film thickness was measured using a surface profiler (DEKTAK 150). Gas sensing characteristics of the fabricated sensors were studied in a specially designed "Gas Sensor Measurement and Caliberation system (GSMCS)" having a glass test chamber. Different concentrations of NOX gas (50 to 500ppm) were introduced into the glass test chamber using calibrated leaks through needle valves. A gas dosing valve was used to control the flow of target gas in the test chamber. Vacuum of the order of $\sim 10^{-3}$ Torr was first created in the test chamber using a rotary pump measured by the pirani gauge and subsequently a mixture of the known concentration of target gas and clean (dry synthetic) air was introduced till the test chamber acquired the atmospheric pressure. The creation of vacuum ensures the removal of any foreign gas molecules from the test chamber. At the time of recovery of the sensor, target gas was flushed out of the test chamber and the clean dry air was introduced. Changes in the sensor resistance due to introduction of target gas were recorded after every second using a data acquisition system consisting of a digital multi-meter (model: Keithley 2700) interfaced with a computer.

3. Results and Discussion

Fig. 1 show the X-ray diffraction (XRD) pattern of annealed barium titanate thin film deposited on corning glass substrate using spin coating technique. It may be seen that the sample shows only XRD peaks corresponding to $BaTiO_3$ and does not show any additional peak related to secondary phase formation indicating the growth of single phase and polycrystalline $BaTiO_3$ thin film. It is observed from Fig.1 that reflection corresponding to (110) plane is relatively intense indicating preferential orientation of the deposited film. Furthermore, the XRD peaks corresponding to (200), (210) and (211) planes are showing splitting into two peaks, which is due to the formation of tetragonal structure that is important for exhibiting ferroelectricity.

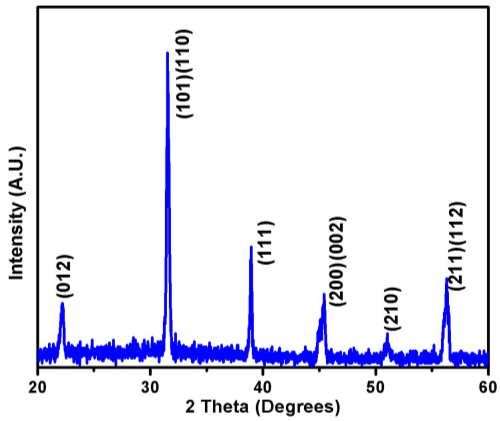


Fig. 1. XRD spectra of BTO Thin film prepared by sol-gel spin coating method

UV-visible transmission spectra of BTO thin film deposited on the quartz substrate under the similar deposition conditions is shown in Fig. 2(a) indicating high transparency (~80%) in the visible region. The Tauc plot of $(\alpha h\nu)^2$ versus photon energy ($h\nu$) of BTO thin film is shown in Fig. 2(b) and a band gap of 3.69 eV is obtained.

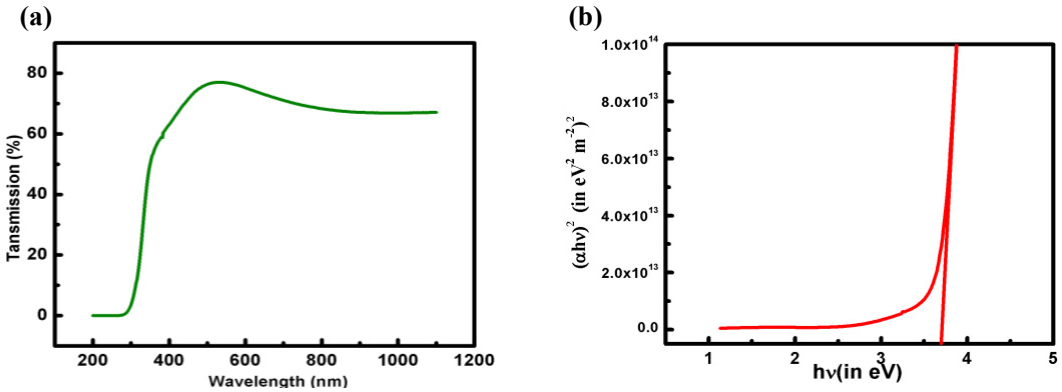


Fig. 2(a): UV-Visible spectra of BTO thin film on quartz substrate; (b): Tauc plot of BTO thin film

Fig. 3 shows the surface morphology of the deposited BTO thin film which can be seen as rough and porous with a particle size of about 40 nm. The rough and porous surface morphology is beneficial for the sensing applications.

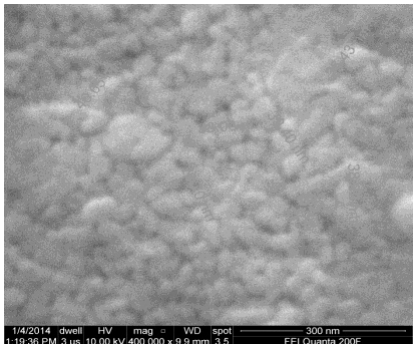


Fig. 3: SEM image of the prepared BTO thin film

Fig. 4 shows the response and recovery profiles of the BTO film (150 nm thin) based sensor towards varying concentration of NO_x gas (50 to 500 ppm) at room temperature. The resistance of sensor decreases on interaction with NO_x gas and regains the initial resistance value after the removal of gas. The response was found to increase from 17.6% to 33.3% with increase in concentration of NO_x gas from 50 to 500 ppm. It is observed that response and recovery times increase as gas concentration increases. Smaller the gas concentration faster would be the oxidation of NO_x gas and hence quick response and immediate recovery of the sensor are obtained.

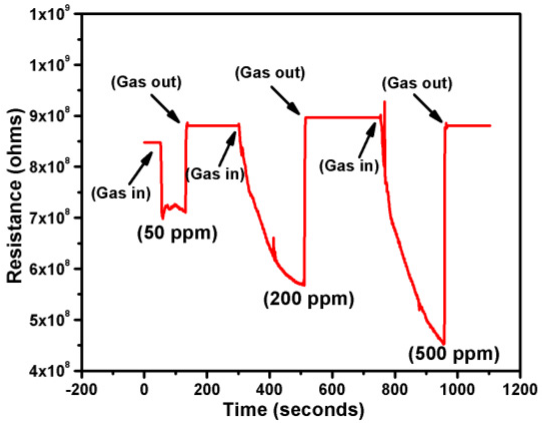


Fig. 4: Response and recovery profiles of the BTO film towards NOx gas in varying concentration

4. Conclusion

Highly transparent barium titanate thin films were prepared by sol-gel spin coating method. High resolution X-Ray diffraction study indicates the formation of single phase and highly crystalline tetragonal structure of barium titanate thin films. The value of optical band gap is about 3.68 eV. The response of $BaTiO_3$ thin film towards sensing NO_x gas at room temperature is relatively high (17.6%) and increases with increase in concentration of gas molecules.

Acknowledgements

The authors are thankful to NPMASS (ADA), GAIL and Delhi University for financial support to carry out this work. One of the author (SS) is thankful to the Delhi Technological University (DTU) for teaching assistantship.

References

[1] G. H. Jain, L. A. Patil, P. P. Patil, U. P. Mulik, K. R. Patil, Studies on gas sensing performance of pure and modified barium strontium titanate thick film resistors, Bull. Mater. Sci. 30(1) (2007) 9–17.
[2] B.T. Marquis, J. F. Vetelino, A semiconducting metal oxide sensor array for the detection of NO_x and NH_3, Sens. Act. B 77 (2001) 100–110.
[3] J. Brunet, V. P. Garcia, A. Pauly, C. Varenne, B. Lauron , An optimised gas sensor microsystem for accurate and real-time measurement of nitrogen dioxide at ppb level, Sens. Act. B 134 (2008) 632–639.
[4] D. J. Kim, J. Y. Jo, Y. S. Kim, Y. J. Chang, J. S. Lee, J. G. Yoon, T. K. Song, T.W. Noh, Polarization Relaxation Induced by a Depolarization Field in Ultrathin Ferroelectric $BaTiO_3$ Capacitors, PRL 95 (2005) 237602.
[5] L. Chen , B.C. Luo, N.Y. Chan , J.Y. Dai, M. Hoffman, S. Li, D.Y. Wang, Enhancement of photovoltaic properties with Nb modified (Bi, Na)TiO_3–$BaTiO_3$ ferroelectric ceramics, J. Alloys and Compounds 587 (2014) 339–343.
[6] G. J. Reynolds, M. Kratzer, M. Dubs, H. Felzer, R. Mamazza, Sputtered Modified Barium Titanate for Thin-Film Capacitor Applications, Materials 5 (2012) 575-589.
[7] H. X. Zhang, C. H. Kam, Y. Zhou, X. Q. Han, Y. L. Lam, Y. C. Chan, K. Pita, Optical and electrical properties of sol-gel derived $BaTiO_3$ films on ITO coated glass, Mater. Chem. Phys. 63 (2000) 174.
[8] A. Sharma, M. Tomar, V. Gupta, SnO_2 thin film sensor with enhanced response for NO_2 gas at lower temperatures, Sens. Act. B 156 (2011) 743– 752.

International Journal of Reliable Information and Assurance
Vol.2, No.2 (2014)

On the significance of Non-Extensivity for the Dynamic Growth of Hidden-Layer Neurons

Seba Susan and Mayank Dwivedi
Department of Information Technology,
Delhi Technological University, New Delhi, India
e-mail: seba_406@yahoo.in

Abstract

In this paper we extend our work on the dynamic growth of hidden layer neurons using the weighted sum of non-extensive entropies in [25] by investigating the significance of the non-extensivity of the entropy measure used. The dynamic neural network in the original work dynamically grows the number of the hidden-layer neurons based on an increase in the entropy of the weights during training. We compare the performance of the non-extensive entropy with Gaussian information gain proposed by Susan and Hanmandlu used in the original paper with that of the non-extensive entropies of Pal and Pal and Tsallis and also the extensive Shannon entropy. Experiments on benchmark datasets from the UCI repository further validate the correctness of our approach and establish the non-linearity of the non-extensive Susan and Hanmandlu entropy as being best suited for this purpose

Keywords: *Hidden layer neurons; Dynamic Neural Network; Dynamic growth of neurons; Multi-layer perceptron; Susan and Hanmandlu entropy; Non-extensive entropy; Weighted sum of non-extensive entropies*

1. INTRODUCTION

The dynamic neural networks [1,2] brought about a revolution in machine learning due to its manifest saving it offers in terms of time and complexity. The number of hidden units or the number of neurons in the hidden layer determines the complexity of the neural network while the converged weights of the network connections determine the accuracy. Statistical inferencing has been used before for improvising the performance of neural networks [3-5]. Dynamic neural networks have been proposed in literature for both RBF [6-9] and MLP [10-12] neural networks with fuzzy extensions [13] in which mostly the growth and pruning of hidden neurons is performed in a recurrent manner consuming time. The axiom followed in static neural network architecture is that more the number of hidden neurons in the hidden layer the higher the accuracy at the cost of increased time and space complexity [14-17]. Extreme Learning Machines (ELM) and its improvisations are recent techniques for dynamically growing the hidden layer [18] which eliminate back-propagation and instead compute hidden weights from the output weights. A new type of dynamic neural network for the conventional feedforward back-propagation configuration was proposed by the authors recently in [25] based on statistical inferencing. It grows the number of hidden neurons from an initial configuration as per requirement as the training progresses. The number of hidden neurons is incremented by one if there is a positive spike in the non-extensive entropy of the network weights. The non-extensive entropy with Gaussian information gain [19] is used for this purpose since it can detect anomalies in a state of order [23].

The paper is organized as follows: The various non-extensive entropies used for the experimentation are described in Section 2. The dynamic growth of hidden layer neurons using the weighted sum of non-extensive entropies proposed by the authors in [25] is described in Section 3. The results are discussed in Section 4 and the overall conclusions are drawn in Section 5.

2. The non-extensive entropies and their role in identifying regularity

Non-extensive entropies are those which are non-additive i.e. the sum of the individual entropies is greater than the joint entropy. For two random variables X , Y and a classical entropy function $H(.)$ the above definition translates to

$$H(X,Y) < H(X) + H(Y) \qquad (1)$$

An example of the non-extensive entropy is Pal and Pal entropy [26] defined by the function

$$H(P) = \sum_{i=1}^{n} p_i e^{1-p_i} \qquad (2)$$

Another example is the non-extensive entropy with Gaussian Information gain proposed by Susan and Hanmandlu defined in [19] as

$$H(P) = \sum_{i=1}^{n} p_i e^{-p_i^2} \qquad (3)$$

The variable P in (2) and (3) is a probability distribution, $P = \{p_1, p_2, ..., p_n\}$, for n possible outcomes. Both (2) and (3) are exponential entropies where the information gain is an exponential function. The difference between the two is that the Susan and Hanmandlu entropy is more non-linear than the Pal and Pal entropy due to the quadratic exponent of the exponential. Hence the former is expected to satisfy the non-additivity property in (1) to a greater extent. The fact can be corroborated by substituting (2) and (3) in (1) to obtain (4) and (5) respectively [19]

$$\begin{aligned} H(X)+H(Y) &= \sum_{x\varepsilon X} p(x_i) e^{1-p(x_i)} + \sum_{y\varepsilon Y} p(y_j) e^{1-p(y_j)} \\ &\cong \sum_{x\varepsilon X}\sum_{y\varepsilon Y} p(x_i,y_j)\left(e^{1-\sum_{y\varepsilon Y} p(x_i,y_j)} + e^{1-\sum_{x\varepsilon X} p(x_i,y_j)} \right) \\ &> \sum_{x\varepsilon X}\sum_{y\varepsilon Y} p(x_i,y_j) e^{1-p(x_i,y_j)} \end{aligned} \qquad (4)$$

$$H(X)+H(Y) = \sum_{x\varepsilon X} p(x_i) e^{-p^2(x_i)} + \sum_{y\varepsilon Y} p(y_j) e^{-p^2(y_j)}$$

$$\cong \sum_{x\varepsilon X}\sum_{y\varepsilon Y} p(x_i, y_j)\left(e^{-\sum_{y\varepsilon Y} p^2(x_i, y_j)} + e^{-\sum_{x\varepsilon X} p^2(x_i, y_j)} \right)$$
$$> \sum_{x\varepsilon X}\sum_{y\varepsilon Y} p(x_i, y_j) e^{-p^2(x_i, y_j)} \qquad (5)$$

The inequality in (5) is more than that in (4) which implies that the entropy in (3) is more non-extensive than that in (2).

Another entropy that comes under the category of pseudo-additive entropy is Tsallis entropy [20] given by

$$H(P) = \frac{1 - \sum_{i=1}^{n} (p_i)^q}{q-1} \qquad (6)$$

The real number q indicates the degree of non-extensivity. Tsallis entropy converges to the extensive Shannon entropy when q=1. The Tsallis entropy is considered non-extensive in a way [27] since it satisfies the condition

$$H(X,Y) = H(X) + H(Y) + (1-q)H(X)H(Y) \qquad (7)$$

The non-extensive entropies are found useful in [19] for the identification of regular textures which contain spatially recurrent patterns that translate to high co-occurrence probabilities. The reason for this is their non-additive nature which does not allow simple addition of component entropies due to unequal significance of the components within regular structures. In contrast the extensive entropies like Shannon entropy adds up the contributions of all components leading to erroneous results when all components are not equally important as in regular textures. It however does perform well in the case of random structures like the Grass texture where all the intensities are equally likely.

In our work we make use of the non-extensive entropy for dynamically growing the hidden layer. The non-additive nature of the non-extensive entropy is exploited here for dynamically growing the neurons since a state of order or regularity is reached in the process of training.

3. dynamical growth of hidden units using the non-extensive entropy of normalized weights [25]

In this section we review the dynamic growth of hidden neurons for a Multi-Layer Perceptron (MLP) neural network proposed in [25]. The weighted sum of non-extensive entropies over two consecutive frame pairs was used in [23] for the detection of video anomalies. The significance of this weighted sum is that any significant departure from the normal will result in a positive spike indicating an anomaly. In our work we compute over time the weighted sum of non-extensive entropies associated with the trained weights of a feedforward network, tuned by back-propagation. A positive spike or an increase in the weighted sum indicates an anomaly in training inputs and increments the number of hidden neurons by one. The weighted sum of non-extensive entropies, also called the entropy of the source $H(S)$ is defined as

$$H(S) = \sum_{x \in X} p(x) H(p(y|x)) \qquad (7)$$

Solving for the entropy $H(p(y|x))$ using (3), we have

$$H(p(y|x)) = \sum_{y \in Y} p(y|x) e^{-p(y|x)^2} \qquad (8)$$

Here $p(x)$ denotes the probability associated with the weight between the output neuron and the xth hidden unit. The set $\{p(y|x)\}$ indicates the probabilities associated with the input connection weights of the xth hidden unit, and $H(p(y|x))$ is the non-extensive entropy associated with $\{p(y|x)\}$ computed using (8).

The multi-layer perceptron architecture 4-3-1 with the actual weights associated with each layer is shown in Fig. 1. Let $w_{ki}^{\ t}$ denote the weight associated with the connection between the kth input dimension and the ith hidden layer neuron after the training of the tth training data sample. The computation of the entropy in (7) from the network weights $\{w_{ki}^{\ t}\}$ and $\{w_{ij}^{\ t}\}$ is explained below. The normalized weights $\{w_{kiN}^{\ t}\}$ are obtained from $\{w_{ki}^{\ t}\}$ by transforming the value of the weights $\{w_{ki}^{\ t}\}$ in the range of 0 to 1, and dividing by the total sum of weights as shown in (9) and (10).

$$w_{kip}^{\ t} = \frac{w_{ki}^{\ t} - \min_{\forall k}(w_{ki}^{\ t})}{\max_{\forall k}(w_{ki}^{\ t}) - \min_{\forall k}(w_{ki}^{\ t})}, \text{k=1,2,3,….,M} \qquad (9)$$

$$w_{kiN}^{\ t} = \frac{w_{kip}^{\ t}}{\sum_{i=1}^{M} w_{kip}^{\ t}}, \text{k=1,2,3,….,M} \qquad (8)$$

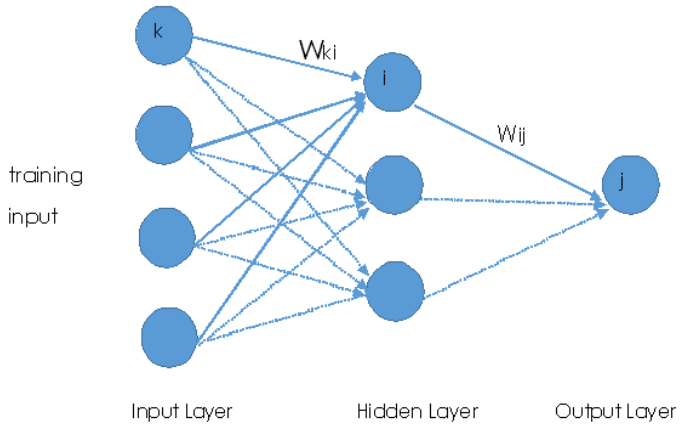


Figure 1 The multi-layer perceptron (MLP) neural network and the connection weights during training

Here M is the number of connection weights between the input layer and the hidden neuron i. The normalized weights $\{w_{1iN}^{\ t}, w_{2iN}^{\ t}, ..., w_{MiN}^{\ t}\}$ are equal to probability values $\{p(y|x)\}$ for a given x, with values in the range of 0 to 1 and $\sum_{k=1}^{M} w_{kiN}^{\ t} = 1$. This probability

distribution can be used for the computation of the entropy $H(p(y|x))$ using (8). The probabilities $\{p(x)\}$ associated with the H hidden neurons and the single output neuron $(j=1)$ are the normalized weights $\{w_{ijN}{}^t\}$ which are computed from $\{w_{ij}{}^t\}$ in a similar manner. The weighted sum of non-extensive entropies given by (7) is generalized for O equally significant outputs as

$$H(S)=\sum_{j=1}^{O}\frac{1}{O}\sum_{i=1}^{H}w_{ijN}{}^t\sum_{k=1}^{M}w_{kiN}{}^t e^{-w^2{}_{kiN}{}^t} \qquad (10)$$

In our example $O=1$. The entropy value computed using (11) for the tth training sample is compared with the entropy value for the previous training data sample $t-1$. If a positive spike in entropy $H(S)$ is encountered, the number of hidden neurons is increased by one and the training proceeds for sample $t+1$. A single memory storage for the previous entropy value is only required for comparison purpose. The steps of the proposed method are summarized below.

1. Initialize the neural network architecture with 3 hidden neurons with all network weights initialized to 0.1.
2. Tune the weights for a training input using BP.
3. Calculate the probabilities of the tuned weights of each layer using (9) and (10).
4. Compute the weighted sum of non-extensive entropies of the tuned network using (11).
5. If this entropy value is greater than that for previous training sample then increment the number of hidden neurons by one, its weights being initialized to 0.1.
6. Repeat the training process for the next sample using the tuned weights of the existing neurons and the newly added neuron.
7. Repeat above steps 2-6 until the training is complete.

The highlight of our method in [25] is that a new computational unit is added whenever an unusual pattern occurs in the training. This trend was also observed before in the case of the Resource-allocating network in [24] which however requires memorizing of specific input patterns that perform poorly, in order to achieve desired accuracy.

4. experimental results

The experiments are performed on benchmark datasets from the UCI repository [28] namely IRIS, DERMATOLOGY, SPECT heart dataset in addition to the linearly separable four dimensional Syntheic dataset used in [25]. The results of dynamically growing the hidden neurons are compared for the Susan and Hanmandlu, Shannon, Pal and Pal, Tsallis entropies. In the case of Tsallis entropy the best results were obtained for q=1.5. The results for the four datasets are summarized in Tables 1-5, with a cross-validation result for IRIS dataset also included. The software platform is C++ on a 2.2 Ghz Pentium processor. As in the original work [25], the single hidden layer Multi-layer Perceptron 4-3-1 shown in Fig. 1 is used as the initial configuration for our experiments, with a learning rate η of 0.2 and an error threshold ε of 0.01. The results in the five tables record a 'slow and steady' rise in the hidden neurons for the Susan and Hanmandlu entropy while the other entropies especially Shannon entropy result in a larger number of hidden neurons. A result which deserves mention is that of the SPECT Heart dataset that grows 38 hidden neurons as compared to 49 hidden neurons using Tsallis entropy. The comparison among the entropies establish that while the non-extensive entropy of Susan and Hanmandlu is certainly superior to Pal and pal and Shannon

entropy, it also provides better results than Tsallis entropy which manages to give comparable results for the easy linearly separable Synthetic dataset but performs badly for a non-linear dataset-SPECT heart. Overall the results in this paper further enhance the utility of the dynamic neural network proposed in [25] and establish the significance of the non-extensivity of the entropy used for the purpose.

Table 1. Performance analysis of the proposed dynamic neural network for the Synthetic dataset using various entropies and various static neural network configurations, in terms of training time in secs (s), number of hidden nodes and the testing accuracy in (%). (Proposed method is shown in gray)

Methods	Dynamic growth of hidden neurons using Susan and Hanmandlu entropy	Dynamic growth of hidden neurons using Shannon entropy	Dynamic growth of hidden neurons using Pal and Pal entropy	Dynamic growth of hidden neurons using Tsallis entropy	Static 3 hidden neuron	Static 7 hidden neuron	Static 11 hidden neuron	Static 22 hidden neuron	Static 34 hidden neuron	Static 40 hidden neuron
Total training time (for 40 samples)	0.39 sec	0.78 sec	0.589sec	0.602sec	0.25sec	0.51sec	0.58sec	0.6sec	0.62sec	0.62sec
Number of hidden nodes	7	11	8	7	3	7	11	22	34	40
Testing Accuracy (for 60 samples)	98.33%	98.33%	98.33%	98.33%	83.43%	83.4%	93.4%	93.4%	83.4%	83.4%

Table 2. Performance analysis of the proposed dynamic neural network for the IRIS dataset (Validation) using various entropies and various static neural network configurations, in terms of training time in secs (s), number of hidden nodes and the testing accuracy in (%). (Proposed method is shown in gray)

Methods	Dynamic growth of hidden neurons using Susan and Hanmandlu entropy	Dynamic growth of hidden neurons using Shannon entropy	Dynamic growth of hidden neurons using Pal and Pal entropy	Dynamic growth of hidden neurons using Tsallis entropy	Static 3 hidden neuron	Static 7 hidden neuron	Static 11 hidden neuron	Static 22 hidden neuron	Static 34 hidden neuron	Static 40 hidden neuron
Total training time (for 75 samples)	0.051 sec	0.136sec	0.152sec	0.168sec	0.090sec	0.082sec	0.173sec	0.129sec	0.107sec	0.116sec
Number of	18	20	20	21	3	7	11	22	34	40

hidden nodes										
Testing Accuracy (for 75 samples)	93.44%	93.44%	93.44%	93.44%	89.44%	89.44%	90.77%	93.44%	93.44%	90.77%

Table 3. Performance analysis of the proposed dynamic neural network for the IRIS dataset (Cross-Validation) using various entropies and various static neural network configurations, in terms of training time in secs (s), number of hidden nodes and the testing accuracy in (%). (Proposed method is shown in gray)

Methods	Dynamic growth of hidden neurons using Susan and Hanmandlu entropy	Dynamic growth of hidden neurons using Shannon entropy	Dynamic growth of hidden neurons using Pal and Pal entropy	Dynamic growth of hidden neurons using Tsallis entropy	Static 3 hidden neuron	Static 7 hidden neuron	Static 11 hidden neuron	Static 22 hidden neuron	Static 34 hidden neuron	Static 40 hidden neuron
Total training time (for 75 samples)	0.115sec	0.163sec	0.186sec	0.170sec	0.1122sec	0.194sec	0.199sec	0.190sec	0.141sec	0.199sec
Number of hidden nodes	19	21	21	20	3	7	11	22	34	40
Testing Accuracy (for 75 samples)	90.77%	89.44%	89.44%	90.77%	88%	89.44%	89.44%	90.77%	90.77%	90.77%

Table 4. Performance analysis of the proposed dynamic neural network for the DERMATOLOGY dataset using various entropies and various static neural network configurations, in terms of training time in secs (s), number of hidden nodes and the testing accuracy in (%). (Proposed method is shown in gray)

Methods	Dynamic growth of hidden neurons using Susan and Hanmandlu entropy	Dynamic growth of hidden neurons using Shannon entropy	Dynamic growth of hidden neurons using Pal and Pal entropy	Dynamic growth of hidden neurons using Tsallis entropy	Static 3 hidden neuron	Static 7 hidden neuron	Static 11 hidden neuron	Static 22 hidden neuron	Static 34 hidden neuron	Static 40 hidden neuron
Total training time (for 183 samples)	0.192 sec	0.242sec	0.196sec	0.198sec	0.198sec	0.198sec	0.156sec	0.184sec	0.236sec	0.472sec
Number										

of hidden nodes	51	51	52	52	3	7	11	22	34	40
Testing Accuracy (for 183 samples)	85.80%	80.00%	84.16%	83.61%	67.22%	67.22%	67.59%	82.52%	83.07%	84.16%

Table 5. Performance analysis of the proposed dynamic neural network for the SPECT HEART dataset using various entropies and various static neural network configurations, in terms of training time in secs (s), number of hidden nodes and the testing accuracy in (%). (Proposed method is shown in gray)

Methods	Dynamic growth of hidden neurons using Susan and Hanmandlu entropy	Dynamic growth of hidden neurons using Shannon entropy	Dynamic growth of hidden neurons using Pal and Pal entropy	Dynamic growth of hidden neurons using Tsallis entropy	Static 3 hidden neuron	Static 7 hidden neuron	Static 11 hidden neuron	Static 22 hidden neuron	Static 34 hidden neuron	Static 40 hidden neuron
Total training time (for 80 samples)	0.136 sec	0.287sec	0.187sec	0.186sec	0.127sec	0.231sec	0.167sec	0.142sec	0.142sec	0.207sec
Number of hidden nodes	38	43	42	49	3	7	11	22	34	40
Testing Accuracy (for 187 samples)	93.05%	92.52%	92.52%	93.05%	83.43%	89.84%	90.38%	90.91%	91.45%	91.45%

5. conclusions

In this paper, the dynamical growth of hidden units proposed recently by the authors in [25] is extended to other non-extensive entropies as well. The non-extensive entropy with the Gaussian information gain being more non-additive than other forms of entropy is proved in this work to be the best measure for dynamically growing the hidden neurons. Experiments on UCI datasets yield the highest accuracy for minimum number of hidden neurons grown by this method. The results further corroborate the claim in our earlier paper that the new technique of dynamically increasing the hidden layer based on statistical inferencing as training progresses provides saving in both time and space and yields high classification accuracy.

References

[1] Yang, Hong, and Jun Ni. "Dynamic neural network modeling for nonlinear, nonstationary machine tool thermally induced error." International Journal of Machine Tools and Manufacture 45.4 (2005): 455-465.

[2] Gupta, Madan M., Liang Jin, and Noriyasu Homma. Static and dynamic neural networks: from fundamentals to advanced theory. Wiley-IEEE Press, 2004.
[3] Erdogmus, Deniz, and Jose C. Principe. "An error-entropy minimization algorithm for supervised training of nonlinear adaptive systems." Signal Processing, IEEE Transactions on 50.7 (2002): 1780-1786.
[4] Ben-David, Arie. "Monotonicity maintenance in information-theoretic machine learning algorithms." Machine Learning 19.1 (1995): 29-43.
[5] Morejon, Rodney A., and Jose C. Principe. "Advanced search algorithms for information-theoretic learning with kernel-based estimators." Neural Networks, IEEE Transactions on 15.4 (2004): 874-884.
[6] Ciabattoni, Lucio, et al. "Supervisory control of PV-battery systems by online tuned neural networks." Mechatronics (ICM), 2013 IEEE International Conference on. IEEE, 2013.
[7] Yingwei, Lu, Narashiman Sundararajan, and Paramasivan Saratchandran. "Performance evaluation of a sequential minimal radial basis function (RBF) neural network learning algorithm." Neural Networks, IEEE Transactions on 9.2 (1998): 308-318.
[8] Huang, Guang-Bin, Paramasivan Saratchandran, and Narasimhan Sundararajan. "An efficient sequential learning algorithm for growing and pruning RBF (GAP-RBF) networks." Systems, Man, and Cybernetics, Part B: Cybernetics, IEEE Transactions on 34.6 (2004): 2284-2292.
[9] Wu, Shiqian, and Meng Joo Er. "Dynamic fuzzy neural networks-a novel approach to function approximation." Systems, Man, and Cybernetics, Part B: Cybernetics, IEEE Transactions on 30.2 (2000): 358-364.
[10] Feng, Guorui, et al. "Error minimized extreme learning machine with growth of hidden nodes and incremental learning." Neural Networks, IEEE Transactions on 20.8 (2009): 1352-1357.
[11]Lan, Yuan, Yeng Chai Soh, and Guang-Bin Huang. "Constructive hidden nodes selection of extreme learning machine for regression." Neurocomputing 73.16 (2010): 3191-3199.
[12] Kurino, Ryusuke, Masanori Sugisaka, and Katsunari Shibata. "Growing neural network with hidden neurons." Proc. 9th Int. Symp. on Artificial Lifeand Robotics (AROB'04). Vol. 1. 2004.
[13] Wu, Shiqian, and Meng Joo Er. "Dynamic fuzzy neural networks-a novel approach to function approximation." Systems, Man, and Cybernetics, Part B: Cybernetics, IEEE Transactions on 30.2 (2000): 358-364.
[13] Robert J.Schalkoff, Artificial Neural Networks, McGraw-Hill, 2011.
[14] Singh, Rampal, and S. Balasundaram. "Application of extreme learning machine method for time series analysis." International Journal of Intelligent Technology 2.4 (2007): 256-262.
[15] Huynh, Hieu Trung, Jung-Ja Kim, and Yonggwan Won. "Performance comparison of SLFN training algorithms for DNA microarray classification." Software Tools and Algorithms for Biological Systems. Springer New York, 2011. 135-143.
[16] Huang, Guang-Bin, Lei Chen, and Chee-Kheong Siew. "Universal approximation using incremental constructive feedforward networks with random hidden nodes." Neural Networks, IEEE Transactions on 17.4 (2006): 879-892.
[17] Huang, Guang-Bin, Lei Chen, and Chee-Kheong Siew. "Universal approximation using incremental constructive feedforward networks with random hidden nodes." Neural Networks, IEEE Transactions on 17.4 (2006): 879-892.
[18] Seba Susan, Madasu Hanmandlu, “A Non-Extensive entropy feature and its application to texture classification”, Neurocomputing, Volume 120, November 2013, pp. 214–225.
[19] Tsallis, Constantino. "Possible generalization of Boltzmann-Gibbs statistics." Journal of statistical physics 52.1-2 (1988): 479-487.
[20] C.E.Shannon, “A Mathematical theory of communication”, The Bell system Technical Journal, Vol.27, pp.379-423 July,1948.
[21] Seba Susan, Madasu Hanmandlu,” A novel Fuzzy Entropy based on the Non-Extensive Entropy and its application for feature selection”, FUZZ-IEEE 2013
[22] Susan, Seba, and Madasu Hanmandlu. "Unsupervised detection of nonlinearity in motion using weighted average of non-extensive entropies." Signal, Image and Video Processing (2013): 1-15.
[23] Platt, John. "A resource-allocating network for function interpolation." Neural computation 3.2 (1991): 213-225.
[24] Susan, Seba, and Mayank Dwivedi. "Dynamic Growth of Hidden-Layer Neurons Using the Non-extensive Entropy." In Communication Systems and Network Technologies (CSNT), 2014 Fourth International Conference on, pp. 491-495. IEEE, 2014.

[25] Nikhil Pal, Sankar Pal , "Entropy- Anew definition and its applications" IEEE Trans. Syst. Man and Cyber, Vol.21, No.5, Sept. 1991.
[26] Albuquerque M., Esquef I.A., Gesualdi Mello, Albuquerque, M.P.," Image thresholding using Tsallis entropy", Pattern Recognition Letters 25(2004), pp. 1059-1065.
[27] Frank, A. & Asuncion, A. (2010). UCI Machine Learning Repository [http://archive.ics.uci.edu/ml]. Irvine, CA: University of California, School of Information and Computer Science.

Spectrochimica Acta Part A: Molecular and Biomolecular Spectroscopy 125 (2014) 53–60

Contents lists available at ScienceDirect

Spectrochimica Acta Part A: Molecular and Biomolecular Spectroscopy

journal homepage: www.elsevier.com/locate/saa

Optical studies of Sm^{3+} ions doped Zinc Alumino Bismuth Borate glasses

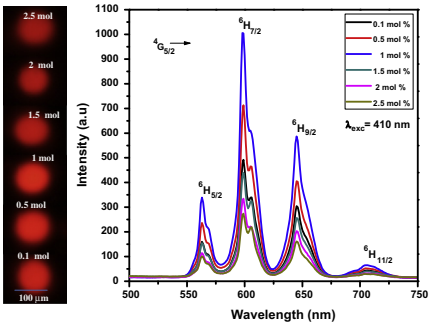
K. Swapna [a], Sk. Mahamuda [a], A. Srinivasa Rao [a,b,*], S. Shakya [c], T. Sasikala [d], D. Haranath [e], G. Vijaya Prakash [c]

[a] Department of Physics, KL University, Green Fields, Guntur (Dt), Vaddeswaram 522 502, AP, India
[b] Department of Applied Physics, Delhi Technological University, Bawana Road, New Delhi 110 042, India
[c] Nano Photonics Laboratory, Department of Physics, Indian Institute of Technology-Delhi, Hauz Khas, New Delhi 110 016, India
[d] Department of Physics, SV University, Tirupathi 517 502, AP, India
[e] CSIR-National Physical Laboratory, Dr. K.S. Krishnan Road, Pusa, New Delhi 110 012, India

HIGHLIGHTS

- ZnAlBiB glasses were prepared by conventional melt quenching technique.
- Emission data coupled with JO analysis were used to measure radiative properties.
- Quantum efficiency of ZnAlBiB glasses were measured from decay curves.

GRAPHICAL ABSTRACT



ARTICLE INFO

Article history:
Received 18 September 2013
Received in revised form 4 January 2014
Accepted 10 January 2014
Available online 24 January 2014

Keywords:
Glasses
Samarium
JO parameters
Radiative properties
Emission cross-section

ABSTRACT

Zinc Alumino Bismuth Borate (ZnAlBiB) glasses doped with different concentrations of samarium (Sm^{3+}) ions were prepared by using melt quenching technique and characterized for their lasing potentialities in visible region by using the techniques such as optical absorption, emission and emission decay measurements. Radiative properties for various fluorescent levels of Sm^{3+} ions were estimated from absorption spectral information using Judd–Ofelt (JO) analysis. The emission spectra and con-focal photoluminescence images obtained by 410 nm laser excitation demonstrates very distinct and intense orange–red emission for all the doped glasses. The suitable concentration of Sm^{3+} ions in these glasses to act as an efficient lasing material has been discussed by measuring the emission cross-section and branching ratios for the emission transitions. The quantum efficiencies were also been estimated from emission decay measurements recorded for the $^4G_{5/2}$ level of Sm^{3+} ions. From the measured emission cross-sections, branching ratios, strong photoluminescence features and CIE chromaticity coordinates, it was found that 1 mol% of Sm^{3+} ions doped ZnAlBiB glasses are most suitable for the development of visible orange–red lasers.

© 2014 Elsevier B.V. All rights reserved.

Introduction

In recent years, there has been an increasing interest to the lanthanide ions doped in different hosts to achieve favorable optical devices such as lasers, fiber amplifiers, light converters, sensors

* Corresponding author at: Department of Applied Physics, Delhi Technological University, Bawana Road, New Delhi 110 042, India. Tel.: +91 85860 39007; fax: +91 01127871023.
E-mail address: drsrallam@gmail.com (A. Srinivasa Rao).

http://dx.doi.org/10.1016/j.saa.2014.01.025
1386-1425/© 2014 Elsevier B.V. All rights reserved.

and hole burning high density memories [1,2]. The optical spectrum of lanthanide ion is closely related to the particular local symmetry of the environment occupied by this ion in solid matrices. In glasses, they usually in homogeneously broadened band due to site-to-site variations in the local field action on the ions [3]. Glasses doped with rare-earth ions are proving to be the best luminescent materials as they have high emission efficiencies. While the emission is originated from both 4f–4f as well as 4f-5d electronic transitions, the 4f–4f transitions gives sharp emission lines covering wide range of spectral region, from the ultraviolet (UV) to the infrared region (IR). These sharp emissions attracted potential applications in solid state lasers, optical fiber amplifiers and three dimensional display devices [4–6]. The emission quantum efficiencies of the rare-earth ions are strongly dependent on phonon energy of the host material and active ion concentration. In recent years, among other oxide based glasses, borate glasses have been the subject of interest due to their high transparency, low melting point, high thermal stability and capability of accommodating large concentrations of rare earth ions [7–9].

The structure of the borate glasses is the gathering of BO_3 triangles and BO_4 tetrahedral units to form well defined and stable borate groups such as di borate, tri borate and tetra borate, resulting into random three-dimensional network [10]. Because of these reasons borate glasses are the best choice for rare earth ion doping. However, borate glasses have large phonon energies due to the stretching vibrations of network-forming oxides, resulting into enhanced non-radiative processes there by reduction in the luminescence efficiency. Such high phonon energies possessed by the borate glasses can be conveniently reduced by adding heavy metal oxides (HMO) such as bismuth and lead oxides [11]. Furthermore, HMO containing glasses show extremely high radioactive resistance because of their high density and atomic number. Bismuth trioxide alone cannot be considered as network former due to small field strength of Bi^{3+} ion [11]. Furthermore, introducing Al_2O_3 as network modifier in a glass improves the chemical stability, thermo-mechanical stability and other emission properties of the rare-earth doped glass [12]. Zinc oxide in a glass host can act as a network former/modifier and gives better chemical durability, low glass transition temperature and wider glass forming compositional range [13]. Hence, for the present work we have prepared a borate glass with the other important oxide based network modifiers containing B^{3+}, Bi^{3+}, Zn^{2+} and Al^{3+} ions.

In recent times, glasses containing Sm^{3+} ions have stimulated extensive interest due to their potential application for high-density optical storage, under sea communication and color displays [14,15]. Additionally, the Sm^{3+} ions exhibit broad emission bands due to $^4G_{5/2} \rightarrow {}^6H_J$ (J = 5/2, 7/2, 9/2, 11/2) transitions in any host matrix. Moreover, the phonon energies of hosts are not so critical to the orange–red emission at ~600 nm, because of the large energy difference of $^4G_{5/2}$ meta-stable level to its next lower lying levels [16,17]. The large gap between the $^4G_{5/2}$ level and its sublevels permits the applications of sm^{3+} ions in different glass hosts with large phonon energy. It is also well known that the intensities of emission bands of Sm^{3+} ion in glasses depend on its concentration and glass composition [18]. In order to obtain optimum emission characteristics for device applications, the characteristic features of host as well as concentration dependent studies of Sm^{3+} are essential.

The present work reports, the preparation and characterization of a new series of trivalent samarium doped Zinc Alumino Bismuth Borate (ZnAlBiB) glasses, by using the techniques such as XRD, FT-IR, optical absorption, luminescence and decay curve measurements. The present study mainly focus on absorption, steady-state and time-resolved emission measurements of Sm^{3+} ions in ZnAlBiB glasses to select a good host material for solid state laser devices.

Experimental

The glasses having composition $20ZnO - 10Al_2O_3 - (10 - x)Bi_2O_3 - 60B_2O_3 + xSm_2O_3$, ($x$ = 0.1, 0.5, 1.0, 1.5, 2.0, 2.5 mol%) were prepared by using normal melt-quenching technique. The glasses were abbreviated as ZnAlBiBSm01, ZnAlBiBSm05, ZnAlBiBSm10, ZnAlBiBSm15, ZnAlBiBSm20, and ZnAlBiBSm25. Analytical reagents of ZnO, Al_2O_3, Bi_2O_3, B_2O_3, and Sm_2O_3 were used as starting materials to prepare the glasses. The reagents were fully mixed and about 10 g batches were taken in a crucible and were put in an electric furnace at a temperature of 1200 °C for 30 min. The melt was stirred frequently for homogeneous mixing of all the constituents. The glass samples were obtained by pouring and quenching the melt in-between two brass plates kept at room temperature (RT). Clear, bubble free and transparent glasses were obtained. Disk shaped samples were polished with different grades of emery powder. The densities and refractive indices were estimated by Archimedes' principle and Brewster angle technique respectively. The absorption spectra were obtained from a JASCO model V-670 UV–vis–NIR spectrophotometer from 800 to 1700 nm with a resolution of 0.1 nm. The photoluminescence (PL) emission and excitation spectra for all these glasses were recorded at room temperature using RF-5301 PC Spectrofluorophotometer. The emission from sample was coupled into a monochromator (Acton SP2300) coupled to CCD (charge coupled detector) through the appropriate lenses and filters. The high-resolution PL images were obtained from a modified 410 nm CW diode laser coupled con-focal microscope (Olympus, BX51) equipped with XY-piezo stage. Time-resolved PL measurements were recorded using an Edinburgh luminescence spectrometer (model F900) equipped with a microsecond xenon flash lamp as the source of excitation at 401 nm.

Result and discussions

XRD spectral analysis

In order to check the amorphous nature of the prepared glasses, the XRD spectral measurement were taken up for an undoped glass using XPERT-PRO diffractometer with Cu $K\alpha_1$ radiation (λ = 1.5406 Å) in the 2θ angle range 5°–70° with step size 0.02° s^{-1} and is shown in Fig. 1. The XRD spectrum shows a broad hump which is continuous in appearance. It is well known that, an amorphous material with short range order will always give a featureless broad hump. Hence the prepared ZnAlBiB glasses have amorphous nature.

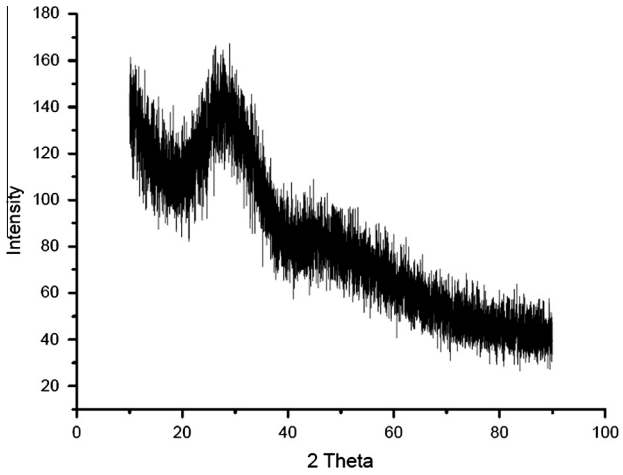


Fig. 1. XRD spectrum for an undoped ZnAlBiB Glass.

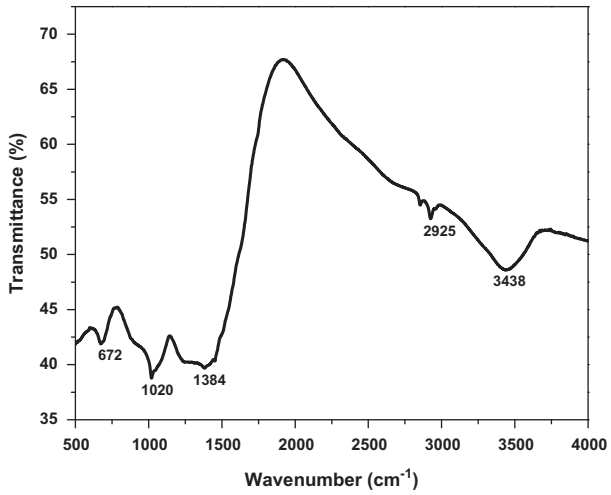


Fig. 2. FT-IR spectrum of 1 mol% Sm^{3+} ions doped ZnAlBiB glass (ZnAlBiBSm10).

FT-IR spectral measurements

To identify the local structure, the FT-IR spectrum for 1 mol% of Sm^{3+} ions doped ZnAlBiB glass has been recorded and is shown in Fig. 2. The observed characteristic functional groups identified from the FT-IR spectrum are given in Table 1. The FT-IR spectral vibrations in the present glass are categorized into five well defined infrared active modes observed around 3438, 2925, 1384, 1020 and 672 cm^{-1}. The broad bands are due to various combinations of high degeneracy vibrational states, thermal broadening of the lattice dispersion and mechanical scattering of samples [19]. The conventional broad band observed at 3438 cm^{-1} is due to the hydroxyl groups of O–H stretching vibrations. A band observed around 2925 cm^{-1} is an indication of the existence of hydrogen bonding. An absorption band at 1384 cm^{-1} is attributed to the B–O stretching vibrations of various network containing planar six membered borate groups in BO_3 units [20]. The peak position around 1020 cm^{-1} confirms the stretching vibration of BO_4 groups in diborate group [21] and broad band at 672 cm^{-1} is due to the oxygen bridges between two trigonal boron atoms and are attributed to B–O–B bending vibrations [22]. These FT-IR spectroscopic analysis results are comparable to other samarium doped alkali/alkaline earth metal oxides [23]. It is well known that, the OH^- content present in glasses can be estimated through FT-IR spectral measurements. The estimation of OH^- content is important as it can increase the non-radiative decay losses and decrease the quantum efficiency of the prepared glasses. The low intensity of OH^- band observed at 2925 cm^{-1} indicates that the present glasses possess low OH^- content. The OH^- content in a glassy materials can be estimated using the equation $\alpha_{OH} = \frac{\ln\left(\frac{T_0}{T_D}\right)}{l}$, where T_0 is the highest transmission, T_D is the transmission of the glass at 3000 cm^{-1} and l is the glass sample's thickness [24]. The OH^- content estimated for the titled glass is 65.20 ppm which is lower than the LBTAF (120.00 ppm) [25], GeS_2 (175.5 ppm) [26] and LHG-8L (128 ppm) glasses [27].

Table 1
Characteristic functional groups present in 1 mol% of Sm^{3+} ions doped ZnAlBiB glass measured from FT-IR spectrum.

S. no	Wave number (cm^{-1})	Assignment
1	672	B–O–B bending in oxygen bridges b/w two trigonal boron atoms
2	1020	Stretching of various borate rings in BO_4 groups
3	1384	Stretching in B–O bonds in BO_3
4	2925	Hydrogen bonding
5	3438	O–H stretching vibration

Absorption spectra and Judd Ofelt analysis

The optical absorption spectra of 1 mol% of Sm^{3+} ions doped ZnAlBiB glass measured in the spectral range 800–1700 nm is shown in Fig. 3. The absorption spectra of all the titled glasses are similar to each other except variation in intensities which are due to variation in concentration of sm^{3+} ions and glass composition [28]. The room temperature optical absorption spectra in NIR region for the titled glasses consists of several inhomogeneous broadened bands assigned to f–f transitions from the ground $^6H_{5/2}$ state to various excited states of Sm^{3+} ions in the host glass. Due to strong absorption of the titled glasses in the UV region, several peaks disappeared in the visible spectral region. The band positions along with their assignments of transitions for the ZnAlBiB glass are given in Table 2. On the other hand, the transitions to ^6H and ^6F spectral terms are spin allowed in the NIR region. Most of the transitions were due to electric dipole interactions only with the selection rule $|\Delta J| \leqslant 0$, but a few transitions contains magnetic dipole contribution following the selection rule $\Delta J = 0, \pm 1$ [29]. To have an idea about the nature of Sm^{3+}-ligand bond, nephelauxetic ratios (β) have also been evaluated using the following expression [30].

$$\beta = \frac{\overline{\vartheta_c}}{\overline{\vartheta a}}$$

where $\overline{\vartheta_c}$ is the wavenumber (in cm^{-1}) of a particular transition for an ion in the host under investigation and $\overline{\vartheta_a}$ is the wavenumber (in cm^{-1}) of the same transition for an aqua-ion. From the average values of β (taken as $\bar{\beta}$) the bonding parameter (δ) can be calculated using the following expression [30].

$$\delta = \frac{1 - \bar{\beta}}{\bar{\beta}}$$

The bonding will be covalent or ionic depending upon the positive or negative sign of δ. The bonding parameters (δ) are found to be negative (−0.0126, −0.0113, −0.0111, −0.0108, −0.0106, −0.0105) for the titled glasses indicates the ionic nature of the Sm–O bond. Moreover, the ionic nature gradually decreases with the decrease in Bi_2O_3 content. Similar ionic nature has been observed in other reported Sm^{3+}-doped glasses [14,31,32].

The Judd–Ofelt (JO) theory [33,34] has been applied for seven well-defined absorption transitions such as $^6H_{5/2} \rightarrow {}^6F_{11/2}$, $^6F_{9/2}$, $^6F_{7/2}$, $^6F_{5/2}$, $^6F_{3/2}$, $^6F_{15/2}$, and $^6F_{1/2}$ observed in the wavelength range 800–1700 nm. The experimental oscillator strengths (f_{exp}) were determined from the absorption spectra by using the procedure outline in our previous paper [35]. From f_{exp} and squared reduced matrix elements using least square analysis, JO intensity parameters (Ω_2, Ω_4 and Ω_6) are obtained for the titled glass matrices and in turn used to obtain calculated oscillator strengths (f_{cal}). Table 2 presents the experimental and calculated oscillator strengths along with δ rms values for all the ZnAlBiB glasses. Very small rms deviations obtained between experimental and calculated oscillator strengths indicates the validity of JO theory. The experimental oscillator strengths (f_{exp}) observed for ZnAlBiBSm10 glass is relatively much higher than the other titled glasses as presented in Table 2. The JO intensity parameters and their trend ($\Omega_6 > \Omega_4 > \Omega_2$) for the titled glasses have been presented in Table 3. According to Jorgensen and Judd [36] and Jorgensen and Reisfeld [37], Ω_2 is a covalency-dependent parameter, whereas Ω_4 and Ω_6 are

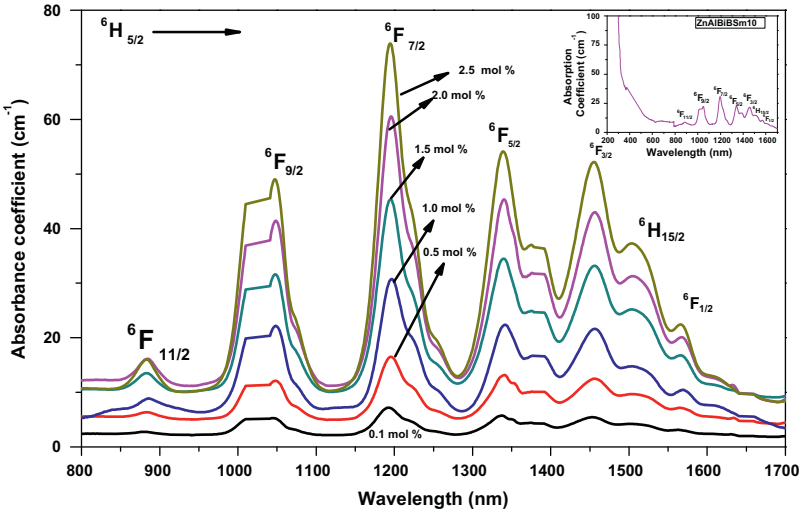


Fig. 3. Absorption spectra of different concentration on Sm^{3+} ions doped ZnAlBiB glasses. The inset shows the absorption edge details of ZnAlBiBSm10 glass.

Table 2
Measured ($f_{exp} \times 10^{-6}$) and calculated ($f_{cal} \times 10^{-6}$) oscillator strengths of Sm^{3+} ions doped ZnAlBiB glasses.

Transitions from $^6H_{5/2}$	Energy (cm^{-1})	ZnAlBiBSm01		ZnAlBiBSm05		ZnAlBiBSm10		ZnAlBiBSm15		ZnAlBiBSm20		ZnAlBiBSm25	
		f_{exp}	f_{cal}	f_{exp}	f_{cal}	f_{exp}	f_{cal}	f_{exp}	f_{cal}	f_{exp}	f_{cal}	f_{exp}	f_{cal}
$^6F_{11/2}$	10,570	0.27	0.56	0.67	0.62	1.71	1.43	0.52	0.71	0.55	0.70	0.57	0.69
$^6F_{9/2}$	9267	3.09	3.38	3.67	3.72	7.57	8.51	3.79	4.31	3.80	4.22	3.91	4.13
$^6F_{7/2}$	8156	4.63	4.41	4.91	4.88	11.3	10.6	5.98	5.60	5.73	5.42	5.84	5.38
$^6F_{5/2}$	7293	1.39	1.44	1.62	1.62	2.23	2.72	1.70	1.80	1.56	1.63	1.71	1.70
$^6F_{3/2}$	6784	0.57	0.64	0.73	0.75	2.03	1.53	0.73	0.80	0.64	0.73	0.61	0.76
$^6H_{15/2}$	6535	0.16	0.02	0.09	0.03	0.30	0.07	0.18	0.03	0.16	0.03	0.16	0.03
$^6F_{1/2}$	6305	0.05	0.003	0.04	0.03	0.16	0.44	0.07	0.006	0.08	0.008	0.10	0.005
δ_{rms} ($\times 10^{-6}$)		±0.186		±0.039		±0.533		±0.269		±0.217		±0.139	
Refractive index (n)		1.790		1.800		1.802		1.804		1.807		1.809	
Density (d) (gm/cc)		3.936		3.935		3.924		3.910		3.911		3.904	
Sample thickness (t) (mm)		1.53		1.53		1.53		1.53		1.53		1.53	

Table 3
Comparison of Judd–Ofelt parameters ($\times 10^{-20}$ cm^2) and their trend for Sm^{3+} ions in different glasses.

Glass composition	J O parameters			Trend	References
	Ω_2	Ω_4	Ω_6		
ZnAlBiBSm01	0.009 ± 0.095	2.27 ± 0.031	3.35 ± 0.012	$\Omega_6 > \Omega_4 > \Omega_2$	Present work
ZnAlBiBSm05	0.091 ± 0.008	2.55 ± 0.001	3.69 ± 0.002	$\Omega_6 > \Omega_4 > \Omega_2$	Present work
ZnAlBiBSm10	1.171 ± 0.231	4.14 ± 0.059	8.52 ± 0.014	$\Omega_6 > \Omega_4 > \Omega_2$	Present work
ZnAlBiBSm15	0.015 ± 0.012	2.82 ± 0.004	4.26 ± 0.004	$\Omega_6 > \Omega_4 > \Omega_2$	Present work
ZnAlBiBSm20	0.021 ± 0.014	2.55 ± 0.005	4.18 ± 0.001	$\Omega_6 > \Omega_4 > \Omega_2$	Present work
ZnAlBiBSm25	0.013 ± 0.188	2.65 ± 0.051	4.07 ± 0.157	$\Omega_6 > \Omega_4 > \Omega_2$	Present work
LPG 12	0.880	3.93	4.66	$\Omega_6 > \Omega_4 > \Omega_2$	[9]
LSG 12	0.770	6.39	7.09	$\Omega_6 > \Omega_4 > \Omega_2$	[9]
CdBiB	0.040	2.84	6.03	$\Omega_6 > \Omega_4 > \Omega_2$	[39]
PbF_2–TeO_2–B_2O_3	0.210	1.42	1.87	$\Omega_6 > \Omega_4 > \Omega_2$	[40]

structure-dependent parameters. From the Table 3 it can be observed that, the Ω_2 value is found to be high for ZnAlBiBSm10 glass. The lower Ω_2 values for the Sm^{3+} ions in the present glasses is an indication of weaker covalency of Sm–O bond under more centro-symmetric or asymmetric environment around Sm^{3+} ions [38]. The high magnitude of Ω_6 indicates low rigidity of the present titled glasses compared to various other glasses presented in Table 3 [9,39,40].

Emission spectra and radiative properties

Fig. 4 shows the excitation spectra of titled glasses in the region 325–500 nm by monitoring the emission at 598 nm. As shown in Fig. 4, the excitation spectra contain several excitation bands in visible region. This indicates that the commercial UV-blue laser diodes and blue-bluish-green light emitting diodes (LEDs) can be used as pumping sources for the Sm^{3+}-doped ZnAlBiB glasses [41]. The emission spectra of the sm^{3+} doped ZnAlBiB glasses recorded in the spectral range 500–750 nm by exciting with 410 nm (24390 cm^{-1}) CW laser is shown in Fig. 5. The con-focal images shown by ZnAlBiB glasses when excited at 410 nm using CW laser are also shown in Fig. 5. The emission spectra exhibit four emission bands corresponding to $^4G_{5/2} \rightarrow {}^6H_{5/2}$ (563 nm), $^4G_{5/2} \rightarrow {}^6H_{7/2}$ (598 nm), $^4G_{5/2} \rightarrow {}^6H_{9/2}$ (645 nm), and $^4G_{5/2} \rightarrow {}^6H_{11/2}$ (704 nm) transition irrespective of variation in concentration. Among the

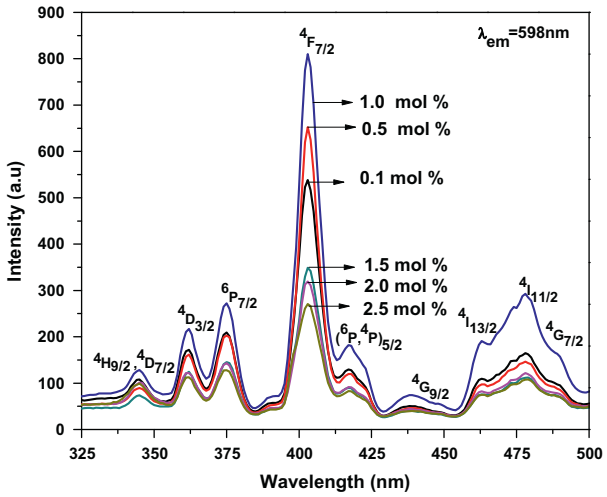


Fig. 4. Excitation spectra of different concentrations of Sm^{3+} ions doped ZnAlBiB glasses.

four observed bands, the $^4G_{5/2} \rightarrow {}^6H_{7/2}$ is more intense and $^4G_{5/2} \rightarrow {}^6H_{11/2}$ is found to be weak in intensity. From Fig. 5, it can be seen that the emission spectral intensity of Sm^{3+} ions in the titled glasses increases gradually up to 1 mol% of Sm^{3+} ions and then decreases gradually for all the peaks. This concentration quenching observed at 1 mol% of Sm^{3+} ions in these glasses may be due to enhanced interaction between Sm^{3+} ions and also between Sm^{3+} ions with host defects leading to the cross-relaxations among the active ions [42]. These samples have a very distinct orange–red luminescence, which is mainly due to the luminescence of the intense $^4G_{5/2} \rightarrow {}^6H_{7/2}$ transition at 598 nm (16722 cm^{-1}) and $^4G_{5/2} \rightarrow {}^6H_{9/2}$ at 645 nm (15503 cm^{-1}). These transitions are useful in high-density optical storage, color displays and medical diagnostics.

The intensity of orange–red luminescence shown by ZnAlBiB glasses increases with the concentration up to 1 mol% of Sm^{3+} ions and then decreasing. To get further confirmation for this, we have recorded con-focal PL images for all the ZnAlBiB glasses. From the con-focal PL images shown in Fig. 5, it can be observed that the orange–red emission intensity is maximum for 1 mol% of Sm^{3+} ions. This result is in consistent with the emission spectra given by the titled glasses. The emission transition may be electric dipole or magnetic dipole allowed that results from an interaction of an electron in an atom with the electromagnetic field. We believe that the $^4G_{5/2} \rightarrow {}^6H_{5/2}$ (563 nm) is predominantly due to magnetic dipole in character where as the transition $^4G_{5/2} \rightarrow {}^6H_{9/2}$ (644 nm) is predominantly due to electric dipole in character. A transition $^4G_{5/2} \rightarrow {}^6H_{7/2}$ (598 nm) is principally present's electric dipole in character, although the transition is magnetic dipole allowed. Higher intensity of the electric dipole transition exhibit more asymmetric nature. In the present work, the spectral intensity of the electric dipole induced transition, $^4G_{5/2} \rightarrow {}^6H_{9/2}$ of the Sm^{3+} ion is higher than the magnetic transition $^4G_{5/2} \rightarrow {}^6H_{5/2}$. The relative intensities of these transitions are known to be sensitive to the variations in the local environment surrounding Sm^{3+} ions [43]. It indicates that the asymmetric nature is predominant in the titled glasses, which is further confirmed through the lower Ω_2 JO intensity parameter. Other emission band located at 645 nm is an electric dipole forced transition and its intensity is also sensitive to the changes in the local field around rare earth ion [44]. Among the four emission transitions, the $^4G_{5/2} \rightarrow {}^6H_{7/2}$ and $^4G_{5/2} \rightarrow {}^6H_{9/2}$ transitions of ZABBSm10 glass are more intense. The JO parameters obtained by least square fit are used to predict the radiative properties such as the radiative transition probability (A_R), total radiative transition probability (A_T), radiative lifetime (τ_R) and branching ratios (β_R) using the expressions collected from the Ref. [45] and are given in Table 4.The peak stimulated emission cross section (σ_{se}) of an emission band having transition probability $A_R(\Psi J,\Psi' J')$ can be expressed as

$$\sigma_{se}(\Psi J,\Psi' J') = \frac{\lambda_P^4}{8\pi c n^2 \Delta\lambda_P} A_R(\Psi J,\Psi' J')$$

Here λ_P is the peak emission wavelength and $\Delta\lambda_P$ is its effective bandwidth found by dividing the area of the emission band by its average height. The values of stimulated emission cross-section (σ_{se}) are given in Table 5, along with emission peak wavelength (λ_P) and effective bandwidth ($\Delta\lambda_P$). The large stimulated emission cross-section is an attractive feature for low- threshold, high gain laser applications, which are utilized to obtain CW laser action. Among the four emission transitions, the $^4G_{5/2} \rightarrow {}^6H_{7/2}$ transition has high stimulated emission cross-section for all the titled glasses. From the same table it can also be seen that ZnAlBiBSm10 glass exhibits higher stimulated emission cross-section among all the glasses studied. The luminescence branching ratio (β_R) is another

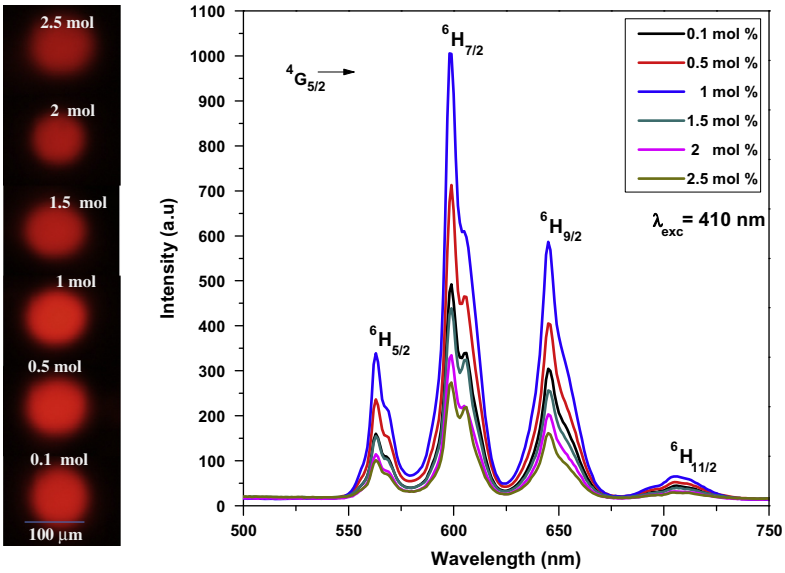


Fig. 5. PL images of sm^{3+} ions doped ZnAlBiB glasses and their corresponding emission Spectra.

Table 4
Radiative transition probability (A_R) (s^{-1}), radiative branching ratio (β_R) and total radiative transition probability (A_T) (s^{-1}) for Sm^{3+} ions doped ZnAlBiB glasses.

Transition $^4G_{5/2}\rightarrow$	ZnAlBiBSm01		ZnAlBiBSm05		ZnAlBiBSm10		ZnAlBiBSm15		ZnAlBiBSm20		ZnAlBiBSm25	
	A_R	β_R	A_R	β_R	A_R	β_R	A_R	β_R	A_R	β_R	A_R	β_R
$^6H_{5/2}$	27	0.08	28	0.08	33	0.04	29	0.07	28	0.07	28	0.07
$^6H_{7/2}$	169	0.53	186	0.53	360	0.54	210	0.54	202	0.54	202	0.54
$^6H_{9/2}$	53	0.16	62	0.17	141	0.21	67	0.17	63	0.17	64	0.17
$^6H_{11/2}$	34	0.11	38	0.11	73	0.10	44	0.11	41	0.11	42	0.11
	$A_T = 315$		$A_T = 348$		$A_T = 668$		$A_T = 386$		$A_T = 370$		$A_T = 372$	

Table 5
Emission peak wavelength (λ_P) (nm), effective band width ($\Delta\lambda_P$) (nm), experimental branching ratio (β_{exp}), stimulated emission cross-section (σ_{se})($\times 10^{-22}$) (cm^2), gain bandwidth ($\sigma_{se} \times \Delta\lambda_P$)($\times 10^{-28}$), optical gain ($\sigma_{se} \times \tau_R$)($\times 10^{-25}$) and O/R ratios for the emission transitions of Sm^{3+} ions doped ZnAlBiB glasses. Experimental, radiative lifetime (τ_{exp}, τ_R) (μs) and quantum efficiency (η%) of $^4G_{5/2}$ transition for different concentrations of Sm^{3+} ions doped ZnAlBiB glasses are given separately.

Transition	Parameters	ZnAlBiBSm01	ZnAlBiBSm05	ZnAlBiBSm10	ZnAlBiBSm15	ZnAlBiBSm20	ZnAlBiBSm25
$^4G_{5/2} \rightarrow {}^6H_{5/2}$	λ_P	563	563	563	563	563	563
	$\Delta\lambda_P$	12.5	10.15	10.15	10.15	10.15	12.5
	β_{exp}	0.09	0.09	0.10	0.11	0.10	0.17
	σ_{se}	0.91	1.15	1.34	1.17	1.15	0.94
	$\sigma_{se} \times \Delta\lambda_P$	1.14	1.16	1.36	1.19	1.17	1.19
	$\sigma_{se} \times \tau_R$	2.88	3.29	2.01	3.02	3.11	2.55
$^4G_{5/2} \rightarrow {}^6H_{7/2}$	λ_P	598	598	598	598	598	598
	$\Delta\lambda_P$	14.06	13.28	12.5	14.06	14.06	15.62
	β_{exp}	0.50	0.53	0.54	0.52	0.49	0.43
	σ_{se}	6.62	7.70	15.8	8.13	7.84	7.08
	$\sigma_{se} \times \Delta\lambda_P$	9.30	10.2	19.8	11.4	11.0	11.1
	$\sigma_{se} \times \tau_R$	21.0	22.1	23.6	21.0	21.2	19.0
$^4G_{5/2} \rightarrow {}^6H_{9/2}$	λ_P	644	644	644	644	644	644
	$\Delta\lambda_P$	15.62	14.06	12.5	14.06	15.62	15.62
	β_{exp}	0.35	0.35	0.33	0.30	0.34	0.35
	σ_{se}	2.42	3.11	7.96	3.36	2.84	2.90
	$\sigma_{se} \times \Delta\lambda_P$	3.78	4.37	9.95	4.72	4.44	4.53
	$\sigma_{se} \times \tau_R$	7.65	8.92	11.9	8.69	7.69	7.77
$^4G_{5/2} \rightarrow {}^6H_{11/2}$	λ_P	706	706	706	706	706	706
	$\Delta\lambda_P$	29.68	16	35.93	21.87	29.68	26.56
	β_{exp}	0.00	0.00	0.04	0.04	0.04	0.03
	σ_{se}	1.20	1.58	2.07	2.03	1.41	1.6
	$\sigma_{se} \times \Delta\lambda_P$	3.55	3.96	7.43	4.44	4.18	4.26
	$\sigma_{se} \times \tau_R$	3.79	4.54	3.09	5.25	3.8	4.3
$(^4G_{5/2} \rightarrow {}^6H_{7/2})/(^4G_{5/2} \rightarrow {}^6H_{9/2})$(O/R)		1.57	1.71	1.67	1.68	1.60	1.65
Emission characteristics of $^4G_{5/2} \rightarrow {}^6H_{7/2}$ transition							
	τ_R	3167	2866	1495	2588	2700	2683
	τ_{exp}	1696	1197	1150	1125	1115	1096
	η	53	42	77	43	41	40

important parameter and plays an important role in deciding the lasing potentiality of an emission transition. It is well known that, an emission transition having the luminescence β_R greater than 50% is consider to be more potential for laser emission [46]. Hence In the present glass systems, $^4G_{5/2} \rightarrow {}^6H_{7/2}$ transition satisfies the above conditions required for a good laser transition. The experimental branching ratios (β_{exp}) are estimated from the ratio of individual area of the corresponding emission band to that of the total integrated area under all the emission peaks. The experimental branching ratios (β_{exp}) of all the titled glasses are given in Table 5. From the magnitude of calculated branching ratios (β_R) given in Table 4, it is evident that the $^4G_{5/2} \rightarrow {}^6H_{7/2}$ and $^4G_{5/2} \rightarrow {}^6H_{9/2}$ transitions are more intense compared to other transitions and therefore the ZnAlBiB glasses may be used for the development of light emitting diodes (LEDs) in optical communication. The laser characteristic parameters such as branching ratio (β_R) and stimulated emission cross-section (σ_{se}) for the ZnAlBiBSm10 glass compared with other different glass hosts are given in Table 6 [23,31,38,40,47–50]. The higher β_R and σ_{se} values obtained for ZnAlBiBSm10 glass speaks the potentiality of that glass for visible lasing action at around 598 nm when compared with other reported glasses (Table 6). The optical gain is a critical parameter to predict the amplification of the laser medium. From the Table 5, it is evident that, the $^4G_{5/2} \rightarrow {}^6H_{7/2}$ transition of ZnAlBiBSm10 glass has the higher stimulated emission cross sections (σ_{se}), optical gain ($\sigma_{se} \times \tau_R$) and gain bandwidth values ($\sigma_{se} \times \Delta\lambda_P$) which could be a favorable feature for the development

Table 6
Comparison of branching ratio (β_R), stimulated emission cross section ($\sigma_{se} \times 10^{-22}$ cm^2) and quantum efficiency (η (%)) of $^4G_{5/2} \rightarrow {}^6H_{7/2}$ transition for sm^{3+} ion in different glass hosts.

Transition ($^4G_{5/2} \rightarrow {}^6H_{7/2}$)	β_R	σ_{se}	η (%)
ZnAlBiBSm10 (Present work)	0.54	15.8	77
LSG [23]	0.41	8.20	–
L5FBS [31]	0.46	5.74	–
N4BS [38]	0.43	8.78	74
30 mol% Pbo [40]	0.51	6.92	–
LCZSFB [47]	0.44	12.6	57
RTFP (LiTFP) [48]	0.53	6.91	–
Tellurite Glass [49]	0.49	3.6	–
ZFBP [51]	–	3.44	–

of visible laser at around 598 nm, which is highly useful in deep-water communications [51].

Emission lifetime analysis

Analysis of emission decay curves gives the information about lifetimes of an excited state of a rare-earth ion in any host composition. The decay curves of the $^4G_{5/2}$ fluorescent level of Sm^{3+} ions in ZnAlBiB glasses with different concentration of Sm^{3+} ions have been carried out at room temperature by controlling the emission at 598 nm corresponding to $^4G_{5/2} \rightarrow {}^6H_{7/2}$ transition upon excitation at 401 nm. Fig. 6 shows the emission decay profiles of 598 nm orange–red emission for all the glasses corresponding to $^4G_{5/2} \rightarrow {}^6H_{7/2}$ transition. An excited rare earth ion may relax to the ground state through radiative transition and/or phonon emission or by transferring the excess energy to a nearby rare earth ion for a combination of relaxation. From Fig. 6, it is observed that the decay profiles of $^4G_{5/2}$ level are single exponential for lower concentration and non-exponential for higher concentration of sm^{3+} ion. The experimental lifetimes (τ_{exp}) measured from the decay curves for $^4G_{5/2}$ levels are presented in Table 5 along with radiative lifetimes (τ_R). The τ_{exp} values for $^4G_{5/2}$ level found to be decreasing with increasing the concentration of sm^{3+} ions. The decrease in the experimental lifetime values and the conversion of decay curves from exponential to non- exponential with increasing concentration of sm^{3+} ions is the characteristic feature for the existence of concentration quenching. These results are also in consistent with the concentration dependent emission spectral study (Fig. 5). The luminescence intensity quenching and non-exponential behavior of decay curves beyond 1 mol% of sm^{3+} ion concentration in the titled glasses are due to non radiative energy transfer between sm^{3+} ions.

From Table 5, it can be observed that the experimental lifetimes (τ_{exp}) are found to be less than radiative lifetimes (τ_R). The deviation of the experimental lifetimes (τ_{exp}) from the radiative lifetimes (τ_R) obtained by using the JO theory was probably not related to the multi-phonon relaxation, considering the larger energy gap between $^4G_{5/2}$ level and the next lower level $^6F_{11/2}$ compared to the phonon energy. The discrepancy of lifetimes between experimental and radiative lifetime values is rather ascribed to the non-radiative energy transfer through cross-relaxation, which increases with the concentration of Sm^{3+} ions [44].

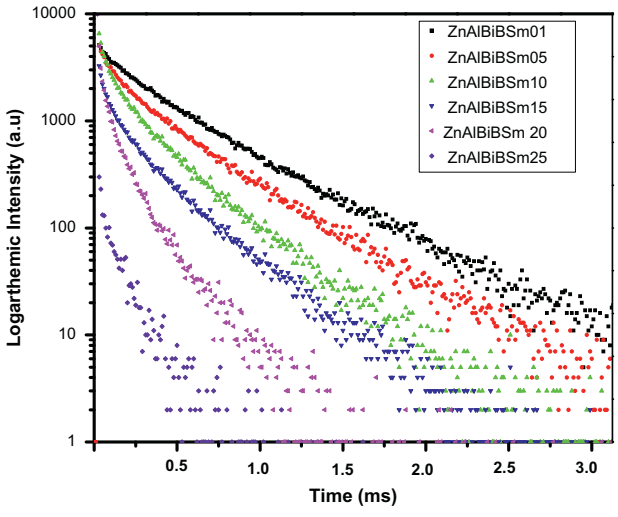


Fig. 6. Decay curves of the prominent emission transition at 598 nm for Sm^{3+} ions doped ZnAlBiB glasses.

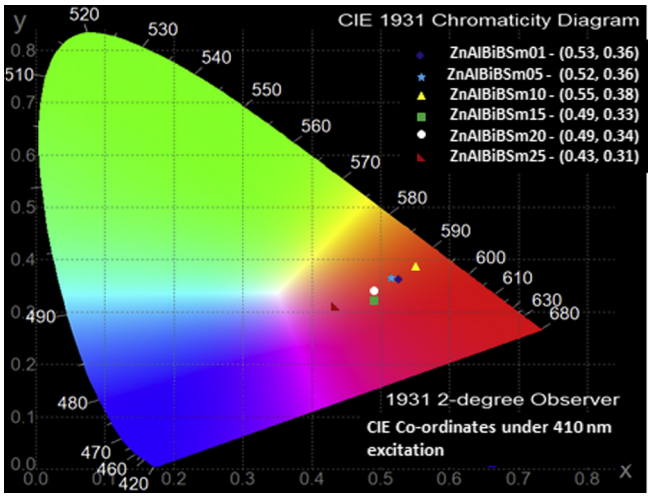


Fig. 7. CIE color chromaticity diagram for Sm^{3+}ions doped ZnAlBiB glasses. (For interpretation of the references to color in this figure legend, the reader is referred to the web version of this article.)

In case of RE^{3+} ions, luminescence quantum efficiency (η) is the ratio of measured lifetime (τ_{exp}) to the radiative lifetime (τ_R), i.e.,

$$\eta = \frac{\tau_{exp}}{\tau_R} \times 100\%$$

The quantum efficiency thus calculated for all the glasses are given in Table 5. Among all the glasses studied, the quantum efficiency obtained for ZnAlBiBSm10 was found to be 77% for $^4G_{5/2}$ level. Such quantum efficiency value observed for ZnAlBiBSm10 glass compared with other glasses are given in Table 6 [23,31,38,40,47–50]. From Table 6, it is evident that ZnAlBiBSm10 glass is competent for visible laser emission at 598 nm with its quantum efficiency value more than the reported glasses.

CIE chromaticity coordinates

In order to understand the color emitted by the Sm^{3+} doped ZnAlBiB glasses, the chromaticity coordinates values are evaluated from the emission spectra following the procedure outlined in the commission International de l'Eclaiage France CIE system [51]. The emission spectra obtained by intrinsic excitation have mainly three parts. A small part spread in green region, a main part spread in the orange to red region and a third part spread in red region. Out of these parts, a main part which is spread in the orange to red is more intense than other parts. Fig. 7 represents the CIE plot with color coordinates of Sm^{3+} in ZnAlBiB glasses when excited at 410 nm wavelength using CW laser. From Fig. 7 it is observed that the CIE coordinates for all the ZnAlBiB glasses falls in orange–red region. As shown in Fig. 7, among all the glasses, the CIE chromaticity coordinates for ZnAlBiBSm10 glass is much nearer to the orange–red region. This result is in consistent with the con-focal images recorded for ZnAlBiBSm10 glass (Fig. 5). This indicates that the present titled glasses are potential materials for the familiar cation of red component of white light emitting diodes in solid state lighting applications.

Conclusion

Zinc Alumino Bismuth Borate glasses doped with different concentration of Sm^{3+} ions were prepared by the conventional melt quenching technique. The JO parameters evaluated from the measured absorption spectra of these glasses are used to calculate radiative properties of Sm^{3+} ions. The excitation spectra for the titled

glasses exhibit several excitation bands in visible region ranging from 325 to 500 nm. This indicates that, the commercial UV-blue laser diodes and bluish-green light emitting diodes are suitable as pumping sources for the titled glasses. The emission spectra recorded by monitoring the excitation at 410 nm using CW laser in the titled glasses gives four emission bands in visible region. Among them $^4G_{5/2} \rightarrow {}^6H_{7/2}$ is more intense and $^4G_{5/2} \rightarrow {}^6H_{7/2}$ is moderate for all the glasses and are responsible for the distinct orange–red emission. This result is in consistent with the con-focal photoluminescence images recorded for all ZnAlBiB glasses. Based on the emission spectra, high stimulated emission cross-sections, branching ratios and quantum efficiencies observed for $^4G_{5/2} \rightarrow {}^6H_{7/2}$ transition for all these glasses suggest the feasibility of using these materials as visible lasers in orange–red (598 nm) visible region. The CIE chromaticity coordinates evaluated from the emission spectra for all these glasses also confirms the same thing. From the measured emission cross-sections, branching radios, quantum efficiencies, con-focal photoluminescence images and CIE chromaticity coordinates evaluated, it was concluded that 1 mol% of Sm^{3+} ion concentration is optimum in ZnAlBiB glasses for the development of orange–red visible lasers (598 nm) in principle.

Acknowledgements

Two of the authors, Swapna Koneru (File No. SR/WOS-A/PS-35/2011) and Mahamuda Shaik, (File No. SR/WOS-A/PS-53/2011) are highly grateful to the Department of Science and Technology (DST), Govt. of India, New Delhi, for providing financial assistance in the form of women scientist scheme (WOS-A) to carry their research work. This work is partly supported by High-impact Research initiative of IIT-Delhi, UK-India Education Research Initiative (UKIERI) and DST, Govt. of India, New Delhi.

References

[1] A.A. Kaminskii, Ann. Phys. FR 16 (1991) 639–706.
[2] G. Blasse, B.C. Grabmaier, Luminescent Materials, vol. 232, Springer Verlag, Berlin, 1994.
[3] M.J. Weber, W.M. Yen, P.M. Selzer, Springer, Berlin, 1986, pp. 189–239.
[4] E. Malchukova, B. Boizot, D. Ghaleb, G. Petite, Nucl. Instru. Methods Phys. Res. A 537 (2005) 411–414.
[5] F. Vetrone, J.C. Boyer, J.A. Capobianco, A. Sepghini, M. Bettinelli, Appl. Phys. Lett. 80 (2002) 1752–1754.
[6] P.R. Biju, G. Jose, V. Thomas, V.P.N. Nampoori, N.V. Unnikrishnan, Opt. Mater. 24 (2004) 671–677.
[7] S. Schweizer, L.W. Hobbs, M. Secu, J.M. spaeth, A. Edgar, G.V.M. Williams, Appl. Phys. Lett. 83 (2003) 449–451.
[8] M.R. Reddy, S.B. Raju, N. Veeraiah, J. Phys. Chem. Solid 61 (2000) 1567–1571.
[9] Y. C Ratnakaram, D. Thirupathi naidu, A.V. Jayakumar, N.O. Gopal, Physica B 358 (2005) 296–307.
[10] V. Lavin, P. Babu, C.K. Jayasankar, I. R Martin, V.D. Rodriguez, J. Chem. Phys. 115 (2001) 10935–10944.
[11] K. Gerth, C. Russel, J. Non-Cryst. Solids 221 (1997) 10–17.
[12] S. Jiang, T. Luo, M. Myers, J. Myers, J. Lucas, N. Peyghambarian, *Proc. SPIE* 3280 (1998) 2–13.
[13] D. Jain, V. Sudharsan, R.K. Vatsa, C.G.S. Pillai, J. Lumin. 129 (2009) 439–443.
[14] V. Venkatramu, P. Babu, C.K. Jayasankar, Th. Troester, W. Sievers, G. Wortmann, Opt. Mater. 29 (2007) 1429–1439.
[15] G. Lakshminarayana, S. Buddhudu, Physica B 373 (2006) 100–106.
[16] M.C. Fearries, P.R. Morkel, J.E. Townsend, Electron. Lett. 24 (1988) 709–711.
[17] G. Turky, M. Dawy, Mater. Chem. Phys. 77 (2002) 48–59.
[18] B.C. Jamalaiah, J. Suresh Kumar, A. Mohan Babu, T. Suhasini, L. Rama Moorthy, J. Lumin. 129 (2009) 363–369.
[19] K. Marimuthu, R.T. Karunakaran, S. Surendra Babu, G. Muralidharan, S. Arumugam, C.K. Jayasankar, Solid State Sci. 11 (2009) 1297–1302.
[20] K. Mahesvaran, K. Linganna, K. Marimuthu, J. Lumin. 131 (2011) 2746–2753.
[21] T. Minami, Y. Ikeda, M. Tanaka, J. Non-Cryst. Solids 52 (1982) 159–169.
[22] F.A. Khalifa, H.A. El-Batal, A. Azooz, Ind. J. Pure Appl. Phys. 36 (1998) 314–318.
[23] I. Arul Rayappan, K. Selvaraju, K. Marimuthu, Physica B 406 (2011) 548–555.
[24] H. Ebendorff-Heideprem, W. Seeber, D. Ehrt, J. Non-Cryst. Solids 163 (1993) 74–80.
[25] T. Suhasini, B.C. Jamalaiah, T. Chengaiah, J. Suresh Kumar, L. Rama Moorthy, Physica B 407 (2012) 523–527.
[26] B.B. Kale, A. Jha, S.K. Apte, P.V. Adhyapak, D.P. Amalnerkar, Mater. Chem. Phys. 78 (2002) 330–336.
[27] T.I. Suratwala, R.A. Steele, G.D. Wilke, J.H. Campbell, K. Takeuchi, J. Non-Cryst. Solids 263 & 264 (2000) 213–227.
[28] A. Mohan Babu, B.C. Jamalaiah, T. Sasikala, S.A. Saleem, L. Rama Moorthy, J. Alloys Compos. 509 (2011) 4743–4747.
[29] C.K. Jorgensen, B.R. Judd, Mol. Phys. 8 (1964) 281–290.
[30] A.S. Rao, Y.N. Ahammed, R.R. Reddy, T.V.R. Rao, Opt. Mater. 10 (1998) 245–252.
[31] C.K. Jayasankar, P. Babu, J. Alloys Compd. 307 (2000) 82–95.
[32] R. Praveena, V. Venkatramu, P. Babu, C.K. Jayasankar, Physica B 403 (2008) 3527–3534.
[33] B.R. Judd, Phys. Rev. 127 (1962) 750–761.
[34] G.S. Ofelt, J. Chem. Phys. 37 (1962) 511–520.
[35] Sk. Mahamuda, K. Swapna, A. Srinivasa Rao, M. Jayasimhadri, T. Sasikala, K. Pavani, L. Rama Moorthy, J. Phys. Chem. Solids 74 (2013) 308–1315.
[36] C.K. Jørgensen, B.R. Judd, Mol. Phys. 8 (1964) 281–290.
[37] C.K. Jørgensen, R. Reisfeld, J. Less Common Met. 93 (1983) 107–112.
[38] S. Shanmuga Sundari, K. Marimuthu, M. Sivraman, S. Surendra Babu, J. Lumin. 130 (2010) 313–1319.
[39] S. Sailaja, C. Nageswara Raju, C. Adinarayana Reddy, B. Deva Prasad Raju, Young-Dahl Jho, B. Sudhakar Reddy, J. Mol. Struct. 1038 (2013) 29–34.
[40] P. Srivastav, S.B. Rai, D.K. Rai, Spectrochim. Acta Part A 60 (2004) 637–642.
[41] B.J. Chen, L.F. Shen, E.Y.B. Pun, H. Lin, Opt. Express 20 (2012) 879–889.
[42] K. Selvaraju, K. Marimuth, J. Alloys Compd. 553 (2013) 273–281.
[43] A. Kurita, T. Kushida, T. Izumitani, M. Matsukawa, Opt. Lett. 19 (1994) 314–316.
[44] O. Ravi, C. Madhukar Reddy, L. Manoj, B. Deva Prasad Raju, J. Mol. Struct. 1029 (2012) 53–59.
[45] R.D. Peakcock, Struct-Bond 22 (1975) 83–122.
[46] J.L. Adam, W.A. Sibley, J. Non-Cryst. Solids 76 (1985) 267–279.
[47] C. Madhukar Reddy, G.R. Dillip, K. Mallikarjuna, Sd. Zulifiqar Ali Ahamed, B. Sudhakar Reddy, B. Deva Prasad Raju, J. Lumin. 131 (2011) 1368–1375.
[48] M. Jayasimhadri, L.R. Moorthy, S.A. Saleam, R.V.S.S.N. Ravi Kumar, Spectrochimi. Acta Part A 64 (2006) 939–944.
[49] Akshaya Kumar, D.K. Rai, S.B. Rai, Spectrochim. Acta Part A 59 (2003) 917–925.
[50] Ki.-Soo. Lim, N. Vijaya, C.R. Kesavulu, C.K. Jayasankar, Opt. Mater. 35 (2013) 1557–1563.
[51] W.M. Yen, S. Shionoya, Phosphors, Hand Book, CRC Press, New York, 1999. p. 805.

Volume 2, Issue 4 (2014) 763-766 ISSN 2347 - 3258
International Journal of Advance Research and Innovation

Optimization of Production and Performance of Biodiesel through Optimization Techniques: A Review

Ashok Kumar Yadav [a], Amit Pal [b], Mohd. Emran Khan [c]
[a] Department of Mechanical Engineering, Raj Kumar Goal Institute of Technology, Ghaziabad, Uttar Pradesh, India
[b]Department of Mechanical Engineering, Delhi Technological University, New Delhi, India
[c] Department of Mechanical Engineering, Jamia Millia Islamia, Jamia Nagar, New Delhi, India

Article Info
Article history:
Received 20 October 2014
Received in revised form
10 November 2014
Accepted 20 November 2014
Available online 15 December 2014

Keywords
Biodiesel,
Engine Performance,
Transesterification,
Optimization Techniques

Abstract
Biodiesel is recently gaining importance as a substitute for petroleum based diesel mainly due to environmental considerations and depletion of vital resources like petroleum and coal. According to Indian petro fuel consumption scenario, the demand for petroleum diesel is increasing day by day hence there is a need to find out an appropriate solution may be biodiesel but the cost of biodiesel produced from vegetable oil through transesterification is higher than fossil fuel, because of high raw material cost. To minimize the biodiesel cost, in recent days, in most cases, NaOH is used as alkaline catalyst, because of its low cost and higher reaction rate. In this review the important process variables for esterification such as concentration of acid catalyst, alcohol/oil ratio, reaction time, temperature, and % of excess alcohol are optimized. The results are also verified with Ganetic Algoritham (GA) method and Taguchi method. Also summarized the research works in optimization of C. I. engineperformance and operating parameters for biodiesel fuel using optimization techniques.

1. Introduction

In recent times there has been an increase in the efforts to reduce the reliance on petroleum fuel for energy generation and transportation and attention is being focused on alternate fuels. Among the alternative fuel, biodiesel and diesohol have receive the much attention for diesel engine due to their advantages as the renewable, domestically produced energy resources and they are environment friendly because there is substantial reduction of unburnt hydrocarbon (UHC), Carbon monooxide (CO) and particulate matter (PM) when it is used in conventional diesel engine. Vegetable oils have been converted to biodiesel via a chemical process, known as transesterification process [1], Resulting fuel is biodiesel, a biodegradable and nontoxic renewable fuel. Furthermore, biodiesels have reduced viscosity, and improved volatility when compared to ordinary vegetable oil. Biodiesel can be produced either from edible or from non- edible oils. Most of the edible oils are produced from the crop land. The idea of using vegetable oil as fuel for diesel engines is not a new one. Rudolph Diesel used peanut oil as fuel in his engine at Paris Exposition of 1900. Inspite of the technical feasibility, vegetable oil as fuel could not get acceptance, as it was more expensive than petroleum fuels. Later various factors as stated earlier, renewed the interests of researchers in using vegetable oil as substitute fuel for diesel engines. In recent years, systematic efforts have been made by several researchers to use vegetable oils of Sunflower, Peanut, Soyabean, Rapeseed, Olive, Cottonseed, Jatropha, Pongamia, Rubber seed, Jojoba etc as alternate fuel for diesel. Many types of vegetable oils are edible in nature. Continuous use of them causes shortage of food supply and proves far expensive to be used as fuel at present [2]. More than 350 oil-bearing crops have been identified, of which only soyabean, palm, sunflower, safflower, cottonseed, rapeseed, and peanut oils are considered potential alternative fuels for diesel engines. Vegetable-oil fuels have not been acceptable because they are more expensive than petroleum fuels. However with recent increase in petroleum prices and uncertainties surrounding in the petroleum availability. Soybeans are commonly used in the United States, as food products, Soyabean oil turned out to be a primary source for biodiesel in that country. In Malaysia and Indonesia, palm oil is the source of biodiesel. In Europe, rapeseed is the source of biodiesel. In India and Southeast Asia, jatropha tree is the source of biodiesel. Major exporters of vegetable oil are Malaysia, Argentina, Indonesia, Philippines, and Brazil. Major importers of vegetable oils are China, Pakistan, Italy, and the United Kingdom. A few countries such as the Netherlands, Germany, the United States, and Singapore are both major exporters as well as importers of vegetable oils. The non-edible oils such as jatropha, microalgae, neem, karanja, rubber seed, mahua, silk cotton tree etc. are easily available in developing countries and are very economical compared to edible oil.

Corresponding Author,
E-mail address: ashokme015@gmail.com
All rights reserved: http://www.ijari.org

2. Production of Biodiesel from vegetable oil

Biodiesel can be produced by esterification followed by transesterification. The oils and fats are filtered and pre-processed to remove water and contaminants. If, free fatty acids are present, they can be removed or transformed into biodiesel using special pretreatment technologies. The pre-treated oils and fats are then mixed with an alcohol (usually methanol) and a catalyst (usually sodium methoxide). The oil molecules (triglycerides) are broken apart and reformed into esters and glycerol, which are thenseparated from each other and purified. The edible oils like soybean, sunflower, mustard, palm, cotton seeds, whose acid values are less than 3.0 are transesterified with methanol in the presence of sodium methoxide as catalyst. Non-edible oil like, Mahua,

karanja and jatropha oils having acid values more than 3.0 are undergoes esterification followed by transesterification. The methyl esters produced by these methods are analyzed to ascertain their suitability as diesel fuels.

3. Chemistry of Esterification and Transesterification

Esterification: In order to eliminate saponification reaction (formation of soap when FFA reacts with homogenous base catalyst) vegetable oil can be pretreated with acid catalyst, which esterifies free fatty acid to form esters of free fatty acid (biodiesel). This reaction is very much useful when raw material contains high percentage of free fatty acid (esterification of free fatty acid to form free acid esters). But this reaction is slower than base catalyzed transesterification reaction. The esterification reaction is given as shown in

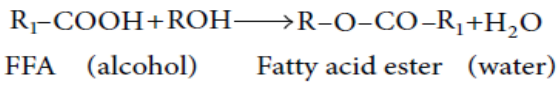


Fig: 1. Esterification Reaction

Esterification is the reaction of an acid with an alcohol in the presence of a catalyst to form an ester. The equation is expressed generally as: Generally, acid catalyst like sulfuric acid is employed. Esterification is a reversible reaction. Thus water produced must be removed to drive the reaction to the right to obtain a higher ester yield.

Transesterification: On the other hand is the displacement of the alcohol from anester by another alcohol in a process similar to hydrolysis, except that an alcohol is used instead of water. This reaction cleavage of an ester by an alcohol is more specifically called alcoholysis and is represented by the general equation:

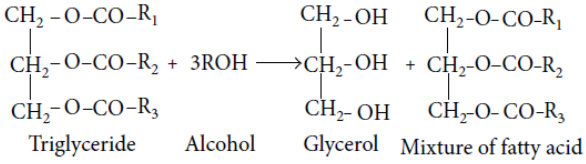


Fig: 2. Transesterification Reaction

In this case, a new ester is formed. Generally alkaline catalysts such as, Sodium hydroxide and Potassium hydroxide can also be used as catalysts. Transesterification is a general term. More specifically, if methanol is used, the reaction is termed methonolysis. Methanol is generally used because it is cheap, however other alcohols can also be used. Although the equation reflects the overall reaction, but the reaction usually consists of a series of consecutive reversible steps. For transesterification reaction a large number of potentially useful catalysts have been investigated as a means to enhance the reaction rate. Without added catalysts some degree of rearrangement can be obtained but only under extreme conditions of temperature and time, leading to undesirable effects such as isomerization, polymerization and decomposition. Apart from the generally preferred acid and alkaline catalysts, Sodium Methoxide and Alcolates, have been claimed to catalyze transesterification reactions. This catalyst has the advantages of reducing the reaction time and temperature, used in small quantity without darkening the color of the oil. Transesterification of vegetable oils using methanol and alkaline catalyst is the most commonly used processes for manufacture of methyl esters.

4. Process VariablesAffecting the Production of Biodiesel

The most important variables which influence the transesterification reaction are: reaction temperature, ratio of alcohol to vegetable oil, catalyst mixing intensity and purity of reactants.

4.1. Reaction Temperature

The literature has revealed that the rate of reaction is strongly influenced by the reaction temperature. However the reaction is conducted close to the boiling point of methanol (60 – 70 ^{0}C) at atmospheric pressure for a given time. Such mild reactionconditions require the removal of free fatty acids from the oil by refining or preesterification. Therefore degummed and de acidified oil is used as feedstock [12]. Pretreatment is not required if the reaction is carried out under high pressure (9000 kPa) and high temperature (240^{0}C), where simultaneous esterification and transesterification take place with maximum yield obtained at temperatures ranging from 60 – 80 ^{0}C at a molar ratio of 6:1 [3-5].

4.2. Ratio of Alcohol to Oil

Another important variable is molar ratio of alcohol to vegetable oil. As indicated earlier, the transesterification reaction requires 3 mol of alcohol per mole of triglyceride to give 3 mols of fatty esters and 1 mol of glycerol. In order to shift the reaction to the right, it is necessary to either use excess alcohol or remove one of the products from the reaction mixture. The second option is usually preferred for the reaction to proceed to completion. The reaction rate was found to be highest when 100% excess methanol was used. A molar ratio of 6:1 is normally used in industrial processes to obtain methyl ester yields higher i.e. 98% (w/w)[3].

4.3. Catalysts

Sodium alkoxides are the most efficient catalysts, although KOH and NaOH can also be used. Transmethylation occurs in the presence of both alkaline and acidic catalysts [5]. Being less corrosive to industrial equipment, alkaline catalysts are preferred in industrial processes. A concentration in the range of 0.5 – 1% (w/w) has been found to yield 94 – 99% conversion to vegetable oil esters [4], and further increase in catalyst concentration does not affect the conversion but adds extra cost, as the catalyst needs to be removed from the reaction mixture after completion of the reaction.

4.4. Mixing Intensity

It has been observed that during the transesterification reaction, the reactants initially form a two-phase liquid system. The mixing effect has been found to play a significant role in the slow rate of reaction. As phase separation ceases, mixing becomes insignificant. The effect of mixing on kinetics of the transesterification process forms the basis for process scale-up and design.

4.5. Purity of Reactants

Impurities in the oil affect the conversion level considerably. It is reported that about 65 – 84% conversion into esters using crude vegetable oils has been obtained as

compared to 94 – 97% yields refined oil under the same reaction conditions [3]. The freefatty acids in the crude oils have been found to interfere with the catalyst. This problem can be solved if the reaction is carried out under high temperature and pressure conditions.The important variables which influence the performance of engine, injection time, injection pressure and heat release rate on engine performance.

5. Optimization Techniques

Some of the researcher had work on the optimization of diesel engine performance and operating parameters using different technique as suitable software [6], as like Taguchi method, Matlab, Artificial Neural Network (ANN). These techniques are computationally efficient for optimization requiring hundreds of function evaluations; this saves cost and time in developing new models and methodologies for overall engine management [7]. For analyzing complex problems of emission analysis of biodiesels and their blends, artificial neural network is suitable, adaptable and flexible computing tool that can be used for diagnostic purposes. There by, time consuming, tedious and costly experiments can be avoided. An overview of applications of artificial neural networks (ANN) in the field of engine development described two back-propagation learning algorithms to predict the torque, power, specific fuel consumption, and smoke emission of diesel engine using different injection pressure and engine speed is given by Garg et al. [8]. Balajiganesh et al. [9] worked on the Optimization of Compression Ignition Engines through advanced artificial neural network using Mat lab. The engine is operated by using diesel and sunflower oil blends and calculate optimized performance as like indicated power, brake power, break mean effective pressure, indicated mean effective pressure and specific fuel consumption. Also Mudgal et al. [10] worked on the Prediction of Emissions from Biodiesel Fueled Transit Buses Using Artificial Neural Networks. Shivakumar et al. [11] had worked on the Experimental investigation on the Performance parameters and Exhaust emissions from the four strokes C.I. engine operated on honge methyl ester. Back-propagation algorithm was used to train the network. In this work they selected the inputs for the ANN are blend percentage (B), load percentage (W), and the compression ratio (CR). The output parameters from the ANN are Brake thermal efficiency (BTE), Brake specific energy consumption, (BSEC), Exhaust gas Temperature and the emissions which include Oxides of nitrogen (NOx), Smoke (SN), Unburnt Hydrocarbon (UBHC), and Carbon Monoxide (CO). Lastly he had investigated the ANN results; showed good correlation between the ANN predicted values and the desired values for various engine performance values and the exhaust emissions. Some researcher had worked on the taguchi approach for the optimization of performance and operating parameters of the diesel engine. For example, Sivarama krishnan and Ravikumar [13] worked on the optimization of the direct injection (DI) single cylinder diesel engine with respect to brake power, fuel economy and emissions through experimental investigations and DOE methods. In the experimental investigations conducted on a single cylinder DI diesel engine using Eucalyptus oil mixed with diesel fuel. Taguchi method of optimization predicted optimum level of parameters within 9 trials and the 40Eu blend found working satisfactorily at optimum setting, also in this work he had investigated the NOx emission found while working with 40Eu blend at optimum level. Here for optimization purpose he had use the orthogonal array with four columns and nine rows were used to design Taguchi experiment. Also lastly he had investigate the 50% smoke reduction was achieved with 40Eu operation [14]. The purpose of analysis of variance (ANOVA) is to investigate the percentage contribution of variance over the response parameter [14]. Lastly he had investigated the Taguchi method of optimization predicted optimum level of parameters within working satisfactorily at optimum setting. Some researchers states that the taguchi is most effective method for optimization of diesel engine performance parameters. For example, [14, 15] in this work consist an experimental study that involves an application of the Taguchi method and grey relational analysis to determine the optimum factor level to obtain optimum multiple performance characteristics of a diesel engine run with different low-percentage thumba biodiesel-diesel blends [16]. Taguchi method of optimization predicted optimum level of parameters within 9 trials and the 40 Turpentine blend found working satisfactorily at optimum setting. Lastly he proved that the blending of turpentine with diesel fuel up to 40% increases the engine Performance without much more effecton emission.

6. Conclusion

Biodiesel produced from vegetable oil (edible and non edible oil) renewable sources, it is a more sustainable source of energy and it will be play an increasingly significant role in providing the energy requirements for transportation. The Properties of biodiesel closely related to diesel fuel. The use of biodiesel will lead to loss in engine power mainly due to the reduction in heating value of biodiesel compared to diesel fuel. Increase in biodiesel fuel consumption, due to low heating value and high density and viscosity of biodiesel, has been found. PM emissions HC, CO emissions for biodiesel are significantly reduced, compared with diesel fuel. But NOx emissions may increases when using the biodiesel, this increase is mainly due to higher oxygen content for biodiesel. From the literature survey it can be concluded that the blends of biodiesel with small Content by volume could replace diesel in order to help in controlling air pollution and improving engine performance of power and economy of engine when using biodiesel blending with diesel fuel. From the literature it may concluded that the Optimization of C.I. engine performance and operating parameters through different software is most suitable technique. Also it is more accurate technique and less time consuming as compaired to experimental method. Use of Artificial Neural networks for optimizing the C.I Engine parameters is most suitable technique. Therefore ANN will be a very good tool to optimize engines parameters in the future. Also the taguchi method can be effectively used for the investigation of multiple performance characteristics of a diesel engine.

Reference

[1] Jon Van Gerpen, Biodiesel processing and production, ElsevierFuel Processing Technology 86 (2005) 1097–1107
[2] S. Jaichandar, K. Annamalai, The status of Biodiesel as an Alternative Fuel for diesel engine, Journal of Sustainable Energy and Environment, 2, 2011, 71-75
[3] C. Carraretto, A. Macor, A. Mirandola, A. Stoppato, S. Tonon, Biodiesel as alternative fuel : Experimental analysis and energetic evaluations, Energy, 29, 2004, 2195-2211
[4] A. Abraham, Artificial Neural Networks, John Wiley & Sons, 2005
[5] Neural Networks: A Comprehensive Foundation (2nd Edition)
[6] M. Venkatraman, G. Devaradjane, Computer Modeling of a CI Engine for Optimization of Operating Parameters Such asCompression Ratio, Injection Timing and Injection Pressure for Better Performance and Emission Using Diesel -Diesel BiodieselBlends, American Journal of Applied Sciences, 8, 2011, 897-902
[7] R. Manjunatha, P. Badari Narayana, K. Hema Chandra Reddy, Application of Artificial Neural Networks for Emission Modelling ofBiodiesels for a C.I Engine under Varying Operating Conditions, modern applied science, 4, 2010
[8] A. Bhaskar Garg, P. Diwan, M. Saxena, Artificial Neural Networks based Methodologies for Optimization of EngineOperations, International Journal of Scientific & Engineering Research, 2012
[9] N. Balajiganesh, B. Chandra Mohan Reddy, Optimization of C.I Engine Parameters Using Artificial Neural', International Journal ofMechanical and Industrial Engineering (IJMIE), 1(2), 2011
[10] A. Mudgal, K. Gopalakrishnan, S. Hallmark, Prediction of Emissions from Biodiesel Fueled Transit Buses using Artificial Neural Networks, International Journal for Traffic and Transport Engineering, 2011
[11] Shivakumar, Srinivas Pai P., Shrinivasa, B. R Rao, B. S. Samaga, Performance and Emission Characteristics of a 4 Stroke C.I.Engine operated on Honge Methyl Ester Using Artificial Neural Network, ARPN Journal of Engineering and Applied Sciences, 2010
[12] Yusuf Cay, Ademcicek, Fuat Kara, SelamiSagiroglu, Prediction of Engine Performance for an Alternative Fuel Using ArtificialNeural Network, Applied hermal Engineering, Elsevier, 2012
[13] K. Sivaramakrishnan, P. Ravikumar, Performance Optimization Karanja Biodiesel Engine Using Taguchi Approach and Multiple Regressions, ARPN Journal of Engineering and Applied Sciences, 2012
[14] A. Karnwal, M. M. Hasan, N. Kumar, A. N. Siddiquee, Z. A. Khan, Multi-Response Optimization of Diesel Engine PerformanceParameters Using Thumba Biodiesel-Diesel Blends by Applying the Taguchi Method and Grey Relational Analysis, International Journal of Automotive Technology, 12(4), 2011, 599−610
[15] D. Tamilvendhan, V. Ilangovan, R. Karthikeyan, Optimization of Engine Operating Parameters For Eucalyptus Oil Mixed Diesel Fueled DI Diesel Engine Using Taguchi Method, ARPN Journal of Engineering and Applied Sciences, 6, 2011
[16] R. Karthikeyan, N. Nallusamy, N. Alagumoorthi, Optimization of Engine Operating Parameters for Turpentine Mixed Diesel FueledDi Diesel Engine Using Taguchi Method, Modern Applied Science, 4, 2010

PHASE SHIFTING TRANSFORMERS CAN OPTIMIZES THE TRANSMISSION INFRASTRUCTURE, REDUCES THE LOSSES, IMPROVES GRID STABILITY, REDUCES CONGESTION, CHANGES THE ACTIVE & REACTIVE POWER FLOW BOTH IN MAGNITUDE AND DIRECTION



SHAGUFTA KHAN
Research Scholar
Delhi Technological University, Bawana



M.I. KHAN
Consultant, BHEL

www.IndianJournals.com
Members Copy, Not for Commercial Sale
Downloaded From IP - 14.139.251.107 on dated 22-Jan-2015

ABSTRACT

In most of the developed countries, there is a very small gap say nil in power generation and the power consumption (Loads connected) and therefore Transmission networks are also not growing much. Little bit addition of small renewable generation or replacement of the aged generation do not justify the addition of transmission network. It is therefore necessary to use the existing network exploiting new devices at meager cost, however the scenario in developing countries is entirely different. Developing countries are struggling to get the power at any cost and have no time to think about the optimization. Any way the increase in the transmission / distribution infra structure will pave the way over a period of time when there will be no right of way left to develop or will not be so easy to develop.

Considering Indian Power System which is growing with a rapid pace and another 100000 MW is planned to be added in next 5 year plan. With the result, the transmission & distribution has to increase many fold. The optimal use of existing infrastructure needs to be done in order to contain investment. It is therefore necessary to load the existing lines to optimal capacity rather than providing the additional corridor where ever it is not absolutely necessary. For reliability reasons in critical areas providing additional transmission corridor can not be ignored. Overloading of subsystem in a power system some times may pose stability issues, which may lead to unwanted tripping, equipment failures which will result long repair/ replacement cycle and heavy revenue losses. Under these conditions, to ensure economical and reliable operation of the grid, power through the lines should be controlled within their capabilities. Application of HVDC systems becomes much simpler to achieve control of both active and reactive power however at all situations the economy may not justify such applications. Application of FACTS(Flexible Alternating Current Transmission Systems) devices could find its place, which are the off shoots of HVDC systems. Most of such devices are location specific and therefore should be carefully chosen and rated for the specific requirements Phase shifting transformer is one of the device from FACTS family, which can be used for power flow control in a network. For demonstrating the ability of the phase shifting transformer in regulating the power flow in an alternate transmission network, various cases involving simulation of Maharashtra zone, Uttar Pradesh zone, a part of Andhra Pradesh zone and inter regional power control of the Indian grid are considered. From power flow solution, various overloaded lines and the alternate under loaded lines are identified. Different cases are simulated to regulate the power using phase shifting transformer in to the actual network of the Indian Grid.

Index Terms – *Phase shifting transformer, FACTS Family power flow control, over loaded lines, PSS/E, EMTDC PSCAD*

1. INTRODUCTION

Indian economy is growing at a fast pace. GDP is expected to grow at a rate of 8 to 10%. Infrastructure including power is the main factor for the growth. The demand for power is increasing steadily. The estimated peak demand amounting to 226 GW in 2016-17 is expected to grow to 592 GW in 2031-32. Thus, the installed capacity of 306 GW in 2016-17 is expected to be 778 GW by 2031.-32 considering GDP growth at 8%. To meet this target, Government has decided to develop large capacity power projects at national level. Already seven Ultra Mega Power Projects (UMPP) of 4000 MW each have been identified and most of them are placed into service. They are all located at pit head such as Sasan in M. P., Akaltara in Chattisgarh and Orissa and at coastal sites in Andhra Pradesh, Gujarat, Maharashtra and Karnataka[1].

Transmission grid has a key function of transporting the bulk power from generation centers to the load centers. Transmission planning has to be done in such a way that besides conserving right of way for new lines, optimum utilization of existing lines has to be made.

Physical path between generation and load centers for power transmission is a group of alternate paths. There could be uneven loading of parallel transmission lines due to different impedances caused by the tower geometry, conductor sizing, number of sub-conductors and line length. The distribution of the power flow between two parallel lines is dictated by their impedances. The line with the smaller impedance carries more power and vice versa. In most situations, one of the two lines will be operating well below its nominal rating because otherwise parallel line with lower impedance would be overloaded[2].

Due to uneven loading of interconnectors in meshed networks, the total power transmission from generation to load center, is lower than expected when looking at the capacities of the lines.

In view of above, the power flows needed to BE controlled in order to achieve the optimum utilization of transmission lines capacity. Similar situation may arise when buses at different voltages are feeding the loads to the common load centers. In this case transmission lines connected to higher voltage bus will have less power losses for the same power flow compared with the transmission line operating at lower voltage level. A phase shifting transformer (PST) can be employed for power flow control in transmission lines / buses. Both the magnitude and direction of power flow can be controlled by varying the phase shift[3].

2. PHASE SHIFTING TRANSFORMER

The active power and reactive power transmission over a transmission line is given by the following equations:

$$P = \frac{|Vs|\ |Vr|}{X_L}\sin\delta \qquad ...(1)$$

$$Q = \frac{|Vs|\ |Vr|}{X_L}\left(\cos\delta - \frac{|Vr|}{|Vs|}\right) \qquad ...(2)$$

Where, Vs, Vr are sending end and receiving end voltages respectively. δ is power angle, XL is line reactance.

The active power is proportional to the voltages on the sending and receiving side and to the sine of the electrical angle between both sides; it is also inversely proportional to the line reactance. Altering the active power can be done by altering the voltages, but this has a bigger influence on the reactive power, so this method is not very effective.

The method discussed is the method of altering the electrical angle, as shown in Fig. 1. The PST is modeled as a reactance in series with a phase shift. The power flow through the line is increased by adding an angle α to the existing angle δ. The phase shift is controllable within certain limits[2]. Equation (1) becomes:

$$P = \frac{|Vs|\ |Vr|}{X_L + X_{PST}}\sin(\delta + \alpha) \qquad ...(3)$$

Where X_{PST} is leakage reactance of PST.

Fig. 2 shows connection diagram of conventional phase shifting transformer. It consists of an excitation transformer (ET), a boosting transformer (BT), and set of mechanical switches. Basic function of PST is to control power flow through the transmission line. This is accomplished by modifying the voltage phase angle by inserting a variable voltage (VB) in series with transmission line. This voltage is provided by the excitation transformer, amplitude is controlled by tap changer. The leakage reactance (XP_{ST}) of boosting transformer is in series with the line impedance[4].

3. MAIN CATEGORIES OF PSTS

PSTs can be designed in different forms and can be classified by these Characteristics:

- Direct PSTs are based on one three phase core. The phase shift obtained by connecting the winding in an appropriate manner.
- Indirect PSTs are based on construction with two separate transformers, one variable tap exciter to regulate the amplitude of the quadrature voltage and one series transformers to inject the quadrature voltage in the right phase.
- Asymmetrical PSTs create an output voltage with an altered phase angle and amplitude compared to the input voltage.

www.IndianJournals.com
Members Copy, Not for Commercial Sale
Downloaded from IP - 14.99.51.17 dated 22-Jan-2018

- Symmetrical PSTs create an output voltage with an altered phase angle compared to the input voltage, but with the same amplitude.

The combinations of these characteristics result in four categories of PSTs are following

1. Direct Asymmetrical PSTs
2. Direct Symmetrical PSTs
3. Indirect Asymmetrical PSTs
4. Indirect Symmetrical PSTs

For influencing the real power flow, the most often used are the quadrature symmetric or the quadrature nonsymmetric PST's.

A quadrature type phase shifter is a unit where the boost voltage, which creates the phase shift between source and load terminals, is perpendicular to the line voltage at one terminal, or to a combination of the line voltages at source and load terminals.

The term "symmetric" means, that under no load condition the voltage magnitude at load side is always equal to the voltage magnitude at the source side, independent from the phase angle.

Quadrature non-symmetric devices add a quadrature voltage to the input voltage. The output voltage is the vector sum of these two perpendicular voltages (therefore the output voltage is boosted by a small amount).

www.IndianJournals.com
Members Copy, Not for Commercial Sale
- 14.99.31.17 dated 23Jan2015

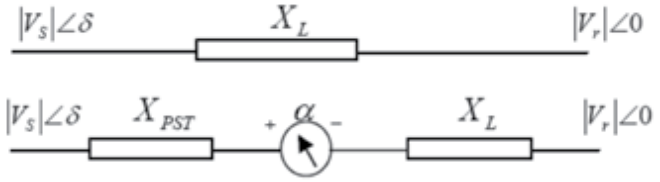


Fig.1 : Model of transmission line without and with a PST[2]

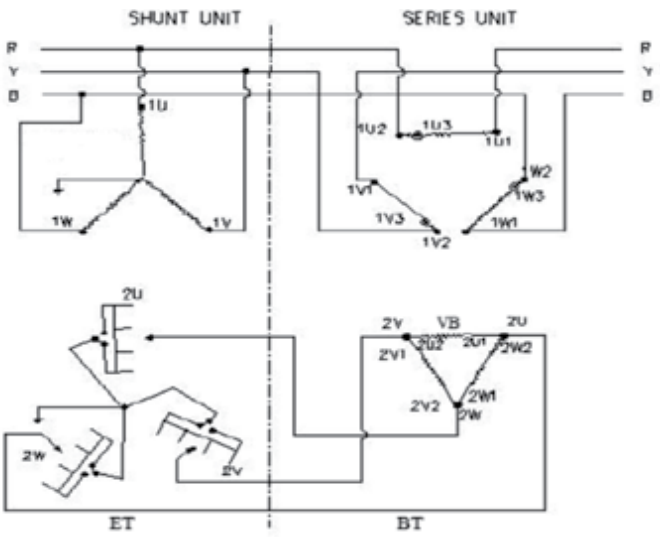


Fig. 2 : Connection diagram of phase shifting transformer[5]

Voltage phasor diagrams for different transformers are shown in the Fig. 3. The voltage control by classical regulating transformer is shown in Fig. 3a, the phase angle control by quadrature symmetric PST is shown in Fig. 3b and Fig. 3c shows the phase angle control by quadrature non-symmetric PST[6].

4. PST MODEL IN PSS/E SOFTWARE

PSS/E software is used for modeling the system. The equivalent circuit of Fig. 4 used to represent adjustable phase shifters. These units use tapped zigzag-connected windings to produce an adjustable phase shift between primary and secondary windings.

PSS/E allows the user to specify both the amplitude of winding ratios and phase shift of transformer. The phase shift angle is the angle by which winding 1 leads winding 2. PSS/E power flow solution includes logic for automatic adjustment of both turns ratio (t) and phase shift. It must be noted that the automatic adjustment of turns ratio does not alter phase shift and, more importantly, that PSS/E assumes that turns ratio is independent of adjustment of phase shift. Power distribution over the lines depends on the voltage shift between the voltage at transformer terminals as well as on the impedances[7].

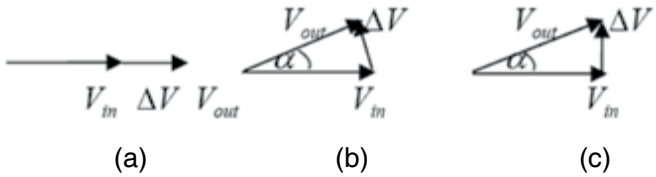


Fig. 3 : Voltage phasor diagrams for different transformers[6]

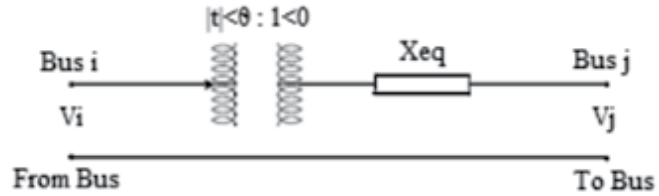


Fig. 4 : Transformer equivalent circuit representing phase shift[7]

5. SIMULATION AND RESULTS

Bulk power generation and heavy loads are situated far away from each other. Existing transmission lines get overloaded with the new generation planning; especially lines with lower impedance will get over loaded. In order to maintain reliability, new transmission lines need to be erected, which requires additional expenditure. Alternatively, the existing infrastructure could be used with optimization using FACTS devices[8]. The device should be placed either in lightly loaded line or in over loaded lines to optimize loading conditions. Many other aspects such as space availability need to be considered.

The aim of this paper is to study various applications of PST in power flow control. The system data for load flow studies consists of the data pertaining to transmission lines, generating transformers, interconnecting transformers, HVDC converters, generation, substation-wise load distribution, shunt compensation and series compensation etc. M/s Power Grid Corporation of India Limited (PGCIL) has provided the network steady state data of 2012 for peak load. The data are also verified by M/s Central Electricity Authority (CEA).

Various cases in Maharashtra zone, Uttar Pradesh zone and a part of Andhra Pradesh zone of Indian grid have been studied, to demonstrate the PST application in order to optimize the utilization of the existing infrastructure without over loading. Also various cases were studied for inter regional power control of Indian power system as an application of PST.

We used PSS/E software for simulation and prepared Single Line Diagrams (SLD) of interest of area as discussed and shown in further sections. In SLD, vertical thick lines represent buses and horizontal lines represent transmission lines. Green arrow and pink arrow indicate active power (MW) flow direction and reactive power flow (MVAR) direction respectively. Buses are given with their name and number on top of bus, voltage (kV) and power angle (degrees) at bottom of bus. Bold pink color represents over loaded lines.

www.IndianJournals.com
Members Copy, Not for Commercial Sale
Downloaded For IP - 14.139.225.10 on Sat, 22 Jan 2022

A. Maharashtra Zone

(1) *SLPR22 Region*

There is a 332 MW load connected at OSMNBD bus, which is being supplied by two lines, (1) from PARL22 to OSMNBD (2) from SLPR22 to OSMNBD. But, line between PARL22 & OSMNBD loaded to 280 MW (full load consideration is 200 MW) and line between SLPR22 & OSMNBD is loaded to 65.3 MW only as shown in Fig. 5.

We could make use of line between SLPR22 & OSMNBD to relieve the overloaded line between PARL22 & OSMNBD. A PST is introduced in line between SLPR22 & OSMNBD at SLPR22 bus and increased power in this line to 150 MW in the same direction. The line between PARL22 & OSMNBD got relieved from over load as shown in Fig. 6. From our study, it was found that 155 MVA, 0 to 15 degrees phase shift and 0.1 p. u. series impedance PST is required for power control in this case.

The very purpose of PST is to change the power angle of bus where it is connected. It can be observed that power angle can be controlled at specific location which will also have an effect in the entire network around PST.

The effect will be maximum at the bus in question and will be comparatively less on further buses. Hence, there will be incremental change in power flow scenario around further buses.

(2) *KOYNA Region*

At LPRSRM bus, 187.2 MW load is connected. The power is flowing from KOYNA2 through 220 kV line which is loaded to 268.9 MW. Balance power of 81.7 MW is flowing from LPRSRM to KNDLG2 as shown in Fig. 7. The capability of line between KOYNA2 to LPRSRM is only 200 MVA, which means, it is loaded to 145 %. In order to relieve this line from over loading, PST is proposed at LPRSRM bus, in the transmission line between LPRSRM and KNDLG2, which can load the line between LPRSRM and KNDLG2 line to 81.6 MW in reverse direction, there by relieving the line between KOYNA2 and LPRSRM to its capability as shown in Fig. 8. Also it is ensured that no other lines in the vicinity are getting overloaded. In this case, the rating of PST is finalized to 90 MVA, 0 to 18 degrees phase shift and 0.1 p. u. impedance of boosting transformer.

B. Uttar Pradesh Zone

We simulated Uttar Pradesh zone of Indian power system, identified an over loaded 400 kV line from UNNAO4 to PANKI4 as shown in Fig. 9. There are alternate lines, which are under loaded. If we limit the power flow in line between UNNAO4 & PANKI4 to $\leq$ 500 MW, it will get relieved from over load. Part of the power is diverted through alternate lines.

PST is considered in line between UNNAO4 & PANKI4 at UNNAO4. PST decreased the power in line between UNNAO4 & PANKI4 from 663.8 MW to 450 MW as shown in Fig. 10.

From our study, it was determined that 460 MVA, 0 to 5 degrees phase shift and 0.1 p. u. series impedance PST is required for power control, in this case.

C. Andhra Pradesh Zone

Generation of 500 MW is added at Kothagudem Thermal Power Station (KTPS) and a double circuit 400 kV line is being erected for evacuation of power. 220 kV network at KTPS is already in operation and it was observed that 3 lines are already over loaded. We can connect 400 kV bus and 220 kV bus using an ICT, study shows that power evacuation from 500 MW generation is further loading the 220 kV lines and 400 kV lines are not getting fully loaded, as shown in Fig. 11. In case PST is connected between 220 kV and 400 kV, 400 kV lines are better utilized and the over all losses are reduced. Also the over loaded 220 kV lines are relieved, as shown in Fig. 12.

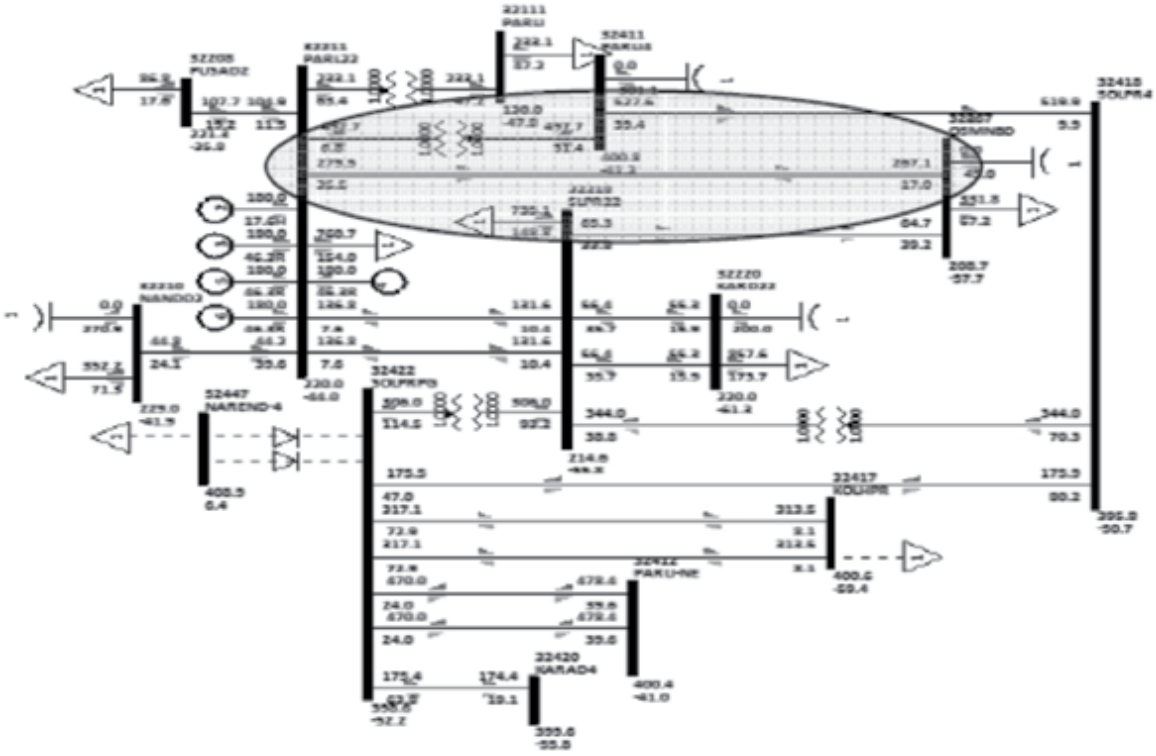


Fig. 5 : Network connected to SLPR22 bus without PST

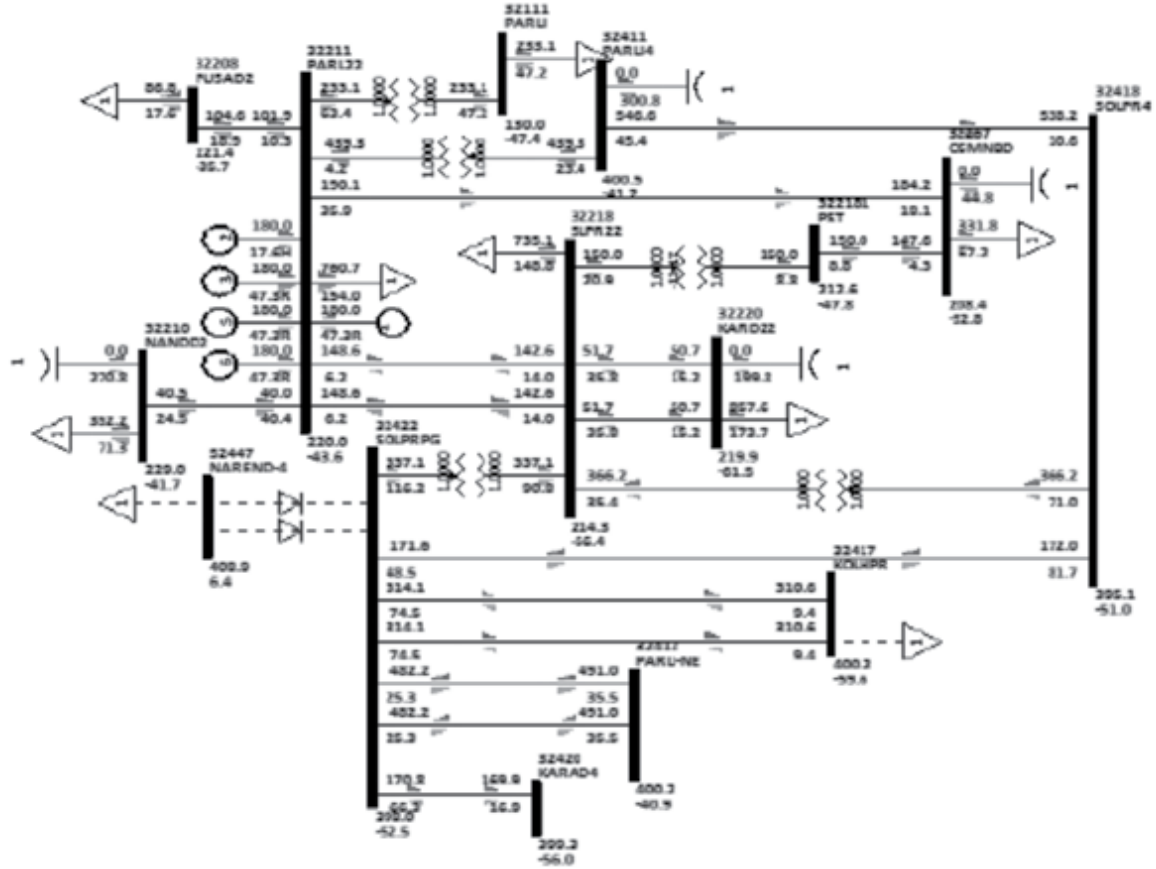


Fig. 6 : Network connected to SLPR22 bus with PST

www.IndianJournals.com
Members Copy, Not for Commercial Sale
Downloaded From IP - 14.139.251.107 on dated 22-Jan-2015

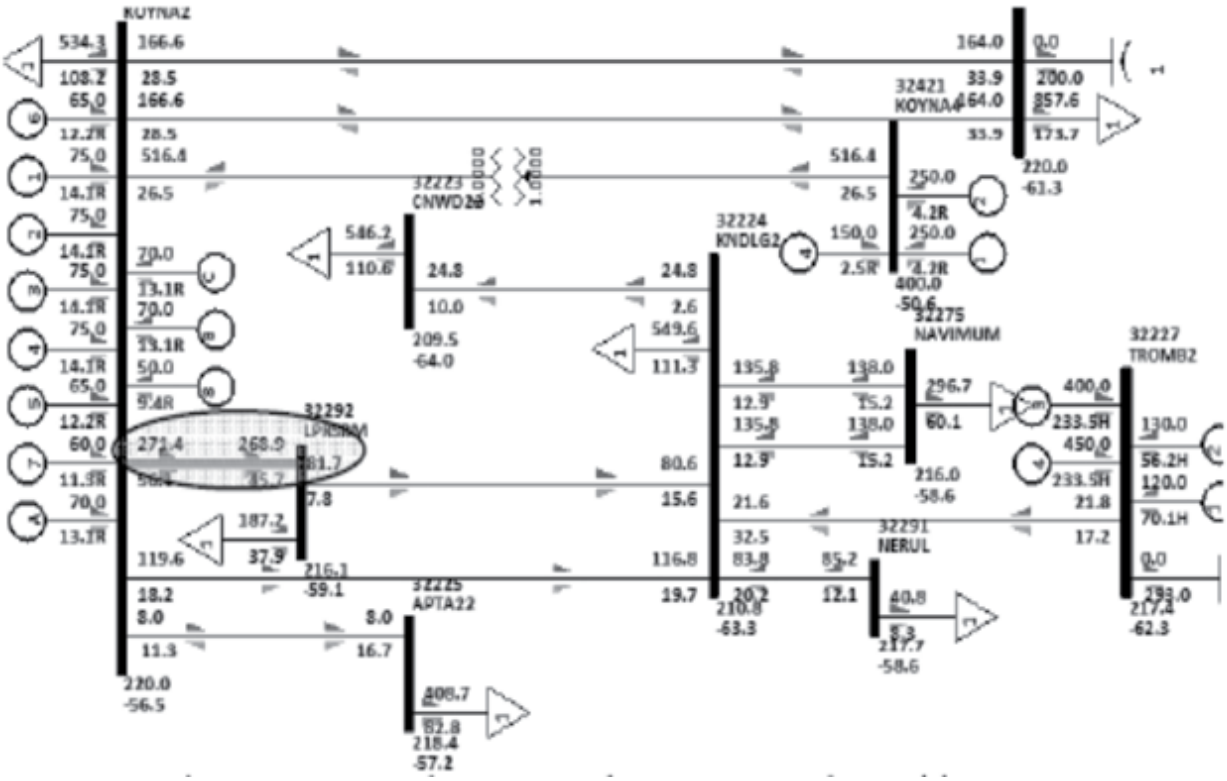


Fig. 7 : Network connected to LPRSRM bus without PST

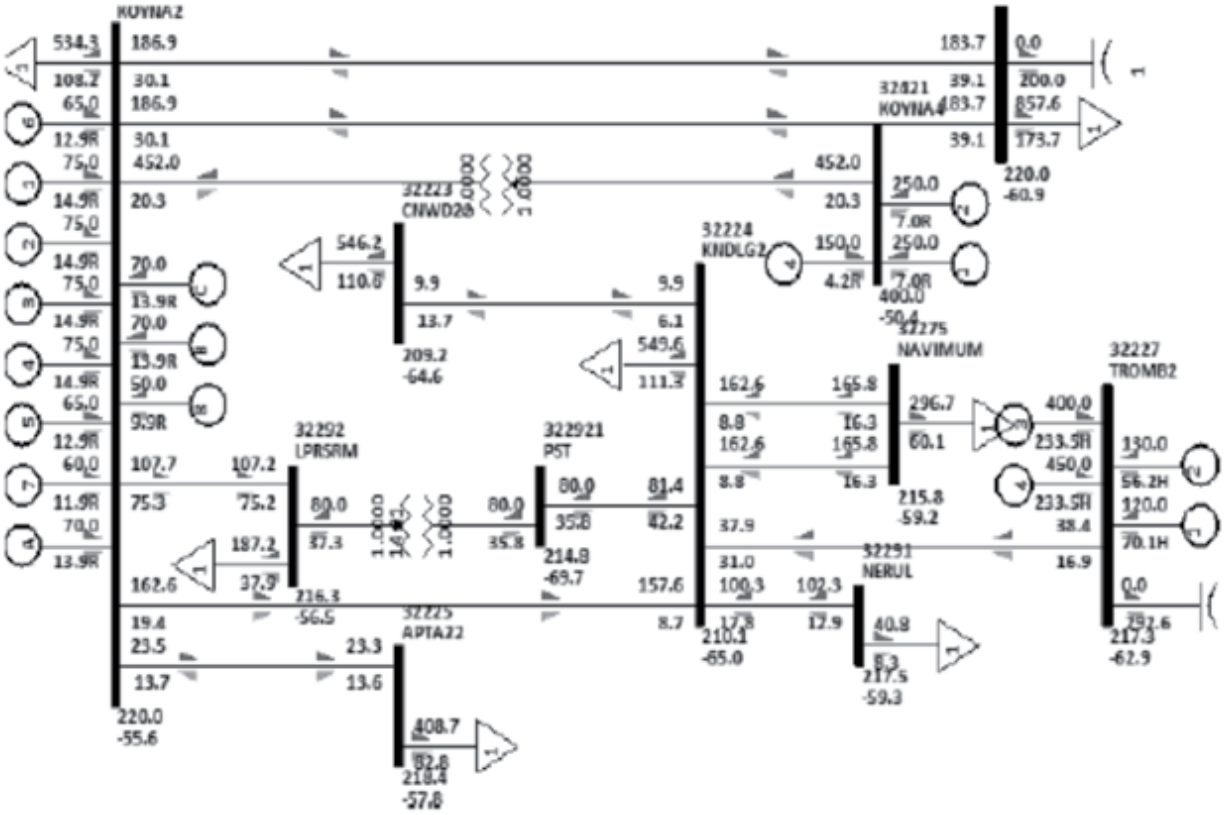


Fig. 8 : Network connected to LPRSRM bus with PST

www.IndianJournals.com
Members Copy, Not for Commercial Sale
Downloaded From IP - 14.139.251.107 on dated 22-Jan-2015

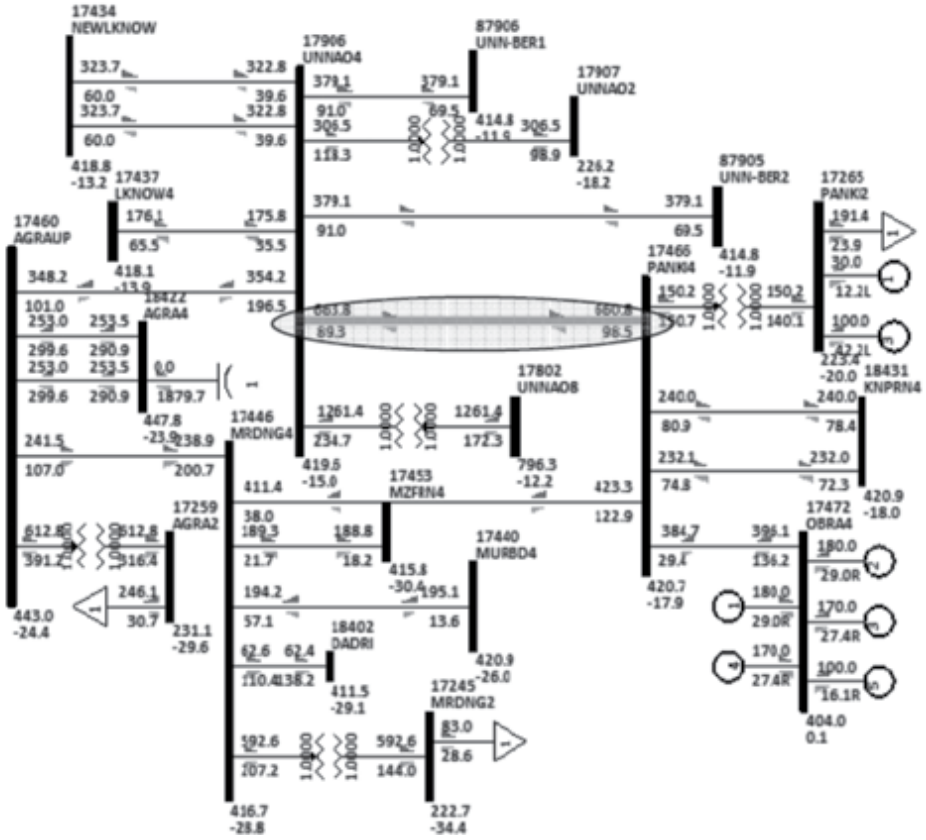


Fig. 9 : Network around UNNA04 bus without PST

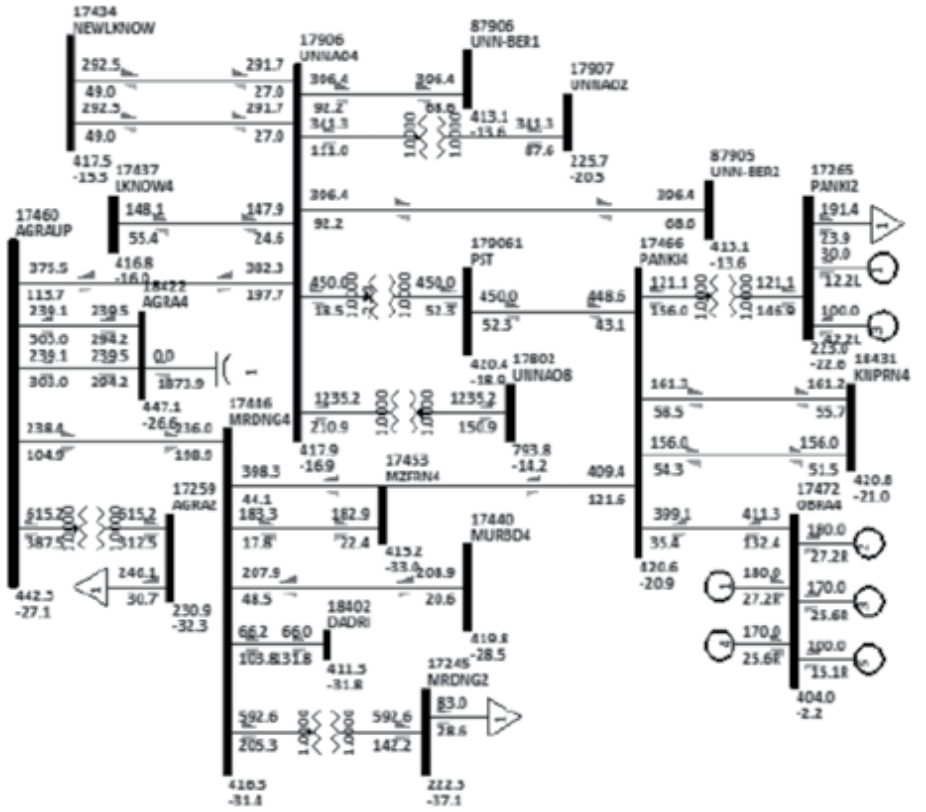


Fig. 10 : Network around UNNA04 bus with PST

www.IndianJournals.com
Members Copy, Not for Commercial Sale
Downloaded From IP - 14.139.251.107 on dated 22-Jan-2015

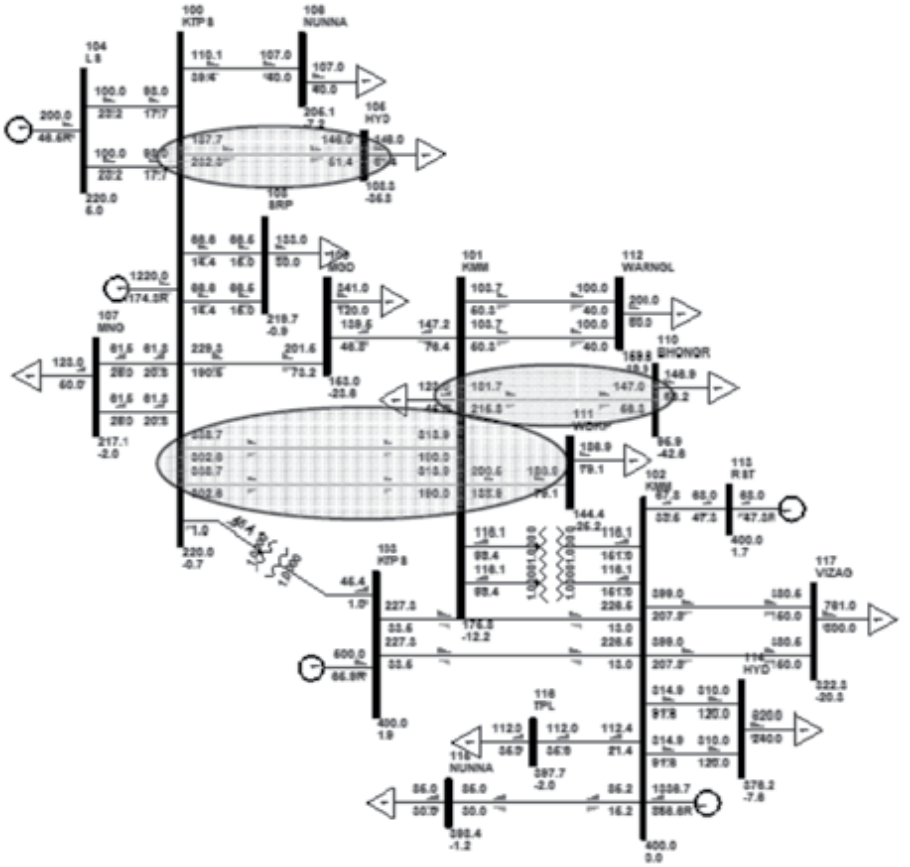


Fig. 11 : Network at KTPS without PST

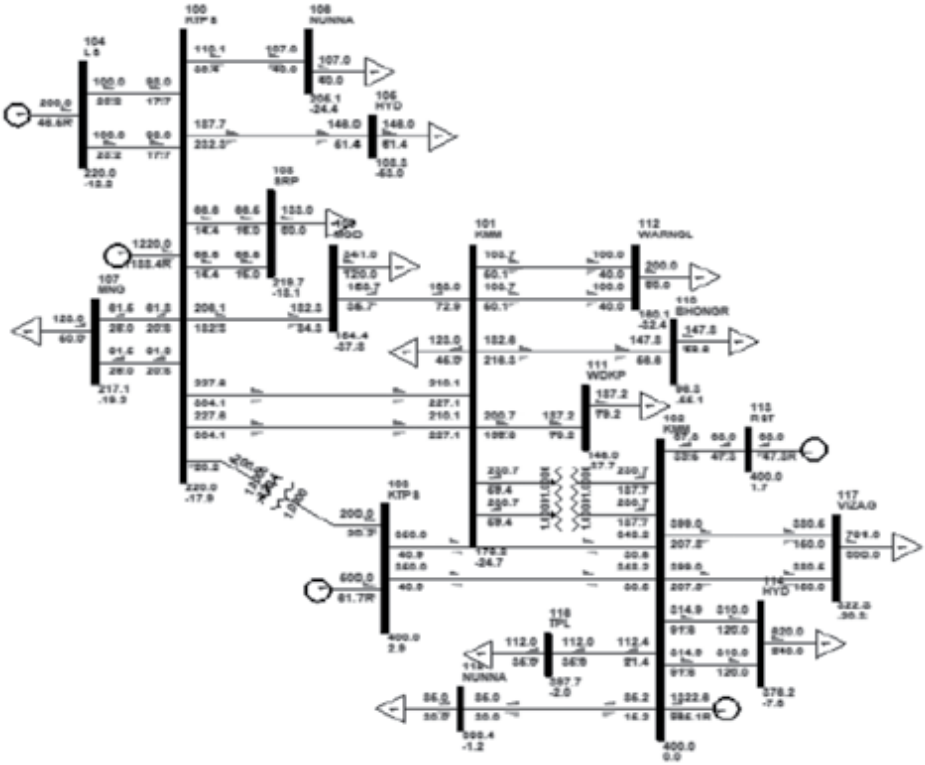


Fig. 12 : Network at KTPS with PST

www.IndianJournals.com
Members Copy, Not for Commercial Sale
Downloaded From IP - 14.139.251.107 on dated 22-Jan-2015

D. Inter Regional Power Control

Indian power system is separated into regions namely North, East, West, North-East and South. North, East, West and North-East regions are synchronized. Southern region still works as asynchronous link. From various literature survey, it is understood that PST can be used for border/regional power control. To demonstrate the PST application in Indian power system for regional power control, the following scenario is studied. The present power flow from Eastern region to Northern region is 10062 MW and Western region to Northern region is 5147 MW.

We studied the following cases for inter regional power control, In c ase (i), power control the power from Eastern region to Northern region is 11000 MW and Western region to Northern region is 4000 MW. In case (ii), power control the power from Eastern region to Northern region is 9000 MW and Western region to Northern region is 6000 MW.

(1) *Eastern Region to Northern Region*

There are two 765 kV lines, (1) Sasaram7 to Fathepr line is loaded to 1700 MW (2) Gaya to Balia line power flow is 1670 MW and 10 No.s of 400 kV lines loaded to 6712 MW between Northern & Eastern regions.

Upon introduction of PST in between Sasaram7 bus & Fathepr bus at Sasaram7, there is an increase of power flow to 3000 MW in the direction from Sasaram7 to Fathepr as shown in Fig. 13. But the overall power increased from East to North is by 201 MW only. In this study over load criteria is not considered.

PST is placed in between Gaya & Balia buses at Balia bus and observed an increase of power flow in direction from Gaya to Balia to 3000 MW as shown in Fig. 14. In this case, the overall power flow increased from Eastern to Northern region is only by 116 MW.

With the two PSTs in operation simultaneously as in earlier cases at Balia and at Sasaram7, then the total power flow in these lines is 6000 MW as shown in Fig. 15. But overall power increased from Eastern region to Northern region is only by 435 MW.

As we increase power flow in 765 kV lines, power flow in parallel 400 kV lines is getting reduced as shown in Table I. Net power flow from East to North is very less due to loop power flows.

Table 1 : Comparison of Power Flow from East to North with PST at Different Locations

Status/Location of PST	Power Flow from East to North (MW)		
	400 kV lines	765 kV lines	Total
No PST	6711.6	3350.2	10061.8
Sasaram7	6014	4249.1	10263.1
Balia	5701.6	4476.2	10177.8
Sasaram7 & Balia	4546.6	5949.5	10496.1

(2) *Western Region to Northern Region*

There are three 765 kV lines, (1) Gwalior[8] to Agra[8] D/C line loaded to 1920 MW (2) Gwalior[8] to Jaipr is loaded to 1256 MW and 4 Nos. 400 kV lines loaded to 1755 MW between West to North regions.

To achieve the desired power flow control another strategy was made to control the power flow from West to North. As three 765 kV lines, which are emanating from Gwalior, are carrying a total power of 3176 MW, A trial simulation is made to locate the PSTs at Gwalior bus for power control.

Case (i), power flow from Eastern region to Northern region is 11235 MW and from Western region to Northern region is 4086 MW is achieved as shown in Fig. 16 and Table 2. with the help of a 2000 MVA, -25 degrees phase shift PST Case (ii), desired power flow from Eastern region to Northern region is 9035 MW and from West to North is 6125 MW is achieved from our study as shown in Fig. 17 and tabulated in Table II. Approx. 2000 MVA, 25 degree phase shift PST is suitable for this application.

It is observed from the Table II, that as decrease in power in 765 kV lines by using PSTs from western region to Northern region, power in parallel 400 kV lines is increased in case (i) and vice versa for case (ii). However, net power control is achieved as desired.

In view of above, PST of 2000 MVA, ±25 degrees phase shift PST is suitable for inter regional power control as desired, which are mentioned in cases (i) and (ii).

Table 2 : Comparison of Inter Area Power Flow with PST at Gwalior

Corridor		Power (MW)		
		No PST	PSTs at Gwalior8	
			Case (ii)	Case (i)
East to North	400 kV lines	6711.6	6321	7571
	765 kV lines	3350.2	2714	3664
	Total	10061.8	9035	11235
West to North	400 kV lines	1755	1325	2286
	765 kV lines	3392	4800	1800
	Total	5147	6125	4086

E. Simulation of UP system using EMTDC/PS CAD

A transient simulation was also done using EMTDC// PS CAD for verification of case study of Uttar Pradesh Zone.

Fig.18 depicts the model of Indirect Asymmetrical PST wherein the single phase units have been considered for the power system application. It may be worth mention here that for power system application the size of the PST could be much bigger and therefore due to transport

www.IndianJournals.com Members Copy, Not for Commercial Sale Downloaded From IP - 14.139.251.107 on dated 3-Jan-2015

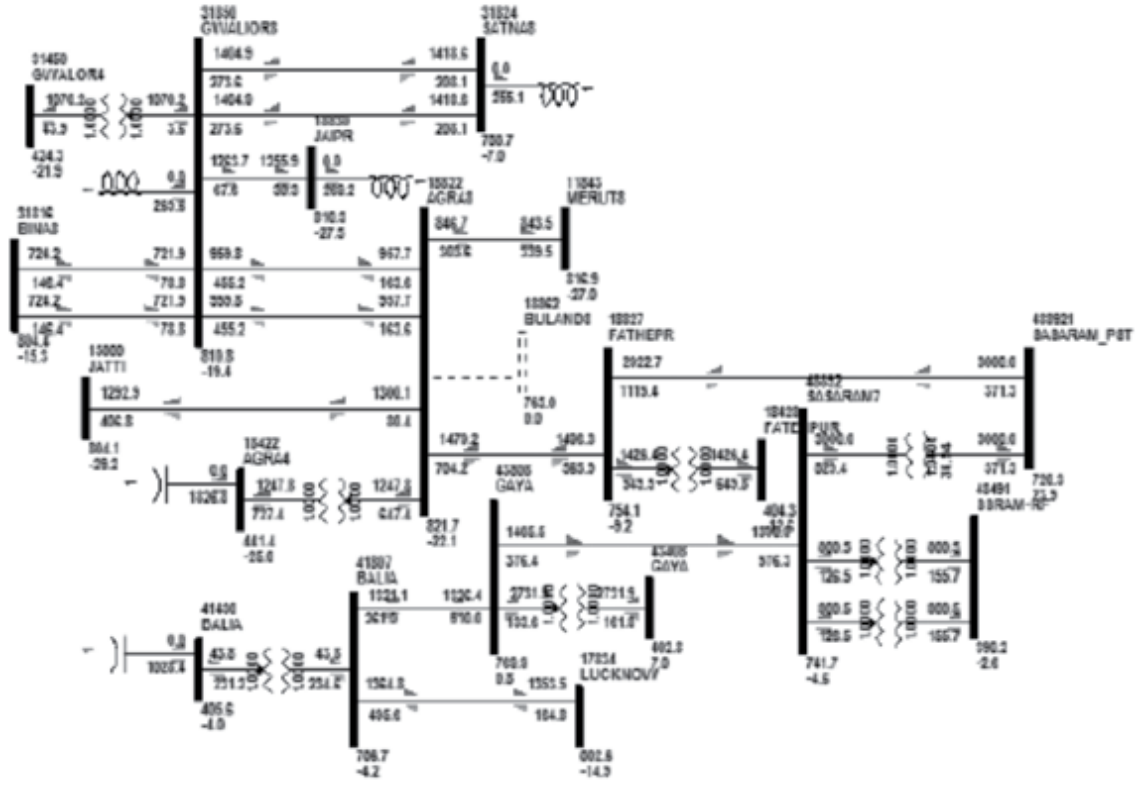


Fig. 13 : Inter regional power control with PST at Sasaram[7]

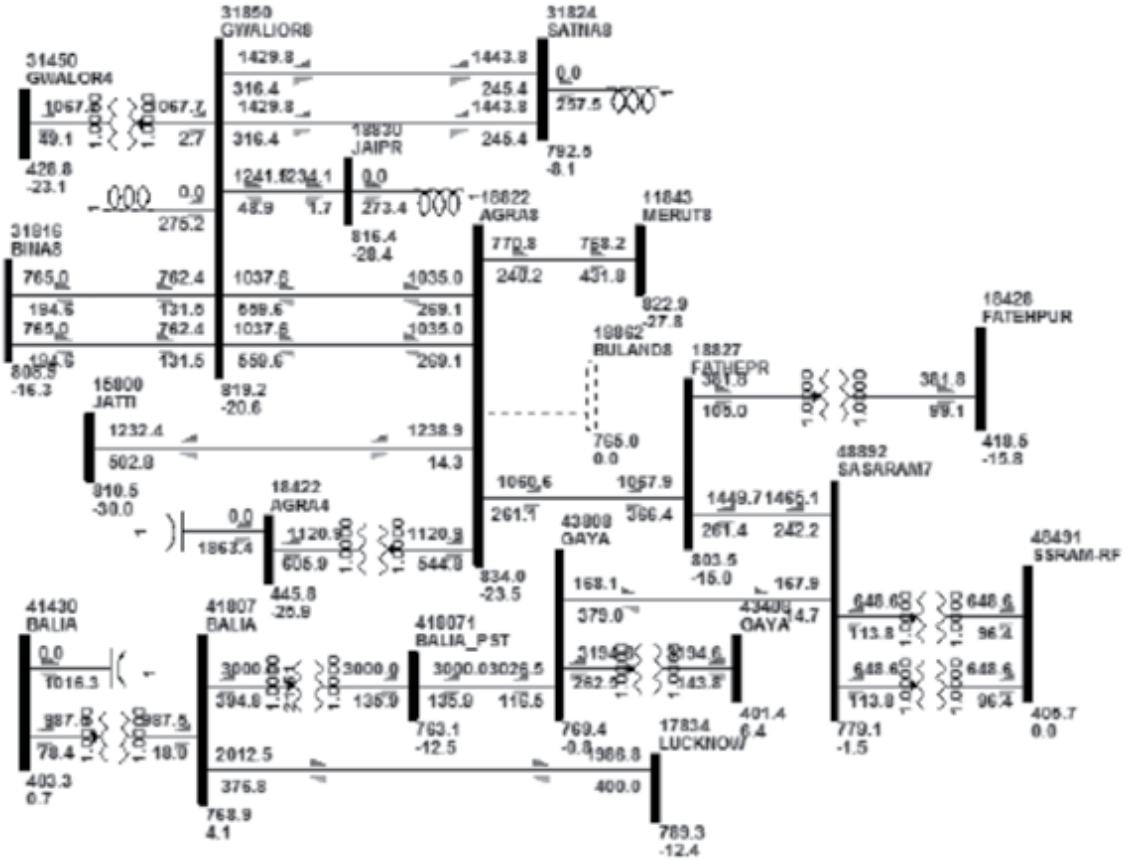


Fig. 14 : Inter regional power control with PST at Balia

www.IndianJournals.com
Members Copy, Not for Commercial Sale
Downloaded From IP - 14.139.251.107 on dated 22-Jan-2015

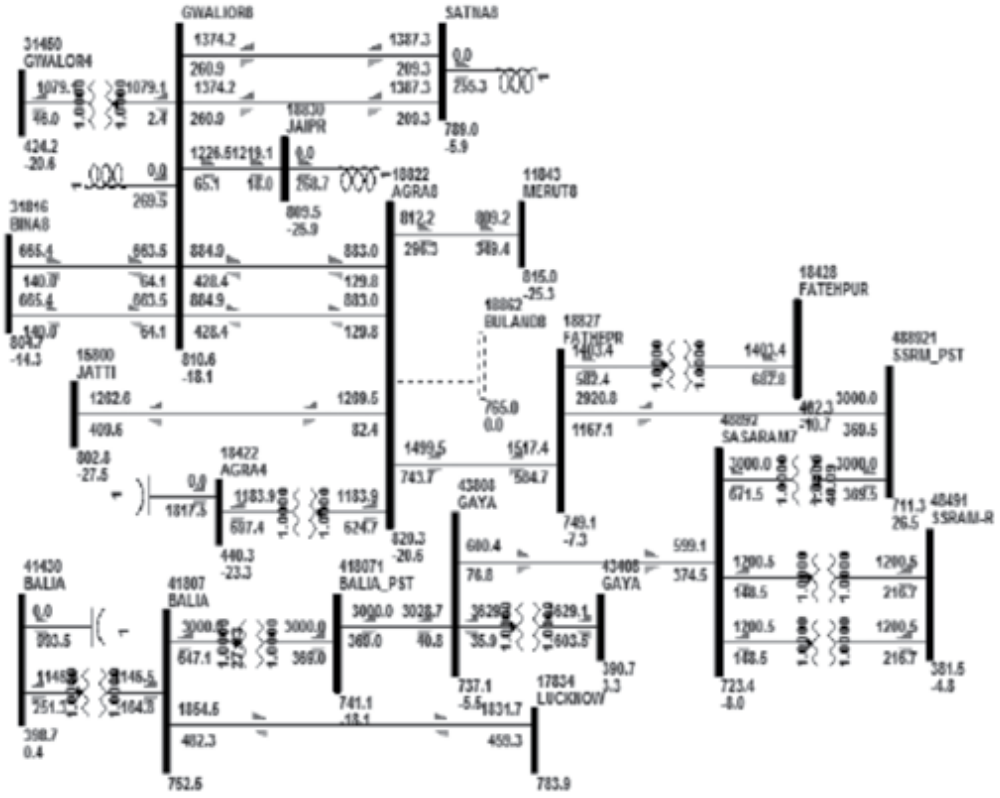


Fig. 15 : Inter regional power control with PST at Sasaram & Balia

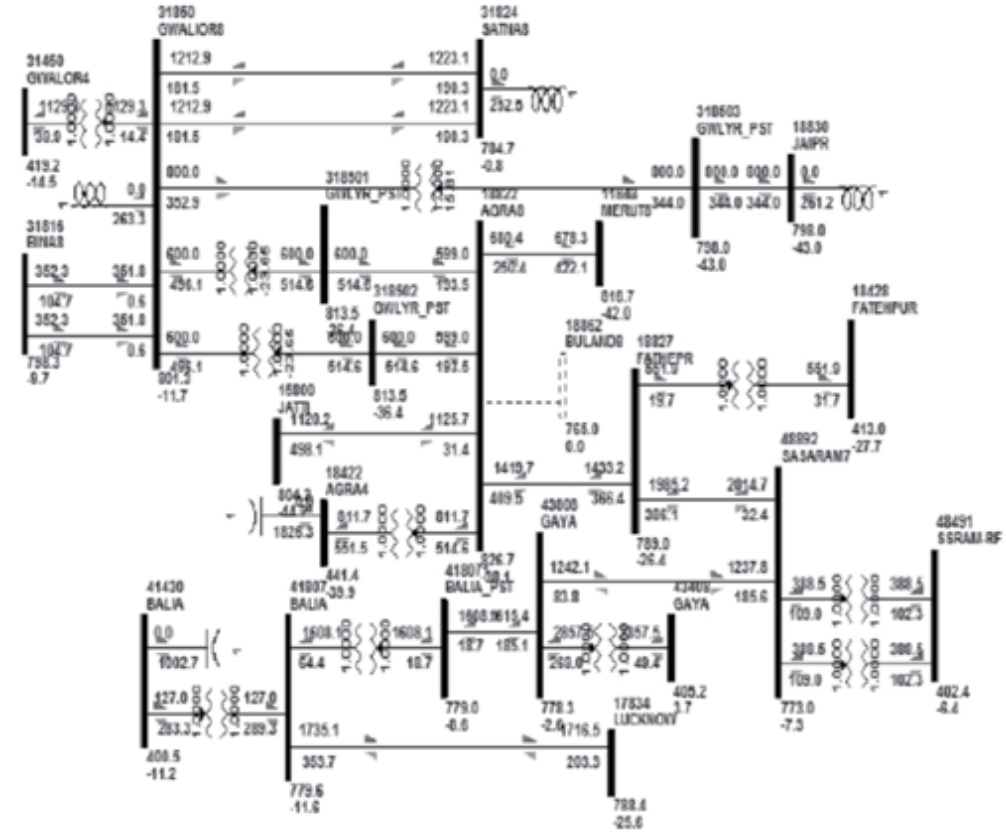


Fig. 16 : Inter regional power control with PSTs at Gwalior[8]

www.IndianJournals.com
Members Copy, Not for Commercial Sale
Downloaded From IP - 14.139.251.107 on dated 22-Jan-2015

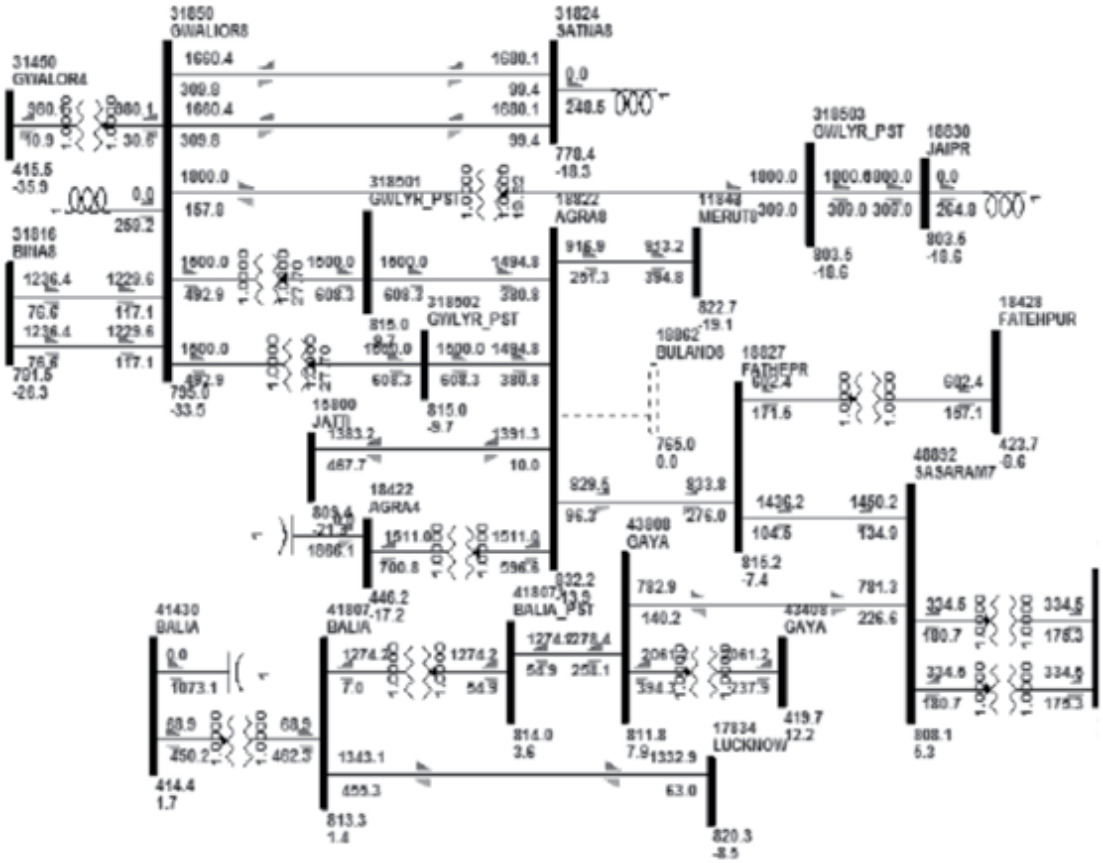


Fig. 17 : Inter regional power control with PSTs at Gwalior[8]

limitation single phase unit may have to be employed. It is assumed that all units will have equal impedances and equal number of taps and OLTC (On Load Tap Changer) shall be ganged operated. Primary winding of PST which is connected to Bus PANKI4 has star connection. Secondary winding connected to Bus UNNAO4 has delta connection. Individual single pole breakers are applied to change the Vector group. Primary winding phases are denoted as RS, YS, and BS. Secondary winding phases are denoted as Rd, Yd, and Bd. Subscript "s" shows star connected and subscript "d" shows delta connected. In Fig.18, at tap setting 0.33, power in overloaded line is flowing in reverse direction.

Entire grid is reduced to generation and load except for the lines which are under study as depicted in Fig.5. Six buses (PANKI4, PANKI2, MRDNG4, OBRA4, UNNAO4 and KNPRN4) are retained for simulation. All generation and load are connected on these buses are shown in the tables. Generation shown in hatched blocks is absorbed in the equielent network also shown in tables therefore they are disconnected. Single line diagram also shows the bus numbers with bus names.

Simulated Uttar Pradesh zone of Indian power system, identified an over loaded 400 kV line from UNNAO4 to PANKI4 as shown in Fig.19. There are alternate lines, which are under loaded. As per CEA limit the power flow

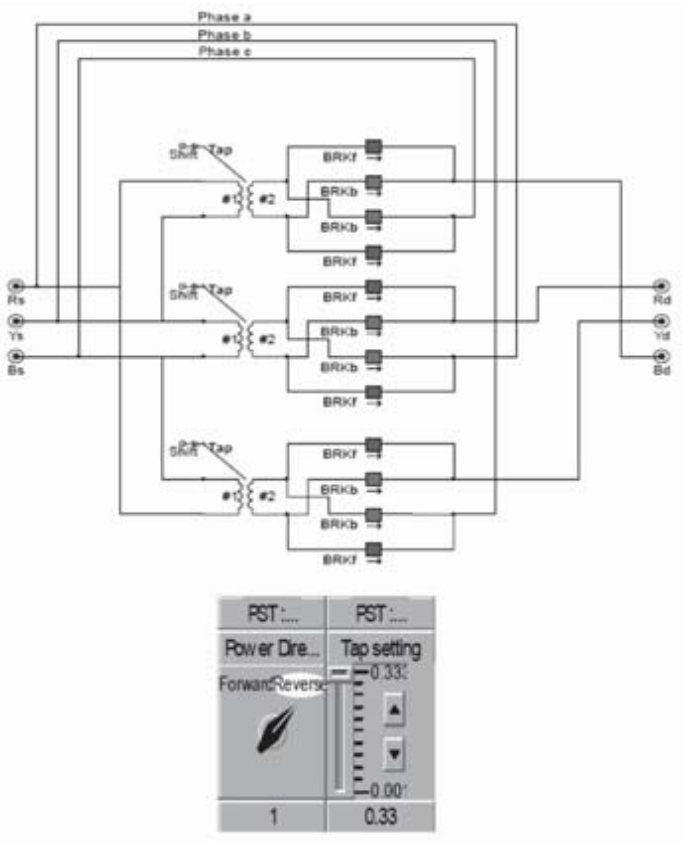


Fig. 18 : Models of PST and Tap Setting in PSCAD

www.IndianJournals.com
Members Copy, Not for Commercial Sale
Downloaded from IP - 14.139.251.107 on dated 22-Jan-2015

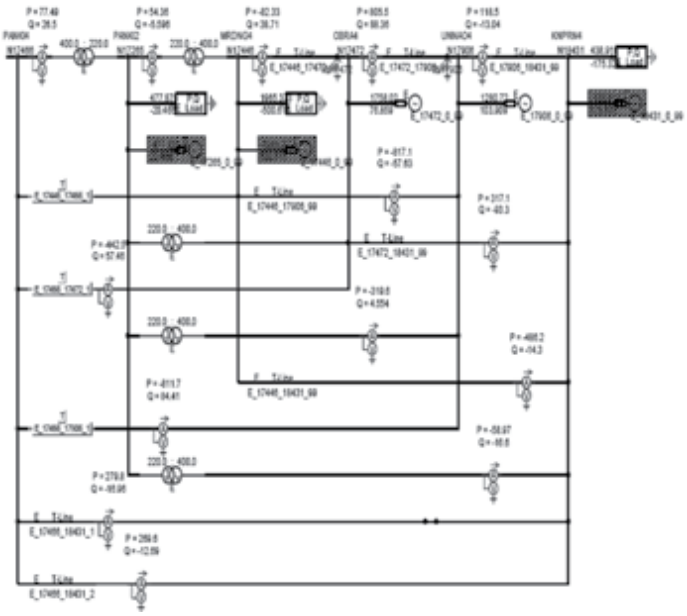


Fig. 19 : Single line diagram of UP Network (without PST) in PSCAD

in line between UNNAO4 & PANKI4 to ≤ 500 MW, it will get relieved from over load. Part of the power is diverted through alternate lines.

PST is considered in line between UNNAO4 & PANKI4 at UNNAO4. PST decreased the power in line between UNNAO4 & PANKI4 from -811.4 MW to 443.4 MW as shown in Fig. 7.

Another alternative could be have a series compensation in the overloaded line for enhancing the power transfer capability however sag may increase reducing the clearance. Unified Power Flow Controller (UPFC) could be another solution for which cost consideration will be needed.

Input data: All input data is taken by power grid. It is 2012 data. This data is in per unit on the base of 100MVA & 400 kV.

Table I : Bus data

Bus Number	Base vV	Voltage (pu)	Angle (deg)
17265	220	0.9923	-27.84
17446	400	0.9983	-44.01
17466	400	0.999	-26.67
17472	400	1.01	-5.81
17906	400	0.9966	-22.76
18431	400	0.9989	-26.83

Table II : Machine data on 100 MVA base

Bus Number	Base kV	Voltage (pu)	Angle (deg)
17265	220	0.9923	-27.84
17446	400	0.9983	-44.01
17466	400	0.999	-26.67
17472	400	1.01	-5.81
17906	400	0.9966	-22.76
18431	400	0.9989	-26.83

Table III : Two winding transformer data

From Bus Number	To Bus Number	Specified X (pu)	Rate A (MVA)
17265	17466	0.026	480

Table IV : Phase shifting transformer

From Bus Number	To Bus Number	Specified X (pu)	Rate A (MVA)
17466	17906	0.145	550

Table V : Load

Bus Number	Pload (MW)	Qload (Mvar)
17265	477.8753	-20.466
17446	1965.373	-500.61
18431	438.9185	-175.32

Table VI :Transmission line

From Bus Number	To Bus Number	Line R (pu)	Line X (pu)	Charging (pu)
17265	17446	0.11215	0.49611	0
17265	17472	0.11069	0.42669	0
17265	17906	0.00295	0.02734	0
17265	18431	0.00291	0.03024	0
17446	17466	0.00735	0.049	2.19
17446	17472	0.0884	0.7157	0
17446	17906	0.00493	0.04448	0
17446	18431	0.00747	0.06079	0
17466	17472	0.00738	0.08217	2.19
17466	17906	0.00074	0.0083	0.22
17466	18431	0.0001	0.001	0.02
17466	18431	0.00009	0.00104	0.02
17472	17906	0.00307	0.03676	0
17472	18431	0.01464	0.10982	0
17906	18431	0.00669	0.05892	0

Fig. 20 depicts the power flow in overloaded line between buses PANKI4 & UNNAO4. This is showing the active power flow (green colour curve) in reverse direction which is 811.4 MW and reactive power flow (blue colour curve) in forward direction is 84.41 MVAr.

Fig. 22 shows the relation of Active and Reactive power flow change, change of tap setting and angle difference. Tap changing block of PSCAD is shown in Fig.18. When tap setting is 0.33 then above graph shows the Active power - 1902.4 MW (reverse direction), Reactive power

www.IndianJournals.com Members Copy, Not for Commercial Sale Downloaded from IP:14.139.251.117, dated 13-Jan-2015

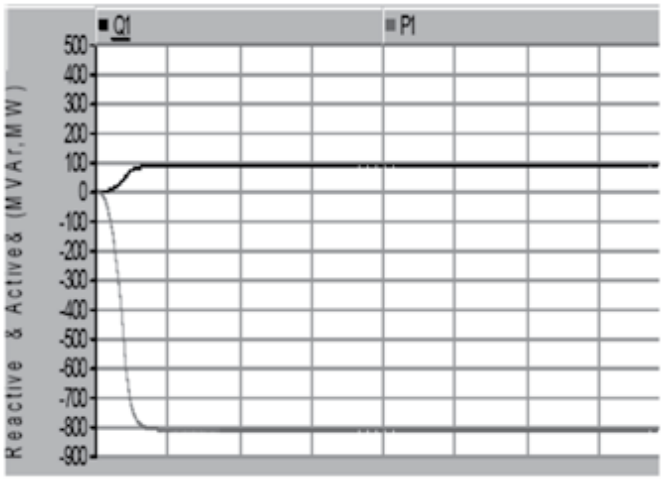


Fig. 20 : Reactive and active power flow in line PANKI4 to UNNA04

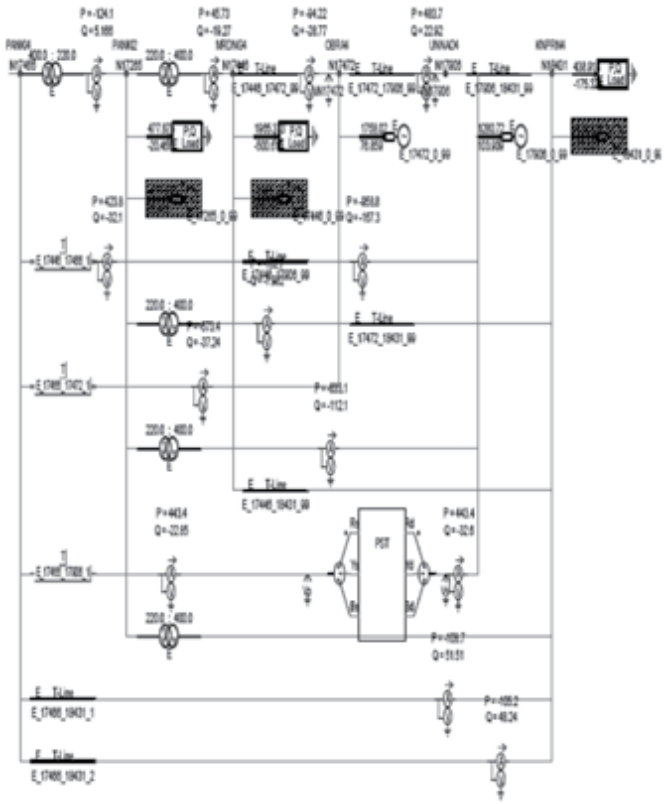


Fig. 21 : Single line diagram of UP Network (with PST) in PSCAD

192.1 MVAr (forward direction) and angle difference 27.5. When tap setting decrease up to 0.0001 then active power (reverse direction), reactive power, angle difference also decreases. After that tap setting increase then active power direction change and it comes to 480.63 MW.

Actual lines-PANKI4 to PANKI2, PANKI4 to OBRA4, PANKI4 to UNNA04, PANKI4 to KNPRN4 (both) After placing PST, all actual lines are not overloaded.

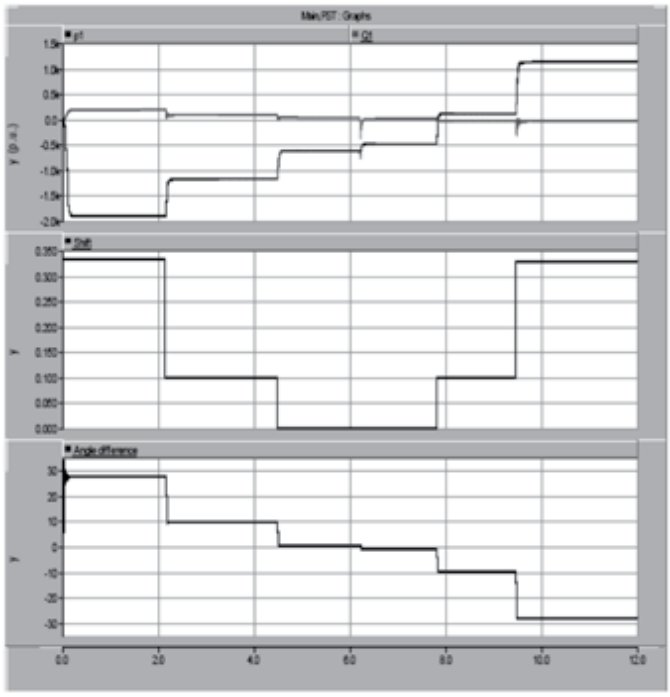


Fig. 22 : Active & reactive power change with tap setting in line PANKI4 to UNNA04

Table VII : PST Results in line PANKI4 to UNNAO4

Active power P(MW)	Reactive power Q(MVAr)	Tap setting	Angle (degree)
-1902.4	192.1	0.33	27.5
-1172.7	87	0.1	9.7
-615.23	28.8	0.001	0.99
480.63	-18.23	0.0101	-0.99
443.4	-22.85	0.01265	-1.239
116.8	-20.73	0.1	-9.8
1126.99	-33.36	0.33	-28.21

Angle Difference

The study has been done for various tap positions from nominal position to + 33% some of the data depicted in table and graph respectively. It is also concluded that 800 MVA single phase unit applied which will have no limitation of transport and manufacturing.

CONCLUSIONS

The paper has discussed the need of PST in growing Indian power system. There could be some more such situations in entire Indian grid where application of PST for control of the power could be justified. From simulation results, it is clear that PST can be used for control of active power over the transmission lines, reducing the congestion there by making the system more stable. In order to have full control over inter

www.IndianJournals.com
Members Copy, Not for Commercial Sale

regional power; we need to install PST in all lines which are connected between areas where the power need to be controlled. Because a single PST, can also shift the power to other lines but can not fully control it, which may not be economical in some cases. However, judicious decision has to be taken depending upon the requirement or alternatively Back to Back HVDC may be considered.

It is also concluded that the over all transmission losses can be reduced if the higher voltage level lines are optimally loaded by reliving the loading of lower voltage level lines.

ACKNOWLEDGEMENT

The authors are thankful to M/s BHEL Management and Delhi Technological University for permitting publication of this paper. Authors are also thankful to M/s PGCIL and M/s CEA for providing network data for enabling the studies.

REFERENCES

1. A.K. Asthana, Transmission Grid – 2022 Perspective, GridTech 2007, New Delhi, India.
2. Jody Verboomen, Dirk Van Herten, Wil L. Kling and Ronnie Belmans, "Phase shifting transformers: Principles and applications", Future Power System, 2005 International Conference on, pp 6.
3. ABB Review: FACTS – solution to power flow control & stability problems. Sweden: ABB Power System AB, 1999, 16p.
4. Nabavi Niaki. S. A., "A Novel Steady-state Model and Principle of Operation of Phase Shifting Transformer Compareable with FACTS New Devices", IEEE Transaction on power system technology. vol. 3, pp. 1450 -1457
5. R.K. Tiwari, J.S. Kuntia and S. Sachdeva, "Development of Phase Shifting Transformers" Presented in International Conference on transformers-2009 held by CBIP in New Delhi, India.
6. Seitlinger, W., "Phase Shifting Transformers Discussion of Specific Characteristic", Paris: CIGRE, 1998, 8P
7. PSSE 32 User Manual, "Program Application Guide: Volume 1"
8. W. L. Kling et al.,"Phase shifting transformers installed in the Netherlands in order to increase available international transmission capacity", in CIGRE Session 2004 – C2-207, 2004.
9. TT Reddy, Aruna Gulati, M.I.Khan, Ramesh Koul Gridtech 2010 " Application of PST in Indian Network"
10. Anwar S.Siddiqui, Shagufta Khan,Shahzad Ahsan, M.I.Khan, Annamalai " Application of PST in Indian Network"presented at IEEE International Conference on clean technology Trivandrum.

www.IndianJournals.com
Members Copy, Not for Commercial Sale
Downloaded From IP - 14.139.251.107 on dated 22-Jan-15

Journal of Production Engineering
Vol.17 No.2

Preliminary Note

Abhimanu S. and Datta C.K

POLICY FOR MINIMIZATION OF SCRAP IN A PRODUCTION LINE WITH IMMEDIATE FEEDBACK AND MULTI SERVER WORKSTATIONS

Received: 01 September 2014 / Accepted: 13 October 2014

Abstract: *In this paper, we are studying to estimate the amount of scrap in a production line caused by unsuccessful processing of items at various processing units. We are studying to obtain mathematical expression to give the scrap amount. We have considered a production line consisting of an arbitrary number of processing units, all arranged in a series along a straight line. At each of the processing units, we have provided the facility of re-processing of a job/item at the same processing unit if its processing is not done correctly at that processing unit, and there is still chance of its processing once more at the same processing unit. We have considered multi server facility at each of the processing units. Arrival of jobs at the first processing unit is supposed to be according to Poisson rule and service times at all the processing units are supposed to be exponentially distributed.*
Key words: *Network of Queues, Processing Units, multi Server Queues, Immediate Feedback, Scrap*

Politika minimizacije otpada na proizvodnoj liniji sa trenutnom povratnom vezom u multi serverskom okruženju za sve proizvodne jedinice. *U ovom radu data je procena količine otpada na proizvodnoj liniji izazvana nakon neuspešne obrade predmeta na različitim proizvodnim jedinicama. Izveden je matematički izraz za dobijanje količine otpada. Proizvodna linija se sastoji od proizvoljnog broja proizvodnih jedinica poređane duž prave linije. Na svakoj proizvodnoj jedinici obezbeđen je objekat za doradu predmet, i ako obrada nije korektna postoji šansa za njegovu doradu na istoj proizvodnoj jedinici. Smatra se da na svakoj proizvodnoj jedinici se nalazi multi server. Dolazeći predmeti na prvoj proizvodnoj jedinici treba da budu u skladu sa Poasonovim pravilom i svim obradnim vremenima proizvodnih jedinica koje imaju eksponencijalnu distribuciju.*
Ključne reči: *Čekajuća mreža, proizvodne jedinice, multi server, trenutna povratna sprega, otpad*

1. INTRODUCTION

A production line is a sequence of a finite number of processing units arranged in a specific order (fig. 1). At each of the processing units, service may be provided by one person or one machine that is called single- server facility, or it can be provided by more than one persons or more than one machines that is called multi-server facility at the respective processing units. In this paper we have considered multi-server facility at each of the processing units. At each of the processing units, a specific type of processing is performed i.e. at different processing units material is processed differently. At a processing unit, the processing times of different jobs or items are independent and are distributed exponentially around a certain value, called mean processing time [1].

In a production line the processing of raw material or a job starts at the first processing unit. It is processed for a certain time interval at the first processing unit and then it is transferred to the second processing unit for other type of processing, if it's processing is done correctly at the first processing unit. This sequence is followed until the processing at the last processing unit is over. In a production line raw material is processed at a series of processing units one after the other and finally it is transformed into finished goods ready for use.

End of processing at each of the processing units give rise to the following three possibilities:

a) Processing at a unit is done correctly and the job or material is transferred to the next processing unit for other type of processing.

b) Processing at a unit is not done correctly but can be reprocessed once more at the same processing unit.

c) Processing at a unit is neither done correctly nor it can be reprocessed at the same processing unit i.e. this job or material is lost, in this situation the job or material is rejected and put into the scrap.

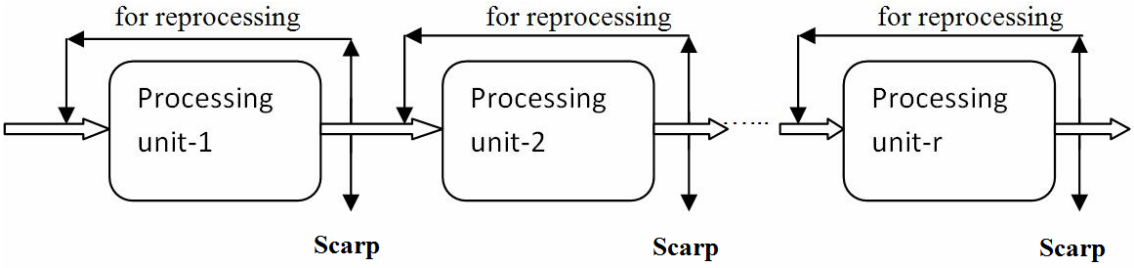


Fig.1. General Production line

2. LITERATURE SURVEY

A Queuing theory is a branch of applied mathematics that deals with phenomenon of waiting lines and arises from the use of powerful mathematical analysis to describe production processes. A lot of work has been done on the applications of Queuing Theory to study and analyze the production systems. After 1920, a lot of work has been done for developing the Queuing Theory as well as on its applications to model various phenomenons. Queuing theory's history goes back nearly 100 years. Johannsen's "WaitingTimes and Number of Calls" (an article published in 1907 and reprinted in Post Office Electrical Engineers Journal, London, October, 1910) seems to be the first paper on the subject. But the method used in this paper was not mathematically exact and therefore, from the point of view of exact treatment, the paper that has historic importance is A. K. Erlang's, "The Theory of Probabilities and Telephone Conversations" (Nyt tidsskrift for Matematik, B, 20 (1909), p. 33). Several researches have made efforts to apply queuing theory to model manufacturing systems. We are making effort to apply this theory to determine a policy to minimize the amount of scrap, which is produced due to ill-processing of material or jobs at various workstations of the production line. Many researchers have considered the queues in series having infinite queuing space before each servicing unit. [2] T. L. Saaty, in his book "Elements of Queuing Theory" has discussed various queuing models and their measures of performances. [3] R. R. P. Jackson, (1954) has found the steady state solution of a network of two queues in series. [4] R. R. P. Jackson, (1956) found the steady state solution of a serial network of arbitrary number of queues. [5] K. L. Arya, had found that the steady state distribution of queue length taking two queues in the system, where each of the two non-serial servers is separately in service with the other two non-serial servers. [6] O. P. Sharma studied the stationary behavior of a finite space queuing model consisting of queues in series. He had found the steady state solution of serial network of queues with multi server facility and infinite waiting space. In our model, we have introduced immediate-feedback at each of the processing units. [7] J. R. Jackson has discussed the network of queues. Arrivals to the first processing unit are according to Poisson rule and service times at each of the processing units are exponentially distributed. . [8] Trivedi, Kishor. S., in his book "Probability & Statistics with Reliability, Queuing and Computer Science Applications" has discussed the network of queues and has found the steady state solution of serial network of queues. [9] U. N. Bhat has discussed the steady state behavior of queues and found the steady state solution of a serial network of an arbitrary number of queues. [10] Leonard Kleinrock in his book "Queueing Systems, Computer Applications" vol.-1, has found the steady state probability distribution of number of units in the system. [11] Gross D , Harris CM in their book "Fundamentals of Queuing Theory" have discussed major queuing models. [12] J. Walrand in his book "An Introduction to Queuing Networks" has discussed a queuing system with immediate feedback and has suggested how the parameters change when immediate feedback is removed. [13] M. P.,GROOVER, in his book "Automation, Production Systems, and Computer-Integrated Manufacturing" has discussed various kinds of assembly line/ production line. [14] Curry Guy L, Feldman Richard M , in their book "Manufacturing System Modeling and Analysis, have discussed the M/M/1 queuing model with applications.

3. MODELING NOTATIONS

Maximum we consider a production line as shown in fig.2 consisting of an arbitrary number(r) of processing units arranged in a series in a specific order. Each of the processing units has multi- server facility and immediate feedback.

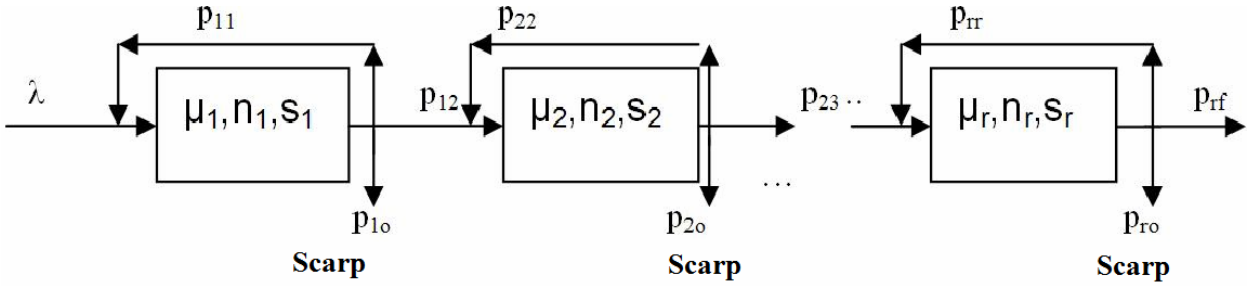


Fig.2. Proposed production line

λ - Mean arrival rate to the first processing unit from an infinite source, following Poisson's rule.

μ_i - Mean service rate of an individual server at the ith processing unit having exponentially distributed service times.

s_i - Number of servers at the ith processing unit

n_i - Number of unprocessed jobs before the ith processing unit waiting for service, including one in service, if any, at any time t

$p_{i,i+1}$ - Probability that the processing of a job or material at the ith processing unit is done correctly and it is transferred to the $(i+1)^{st}$ processing unit $p_{i,i}$ - Probability that the processing of a job or material at the ith processing unit is not done correctly but it can be reprocessed once more, so, it is transferred to the same processing unit for processing once more.

$p_{i,o}$ - Probability that the processing of a job or material at the ith processing unit is neither done correctly nor it remains suitable for reprocessing.

$P(n_1, n_2, ...n_r, t)$ - Probability that there are n_1 jobs waiting for processing before the first processing unit, including one in service, if any, n_2 jobs before the second processing unit waiting for service including one in service, if any, and so on, n_r jobs before the rth processing unit waiting for service including one in service, if any at time t, with $n_i \geq 0 (1 \leq i \leq r)$, and $\mathrm{P}(n_1, n_2, ...n_r, t)$=0, if some n_i <0 (because number of jobs cannot be negative).

Queuing Network: An interconnected collection of stations in which customers move from one station to another requesting service called queuing network, where each station consists of a queue where customers (or jobs) wait for service.

The above production line can be represented by a serial network of queues (Fig. 3) in which each workstation is equivalent to a queue with the same number of similar servers and the same numbers of jobs waiting for service.

In the above serial network of queues, each queue has immediate feedback. To analyze this serial network of queues firstly we remove the immediate feedback.

After removing the immediate feedback, the above serial network of queues is replaced by one, as follows:

Here $\mu_i^{'} = \mu_i (1 - p_{i,i})$, [11] is the effective service at the ith processing unit after the removal of the immediate feedback.

And the respective probabilities become as follows:

$$q_{i,o} = \frac{p_{i,o}}{(1 - p_{i,i})}, q_{i,i+1} = \frac{p_{i,i+1}}{(1 - p_{i,i})} \quad (1)$$

Under the steady state conditions, we have [1, 8, 10]:

$$\left[\lambda + s_1\mu_1^{'} + s_2\mu_2^{'} + ... + s_r\mu_r^{'}\right].$$

$$\mathrm{P}(n_1, n_2, ...n_r) = \lambda \mathrm{P}(n_1 - 1, n_2 n_3, ...n_r) +$$

$$\sum_{i=1}^{r} s_i\mu_i^{'}.q_{i,i+1}.P(n_1, n_2, ...n_i + 1, n_{i+1} - 1, ...n_r) +$$

$$\sum_{i=1}^{r} s_i\mu_i^{'}.q_{i,o}.P(n_1, n_2, ...n_i + 1.n_{i+1}, ...n_r) \quad (2)$$

4. SOLUTION FOR INFINITE QUEUING SYSTEM

Under the steady state conditions all the queues behave independently and thus the solution of steady state equation in product form is given by

$$\mathrm{P}(n_1, n_2, ...n_r) = \prod_{i=1}^{r} (1 - \rho_i)\rho_i^{n_i} \quad (3)$$

where $n_i \geq 0 (1 \leq i \leq r)$ and $\rho_i < 1 \ (1 \leq i \leq r)$.

If any $\rho_i \ (1 \leq i \leq r) > 1$ then the stability is disturbed and the behavior of the system will not remain stationary consequently solution will not be given by Eq. (3) [1, 5, 7, 8, 10, 13].

Here, we have

$$\rho_i = \frac{\lambda_i}{s_i\mu_i^{'}},$$

where $\lambda_i = \lambda \prod_{k=1}^{i} \frac{p_{k-1,k}}{(1 - p_{k-1,k-1})}, \quad p_{0,0} = 0$

Thus

$$\rho_i = \frac{\lambda}{s_i\mu_i} \prod_{k=1}^{i} \frac{p_{k-1,k}}{(1 - p_{k,k})}, \quad (4)$$

with $p_{0,1} = 1$.

It is observed that

$$\sum_{i=1}^{r} \lambda_i.q_{i,o} + \lambda_r.q_{r,f} = \lambda \quad (5)$$

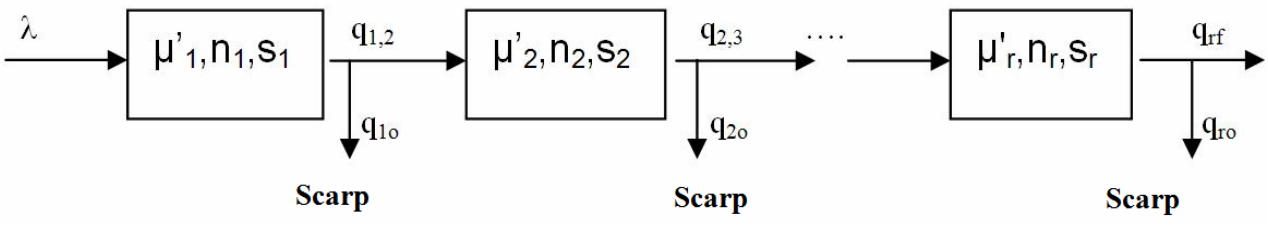


Fig.3. Equivalent serial network of queues representing the production line

5. AVERAGE AMOUNT OF SCRAP

As we start the production line, its first workstation starts working and the output of this workstation is checked for quality. If the processing of the job is done correctly, then it is transferred to the second workstation. If its processing is not done correctly, but it still possesses the quality for reprocessing once more at the same workstation, then it is reprocessed at the first workstation. If the processing at the first workstation is neither done correctly nor it possesses the quality for reprocessing at the first workstation, then it is rejected and put into the scrap. This quality check is performed at all the workstations in the production line. Finally, the work part/a job/material is processed at the last workstation. In this way, the jobs/work parts, which are not processed correctly as well as they do not have the quality required for reprocessing, are useless and put into the scrap.

Under steady state condition, A, the amount of scrap produced per unit of time is:

A= The amount of scrap obtained from all the workstations of the production line (due to unsuccessful processing of material/a job/a work part),
= Sum of amounts of scrap obtained at all of the workstations of the production line,
= amount of scrap obtained at the first workstation + amount of scrap obtained at the second workstation + ...,
... + amount of scrap obtained at the last workstation.

$$A = \lambda\, q_{1,o} + \lambda\, q_{1,2}\, q_{2,o} + \ldots + \lambda\, q_{1,2}\, q_{2,3} \ldots q_{r-1,r}\, q_{r,o}$$

$$= \sum_{i=1}^{r} \lambda\, q_{1,2}.q_{2,3}...q_{i-1,i}q_{i,o}\,, \text{ with } q_{0,1} = 1$$

$$= \lambda \sum_{i=1}^{r} \frac{p_{1,2}}{(1-p_{1,1})} \frac{p_{2,3}}{(1-p_{2,2})} \cdots \frac{p_{i-1,i}}{(1-p_{i-1,i-1})} \frac{p_{i,o}}{(1-p_{i,i})},$$

with $p_{0,0} = 0$, *and* $p_{0,1} = 1$

$$= \lambda \sum_{i=1}^{r} \prod_{k=1}^{i} \left(\frac{p_{k-1,k}}{1-p_{k-1,k-1}} \right) \frac{p_{i,o}}{(1-p_{i,i})} \qquad (6)$$

6. MINIMIZATION OF SCRAP

The scrap as given by the equation (6) can be minimized by minimizing each term in the summation given by the equation (6).

This we can do in two ways:

(i) By minimizing the numerator i.e. by minimizing the terms. Thus, one way of minimizing the scrap is the installation of machines with minimum rejection rate.

(ii) By maximizing the denominators i.e. by maximizing the terms in the denominators or by minimizing the values of scarp. Thus, another way of minimizing the scrap is the installation of machines with minimum reprocessing rate.

Finally, the scrap in the production line can be minimized by installing machines with minimum rejection rate and minimum reprocessing rate.

7. ACKNOWLEDGEMENT

I am thankful to the management and director of BPIT for providing a very conducive environment as well as to my colleague faculty members for invaluable suggestions and discussions.

8. REFERENCES

[1] Singh, A., Datta, C.K.: *Loss Minimization Policy for a Production Line with Immediate Feedback and Multi Server Facility at all Processing Units*, Journal of Production Engineering, vol. 16, No. 2013.

[2] Saaty, T. L.: Elements of Queuing Theory. McGraw-Hill, New York, 1961.

[3] Jackson, R. R. P.: *Queuing Systems with Phase Type Service,* Operations Research Quarterly, Vol. 5, No. 2, pp. 109-120, 1954.

[4] Jackson, R. R. P.: *Some equilibrium Results for the Queueing Process Ek/ M/I*, Journal of the Royal Statistical Society, 1956.

[5] Arya,K. L.: *Study of a Network of Serial and Non-serial Servers with Phase Type Service and Finite Queuing Space*, Journal of Applied Probability, Vol. 9, No.1, pp. 198-201, 1972.

[6] Sharma,O. P.: *A Model for Queues in Series*, Journal of Applied Probability, Vol.10, No.3, pp. 691-696, 1973.

[7] Jackson, J. R.: *Networks of waiting lines*, Oper. Res., 5, pp. 518-521, 1957.

[8] Trivedi, Kishor. S.: *Probability & Statistics with Reliability,* Queuing and Computer Science Applications. Wiley India, (P.) Ltd., 4435/7, Ansari Road, Daryaganj, New Delhi, 2002.

[9] Bhat, U. Narayan: *An Introduction to Queuing Theory*. Birkhäuser Boston, pp.144-147, 2008.

[10] Leonard Kleinrock: *Queueing Systems*, Computer Applications, Volume 2 , Wiley Interscience, pp. 147-152, 1976.

[11] Gross. D, Harris C.M.: *Fundamentals of Queuing Theory.* John-Wiley, New York, pp.220-226, 1985.

[12] Warland, J.: *An Introduction to Queuing Networks*, Prentice Hall, Englewood Clifs, New Jersey, USA, pp.160, 1998.

[13] GROOVER, M. P.: *Automation, Production Systems, and Computer-Integrated Manufacturing*, Pearson Education, Delhi, India, 2004.

[14] Curry Guy L., Feldman Richard, M.: *Manufacturing System*, Springer-Verlag Berlin Heidelberg, pp.77-80, 2011.

Authors: **Mr. Abhimanu Singh**, Research Scholar at Faculty of Technology, university of Delhi, Delhi, India, Assistant Professor at BPIT, Rohini, Delhi, India. **Prof., Dr., C. K. Datta,** Deptt. of Mechanical Engineering, PDM College of Engineering, Bahadurgarh, Haryana, India(Formerly Professor in Production Engineering at Delhi Technological University, Delhi, India).

E-Mail: asingh19669@yahoo.co.in

Review of the Concentrated Solar Thermal Technologies: Challenges and Opportunities in India

Dr. J.P Kesari*, Mohit Gupta*, Aadish Jain*, A.K Ojha**

* *Department of Mechanical Engineering, Delhi Technological University Bawana Road , Delhi -110042,India*

***Saraswati Institue of Engineering and Technology, Ghaziabad*

Abstract- **This paper starts with the introduction of energy scenario in India and realising the huge potential of Solar Concentrated Power to fill in the deficit. Further, we have mentioned some of the government initiatives to promote the solar concentrated power. Continuing with the basic discussion on the various types of solar thermal techniques such as Flat Plate Collector, Cylindrical Trough Concentrator, Parabolic Trough, Parabolic Dish Reflector, Compound Parabolic Concentrator, Fresnel Concentrator, Hemispherical Bowl Mirror Concentrator, Tower Receiver and there application. We have also listed some of the large scale application of Concentrated Solar Energy by private institutions and industry. We have also tried to point out the reason for low confidence of masses in the Solar Energy sector and also pointed out the advantages of the solar energy use for rural areas. As solar energy can have wide range of applications and India have ample amount of solar irradiance we must try and utilize this source to maximum extent and thereby reduce our dependence on the fossil based energy resources at least during the day time or sunshine hours.**

Keywords- Solar Concentrated Power; Flat plate collector; Space Heating Applications; Parabolic Concentrator ; Non-Conventional Energy Sources

I. INTRODUCTION

The demand for power is increasing day by day. It's a high time we should stop our dependence on the conventional sources of energy and adopt renewable sources of energy to meet our energy demands. The emission of Carbon dioxide (CO_2) is almost unstoppable as a result of dependence on conventional sources of energy. Hence using fossil fuels is directly related to the rising environmental problems [1].It can be estimated that with the increasing concentration of CO_2 the earth can get warmer by (1-5°C) with the advent of the next century [2].The oil crisis of 1973 and the rising environmental concerns attributed to the use of fossil fuels have resulted in certain outstanding efforts in adopting alternative energy sources [4]. India has a tremendous potential for solar power. A $6 billion to $7 billion capital equipment market for grid-connected solar generators is estimated [5]. In a typical Indian scenario, where there is a tremendous increase in the population in the cities, a need arises to develop clean energy technologies and innovations have to be adopted to ensure the healthier habitat for this population [3].

II. REALİSİNG THE POTENTİAL OF NON-CONVENTİONAL ENERGY SOURCES

The importance of renewable energy sources was realized in March, 1981, when the government of India made a Commission for Additional Sources of Energy (CASE) in the Department of Science and Technology. In 1982, CASE was taken under the Department of Non-Conventional Energy Sources (DNES), Ministry of Energy. IREDA (Indian Renewable Energy Development Agency Ltd.) got established in 1987. The DNES was converted to MNES (Ministry of Non- Conventional Energy Sources) in 1992. Finally in 2006 the ministry was named as the Ministry of New and Renewable Energy (MNRE) [4].

2.1 Focus on deployment of Solar Power

The Jawaharlal Nehru National Solar Mission (JNNSM) which was launched in Januray,2010 has set the target of generating 20,000 MW of grid connected solar power by 2022 and also aimed at reducing the cost for the generation of solar power in the country through long term policy, large scale deployment goals, aggressive R&D, domestic production of critical raw materials, components and products, as a result to achieve grid tariff parity by 2022 [6].With the current pace of progress JNNSM will be able to achieve this objective and transform India into a green and solar powered Nation.

III. SOLAR THERMAL TECHNOLOGİES

Solar power has a low density per unit area (1KW/sq. to 0.1 Kw/sq.m.), therefore requires a large ground area by the collectors to harness it [4]. The collectors can be concentrating type or non-concentrating type. In the present discussion we will focus on the concentrated types of solar collectors.

3.1 Flat Plate Collector

A flat-plate collector(Figure 1) is a heat exchanger device which converts Solar radiation energy to Thermal energy by absorbing energised radiation from a distant object (Sun) and delivering heat to fluid (Air , Gas , Water etc.). Flat plate collector absorbs both direct and diffuse radiation, has very low maintenance and no sun tracking is required. Temperatures of around 80°C to 100°C can be achieved using this type of solar collector. [19]

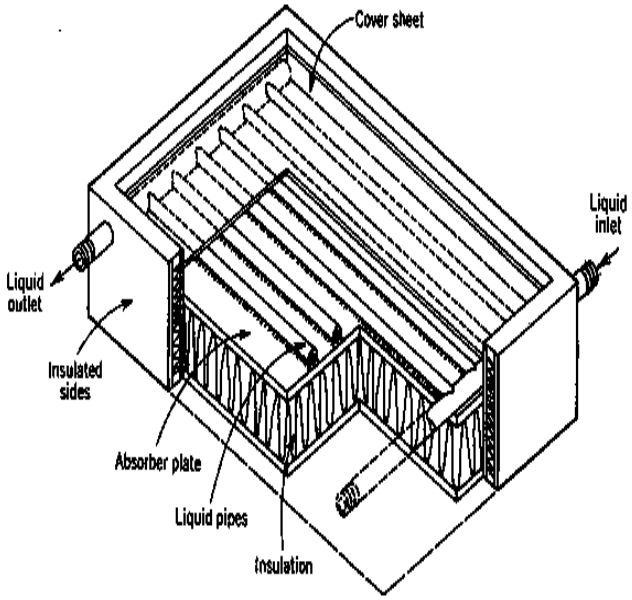


Figure 1: A cross-section of the flat plate collector showing inlet and outlet flow of liquid

Image source: www.powerfromthesun.net

Applications: Flat plate collector can be used for space heating applications by using air heaters, can be used for heating water for various purposes, Source of Heat for low temperature applications.

3.2 Modified Flat Plate Collector

A flat-plate collector can be modified by incorporating plane reflectors at the edge of the flat plate collector so that the additional radiation can be reflected into the receiver [4]. This type of arrangement increases the concentration of solar radiation. The plane reflectors (mirrors) are also called booster mirrors. A modified flat plate collector is shown in Figure 2. The concentration ratio so obtained has a maximum value of 4.

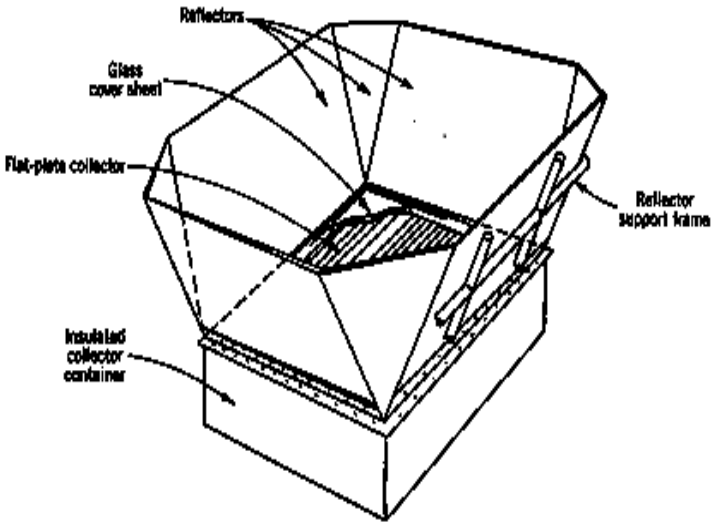


Figure 2 : A modified flat plate collector to increase the concentration ratio is shown.

Image source: www.powerfromthesun.net

Applications: Modified flat plate collectors can be used for water heating applications, grain and vegetable drying purposes to reduce the moisture content and for space heating applications with incorporation of rock-bed storage.

3.3 Cylindrical Trough Concentrator (CTC)

It CTC(Figure 3) is a cylindrical trough with spherical profile reflector is very similar to Parabolic Trough with a metal tube (blackened) receiver placed at its focal line. These types of concentrators can be rotated about an axis to track the sun. The black coating of the tube increases the absorption. However after the development of the parabolic concentrators the use of spherical concentrator is reduced as with same space parabolic concentrators can deliver more energy and temperature. The concentration ratio ranges from 5-25.

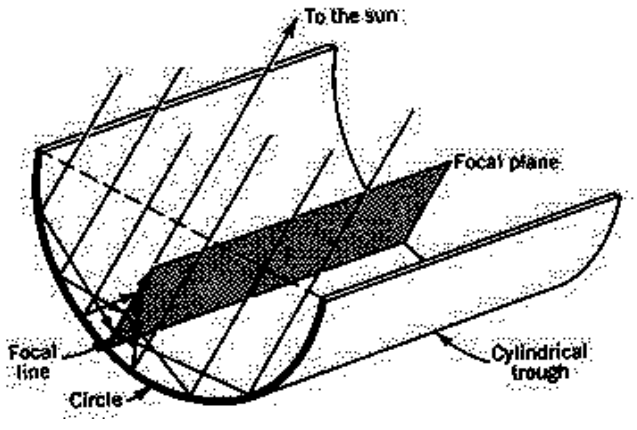


Figure 3: Cylindrical Trough Concentrator
Image source: www.powerfromthesun.net

Applications: This technology can be used for water purification, steam generation purposes and solar chemistry.

3.4 Parabolic Trough

It is the most employed concentrated technology accounting a major share in the CSTs [7]. This technology(Figure 4) is based on the fact that when sun rays falls on the parabolic mirrors they are directed towards the receiver placed at the focal line. The receivers have a special coating ensuring maximum energy absorption and minimum infrared re-radiation. The heat produced in the receiver carried by the heat transfer fluid which is transferred to the steam generator producing steam which runs the turbine. Single axis tracking of the sun in sufficient thereby producing long collector modules [8] .The temperature of around 400°C can be produced with this technology [10].

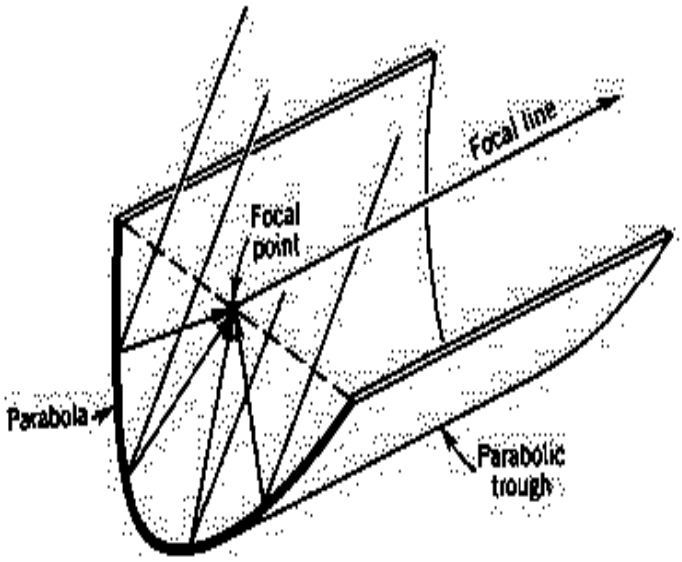


Figure 4: Parabolic Trough

Image source: www.powerfromthesun.net

Applications: Parabolic trough can be used for desalination, water purification and steam generation purposes [22].

3.5 Parabolic Dish Reflector

It has a point focus and tracks the sun in two axes, concentrating the solar energy at the focal point. The receiver placed at the focal point stores the thermal energy which is absorbed by the heat transfer fluid. The temperatures of around 1500°C can be achieved with this arrangement(Figure 5) [9]. The concentration ratio is in the range of 600-2000[8].

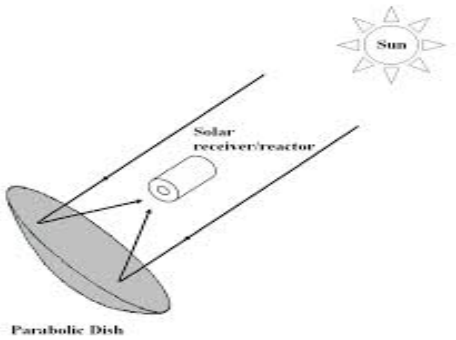


Figure 5: A dual-axis parabolic dish reflector is shown.

Image source: www.powerfromthesun.net

Applications: On the account of high temperature produced, parabolic dish can be used for power generation, cooking, high temperature water for laundry, solar furnaces and desalination purposes.

3.6 Compound Parabolic Concentrator

The booster mirrors in case of a modified flat plate collectors are replace by parabolic mirrors in this case as shown in Figure 6. These mirror segments are oriented such that the focus of one segment lies at the base of the other segment which is in contact with the receiver. The acceptance angle is large for this arrangement. With this type of arrangement the rays which falls in the central region reaches the absorber directly whereas those falling near the edges undergo certain reflections. The concentration ratio that can be achieved ranges from 3-7[4].

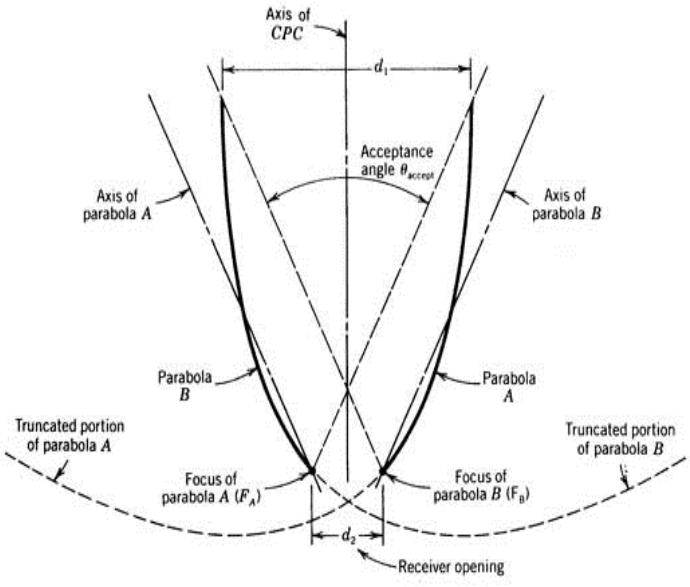


Figure 6: Compound Parabolic Concentrator

Image source: www.powerfromthesun.net

Applications: It has applications in integrated collector storage, direct circulation, indirect water heating systems, heat pumps, absorption systems and solar chemistry systems [21].

3.7 Fixed Mirror Solar Concentrator

There is a practical difficulty in manufacturing a large cylindrical parabolic shape mirror, therefore long narrow mirror strips are used in this type of concentrator(Figure 7). These mirror strips are arranged on a circular reference cylinder while the receiver tube is tracked. The receiver tube rotates about the centre of curvature of the reflector module to track the sun. The concentration ratio is approximately equal to the number of mirror strips [4].

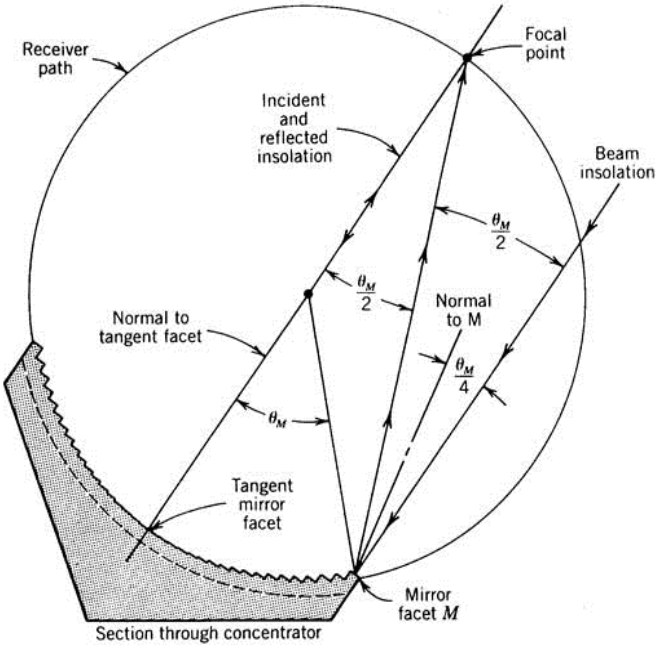


Figure 7: Fixed Mirror Solar Concentrator

Image source: www.powerfromthesun.net

Applications: This technology finds use in water heating, drying and space heating requirements.

3.8 Fresnel Concentrator

3.8.1 Linear Fresnel lens Refractor

This type of collector(Figure 8.1) consists of fine, linear grooves on the surface of a refractory material (generally optical quality plastic) on one side and flat on the other side. The angle of the groove is such that it behaves similar to a spherical lens. Temperature ranges between 150°C to 300°C with a concentration ratio of 10 to 30. The incident radiation is converged to a focal line where a receiver tube is provided [4].

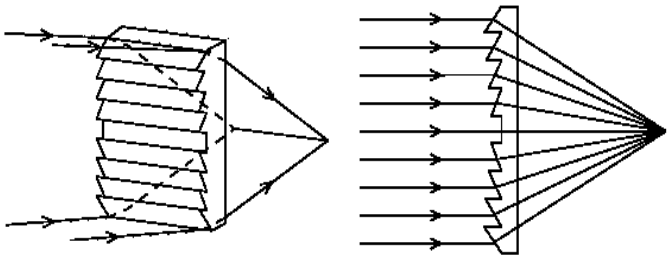


Figure 8.1: Linear Fresnel Lens Refractor in two different views

Image source: www.powerfromthesun.net

3.8.2 Linear Fresnel Mirror Reflector

This type of concentrator as shown in Figure 8.2 is an array of linear mirror strips which have a same focus and concentrate light on to a fixed receiver mounted on a tower, large absorbers can be constructed as absorbers are generally stationary. However the reflectors are moving about its linear axis to focus the sunlight to the fixed absorber. The greatest advantage of this type of system is that it uses flat or elastically curved reflectors which are cheaper compared to parabolic glass reflectors [21].

Additionally, these are mounted close to the ground, thus minimizing structural requirements. The first to apply this principle was the great solar pioneer Giorgio Francia[20] who developed both linear and two-axis tracking Fresnel reflector systems at Genoa, Italy in the 60s.

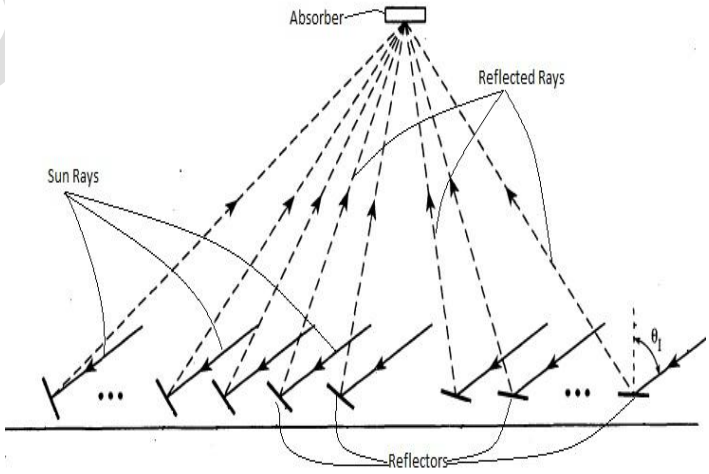


Figure 8.2: Linear Fresnel Mirror Reflector

3.8.3 Circular Fresnel lens Concentrator

These lenses are used where high flux is required, such as with silicon solar cells or with gallium arsenide solar cells. The Fresnel lens here is divided into thin circular zones. The tilt of each zone is adjusted to make the lens approximately a spherical one. The concentration ratio of 2000 can be achieved.

Applications: Fresnel reflector can be used for various thermal applications including power generation by steam and solar chemistry systems [21].

3.9 Hemispherical Bowl Mirror Concentrator

It is an example of linear focal optics and uses two-axes tracking. In this arrangement hemispherical bowl is fixed while the receiver tracks [11]. The rays entering the hemisphere crosses the paraxial line after the reflection at a point between the focus and the mirror surface. The absorber is driven around a polar axis at a constant angular speed or adjusted periodically(Figure 9).

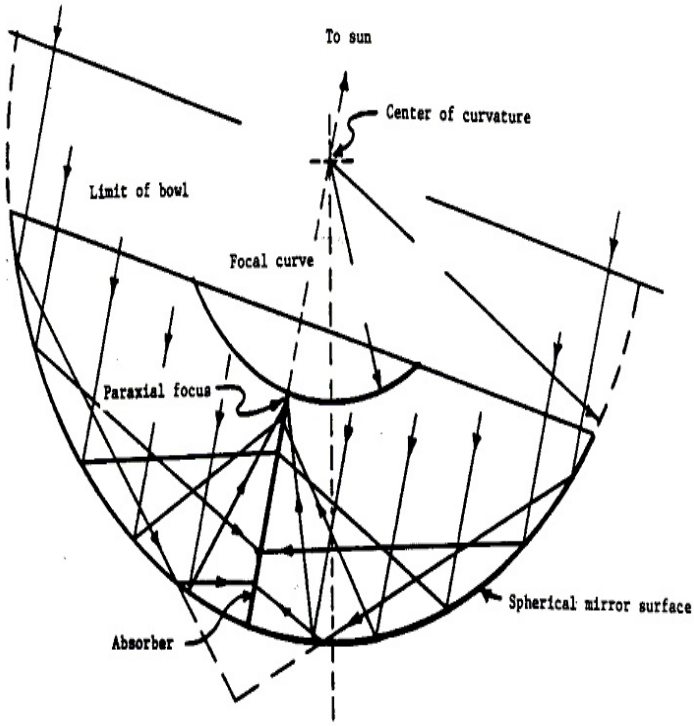


Figure 9: A two-axes Hemispherical Bowl Mirror Concentrator

Image source: [11]

Applications: This technology has applications in cooking, process heat and solar drying purposes.

3.10 Tower Receiver

A tower receiver (Figure 10) or a solar power tower has an arrangement of heliostats (dual-axes tracking reflectors) which are used to concentrate the rays falling on them to the top of a tower. The temperature generated at the receiver is 500°C to 1000°C in which working fluid is used as a heat source for power generation or for storage systems [12].

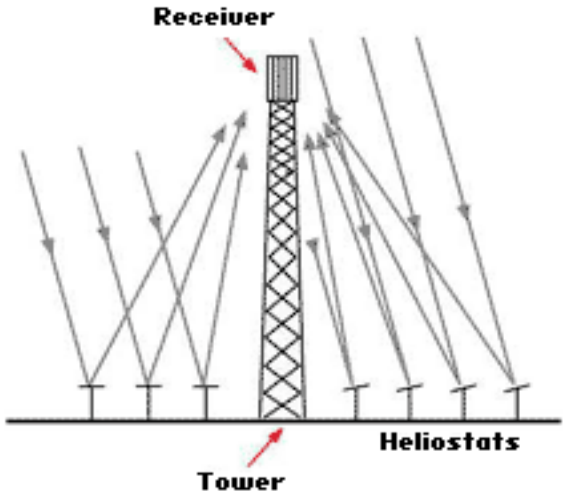


Figure 10 : Tower Receiver

Applications: Tower receiver has exclusive applications in solar furnace and generating power by producing steam in a solar power plant on the account of very high temperatures .The waste heat from a solar power plant can be used to run a solar desalination process.

3.11 Dish Stirling

Dish Stirling(Figure 11) has a large reflective dish to concentrate the incoming solar radiation at the focal point of the reflector. It also uses a two-axes tracking system. The working fluid in the receiver has a temperature between 250°C to 700°C and is used by Stirling engine for the generation of power [12].Dish Stirling has the highest efficiency of all the solar technologies available. It has an efficiency of 30% compared to 15% efficiency of solar photovoltaic [13].

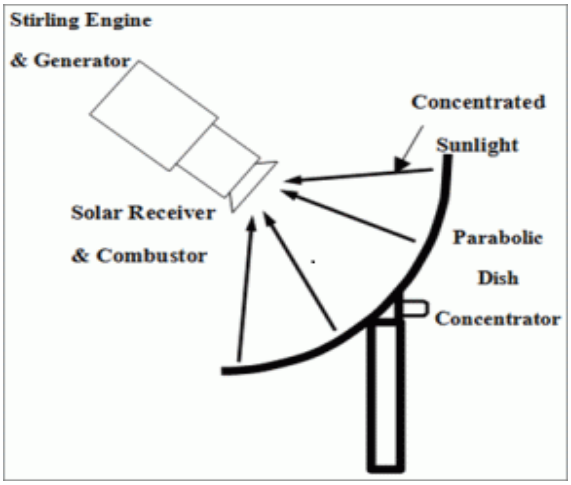


Figure 11: A dish Stirling

Image source: www.solardryer.com

Applications: The Stirling engine has many applications from heating and cooling to underwater power systems. A Stirling engine can function in reverse as a heat pump for heating or cooling. Other uses include: combined heat and power, solar power generation, Stirling cryo-coolers, heat pump, marine engines, and low temperature difference engines.

3.12 Enclosed Trough

An enclosed trough consists of a solar thermal system within a greenhouse-like glasshouse. The purpose of the glasshouse is to make sure that the solar thermal system is from negative impacts and its efficiency is not effected [14]. Curved shaped reflecting mirrors are used which are suspended by wires from the ceiling. A single axis tracking system is used and the sunlight is concentrated on a network of steel pipes which are also suspended from the glasshouse structure [15]. Water is made to flow through these pipes to produce steam. Creating a protecting environment helps the mirror from the effects of wind and higher temperature is achieved with prevention from dust deposits on the mirrors [14].

Applications: These systems have applications in the process heat requirement and power generation purposes.

IV. INTEGRATİON OF CST WİTH OTHER TECHNOLOGİES

4.1 Concentrated Solar Thermoelectricity Generation

It is a well-known fact that when junctions between two dissimilar metals and exposed to different temperatures they can deflect a compass [16]. In other words a potential differ an electric potential is set up and a current flows if the closed circuit. This Seebeck effect can be initiated by using a concentrating mirror arrangement which directs the incoming solar radiation at a fixed point where we want to make the junction hot for a given pair of metals [18]. Thus a suitable temperature difference can be generated which further creates the potential difference across the junction.

4.2 Solar Vapour Compression Refrigeration

The compressor of an air-conditioner raises the temperature of the refrigerant fluid. If a concentrator is incorporated with the existing vapour compression system, the rays falling on the solar concentrator can be used to provide a portion of the temperature increase thereby reducing the workload on the compressor considerably. This will enable the system to consume less electricity.

V. CONCENTRATED SOLAR THERMAL (CST) İN INDİA

India has an immense potential of solar energy. A fairly large amount of fossil fuels, especially electricity & fuel oil are being consumed for process heat, space cooling and various other thermal applications. In the majority of the cases, heat is required in the form of high pressure steam/air/oil between 90°C to 350°C.

Solar water heating is a well-established technology and is used exclusively but is limited to the temperature of 90°C. Whereas CST can provide temperatures in the range of 100°C to 450°C [17].

5.1 Status of CST Technology

In India there are mainly three types of CSTs.

i) Dish Solar Cooker to cook food for 10 to 40 people which are manually tracked.
ii) Fixed focus E-W automatically tracked elliptical dishes (Scheffler) for direct indoor cooking for about 50 to 100 people and generation of steam for laundry, space cooling of any capacity.
iii) Fully tracked dual-axes Fresnel dishes.

All the above mentioned technologies are in operation with the support of MNRE in the recent past years.

5.2 Large Scale Applications at Present

- *For cooking food:* The system consists of 73 fixed focus single axis automatically tracked elliptical dishes, each of 16 sq.m. area and generates about 3500 kg of steam per day to prepare food for hundreds and thousands of people in the community kitchens at the institutional canteens and religious centres. It is the world's largest solar concentrating system at Shirdi, Maharashtra which makes food for 20,000 people per day. The plant was commissioned in July, 2007. This system saves around 263 kg of LPG per day.

- *For Industrial Application*: Another big CST system is installed at Hindustan Products Ltd., Faridabad, Haryana which consists of 20 parabolic dishes 16 sq.m. each and is able to produce 0.4-0.45 million kcal of heat per day and is used for vulcanization of cables. The vulcanization is done by dipping the cable-core for 18-24 hours in a heated tank with a maintained temperature of 85°C.

- *For Heat Ventilation & Air Conditioning (HVAC):* Integration of CST with vapour absorption machines (VAM) is also done now-a-days primarily in the areas where power cuts are high or the electricity rates are expensive. One of the 213 Ton Refrigeration (TR) system is at Civil Hospital, Thane with a combination of 160 TR with VAM and 52 TR through liquid desiccant, each of 13.5 sq.m. area. As it is a coastal region, the combined VAM and the desiccant system makes it economic as the desiccant system firstly dehumidifies the moist air which is further

cooled using VAM. The system has been integrated with a briquette fuelled biomass boiler which runs 24x7. Various other examples of solar cooling include 100 TR AC plant at Muni Seva Ashram, Vadodara, 92 TR systems at TVS, Suzuki factory near Chennai, 50 TR systems at NTPC, Noida [17].

VI. SAVİNG OF FUEL WİTH THE PRESENT CST INSTALLATİON

Total of 144 steam generating systems have been installed so far with a cumulative figure of 28,000 sq.m. of dish area, 23 systems with 8100 sq.m. of CST area are at execution stage (figures till September, 2013). For instance a 100 sq.m. System can save 5,000 to 10,000 litres of diesel per year and 600 to 1200 LPG cylinders per year depending on the type of technology used and availability of DNI (Direct Normal Irradiance). If it is assumed to be 80% functional, it can be inferred that about 18 lakh litres of fuel oil would have been saved per year from CST installation. Besides this a lot of GHG (Green House Gas) load will be reduced touching 8500 tons per year [17].

VII. CST TECHNOLOGY ASPECTS OBSERVED:

Limitations: Lack of awareness about the technology, problems in large-scale promotion of CSTs, deficiency of information on successful projects, fool-proof technology, requirement of large space, performance data on CSTs with varying DNI is not available, high input cost, long gestation periods and inconsistent performance on small scale level are the major reasons for the low confidence about solar power among the masses. Efforts are required to promote CST on a bigger scale and technological advancements are needed to overcome the existing difficulties.

Advantages: However there are many limitations to the technology even then the solar power is proving to be boon for the rural applications and standalone system for powering far flung rural areas where grid connectivity is still a far cry, supply of LPG cylinders is very low. Various CSR activities have promoted the use of solar power for providing power through Solar Power.

VIII. CONCLUSİON

It is very important to understand the technologies discussed in this paper so that we can employ them in practical use. It should be realized that the increasing demand for power can be met with the above discussed methods. In India some of the technologies in this paper have been employed but many are only at the research stage, so this work emphasizes the use of these solar concentrating arrangements. Awareness should be spread about their applications as we cannot depend upon a single method for producing power through sun rather we need to have a holistic approach while incorporating them.

REFERENCES

[1] KLAUS S. LACKNER (2010), Comparative Impacts of Fossil Fuels and Alternative Energy Sources.

[2] Donald J. Wuebbles, Atul K. Jain,(2001),Concerns about climate change and the role of fossil fuel use,.

[3] J.P.Kesari, Uk Sahoo, Sk Singh, P.B.Sharma,(2014)Transforming India Into a Green Nation: Bottom Up Approach through Solar Energy Education, Training and Innovations.

[4] A Text book of "Non –Conventional Energy Resources", B H KHAN, ISBN. 9780070142763.

[5] A.T. Kearney,(2013),Solar Power and India's Energy Future.

[6] Ministry Of New and Renewable Energy ,GoI,mnre.gov.in.

[7] IEA-ETSAP and IRENA,(2013),Concentrating Solar Power, Technology Brief

[8] Yinghao Chu, Global Energy Network Institute (GENI),(2011),Review and Comparison of Different Solar Energy Technologies

[9] Sorenson, B., Breez, P.,(2009), Renewable Energy Focus Handbook, Academic Press

[10] Kalogirous, Soteris,(2004) "Solar Thermal Collectors and Applications", Progress in Energy and Combustion Science.

[11] George M. Kaplan,(1985), Understanding Solar Concentrators.

[12] Christopher L. Martin., Yogi Goswami (2005). Solar energy pocket reference. Earthscan. p. 45. ISBN 978-1-84407-306-1.

[13] Akshay Urja , Ministry of New and Renewable Energy,GoI,Volume 7,Issue 5,April 2014

[14] Deloitte Touche Tohmatsu Ltd, (2011), "Energy & Resources Predictions 2012".

[15] Helman,Christopher, (2011),"Oil from the sun", "Forbes",

[16] Seebeck, T. J., (1825) "Magnetische Polarisation der Metalle und Erze durch Temperatur-Differenz" (Magnetic polarization of metals and minerals by temperature differences), Abhandlungen der Königlichen Akademie der Wissenschaften zu Berlin (Treatises of the Royal Academy of Sciences in Berlin), pp. 265-373.

[17] Sun Focus, (2013),UNDP-GEF Project on CSH,Ministry of New and Renewable Energy, Government of India

[18] Daniel Kraemer, Bed Poudel, Hsien-Ping Feng, J. Christopher Caylor, Bo Yu, Xiao Yan, Yi Ma,Xiaowei Wang, Dezhi Wang, Andrew Muto, Kenneth McEnaney,Matteo Chiesa4, Zhifeng Gang Chen, (2011),High-performance flat-panel solar thermoelectric generators with high thermal concentration.

[19] John A. Duffie & William A. Beckman, 2006Solar engineering of thermal processes, third edition,

[20] Francia G.,(1968), Pilot plants of solar steam generation systems.Solar Energy;12:51 – 64.

[21] Soteris A. Kalogirou ,(2004),Solar thermal collectors and applications .

[22] Soteris Kalogirou,(1998),Use of parabolic trough solar energy collectors for sea-water desalination

Available online at www.sciencedirect.com

ScienceDirect

Procedia Engineering 97 (2014) 2213 – 2221

Procedia Engineering

www.elsevier.com/locate/procedia

12th GLOBAL CONGRESS ON MANUFACTURING AND MANAGEMENT, GCMM 2014

Simulation Modelling and Analysis of Network Design for Closed-Loop Supply Chain: A Case Study of Battery Industry

A. Jayant[a*], P.Gupta[b] and S.K.Garg[c]

[a,b]*Mechanical Engineering Department, SLIET Deemed University, Longowal, Sangrur, Punjab, INDIA*
[b]*Department of Mechanical Engineering, Delhi Technological University, Delhi-110042, INDIA*

Abstract

Reverse logistics has evolved to assist companies in recognizing potential benefits and overcoming challenges associated with its operations and strategies. Reverse logistics has a considerable influence both on production planning and management and on the determination of optimal production and storage capacities. Product recovery, which encompasses reuse, remanufacturing and materials recycling, requires a structured reverse logistic network in order to collect products efficiently at the end of their life cycle. Present work describes simulation modelling of reverse logistics networks for collection of EOL products for XYZ Limited Company of North India. This company is involved in production of acid batteries for commercial use. Simulation model presented in this work, allows the user to analyze the future performance of the network and to understand the complex relationship between the parties involved. The findings from the simulation suggest that the model calculates cycle time, transfer time, transfer cost, and resource utilization in a predictable manner. Simulation model was developed using Arena 11.0 simulation package.

© 2014 Published by Elsevier Ltd. This is an open access article under the CC BY-NC-ND license (http://creativecommons.org/licenses/by-nc-nd/3.0/).
Selection and peer-review under responsibility of the Organizing Committee of GCMM 2014

Keywords: Reverse logistics; recycling; simulation modelling, supply chain networks

1. Introduction

The business of logistics has considerably changed due to globalization, modern information technology, and especially increasing ecological awareness and development of sustainable supply chain systems. The location of production facilities, storage concepts, and transportation strategies are major determinants of closed loop supply chain performance. There is a trend nowadays in interest towards firms' environmental sustainability activities for the society welfare and improvement environmental practices in company supply chains. Reverse logistics

*Corresponding Author: A.Jayant Tel. No.:01672-253276,09417666112
E-mail.ID: arvindjayant@sliet.ac.in

1877-7058 © 2014 Published by Elsevier Ltd. This is an open access article under the CC BY-NC-ND license (http://creativecommons.org/licenses/by-nc-nd/3.0/).
Selection and peer-review under responsibility of the Organizing Committee of GCMM 2014
doi:10.1016/j.proeng.2014.12.465

practice has been gaining growing interest among researchers and practitioners of operations and supply chain management over the last decade. Nevertheless few works on reverse logistics have addressed the relationship between the manufacturing strategies and environmental issues [1].This situation, which accompanies consumers developing disposable habits, has caused a large amount of waste, rapid depletion of resources, and serious damage to the environment. To deal with these critical problems, many governments have announced environmental legislation associated with green product designs and encouraged enterprises to implement green supply chains and reverse logistics to improve customer satisfaction, extend product life, and decrease resource investment. Reverse logistics is a recoverable system that increases product life by means of recycling, repair, refurbishment, and remanufacturing [2-4]. In 2011, Benjamin T. Hazen [5] defined reverse logistics as the processes associated with the flows of product returns, source reduction, recycling, material substitution, material reuse, waste disposal, material refurbishment, repair, and remanufacturing. Hence, the recoverable system deals with the physical flows of products, components and materials from end users to re-users. Efficient management of reverse logistics will benefit enterprises and contribute to environmental protection [6].

In this paper, a reverse logistics network for used inverter batteries collection in north India is presented, including the corresponding simulation model. The aim of the paper is to provide a flexible model to address some of the aforementioned problems associated with reverse logistics networks. In order to achieve this, firstly, a reverse logistics network was designed to establish transfer stations, drop-off points and a disassembly plant. Secondly, a simulation model was developed using the Arena 11.0 simulation package. Thirdly, the simulation model was tested for the waste inverter batteries collection process in north India. The certainty of the results was statistically defined using a confidence interval of 95%. The model was then validated using t-distribution in order to find out the number of simulation runs required so that the results are within the 95% confidence interval. Finally, a sensitivity analysis was carried out to analyze the effect of incoming goods, the fixed and variable costs of transport.

2. Literature survey

The rapid advance of technology results in a shortened product life cycle. This situation, which accompanies consumers developing disposable habits, has caused a large amount of waste, rapid depletion of resources, and serious damage to the environment. To deal with these critical problems, many governments have announced environmental legislation associated with green product designs and encouraged enterprises to implement green supply chains and reverse logistics to improve customer satisfaction, extend product life, and decrease resource investment. Reverse logistics is a recoverable system that increases product life by means of recycling, repair, refurbishment, and remanufacturing. Efficient management of reverse logistics will benefit enterprises and contribute to environmental protection [6]. Awareness among the customers for the green products through green supply chains is increasing and industries become concerns for the sustainable development in business environment today, increasing attention is given to managing the waste streams and depletion of non-renewable resources [7].

Environmental management aims primarily to reduce waste volume by moving away from one-time use and disposal to having control of the product's recovery. This encompasses reuse, remanufacturing and materials recycling, which can be the three end-of-life (EOL) alternatives determined by the product's characteristics at the end of the product life cycle [8]. As these concerns start to affect the customer's purchasing decisions, manufacturers are increasingly forced to consider their product's impact on the environment. This changing trend extends the responsibility of OEM beyond the production and distribution to the responsibility for their products at the end of their life cycle. A major issue in the reverse distribution is integration of forward and reverse supply chain. Returns information captured should be integrated with forward supply chain information to achieve optimum planning and reduction of costs. The whole support network can then be designed in such a way that it can service both the forward and reverse logistics processes efficiently. This is in line with the concept of a closed-loop supply chain design [9]. G. Kannan et. al. [9] developed an integrated, multi-echelon, multi-period, multi-product mixed integer linear programming model to optimize the distribution and inventory level for a closed loop supply chain network for waste batteries using a genetic algorithm. The modelling of this closed loop supply chain network is done in the context of a lead-acid battery (SLI batteries) production. Gengui Zhou and Hokey Min [10] proposed a

non-linear mixed-integer programming model and a genetic algorithm (GA) that can solve the stochastic network design problem in a closed-loop supply chain.

Benjamin T. Hazen [5] proposed a concept to synthesize the fundamental factors established in extant conceptual reverse logistics frameworks in order to provide a synopsis of these factors to business decision makers who are looking to adopt or improve their firms' reverse logistics functions.

Based on the above literature, it is identified that there is a research potential to design reverse logistics network for End-of-Life (EOL) product management (to recover the value from used products). The purpose of this research work is to develop an integrated model of forward and reverse supply chain for battery recycling using simulation approach. The modeling of this closed loop supply chain network is done in the context of a lead acid battery automobile batteries production.

3. Reverse logistics practice in XYZ limited

XYZ Limited is one of the leading global business groups of north India, operating as manufacturer and exporter of lead metal and its products. The company manufactures lead metal by smelting and recycling processes, which are further extended to lead refining, lead alloying and lead oxide (litharge, red lead and lead sub-oxide). Aside from lead processing, XYZ Limited is engaged in trading of lead scrap, lead ore, lead concentrates, lead battery scrap and lead products globally. The company's 15 years' experience in the lead industry has sharpened its expertise in producing quality products such as lead metal and lead by-products, which gives it an edge to gain trust on quantitative grounds. The refining plan uses a pyro-metallurgical process for lead refining, producing 5-10 tons/day of lead with a minimum purity level of 99.97% from furnace-tapped crude lead. Most lithium batteries are non-rechargeable and are used in cameras, hearing aids and defense applications. For proper disposal, the batteries must first be fully discharged to consume the metallic lithium content. Battery recycling plant requires that the batteries be sorted according to chemistries. Some sorting must be done prior to the battery arriving at the recycling plant. Nickel-cadmium, nickel-metal-hydride, lithium-ion and lead acid are placed in designated boxes at the collection point. Battery recyclers claim that if a steady stream of batteries, sorted by chemistry, were available at no charge, recycling would be profitable. But preparation and transportation add to the cost. The recycling process starts by removing the combustible material, such as plastics and insulation, with a gas fired thermal oxidizer. Gases from the thermal oxidizer are sent to the plant's scrubber where they are neutralized to remove pollutants. The process leaves the clean, naked cells, which contain valuable metal content. The cells are then chopped into small pieces, which are heated until the metal liquefies. Non-metallic substances are burned off; leaving a black slag on top that is removed with a slag arm. The different alloys settle according to their weights and are skimmed off like cream from raw milk. Cadmium is relatively light and vaporizes at high temperatures. In a process that appears like a pan boiling over, a fan blows the cadmium vapor into a large tube, which is cooled with water mist. This causes the vapors to condense and produces cadmium that is 99.95 percent pure. Current battery recycling methods requires a high amount of energy. It takes six to ten times the amount of energy to reclaim metals from recycled batteries than it would through other means [11].

A series of interviews and discussion sessions has been conducted in the plant with company management during this project and following problem areas are identified for improvement in reverse logistics operation of the plant.

- Supply of used batteries is irregular and company is unable to forecast collection of EOL products.
- The company does not having any well-structured model of reverse logistics practice.
- Performance evaluation criteria are undefined in the existing model of the company.
- Under utilization of existing workstations of the reverse supply chain.

To solve aforesaid problems and performance improvement an integrated model of reverse supply chain has been developed for the company in simulation environment, which is capable enough to predict the future performance of the company.

4. Design of integrated supply chain logistics network

At the current stage, the company is not using a well-defined structured approach to get EOL product in the company. Automobile batteries are collected at battery collection center, from collection center they are transported to the recycling plant where recycling is done and finally converted to new battery production and other lead products. Recycling involves processing used materials into new products to prevent waste of potentially useful materials, reduce the consumption of fresh raw materials, reduce energy usage, reduce air pollution (from incineration) and water pollution (from land filling) by reducing the need for "conventional" waste disposal, and lower greenhouse gas emissions as compared to virgin production. Recycling is a key component of modern waste reduction and is the third component of the "Reduce, Reuse, and Recycle" waste hierarchy. Therefore, we have designed and developed an integrated model of forward and reverse logistics supply chain networks. Prior to model construction with the Arena simulation package, it is first fundamental to obtain an appropriate conceptual model, by which the reverse logistics infrastructure can be described. When designing a network structure of reverse logistics, there are many factors to be considered .The factors include inverter batteries, the number and the type of participants in the system, battery collection centre, battery recyclers, consumers, characteristics of the material flow and product characteristics. The retailers will deliver the inverter battery directly to the disassembly centre. At the centre, the parts that can be manufactured or recycled will be extracted and transferred either to the recycling facility or to remanufacturing plant.

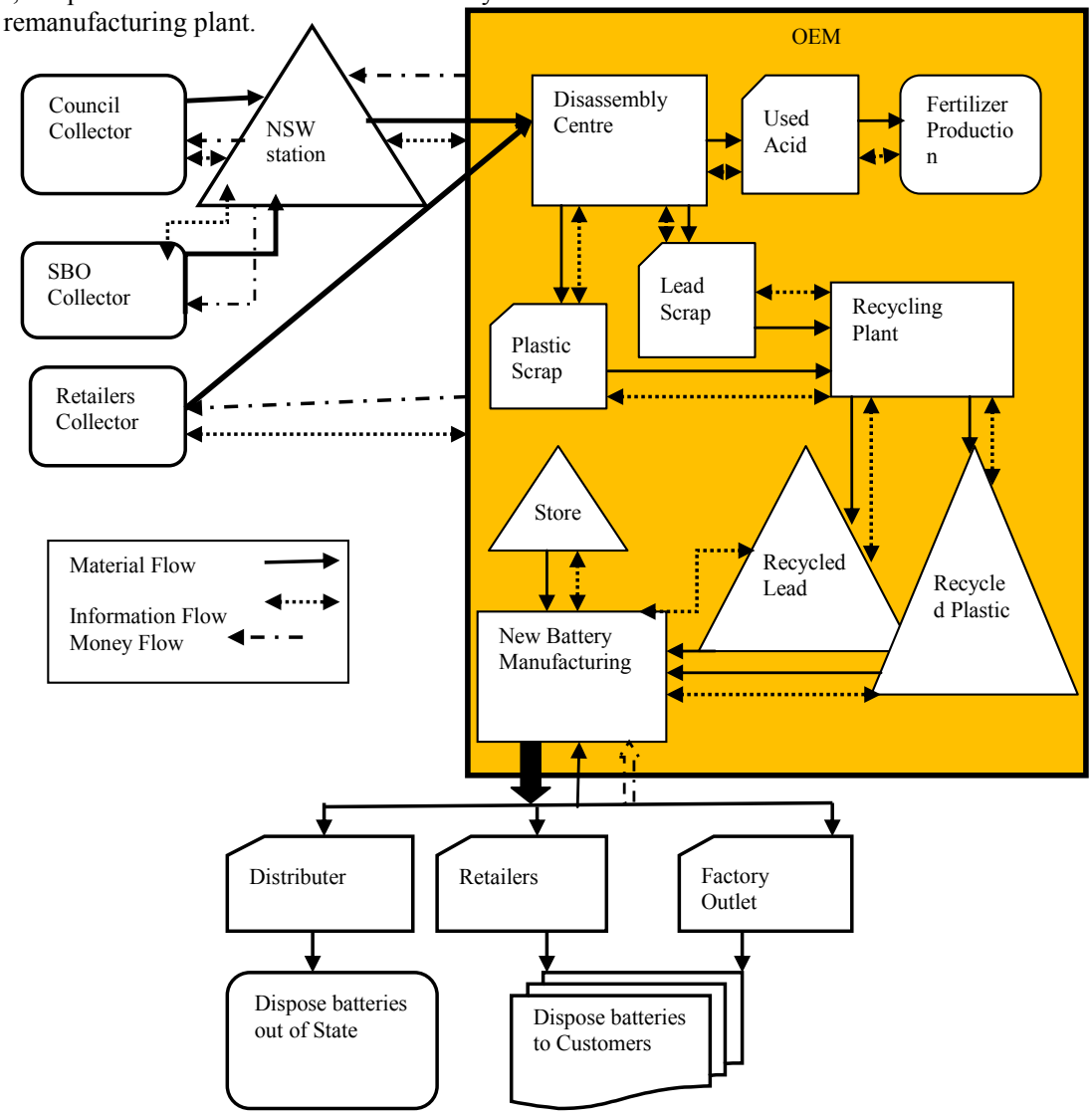


Figure 1 Reverse Logistic Network simulation model of forward and reverse supply chain

5. Simulation modelling of the reverse logistics network

The Arena simulation package by Rockwell Inc, which allows such modular design, has been used to create the simulation model. Figure 1 shows the structure of simulation model and show simulation model logic in ARENA simulation environment. The starting point of simulation is in the" Creation and Assigning of Collector" sub model, where inverter batteries are created and then assigned to the three collectors. The first process in the council sub-model is to determine the area of the council in which inverter batteries are discarded in accordance with the council's population. Then collection of EOL batteries is assigned to the council, retailer and SBOs area in the area by using the probability distribution. Inverter batteries are then delivered either to the NSW "Transfer station" sub-model if the collector is a council or a SBO or to the "Disassembly Plant" sub-model if the collector is a retailer. The inverter batteries coming from NSW station are brought in by the disassembly plant where they are disassembled and separate different components of batteries and finally transfer lead scrap and plastic scrap to the recycling plant.

6. Simulation model development

The system represents the final operation of manufacturing of batteries after recycling. The arriving parts are inverter batteries that are collected by council, SBOs, retailer. The first units called, council collector with inter arrival times to our model being exponentially distributed with a mean 7 (all times are in minutes). Upon arrival, they are transferred to NSW- station with a route time 35 minutes. The second units called, SBO collector with inter arrival times to our model being exponentially distributed with a mean 8. Upon arrival, they are transferred to NSW-station with a route time 35 minutes. The third units called, retailer collector with inter arrival times to our model being exponentially distributed with a mean 8. Upon arrival, they are transferred to NSW- station with a route time 50 minutes. The inverter batteries collected at NSW-Station are transferred to Disassembly centre. At Disassembly centre, the batteries are dismantled and separate out into different parts by "N-way by chance" distribution where 70% lead scrap, 20% Plastic scrap and 10% spent acid is obtained. The spent acid is directly reclaimed by acid reclamation process and the process time for the combined operation at acid reclamation follows a TRIA (7, 9, 10) distribution and used for chemical fertilizer production. 70% lead scrap is recycled by refining through pyrometallurgical process and the process time follows a TRIA (35, 35, 50) distribution and gets 99% pure lead. Similarly, the plastic scrap is recycled by plastic recycling process and the process time follows a TRIA (25, 30, 35) distribution and manufacture outer bodies of batteries.

The stores release new plastic body, purified lead and new acid for manufacturing of new batteries by battery manufacturing process and the process time follows a TRIA (35, 45, 55) distribution. In the last, the decision how these batteries are distributed should be taken. It should be distributed through N-way by chance distribution i.e., 45% through distributor, 40% through retailer and remaining 15% through factory outlet. Distributor dispenses batteries to out of states while retailer and factory out-let dispense batteries to customers. Simulation model collects statistics in each area on entity, transfer time and transfer cost (councillor, SBOs, retailer and disassembler), process and resource utilization. The random nature of simulation inputs renders the simulation run able to produce a statistical estimate of the performance measure, not the measure itself. So that estimates can be statistically precise (have a small variance) and free of bias, the following parameters were specified:

(i) Length of each simulation run= 30 days (one month).
(ii) Number of independent simulation runs = 70

7. Verification and validation

Verification concerns the operational model (whether it is performing properly). It is done to ensure that:

- The model is programmed correctly.
- The model does not contain errors, oversights, or bugs.

In recycling process, model verification took place as a continuing process. In this case, the percentage error is at an acceptable level of less than 5%.

In this study, comparisons between the simulation and calculated results are made. The associated parameters are set constant for calculating the transportation costs by using deterministic data. This includes average truck load size, average speed of transporter, transporter cost per hour, and its travel distance. The transfer times and costs per part are calculated by using,

$$\textbf{Transportation cost/part} = \frac{\textbf{Transportation time} \times \textbf{Transportation cost/hr}}{\textbf{No. of transported part per trip}}$$

In order to make sure that the model data accurately represent the actual process, hence enhance model validity, a confidence interval analysis was carried out. A 95% confidence interval was determined and the required number of simulation replications calculated by the following equation [12]

$$n = \frac{Z_{\alpha/2}\, S^2}{d^2} \qquad \ldots\ldots\ldots\ldots\ldots\ldots (1)$$

Where n is the number of desired replications, d is the accuracy expressed, Z is the critical value from the standard normal table at given confidence interval & S is the standard deviation estimated.

8. Results & discussion

Statistics from simulation of the designed model are summarized in the tables 1-7 given below which focus on main performance indicators in our process that are: transfer time, transfer cost, process, total time for the process (VA), resource utilization and the number of entities processed in the process. Simulation results show tremendous improvement in the designed reverse logistics network parameters and improve system performance and product supply planning function. The results of simulations are summarized in table 1-7. The Model calculates the values in predictable manner of the main performance indicators in designed processes that are: transfer time, transfer cost, recourse utilization for the process and number of entities processed in the process. Product transfer cost of all the players in the supply chain has been reduced by operating the business in the developed model. The Council's product transfer cost reduced by 31.71%, SBO's transfer cost reduced by 31.42%, retailer's cost by 24.07% and Disassembly cost reduced by 37.91%. Product transfer time among the players also reduced after the simulation analysis. The Council's by 16.66%, SBO's by 16.66%, Retailer's by 23.91% and Disassembly centre's by 30.55%.Resources (Work Station) utilization increases by the simulation analysis of the designed networks model. Acid reclamation by 57.50%, Battery manufacturing by 21.33%, Plastic body manufacturing by 23.07%, Disassembly centre by 60%, Lead scrap by 27.14%, Plastic recycling by 44%, pure lead production by 75%, Pyro-metallurgical Process by 16.47%, Scrap plastic by 54.76% and Spent acid utilization by 32.25%.

Table 1 Total Time per Entity

S. No.	Work Station	Processing Time (Minutes)
1.	Lead Refining Process	37.85
2.	Lead Scrap Process	24.73
3.	New Battery manufacturing	21.22
4.	Plastic Recyclers	25.37
5.	Scrap plastic process	20.21
6.	Spent acid process	12.27

Table 2 Total cost per entity

S. No.	Process Name	Unit Processing Cost (Rs.) Average
1.	Acid reclamation	6.13
2.	Battery Manufacturing	3.35
3.	Plastic Body Manufacturing	15.22
4.	Disassembly	10.20
5.	Lead Scrap	15.60
6.	Plastic recycling	10.00
7.	Pure lead	8.90
8.	Pyro-metallurgical Process	10.67
9.	Scrap plastic	8.60
10.	Spent acid	5.50

Table 3 Number busy during resource queue

S. No.	Work Station (Process)	Average busy (%)
1.	Acid reclamation	42.40
2.	Battery Manufacturing	81.07
3.	Plastic Body Manufacturing	86.36
4.	Disassembly	78.42
5.	Lead Scrap	79.83
6.	Plastic recycling	35.75
7.	Pure lead	24.66
8.	Pyro-metallurgical Process	99.26
9.	Scrap plastic	55.00
10.	Spent acid	68.17

Table 4 Queue in the system

S. No.	Key Work Station (Process)	Avg. Waiting Time (Minutes)
1.	Disassembly	38.00
2.	Battery Manufacturing	5.00
3.	Lead Recycling	45.00
4.	Plastic recycling	44.00
5.	Plastic Body Manufacturing	22.00

Table 5 Comparison of Transfer Cost

Transporters	Transfer Cost (Rs.)			
	Council	SBO	Retailer	Disassembly centre
Manual (Average)	7.00	7.00	5.40	5.46
Simulation (Average)	4.78	4.80	4.10	3.39
Improvement	31.71%	31.42%	24.07%	37.91%

Table 6 COMPARISON OF TRANSFER TIME

Transporters	Transfer time (minutes)			
	Council	SBO	Retailer	Disassembly centre
Manual (Average)	72	72	46	36
Simulation (Average)	60	60	35	25
Improvement	16.66%	16.66%	23.91%	30.55%

Table 7 Comparison of Resource Utilization

Resource Utilization(Number Busy)	Manual (Average)	Simulation (Average)	Improvement (%)
Acid reclamation	0.40	0.63	57.50
Battery Manufacturing	0.75	0.91	21.33
Plastic Body Manufacturing	0.78	0.96	23.07
Disassembly	0.55	0.88	60.00
Lead Scrap	0.70	0.89	27.14
Plastic recycling	0.25	0.36	44.00
Pure lead	0.20	0.35	75.00
Pyro-metallurgical Process	0.85	0.99	16.47
Scrap plastic	0.42	0.65	54.76
Spent acid	0.62	0.82	32.25

10. Conclusions & scope of future research

The present work provides a flexible model to address some of the aforementioned problems associated with reverse logistics networks. In order to achieve this, firstly, a reverse logistics network was designed to establish transfer stations, drop-off points and a disassembly plant. Secondly, a simulation model was developed using Arena 11.0 simulation package. Thirdly, the simulation model was tested for the spent battery collection process at XYZ limited of northern India. The certainty of the results was statistically defined using a confidence interval of 95%. The model was then validated using t-distribution in order to find out the number of simulation replications required so that the results are within the ±5% error level. Finally, a sensitivity analysis was carried out to analyze the key performance indicators, transfer time, transfer cost, process, resource utilization and the number of entities in the process. The following conclusions have been made from this project:

- An integrated network in view of forward and reverse supply chain logistics has been designed for the Battery manufacturing company which simulates to optimize the supply planning function.
- To perform simulation modelling, the integrated model has been developed in simulation environment of ARENA-11 software to allow the user to analyze the future performance of the network and to understand the complex relationship between the parties involved in business.
- The developed simulation model in ARENA environment calculates cycle time, transfer time; transfer cost, service level and resource utilization in a predictable manner in the designed logistics networks.
- Simulation model of a reverse logistics networks for collecting EOL inverter batteries in the XYZ Limited Company, successfully represents dynamic processes of order arrivals, distribution centre operations, and delivery transportation.
- Experimental runs through simulation are made to evaluate the system performance under different strategies with regard to different criteria such as cycle time, cost, servicing level and resource utilization.
- Product transfer cost of all the players in the supply chain has reduced by operating business in the developed model. The Council's product transfer cost reduced by 31.71%, SBO's transfer cost reduced by 31.42%, retailer's cost by 24.07% and Disassembly cost reduced by 37.91%.
- Product transfer time among the players also reduced after the simulation analysis. The Council's by 16.66%, SBO's by 16.66%, Retailer's by 23.91% and Disassembly centre's by 30.55%.
- Resources (Work Station) utilization increases by the simulation analysis of the designed networks model. Acid reclamation by 57.50%, Battery manufacturing by 21.33%, Plastic body manufacturing by 23.07%, Disassembly centre by 60%, Lead scrap by 27.14%, Plastic recycling by 44%, pure lead production by 75%, Pyro-mettallurgical Process by 16.47%, Scrap plastic by 54.76% and Spent acid utilization by 32.25%. The results clearly illustrate the dramatic improvement in the some performance indicators of reverse logistics operation by using developed reverse logistics network model.

Supply chain is a continuous process, it has to be modified to suit the new challenges faced by the company with the newer approach considering the advanced technology and market. The study can be extended in several ways as given below:

- The scope of work can be extended to improve the efficiency of distribution network by developing the efficient network by connecting the all distributors by the net.
- The model can be expanded to include the element of risk and uncertainty involved in the reverse logistics network design problem.
- To avoid carrying out further simulation experiments, simulation optimization techniques such as meta-models or variance analysis techniques can be applied.

Acknowledgements

The authors express their deep sense of gratitude to management and staff of XYZ Enterprises for providing an opportunity to carry out the project and extending their cooperation for data collection and providing all kind of support for the present research work. The authors are also thankful to the editor-in-chief and anonymous referees for their constructive comments and valuable suggestions that led to a considerable improvement of the paper over its earlier version.

References

[1] Chiou, C.C, A system dynamic model for an open-loop reverse logistic channel, 2010 IEEE International conference on Industrial Engineering and Engineering Management, 2010.

[2] Jayant, P. Gupta, S. K. Garg,Closed Loop Supply Chain for Spent batteries: A Simulation Study, *International Journal of Advanced Manufacturing Systems,* Volume 3, No.1, pp 89-99.

[3] Jayant, P. Gupta, S.K. Garg, Perspectives in Reverse Supply Chain Management(R-SCM): A State of the Art Literature Review, *Jordan Journal of Mechanical and Industrial Engineering***,** Volume 6, Number 1, pp-87-102

[4] Jayant, Sanjeev Kumar, Simulation Modelling of Integrated Supply Chain Logistics Networks, *proceedings of the International Conf. on Soc-Pros 2011, AISC* 131, pp. 87–97.springerlink.com © Springer India 2012.During December 20-22, 2011 at Roorkee.662

[5] Benjamin T. Hazen, Strategic reverse logistics disposition decisions: from theory to practice, *Int. J. of Logistics Systems and Management*, 2011 Vol.10, No.3, pp. 275 - 292 D.S.

[6] Jayant Arvind, P.Gupta and S.K.Garg, Design and Simulation of Reverse Logistics Network: A Case Study, proceedings of *World Congress on Engineering (WCE-2011), London*, U.K., during July 6-8, 2011.

[7] Gungor, A. and Gupta, S.M., Issues in environmentally conscious manufacturing and product recovery: a survey, *Computers and Industrial Engineering*, Vol.36, No.4, pp.811-853.

[8] Dowlastshahi, S., A strategic framework for the design and implementation of remanufacturing operations in reverse logistics, *International Journal of Production Research*, Vol.43, No.16, pp.3455-3480.

[9] G. Kannan, P. Sasikumar, K. Devika, A genetic algorithm approach for solving a closed loop supply chain model: A case of battery recycling, *Applied Mathematical Modelling,* Vol. 34, pp 655–670

[10] Gengui Zhou, Hokey Min, Designing a closed-loop supply chain with stochastic product returns: a Genetic Algorithm approach, *Int. J. of Logistics Systems and Management*, 2011 Vol.9, No.4, pp.397 - 418

[11] www.gravitatechnomech.com

[12] S. Kara, F. Rugrungrang, H. Kaebernick, Simulation modelling of reverse logistics networks, *Production Economics*, Vol.106, pp.61-69.

International Conference on Innovative Applications of Computational Intelligence on Power, Energy and Controls with their Impact on Humanity (CIPECH14) 28 & 29 November 2014

Supervised Pixel Classification into Arteries and Veins of Retinal Images

Smriti Chhabra
Electrical Engineering Department
Delhi Technological University
Delhi, India
smritichhabra1407@gmail.com

Bharat Bhushan
Electrical Engineering Department
Delhi Technological University
Delhi, India
bharatdce@yahoo.co.in

Abstract— **With the emerging computation techniques in the field of medical science such as in Ophthalmology; it is often required an automated technique for identification of pathological condition such as diabetic retinopathy which might cause serious problems like blindness. Retinal diseases are often characterized by modification in retinal vessels. Retinal blood vessels observed with fundus imaging provides important indicators not only for clinical diagnosis and treatment of eye diseases but also for systemic diseases such as diabetes, hypertension etc. which manifest themselves in the retina. Quantitative structural analysis of the retinal vasculature not only helps in the diagnosis of retinopathies but also provides potential biomarkers of systemic diseases. Such as arteriole to venule width ratio (AVR) is a parameter indicative of microvascular health and systemic disease. In this paper we performed retinal vessel's pixel classification into arterioles and venules using Neural Network on DRIVE database. Two types of feed-forward Neural Network are used: Back Propagation Network (BPN) and Probabilistic Neural Network (PNN). BPN gives 83.9% and where as PNN gives 85.1% pixel classification on 20 images. The ROC curve for BPN and PNN has value 0.83 and 0.87 respectively for the DRIVE dataset.**

Keywords— Retinal images, arteries, veins, classification, neural network

I. INTRODUCTION

Retinal blood vessels observed with fundus imaging, provide important indicators not only for clinical diagnosis and treatment of eye diseases but also for systemic diseases such as diabetes, hypertension etc. which manifest themselves in the retina. For example narrowing of retinal blood vessels are the early makers of cardiovascular risk [1]. It is important to classify retinal blood vessels into arterioles and venules for computerized analysis of the vasculature and for biomarker discovery such as AVR. Conventionally, AVR and other retinal vascular parameters are drawn from zone B - an annulus 0.5 to 1 optic disc (OD) diameter from the OD boundary [2,3]. Changes in vessel structure can affect arteries and veins differently and thus in (semi-) automatic retinal image analysis conclusion is drawn from the quantification of venular and arteriolar components distinctly. For instance, measuring the central retrial arterial equivalent (CRAE) and the central retrial venular equivalent (CRVE), which are used to calculate the arteriolar to venular width ratio (AVR) [4].

Developments in automated diagnostic systems offer great potential for retinal fundus imaging to be used in biomarker discovery studies. To this end, in this paper we classify vessel's pixels into arteries and veins in zone B of the retinal images from DRIVE dataset using neural network with only four discriminative features. In section II, literature review has been given and Methodology is explained in section III followed by Results in section IV. Finally, the results are discussed in section V.

II. RELATED WORK

Several authors reported various methods to classify retinal vessels into arterioles and venules in images from DRIVE dataset using different classifier and framework. In 2003, Huiqi, et al. [5] uses minimum Mahalanobis distance classifier for classification of 505 segments of vessels of 35 images obtained from a population-based study in Wisconsin. The success rate is 82.46% and 89.03% for the arteries and veins respectively in Zone B. In 2007, C.Kondermann et al. [6] classified vessels as arteries and veins using Neural Network and Support Vector Machine. The test is performed on 1024*1280 retinal images containing 10132 different vessel skeleton pixels. NN with the combination of Region of Interest (ROI) resulted in 95.23% vessel pixel classification and SVM with ROI resulted in 92.84% vessel pixel classification within three diameters of the optic disk region.In another study, N.Karssemijer et al. presented a supervised, automatic method which determined artery or vein in a vessel based on intensity and derivative information [7]. They extracted features using steered Gaussian filter from the images in DRIVE database. ROC for 20 testing images was 0.88 for correctly classified pixels. In 2011, G.Mirsharif et al. in [8] performed the vessel classification on DRIVE database using 6 features which were selected via features selection method. The best result was achieved using LDA when classification was found on major vessels. Their method resulted in accuracy of 86% on major vessels and 87.53% on main pair vessels in upper and lower region. The classification of major arteries was performed on whole image but not in specific zone. Diego Marin, et al. [9] presented a supervised method using Neural Network for pixel classification on DRIVE and STARE databases. Their methodology computes 7-D vector composed of Gray-level and moment invariants-based features for pixel representation. The area under curve measured for both curves was 0.9769 for DRIVE and 0.9588 for STARE databases. In [10] Jihene, et al. classifies vessel's pixels into arteries and veins using Multi Layer Perceptron. They use Principle Component Analysis for

©2014 CIPECH14.

feature selection. Their approach of feature selection and classification resulted in 95.32% on DRIVE database. In [11] the author performed multifeature analysis for identification of vessels using multiscale vesselness measures and Gabor filters [11]. Adaptive threshold selection method was used with a post processing technique giving ROC curve value up to 0.9616 on DRIVE database.

III. METHODOLOGY

A. Material

In this paper we have used DRIVE dataset for retinal vessel classification. The total 40 images from DRIVE dataset are divided into 20 Training and 20 Testing images. Classification was performed on 171 vessels extracted in similar manner as explained in [12]. Ground truth was generated to compare the final classification results.

B. Pre-processing of images and extraction of centerline pixels

The contrasts or color variability would affect the classification results adversely thus all images were first pre-processed. We preprocessed red, green and hue channel images for background illumination using a method explained in [13]. The Hue channel was also pre-processed to improve the contrast of vessels against background before illumination correction by mapping the original intensity values such that values between 0.01 and 0.8 maps to values between 0 and 1. Four distinctive features were then extracted from centerline pixels of illuminated corrected image. Centreline pixels of vessels in zone B were extracted as previously reported in [12]. In order to extract centerline pixels from zone B first the intensity profile across the vessel axis is obtained. Next the canny edge detection method is applied to each of these profiles to locate vessel edges and finally the centerline pixels are located as the midpoint of pair of edges selected. Canny detection method is explained below:

Areas with strong intensity contrasts in an image are edges. Edge detection method in images suppresses the useless information and preserves the important structural properties in an image. It is an optimum edge detector because of its low error rate. All the edges in an image should be noticed, edge-points should be well localized. The algorithm aims at finding the minimum distance between edge pixels and actual edge. It is required that each single image should have only one response. Based on the above criteria's, firstly the detector smoothens the image to eliminate noise. Edges are marked where the gradients of image have large magnitudes. Local maxima are only marked as edges. The gradient error is further reduced by hysteresis. Pixels which are not suppressed, hysteresis track them using two thresholds. If magnitude is below first threshold, it set to zero therefore a non- edge. If it is above threshold, it is made an edge. If it's between the two thresholds, it is set to zero unless a path is present from this pixel to a pixel with the gradient above.

C. Feature Extraction

Retinal vessels can be distinguished into arterioles and venues using different colours features. The four colour features used in our study are set of colour features which are proven statistically important in differentiating between arteries and veins [14]. After the centreline pixels were found, four colour features viz. MR (mean of red), MH (mean of hue), MG (mean of green) and VR (variance of red) were extracted from illuminated corrected channels. These were extracted around the centre of centreline pixels, with diameter 60% of the mean vessel diameter [15]. Finally Neural Network classifier was applied to classify vessel's pixels into arterioles and venules using these features. Figure 1 shows the flowchart representing the procedure undertaken for the pixel classification into arteries and veins representing the original DRIVE dataset image and illuminated images.

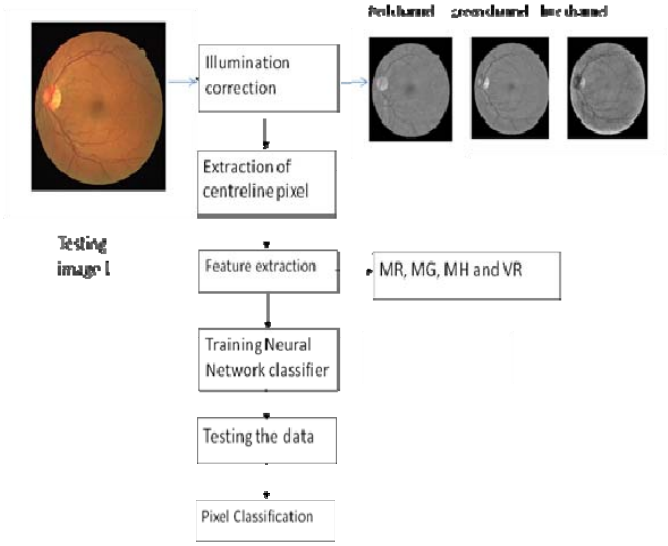


Figure 1: Flowchart representing Methodology

IV. RESULT

The vessel's pixel classification was evaluated on publicly available DRIVE database. The efficiency analysis was evaluated using Receiver Operating Curve (ROC). It plots variation of false ratio versus true ratio. The closer the curve approaches the top left corner, the better the performance of the system. ROC for BPN and PNN is 0.83 and 0.87 respectively.

Total 1730 pixel vessels from 171 vessels were classified. BPN results in correct classification of 83.9% whereas PNN resulted in correct classification of 85.1% as shown in figure 2 and 3 respectively.

Confusion matrix tells us about the classification result or the performance of an algorithm. High numbers of responses are shown in the green squares and the low numbers of correct incorrect responses in the red squares. The lower right blue

squares illustrate the overall accuracies Table I shows the result obtained by each classifier.

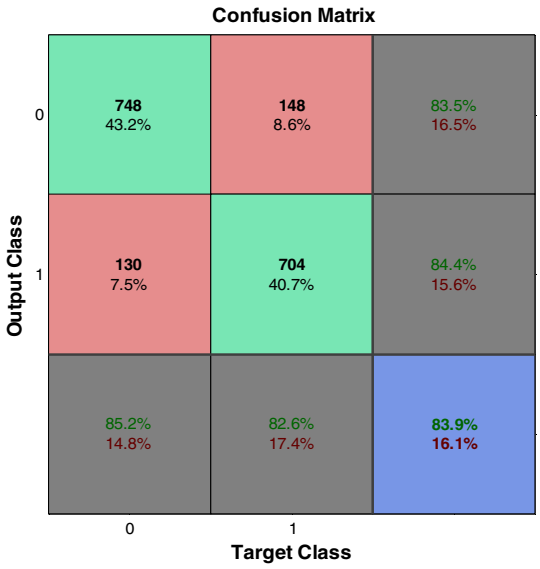


Figure 2.Confusion Plot for BPN for DRIVE dataset

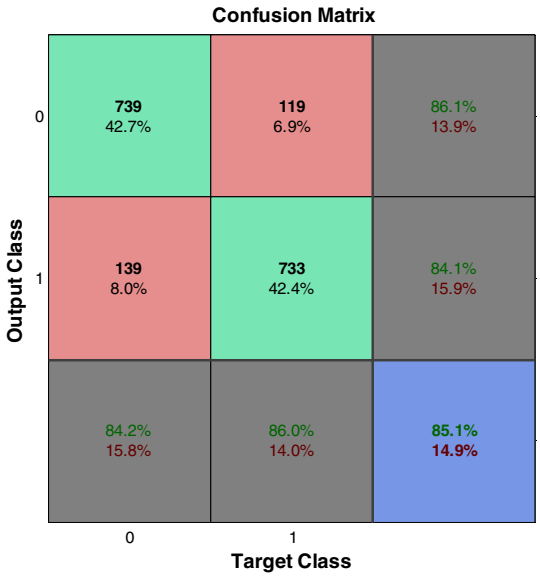


Figure 3: Confusion Plot for PNN for DRIVE dataset

TABLE I : CLASSIFICATION RATE

	BPN	PNN
ROC	0.83	0.87
Overall Pixel classification	83.9%	85.1%

V. DISCUSSION AND CONCLUSION

It is very time consuming to annotate vessels manually hence it is required to design a method which can classify vessels into arterioles and venules automatically. In this paper we proposed a supervised method using four colour features to classify arteries and veins automatically using Neural Network.

Many authors have performed vessel classification on DRIVE dataset using different classifier, features and framework [9, 10, 11]. We have used a simple and widely used supervised Neural Network classifier with only four colour features unlike those work which uses feature selection method [8,10] which is often time consuming. As we have used only fixed four features for classification which make our classification framework faster as extracting and then selecting distinctive features from bank of features is time consuming task.

Our approach resulted in similar result with PNN classifier as compared to [7] who uses different features and supervised classifier. PNN is giving better classification result in comparison to BPN. PNN is a Bayesian classifier implemented in parallel unlike BPN which is trained iteratively. This makes training of parameters faster as compared to traditional Neural Networks. PNN is robust over standard Neural Network.

We conclude that the performance of our system is very promising and producing similar result as compared to recently reported methods even by using only four colour features and simple Neural Network classifier as compared to others recently reported work yet results in a similar classification rate. However, the classification performance may differ on different datasets. The results are highly dependent on locating center line pixels. Also pixel classification on different retinal zone also affects the classification performance. Moreover different classifier and framework would also have an impact on classification rate. Further tests on large, ideally public, are needed to assess comparatively and reliably classification algorithms.

Acknowledgment

Smriti Chhabra would like to thank Mrs. Devanjali Relan of Clinical Research Imaging Centre, University of Edinburgh, U.K. for her significant help for providing and explaining the center line pixel extraction and feature extraction algorithms.

References

[1] T. Y. Wong, R. Klein, B. E. Klein and J. M. Tielsen, "Retinal microvascular abnormalities and their relation to hypertension,

cardiovascular diseases and mortality", Survey Opthalmol,vol.46,pp.59-80, IEEE 2001.

[2] H. Li et al., "Automatic grading of retinal vessel calibre",IEEE transactions on bio-medical engineering, vol. 52, pp.1352-5, 2005.

[3] M. K. Ikram, et al., "Retinal vessel diameters and risk of hypertension: the Rotterdam Study," Hypertension: Journal of the American Heart Association, vol. 47(2), pp.189–94, 2006.

[4] T. Y. Wong, M. D. Knudtson, et al, "Computer-assisted measurement of retinal vessel diameters in the Beaver Dam Eye Study: methodology, correlation between eyes, and effect of refractive errors," American Academy of Ophthalmology, pp. 1183–90, 2004

[5] Li Huiqi, H. Wyne, L. Mong lee and W.Hongyu, "A piecewise Gaussian model for profiling and differentiating vessels" in ICIP03, vol.1,pp.1069-1072,2003.

[6] C. Kondermann ; D. Kondermann and M. Yan "Blood vessel classification into arteries and veins in retinal images", Proc. SPIE6512, Medical Imaging 2007: Image Processing, 651247 (March 02, 2007)

[7] M. Niemeijer ; B. Ginneken and M. D. Abràmoff, "Automatic classification of retinal vessels into arteries and veins", Proc. SPIE7260, Medical Imaging 2009: Computer-Aided Diagnosis, 72601F (February 27, 2009)

[8] G.Mirsharif, F.Tajeripour, F.Sobhanmanesh, H.Pourreza, T.Banaee "Developing an automatic method for separation of arteries and veins in retinal images",1st International Conference ICCKE, October 13-14,2011

[9] D.Martin, A.Aquino, M.Emilio, G.Arias and J.B.Manvel, "A New Supervised Method for Blood Vessel Segmentation in Retinal Images by Using Gray-Level and Moment Invariants-Based Features", IEEE Transactions on Medical Imaging, Vol.30,Jan 2011

[10] J.Malek, R.Tourki, "Blood Vessels Extraction and Classification into Arteries and Veins in Retinal Images", IEEE International Multi-Conference on SSD, March 18-21,2013

[11] A.K.Dhara, R.M.Rangayyan, F.Oloumi, S.Mukhopadhyay, " Methods for the Detection of Blood Vessels in Retinal Fundus Images and Reduction of False-Positive Pixels around the Optic Nerve Head", IEEE International Conference on E-Health and Bioengineering, November 21-23, 2013

[12] D. Relan, T. Macgillivray, L. Ballerini and E. Trucco, "Retinal vessel classification: sorting arteries and veins", in 35th Annual International Conference of the IEEE EMBS,pp.7396-7399, OSAKA,JAPAN,3-7 July 2013.

[13] R.Crastek, M.Wolf, K.Donath,et al. "Automated Segmentation of the optic nerve head for diagnosis of glaucoma. Medical Imaging Analysis,"9(4),297-314,2005.

[14] H.F.Jelinek, C.Depardieu, C.Lucas, D.J.Cornforth, W.Huang and M.J.Cree, "Towards Vessel Characterization in the vicinity of the Optic Disc in Digital Retinal Images" In Proceedings of the Image and Vision Computing, New Zealand ,28-29 November 2005

[15] V. S.Joshi, M.K. Garvin, J.M. Reinhardt, M.D.Abramoff, " Automated artery-venous Classification of Retinal Blood Vessels based on Structural Mapping Method", Medical Imaging 2012:Computer Aided Diagnosis, Proceedings of SPIE vol.8315,pg.3

INTERNATIONAL JOURNAL OF ELECTRICAL ENGINEERING & TECHNOLOGY (IJEET)

ISSN 0976 – 6545(Print)
ISSN 0976 – 6553(Online)
Volume 5, Issue 12, December (2014), pp. 321-327
© IAEME: www.iaeme.com/IJEET.asp
Journal Impact Factor (2014): 6.8310 (Calculated by GISI)
www.jifactor.com

IJEET

© I A E M E

THEFT DETECTION SCHEMES FOR SMART GRID APPLICATION

Palak Kalra

Electrical Engineering, Delhi Technological University
Formerly Delhi College of Engineering, New Delhi, India

ABSTRACT

Energy theft is one of the most important concerns related to the smart grid implementation. It is estimated that utility companies lose more than $25 billion every year due to energy theft around the world. With the smart grid being proposed to modernize current power grids, energy theft may become an even more serious problem since the "smart meters" used in smart grids are vulnerable to more types of attacks compared to traditional mechanical meters especially the Advanced Metering Infrastructure. Therefore, it is important to develop efficient and reliable methods to identify illegal users who are committing energy theft. Although some schemes have been proposed for the UCs to detect energy theft in power grids, they all require the users to send their private information, e.g., load files or meter readings at certain times, to the UCs which invades users' privacy and raises serious concerns about privacy, safety, etc. In this paper, we are analysing how energy theft can be monitored and highlight the current AMI energy-theft detection schemes.

Keywords: Losses; Smart Grid; Advanced Metering Infrastructure (AMI); Energy-Theft Detection

INTRODUCTION

Electricity was sure the greatest invention of 20th century. But people no longer consider it as an asset but a mere liability. Electricity theft needs no introduction, as we are all aware of the prevalence and significance of Electricity theft especially in smart grid applications. It is increasing in most countries with increase in power rates. In a way, stopping these practices is as important as generating electricity. Also it's a wrong thought that uneducated people are responsible for this, as a matter of fact it's mostly educated people who use these practices and cost government huge loss. Electricity theft in smart grid applications especially the Advanced Metering Infrastructure is a major concern these days.

It is one of the principal components of smart grid. Which replaces the normal analog meters with computerized systems that report usage over digital communication interfaces e.g. phone lines. However, with this comes the new risk. With the help of strict rules and a simple yet effective plan, the electricity theft can be reduced effectively.

OVERVIEW

Monitoring electricity theft begins with the analysis of losses in electrical power systems. Losses occur at all levels, from generation, through transmission and distribution, to the consumer and the meter. It is normally at the distribution level where the majority of avoidable losses occur. All electrical power distribution companies operate with some accepted degree of losses. Basically losses incurred in electrical power systems have two components: technical and non-technical.

Technical losses consist mainly of power supply dissipation because of faulty transmission and distribution lines, transformers and measurement systems. They are naturally occurring losses mainly caused by actions internal to the power system. It is possible to monitor and compute these losses provided the power system in question has known quantities of loads. Optimization of technical losses in electricity transmission and distribution grids involves classic tools of power systems planning and modelling. The driving criterion is minimization of the net present value (sum of costs over the economic life of the system discounted at a representative rate of return for the business) of the total investment cost of the transmission and distribution system plus the total cost of technical losses. Technical losses are valued at generation costs and they represent an economic loss for the country, and its optimization should be performed from a country's perspective, regardless of the institutional organization of the sector and ownership of operating electricity utilities.

Non-technical losses are caused by actions external to the power system and consist primarily of electricity theft, non-payment by customers, and errors in accounting and record-keeping.

A NTL is basically any consumed energy which is not included in the bill because of measurement device failure or fraudulent manipulation of said device. This is where electricity theft comes into picture. As the name suggests, it means stealing of electric power. The basic method of stealing electricity is a direct wire-connection to a main power route passing by a house so that electricity can flow to the consumer without crossing the electric meter installed by a governmental agency which is responsible for providing electrical services to customers.

Metering and billing for electricity actually consumed by users is integral to commercial management of an electricity utility. Another critical task is collection of the billed amounts. Effective performance in both functions is critical to ensure the financial viability of the company. From the operational point of view, metering-billing and collection are separate functions and they require specific management approaches.

The two common examples of sources of such losses are component breakdowns that drastically increase losses before they are replaced and electricity theft.Other probable causes of commercial losses are:

- Non-payment of bills by customers
- Errors in technical losses computation
- Errors in accounting and record keeping that distort technical information.
- Inaccurate or missing inventories of data on customers.

GENERAL PRACTISES

There are many ways, local people try to outsmart meters and skip heavy electricity bills. The various types of electrical power theft are:

1. Direct Hooking from Line

It is the most used method for theft of power. 80% of total power theft all over the world is done by direct tapping from line. The consumer taps into a direct power line from a point ahead of the energy meter. This HYPERLINK "http://en.wikipedia.org/wiki/Energy" \o "Energy" energy source therefore is unmeasured in its consumption and procured with or without switches.

2. Bypassing the Energy Meter

In this method the input terminal and output terminal of the energy meter has been shorted by a wire. So energy cannot be registered in the energy meter.

3. Injecting Foreign Element into the Energy Meter

Sometimes skilled individuals inject foreign elements such as transistors, resistors or IC chips into the electrical meter which causes a lower consumption of electricity. Also some meters are manipulated with a remote control circuit by installing the circuit inside the meter which can be operated remotely and the meter can be slowed down at any time consumer desires. If someone tests the meter for its accuracy by external inspection, it always found correct unless the remote is turned on.

4. Drilling Holes in Electromechanical Meter

Drilling holes is a visible type of manipulating an electrical meter. This type of tampering is done to electromechanical types meters. The individual inserts foreign material inside the meter to obstruct the free movement of the rotating disc.

SCHEMES

Different from other issues in smart grid, energy theft seems more intractable. This is partly because it involves human nature and economic considerations which are difficult to observe and control even by advanced measurement equipments. The detection and identification of frauds in power systems has been initially addressed with statistical techniques[7,8]. A variety of solutions to energy theft have been proposed recently due to the fast development of AMI in smart grid. Their explanation in brief is aforementioned.

1. Vector based data classification method

The basic procedure for classification-based energy-theft detection consists of seven parts: data acquisition, data preprocessing, feature extraction, classifier training and parameter optimization, classification, data post processing, and suspected customer list generation. A dataset of customer energy consumption pattern is developed based on the historical data. Then, support vector machines (SVMs) are trained with the data collected from smart meters, that represents all possible forms of theft and are tested on several customers. This data is classified based on rules and the suspicious energy consumption profiles are grouped.

2. Specification based intrusion detection technique

Another common solution for energy-theft detection is state-based detection technique, which uses monitoring state to improve the detection rate. The monitoring state can be derived from wireless sensor networks [10-12, 17], RFID[13], mutual inspection[14], AMI[18], etc. Since wireless sensor networks are cheap and easy to implement [19], they are popular to assist detecting energy theft. McLaughlin et al. proposed an AMI Intrusion Detection System (AMIDS) that uses information fusion to combine the sensors and consumption data from a smart meter to more accurately detect energy theft [10, 11]. AMIDS combines meter audit logs of physical and cyber events with consumption data to more accurately model and detect theft-related behaviours.

3. Game theory based detection technique

Game theory-based energy-theft detection schemes are proposed recently and provide a new perspective to solve the energy-theft issue [15, 16]. In Ref. [15], Amin et al. investigated incentive problems in electricity distribution when customer energy usage is imperfectly observable by the distributor. From the perspective of privacy protection, each customer has private information about the amount of his consumed electricity, and therefore distributor cannot observe customers' energy usage precisely, which results in non-technical energy losses, especially by energy theft. Although installing AMI can reduce such losses to a large extent, it requires substantial cost for distributor. These were some of the established techniques for theft detection. We'll present two schemes having varying, fixed and running costs.

Differential Scheme

Here sensors are put on heavy appliances drawing large powers and are responsible for 90% of the whole consumption like Fridge, AC, TV, Fans etc. And for rest of the appliances, their power consumptions are sensed by one single sensor.

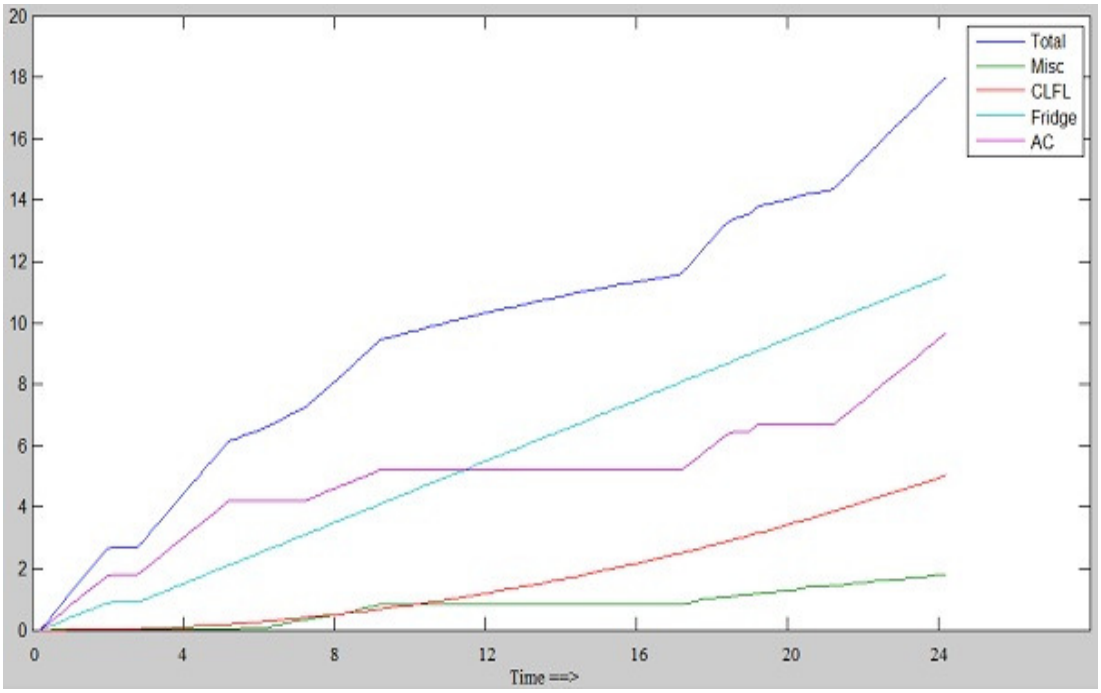


Fig 1. Load curve of a general household meter.

If we know readings of all individual appliances and other small loads. Then we can subtract sum of their readings from actual reading of meter. If result is within the margin of errors relative to its Class type, then it'll be considered a theft-free operation of supply. And if it's not then we would know the exact percentage of electricity thefts going on. Sensors sensing power need not be very accurate, hence cheap CTs or ADCs can be used to save the cost.

Integrated Scheme

This is a very cheap but very effective scheme. In this scheme, a communication module of the sorts of X-bee is embedded into the meter that communicates with the module present in distributor sensing total power going out of it.

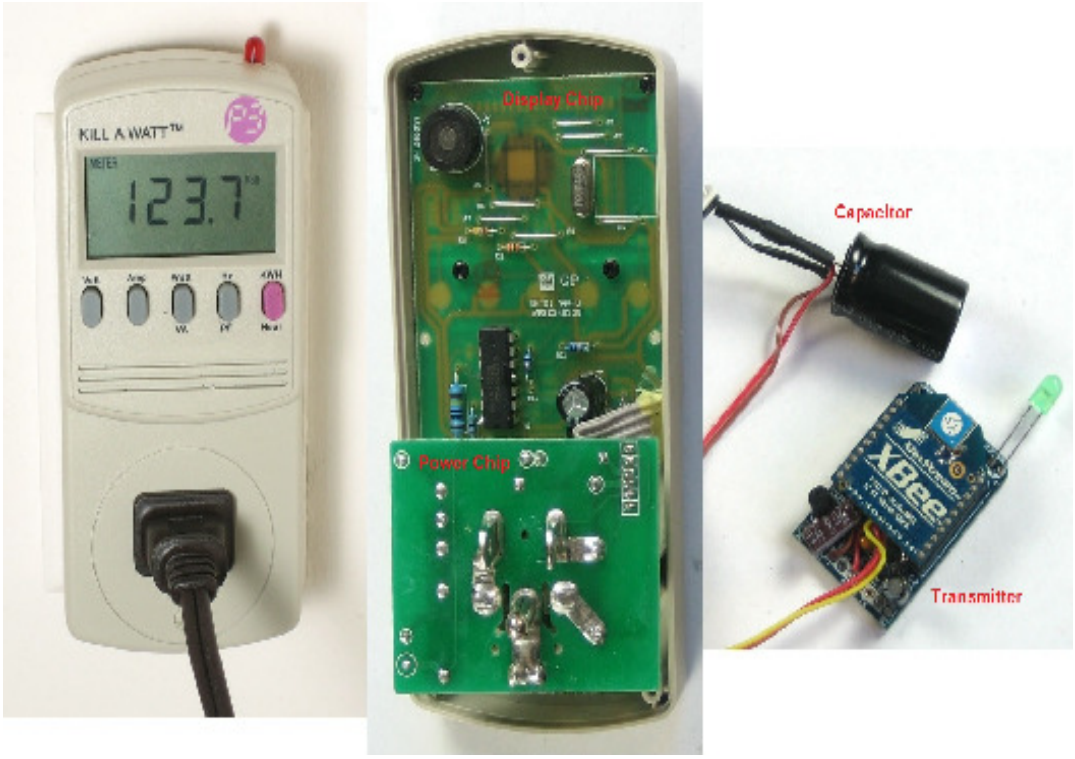


Fig. 2. X-bee embedded inside Conventional Meters connections

Let's assume that normally power is flowing smoothly without any signs of theft so far. All the meters are synced and giving agreeable readings. Now let's suppose that one connection in the distributor box supplies power to three homes each.

When contrasting readings appear, simply switch off the supply of houses from remote utility one at a time for few minutes and see if differences in readings are acceptable during that time. Do this for each house until this problem is resolved, this way we would know exactly which home initiated theft practises and at what time.

Fig. 2 Before I, both meters were running synchronously. At I & II, MCU notified the difference. At IV, utility turned OFF supply in house 1 but still both meters were not in sync. So in V, utility turned OFF supply in house 2 and now both meters are in sync which assures that house 2 is tinkering with meter system.

CONCLUSION

Energy theft detection is surely a very difficult problem in power grid. Though Advanced Metering Infrastructure has digitalised the metering system over the existing analog system, it has raised more complications in the energy theft. In this paper, I mentioned about the existing schemes that have been used to detect energy theft in AMI which is a smart grid application. Also, I added two new schemes for the detection of energy theft in basic power grid network. Smart grid requires some concrete and efficient theft detection techniques designed mainly for advanced metering infrastructure.

REFERENCES

1. Potuganti Prudhvi, Dhruv Balodhi, Manikant, Vamshi, Sudarshan, A smart energy meter Architecture in Indian context 2012
2. Final Report Development of Best Practice Recommendations for Roll out of Smart Meters by Kema International,Netherlands
3. http://siteresources.worldbank.org/EXTESC/Resources/Background_paper_Reducing_losses_in_the_power_sector.pdf
4. http://www.dawn.com/news/742325/electricity-technical-losses
5. https://www.google.co.in/?gws_rd=ssl#q=Theft+Detection+Schemes+for+Smart+Grid+Application
6. http://www.leonardo-energy.org/sites/leonardoenergy/files/root/Documents/2009/ dan_ suriya mongkol_thesis.pdf
7. R. J. Bolton and D. J. Hand, Statistical fraud detection:A review, Statistical Science, vol. 17, no. 3, pp. 235-249,2002.
8. Y. Kou, C.-T. Lu, S. Sirwongwattana, and Y.-P. Huang, Survey of fraud detection techniques, in Proc. IEEE International Conference on Networking, Sensing and Control, 2004, vol. 2, pp. 749-754.
9.]. J. Nagi, K. S. Yap, S. K. Tiong, S. K. Ahmed, and F. Nagi, Improving SVM-based nontechnical loss detection in power utility using the fuzzy inference system, IEEE Transactions on Power Delivery, vol. 26, no. 2, pp. 1284-1285, 2011
10. S. McLaughlin, B. Holbert, S. Zonouz, and R. Berthier, AMIDS: A multi-sensor energy theft detection framework for advanced metering infrastructures, in Proc. IEEE Third International Conference on Smart Grid Communications (SmartGridComm), 2012, pp. 354-359.
11. S. McLaughlin, B. Holbert, A. Fawaz, R. Berthier, and S. Zonouz, A multi-sensor energy theft detection framework for advanced metering infrastructures, IEEE Journal on Selected Areas in Communications, vol. 31,no. 7, pp. 1319-1330, 2013
12. C.-H. Lo and N. Ansari, CONSUMER: A novel hybrid intrusion detection system for distribution networks in smart grid, IEEE Transactions on Emerging Topics in Computing, vol. 1, no. 1, pp. 33-44, 2013.
13. B. Khoo and Y. Cheng, Using RFID for anti-theft in a chinese electrical supply company: A cost-benefit analysis, in Proc. IEEE Wireless Telecommunications Symposium (WTS), 2011, pp. 1-6
14. Z. Xiao, Y. Xiao, and D. H.-C. Du, Non-repudiation in neighborhood area networks for smart grid, IEEE Communications Magazine, vol. 51, no. 1, pp. 18-26, 2013
15. S. Amin, G. A. Schwartz, and H. Tembine, Incentives and security in electricity distribution networks, in Decision and Game Theory for Security, Springer, 2012, pp. 264-280

16. A. A. Cardenas, S. Amin, G. Schwartz, R. Dong, and S. Sastry, A game theory model for electricity theft detection and privacy-aware control in AMI systems, in Proc. IEEE 50th Annual Allerton Conference on Communication, Control, and Computing (Allerton), 2012, pp. 1830-1837
17. R. V. P. Yerra, A. K. Bharathi, P. Rajalakshmi, and U. Desai, WSN based power monitoring in smart grids, in Proc. IEEE Seventh International Conference on Intelligent Sensors, Sensor Networks and Information Processing (ISSNIP), 2011, pp. 401-406
18. P. Kadurek, J. Blom, J. Cobben, and W. Kling, Theft detection and smart metering practices and expectations in the Netherlands, in Proc. 2010 IEEE/PES Innovative Smart Grid Technologies Conference Europe (ISGT Europe), 2010, pp. 1-6.
19. R. Jiang, J. Luo, and X. Wang, HRKT: A hierarchical route key tree based group key management for wireless sensor networks, KSII Transaction on Internet and Information Systems, vol. 7, no. 8, pp. 1754-1773, 2013
20. M. S. Sujatha, Manoj Kumar.N, Dr.M. Vijay Kumar, "Pilferage/Theft Management of Industrial Energy Using Wireless Communication Technology" International Journal of Electrical Engineering & Technology (IJEET), Volume 3, Issue 2, 2012, pp. 250 - 261, ISSN Print : 0976-6545, ISSN Online: 0976-6553.
21. Dr. Damanjeet Kaur, "Smart Grids and India" International Journal of Electrical Engineering & Technology (IJEET), Volume 1, Issue 1, 2010, pp. 157 - 164, ISSN Print: 0976-6545, ISSN Online: 0976-6553.
22. Mamatha Sandhu and Dr.Tilak Thakur, "Innovative Technologies and Challenges in the Field of Smart Grid" International Journal of Electrical Engineering & Technology (IJEET), Volume 4, Issue 4, 2013, pp. 129 - 143, ISSN Print: 0976-6545, ISSN Online: 0976-6553.

Available online at www.sciencedirect.com

ScienceDirect

Procedia Engineering 97 (2014) 2147 – 2156

Procedia Engineering

www.elsevier.com/locate/procedia

TOPSIS-AHP Based Approach for Selection of Reverse Logistics Service Provider: A Case Study of Mobile Phone Industry

***A. Jayant[a], P.Gupta[a], S.K.Garg[b], M.Khan[a]**

[a] *Department of Mechanical Engineering, SLIET Deemed University, Longowal, Sangrur, Punjab, INDIA*
[b] *Department of Mechanical Engineering, Delhi Technological University, Delhi-110042, INDIA*

Abstract

Reverse supply chain logistics, means mobility of goods from end consumers towards core manufacturer in the channel of product distribution. In the turbulent business environment, the companies must promote alternative uses of resources that may be cost-effective and ecology friendly by extending products' routine life cycles. Reveres logistics activities i.e. storing, transporting and handling of used products poses a great challenge to reverse logistics managers as there is always chances of uncertainty in terms of quantity, quality and timing of return of EOL products in case of reverse supply chains. Business organizations including those of white/electronics goods manufacturing industries would like to focus on their core competency areas and there is need of making outsourcing decisions of their reverse logistics process to Third-Party reverse Logistics Providers (3PRLPs). Thus, most important strategic issue for top management is the evaluation and selection of third party logistics service provider who can effectively provide reverse logistics operation services to the firms. The objective of this work is to develop decision support system to assist the top management of the company in selection and evaluation of different 3PRL service providers by hybrid approach using Analytical Hierarchy Process (AHP) and Technique for Order Preference by Similarity to Ideal Solution (TOPSIS) method. A real life case study of a mobile phone manufacturing company is presented to demonstrate the steps of the decision support system. Present study also enables the logistics managers to better understand the complex relationships of the key attributes in the decision making environment and subsequently improve the reliability of the decision making process.

Keywords: **T**echnique for order preference by similarity to ideal solution; Mobile industry; Analytical hierarchical process; reverse logistics operation.

1. Introduction

Supply chain management systems have seen a dynamic change in operational style since last two decades. In earlier business practices, supply chain flow happens in the forward direction only. In current business environment industries are facing the problem of return flow of the products in the supply chain for a variety of reasons like product recalls, warranty failure, service failure, commercial returns, manufacturing returns, end-of-life (EOL) and end-of-use returns. Reverse logistics is the process of return product handling mechanism in forward supply chain. The industries may have earned more benefits during the process of reuse recycle and remanufacturing of the used products. In general, the producer collects their used products from consumers and then again sells to new customers as new ones after reprocessing or remanufacturing process. Closed loop supply chain mainly focuses on how to take back the used products and recover the useful components efficiently and economically in eco-friendly manners. It is beneficial to save environment, natural resource, increase financial benefits, enhance enterprises competition, for the industries to implement reverse logistics activities in their supply chain. However, reverse logistics activities collection, inspection/testing, transporting and handling of used products/components poses a great challenge to reverse logistics supervisors as there is very high level uncertainty involves in terms of quantity, quality and timing of return of end-of life products in case of close loop supply chains. Diversion of electronics and white goods products from landfills is important issue, because they contain substances various hazardous elements like cadmium, lead, and mercury which may have ill effects on human health if dispose off in appropriately manner. Day by day increasing volume and rapid rates of obsolescence of these used products only serves to enhance the problem. PCs alone contribute 300 million pounds of lead to the waste stream each year (V. Ravi, 2012).

*Corresponding Author :A.Jayant
E-mail.ID: arvindjayant@sliet.ac.in

1877-7058 © 2014 Published by Elsevier Ltd. This is an open access article under the CC BY-NC-ND license (http://creativecommons.org/licenses/by-nc-nd/3.0/).
Selection and peer-review under responsibility of the Organizing Committee of GCMM 2014
doi:10.1016/j.proeng.2014.12.458

The productive utilization of 3PLS providers for reverse logistics activities may lead to enhancement of profit margin and effective integrated supply chain network for organizations. An efficient collection & processing used products is important for maintaining sustainability. Therefore, a very important strategic issue for company management is the evaluation and selection of 3PL logistics service providers who can efficiently provide reverse logistics services to organization. In this paper, a hybrid approach (a combination of TOPSIS and AHP) has been used for making strategic decision in multi-attribute decision environment for selection of 3PL service providers for collection of end-of-life (EOL) mobile phones. This paper organized as follows. In Section 2, AHP-TOPSIS approach for decision making is presented. Subsequently, section 3 presents a case study of mobile industry. In the section 4, proposed decision support system steps are explained. The section 5 evaluates 3PL service providers. In the section 6, managerial implications of the model discussed. Finally, section 7 discusses conclusion & future research directions.

2. TOPSIS-AHP Method

The foundation of the Analytic Hierarchy Process (AHP) is a set of axioms that carefully delimits the scope of the problem environment (Saaty, 1988). It is based on the well- defined mathematical structure of consistent matrices and their associated eigenvector's ability to generate true or approximate weights (V. Ravi, 2012). The analytic hierarchy process compares criteria, or alternatives with respect to a criterion, in a natural, pair wise mode. The analytic hierarchy process uses a fundamental scale of absolute numbers that has been proven in practice and validated by physical and decision problem experiments. The fundamental scale has been shown to be a scale that captures individual preferences with respect to qualitative and quantitative attributes just as well or better than other scales (Saaty1980, 1994). It converts individual preferences into ratio scale weights that can be combined into a linear additive weight for each alternative. The resultant can be used to compare and rank the alternatives and, hence, assist the decision maker in sound decision making. (Saaty1980, 1994). In year 1981 Yoon and Hwang developed TOPSIS method that simultaneously considers the distance to the ideal solution and negative-ideal solution regarding each alternative and selecting the closest relative to the ideal solution as the best alternative. One of the unique features of AHP is that it provides a powerful procedure to determine the relative importance of different attributes with respect to the objective. A hybrid MADM approach using TOPSIS and AHP has been used in this research for selection of 3PL service providers for collection of used mobile/end-of-life cell phones. The MCDM approach based on AHP-TOPSIS is explained in the following steps:

Step 1: TOPSIS method begins with decision matrix having 'n' criteria/attributes and 'm' alternatives and decision matrix can be represented as:

$$D = \begin{pmatrix} X_{11} & X_{12} & X_{13} & \ldots & \ldots & X_{1n} \\ X_{21} & X_{22} & X_{23} & \ldots & \ldots & X_{2n} \\ X_{31} & X_{32} & X_{33} & \ldots & \ldots & X_{3n} \\ \ldots & \ldots & \ldots & \ldots & \ldots & \ldots \\ \ldots & \ldots & \ldots & \ldots & \ldots & \ldots \\ X_{m1} & X_{m2} & X_{m3} & \ldots & \ldots & X_{mn} \end{pmatrix} \quad (1)$$

Where, x_{ij} is the performance of the ith alternative with respect to j^{th} attribute.

Step 2: The normalized decision matrix is obtained, which is given herewith:

$$r_{ij} = \frac{x_{ij}}{\sqrt{\sum_{i=1}^{m} x_{ij}^2}} \qquad \text{Where j = 1 , 2 , 3 ……m} \quad (2)$$

Step 3: In this step, relative importance of different attributes with respect to the overall objective is determined, and weights for attributes are given according to their importance. A nine-point preference scale of Saaty (1980) has been used for construction of pair-wise comparison matrices. One of the salient properties of this scale is reflexive property between the relatedness of two criteria being compared. For example, if a criterion 'B' is 7 times more important compared to another criterion 'C', then 'C' will be 1/7 times as important as 'B'.

Let P represent an n X n pair-wise comparison matrix,

$$P = \begin{pmatrix} 1 & p_{12} & \ldots\ldots & p_{1n} \\ p_{21} & 1 & \ldots\ldots & p_{2n} \\ \ldots. & \ldots. & \ldots\ldots & \ldots. \\ p_{n1} & p_{n2} & \ldots\ldots & 1 \end{pmatrix} \quad (3)$$

In matrix P, diagonal elements are self-compared and those elements have equal importance. Thus, $p_{ij} = 1$, where i = j, and i, j = 1, 2,…n.

The strength of relative importance of the ith variable compared with the jth attribute is the values on the left and right sides of the matrix diagonal. Thus, $p_{ij} = 1/p_{ij}$, where $P_{ij} \neq 0$, $i \neq j$ as p is a positive reciprocal square matrix.

For normalization the Geometric Mean method is used to determine the importance degree of the considered attributes. If W_i denotes the importance degree for the ith attribute, then:

$$W_i = \frac{\prod_{j=1}^{n} (a_{ij})^{1/n}}{\sum_{i=1}^{n} \prod_{j=1}^{n} (a_{ij})^{1/n}} \quad (4)$$

Consistency check is then performed to ensure that the evaluation of the pair-wise comparison matrix is reasonable and acceptable.

Let us denote Q as an n-dimensional column vector, which describes the sum of the weighted values of the importance of degrees of attributes, then,

$$Q = [q_i]_{nx1} = PW^T \quad i = 1, 2, 3 \ \ldots \ \ldots. \ N \quad (5)$$

Where,

$$PW^T = \begin{pmatrix} 1 & p_{12} & \ldots\ldots & p_{1n} \\ p_{21} & 1 & \ldots\ldots & p_{2n} \\ \ldots. & \ldots. & \ldots\ldots & \ldots. \\ P_{n1} & p_{n2} & \ldots\ldots & 1 \end{pmatrix} \begin{bmatrix} W1, & W2 \ldots\ldots, & Wn \end{bmatrix} C_n = \begin{pmatrix} C_1 \\ C_2 \\ \ldots \end{pmatrix} \quad (6)$$

Consistency values of attributes can be represented by vector:

$QV = [qv_i]_{1\times n}$ with a typical element qv_i defined as: $qv_i = (q_i/w_i)$, $i = 1, 2, \ldots\ldots\ldots, n$.

It should be ensured that inconsistency in pair-wise comparison matrix is avoided. Saaty (1980) has suggested use of maximum Eigen value (λ_{max}) to calculate the Effectiveness of the judgment for this purpose.

λ_{max} is calculated as:

$$\lambda_{max} = \left(\frac{\sum_{i=1}^{n} qVi}{n}\right), \quad i=1, 2,\ldots.n \quad (7)$$

Consistency Index (CI) is estimated as:

$$CI = \left(\frac{\lambda_{max} - n}{n-1}\right) \quad (8)$$

The closer the λ_{max} is to n, the more consistent is the evaluation. In most cases, Consistency Ratio (CR) is used as a guide for checking consistency of evaluation. CR is calculated as:

$$\text{Consistency Ratio (CR)} = \frac{CI}{RI} \quad (9)$$

Where random consistency index (RI) obtained from a large number of simulation runs and varies depending upon the order

of the matrix (Saaty, 1980). Research has shown that if value of consistency ratio is below the threshold of 0.10, the evaluation of importance of degrees of attributes is considered to be reasonable.

Step 4: The weighted normalized matrix is constructed by multiplying each column of the Matrix r_{ij} by weight w_j, thus,

$$V_{ij} = w_j . r_{ij} \quad (10)$$

Step 5: In this step, ideal solutions (v+) and negative-ideal solutions (v–) are calculated It can be expressed as:

$$v^+ = \{v_1^*, v_2^*, v_3^*, \ldots\ldots\ldots v_n^*\} = \{(\max_i v_{ij} \mid j \varepsilon J), (\min_i v_{ij} \mid j \varepsilon J'), i = 1,2,3.....m\} \quad (11)$$

$$v^- = \{v_1^*, v_2^*, v_3^*, \ldots\ldots\ldots v_n^*\} = \{(\min_i v_{ij} \mid j \varepsilon J), (\max_i v_{ij} \mid j \varepsilon J'), i = 1,2,3.....m\} \quad (12)$$

Here J and J′ are associated with beneficial and non-beneficial attributes, respectively.

Step 6: The Euclidean separation distance between the ideal solution (S_i^+) and the Negative-ideal solution (S_i^-) for each alternative is calculated as:

$$S_i^+ = \sqrt{(v_{ij} - v_j^+)^2}\ , \text{i} = 1,2,3,\ldots\ldots\ldots\text{m} \quad (13)$$

$$S_i^- = \sqrt{(v_{ij} - v_j^-)^2}\ , \text{i} = 1,2,3,\ldots\ldots\ldots\text{m} \quad (14)$$

Step 7: The relative closeness to the ideal solution of each alternative is calculated as:

$$C_i = \frac{S_i^-}{S_i^- + S_i^+} \quad (15)$$

Step 8: A set of alternatives can be preference ranked in descending order of C_{i*}. In this, larger index values indicate better performance of the alternatives.

3. Problem Description

Profitable reuse and remanufacturing of cell phones must meet the challenges of turbulent business environment which may includes continuous change in design pattern, frequent price fluctuations of new cell phone models, disassembly of unfriendly designs, short life cycles, and prohibiting transport, labor and machining costs in high-wage countries. In current business environment, the remanufacturing of expensive, long-living investment machine/equipments, e.g., jet fans, machine tools, defense equipment or automobile engines, is extended to a large number of consumer goods with short life cycles and relatively low values. Reuse is an alternative to material recycling to comply with recovery rates and quantities as well as special treatment requirements (Franke, 2006). The company segment selected for this research is mobile phones manufacturing industry situated in the north India. The aim of present research is to evaluate logistics service providers for hiring their service to collect & supply the end-of-life (EOL) mobile phones to the company door step for reclaiming the useful components for remanufacturing of mobile phones. According to Greenpeace report, few mobile phones having toxic materials like polyvinyl Chloride plastic (PVC) bars, phthalates antimony tried, beryllium oxide and Brominates Frame Retardant (BFR).These toxic materials posses a great threat to environment and human health if not disposed off in a proper method. E-waste rule 2011 (Management and handling Rules) came into effect in May 2012 in India. It places responsibility on the producers for the entire life cycle of a product. Under electronic waste management rules producer/ original equipment manufacturer (OEM) will set up collection centers to dispose of e- waste, and fix the duty of manufacturers to collect electronic waste of their products. Till now, three years has been completed since the rules were notified by government, but most of the companies have failed to set up their collection centers. An old non working mobile may fetch up anything between Rs.200 to Rs.1000 depending on its condition. A laptop may get you a little more; but your old fridge or a television may not get you much primarily because of its high transportations cost to the electronic recycling unit. These new rules, however, may put any law–abiding citizen in a fix because the designated centers, where they are actually meant to dispose of the e–waste have not come up in most cities. The effective implementation of the rules looked very unlikely in light of the present circumstances. Mostly consumers even today, do not how to dispose off their e-waste (Toxics-link).

E- Waste is turning out to be one of the greatest threats to the environment. Around 1.46 lakh tones of e–waste were generated in India in 2005 and 2013, the quantity is expected to grow up to 8.5 lakh tones. More than 60% of India's e-wate is generated by 65 cities in India-the foremost being Delhi, Bangalore, Chennai, Kolkata, Ahmadabad, Hyderabad, Pane, Surat and Nagpur. In the internal supply chain of cell phones, the major components such as printed circuit board (PCB), Display Unit, SIM IC, Battery, Charging Jack, Speaker & MIC and plastic body are procured from different suppliers for

new mobile phones production. Once the mobile phones are assembled in different production units it has to be shipped through distributors, wholesalers, retailers and end users. After end of life of the products, end users do not know how to e-waste is to be disposed. As there is no authentic mechanism is available in Indian business environment to collect e-waste from homes, it is mostly lands in municipal bins. Generally used mobile phones are collected at the retailers and should be quickly transported to centralized collection center, where returned mobile phones are inspected for quality failure, sorted for potential reuse, repair or recycling. After inspection, the useless phones/batteries (not able to recycle) are disposed off by eco-friendly manner and reusable components are transported to disassembly/recycling plants and recovered components are used in new phones assembly.

A series of interviews and discussion sessions were held with the mobile phone industry managers, retailers, state pollution control boards officials during this project and following problem areas are identified for improvement in reverse supply chain of the mobile phones.

- Uncertainty is always involved in the supply of used mobile phones to the OEM and industries are unable to forecast collection of EOL mobile phones quantity.
- Most of the e- waste generated in India is recycled but recycling operations has been conducted in hazardous manner by informal sector.
- Presence of illegal recycling operators in the recycling business and there is no government control in the state for unauthorized mobile collection & PVC recycling operation.
- The case company does not have any well-structured business model of reverse logistics practice.
- Huge cost involved in setting of mobile collection centers at prime locations under the directions of new management & handling rules, 2011, Government of India.

To solve aforesaid problems and business performance improvement mobile phones manufacturing industry is ready to assign the work of regular supply of end-of-life (EOL) phones to logistics service provider. The team of industry managers must have enough knowledge to define the aims and benefits from outsourcing of logistics service and may be able to convince about the goal and desired objectives of the company to the service provider. The top management must exactly understand the goals and objectives of the company want to achieve. An accurate estimation of business and service requirements of the company would minimize the need of assumptions on the part of the service provider and ensure a high service level. Service level desired from the logistics service providers must include both the present and the future service standards of the industry. The problem addressed here is to build a sound decision support methodology to evaluation & selection of best reverse logistics service provider. It will help to minimize the forward and reverse supply chain cost including procurement, production, distribution, inventory, collection, disposal, dis-assembly and recycling costs.

4. Decision Support System for the Selection of a Logistics Service Provider

The proposed decision support system require for the assessment of alternative logistics service providers in two steps: (i) Initial screening of the providers by a team of concerned managers from industry and (ii) AHP-TOPSIS based decision support system for the final evaluation of the service providers. Often, the initial screening of the service providers is an easy task but the final selection from the list of short-listed providers is a difficult task. In this section, we present a methodology for the initial screening of the providers. Later, these short-listed providers would be ranked by the AHP-TOPSIS based approach.

The steps of decision support methodology are enlisted as follows:

1. Constitution of a team of senior managers & consultants.
2. Decision regarding type of outsourcing service level required and collection target.
3. Preparation of the functional specifications of the proposed task.
4. Identification of potential reverse logistics service providers in the business environment.
5. Evaluation of proposal of the RL logistics service providers (RLLSP).
6. Submission of request for proposal offer submission from 3PL reverse logistics service providers
7. Evaluation of service proposal offer supplied by the logistics service providers.
8. Field visits and inspection of facilities of the logistics service providers by the team of industry senior managers.
9. Collection of feed backs from the exiting customers of the service providers
10. Final selection using AHP-TOPSIS approach and agreement of services offered by the service providers.

AHP-TOPSIS based decision modeling methodology, which is discussed in the next section of the paper, is recommended for the final selection of a RL service provider. For any long term business relationship a business contract between two parties must address scope of work, responsibilities, liabilities, rate adjustments, service compensations limitations, compensation, insurance, risks and rewards, remedies, extra services, damages types, individual status, termination, agreement modification, performance measurement issues, etc.

5. Evaluation of 3PLRL Service Provider Using AHP-TOPSIS Hybrid Approach

The TOPSIS-AHP based MCDM approach presented in this work and applied in evaluation & selection of 3PL for a mobile phone manufacturing industry. There are 20 outsourcing service providers were interested to conduct reverse logistics operation for the cell manufacturing industry. In the preliminary screening 11 service providers were rejected easily by the company management. The final selection from the remaining nine potential 3PRLPs (A, B, C, D, E, F, G, H and I) was very tough task because almost all the service providers fulfill the requirement of the company. Due to fund limitations and other operational constraints, the case company was keen interested to apply a scientific technique to evaluate all eligible 3PL service providers and determine the best 3PL service providers among the nine bidding submitted for the deal.

The company management identified 10 important parameters/attributes that were relevant to their business. These attributes are E-Waste Storage Capacity (EWSC), Availability of Skilled Personnel (AOSP), Level of Noise Pollution (LNP) and Impacts of Environmental Pollution (IEP), Safe Disposal Cost (SDC), Availability of a covered and closed Area (ACCA), Possibilities to work with NGOs (PWNGO), Inspection/sorting and disassembly cost (ISDC), Mobile phone Refurbishing cost (MPRC), Mobile recycling cost (MRC). Among these attributes, ISDC (thousands of Rupees), EWSC (in tones), MPRC (INR/hour), MRC (thousands of INR) and final disposal cost (thousands of INR) are quantitative in nature, having absolute numerical values. Attributes AOSP, LNP, ACCA, IEP and PWNGO have qualitative measures and for these a ranked value judgment on a scale of 1–5 (here 1 corresponds to lowest, 3 is moderate and 5 corresponds to highest) has been recommended. The cost of recycling of EOL or used mobiles phones ranges from INR.1000 to INR.1600 per unit and INR.1200 to INR.2000 per unit for safe disposal of hazardous waste from mobile. A single mobile refurbishing technician can test and troubleshoot a used mobile, make necessary repairs and upgrade and package it for reuse in 3 hours at a cost of on an average INR.1500 (Techsoup, 2008). These data was provided by various remanufacturing companies during this research project and has been used as the reference for the formulation of reverse logistics data for the case company dealt in this work. The data for all 3PL with respect to various attributes are provided in Table 1.

Table 1 Decision matrix representing the performance of various RLSP

3PRLSPs	EWSC	ISDC	MPRC	MRC	SDC	ACCA	PWNGO	AOSP	LNP	IEP
A	150	160	130	1200	1400	3	4	3	4	5
B	140	170	150	1300	1800	5	5	4	3	4
C	170	160	180	1350	1480	4	3	5	5	5
D	180	165	160	1500	1600	2	3	3	1	2
E	110	150	160	1500	1400	1	3	5	2	5
F	120	180	130	1400	1400	5	3	4	4	2
G	130	165	150	1300	1750	3	2	4	3	5
H	200	160	130	1550	1800	4	1	2	4	4
I	150	110	140	1200	1650	5	2	2	4	5

The implementation of the TOPSIS-AHP model and analysis are explained in the following eight steps:

Step 1: Based upon the information provided by concerned industry segment, the decision matrix has been prepared as shown in table 1, which illustrates the performance of service providers with respect to all 10 attributes:

Step 2: The normalization of decision matrix by using equation (2) as shown below in table 2:

Table 2 Normalized decision matrix

3PRL SPs	EWSC	ISDC	MPRC	MRC	SDC	ACCA	PWNGO	AOSP	LNP	IEP
A	0.3279	0.3357	0.2915	0.2915	0.2926	0.2631	0.0465	0.2694	0.3780	0.3892
B	0.3060	0.3567	0.3363	0.3159	0.3762	0.4385	0.0581	0.3592	0.2835	0.3114
C	0.3716	0.3357	0.4036	0.3280	0.3093	0.3508	0.03490	0.4490	0.4725	0.3892
D	0.3934	0.3462	0.3587	0.3643	0.3344	0.1754	0.0348	0.2694	0.09450	0.1557
E	0.2404	0.3147	0.3587	0.3644	0.2926	0.0877	0.0348	0.4490	0.1890	0.3892
F	0.2623	0.3777	0.2915	0.3401	0.2925	0.4385	0.0348	0.3592	0.3780	0.1557
G	0.2842	0.3462	0.3364	0.3158	0.3658	0.2631	0.02325	0.3592	0.2835	0.3892
H	0.4372	0.3357	0.2914	0.3765	0.3762	0.3508	0.0116	0.1796	0.3780	0.3114
I	0.3279	0.2308	0.3140	0.2915	0.3449	0.4385	0.0232	0.1796	0.3780	0.3892

Table 3 Pair-wise comparison of attributes

Attributes	EWSC	ISDC	MPRC	MRC	SDC	ACCA	PWNGO	AOSP	LNP	IEP	Wi
EWSC	1	5	1/3	1/2	6	6	8	9	1/2	1/5	0.1078
ISDC	1/5	1	1/3	1/3	4	5	6	7	1/5	1/5	0.0611
RFB	3	3	1	4	6	8	9	8	1/3	1/4	0.1588
MPRC	2	3	1/4	1	6	6	8	9	1/3	1/4	0.1123
MRC	1/6	1/4	1/6	1/6	1	4	5	6	1/6	1/6	0.0361
ACCA	1/6	1/5	1/8	1/6	1/4	1	4	5	1/7	1/8	0.0239
PWNGO	1/8	1/6	1/9	1/8	1/5	1/4	1	5	1/8	1/7	0.0162
AOSP	1/9	1/7	1/8	1/9	1/6	1/5	1/5	1	1/9	1/8	0.0107
LNP	2	5	3	3	6	7	8	9	1	4	0.2529
IEP	5	5	4	4	6	8	7	8	1/4	1	0.2199

Step 3: In present research project, five experts, three from the mobile manufacturing/ recycling companies and other two from academia, were consulted for making required pair-wise comparison of attributes. Two senior executives from industry

were the members of the team. The team members from industry and academia having life long experience in the field of reverse logistics practices in electronics goods industry. The pair-wise comparison matrix is given herewith:
The normalized weights of the attributes computed using equation (4) is given in table 3:
EWSC = 0.1078, ISDC = 0.0611, MPRC= 0.1588, MRC = 0.1123, SDC = 0.03613, ACCA = 0.02390, PWNGO = 0.0162, AOSP = 0.0107, LNP = 0.2529 and IEP= 0.2199.
λmax value is 10.81 and that of CR is 0.08, which is less than allowable value 10%. Thus, there is no inconsistency in judgments made by the team and the pair-wise comparison matrix is free from any undue bias.
Step 4: The weighted normalized matrix has been computed and given in table 4:
Table 4 Weighted normalized matrix

	EWSC	ISDC	MPRC	MRC	SDC	ACCA	PWNGO	AOSP	LNP	IEP
A	0.0353	0.0205	0.0463	0.0327	0.0106	0.0063	0.0007	0.0029	0.0956	**0.0856**
B	0.0333	0.0218	0.0534	0.0355	**0.0136**	**0.0105**	**0.0009**	0.0038	0.0717	0.0685
C	0.0401	0.0205	**0.0641**	0.0369	0.0112	0.0084	0.0006	**0.0048**	**0.1195**	**0.0856**
D	0.0424	0.0211	0.0570	0.0409	0.0121	0.0042	0.0006	0.0029	0.0239	0.0342
E	0.02593	0.0192	0.0570	0.0409	0.0106	0.0021	0.0006	**0.0048**	0.0478	**0.0853**
F	0.0283	**0.0231**	0.0463	0.0382	0.0106	**0.0105**	0.0005	0.0040	0.0956	0.0342
G	0.0306	0.0212	0.0534	0.0355	0.0132	0.0063	0.0004	0.0040	0.0717	**0.0856**
H	**0.0471**	0.0205	0.0463	**0.0423**	**0.0136**	0.0084	0.0002	0.0019	0.0956	0.0685
I	0.03535	0.0141	0.04990	0.0327	0.01246	**0.0105**	0.0004	0.0019	0.0956	**0.0856**

Step 5: By the use of equations (11) and (12) the ideal (best) and negative-ideal (worst solutions are calculated and given in table 5.

Table 5 Ideal (best) solution matrix and Negative-ideal (Worst solution matrix)

	Ideal (best)		Negative-ideal
v_{1+}	0.047142562	v_{1-}	0.025928409
v_{2+}	0.023107555	v_{2-}	0.014121284
v_{3+}	0.064098721	v_{3-}	0.046293521
v_{4+}	0.042285422	v_{4-}	0.032737101,
v_{5+}	0.013594477	v_{5-}	0.010573482,
v_{6+}	0.01048479	v_{6-}	0.002096958,
v_{7+}	0.0009439	v_{7-}	0.0001888,
v_{8+}	0.004814769	v_{8-}	0.001925908,
v_{9+}	0.1195015	v_{9-}	0.0239003
v_{10+}	0.085604133	v_{10-}	0.034241653

Table 6 Euclidean separation distance

	Ideal (best)		Negative-ideal (worst)
s_{1+}	0.033991	s_{1-}	0.08904
s_{2+}	0.054233	s_{2-}	0.060899
s_{3+}	0.009836	s_{3-}	0.11136
s_{4+}	0.109096	s_{4-}	0.022604
s_{5+}	0.07575	s_{5-}	0.058526
s_{6+}	0.062521	s_{6-}	0.073016
s_{7+}	0.05235	s_{7-}	0.071285
s_{8+}	0.034659	s_{8-}	0.083334
s_{9+}	0.033089	s_{9-}	0.089189

Step 6: The euclidean separation distances has been computed using equations (13) and is given in table 6.
Step 7: The relative closeness to the ideal solution of each alternative has been calculated using equation (15) and given in table 7.

Table 7 Relative closeness to the ideal solution to each Alternative

Relative Closeness	Value	Alternatives
c_1	0.723720499	A
c_2	0.528946401	B
c_3	0.918842279	C
c_4	0.171635183	D
c_5	0.435862761	E
c_6	0.538715407	F
c_7	0.576578637	G
c_8	0.706260564	H
c_9	0.72939389	I

Table 8 Ranking of 3 PL service providers

Alternatives (3PRLPs)	Value	Rank
A	0.723720499	3
B	0.528946401	7
C	**0.918842279**	**1**
D	0.171635183	9
E	0.435862761	8
F	0.538715407	6
G	0.576578637	5
H	0.706260564	4
I	0.72939389	2

Step 8: On the basis of the relative closeness values, the case company can be ranked and choose 3PL for their operations as **C-I-A-H-G-F-B-E-D** in the decreasing order of preference as shown in table 8. It is clear here that these results must be seen in the light of the business environment of mobile manufacturing company and the inputs provided by a team of experts in the pair-wise comparison of the attributes.

6. Discussion and managerial implications

A good number of electronics products contain large volumes of waste and substantial quantities of toxic materials. Industries under tight regulatory pressure from both governments and environmentally focused NGOs 'reduce', 'recycle', and 'reuse' their industrial waste. The results from mobile phones case study indicate that 3PL service provider ‘C’ is the first choice for the case company. An analysis of data provided by 3PL service provider ‘C’ reveals that the logistics firm ‘C’ has been take care about environmental aspects like proper disposal of end of life and used products. Results indicates that logistics firm ‘C’ have scored high values on almost all quantitative attributes as compared to other logistics service providers. Day by day environmental issues are gaining more importance in Indian business environment. So, most important managerial implication of the developed model is that only the firms who are dealing with environmental issues significantly will get success in competitive business environment. The proposed hybrid model in the present research has find out several significant attributes for evaluation of logistics firms for conduct of reverse logistics operation with respect to mobile phones manufacturing companies. This may provide support to management and consultants for making strategic decisions like selection of logistics firm, selection of new plant site, selection of business partner in competitive business environment. In the present work 10 relevant attributes has been identified for evaluation and selection of 3PL service provider for reverse logistics operation for the mobile phone manufacturing industry. The developed model provide flexibility in accommodating new attributes according to industry needs time to time for sound decision making.

7. Conclusions & future research scope

The evaluation and selection of the 3PL for mobile industry segment is a top management level strategic decision. The quantity of e-waste is tremendously increasing and it has become menace to society and environmental burden. The legislations like Restriction on Hazardous Substances (RoHS) Directive and Waste Electrical and Electronic Equipment Directive (WEEE) gaining importance in current business environment. The electronics appliances manufacturing companies

are more interested to focus upon their core competencies and services of 3PL is a right choice for them to separate reverse logistics operations. Therefore, hiring the services of 3PL is an importance issue and present work is very significant in this regards. Now-a-days, efficient reverse logistics operation is regarded as a focused problem. Development of a sound reverse logistics system is beneficial to environmental protection, and the companies may improve their financial health also by handing the return in a professional way. Mostly the manufacturing industries does not have enough competence to manage their product reverse flow in supply chain, thus they have to only option to outsource their reverse logistics operations to the 3PL service provider for conduct of reverse logistics (RL) activities. To make AHP-TOPSIS model more effective, top management must establish key criteria for evaluation and selection of third party logistics service providers. The attributes may be increase or decrease as per the needs of the industry. In real life business environment it is very difficult to find suitable criteria for the evaluation and selection of outsourcing partner. In the present work, a decision model has been developed for the mobile phones manufacturing company only. However, the same decision model may be applicable for different market segment with minor modification.The hybrid AHP-TOPSIS method presented in this research properly guides policy makers for evaluation of 3PL reverse logistics service providers and support them visualize the intensity of impact of various criteria on the alternatives available before reaching at the final decision.

There is always a scope for further improvement in the research, so a comparative study may be conducted by using other multi-criteria decision-making methods to validate the results obtained by present method. An analytic network process (ANP) approach may be used for consideration the interactions between attributes and the results could be compared by using interpretive structural modeling (ISM) based approach. Matlab version 11 has been used for calculation purpose in this work. Customized software may be developed to reduce computational speed and simplification of calculations.

Acknowledgements

The authors express their sincere thanks to the management and staff of XYZ Enterprises for providing an opportunity to carry out the project and extending their cooperation for data collection and providing all kind of support for the present research work.
The authors are also thankful to the editor-in-chief and anonymous referees for their constructive comments and valuable suggestions that led to a considerable improvement of the paper over its earlier version.

References

[1] Franke, C., B. Basdere, M. Ciupek, and S. Seliger(2006) ‘Remanufacturing of Mobile Phones—Capacity, Program and Facility Adaptation Planning" Omega, 34 (2006) 562 – 570.
[2] Hwang, C.L. and Yoon, K. (1981) Multiple Attribute Decision Making-Method and Applications: A State-of-the-Art Survey, Springer-Verlag, New York.
[3] Knemeyer, A.M., Ponzurick, T.G. and Logar, C.M. (2002) ‘A qualitative examination of factors affecting reverse logistics systems for end-of-life computers’, International Journal of Physical Distribution and Logistics Management, Vol. 32, No. 6, pp.455–479.
[4] Qureshi, M.N., Kumar, P. and Kumar, D. (2009) ‘Selection of Logistics Services Provider (LSP) under fuzzy environment: a graph-theoretic and matrix approach’, International Journal of Logistics Systems and Management, Vol. 5, No. 5, pp.551–573.
[5] Ravi, V., Shankar, R. and Tiwari, M.K. (2005) ‘Analyzing alternatives in reverse logistics for end-of-life computers: ANP and balanced scorecard approach’, Computers and Industrial Engineering, Vol. 48, No. 2, pp.327–356.
[6] Ravi, V., Shankar, R. and Tiwari, M.K. (2008) ‘Selection of a reverse logistics projects for end-of-life computers: ANP and goal programming approach’, International Journal of Production Research, Vol. 46, No. 17, pp.4849–4870.
[7] Saaty, T.L. (1980) The Analytic Hierarchy Process, McGraw-Hill, New York.
[8] Sasikumar, P. and Haq, A.N. (2010) ‘A multi-criteria decision making methodology for the selection of reverse logistics operating modes’, International Journal of Enterprise Network Management, Vol. 4, No. 1, pp.68–79.
[9] Schultz, G. (2002) ‘The recurring side of supply chain management’, APICS – The Performance Advantage, Vol. 10, pp.35–38.
[10] Saaty, T. L. (1988). Multicriteria decision making: The analytic hierarchy process. New York: McGraw-Hill.
[11] Saaty, T. L. (1994). Highlights and critical point in the theory and application of the analytic hierarchy process. European Journal of Operational Research, 74, 426–447.
[12] Vijayvargiya, A. and Dey, A.K. (2010) ‘An analytical approach for selection of a logistics Provider’, Management Decision, Vol. 48, No. 3, pp.403–418.

PS-IV-30

Trait association analysis for yield and yield attributing traits in niger germplasm

P. K. Jagtap[1], P. B. Sandipan, K. M. Patel and M. C. Patel

Niger Research station, NAU, Vanarasi 396 580, Tal. Vansda Dist. Navsari (G); e-mail: pacific7@rediffmail.com

Abstract

A field experiment was conducted during the *kharif* season of 2013-14 at Niger Research Station, Navsari Agricultural University, Vanarasi (Gujarat), India, to determine the interrelationship between yield and its contributing components in 200 germplasm accessions niger (*Guizotia abyssinica*). Total the results revealed that phenotypic correlation was higher in magnitude than genotypic ones due to effect of environmental factors on the associations of characters. Seed yield per plant exhibited the highest significant positive genotypic correlations with days to 50% flowering, number of capsules on branches followed by test weight. However, an interrelation study indicates that plant height and number of branches had a significant positive correlation with capsules per plant and number of seeds per capsule whereas negative significant correlation was observed between branches per plant and test weight (g).

Key words: Niger, germplasm, trait association, yield

Niger [*Guizotia abyssinica* (L.f.) Cass.] commonly known as ramtil, kalatil, gurellu, tilangi, and noog, is a minor oilseed crop of India, indigenous to tropical Africa particularly to Ethiopia islands which occupies an area of one lakh ha with a production of 0.39 million tonnes and productivity of 320 kg per ha. In India, South Gujarat heavy rainfall zone particularly comprising of Dang, Navsari and Valsad districts are very potential areas where this crop is already being grown to some extent. The important feature of this crop is that it gives reasonable seed yield even under poor marginal growing conditions. Further, lack of improved seed production technology and suitable high yielding varieties are the major causes for the low seed yield. Production potentiality of niger can be fully exploited with identifying the association among the yield contributing traits and thus selection of suitable genotypes for further improvement. Knowledge of interrelationship between yield and its contributing components can improve the efficiency of breeding programme through the use of appropriate selection indices. However, yield is a complex quantitative character having low heritability and is influenced by many other components both in positive and negative directions. A rational approach towards improvement of yield necessitates the selection of important yield components and to study their extent and nature of association with yield which would provide effective basis of selection. The present investigation is therefore carried out to study the correlation coefficients between yield and yield contributing characters to developing suitable selection criterion for niger breeding programme.

Materials used in the present study consisted of 200 germplasm accessions received from All India Coordinated Improvement Project on Niger, Jabalpur (MP). These accessions were evaluated in Augmented Block Design at Niger Research Station, NAU, Vanarasi (GJ) during *kharif* 2013. Data were recorded on days to 50% flowering, days to maturity, plant height (cm), number of branches, number of capsules on branches, number of capsules per plant and seed yield per plant. The correlation coefficients were calculated [2].

The results indicated that phenotypic correlation was higher in magnitude than genotypic ones. The high phenotypic correlation could have resulted due to effect of environmental factors on the associations of characters. Seed yield per plant exhibited the highest significant positive genotypic correlations with days to 50% flowering, number of capsules on branches followed by test weight (g) (Table 2). Similar results were also reported earlier [3, 4] in sesame. Studies on inter correlations among yield components showed that days to maturity had significant

and positive correlation with plant height, number of branches per plant, number of capsules per plant and number of seeds per capsule. Plant height and number of branches had a significant positive correlation with capsules per plant and number of seeds per capsule whereas negative significant correlation was observed between branches per plant and test weight (g). Number of capsules on branches per plant had significant and positive correlation with number of seeds in the capsules. However, negative correlation of seeds in the capsules with test weight and seed yield was also noticed. Test weight (g) also had significant and positive correlation with seed yield per plant (g) which is in agreement with earlier findings [1, 5]. In general, trait association study indicates that days to 50% flowering, number of capsules per plant and test weight (g) influences the seed yield more than any other characters. Hence, more emphasis would be given to these characters during selection to improve the seed yield in niger.

Table 1. Seed yield and other ancillary traits of niger germplasms

Characters	Mean	SE±	Range	Skewness	Kurtosis
Days to 50% flowering	82.70	0.296	68-89	0.742	0.811
Days to maturity	132.19	0.378	121-183	4.276	41.82
Plant height (cm)	158.27	1.204	105-206	0.179	0.081
Number of branches per plant	5.61	0.144	9-10	0.605	-0.587
Number of capsules per plant	26.78	0.758	11-61	0.892	0.278
Number of seeds per plant	12.00	0.269	9-10	0.501	1.086
Test weight (g)	3.70	0.019	2.9-4.2	0.587	0.397
Seed yield (g)	216.79	9.268	89-100	0.631	-0.181

Table 2. Correlation analysis for yield contributing traits in niger germplasms

Characters	Days to 50%	Days to maturity	Plant height	Branches/ plant	Capsules/ plant	Seeds/ plant	Test weight (g)	Seed yield (g)
Days to 50% flowering	1.000	-0.111	-0.028	0.072	-0.137	-0.118	0.121	0.236**
Days to maturity		1.000	0.661**	0.216**	0.339**	0.269**	-0.046	-0.084
Plant height (cm)			1.000	0.114	0.309**	0.336**	-0.034	-0.014
Number of branches per plant				1.000	0.257**	0.362**	-0.240**	-0.064
Number of capsules per plant					1.000	0.704**	-0.138	0.215**
Number of seeds per plant						1.000	-0.139	-0.078
Test weight (g)							1.000	0.187**
Seed yield (g)								1.000

References

1. Muralidharan V., Vijayabharathi A., Manivannan N. and P. Vindhiyavarman. 2009. Character association for seed yield and yield attributes in sesame, *Sesamum indicum* L. J. Oilseeds Res., 26: 91-92.
2. Dewey, D.R. and Lu, K.H. 1959. A correlation and path coefficient analysis of components of crested wheat grass seed production. Agronomy J., 57: 515-518
3. Sahu, D.P. and Patnailk, M.C. 1981. Variability, correlation and path anysis in niger. Indian J. Agric. Sci., 51: 287-291.
4. Patil, H.S. 2003. Nature of variability, association and path analysis in niger. Crop Improvement, 30(20): 212-215.
5. Goyal, S.N. and Kumar, S. 1985. Correlation and path analysis in niger. Journal of Oilseeds Research, 2: 34-38.

PS-IV-31

Potential sorghum genetic resources for utilization

M. Elangovan*, G. Premalatha and P. Kiran Babu[1]

Directorate of Sorghum Research; Rajendranagar, Hyderabad 500 030; [1]Indian Agricultural Research Institute, New Delhi; e-mail: elangovan@sorghum.res.in

Abstract

A total of 3585 accessions were identified based on their uniqueness of traits and reported in the annual report. The popular *rabi* landrace M 35-1 released as variety during the past was the most frequently identified sorghum accession with 16 occasions. The breeding material recorded the highest frequency of 804 accessions identified as potential genetic resources. The plant breeding division stands first with the maximum utilization and identification of 1441 accessions. The maximum frequency of 624 accessions was observed for high grain yield. The Eighteen accessions were identified as potential genetic resources for multiple shoot pests resistance to stem borer and shoot bug, whereas 8 accessions were observed to have high brix and stalk yields sweet sorghum group.

Key words: Sorghum, utilization, trait-specific, genetic diversity

Plant genetic resources can be defined as the “Genetic material of plants that use of value as resource for the present and future generations of people” [1]. Sorghum (*Sorghum bicolor* L. Moench) is one of the five major cereals of the world. The identification of potential germplasm for utilization in crop improvement is an important objective to make the raw germplasm into useful with their trait-specific tags. This status report is made from the available last 14 years of published annual reports from 2000-01 to 2013-14. The paper will reveal the different kind of trait-specific sorghum genetic resources and the programme, division and the scientists who developed the germplasm etc.

A database on the utilization of sorghum genetic resources in the last 14 years was made based on the Annual Report of DSR during 2000 – 2014. A total of 3585 accessions identified based on its uniqueness of trait identified and reported in the annual report. The database was developed with the details of the accession number, category of material, traits identified, division in which the material used, programme under which material identified, scientists used the material, season were utilized, year of annual report and page numbers. The data is entered in the MS-Excel and used for filtering the data according to the objective of the study.

A total of 3585 accessions were identified as potential donor for different traits in the last fourteen years. The accession M 35-1 was used and identified as potential material for maximum of 17 times during 2000 – 2014 followed by SSV 74 (15) and SLB 19 (14). A total of 804 accessions of breeding material were reported maximum utilized followed by indigenous germplasm (683) and variety (616). High grain yield was the top most traits with 624 accessions identified during 2000 – 2014 followed by resistance to shoot fly (404) and resistance to stem borer (267). Plant breeding division has identified 1441 accessions as potential donors followed by Agricultural Entomology (922) and Plant Physiology (523). The research programme entitled “Evaluation of dual type sorghum resistant to stem borer, *Chilo partellus”* resulted an identification of 199 accessions as potential donor for stem borer followed by programme on “Improvement of B and R Lines” with 102 accessions. The maximum potential donors were identified during post-rainy season of 2013-14 with 287 accessions followed by rainy season in 2010 with 279 accessions and post-rainy season of 2011-12 with 239 accessions. The accessions with multiple potential traits are presented in Table 1.

Table 1. The multiple trait accessions identified during 2000 – 2014

S.No.	Accessions	Multiple traits
1	M 35-1	Resistance to shoot fly, positive GCA for panicle length, days to 50% flowering, 100-seed weight, high GCA for grain yield, high stover yield and 100 seed weight, high grain yield, resistance to shoot bug, stay green, resistance to shoot fly and charcoal rot with high grain yield, high grain yield, high degree of antixenosis for oviposition by shoot fly
2	SSV 74	Salinity tolerance, high green fodder yield, high brix, sugar, sucrose, computed ethanol yield, sugar yield; high grain yield, high stalk yield, good plant vigour, high biomass and bagasse yield, high seed longevity and viability potential
3	SLB 19	High grain and fodder yield, improved B & R Lines, less damage of aphids
4	IS 2312	Resistance to shoot fly and charcoal rot; restorer lines in shoot fly resistance, more leaves, high degree of antixenosis for oviposition by shoot fly, stay green, high leaf N concentration, superior in total chlorophyll and CSI, drought tolerant
5	SLB 9	High grain and fodder yield, high total dry matter yield, high grain yield than 104B, post-flowering drought tolerance, improved B & R Lines
6	RSSV 9	Resistance to stem borer, forage and resistance to shoot fly, high CHI and fresh cane weight, high total biomass, high grain yield
7	ICSV 93046	Resistance to shoot fly, aphid and stem borer
8	Katarkhatav	Forage and resistance to shoot fly and stem borer; high biomass, fodder yield and grain yield
9	C 43	High grain yield under mid-season drought stress, susceptible to low temperature, plant metabolism, biotic and abiotic stress, resistance to grain mold, shoot bug and aphids; low endosperm utilization, high grain yield and biomass
10	EP 87	Post-flowering drought tolerance, high grain and total dry matter yield, high LAI, high biomass and grain yield under post flowering, moisture stress conditions, high biomass and grain yield, larger LAI under stress conditions

Only few sorghum germplasm reported as potential donor for multiple traits during 2000-2014 such as M 35-1, SSV 74, RSSV 9 (varieties); SLB 9, SLB 19, C 43 (parental lines); ICSV 93046 (breeding material); IS 2312 (international sorghum); EP 87 – IC 343586 (indigenous germplasm). Upadhyaya *et al* [2] also revealed the similar conclusion such as IS 18758, IS 1054 and IS 33844 have proved to be an excellent source of desirable plant height, high grain yield, good grain quality, resistant to leaf diseases, and used extensively in breeding programme at ICRISAT and elsewhere.

Useful traits, such as increased seed number, larger panicles, greater total biomass, drought tolerance, disease resistance, greater plant height, longer maturity, greater leaf area indices, increased green leaf retention and greater partitioning of dry matter have contributed to increased yield [2]. The present study also observed that the following traits with more frequency *viz*., high grain yield / grain weight, resistance to abiotic / biotic stresses, early maturity, high biomass, long panicle, high brix / sugar / sucrose / stalk yield, malt quality, leaf area index, high protein/ amylose / proline etc. The amount of genetic variability available in sorghum is immense. Sorghum landraces and wild relatives of cultivated sorghum from the centres of diversity have been rich sources of resistance to new pathogens, insect pests and other stresses such as high temperature and drought, as well as sources of traits improve food and fodder quality, animal feed and industrial products [4].

Early work on sorghum germplasm was confined to pure line selection within cultivated landrace populations in Africa and India that resulted in improved cultivars, some of which continue to be widely grown. Crossing and/ or backcrossing between adapted introductions and local germplasm has been used to derive improved pure-line varieties and parental lines [5]. The direct selection is the fastest adaption process for the variety developed from the landrace. This can also address the local problems where they were existing. The pre-breeding concept also helps the breeders to broaden their genetic base by using the diverse germplasm. Sorghum is considered as an industrial and high-energy crop with its diverse uses. Sorghum alcohol, syrup, liquor, beer, and malt play an important role for small industries. Commercialization of sorghum lies in proper utilization of its diverse economic

importance [5].

References

1. IPGRI. 1993. Diversity for Development. Rome: IPGRI.
2. Upadhyaya, H. D., Sharma, S., Dwivedi, S. L., and Singh, S. K. 2014. Sorghum Genetic Resources: Conservation and Diversity Assessment for Enhanced Utilization in Sorghum Improvement. Genetics, Genomics and Breeding of Sorghum, 28.
3. Miller, F.R and Kebede, Y. 1984. Genetic contributions to yield gains in sorghum, 1950 to 1980In: Fehr W.R. ed. 1984. Genetic Contributions to yield gains of Five Major Crop Plants, CSSA Special Publication 7, Madison, WI: CSSA, ASA. P1-14.
4. Belum VS Reddy, Ashok Kumar, A., Sanjana Reddy, P. and Elangovan, M. 2008. Sorghum germplasm: diversity and utilization. In: Reddy Belum VS, Ramesh S, Ashok Kumar A and Gowda CLL (eds.) 2008. Sorghum Improvement in the New Millennium. Patencheru 502324, Andhra Pradesh, India: International Crops Research Institute for the Semi-Arid Tropics. P153-169. ISBN 978-92-9066-512-0.
5. Prasada Rao K.E., Mangesha M.H. and Reddy, V.G. 1989. International use of sorghum germplasm collection. In: Brown AHD, Frankel OH, Marshal DR and Williams JT,(eds.) 1989. The use of Plant Genetic Resources, Cambridge, UK: Cambridge University Press. P150-167.
6. Elangovan, M. 2005. Diverse use of sorghum. Course material for the training on alternate Uses of Sorghum and Pearl millet, 16-23 February 2005, NRCS, Hyderabad.

PS-IV-32

Characterization of sorghum germplasm from Khammam regions of Telangana

M. Elangovan*, N. Sivaraj[1] and G. Premalatha

Directorate of Sorghum Research; Rajendranagar, Hyderabad 500 030; [1]National Bureau of Plant Genetic Resources, New Delhi; e-mail: elangovan@sorghum.res.in

Abstract

The preliminary characterization and evaluation of 40 accessions collected from Khammam regions of Telangana was done characterized for 14 quantitative and 16 qualitative traits. The descriptive statistics showed maximum variability in stem biomass followed by stem dry weight, plant height and grain yield. The accessions IC 0596007 (SE 2) with tall plant height, ear head length and leaf length may be used as high biomass sorghum. IC 0596013 (SE 24) may be used as sweet sorghum for its high brix, tall plant height and ear head length. Three accession *viz.*, IC 0596014 (SE 25), SE 53, IC 0596024 (SE 54) and IC 0596026 (SE 62) may be used in the grain sorghum programme for its good grain yield per plant and 100-seed weight. *Durra* (12 acc.) is the dominant in these collections followed by *bicolor* and *durra bicolor* (3 acc. each). Light red glume colour (6 acc.) is dominant followed by red and purple (5 each). The maximum proportion of the races studied are six from Andhra region of Andhra Pradesh.

Key words: Sorghum, characterization, races, biomass

Sorghum is one of the five major cereals of the World. It is a staple food crop for middle and poor people and also a main source of fodder, feed and industrial raw material. The first major effort in the assembly of a World collection of sorghum was made in the sixties by the Rockefeller Foundation Agricultural Research Programme in India [1-3]. The sorghum germplasm collection was undertaken in the Telangana regions of Andhra Pradesh in collaboration with the National Bureau of Plant Genetic Resources Institute (NBPGR), Regional Station, Hyderabad. The accessions were evaluated to identify the potential donors for use in the crop improvement programme. The Eastern Ghats district of Khammam in Telangana is rich in sorghum diversity particularly landraces [4]. Maximum

racial diversity of sorghum exists in the state of Andhra Pradesh followed by Maharashtra [4, 5].

The preliminary characterization and evaluation of 40 accessions collected from Khammam regions of Telangana collected were characterized for 30 agro-morphological traits which include 14 quantitative and 16 qualitative traits. The accessions were evaluated during rabi 2013-14 along with checks at Directorate of Sorghum Research (DSR), Hyderabad, GTC Research Farm. The centre is located at $17^0$19' N latitude and $78^0$24' E longitude and at an altitude of 538 m above MSL with temperature varying from 10^0 C to a maximum of 30^0 C during the cropping season. The soil type was of red sandy. The accessions were raised in an Augmented Randomized Block Design (ARBD) with check varieties in each block. The accessions were grown in 4 m rows with a row spacing of 60 cm and plant to plant spacing of 10 cm. Standard agronomic and plant protection practices were followed during the cropping season. The data on qualitative and quantitative descriptors were recorded using minimal descriptor developed by NBPGR [6] and list of sorghum descriptors released by IBPGR/ ICRISAT. Five representative plants in each accession were tagged for recording the qualitative and quantitative characters. Brix percentage of each accession was estimated by refractometer. The quantitative data were analysed statistically. Out of forty accessions evaluated, only 26 accessions could flower and data collected for analysis.

The descriptive statistics showed maximum variability in stem biomass followed by stem dry weight, plant height and grain yield (Table 1). The frequency of qualitative traits is presented in (Table 2). The potential germplasm accessions identified from Khammam region collection is presented in (Table 3). Based on the analysis, accessions with distinct traits were identified for utilization in the crop improvement programme. The accessions IC 0596007 (SE 2) with tall plant height, ear head length and leaf length may be used as high biomass sorghum. IC 0596013 (SE 24) may be used as sweet sorghum for its high brix, tall plant height and ear head length. Three accessions *viz.*, IC 0596014 (SE 25), SE 53, IC 0596024 (SE 54) and IC 0596026 (SE 62) may be used in the grain sorghum programme for its good grain yield per plant and 100-seed weight. *Durra* (12 acc.) is the dominant in these collections followed by *bicolor* and *durra bicolor* (3 acc. each). Light red glume colour (6 acc.) is dominant followed by red and purple (5 each).



Fig. 1. Variation in ear head compactness



Fig. 2. Variation in grain colour



Fig. 3. Variation in glume coverage

Table 1. Descriptive statistics of quantitative characters of sorghum germplasm collections from Khammam regions of Telangana

Characters	Mean	SE	SD	Variance	Range	Min.	Max.
Days to 50% flowering (days)	77.58	0.77	3.76	14.17	12.00	71.00	83.00
No. of leaves	6.43	0.21	1.05	1.10	4.00	4.80	8.80
Leaf length (cm)	61.83	1.20	5.89	34.67	27.62	44.92	72.54
Leaf width (cm)	6.65	0.21	1.10	1.04	3.92	4.86	8.78
Ear head length (cm)	20.67	1.75	8.60	73.89	22.22	11.88	34.10
Ear head width (cm)	7.75	0.25	1.22	1.50	4.26	5.04	9.30
Plant height (cm)	181.63	5.47	26.78	714.68	106.00	129.00	235.00
Stem thickness (mm)	1.41	0.03	0.15	0.02	0.66	1.10	1.76
Stem brix (%)	13.38	0.64	3.12	9.73	12.30	7.50	19.80
Stem biomass (g/pl)	263.21	19.21	94.11	8850.70	400.00	150.00	550.00
Stem dry weight (g/pl)	94.88	9.59	46.98	2204.80	180.00	20.00	200.00
Grain yield (g/pl)	62.82	4.26	20.88	436.24	72.80	31.20	104.00
100-Seed weight (g)	2.57	0.10	0.48	0.23	1.74	1.85	3.59

Table 2. Frequency distribution of qualitative traits of sorghum germplasm from Khammam, Telangana

S.No.	Character	Status
1	Plant vigour	Good (13acc.), Poor (8), Very good (5)
2	Leaf colour	Light green (22), Pale green (3), Dark green (1)
3	Leaf sheath pigmentation	Non-tan (26), Tan (0)
4	Leaf orientation	Drooping (15), Erect (11)
5	Leaf midrib colour	White (24), Green (2)
6	Ear head compactness	Compact (12), Loose (10), Semi compact (2)
7	Ear head shape	Ovate (10), Cylindrical (7), Elliptical (3), Symmetrical (2), Oblong (1)
8	Race	(D)Durra (12), (B)Bicolor (3), (DB)Durra bicolor (3), (DC)Durra caudatum (1), (BC)Bicolor caudatum (1), (CB)Caudatum bicolor (1), (GB)Guinea bicolor (1), (GC)Guinea caudatum (1), (K)Kafir (1)
9	Glume colour	Light red (6), Red (5), Purple (5), Brown (4), Black (3), Yellow green (1)
10	Glume coverage	25% (12), 50% (2), 75% (6), 100% (4)
11	Grain colour	Yellow (8), Red (6), Light red (4), White (2), Yellow green (2), Orange (1), Yellow white (1)
12	Grain shape	Round (16), Elliptical (8)
13	Grain size	Very bold (12), Bold (12)
14	Presence of Awn	Present (16), Absent (8)
15	Grain lusture	Lustrous (15), Non-lustrous (9)
16	Stay green	Stay-green (19), Non-tan (5)

The maximum proportion of the race collected from the present study is six from Andhra region of Andhra Pradesh. This reports the maximum diversity of races available in the state of Andhra Pradesh. Appa Rao *et al*. [4] also studied that racial diversity is maximum in the state of Andhra Pradesh followed by Maharashtra. The present study also revealed the similar results and 9 races were collected from the region.

Sorghum landraces are consistent for morphological characters, the importance of the midrib color, grain color, grain size, glume color, glume hairiness, and grain shape were used by the farmers in naming the sorghum landraces. In these collections also the landrace *konda jonna* is named to indicate topography of the crop grown. The landrace *tella jonna and erra jonna* indicated the white and red colour of the grain. Audilakshmi *et al.* observed that the twenty-two sorghum genotypes evaluated for grain mold response. They found that harder grain, higher levels of seed phenols and darker glumes contributed to grain mold resistance. The variability of glume colour (7 types) available in the present study may be utilized for screening for grain mold resistance in sorghum.

Table 3. Promising entries identified from sorghum germplasm collections from Khammam regions of Telangana

Trait	Promising accessions indigenous collection No. (Collector No.)	No. of acc.
Leaf length (>70 cm)	IC 0596006 (SE 1), IC 0596007 (SE 2)	2
Leaf width (>8 cm)	IC 0596012 (SE 22), IC 0596014 (SE 25), IC 0596015 (SE 26)	3
Plant height (>200 cm)	IC 0596007 (SE 2), IC 0596015 (SE 24), IC 0596014(SE 25), IC 0596022(SE 45)	4
Ear head length (>30 cm)	IC 0596007 (SE 2), IC 0596013 (SE 24), IC 0596027 (SE 63), IC 0596028 (SE 64), IC 0596030 (SE 66)	5
Ear head width (>9 cm)	SE 13, IC 0596012 (SE 22), IC 0596022 (SE 45)	3
Brix (>18%)	IC 0596015 (SE 24), SE 56	2
Stem fresh weight (>500g/plant)	IC 0596012 (SE 22)	1
Stem dry weight (>180g/plant)	IC 0596006 (SE 1), IC 0596030 (SE 66)	2
Grain yield (>80 g)	IC 0596014 (SE 25), SE 41, SE 53, IC 0596024 (SE 54), IC 0596026 (SE 62)	5
100-seed weight (>3.0g)	IC 0596014 (SE 25), IC 0596015 (SE 26), SE 53, IC 0596024 (SE 54), IC 0596026 (SE 62)	5
	Total	32

References

1. House L. R. 1980. A guide to sorghum breeding. ICRISAT, Patancheru, Andhra Pradesh, India.
2. Murty B. R., Arunachalam V. and Saxena M. B. L. 1967. Classification and catalogue of a world collection of sorghum. Indian Journal of Genetics and Plant Breeding., 27 (*S. bicolour* var. *bicolor* race guinea: Special Number): 1 – 312.
3. Rockefeller Foundation. 1970. World collection of sorghums. List of pedigrees and origins. Rockefeller Foundation, Indian Agricultural Program, New Delhi, India.
4. Appa Rao S., Prasada Rao K. E., Mengesha M. H. and Gopal Reddy V. 1999. Morphological diversity in sorghum germplasm from India. Genetic Resources and Crop Evolution., 43(6):559-567.
5. Elangovan M. 2004. Diversity in Sorghum Races. The Andhra Agricultural Journal., 50: 549-551.
6. Mahajan R. K., Sapra R.L., Umesh Srivastava, Mahendra Singh and Sharma G. D. 2000. Minimal Descriptors (for characterization and evaluation) of agri-horticultural crops (Part I). National Bureau of Plant Genetic Resources, New Delhi., 230 p.
7. Audilakshmi S., Stenhouse J. W., Reddy T. P. and Prasad M. V. R. 1999. Grain mould resistance and associated characters of sorghum genotypes. Euphytica, 107(2): 91-103.

PS-IV-33

Genetic diversity of *Moringa oleifera* in shiwalik foothills of Uttarakhand: Prospects of cultivation

A. K. Trivedi[*], S. K. Verma and R. K. Tyagi[2]

NBPGR, Regional Station Bhowali (Niglat) 263 132, District Nainital (Uttarakhand), National Bureau of Plant Genetic Resources, Pusa Campus, New Delhi 110012; e-mail: ajayakumartrivedi@gmail.com

Abstract

Genetic diversity of *Moringa oleifera* was explored and collected from remote and far-flung areas of Shiwalik foothills. Ample diversity in fruits of different habitats has been found. Based on plant type, size, color, thickness of fruits and agro-eco niches, a total of 23 accessions were collected from altitudinal range of 206 – 1010 m asl. In spite of genetic diversity of *Moringa oleifera* available in the Shiwalik foothills, its potential has not been harnessed for cultivation. Cultivation of *Moringa* in the tarai and bhabar areas may help to overcome problem of malnutrition and generate additional source of income.

Key words: Drumstick, *Moringa oleifera*, genetic diversity, vitamin A

Moringa oleifera Lam., commonly known as drumstick tree, horseradish tree, ben tree, 'miracle tree', and several other names is a fast growing evergreen or deciduous tree. It is extensively used in traditional medicine and valued for leaves, flowers, fruits, roots and seed oil. It is indigenous to South Asia, where it grows in Himalayan foothills. It grows in areas having large fluctuations in annual minimum (-1-3^{0}C) and maximum (38-48^{0}C) temperatures during coldest and warmest months. It is highly drought tolerant [1] and grows at elevations up to approximately 1400 m.

The soft wood of *Moringa* is used as fuel wood and it is suitable for pulp production for news print, cellophane and textiles. Its edible tender pods are eaten as a nutritious vegetable either cooked or pickled. The tender leaves are rich in protein, minerals, beta carotene, thiamine, riboflavin and vitamin 'A' [2]. It is rich source of ascorbic acid; in green pods ascorbic acid ranges 92-126 mg per 100 g of pulp. Protein content in young fruit, flowers and leaves ranges 5-10 percent. Oil content in seeds ranges 19-47 percent. Oil is rich in palmetic, stearic, behmic and oleic acids. Oil is highly useful for its power of absorbing and retaining odors. It is used as lubricant by watchmakers and oil cake is used as fertilizer. In spite of its nutritional and medicinal importance, the crop still remains underexploited.

An exploration and germplasm collection tour was conducted in Shiwalik foothills of Uttarakhand w.e.f., June 16-20, 2014 to collect the genetic diversity of *Moringa oleifera*. In view to explore and collect the maximum diversity of wild Moringa 5-6 farmers of the near by area have been contacted at each site and samples representing the distinct agro-eco-niches were collected. In all the sites emphasis was to first make the inventory of the wild *Moringa* germplasm with the help of farm folks after that germplasm was collected along with associated traditional knowledge. Method of sites selection was selective on the basis of availability of germplasm and to avoid the duplicity of samples. All the samples were collected from partly disturbed habitats. Fresh leaves and fruits of collected germplasm were used for estimation of Vitamin A [3] and C [4] concentrations.

Rich diversity of flora in general and underutilized plants in particular is available in the CHR i.e., Uttarakhand state of India which spreads from 28^{0}43' - 31^{0}27' N latitude and 77^{0}34' - 81^{0}02' E longitude covering 53484 sq km area. *Moringa oleifera* is an underutilized multipurpose plant native to this region. Vegetative propagation such as through cuttings is easy and effective in *Moringa oleifera*. Plants raised from seeds produce inferior quality fruits

and are slower to produce fruits. Germination in *Moringa* is epigeal. Scarification does not positively affect germination rate.

Table 1. Genetic diversity of *Moringa oleifera* in the Shiwalik foot hills

S.No.	Collector's No.	Altitude (m)	Latitude	Longitude	Specific characters
1	T-123	1010	$29^0$11'17.7"	$79^0$34'0.6"	Luxuriant growth in natural condition, long fruits, good fruiting
2	T-124	218	$28^0$55'56.3"	$79^0$44'24.8"	Small plants, heavy fruiting, long fruits
3	T-125	206	$28^0$52'24.1"	$79^0$57'11.9"	Medium size plant, thick fruits, heavy fruiting
4	T-126	251	$29^0$07'28.61"	$80^0$11'27.93"	Plant tall, fruits are thick, seeds bold, fruits soft
5	T-127	211	$29^0$01'38"	$79^0$29'35.5"	Medium size plant, thick and soft fruits
6	T-128	953	$29^0$04'12"	$79^0$03'26"	Small plants, heavy fruiting
7	T-129	223	$29^0$15'07"	$79^0$12'09"	Small plants, thick fruits
8	T-130	214	$29^0$19'17"	$78^0$95'39"	Small plant, heavy fruiting
9	T-131	333	$29^0$21'59.9"	$79^0$08'38.4"	Plants with luxuriant vegetative growth, long fruits, heavy fruiting
10	T-132	425	$29^0$26'40.4"	$79^0$07'54.4"	Plants are tall, heavy fruiting with long fruits
11	T-133	246	$29^0$16'34.8"	$79^0$01'11.4"	Small plant, fruits are small and thick
12	T-134	233	$29^0$17'57.5"	$79^0$49'2.3"	Medium size plant, long fruits
13	T-135	405	$29^0$45'32.8"	$78^0$32'12"	Small plant, long fruits
14	T-136	270	$29^0$86'54"	$78^0$18'14"	Medium plant, long fruits
15	T-137	333	$30^0$03'1.3"	$78^0$12'59.4"	Small plant, long and thick fruits
16	T-138	346	$30^0$07'18.1"	$78^0$18'7.1"	Long plant, long fruits
17	T-139	379	$30^0$07'9.7"	$78^0$17'20.6"	Small plants, long fruits
18	T-140	535	$30^0$21'7.5"	$77^0$53'13.5"	Medium plant, long thin fruits
19	T-141	487	$30^0$28'44.2"	$77^0$47'26.1"	Medium plant, long fruits, bold seeds
20	T-142	296	$29^0$59'36.6"	$78^0$11'21.2"	Long plant, medium fruit
21	T-143	294	$29^0$41'39.4"	$78^0$31'26.1"	Small plant, medium fruits
22	T-144	275	$29^0$36'0.5"	$78^0$34'3.2"	Long plant, long fruit
23	T-145	265	$29^0$29'46.4"	$78^0$45'31.2"	Long plant, long and thick fruits

Ample diversity of this plant is available in Shiwalik foothills (Table 1). Besides diversity in flowering and fruiting traits leaves and fruits are rich source of vitamin 'A' and 'C' (Table 2). It has numerous medicinal uses that have been appreciated for centuries. In ancient Sanskrit texts on medicine uses of its roots, root bark, stem bark, stem exudates, leaves, flowers and seeds in the treatment of wide variety of ailments have been mentioned [5]. The juice extracted from the leaves has strong antibacterial and antimalarial properties. The crushed seeds are effective and low cost method for removing turbidity and reducing bacterial

Table 2. Diversity in flowering and fruiting traits of *Moringa oleifera* from Shiwalik foot hills

S.No.	Parameter	Mean	Max	Min
1.	Flowers/inflorescence (No.)	34.66	49.33	27.40
2.	Fruit length (cm)	43.50	62.55	27.33
3.	Fruit girth (cm)	4.33	5.22	2.10
4.	Fruits/plant^{-1}	212	285	109
5.	Fruit weight (g)	44.23	60.50	22.33
6.	Seeds/fruit^{-1}	18.66	22.50	12.00
7.	Leaf vitamin A (I.U.)	9512	11225	7650
8.	Fruit vitamin A (I.U.)	122	145	86.50
9.	Leaf vitamin C (mg 100 g^{-1})	198.50	209.33	172.20
10.	Fruit vitamin C (mg 100 g^{-1})	104.66	112.33	82.55

contamination from drinking water in rural areas [6]. Leaf extract is effective in increasing root nodulation, nodule weight and *Rhizobium* nitrogenase activity. In view of uncertainty in climatic condition, particularly rainfall this may be a suitable plant for areas prone to drought and where malnutrition is a challenge. Diversity of such perennial plants will help to provide nutrition besides its role in improving properties of soil.

Acknowledgement

Authors are thankful to Director, NBPGR, Pusa Campus, New Delhi, for providing necessary facility.

References

1. Booth E.F.E.M. and Wickens G.E. 1988. Non-timber uses of selected arid zone trees and shrubs in Africa. FAO Conservation Guide 19. Rome : Food and Agriculture Organization. 176 p.
2. Dahot M. U. 1988. Vitamin contents of the flowers of *Moringa oleifera.* Pak. J. Biochem., 211-2): 21-24.
3. Srivastava R. P. and Kumar S. 1998. *Fruit and Vegetable Preservation- Principles and Practices*. 2nd edn. International Book Distributing Co., Lucknow, 444p.
4. Sadasivam S. and Manickam A. 1992. *Biochemical Methods for Agricultural Sciences*. Wiley Eastern Ltd., New Delhi, 246p.
5. Ramachandran C., Peter K. V. and Gopalkrishnan P. K. 1980. Drumstick (*Moringa oleifera*): a multipurpose Indian vegetable. Econ. Bot., 34(3): 276-283.
6. Sreeramulu N., Ndossi G. D. and Mtotomwema K. 1983. Effect of cooking on the nutritive value of common food plants of Tanzania. 1: Vitamin C in some of the wild green leafy vegetables. Food Chemistry, 10(3): 205-210.

PS-IV-34

Assessment of genetic diversity in aerobic rice genotypes using microsatellite markers

Puja Kumari* and V. K. Sharma

Department of Agricultural Biotechnology and Molecular Biology, Rajendra Agricultural University, Bihar, Pusa (Samastipur) 848 125; e-mail: pjkm1987@gmail.com

Abstract

A study was undertaken to evaluate the nature of microsatellite sites based simple sequence length polymorphism in 18 aerobic rice entries in order to characterize them on the basis of simple sequence length polymorphism and to determine the nature and extent of genetic differentiation and diversity among them using twenty six microsatellite primer pairs, covering all the chromosomes in the genome of aerobic rice. A total of 110 shared and 115 unique allelic variants were generated in the form of amplified products. Altogether 225 allelic variants were detected at 33 microsatellite loci amongst the entries and the number of alleles per locus ranged from 5 to 13, with an average of 6.81 alleles per locus. The polymorphism information content value, a measure of gene diversity, varied from 0.607 to 0.913 with an average value of 0.795 per microsatellite primer. A dendrogram generated from allelic diversity data using similarity coefficient based sequential agglomerative hierarchical non-overlapping clustering module indicated that the aerobic rice entries AER-05 and AER-06 were relatively more closely related with the highest similarity coefficient amongst eighteen aerobic rice entries under evaluation in the present study, which were broadly divided into three clusters. The use of 26 microsatellite markers in the analysis exhibited a remarkably higher level of genetic polymorphism and revealed unique or entry specific allele which could be useful as DNA fingerprints in the identification and preservation of these aerobic rice entries as well as invaluable genetic resources for improving economically important traits in rice, such as tolerance to drought stress.

Key words: Aerobic rice, genetic diversity, polymorphism, microsatellite

Rice is one of the most important food crops in the world with regard to human nutrition and caloric intake, providing more than one fifth of the calories consumed worldwide by the human species. Production of rice requires a great deal of water. But, when the rice is grown in non-puddled aerobic soils or grown on rain-fed, naturally well-drained fields without surface water accumulation, it saves water considerably and protects soil health as well. Molecular marker assisted selection and determination of genetic differentiation and genetic diversity facilitate to a great extent in the breeding programs directed towards the improvement of available varieties or development of elite varieties in short time period and more easy way. The SSR markers are known to detect a significantly higher degree of polymorphism in rice which becomes ideal for studies on genetic divergence. A carefully chosen set of microsatellite markers is considered to provide genome-wide coverage, facilitating an unbiased assessment of genetic difference and genetic divergence, besides enabling an unambiguous description of the entries and molecular profiling of genotypes of rice. Therefore, in the present investigation, an attempt was made to characterize and estimate the extent of genetic divergence among these aerobic rice genotypes using microsatellite markers for their further utilization in future hybridization programme.

A total of 18 aerobic rice entries were used as experimental material for isolation of genomic DNA from their young leaves using modified CTAB method [1]. The amplification of the extracted DNA was carried out using a panel of twenty six primer pairs specific to the unique flanking sequences of the microsatellites distributed among all the twelve chromosomes present in the genome of rice. The polymerase chain reaction was performed in the Eppendorf Master Cycler gradient in a total volume of 15µl containing 1.5µl template DNA, 10X buffer, 25mM $MgCl_2$, 2mM dNTPs, 10µM of each primers and 1.25U/µl Taq DNA polymerase. The thermal profile cycling conditions of denaturation at 94^0C for 1 min; annealing at $53^{0-}58^0$C for 1 min and extension at 72^0C for 2 min for 35 cycles was preceded by an initial denaturation at 94^0C for 5 min. In the end, a final extension at 72^0C for 7 min was given. The amplicons were resolved on 2% agarose gel containing ethidium bromide (0.5µg/ml) in 0.5X TBE buffer at 100 volts. Frequencies of incidence of amplified allelic variants were calculated and used for determination of polymorphism information content of each primer pair. The efficacy of the individual primer pairs in differentiation of the genotypes was assessed by computing polymorphism percent, discrimination coefficient and non-discrimination coefficient. The similarity matrix was subjected to construct a dendrogram to produce an agglomerative hierarchical classification [2].

By using a panel of 26 microsatellite markers, 225 allelic variants were detected at 33 SSR loci with an average of 6.82 alleles per locus. Among the primer pairs used in present study, the nineteen primer pairs namely, RM 5359, RM 250, RM 60, RM 114, RM 280, RM 335, RM 538, RM 153, RM 461, RM 510, RM 427, RM 219, RM 524, RM 591, RM 5373, RM 332, RM 224, RM 7003 and RM 558 produced single but polymorphic amplicons in combination with the eighteen aerobic rice entries evaluated. These 19 primer pairs amplifed the targeted regions in the genome of rice, which belonged to simple sequence repeats located on chromosome 1, 2, 3, 3, 4, 4, 5, 5, 6, 6, 7, 9, 9, 10, 10, 11, 11, 12 and 12, respectively. The number of allelic variants per locus ranged from five in the case of RM 524 to thirteen in the case of RM 538. Altogether 225 allelic variants were detected at 33 SSR loci with an average of 6.82 allele per locus. However, the proportion of alleles per locus recorded in the present study is comparatively lower than that documented earlier [3]. A total of 110 shared and 115 unique allelic variants were generated in the form of amplified products by using the twenty six primer pairs. The number of shared alleles per locus ranged from three out of five alleles in RM 524, six alleles in RM 289 and RM 407, seven alleles in RM 3873, RM 461 and RM 510, nine alleles in RM 219 and RM 335, eleven alleles in RM 591and thirteen alleles in RM 538 to seven out of twelve alleles in the case of RM 337. The number of unique alleles per locus ranged from one out of six alleles in the case of primer pairs RM 114 and RM 5373 to ten out of thirteen and sixteen alleles in the cases of primer pairs RM 538 and RM 234, respectively. The primer pairs RM 538, RM 591, RM 263, RM 335, RM 234, RM 5359, RM 3530 , RM 3873, RM461, RM 510, RM 219, RM 332, RM 280, RM 7003 and RM 407 generated considerably greater polymorphism percentage in descending order of magnitude. Considerably greater magnitude of PIC value was obtained in the cases of primer pairs RM 591, RM 5359, RM 538, RM 263, RM 224, RM 153, RM 337, RM3530, RM 114, RM 60, RM 332, RM 335 and RM 219 in descending order of magnitude. Among these, the primer pairs RM538, RM 5359, RM 263, RM 337, RM 591, RM 224, RM 153, RM 3530, RM 332, RM 335and RM 219 generated considerably greater number of allelic variants

and appeared to be more informative primers. Occurrence of null allele for a particular repeat locus was noticed reflecting failure of locus specific generation of amplified products. The repeat locus associated with primer pairs RM 3873, RM 280, RM 114 and RM 591 showed null allele in some of the entries evaluated. The number of entries showing null allele varied from one in combination with RM 280, two in combination with RM 3873 and three in combination with RM 114 and RM 591. Occurrence of null alleles has also been reported by earlier researchers. Therefore, the result of the present study corroborates the previous reports [46]. The estimates of discrimination coefficient ranged from 0.647 in the case of primer pair RM 407 to 0.960 in the case of primer pair RM 591. Considerably greater ability to discriminate pair-wise combinations of entries was exhibited by the primer pairs RM 591, RM 5359, RM 538, RM 263, RM 335, RM 153, RM 337, RM 224, RM 3530, RM 114, RM 60 and RM 332 in descending order of magnitude. The estimates of non-discrimination coefficient ranged from 0.039 in the case of primer pair RM 591 to 0.719 in the case of primer pair RM 263. Comparatively greater inability to discriminate pair-wise combinations of entries was exhibited by the primer pairs RM 263, RM 524, RM 537, RM 510, RM 427, RM 280 and RM 3873. The repeat loci with di, tri nucleotide and complex repeat motifs tended to detect greater number of alleles than the repeat loci with tetra-nucleotide repeat motifs. The results did not indicate any relationship between the repeat number involved in the simple sequence repeat and the number of identified alleles. Appearance of more than one band in the same entry was noticed reflecting the existence of the duplicated region in the genome of some of the entries. Taking into consideration the number of alleles generated by different primer pairs in concomitance with the level of polymorphism detected in the present investigation, the primer pairs primer RM538, RM 5359, RM 263, RM 337, RM 591, RM 224, RM 153, RM 3530, RM 332, RM 335and RM 219 appeared to be more informative primers. The estimates of similarity coefficient clearly indicated the existence of a considerably greater extent of genetic variation at the molecular level. The genetic relationships among the entries were evaluated by matrix based on Dice's similarity coefficients [7]. The magnitude of similarity coefficient between AER-05 and AER-06 (0.542) was found to be the maximum amongst pair-wise combinations of entries. The clustering analysis was conducted based on the similarity matrix by UPGMA method and dendrogram has been constructed (Fig. 1). Considering broad classification of entries, as indicated by dendrogram, basically the entries were divided into three groups and mainly grouped into seven main groups with different subgroups viz., IA, IB, IIA, IIB, IVA, IVB, VA and VB and sub-sub groups viz, IAa, IAb, IIAa, IIAb, IIBa and IIBb (Table 1 and Fig. 1).

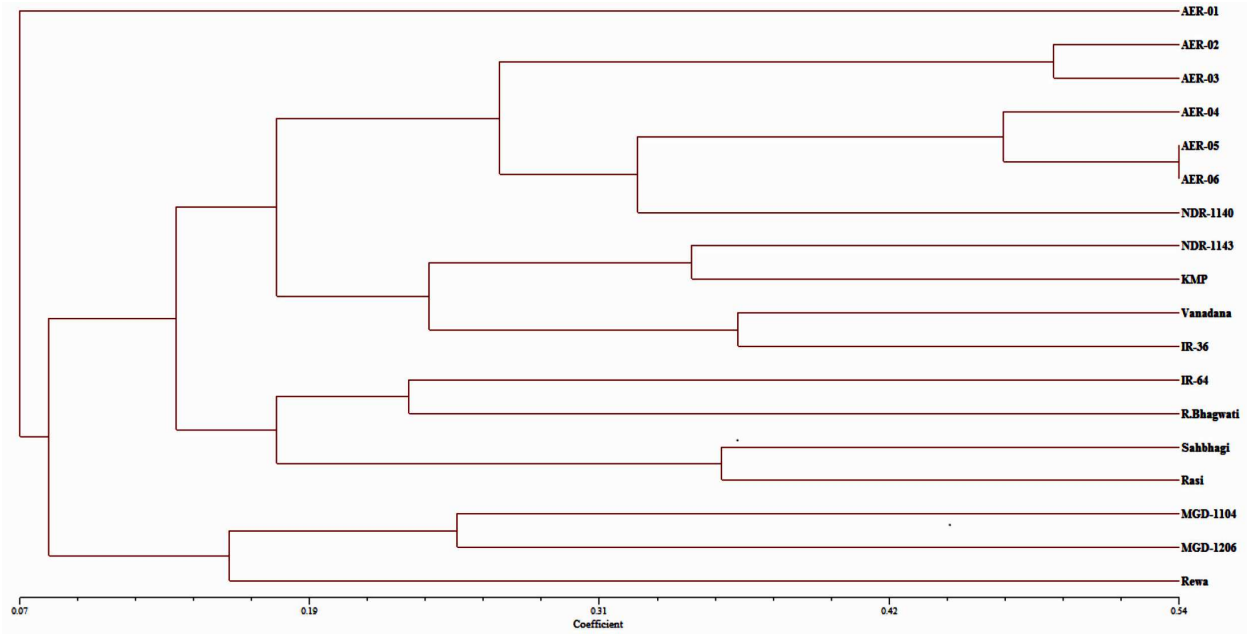


Fig. 1. Dendrogram of 18 aerobic rice varieties based on average similarity coefficients for 26 microsatellite primer pairs dependent allelic diversity

Among the aerobic rice entries under evaluation in the present study, AER-05 and AER-06 exhibited the maximum extent of similarity. The microsatellite site specific SSR primer based analysis revealed unique or entry specific allele which could be useful as DNA fingerprints in the identification and preservation of aerobic rice entries. The use of twenty six SSR markers in the evaluation of aerobic rice entries exhibited a remarkably higher level of genetic polymorphism, which allowed unique genotyping of eighteen aerobic rice entries included in the analysis.

Table 1. Composition of clusters based on similarity coefficient in numerical taxonomic approach of cluster analysis.

Clusters identified at different phenon levels			Entries included in each cluster
25	50	75	
I (6)	IA(4)	IAa(3)	AER-04, AER-05, AER-06
		IAb(1)	NDR-1140
		IB(2)	IB(2) AER-02, AER-03
II(4)	IIA(2)	IIAa (1)	Vandana
		IIAb (1)	IR-36
	IIB(2)	IIBa(1)	KMP
		IIBb (1)	NDR-1143
III(2)	III(2)	IIIA(1)	Sahbhagi
		IIIB(1)	Rasi
IV(2)	IVA(1)	IVA(1)	IR-64
	IVB(1)	IVB(1)	Rajendra Bhagwati
V(2)	VA(1)	VA(1)	MGD1104
	VB(1)	VB(1)	MGD1206
VI(1)	VI(1)	VI(1)	Rewa

The microsatellite markers manifested a high level of polymorphism was observed as revealed by the use of twenty six primer pairs specific to the unique flanking sequences of the repeats providing a molecular database of the eighteen aerobic rice entries evaluated, in the present investigation. The marker based identification and differentiation of aerobic rice could be helpful to preserve the integrity of these high quality aerobic rice genotypes to benefit farmers, breeders and consumers.

References

1. Murray M. G. and Thompson W. F. 1980. Rapid isolation of high molecular weight plant DNA. Nucleic Acids Res.8: 4321-4325.
2. Rohlf F. J. 1997. NTSYS-pc numerical taxonomy and multivariate analysis system version 2.0 New York, Exiter Software.
3. Jayamani P., Negrão S., Martins M., Maçãs B. and Oliveira M. M. 2007. Genetic relatedness of Portuguese rice accessions from diverse origins as assessed by microsatellite markers. Crop Sci., 47(2): 879-884.
4. Lapitan Victoria C., Brar Darshan S., Abe Toshinori and Redofla Edillerto D. 2007. Assessment of genetic diversity of Phillipine rice cultivars carrying good quality traits using SSR markers. Breeding Sci., 57: 263-270.
5. Pervaiz Zahida H., Rabbani Malik A., Pearce Stephen R. and Mali Salman A. 2009. Determination of genetic variability of Asian rice (*Oryza sativa* L.) varieties using microsatellite markers. African J. Biotechnol., 8(21): 5641-5651.
6. Zeng L., Kwon T. R., Liu X., Wilson C., Grieve C. M. and Gregorio G. B. 2004. Genetic diversity analysed by microsatellite markers among rice (*Oryza sativa* L.) genotypes with different adaptation to saline soils. Plant Sci., 166: 1275-1285.
7. Dice Lee R. (1945). Measure of the amount of ecological association between species. Ecology, 26(3): 297-302.

PS-IV-35

Evaluation of wheat germplasm for powdery mildew and stripe rust resistance

Vikas Gupta, Satish Kumar, C. N. Mishra, R. Selvakumar, Vinod Tiwari and Indu Sharma

Directorate of Wheat Research, Karnal, Haryana 132001; e-mail: vikasdwr@gmail.com

Abstract

A set of 240 indigenous wheat germplasm accessions evaluated for powdery mildew and stripe rust resistance along with three released varieties PBW 343, DPW 621-50 and PBW 550 at Dhaulakuan and Malan which are hot spot locations for both the diseases. 100 and 82 accessions were found resistant for powdery mildew whereas 40 and 64 accessions were found resistant to stripe rust at Malan and Dhaulakuan, respectively. Only ten accessions were found resistant to both the diseases at both locations. These accessions will be used as donor for transferring new resistance genes in the future breeding lines.

Key words: Wheat, germplasm, powdery mildew, stripe rust

Wheat (*Triticum aestivum* L.) is one of the major sources of energy, protein and fibre in human diet and is the second most important crop after rice in India. During 2011-12, the annual wheat production in India was 93.90 million tonnes and global wheat production was estimated at 704.08 million tonnes [1, 2]. Development of high yielding and resistant varieties is an important objective of any wheat breeding programme. Wheat production is globally hampered by several biotic factors of which rusts and powdery mildew are the most important. Heavy economic losses around the globe have reported due to stripe rust (caused by *Puccinia striiformis*) and powdery mildew (caused by *Blumeria graminis* f. sp. *tritici*) diseases of wheat [3,4]. North Western Plains Zones has been the seat of the historical green revolution and at present it contributes over 45% of the total wheat production in the country. The major challenge in this zone is to sustain the wheat production by higher yield potential coupled with disease resistance in the wheat varieties. Stripe rust and powdery mildew are the major diseases of Northern Hills Zone and North Western Plains Zones of India. Intensive cultivation single high yielding varieties having major genes of resistance led to the problem of resistance breakdown. In India, PBW 343 mega variety of wheat has become susceptible to yellow rust. Susceptibility to yellow rust has also been reported in newly released cultivars DPW 621-50 and HD 2967. In addition to this most of the *T. aestivum* and *T. durum* varieties are highly susceptible to powdery mildew. It is also by and large accepted that in the absence of diverse genetic pool, the breeding approach may not prove successful. The genetic diversity for resistance to rusts and powdery mildew within wheat needs to be enriched with identification and mobilization of new genes from unexploited germplasm collection. Therefore, the present study was taken to identify new sources for stripe rust and powdery mildew resistance for use in breeding programmes.

Wheat indigenous germplasm comprising 240 accessions obtained from National Bureau of Plant Genetic Resources, New Delhi along with three released varieties PBW343, DPW 621-50 and PBW550 were screened against natural incidence of stripe rust and powdery mildew at hot spot locations Dhaulakuan and Malan during 2012-13. The accessions were timely sown in one metre rows with spacing of 20cm following all the recommended package of practices for raising a good wheat crop. The stripe rust severity was recorded according to the modified Cobb's Scale as % of rust infection on the plants [5]. Powder mildew reactions were recorded following the scale developed by Leath and Heun (1990) [6].

Stripe rust reaction varied from immune (0) to highly susceptible (80S) among germplasm at both the locations. Stripe rust reaction of 80S, 20S and 40S and 60S, 20S and 30S was reported for checks PBW 343, DPW 621-50 and PBW 550 at Malan and Dhaulakuan locations respectively. Out of 240 accessions, 100 accessions

have shown immune reaction at Malan and 82 accessions at Dhaulakuan where as for other accessions reaction varied form moderately resistant to 80S (Table 1). Only 61 accessions have shown immune reaction at both locations. Similarly, for powdery mildew the checks PBW343, DPW 621-50 and PBW550 have shown susceptible reaction of 8, 7and 8 at Malan and susceptible reaction of 9, 8, 8 at Dhaulakuan. Out of 240 accessions, 40 and 64 accessions have sown immune and resistant reaction whereas reamiaing accessions have shown moderately susceptible to highly susceptible reaction at Malan. 156 accessions have shown immune reaction to powdery mildew disease at Dhaulakuan while only 35 accessions have shown moderately resistant reaction. Remaining accessions have shown moderately susceptible to highly susceptible reaction (Table 2).

Table 1: Stripe rust reaction of germplasm accessions alongwith checks at Malan and Dhaulakuan locations

S.No.	Field response	No. of acc.		Stripe rust reaction
		Malan	Dhaulakuan	
1	0	100	81	Immune
2	tR	-	09	Traces
3	MR	17	-	Moderately resistant
4	S	104	150	Susceptible
5	MS	19	-	Moderately susceptible
Checks		Stripe rust reaction		
6	PBW 343	80S	60S	Susceptible
7	DPW 621-50	20S	20S	Susceptible
8	PBW 550	40S	30S	Susceptible

Table 2. Powdery mildew reaction of germplasm accessions alongwith checks at Malan and Dhaulakuan

S.No.	Powdery mildew scale	No. of acc.		Powdery mildew reaction
		Malan	Dhaulakuan	
1	0	40	156	Immune
2	1	-	-	Resistant
3	2	-	19	Resistant
4	3	64	16	Resistant
5	4	-	15	Moderately Susceptible
6	5	132	13	Moderately Susceptible
7	6	01	10	Moderately Susceptible
8	7	4	06	Highly susceptible
9	8	-	03	Highly susceptible
10	9	-	03	Highly susceptible
Checks		Powdery mildew scale		
11	PBW343	8	9	Highly susceptible
12	DPW 621-50	7	8	Highly susceptible
13	PBW550	8	8	Highly susceptible

At both the locations, only 10 accessions (IC 535228, IC 535240, IC 415949, IC 415981, IC 416229, IC 252344, IC 252431, IC 252447, IC252493 and IC 252975) have shown immune reaction to both stripe rust and powdery mildew whereas 20 accessions (IC 36900, IC535198, IC 535200, IC 535241, IC 535557, IC 128643, IC 279889, IC 397999, IC 398039, IC 415962, IC 415971, IC 415977, IC 415984, IC 416012, IC 416025, IC 416220, IC 416249, IC 416256, IC 416278 and IC 145961) have shown immune reaction to stripe rust and moderately resistant reaction to powdery mildew. These lines can be used as parental lines/base material for developing disease resistant genotypes in the wheat improvement programmes.

References

1. Anonymous. 2012. *Progress Report of All India Coordinated Wheat & Barley Improvement Project*. Ed: Indu Sharma, DWR, Karnal, India.

2. Arya R.K, Munjal R and Dhanda S.S. 2012. Evaluation of bread, durum and synthetic wheats and triticale for physiological traits under heat stress conditions. In: *National seminar on sustainable agriculture and food security: challenges in changing climate*, March, 27-28, 2012 at CCSHAU, Hisar.

3. Alam M.A, Mandal M.S.N, Wang C and Ji W. 2013. Chromosomal location and SSR markers of a powdery mildew resistance gene in common wheat line N0308. Afric. J. Micro. Res. 7(6) 477-482.

4. Chen X.M. 2005. Epidemilogy and control of stripe rust (*Puccinia striiformis* f.sp. *tritici*) on Wheat. Canadian J. Plant Pathology, 27:314-37.

5. Peterson R.F., Campbell A.B., and Hannah A.E. 1948. A diagrammatic scale for estimating rust intensity of leaves and stem of cereals. Can J. Res., 26: 496-500.

6. Leath S., and Heun M. 1990. Identification of powdery mildew resistance genes in cultivars of soft red winter wheat. Plant Dis., 74:747-752.

PS-IV-36

Diversity distribution mapping in collected rice (*Oryza sativa*) germplasm from Chhattisgarh, Odisha and West Bengal

D. P. Semwal*, Soyimchiten and Shashi K. Sharma

Division of Plant Exploration and Germplasm Collection, National Bureau of Plant Genetic Resources, New Delhi 110 012; e-mail: dinusem@rediffmail.com

Abstract

Based on gaps identified in collections, it is concluded that the unexplored/underexplored area identified needs to be surveyed for future rice germplasm collection particularly Mungeli, Bemetara and Balod districts of Chhattisgarh; Bargarh, Gajapati and Subarnapur districts of Odisha and Birbhum, Murshidabad, Nadia and Howrah districts of West Bengal.

Key words: Rice, germplasm, distribution, GIS, geo-referencing

Diversity collected analysed using exploration database vis-a-vis their areas of availability, is a priority activity in planning and execution of exploration programmes. Identifying gaps in collections is the main focus for major prioritized crops. Although geo-referenced data are currently negligible for diversity mapping hence using Geographic Information System (GIS) tools for geo-referencing of passport information, diversity analysis, mapping trait-specific germplasm for management of genetic resources will provide strong inputs for explorers to improve the quality and quantity of information recorded in passport data.

The germplasm collected from different agro-ecological regions belonging to more than 200 collection sites was examined using information mentioned in plant exploration database, plant collection reporter, annual reports and other published literature [1]. Geo-referencing was done in order to know the spatial distribution and diversity assessment of collected rice germplasm using GIS tools [2, 3].

Geo-referencing methodology was applied for analysis of passport data of *Oryza sativa* (12,047 acc.) collected from Chhattisgarh, Odisha and West Bengal which were compiled using available information in the database of NBPGR. On the basis of rigorous screening, 11,632 accessions were short-listed with details on state, district, village, collector number, latitude (N) and longitude (E) of the collection sites. A total of 8,073 acc. of rice germplasm collected from 27 districts of Chhattisgarh and 6,075 acc. with locality information screened for gap analysis studies. Though all 27 districts have been explored during last four decades, however maximum accessions were collected from Raipur (1,536), Bastar (1,310), Gariaband (740) and Raigarh (541) districts while accessions collected from Mungeli (15), Bemetara (21) and Balod (11) districts were less to map the diversity for identify gaps in collection. Similarly, a total of 3,491 rice germplasm accessions were collected from 30 districts of Odisha and 3,161 acc. with locality information screened, which indicate that maximum accessions were collected from Cuttack (542), Puri (202), Sundergarh (195) and Kandhamal (191) districts while Bargarh, Gajapati and Subarnapur districts of Odisha were with minimum accessions. While only 483 acc. were collected from

West Bengal and 423 acc. with locality information were screened for gap analysis studies. Some locally important germplasm/landraces were identified with specific traits.

References

1. Plant Germplasm Reporter 2001-2010. Indigenous collections. National Bureau of Plant Genetic Resources (NBPGR), New Delhi, India.
2. Hijmans R.J., Guarino L., Cruz M. and Rojas E. 2001. Computer tools for spatial analysis of plant genetic resources data: 1. DIVA-GIS. Plant Genet. Resour. Newslett., 127: 15-19.
3. Semwal D.P., Bhandari D.C., Bhatt K.C. and Singh R. 2013. Diversity distribution pattern in collected germplasm of rapeseed-mustard using GIS in India, Ind. J. Plant Genet. Resour., 26: 76-81.

PS-IV-37

Global status of sorghum patents

M. Elangovan* and G. Premalatha

Directorate of Sorghum Research Rajendranagar, Hyderabad 500 030; e-mail: elangovan@sorghum.res.in

Abstract

Compiled information on patents on any particular crop is not available for cross checking the repetition of research in that area. A total of 143 unique patents were documented based on its utility and area reported in the WIPO. China has the maximum frequency of 71 patent grants. Apart from this 11 applicants have filed their patent in individual country as well as in PCT to protect their patents in multiple countries. USA has protected its patent both in USA and PCT through WIPO with maximum frequency of 5 patent grants. Republic of Korea has been granted a maximum of 8 patents. Five patents were granted to Dr Tuinstra Mitchell R. as inventor. A maximum of 61 patents in sorghum was granted in the area of agriculture followed by industry with 52 patents. Biochemistry division has been granted a maximum of 33 patents in sorghum followed by post-harvest technology with 20 and food technology with 15.

Key words: Sorghum, patents, WIPO, IPR

The mere discovery of a new form of a known substance which does not result in the enhancement of the known efficacy of that substance or the mere discovery of any new property or new use for a known substance or of the mere use of a known process, machine or apparatus unless such known process results in a new product or employs at least one new reactant [1]. The research results obtained in any field of technology, whether processes or products which are new inventive (non-obvious) and useful (industrially applicable) are patentable under the patent act [2]. Patents and publications are important outputs of any research project. Compiled information on patents on any particular crop is not available for cross checking the repetition of research in that area. Sorghum is considered as one of the bio-energy crops, because the grain can be used to make food, feed and drinks, the stalk can yield sugar, fuel, forage and fibre, mat, hat, building material, frame material and barrier, the roots can be used as fuel, the peduncle is used as cover, the threshed spike are used as broom and pot scouring brush. Minor uses include molasses (syrup), construction and basketry material and alcoholic beverages (Elangovan, 2005). In this paper, an attempt has been made to document all the patents granted in different areas of research in sorghum during the past five years.

A database on the patents granted in sorghum research areas is prepared from 2010 to 2014. A total of 143 unique patents were documented based on its utility and area reported in the World Intellectual Property Organization [3]. The database was developed with the details of the applicant country of origin, title of the patent, publication date, international classification number, application number, other [3] application number, individual or company

who applied for the patent, name of the inventor and area in which the patent was granted. The data is entered in the MS-Excel and used for filtering the data according to the objective of the study.

A total of 143 unique patents granted in sorghum were documented from 2010 to 2014. China has the maximum frequency of 71 patent grants followed by United States of America (27) and Korea (22). It has been observed from the documentation that all the 143 are unique patents with unique title. Apart from this 11 applicants have filed their patent in individual country as well as in PCT to protect their patents in multiple countries. USA has protected its patent both in USA and PCT through WIPO with maximum frequency of 5 patent grants. Coincidentally, on the publication date of 6/3/2014, USA has been granted 2 patents; on the publication date of 12/05/2011, 2 grants were given to CERES, INC. of USA. Forty-nine patents in sorghum were granted during 2013 followed by 46 in 2012 and 39 in 2011. Republic of Korea has been granted a maximum of 8 patents. A maximum of 5 patents were granted to Dr Tuinstra Mitchell R. as inventor followed by Dr Han, Sang IK with 3 patents. A maximum of 61 patents in sorghum was granted in the area of agriculture followed by industry with 52 patents. Biochemistry division has been granted a maximum of 33 patents in sorghum followed by post-harvest technology with 20 and food technology 15. The list of potential patents and the parts of sorghum used is presented in Table 1.

Sorghum has been successfully used in feeding programmes after fortification with legumes. Patent on sorghum porridges and sorghum noodles are granted to China during 2011. Patent on method of

Table 1. List of potential patents in sorghum

Health problems	**Parts and methods**
Sickle cell disease	Botanical formulation
Bone reunion powder	Leaf sheath
Health care	Sorghum rice
Cancer	Sorghum extract
Antibacterial and antiviral	Sorghum glume pigment
Diabetics	Active ingredient
Lipid absorption	Sorghum extract
Anti-thrombotic	Sorghum powder
Anti-oxidant	Grain powder
Warming spleen and stomach to dispel cold	Sorghum flour
Industrial and commercial uses	**Sorghum Parts**
Composite boards, strand boards	Stalk
Wine, Red wine	Grains
Liquor, ethanol, alcohol	Stalk
Natural pigment, colored plastic	Straw
Citric acid	Sorghum powder
Glutathione	Stalk juice
Liquid fertilizer	Stalk juice
Maltose	Grain
Feed	Straw powder
Healthy bread	Sorghum powder
Edible yeast	Stalk juice
Color enhancer	Sorghum bran
Wood plastic	Sorghum stalk
Feed	Sweet sorghum
Devices	**Sorghum Parts**
Sorghum harvester	Whole plant
Dehulling machine	Grain
Seed metering	Sowing
Stalk cutting device	Sweet sorghum
Gene	**Trait**
MA5/MA6	Photoperiod sensitivity
SbDES2 and SbDES3	Desaturation reaction
Terminator sequences	Polynucleotide sequences
SCAR Marker	High sugar
SbSAP14	Salt-resistant gene
MC with novel compositions	Transformation of plant cells
TS304T, TS050	Restorer line identification
SbbHLH1 gene	Sorghum lignin synthesis regulatory
Ma 1	Sorghum maturity gene 1
SEQ ID NO 2 and SEQ ID NO 1.	Altered lignin composition
DW_3 Allele	Plant height
ARSl and ARS2	Biosynthesis of sorgoleone

manufacturing sorghum slices is granted to China during 2012. Malted grain sorghum is used for food in many parts of the world. Sorghum malt could be used to make biscuits, weaning foods and beer wort. Patent on method of manufacturing corn or sorghum maltose is granted to China during 2013. Sorghum is a new potential substitute for traditional brewing ingredients *viz*., barley and rice. It can solve the ingredient problem and also raise the economic benefits. Sorghum liquor is a unique chinese alcoholic drink with a history of about 1500 years. Chinese sorghum beer is similar to European beer. Its colour, flavour and quality are similar to barley beer. The characteristics of Chinese sorghum liquor are strictly selected materials, meticulous processing, excellent quality, special flavour and very strong prepared from the grains. The famous sorghum liquors are *Maotai, Fen Liquor, Wuliangye, Jiannanchun, Xi Feng* and *Luzhoutequ*. Sweet sorghum stalks have a high sugar content good for making liquor. China has been granted 10 patents in making of wine, liquor and alcohol from sorghum during 2011 and 2012. The sorghum sweet stalks can be utilised comprehensively, the juice of the stalk cane used to produce alcohol and nitrogenous fertilizer which can satisfy the need of crops or herbage. Sorghum leaves and residue may be used as feed, waste is used to produce methane to generate electricity. China has been granted one patent in making method of liquid fertilizer during 2013. The cellulose content in sorghum stalk is very high, at about 48 percent of dry weight. Sorghum stalks are not only light, but also pliable and hard. It can be used to produce sorghum plywood which has many advantages. It can be used as a substitute for wood board. Alternatively, sorghum can reduce the use of wood materials to conserve acres of forests. The sorghum plywood can be used to construct tables, doors, furniture and decorative materials. United States of America has been granted 2 patents during 2013 one each on making composite board and strand board using sorghum stalks.

Sorghum pericarp and glumes are coloured. The glume colour can be dark to light, such as brown, red, yellow and white based on the type of variety. Sorghum pigments belong to iso-xanthoketone galactoside, which has many kinds of components. In ancient China, people found glume pigment sorghum to be very stable useful to dye woollens, cotton, linen, and other textiles. However, most of sorghum glumes are either discarded or used as fertilizer, because no suitable pigment extracting method was found earlier. Chinese successfully extracted pigments from sorghum glumes and named *Sorghum Red Pigment*. Along with improvement of people's living standards, edible pigments are evolving from synthetic pigments to natural pigment. It is because synthetic pigments are harmful to human's health. People are more and more interested in natural pigments. Sorghum Red Pigment is dark red powder with natural soft colour, containing no toxin or special odour, which can be used in foods, meat products, beverage, cosmetics, medicine and textiles. Korea has been granted 6 patents in extraction and utilization of natural pigments from sorghum.

References

1. The Patents (Amendment) Act, 2005.
2. ICAR. 2006. ICAR guidelines for Intellectual Property Management and Technology Transfer/Commercialization. Indian Council of Agricultural Research, New Delhi.
3. WIPO. 2014. PCT, The International Patent System, www.wipo.int/pct/en/.

PS-IV-38

New report of citral rich *Ocimum* for tropical and sub-tropical regions of India

S.C. Singh*, Bhaskar Datt[1], A. Samad and Birendra Kumar

CSIR- Central Institute of Medicinal and Aromatic Plants, Lucknow 226 015, [1]CSIR- National Botanical Research Institute, Lucknow 226 001; e-mail: sc.singh@cimap.res.in

Abstract

The taxonomy of *Ocimum* is in a state of confusion and the same species is often referred to by more than one name or *vice-versa*. The circumscription of *Ocimum* itself is also a matter of disputes among taxonomists. The camphor type is *O. basilicum* L. and the citral type is *O. africanum* Lour. The main difference is in the relative size of the mature calyx. *O. basilicum* has fruiting calyx 6-8 mm long while in *O. africanum* up to 5.5 mm long. Furthermore, it is hoped the present report will attract other Indian taxonomists for the correct appraisal of citral and camphor rich *Ocimum* in India.

Key words: Essential oil, citral, diversity, *Ocimum africanum*, *O. basilicum*

Ocimum is an important economic and medicinal herb due to presence of essential oils which consist of monoterpenes, sesquiterpenes and phenylpropanoids [1]. Its oil is the natural source of methyl chavicol, methyl cinnamate, camphor, neral, geranial, linalool, eugenol, etc. which are used in pharmaceutical, cosmetic and flavouring industries. In addition to these uses, *Ocimum* is widely cultivated as a pot herb for culinary uses, and for the fresh herb market, the export of *Ocimum* from Israel alone is worth 4 million US dollars per year [2]. In India as well it constitutes an important component of ever growing herbal market. Basil is an important essential oil crop with around 350 tonnes of essential oil being produced throughout the world annually. About half of this is produced from *Ocimum basilicum* L. and its close relatives.

The genus *Ocimum* L., collectively called basil, which is annual and perennial herbs and shrubs native to the tropical and subtropical regions of Asia, Africa, and Central and South America [1,2]. The taxonomy of *Ocimum* is in a state of confusion. In the literature concerning *Ocimum*, particularly the work pertaining to economic and industrial fields, same species is often referred to by more than one name or *vice-versa*. The circumscription of *Ocimum* itself is also a matter of dispute among taxonomists. Estimates of species in the world vary from 30 to 160 [3]. *Ocimum africanum* (Lemon basil) was described by Joao de Loureio in 1970. Over the next 50 years separate systematic botanists gave it two names, *O. citriodorum* Vis. and *O pilosum* willd. The same species is also found as *O. basilicum* var. *anisatum, O. americanum sensu* Pushpangadan & Sobti non L., etc. Although *O. americanum* is well known in Indian Floras, the following nomenclature (author citation), dichotomous key and description will facilitate to distinguish it from other closely related species. It is hoped that the present report will attract other Indian taxonomists for the correct appraisal of *O. africanum* in India.

Ocimum africanum Lour., Fl. Cochinch. 2; 270. 1790; Suddee, S. *et al*. in Kew Bull. 60: 28–29. 2005. *O. citratum* Rumph. in Herb. Amboin. 5: 266, t. 93, f.1. 1747. *O. pilosum* Willd., Enum. Pl. 2: 629. 1809. *O. basilicum* L. var. anisatum Benth., Labiat. Gen. Sp. 4. 1832. *O. basilicum* L. var. *pilosum* (Willd.) Benth., Prodr. 12:33. 1848. *Ocimum* × *citriodorum* Vis. in Linnaea 15: Litt. Ber. 102. 1841. *Ocimum americanum* L. var. pilosum (Willd.) A. J. Paton in Kew Bull. 47:426. 1992. *O. americanum* sensu Pushpangadan & Sobti non L. in Cytologia 47: 575. 583. 1982. 'Lemon basil'. The characteristic features are:

Fruiting calyx up to 5 mm long; corolla 4 – 5.5 mm long,

...*O. americanum* Fruiting calyx 2 – 3 mm long; stem internodes with short adpressed

or retrorse hairs

... *O. africanum* Fruiting calyx 4 – 5.5 mm long; stem internodes with long, spreading and sometimes

retrorse hairs, and

... *O. basilicum* Fruiting calyx 6 – 8 mm long; corolla 7 – 8 mm long

Ocimum africanum was described by Joao de Loureio in 1970. Over the next 50 years separate systematic botanists gave it two names, *O. citriodorum* Vis. And *O pilosum* willd. The same species is also found as *O. basilicum* var. *anisatum, O. americanum sensu* Pushpangadan & Sobti non L., etc.

Aromatic, annual or short lived perennial herbs, up to 50 cm high; stems densely pubescent with long, spreading and sometimes retrorse hairs. Leaves elliptic-lanceolate or ovate-lanceolate, 0.8-3.5 x 0.6-2 cm, entire or shallowly serrate at margins, apex acute, base cuneate or obtuse, glandular punctuate, glabrescent above, hairy on veins beneath, sometimes pubescent on both surfaces with longer hairs on veins beneath; petioles 0.2-1.8 cm long, pubescent. Verticels up to 1 cm apart; axis densely pubescent with retrorse hairs; bracts ovate, up to 5 mm long; pedicels 1-2 mm long, recurved, finely pubescent. Calyx campanulate, 2-2.5 mm long, 4-5.5 mm long in fruit; posterior lip rounded, decurrent on tube; anterior lip with 2 median lanceolate teeth; tube with a ring of dense hairs at throat. Corolla white or light purple, 4-5.5 mm long; posterior lip with 4-lobed with oblong obovate villous lobes, anterior lip boat-shaped; tube straight, glabrous. Stamens 4, slightly exserted, posterior 2 shorter. Nutlets oblong, 1-1.5 mm long, black, minutely tuberculate.

Apart from taxonomic reasons, these differences are on account of high levels of both morphological and chemical variability exist within the genus due to inter-specific hybridization, polyploidy, and the existence of chemotypes or chemical races that do not differ significantly in morphology [4]. To get better insight into intra- and inter-speci?c taxonomy, a variety of different approaches based on geographic origin, morphology, karyotype, chemical composition, and crossability have been used by some workers [5, 6]. Despite these efforts, taxonomy and phylogenetic relationships within *Ocimum* genus are still in question.

The taxonomy of *Ocimum* in India is itself in confusion, with some Indian literature [7] providing detailed information on cytology and phytology using a different infrageneric classification from that used in recent taxonomic literature. Due to polymorphism, much confusion has still surrounding the identification of the species of *O. basilicum* and *O. americanum* which have a wide range of distribution in India with enormous diverse ecological settings. The confusion surrounding the name of *O. americanum* also arises because the type specimens of *O. americanum* and *O. canum* do not reveal the characters necessary to decide to which entity they belong. The Type of the former species is a young specimen lacking calyx, whereas the Type of the later species is an illustration [6]. After exhaustive survey and collection of *Ocimum* species in India, we have found various genetic and chemotypic diversities in natural population. Some species of *Ocimum* are citral rich, camphor rich, methyl cinnamate, methyl chavicol and linalool rich. On the basis of chemotypic variability various authorities named it as *Ocimum basilicum* and *O. americanum* (syn. *O. canum*).

The populations of *O. americanum* and *O. afrinanum* are often intermixed and erroneously identified as *O. americanum* in most of herbaria in India. Chemical profiling worked out at CIMAP also indicates their distinctiveness. The results of chemical analysis of *O. africanum* essential oil by gas liquid chromatography exhibited the presence of neral (31.66%), geranial (40.23%), 1, 8 cineole (1.34%), ocimene (0.59%), linalool (2.29%), methyl chavicol (3.46%), citronellal (2.82%) and geraniol (2.26%) as major aroma chemicals. During the survey, the population of *O. africanum* in Lucknow and adjoining areas was also found infected with virus and showed mosaic, yellowing, deformation of leaves and over all stunted growth. The associated pathogen seems to be a begomovirus on the basis of molecular studies. From above studies it is revealed that this citral rich *O. africanum* or lemon basil can be commercially cultivated in tropical and sub tropical regions of India as an annual crop in two seasons (June-September and February-April). The authors are grateful to the Directors, CSIR-CIMAP, and CSIR-NBRI, Lucknow for providing necessary facilities. We are thankful to Dr. Alan Paton, Royal Botanical

Gardens, Kew, United Kingdom for critical suggestions. The study was financially supported by Uttar Pradesh State Biodiversity Board, and CSIR-CIMAP CHEM-BIO (BSC 0203), Lucknow, India.

References

1. Paton A., Harley M.R. and Harley M.M. 1999. *Ocimum*: an overview of classi?cation and relationships. In: Basil: the genus *Ocimum* (eds. Hiltunen R., Holm Y.). Harwood, Amsterdam, pp. 1-38.
2. Darrah H. 1980. The cultivated basils. Thomas Buckeye, Independence, M.O.
3. Pushpangadan P. and Bradu B.L. 1995. Basil. In: Advances in Horticulture, Medicinal and Aromatic Plants (eds. Chadha, K.L., Gupta, R.). Malhotra Publishing House, New Delhi, pp. 627-657.
4. Simon J.E., Quinn J. and Murray R.G. 1990. Basil: a source of essential oils. In: Advances in new crops (eds. Janick J, Simon J.E.). Timber, Portland, pp. 484-989.
5. Khosla, M.K., 1995. Study of inter-relationship, phylogeny and evolutionary tendencies in genus Ocimum. Ind. J. Genet., 55: 71-83.
6. Paton A. and Putievsky E. 1996. Taxonomic problems and cytotaxonomic relationships between and within varieties of *Ocimum basilicum* and related species (Labiatae). Kew Bull., 51: 509-524.
7. Khosla M.K. 1993. Study on inter-relationship, phylogeny and evolutionary tendencies in genus *Ocimum*. J. Plant Anat. Morphol., 6: 93-106.

PS-IV-39

Assessment of endophytic bacteria from cultivated and wild species of soybean (*Glycine max* (L.) Merrill)

K. C. Kumawat*, Poonam Sharma[1] and B. S. Gill[1]

*Department of Microbiology, [1]Department of Plant Breeding and Genetics, Punjab Agricultural University, Ludhiana, Punjab 141 004; e-mail: kailashkumawat02@gmail.com

Abstract

The present study was conducted to assess the genetic diversity of endophytic bacteria from wild species and cultivated variety of soybean. All endophytic bacterial isolates were assessed for morphological, biochemical and plant growth promoting (PGP) traits *in vitro*. Two endophytic bacterial isolates LSKL-4 and LSBL-4 from wild sp. (*G. tomentella*) and LSKL-1 from cultivated variety (SLE-27) have been identified as potential strains. Endophytic bacterial isolates from wild species can be exploited in mordern varieties for improving growth symbiosis and yield in soybean along with *Bradyrhizobium* as future consortium biofertilizer for sustainable agriculture production.

Key words: Endophytic bacteria, IAA, P-solubilization, soybean, Zn- solubilization

Soybean (*Glycine max* (L.) Merrill) is one of the most important legume crops in India. It fulfills it's own nitrogen (N) requirement through nitrogen fixation in symbiosis with soil bacteria collectively known as rhizobia. The nitrogen fixed by rhizobia in legumes can also benefit associated non-legumes via direct transfer of biologically fixed nitrogen to cereals grown after legumes. Diverse endophytic bacteria has been isolated from roots and stem of soybean, but wild soybean is likely to harbor unique populations of endophytic bacteria that differ from those in extensively bred modern varieties of soybean subjected to application of fertilizers and agrochemicals. No information is available on root and nodule endophytic bacteria of soybean in present agro-climatic zone. There is need to identify the predominant diversity of endophytic bacteria of soybean for sustainable agriculture in Punjab.

Healthy samples of soybean were collected from three genotype (cultivated variety, SLE-27 and two wild species, *Glycine soja* and *Glycine tomentella*) during *Kharif* 2013 from breeder's field, Department of Plant Breeding & Genetics, PAU, Ludhiana. Bacterial endophytes from nodules, stems, leaves and roots were isolated on Nutrient agar (NA) and *Pseudomonas* agar media as described by [1]. Further, bacterial isolates were also maintained on specific media for future study. All the endophytic bacterial isolates were characterized on the basis of morphological, biochemical and Plant Growth Promoting (PGP) traits *viz*. P- solubilization, Zn solubilization and Indole acetic acid production as per standard procedure [2].

A total 28 isolates of endophytic bacteria from each of cultivated (SLE27) variety and two wild species *Glycine soja* and *Glycine tomentella* were isolated from four different tissues (stems, roots, nodules and leaves) of soybean. All isolates were grown on nutrient agar and *Pseudomonas* agar media for isolating *Bacillus* sp., *Pseudomonas* sp. and *Klebsiella* sp. Out of 28 endophytic isolates, 32.1% each from stems and leaves and 17.9% each from roots and nodules were isolated from different sorces of soybean.

Table 1. Isolation of endophytic bacteria from different tissue samples of soybean

Sources	No. of Isolates	Designated endophytes bacteria
Cultivated varieties(SLE27)	11	LSBR-1, LSPR-1, LSBN-1, LSPN-1, LSKN-1, LSBS-1, LSPS-1, LSKS-1, LSBL-1, LSPL-1, LSKL-1
Wild species		
Glycine soja	11	LSBR-3, LSPR-3, LSKR-3, LSBN-3, LSPN-3, LSBS-3, LSPS-3,LSKS-3, LSBL-3, LSPL-3, LSKL-3
Glycine tomentella	6	LSBS-4, LSPS-4, LSKS-3, LSBL-4, LSPL-4, LSKL-4
Grand total	28	

Table 2. Morphological and biochemical characteristics endophytes.

Bacterial isolates	*Bacillus* sp.	*Pseudomonas* sp.	*Klebsiella* sp.
Cell shape	Rods	Rods	Rods
Motility	Motile	Motile	Non-motile
Colony shape	Polymorphic	Round	Round
Elevation	Umbonate	Raised	Raised
Texture	Mucoid	Mucoid	Mucoid
Margin	Irregular	Smooth	Entire
Colour	Cream	Light yellow	Cream
Odour	Odourless	Odourless	Odourless
Size	Large	Medium	Medium
pigmentation	None	Few isolates produced fluorescent green pigment	None
Gram's reaction	Gram positive	Gram negative	Gram negative
Oxidase	+	-	+
Catalase	+	+	+
Citrate utilization	+	+	+
Methyl red (MR)	-	-	-
Voges Proskauer(VP)	+	+	-
Nitrate reduction(NR)	+	+	+
Carbohydrate utilization test	+	+	+

Table 3. Screening of endophytic isolates for PGP traits in soybean

IAA production	P-solubilization	Zn solubilization efficiency	
		Zno	Zn_3PO4
LSKL-1(40.7 µg/ml)	LSKL-1(20.17mg/100ml^{-1})	LSKL-1(443.8)	LSKS-3(344.4)
LSKL-4(43.9 µg/ml)	LSPL-4(18.18mg/100ml^{-1})		
LSBL-4 (42.9 µg/ml)			

On the basis of morphological and biochemical tests, out of 28 endophytic isolates 35.7%, 35.7%, and 28.6% were tentatively identified as *Bacillus* sp., *Pseudomonas* sp., *Klebsiella* sp., respectively. IAA is the chief phytohormones with broad physiological activities and enhances lateral root growth formation and thus increase nutrient uptake by plants and root. Results showed that all endophytic bacterial isolates produced IAA ranging from 35.6 to 43.9µg/ml after 3 days of incubation in Luria broth amended with 0.01% tryptophan as substrate. Maximum amount of IAA production were observed in LSKL-4(43.9 µg/ml) and LSBL-4(42.9 µg/ml) isolate from leave of *Glycine tomentella*. These results that are similarly with [3] who also reported that out of 40 *Pseudomonas* isolates obtained from rhizosphere of chickpea and green gram, respectively, only 11 produced IAA in LB broth and highest amount of IAA produced was observed in *Pseudomonas* isolates CPS72 and MPS77.

Endophytic bacteria possess the capacity to solubilize immobilized mineral phosphate. All the 28 isolates were subjected for their phosphate solubilising activity on NBRIP medium amended with 0.5% tri calcium phosphate as inorganic source of phosphorous. 10 out of 28 endophytic isolates showed as clear halo yellow zone on NBRIP medium indicated the positive test for P-solubilization.

Ten endophytic bacterial isolates, out of 28 isolates, which showed zone of solubilization on NBRIP (medium), were further tested in flask containing TCP (0.1%) as inorganic substrates in 100ml of Pikovaskaya's broth having initial pH 7.0. The quantitative estimation of P- solubilization was observed up to 15th days at 3 days of time intervals with decrease in pH of medium. Maximum P-solubilization at 12th days ranged from 1.13 to 20.17mg/100ml^{-1}. Significantly high P-solubilization was recorded by LSKL-1(20.17mg/100ml^{-1}) strain isolated from leaves of cultivated variety (SLE-27) followed by LSPL-4(18.18mg/100ml^{-1}) strain isolated from leaves of wild species (*Glycine tomentella*). Our results are in harmony with [4] who also reported that all the strains solubilized tricalcium phosphate and rock phosphate in broth. In the presence of tricalcium phosphate, the concentration of soluble P was between 12.12 to107 mgL^{-1} and supplemented with phosphate rock. Several researchers demonstrated that P-solubilizing strain of rhizobacteria [5] as an inoculant increases phosphorous uptake, crop yield, induce resistance against salinity and pathogen in legumes.

Zinc deficiency is major problem that affects soil health and crop yields in agriculture. Microorganisms play an important role in solubilization of zinc in soil. In plate assay, all the endophytic bacterial isolates were subjected to measure the magnitude of Zn solubilization on Tris- minimal medium amended separately with zinc oxide and zinc phosphate as inorganic source of zinc. Nine isolates out of total 28 endophytic bacterial isolates from soybean rhizosphere were able to solubilize zinc oxide (insoluble) incorporated in Tris- minimal medium whereas, 6 endophytic bacterial isolates were able to solubilize zinc phosphate (insoluble) supplemented in Tris- minimal medium.

Highest zinc solubilization efficiency for zinc phosphate was recorded in LSKS-3 strain isolated from stem of wild species (*Glycine tomentella*) whereas, Zinc oxide solubilization efficiency was highest in LSKL-1 strain isolated from cultivated variety (SLE-27). Our results are in close agreement with the findings of [6] who have also reported that three *Bacillus aryabhattai* strains MDRS7, MDRS11 and MDRS14 possessed IAA, siderophores and ammonia producing traits. On the basis of PGP traits endophytic bacterial isolates can be further assessed to prove the endophytic nature of these isolates under field condition can be employed as future consortium bioferitlizer for better crop production and soil health.

References

1. Hung P. Q., Senthil M., Kumar V., Govindsamy and Annapurna K. 2007. Isolation and characterization of endophytic bacteria from wild and cultivated soybean varieties. Biol. Fertil, Soils, 44: 155-162.
2. Arora D. K. 2007. Microbial identification modules for some agriculturally important micro-organism Pp. 97-107. National Bureau of Agriculturally important micro-organism (NBAIM) Mau, U.P.
3. Malik D. K. and Sindhu S. S. 2011. Production of indole acetic acid by *Pseudomonas* sp. effect of coinoculation with *Mesorhizobium* sp. *Cicer* on nodulation and plant growth of chickpea (*Cicer arietinum*). Physiol. Mol. Biol. Pants., 17: 25-32.
4. Lopez-Ortega M. P., Criollo-Campos P. J., Gomez-Vargas R. M., Camelo-Rusinque M., Estrada-Bonilla G., Garrido-Rubiano M. F., and Bonilla-Buitrago R. 2013. Characterization of diazotrophic phosphate solubilizing bacteria as growth promoters of maize plants. Rev. Colomb. Biotechnol., 15: 115-123.
5. Kaur N. and Sharma P. 2013. Phenotypic characterization of rhizobacteria associated with mungbean rhizosphere. J. Food legumes., 26:84-89.
6. Sharma P., Kumawat K. C., Kaur S. and Kaur N. 2014. Assessment of Zinc solubilisation by Endophytic Bacteria in Legume Rhizosphere. Indian J. Appl. Res., 4: 439-441.

PS-IV-40

Exploration, collection, characterization and conservation of landraces of desi cotton and perennials from different regions of India

M. Saravanan, Punit Mohan, R. C. Mishra[1] and T. R. Loknathan

Central Institute for Cotton Research (CICR), Nagpur, Maharashtra, [1]National Bureau of Plant Genetic Resources (NBPGR), Regional Station, Cuttack, Orissa; e-mail: msaraniari@gmail.com

Abstract

India is the ancient home of some of the important races of desi cotton. India was known to produce world's best cloths which were traded across the globe. The landraces of desi cotton and perennials possesses many desirable traits such as resistance to biotic and abiotic stresses. Utilization of few elite genotypes leads to narrow genetic base in the cotton gene pool. The introduction of Bt cotton hybrids also aggravated genetic erosion of cotton landraces. So there is urgent need to explore, collect, characterize and conserve the landraces of desi cotton and perennials from different regions of India. Based on the information collected from literature and from Krishi Vigyan Kendras (KVKs), the expedition survey was conducted to collect the landraces of desi cotton and perennials. Eighty nine cotton germplasm samples were collected from different regions of India. Morphological and molecular characterizations are being carried out for the collected cotton samples.

Key words: Perennial cotton, germplasm, diversity analysis, fiber quality

Desi cotton species have originated in India particularly the three geographical races of *Gossypium arboreum* L. namely bengalense, cernuum and indicum and also *G. herbaceum* L. race wightianum. The wild and cultivated cotton plants of the world have been well compiled and documented by Watt (1907) (3).Perennial trees of the cotton species were cultivated in the country by farmers and also in backyard for at least five thousand years. The farmers in some region have domesticated the seeds to convert them into landraces. Comilla, Ponduru, Uppam, Karuganni, Mathio, Wagad are some of important landraces present in India. India was known to produce the world's best cotton cloth known as 'Dhaka muslins' and 'calicoes' which were traded by the 'British East India company' to be exported across the globe. Excavations of Mahenjodaro and Harappa have shown that cotton cloth of finest quality of about 300 counts was produced from the *desi* cotton species (*G. arboreum*) that

was being cultivated in India. Perennial trees and landraces of desi species are invaluable resources of innumerable genes that confer resistance to drought, water logging, insect pests and diseases (1,2). The cotton breeding programme primarily rely on crossing of a few elite lines of closely related genotypes leads to narrow genetic base in the cotton gene pool. Rapid urbanisation and extensive cultivation of Bt cotton hybrids also aggravated genetic erosion of cotton landraces. Global climate change is nowadays a regular phenomenon. Because of climate change, water logging and drought intensity are becoming severe every year. Minor insects and diseases are becoming major problems in the cropping systems. There is possibility many of these precious tree cottons and landraces would become extinct if we do not collect and conserve them. So it is necessary to explore, collect, characterise, conserve and utilize perennials and landraces of cotton.

National Bureau of Plant Genetic Resources (NBPGR), New Delhi and Central Institute for Cotton Research (CICR), Nagpur, have taken initiative to collect and conserve the perennials and landraces of cotton from different regions of India like North eastern Hill Region, Gujarat and Tamil Nadu. Morphological and molecular characterization of perennials and landraces of cotton is being carried out for the collected materials. Eighty nine cotton germplasm belonging to *G. arboreum*, *G. herbaceum* and *G. barbadense* were collected from the states of Tripura, Manipur, Mizoram, Assam, Nagaland, Meghalaya, Tamil Nadu, Gujarat and Maharashtra.

Fibre quality traits were completed particularly samples collected from Tripura. Fourteen collections consisting of *G. arboreum* – 8 (white linted), *G. arboreum* – 2 (brown linted) and *G. barbadense* perennials – 4 were made from tribal area of Gomati, Khowai & Dhalai Districts. The lint samples of the 14 collections were evaluated for fibre quality traits. The staple length ranged 17.2 – 19.1 mm (*G. arboreum)*, 32.6 mm to 34.9 mm (*G. barbadense* perennials), fibre bundle strength 15.0 g/tex to 16.7 g/tex (*G. arboreum)*, 21.6 g/tex to 24.7 g/tex (*G. barbadense* perennials). However, economic characters reveals broad variability spectrum viz; Ginning outturn % (34.5 % - 46.0%) and boll weight (1.3g to 5.0g). The diversity within the single region provides ample evidence to cultivate improved cultivars of *Gossypium arboreum* race *cernuum* in Tripura region. Molecular characterization was carried out for 31 collected cotton samples by using 19 SSR markers. Out of nineteen, five SSR markers were polymorphic. A dendrogram was constructed for 31 collected cotton germplasms using UPGMA method based on genetic similarity (Fig. 1).

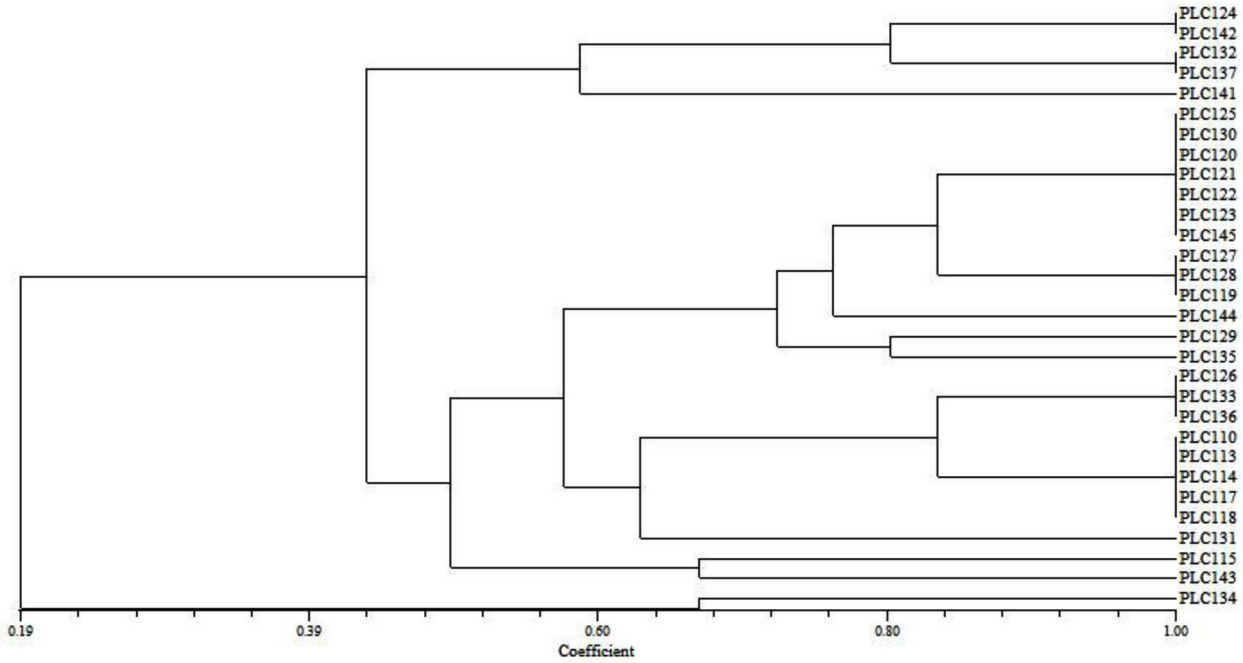


Fig. 1. Dendrogram depicting genetic diversity among cotton landraces

References

1. Punit Mohan and Pandravada S.R. 1996. Perpetual cottons of Andhra Pradesh. Indian J. Plant. Genet. Resour., 9(2): 313-317.
2. Samba Murthy J.S.V, Ranganadha N. Charyulu and Reddy K.H.G. 1994. Perennial cottons of Andhra Pradesh. Paper presented in national seminar on cotton production challenges in 21st century, 18-20 April at CCS Haryana Agricultural University, Hissar.
3. Watt S.G. 1907. The wild and cultivated cotton plants of the world. First Indian Edition (1989) P.1-885.

PS-IV-41

Agro-morphological diversity in *Canavalia* germplasm: promising food and fodder legume

Archana Singh*, S. K. Mahanta and D. Deb

Indian Grassland and Fodder Research Institute, Jhansi; e-mail: archanasingh.igfri@gmail.com

Abstract

Eighteen accessions comprised of four species of *Canavalia,* namely, *C. ensiformis, C. gladiata, C. brasiliensis* and *C. virosa* were evaluated for qualitative and quantitative traits. *C. ensiformis* gave best response for green vegetable pods with maximum number of pods per plant (20.6), pod length (23.8cm) and pod width (3.0cm), respectively. However, for grains, *C. virosa* and *C. gladiate* gave good response for number of seeds/pod (9.3) and (7.3), respectively. 10-seed weight was found maximum (19.4g) in *C. gladiate*. Whereas, *C. brasiliensis* gave maximum forage potential with highest number of branches (20.6) and leaves (385.0). Promising accessions of the species could be improved for green pods, grain and forage yielding attributes through selection and breeding methods to have an alternative protein source.

Key words: Green pods, grain, protein, tribal legume, vegetable

Canavalia is an under-exploited food and fodder legume. It is considered to be a cheap source of protein, vitamins and minerals. The young pods are extensively utilized in Asia as a green vegetable [1]. Ttribal people of ancient India used to eat this traditionally but are less popular among the general population. The mature dry beans are cooked and eaten as food. Besides, the whole plant, the pods and seeds are also used to feed animals. Sword bean (*C. gladiata*) has several other potentials as nutraceuticals and phytopharmaceuticals [2]. The protein content in *Canavalia* species ranges from 21- 31 % which is higher than in any average food legume [3]. These are now cultivated on a limited scale throughout Asia, West Indies, Africa and America. The seeds of *C. ensiformis* are considered as one of the lesser-known grain legumes that grew well on nutrient-depleted lowland tropical soils under drought conditions. It is also reported to be tolerant to water logging and salinity. Average grain yield of *C. gladiata* ranges from 720-150 Kg / ha which is comparable with the soybean yield of 600-1000 Kg / ha [3]. Owing to its economical importance and in view of scanty reports on morphological evaluation of *Canavalia* germplasm, an attempt has been taken to collect, conserve and evaluate the germplasm of *Canavalia* species for food and forage purposes in semi-arid region of the central India.

Eighteen germplasm of exotic and indigenous origin comprised of four species were grown in RBD in two replications in July 2011-2013 in *kharif* at IGFRI, Jhansi, India. Observations were recorded for growth and morphology on five randomly chosen plants for ten quantitative traits *viz*., plant height, number of branches, number of leaves, leaf length, leaf width, pod length, pod width, seed length, seed width, 100 seed weight and seed hilum length and six qualitative traits viz., stem colour, leaf colour, flower colour, pod colour, seed colour and seed shape. Among the qualitative traits, germplasm of *C. gladiata* exhibited more variation for stem colour

(green and red), leaf colour (light and dark green), flower colour (white and pink), seed colour (white, cream, light brown and light / dark pink) and seed shape (long, ovoid) (Fig.1) as compared to germplasm of other three species, namely, *C. virosa, C. brasileinsis* and *C. ensiformis* showed least variation (Table 1).

Table 1. Variation for qualitative traits in four species of *Canavalia*

Trait	*C. gladiata*	*C. virosa*	*C. ensiformis*	*C. brasiliensis*
Stem colour	White / red	Purple	Purple	Purple
Leaf colour	Green	Green/Dark green	Dark green	Dark green
Flower colour	Pink, white	Pink	Pink	Pink
Pod colour	Green	Green, Dark green	Green-purple	Green-purple
Seed colour	Pink, White, Cream-brown	Cream-brown, Black-brown	White	Brown
Seed shape	Long, ovoid, smooth	Long, ovoid	Small, ovoid	Small-medium ovoid
Grazing preference	High	Low	Medium	High

Out of four species evaluated*, C. virosa* exhibited maximum plant height (8.8 m) followed by *C. gladiata* (8.4m) however *C. ensiformis* gave lowest response (2.13m). In case of food potential (green vegetable pods and grain), *C. ensiformis* gave maximum response to pod number (20.6), pod length (23.8cm) and pod width (3.0cm) followed by *C. gladiata* (19.9cm, 18.7cm and 4.8cm). Maximum seed number per pod was observed in *C. virosa* (9.3) followed by *C. gladiata* (7.3) and *C. ensiformis* (6.3). 10-seed weight was found maximum in *C. gladiata* (19.4g) followed *by C. brasiliensis* (13.2 g) and *C. virosa* (11.4g) whereas *C. ensiformis* showed minimum seed weight (5.8 g) due to small size of seed. For forage traits, *C. brasiliensis* showed highest number of branches (20.5) followed by *C. virosa* (18.7) and *C. gladiata* (12.8). Further, maximum Number of leaves was recorded in *C. brasiliensis* (385) followed by *C. gladiata* (213) Table 2. In general, accessions within species did not show much variation for quantitative traits but accessions of *C. gladiata* showed maximum variation for qualitative traits. However at species level, *C. gladiata* gave maximum response to grain and vegetable yielding traits followed by *C. ensiformis*. Whereas, *C. brasiliensis* showed poor response for grain and vegetable yielding traits but it gave good response to forage yielding components.

Table 2. Variations for quantitative traits in germplasm of *Canavalia* species.

S.No.	Traits	*Canavalia brasiliensis*		*Canavalia gladiata*		*Canavalia ensiformis*		*Canavalia virosa*	
		Mean ± SD	Range Min-Max	Mean ± SD	Range Min-Max	Mean ± SD	Range Min-Max	Mean ± SD	Range Min-Max
1.	Plant length	5.7±0.84	5.1-6.3	8.40±3.33	4.4-12.10	2.13±0.53	1.8-2. 5	8.8±5.93	2.0-12.6
2.	No.ofBranches	20.5±29.03	9.0-41.0	12.8±5.57	80-92	7.0±1.41	6.0-8.0	18.7±4.72	15.0-24.0
3.	No. Leaves	385.0±23.33	364.0-397.0	213.2±134.61	63-393	93.0±5.65	89-97	42.0±30.51	21.0-77.0
4.	Pods/plant	19.3±1.76	18.0-20.0	19.9±9.44	11-33	20.6±29.15	23.0-41.2	-	-
5.	Pod length	13.4±0.07	13.5-13.6	18.7±1.90	16.5-20.6	23.8±0.77	23.2-24.3	19.7±3.44	15.8-22.2
6.	Pod width	2.6±0.24	2.4-2.8	4.8±0.43	4.30-5.45	3.0±0.14	2.9-3.1	4.15±0.32	3.8-4.5
7.	Seeds/pod	5.6±0.70	2.0-9.0	7.3±0.41	2-12	6.3±0.53	2.0-9.0	9.3±0.84	6.0-8.0
8.	Seed length	1.8±0	1.7-1.8	2.5±0.39	1.95-2.85	1.6±0.38	1.4-1.9	1.8±0.57	1.2-2.4
9.	Seed width	0.3±0.03	0.30-0.35	1.7±0.31	1.20-1.95	0.4±0.07	0.3-0.4	0.9±0.62	0.6-1.7
10	10 seed weight	13.2±1.27	12.3-14.1	19.42±3.99	15.7-25.2	5.8±4.03	2.9-8.6	11.4±7.06	4.6-18.7
11	Hilum length	1.3±0.07	1.3-1.4	1.9±0.60	1.3-2.8	0.7±0.14	0.6-0.8	0.9±0.52	0.5-1.5



(a) (b) (c)

Fig. 1. Variability for morphological traits in *Canavalia* species. (a) Foliage with white flower (b) Green vegetable pods (c) Variation in seed colour

Morpho-agronomic traits clearly distinguished the germplasm of *Canavalia* species [4]. The results indicated that promising germplasm of *C. gladiata* and *C. ensiformis* could be selected and improved for high pod yield to be used as vegetable whereas high seed yielding could be the good option for grains. Selection for the character and other yield component have greatly aided advances in plant breeding for yield. Similarly, few accessions of *C. brasiliensis* and *C. virosa* showed the promise for forage yielding attributes [5]. Recently NBPGR also reported that *C. gladiate* has been considered as vegetable under wild economical plants of Orissa whereas *C. virosa* was regarded as wild relative of crop plants as a source of biotic and abiotic stresses [6]. *Canavalia gladiate* is also reported to be good sources of nutraceuticals and for other agricultural uses [2].

(a) Based on the results, it may be concluded that systematic research on production potential, nutritional quality and anti-nutritional factors could be taken to popularize these species as an alternative leguminous crop to overcome the problem of malnutrition worldwide.

References

1. Purseglove J. W. 1968. *Canavalia gladiata* (Jacq.) DC. *Tropical Crops :* Dicotyledons 1, 245. London: Longmans, Green and Co Ltd, 332p.
2. Morris J. B. 1997. Special-purpose legume genetic resources conserved for agricultural, industrial, and pharmaceutical use. Econ. Bot., 51: 251-263.
3. Ekanayake S., Jansz E. R., Nair B. M. and Abeysekera A. M. 2000. Literature review of an underutilized legume: *Canavalia gladiate.* Plant Foods Human Nutr., 55: 305-312.
4. Vadivel V. and Janardhnan K. 2005. Nutritional and Antinutritional Characteristics of Seven South Indian Wild Legumes. Plant Foods Human Nutri., 60: 1-7.
5. Singh Archana and Roy A. K. 2013.Variability for forage potential yielding traits in exotic grasspea (*Lathyrus sativus* L.). Forage Res., 38(4): 230-233.
6. Rani D. R., Mishra R. C., Bhandari D. C., Pandey A., Dixit N. and Sharma S. K. 2010. Wild Economical Plants, *In*: Plant Genetic Resources of Orrissa: Accomplishments and Future strategies, NBPGR Publication, New Delhi, p.22-23.

PS-IV-42

Variability and performance of maize accessions collected from North-East Himalayan region at Delhi location

Jyoti Kumari*, Ashok Kumar, K. C. Bhat and T. P. Singh

National Bureau of Plant Genetic Resources, New Delhi 110 012; e-mail: jj.gene@gmail.com

Abstract

This study pertains to evaluation of maize accessions collected from Manipur and Nagaland states of North-East Himalayan region at Delhi location. The maize landraces collected were known by various local names such as Seko, Metata, Mikreta, Mendi, Tesu, Tsungro, Kholithi, Ongpok and used by local tribes in various forms. The collection from Nagaland, KC/S/I-67 was early maturing, medium statured with deep brown grains and multicob nature. There were ample variability for kernel colours in this set of collection, as we found white, yellow, Purple, orange, red, gray, light brown, mottled and black coloured grain. Based on coefficient of variance, accessions of Nagaland were more diverse for characters such as plant height (21.13%), ear height (31.43%), number of ears per plant (34.70%), ear length (22.61%), ear width (18.87%), number of kernels per row (25.47%) and yield per plant (56.05%). The yield per plant varied from 23.78 to 128.62 g in Manipur accessions while it was 24.56 to 104.49g in Nagaland collections. We could found collections performing better than best check for each agronomic character for example the collection KC/S/I-72 from Okha had maximum ear length (24.40 cm) whereas DS/NP/RS-25 Churchandpur had maximum ear width (4.20 cm). Thus, the study clearly demonstrated that despite environment-specific adaptations, many of the accessions are capable of showing high adaptability across agro-ecologies.

Key words: Maize, NEH region, landarces, descriptor

Genetic erosion and ecological destruction by modern agriculture has increased the importance of germplasm collection and characterization, as genetic variability is essential for present and future plant breeding programmes. Maize (*Zea mays* L.) is grown under diverse environmental conditions ranging from the tropical to the temperate regions [1-3]. Owing to tremendous diversity in the Indian Himalayan regions, Anderson [4] considered maize to have an Asiatic origin while Dhawan [5] defined several landraces from NE Himalayan regions as Sikkim primitives, which have primitive character of popcorns and high prolificacy. The primitive group comprised of several races of popcorn, which had differentiated at various altitudes and under diverse conditions, was distributed throughout the eastern Himalayan region. This group included Poorvi Botapa, Murli sub-race of Poorvi Botapa, Tirap Nag-Sahypung, Arun Tepi and Alok Sapa. Extensive surveys were made to collect the indigenous diversity of maize from NEH region following proper sampling procedure. A total of 75 maize accessions were collected from Nagaland (58 acc.) and Manipur (17 acc.) states of North Eastern region during year 2011. The maize accessions from Nagaland were collected from different villages of Phek, Longleng, Mokokchung, Zunheboto, Tuensang, Okha and kohima districts and from Manipur the collections were made from Thoubal, Churchandpur, Senapati, Chandel and East Imphal districts (Fig 1). The altitude of collection varied from 696 m above sea level (Lanye, Phek, Nagaland) to 2077 m above sea level (Reku, Phek, Nagaland).The local name of maize landraces were Seko, Metata, Mikreta, Mendi, Tesu, Tsungro, Kholithi, Ongpok and these were used by local tribes in various forms. The collected accessions were very diverse in grain colour, ear shape, ear length and grain type. The young cobs of collection KC/S/I-22 were used as vegetable types; KC/S/I-19 and KC/S/I-35 as popcorn. These accessions were evaluated in Delhi condition at NBPGR Farm, New area of IARI during *Kharif* 2012. Apart from the data related to agro-morphological descriptors, the various yield contributing traits like grain yield, 100-kernel weight, ear length, ear diameter, number of kernel-rows per ear and number of kernels per ear were also recorded. Out of them, five accessions KC/S/I-30 and KC/S/I-32 (Mokokchung), KC/S/I-36 (Zunheboto), KC/S/I-58 and KC/S/I-73 (Okha) did not come into flower under Delhi condition. The average value of days to tasseling for accessions of Nagaland was 56.45 with range of 39 to 68 days whereas it was 54.76 for accessions collected

from Manipur with range of 46 to 60 days. Days to silk ranged from 52 to 69 days (mean value, 60.71) in accessions belonging to Manipur while it was 46 to 74 days in accessions of Nagaland. Based on coefficient of variance, it was observed that accessions of Nagaland were more diverse for characters as plant height (21.13%), ear height (31.43%), number of ears per plant (34.70%), ear length (22.61%), ear width (18.87%), number of kernels per row (25.47%) and yield per plant (56.05%). Only for 100 grain weight accessions from Manipur were more diverse with 30.91% CV, but mean value of grain weight was more in Nagaland as collection KC/S/R-9 had 100 grain weight of 30.60 g. We could also find multicob accessions KC/S/R-10 with mean ears per plant (1.6), KC/S/I-21 (3.2) and KC/S/I-28 (3.6). The collection KC/S/R-3 had maximum plant height of 278 cm with ear height of 202 cm.

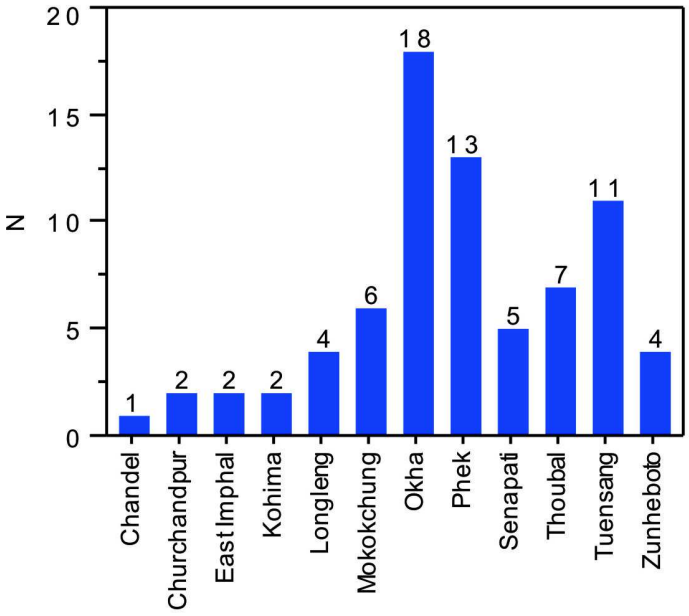


Fig. 1. Bar diagram showing number of accessions collected from different districts of NEH region

Table 1. Descriptive statistics of maize accessions collected from Nagaland and Manipur

	DT	DS	NTB	PH	EH	NEP	DM	EL	EW	KR	GW	NKR	YP
Nagaland													
Mean	56.45	63.08	19.82	195.57	121.55	1.34	110.77	14.05	2.87	10.88	19.08	19.09	45.75
Standard Error	0.59	0.62	0.39	5.43	5.02	0.06	0.80	0.44	0.08	0.19	0.64	0.68	3.37
Kurtosis	5.34	3.74	1.47	0.30	0.17	14.69	4.21	1.30	0.05	-0.69	0.23	-0.53	-0.23
Skewness	-0.67	-0.66	0.40	-0.21	-0.13	3.56	-0.40	0.50	-0.53	-0.45	0.05	0.41	-0.02
Minimum	39.00	46.00	11.20	79.20	9.30	1.00	89.00	6.20	1.30	8.00	8.30	9.60	24.56
Maximum	68.00	74.00	28.30	278.90	202.20	3.60	127.00	24.40	3.90	13.20	30.60	29.60	104.49
CV	7.62	7.15	15.00	21.13	31.43	34.70	5.22	22.61	18.87	12.80	24.17	25.47	56.05
Manipur													
Mean	54.76	60.71	17.16	181.77	104.40	1.44	101.47	13.63	3.31	11.88	15.97	22.40	63.06
Standard Error	0.96	1.14	0.68	6.51	5.50	0.05	1.64	0.61	0.10	0.28	1.20	1.30	7.57
Kurtosis	0.10	-0.44	0.09	-0.27	3.03	2.03	-0.84	0.74	0.09	0.67	0.63	1.52	0.16
Skewness	-0.75	-0.44	-0.74	0.81	1.48	1.32	0.28	0.50	0.53	-1.13	1.12	1.16	0.92
Minimum	46.00	52.00	11.20	151.10	79.20	1.20	92.00	9.10	2.60	9.20	10.30	16.00	23.78
Maximum	60.00	69.00	21.20	238.20	169.10	2.00	114.00	19.40	4.20	13.20	27.20	36.40	128.62
CV	7.20	7.77	16.36	14.76	21.73	14.97	6.68	18.33	12.45	9.80	30.91	23.87	49.50
C1-Vivek-17	40.00	44.00	15.50	143.65	64.10	1.10	91.00	15.15	3.55	11.80	22.95	19.00	56.11
C2-HM-4	47.00	50.50	17.80	148.20	77.70	1.30	94.00	15.75	3.65	12.40	23.65	28.60	109.23
C3-HQPM-1	54.00	60.33	18.33	164.20	79.23	1.33	93.33	15.20	3.50	11.60	24.17	24.53	97.93

The collection from Nagaland, KC/S/I-67 was early maturing, medium statured with multicob nature. Most of the traits had left skewed distribution except number of tassel branches, number of ears per plant, ear length,

grain weight and number of kernel rows in the Nagaland collection. Whereas in Manipur accessions days to tassel, days to silk, number of tassel branches and kernel rows are left skewed which meant most of the values are concentrated in right side of the mean in these traits. There were variability for kernel colours in this collection, as we found white, yellow, Purple, orange, red, gray, light brown, mottled and black. The yield per plant varied from 23.78 to 128.62 g in Manipur accessions while it was 24.56 to 104.49g in Nagaland collections. We could found collections performing better than best check for each agronomic character for example the collection KC/S/I-72 from Okha had maximum ear length (24.40 cm) whereas DS/NP/RS-25 Churchandpur had maximum ear width (4.20 cm). Singode et al., 2009 also identified promising accessions from NEH region for yield related traits at Delhi and/or Hyderabad location. Thus, the study clearly demonstrated that despite environment-specific adaptations, many of the accessions are capable of showing high adaptability across agro-ecologies.

References

1. Singh B. 1977. Races of Maize in India. Indian Council of Agricultural Research (ICAR), New Delhi.
2. Prasanna B.M. and Sharma L. 2005. The landraces of maize (*Zea mays* L.) diversity and utility. Indian J. Plnat. Genet. Resour., 18: 155-168.
3. Prassana B.M. 2010. Phenotypic and molecular diversity of maize landraces: Characterization and utilization. Indian J. Genet., 70: 315-327.
4. Anderson E. 1941 Antithetical Dominance in North American Maize. Proceed. Nat. Acad. Sci,. 27(9): 436-440.
5. Dhawan N.L. 1964. Primitive maize in Sikkim. Maize Genet. Coop. Newslett., 38: 69-70.

PS-IV-43

Exploring the plant genetic resources potential of Lakshadweep Islands

K. Joseph John, R. Asokan Nair, A. Suma, M. Unnikrishnan[1] and V. Arunachalam[2]

National Bureau of Plant Genetic Resources, Regional Station, KAU P.O., Thrissur 680 656, Kerala, [1]Central Tuber Crops Research Institute, Sreekaryam P.O., Thiruvananthapuram 695 017, Kerala, [2]ICAR Research Complex for Goa, Ela, Old Goa, Goa 403 402; e-mail: nbpgrtsr@gmail.com

Abstract

The Union Territory of Lakshadweep was explored for plant genetic resources assessment. Variability in Noni (*Morinda citrifolia*), Fiji Arrowroot (*Tacca leontopetaloides*), Indian laurel (*Calophyllum inophyllum*), Betel leaf (*Piper betle*), Indigo (*Indigofera tinctoria*), Brahmi (*Bacopa monnieri*), Bread fruit (*Artocarpus communis*) and Giant taro (*Alocasia macrorrhiza*) was found. Unique economic plants like *Colubrina asiatica* (shampoo), *Cordia bicordata* (timber) and *Macaranga roxburghii* (multi-purpose) were collected. Minicoy Island is righ in Noni variabilitya nd local betel leaf plants are highly pungent. *Vigna marina*, *Cajanus scarabaeoides*, *Canavalia cathartica*, *Corchorus trilocularis* and *Cucumis melo* var. *agrestis* were the wild relatives of crop plants collected from the islands. Genetic erosion status and ITK on local flora are also dealt with.

Key words: Plant genetic resources, Lakshadweep, flora, Minicor, wild relatives, distribution record

The Union Territory of Lakshadweep consists of 10 inhabited Islands and 17 uninhabited Islets with a total land area of 28.5 Sq. Km. lying between 8° and 12°N Latitudes and 71° and 74°E Latitudes. Soils of these coral formulations are calcareous and the height of the land above sea level is about 1-2 meters. Average annual rainfall is about 1,640mm which is the only source of fresh water and the water table is about 2-3m deep. Climate is humid tropical [1, 2].

Soils are poor in humus and nitrogen deficient. The agriculture of the islands has a recent history dating back to only a few hundred years, when the first inhabitants from Kerala arrived. There is a high preponderance of Australian-Polynesian elements in the flora of the region and as such is interesting for economic exploitation. Lakshaweep flora consists of about 150 species out of which 134 occur in Minicoy itself. Total wild and feral plant wealth is 114 species, of which 85 species occur in Minicoy [3]. The Territory was under Portuguese rule for a short stint. The state is declared fully organic permitting no agro-chemicals except rodenticides. Fragmentation of land holdings and density of population is one of the highest with less than a handful of people having more than 1.0 ha size holding. There is no government land or forest, the entire territory is private deed land. There are no honey bees and there is a heavy infestation of burrowing nematodes. Rice and fish are the staple food items and vegetables are not normal dietary items [4].

In order to assess the plant genetic resources collection potential of these islands, two exploration trips, the first in January 2009 and the second in March 2010 were undertaken. A total of 106 germplasm samples were collected. The inhabited islands of Agathy, Amini, Androth, Kadamath, Kalpeni, Kavaratty and Minicoy, and uninhabited Cherium, Suheli and Viringili islets were extensively surveyed. This paper pertains to the findings of the first field study on scope of plant genetic resources collection (other than coconut) from Lakshadweep islands. Coconut based homestead agro-ecosystems consisting of a few vegetables, tropical tubers and banana predominate. Variability in cultivated crops is scanty except in coconut, where high variability occurs [5]. However, medicinal and aromatic plants and a few wild relatives of crop plants occur in home gardens and as part of littoral vegetation. Minicoy is floristically rich compared to other islands.

All the islands, Minicoy in particular, have tremendous variability for fruit and tree characters in Noni (*Morinda citrifolia*). Noni has one of the highest fruit variability and population densities in Minicoy Island. Other indigenous/ naturalized economic plants showing high population are Fiji Arrowroot (*Tacca leontopetaloides*), Indian laurel (*Calophyllum inophyllum*), Brahmi (*Bacopa monnieri*), Glory lily (*Gloriosa superba*), Betel leaf (*Piper betle*), Indigo (*Indigofera tinctoria*), Giant taro (*Alocasia macrorrhiza*) and Bread fruit (*Artocarpus communis*). Prolific bearing plants of *Cajanus scarabaeoides*, bitter less *Cucumis melo* var.*agrestis*, saline tolerant *Canavalia cathartica*, *Vigna marina* and *Corchorus trilocularis* were the unique wild relatives collected. *Launea sarmentosa* is a wild gathered leafy vegetable cum salad plant of the saline sandy coast. 'Bagga' (*Colubrina asiatica*) is a promising economic plant reared in home gardens for its leaves used as shampoo and also to polish brassware. It may be tested for its efficacy as a safe botanical for cleansing vegetables and fruits from pesticide residues.

Unique PGR includes highly pungent betel leaf cultivated in homesteads for chewing, as mainland supply of betel leaf during rough monsoon season is not dependable. Breadfruit is another potential food cum vegetable of all the Islands which has one of the highest population compared to mainland [4]. Jackfruit and other *Artocarpus* species common in mainland and Andaman & Nicobar Islands are conspicuously not adapted to these Islands. The 'dweep teak', *Cordia bicordata*, is a unique timber adapted to cultivation in coastal shores. *Cordia bicordata* needs to be studied for its utilization as cultivable timber source in the whole of Lakshadweep, besides west and east cost of India. Unlike *Casuarina*, it can be reaped to pieces and worked out for various wood works. Presently, the Islanders depend on imported wood for all their timber needs, with indigenous coconut trees to a certain extent. Figi Arrow root is another potential food plant for high value arrowroot. The harvested tubers from senescent plants are crushed and washed in 7 changes of water before drying to a fine starch powder. Acclaimed with many health benefits and highly adapted to cultivation as intercrop in coconut plantations, it is one of the worth candidate species for improvement and cultivation. Contrary to the use of kernel as edible material in Indian almond, mesocarp is a delicacy fruit item in all the Islands. Goat fodder is in high demand for which cultivated trees and fallen litter form the main sources. Genetic erosion of crops like rice, ragi and taro are 100% complete. *Macaranga roxburghii,* locally called *Patti*, is cultivated in homesteads for its leaves used for cooking (wrapping) *pathiri* (rice roti). Its wood is used for making decorated coconut scraper stand, leaf as fodder and fruits as fishing net float and adhesive for cordage fibre. The Chinese water chest nut (*Eleocharis dulcis*) which emerge with the first rain is a delicacy food item in almost all Islands [6].

The import of horticultural plant materials with soil may be restricted for fear of quarantine issues. Instead, the Agriculture Department may establish scion banks and train local population in nursery techniques. The existing *Casuarina* belt in the coast may be enriched with multiple species like *Thespesia populnea* and *Cordia bicordata* as the islanders require construction wood for housing. Concrete construction in addition to high level of corrosion of iron and exorbitant cost of imported sand, cement and stone impart heavy load on the fragile island strata. The spread of alien invasive weeds like *Mikania micrantha* and *Lantana camara* needs to be checked and the only small patch of marshland existing in Kalpeni needs to be protected for ecological reasons and drinking water security. There is a need to conserve local tree resources like breadfruit, *Macaranga, Cordia*, etc. at one place. ITK (Indigenous Traditional Knowledge) on plants used as vegetable, fruit, fodder, medicinal plant, fuel, water purifier, soil binder, timber and cottage industry were also recorded. Spotting and collection of *Vigna marina*, *Cajanus scarabaeoides* and *Lea sambusina* are new distribution records for the Islands.

References

1. Vadivelu S., Muraleedharan A. and Bandyopadhyay A. K. 1993. Soils of Lakshadweep Islands. CARI Research Bulletin No.9, CARI, Port Blair.
2. Jones S. 1986. Lakshadweep - General features and some considerations. *In*: Marine Fisheries Information Services, Technical & Extension Series., No. 68.Central Marine Fisheries Research Institute, Cochin, India: 3-6.
3. Willis J.C. and Stanley Gardner J. 1901. The Botany of the Maldives Islands. Annals of Royal Botanical Gardens, Peredeniya, Sri Lanka. 1:1-120.
4. Mannandiar N.S. 1971. Gazetteer of India – Union Territory of Lakshadweep. Administration of the UTL, GOI i-375, pp. 119-130.
5. Samsudeen K., Jacob P. M., Niral V., Kumaran P. M., Radha Salooja and Moosa H. 2006. Exploration and collection of Coconut Germplasm in Kadmat and Amini Islands of Lakshadweep, India. Genet. Resou. Crop Evol., 53(8): 1721-1728.
6. Mukundan T.K. 1979. Lakshadweep: A hundred thousand Islands. Academic Press. pp. 100-103.

PS-IV-44

In vitro genebank : management of genetic resources of tuber crops at National Bureau of Plant Genetic Resources, India

N. Sharma[*], Z. Hussain[1], R. Chamola, D. K. Nerwal and R. K. Tyagi

CAR-National Bureau of Plant Genetic Resources (NBPGR), Pusa Campus, New Delhi 110012, Division of Vegetable Crop Science, Indian Institute of Agricultural Research, Pusa Campus, New Delhi 110 012; e-mail: neelam@nbpgr.ernet.in

Abstract

A total of 620 accessions of five tuber crops (mainly sweet potato, yams and taro), representing diversity collected from various ecogeographic regions, have been conserved in the *in vitro* genebank at National Bureau of Plant Genetic Resources, India. Regarding genetic stability, *in vitro* conserved germplasm of these crops have been tested for genetic stability and these were found to be true to type.

Key words: Cryopreservation, genetic stability *in vitro* genebank, tuber crops

Conservation of tuber crops in their original habitat has not received much attention. On-farm conservation in tuber crops exists in India among tribals and marginal farmers because of their preference for specific local cultivars and also non-access/exposure to new technologies. *Ex situ* conservation of these crops require special

attention as these are asexually propagated and storage of vegetative propagules is extremely difficult. Field genebanks have its own limitation as it requires maintenance by repeated planting. Besides being labour intensive, it is constrained by chances of loss of accessions due to natural vagaries (climate change may further aggravate this loss) and mixing of germplasm.

Thus, for conservation of vegetatively propagated species of tuber crops use of biotechnological approaches was considered a valuable adjunct to field genebanks. *In vitro* conservation is recognized as a viable option for medium-term conservation, while cryopreservation is the only long-term option [1]. The *In Vitro* Genebank at NBPGR initiated conservation of tuber crops in 1988 and at present maintains a total of 620 accessions of tuber crops (mainly sweet potato, yams and taro) as shoot cultures. This paper highlights various issues related to management of *in vitro* conservation of germplasm of tuber crops including the strategies adopted, success achieved, technical limitations and future thrust to ensure sustainable utilization.

Germplasm of tuber crops, from various ecogeographic regions through explorations and maintained *ex situ* in the field genebanks/net house or exotic collections served as the source of explants. Depending on the species various explants (viz. shoot tips, buds, nodal cuttings) were used to initiate aseptic cultures. The explants were washed thoroughly to remove soil, surface sterilized with 0.1 or 0.2% solution of mercuric chloride and washed five times with sterile distilled water. The explants were vertically implanted onto the nutrient medium (MS+growth regulators) [2] selected for each species. The regenerated shoots were subcultured after 4-8 weeks. At each subculture the individual shoots were cut into 1.0 cm segments and transferred to multiplication medium. Single explants were transferred to glass tubes (25x150mm) containing 15 ml of culture semi-solid medium. Survival of cultures was periodically assessed by visual examination and by the ability of explant to resume growth on fresh medium. For multiplication and maintenance cultures were maintained at 25 ± 2°C and 16 h photoperiod. For long term conservation, shoot tips of yams were cryopreserved using encapsulation-dehydration and vitrification technique [3].

Rapid clonal multiplication is an important prerequisite and integral activity for *in vitro* conservation. Standardization of a single medium each effective for *in vitro* propagation of large array of accessions in sweet potato and yams has been a significant achievement [1]. A single medium applicable for propagation of taro, tannia and giant taro was standardised (see Table 1). Thus standardised methods of *in vitro* multiplication have been applied to establish a large number of accessions in each species.

Various slow growth strategies such as low temperature incubation, use of osmotic agents, growth retardant, nutritional or hormonal manipulations etc. were evaluated for different tuber crops [1]. Mannitol at low levels prolonged the subculture intervals to 12 to 16 months at 25°C in sweet potato. Although genotypic variation in response to mannitol did exist, 1-2% mannitol was suitable for >150 accessions [1]. Most of the *Dioscorea* species were relatively slow in growth under *in vitro* conditions. Germplasm of various *Dioscorea* spp. could be maintained on MS+0.15mg/l NAA at 25 ± 2°C for 10-12 months without subculture. Induction of *in vitro* tubers increased the shelf life of cultures for additional 4-6 months in *D. alata*, *D. bulbifera* and *D. pentaphylla*. In taro induction of *in vitro* corm on MS+6% sucrose was beneficial in extending conservation period from six to 15 months. This method has been applied for >100 accessions [4].

Table 1. Status of *in vitro* conservation of tuber crops in the *in vitro* genebank at NBPGR

Plant	Common name	No. of acc.	Maintenance medium
Alocasia indica	Giant taro	4	MS + 0.5 mg/l BAP + 0.1 mg/l NAA
Colocasia esculenta	Taro	195	MS + 0.5 mg/l BAP + 0.1 mg/l NAA
Dioscorea spp.	Yams	152	MS + 0.15mg/l NAA or MS + 0.05 mg/l BAP + 0.1 mg/l NAA
Ipomoea batatas	Sweet potato	259	MS + 0.2mg/l Kn + 0.1mg/l IAA + 4% sucrose
Xanthosoma sagitifolia	Cocoyam	10	MS + 0.5 mg/l BAP + 0.1 mg/l NAA

A total of 620 accessions (~9500cultures) of tuber crops (sweet potato, yams and taro) have been maintained in the *in vitro* genebank at NBPGR at 25^0C with a subculture interval of 8-12 months (Table 1) [5]. Though, reduced temperature incubation (18^0C) was effective in increasing the shelf-life of cultures but conservation at culture room temperature (25^0C) was found to be more economical.

Cryopreservation is potentially the most appropriate strategy for long term conservation of *in vitro* cultures. Although limited success has been reported in the past with some subtropical and temperate plant species, this technique is now considered suitable for general application. Application of cryopreservation for the long-term conservation of germplasm has not been very satisfactory in sweet potato. However in yams, successful cryopreservation has been achieved in seven species including *D. alata, D. bulbifera, D. deltoidea* and *D. floribunda* using encapsulation-dehydration and/or vitrification technique with high rate of recovery. [3, 6]. Regarding genetic stability, using morphological, isozyme and molecular markers, after conservation, no significant differences were observed in selected accessions [4, 7].

The feasibility of conserving germplasm of tuber crops using *in vitro* techniques has been successfully demonstrated. Appropriate protocols for *in vitro* multiplication and medium-term conservation of large number collections of tuber crop species enabled their practical use for the conservation of indigenous as well as exotic germplasm diversity. Significant success achieved in cryopreservation of shoot tips in yams has led to initiation of cryobanking of germplasm. Role of *in vitro* conservation becomes very crucial to mitigate the risk of environmental instability particularly on climatically vulnerable vegetatively propagated crops. In this context, *in vitro* conserved collections with traits such as drought tolerance, salt tolerance, early/late maturity etc. will be very useful in future.

References

1. Mandal B. B., Tyagi R. K., Pandey R., Sharma N. and Agrawal A. 2000. *In vitro* Conservation of Germplasm of Agri-horticutural Crops at NBPGR : An Overview. *In*: Razdan M.K. and Cocking E.C. (eds) Conservation of Plant Genetic Resources In vitro, Vol.2, Oxford & IBH Publishing Co. Pvt. Ltd., New Delhi, pp 279-307.
2. Murashige T. and Skoog F. 1962. A revised medium for rapid growth and bioassays with tobacco tissue culture. Physiol. Plant., 15: 473-497.
3. Mandal B. B. 2003. Cryopreservation techniques for plant germplasm. *In*: Mandal B. B., Chaudhury R., Engelmann F., Bhag Mal, Tao K. L. and Dhillon B. S. (eds) Conservation Biotechnology of Plant Germplasm. Proceedings of Regional Training Course on *In vitro* Conservation and Cryopreservation, National Bureau of Plant Genetic Resources, New Delhi, India, pp 187-208.
4. Hussain Z. and Tyagi R. K. 2006. *In vitro* corm induction and genetic stability of regenerated plants in taro [*Colocasia esculenta* (L.) Schott]. Indian J. Biotechnol*.,* 5: 535-542.
5. Sharma N., Hussain Z. and Mandal B. B. 2009. Management of genetic resources of tuber crops in the *in vitro* genebank at NBPGR as an aid to meet the challenge of climate change. *In*: Abstr., National Symposium on Recent Global Developments in the Management of Plant Genetic Resources, 17-18 December, 2009, NBPGR, New Delhi, , 303.
6. Mandal B. B. and Dixit S. 2000. Cryopreservation of shoot-tips of *Dioscorea deltoidea* Wall - an endangered medicinal yam, for long-term conservation*.* International Plant Genetic Resources Institute Newsl. for Asia, the Pacific and Oceania 33:23.
7. Ahuja S., Mandal B. B., Dixit S. and Srivastava P. S. 2002. Molecular, phenotypic and biosynthetic stability in *Dioscorea floribunda* plants derived from cryopreserved shoot tips. Pl. Sci., 163: 971-977.

PS-IV-45

Evaluation of rice germplasm for multiple disease resistance under artificial inoculation conditions

Jagjeet Singh Lore, Jyoti Jain and G. S. Mangat

Department of Plant Breeding and Genetics, Punjab Agricultural University, Ludhiana (Pb.) 141 001; e-mail**:** jagjeetsingh-pbg@pau.edu

Abstract

A total of 1,018 rice germplasm lines received from Directorate of Rice Research, Hyderabad were evaluated against highly virulent pathotypes *viz*. PbXo-7 and PbXo-10 (Tar-950) of the BB pathogen, sheath blight and brown spot under artificial inoculation conditions during the year 2012-13. Out of 1,018 germplasm lines tested, 46 lines showed resistant reaction to pathotype PbXo-7 and 30 lines showed resistance to newly emerged pathotype PbXo-10. These sources of resistance after determining their genetics can be exploited in disease resistance breeding programmes for the development of resistant commercial cultivars.

Key words: Rice, disease, resistance, bacterial blight

Rice crop is affected by various diseases, out of which Bacterial Blight (BB) caused by *Xanthomonas oryzae* pv. o*ryzae*, sheath blight caused by *Rhizoctonia solani* and brown spot caused by *Drechslera oryzae* are of major concern. Bacterial bligh can cause losses up to 50% depending on stage, weather, location and varieties [1]. On the other hand it has been reported that sheath blight and brown sopt account for highest yield loss across all the production situations in South and Southeast Asia [2]. Although, rice resistance breeding has made large achievements in managing BB disease, but, due to emergence of new races of the pathogen, breeding of resistant cultivars always confronts difficulties in terms of durability of resistance. To date, no complete resistance against sheath blight [3] and brown spot has been reported. So in view of this, rice germplasm/landraces were evaluated for multiple disease resistance under artificial inoculation conditions.

A total of 1,018 rice germplasm lines received from Directorate of Rice Research, Hyderabad were evaluated against highly virulent pathotypes *viz*. PbXo-7 and PbXo-10 (Tar-950) of the BB pathogen, sheath blight and brown spot under artificial inoculation conditions during the year 2012-13. The cultivar TN1 was used as susceptible check for BB and PR116 was used as susceptible check for sheath blight and brown spot diseases. The selected resistant entries were re-evaluated during the year 2013-14. Seventy two hour old single colony virulent culture of the two pathotypes was used for artificial inoculations using clip-inoculation technique with bacterial suspension of approximately 10^{-9} cells/ ml. For sheath blight, the pathogen was mass multiplied on *Typha* bits. Ten-days-old growth of *R. solani* was inoculated on plants by placing 3-4 *Typha* bits per hill in the whorl of each test genotype**.** For brown spot the pathogen was mass multiplied in 250 ml conical flasks containing 100 ml potato dextrose broth. Conidial concentration was adjusted to $1x10^6$ conidia per ml with the help of a haemocytometer and sprayed on the plants with hand sprayer at the booting stage. The disease data were recorded 15 days after inoculation based on 0-9 scale of Standard Evaluation System (SES) for rice. Plants were characterized as resistant (R) where score ranged from 0-3, moderately resistant (MR) for score of 5 and susceptible (S) for score of 7-9.

Out of 1,018 germplasm lines tested, 46 lines showed resistant reaction to pathotype PbXo-7 and 30 lines showed resistance to newly emerged pathotype PbXo-10. Twenty two lines viz. IC Nos. 450499, 461818, 450574, 544851, 449553, 449621, 449706, 449598, 449607, 449782, 449756, 544893, 449829, 449798, 145446, 449935, 450036, 381978, 114180, 252166, 330813, 320824 showed resistant reaction to both the pathotypes (Table 1),

however, 14 lines i.e. IC Nos. 450130, 449555, 449575, 449673, 449679, 450100, 449984, 450010, 347244, 400034, 413639, 334173, 460015 including IR 64 showed resistance to PbXo-7 but susceptible to PbXo-10. On the other hand four lines 17065, 450481, 450597, 450544 showed resistant reaction to PbXo-10 but susceptible to PbXo-7. Germplasm line IC No.346207 showed resistant reaction and two lines IC Nos. 114315 and 320826 showed MR reaction to brown spot (Table 1). Though some of the lines showed R/MR reactions to sheath blight during the first year (2012-13) testing, but none of the entries showed R/MR reactions to sheath blight during second year (2013-14) (Fig. 1).

Ten pathotypes of the *X. oryzae* pv. *oryzae* have been reported in Punjab state of India [4]. The pathotype PbXo-7 is predominant with frequency distribution of 40.1% in Punjab and virulent to known *Xa* genes namely *Xa 1, Xa 3, Xa 4, xa 5, Xa 7, xa 8, Xa 10 and Xa 11* and cultivars PR 114, PR 116 and PR 118 growing in Northern regions of India [5]. In the present study out of 1018 germplasm lines evaluated, 4.5% (46 lines) showed resistant reaction to the PbXo-7 (Fig. 1), however, among these 46 lines, 14 including IR 64 showed susceptible reaction to the emerging pathotype PbXo-10. In the present study, only 2.9% (30 lines) lines showed resistance to the pathotype PbXo-10 (Fig.1). The pathotype PbXo-10 is highly virulent to all the above said BB resistance genes as well as to newly designated gene *Xa 38* from *Oryza nivara* [6]. None of the germplasm line showed resistance to sheath blight. Similarly, large scale screening of the national rice elite material and germplasm has been done in the past against sheath blight and so far none of the material has been found to possess clear cut resistance [3]. Very few germplasm lines showed R/MR reaction to brown spot in this study.

References

1. Mew T.W., Alvamz A.M., Leach J.E. and Swings J. 1993. Focus on bacterial blight of rice. Plant Dis., 77: 5-12.
2. Savary S., Willocquet L., Elazegui F. A.,

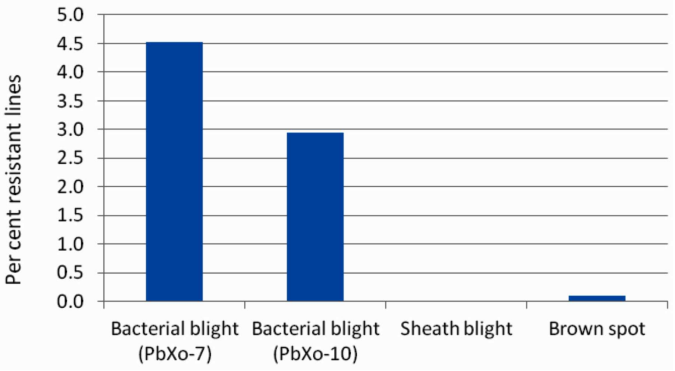


Fig. 1. Resistant germplasm lines entries against two pathotypes of *Xanthomonas oryzae* pv. *oryzae* (bacterial blight), sheath blight and brown spot

Table 1. Some rice germplasm promising lines showed disease score to pathotypes of *Xanthomonas oryzae* pv. *oryzae* (bacterial blight), sheath blight and brown spot

IC No.	Bacterial blight (Pathotypes)		Sheath blight	Brown spot
	PbXo-7	PbXo-10		
450499	3	3	**7**	**7**
461818	3	3	**7**	**7**
450574	3	3	**7**	**7**
544851	3	3	**7**	**7**
449553	3	3	**7**	**7**
449621	3	3	**7**	**7**
449706	3	3	**7**	**7**
449598	3	3	**7**	**7**
449607	3	3	**7**	**7**
449782	3	3	**7**	**7**
449756	3	3	**7**	**7**
544893	3	3	**7**	**7**
449829	3	3	**7**	**7**
449798	3	3	**7**	**7**
145446	3	3	**7**	**7**
449935	3	3	**7**	**7**
450036	3	3	**7**	**7**
381978	3	3	**7**	**7**
114180	3	3	**7**	**7**
252166	3	3	**7**	**7**
330813	3	3	**7**	**7**
320824	3	3	**7**	**7**
450123	**7**	7	**7**	5
449906	**7**	5	**7**	5
346207	**7**	**7**	**7**	3
IR64 (Check)	3	7	**7**	7
TN-1	9	9	**7**	7
PR116	9	9	9	9

Castilla N. and Teng P.S. 2000. Rice pest constraints in tropical Asia: quantification of yield losses due to rice pest in a range of production situations. Plant Dis., 84: 341-356.

3. Srinivasachary, Willocquet L. and Savary S. 2011. Resistance to rice sheath blight (*Rhizoctonia solani* Kuhn) [(Telemorph : *Thanatophorus cucumeris* (A.B. Frank) Donk.] disease: current status and perspectives. Euphytica 178: 1-22.
4. Lore J.S., Hunjan M.S., Singh P.P. and Mangat G.S. 2013. Distribution of *Xanthomonas oryzae* pv. *oryzae* strains virulent to rice cultivars/ lines containing bacterial blight resistance single gene and gene combinations in Punjab state of India. 4th International Conference on Bacterial Blight of Rice, Hyderabad, India, Pp 41 (Abstract).
5. Lore J.S., Vikal Y., Hunjan M.S., Goel R.S., Bharaj T.S. and Raina G. L. 2011. Genotypic and pathotypic diversity of *Xanthomonas oryzae* pv. *oryzae*, the cause of bacterial blight of rice in Punjab state of India. J. of Phytopathol. 159: 479-487.
6. Cheema K.K., Grewal N.K., Vikal Y., Das A., Sharma R., Lore J.S., Bhatia D., Mahajan R., Gupta V. and Singh K. 2008. A novel bacterial blight resistance gene from *Oryza nivara* mapped to 38 Kbp region on chromosome 4L and transferred to *O. sativa* L. Genet. Res., 90: 397-407.

PS-IV-46

Genetic variability in sucking type of mango genotypes

Mandeep S. Gill* and Nav Prem Singh[1]

Punjab Agricultural University Fruit Research Station Gangian 144 205, [1]Department of Fruit Science, Punjab Agricultural University, Ludhiana 141 004, PAU Regional Research Station, Bathinda 151 001; e-mail: mandeepgill21@pau.edu

Abstract

Genetic variability present among the sucking mango genotypes may be further studied and utilized for future crop improvement programme. Mango is cultivated in tropical and sub tropical regions of the world and ranks 3rd both in term of area and production after citrus and guava fruit crops in the Punjab state. It is highly heterozygous in nature and exhibits a wide variability among wild seedlings strains/genotypes and grafted mangoes varieties growing in diverse regions of the country in term of vegetative, floral and physico-chemical characters. Mango was cultivated on large scale plantation as wild, isolated, scattered and solid plantation in Hoshiarpur, Gurdaspur and Ropar Districts of Punjab but relegated due to popularization of kinnow, guava and amla in both *Kandi* and sub mountane zone of Punjab. It is opined that many mono embryonic mango seedlings growing on roadsides, riverbanks, isolated places and government lands are being uprooted for the last few decades by mankind to meet the local requirements for fodder, fuel, widening of roads, construction of check dams for ensured irrigation facilities in undulated terrains, aberrations in various abiotic and biotic components etc. [1]. In order to diversify the fruit cultivation in the state and to minimise the monoculture of kinnow in the sub montane area, there is a need of the hour to explore the alternate option or initiate a breeding programme to improve the existing and available mango germplasm. To achieve this objective, it is essential to initiate survey, identification, documentation and collection of natural variation which exists throughout the region among seedling mangoes. Hence, genetic diversity has been harness among the collected sucking mango genotypes planted at PAU-Fruit Research Station Gangian (Hoshiarpur). The information on characterization and classification of sucking type of mango genotypes on the basis of their vegetative and flowering attributes is meagre; therefore, the present studies were planned.

Key words: *Mangifera indica* L., characterization, variability

Ten sucking type of mango strains *viz*., GN_{51}, GN_{52}, GN_{53}, GN_{54}, GN_{55} GN_{56}, GN_{57}, $GN_{58,}$ GN_{59} and GN_{60} budded on *desi* mango seedlings were evaluated at Fruit Research Station, Gangian. Fully mature twenty mango leaves were collected randomly after growth cessation from the middle of current season shoot. Vegetative and flowering traits were recorded as per IPGRI 'Mango Descriptor'. Colour of young emerging leaves was noted visually and with Hunter Lab Colour Flex EZ, USA. Reflectance 'L' measures luminosity that varies from zero (black) to 100 (pure white), 'a' and 'b' values represent the levels of tonality and saturation; with +a (indicating red); -a (indicating

Table 1. Leaf and flower characteristics of sucking mango strains.

Characters/strains	GN_{51}	GN_{52}	GN_{53}	GN_{54}	GN_{55}	GN_{56}	GN_{57}	GN_{58}	GN_{59}	GN_{60}
Leaf shape	Elliptical	Elliptical	Elliptical	Elliptical	Ovate	Elliptical	Ovate	Elliptical	Ovate	Elliptical
Leaf length (cm)	13.26	31.8	17.66	21.94	18.8	15.87	16.82	13.06	20.9	19.38
Leaf breadth (cm)	3.9	3.92	4.62	4.52	4.48	4.50	4.54	3.86	5.44	4.52
Petiole length (cm)	2.8	2.48	2.56	3.18	2.34	2.27	2.45	2.16	3.28	3.45
Leaf apex	Acuminate	Acuminate	Acuminate	Attenuate	Acute	Acuminate	Attenuate	Acuminate	Attenuate	Acuminate
Leaf base	Acute	Acute	Acute	Acute	Obtuse	Acute	Obtuse	Acute	Acute	Acute
Leaf margin	Entire	Wavy	Entire	Wavy	Wavy	Wavy	Wavy	Wavy	Entire	Wavy
Leaf Venation	Narrow	Wide	Wide	Wide	Wide	Medium	Medium	Medium	Medium	Medium
Mature leaf colour	Green	Pale green	Pale green	Pale green	Pale green	Dark green	Dark green	Green	Dark green	Green
Emerging leaf colour	Light green	Purple brown	Light green with brown tinge	Green red	Light brick	Light green	Light brick red	Greenish with brownish tinge	Pale green	Greenish brown
Reflectance 'L'	25.9	29.4	28.8	27.7	31.3	30.5	29.6	28.4	34.9	31.6
'a'	-0.84	-2.67	-1.47	2.06	0.34	-1.78	-4.08	0.55	-2.84	-3.32
'b'	6.14	11.24	6.76	8.23	4.61	8.33	9.65	7.91	11.42	11.03
Panicle length (cm)	21.8	17.6	16.3	14.2	12.5	11.9	15.4	17.9	12.3	13.7
Panicle breadth (cm)	11.5	6.2	7.4	7.0	8.9	4.6	9.1	8.7	5.8	4.6
Number of rachis	33.8	22.3	29.0	21.4	26.4	15.9	26.1	30.6	24.7	22.8
Hermaphrodite flowers (%)	22.4	18.6	25.7	39.1	23.7	57.4	29.6	26.6	37.1	27.4

green); +b (indicating yellow) and –b (indicating blue). Twenty panicles growing in different directions were tagged after their emergence for recording various inflorescence parameters. Male (M) and hermaphrodite (H) flowers were counted from randomly selected 400 flowers.

It is clear from Table I that leaf shape was ovate ($GN_{16,}$ GN_{57}) and rest of strains had elliptical shape. Leaf length varied between 13.06 cm in GN_{58} to 31.8 cm in GN_{52} ; leaf breadth from 3.86 cm in GN_{58} to 5.44 cm in GN_{59}; petiole length from 2.16 cm in GN_{58} to 3.45 cm in GN_{60}. Significant variability was observed in different sucking mango strains with respect to leaf apex, leaf base, leaf margin, panicle size and number of rachis. Colour of emerging and mature leaves varied from light green to light brick red and pale green to dark green respectively. Reflectance measurements for 'L', 'a' and 'b' were ranged from 25.9 to 34.9; -4.08 to 2.06 and 4.61 to 11.42, respectively. Hermaphrodite flowers per cent was ranged from 18.6 in GN_{52} to 39.1 in GN_{54} . Sharma and Singh [2] reported that hermaphrodite flowers per cent in mango depends upon the cultivar and climatic conditions.

References

1. Navprem S., Jerath N., Singh G and Gill P.P.S. 2012 Physico-chemical characterization of unexploited mango diversity in sub-mountane zone of northern India. Indian J. Plant Genet. Resour., 25: 261-69.
2. Sharma K. K. and Singh N. P. 2011. Orchard and Soil Management. Daya Publishers, New Delhi.

PS-IV-47

Efficacy of HMO against sooty mould on Kinnow

P. K. Arora, Krishan Kumar and Anil Kumar

Punjab Agricultural University, Regional Research Station, Abohar 152 116; e-mail: parshotamarora@pau.edu

Abstract

HMO @ 1.25% and 1.0% proved more effective against sooty mould than already recommended pesticides (ethion+ziram). Sucking pests viz. psylla, aphids, whiteflies and mealybugs are posing a serious threat to citrus industry in Punjab. These affect the plant performance by sucking the cell sap while sooty mould developed on the honey-dew excreted by these pests interferes with the photosynthetic activity of the plant leading to poor growth and yield. Sooty mould is caused by fungus *Capnodium citri* which produces black velvety superficial coating on leaves, twigs, stems and fruits. The affected leaves exhibit curling and shriveling symptoms. The mould deposited on the fruit rind may delay the fruit colouring and also become difficult to remove resulting in poor market acceptability. Heavy infestation leads to poor growth flushes, less flowers and fruits in next cropping season.

Key words : HMO, kinnow mandarin, sooty mould, sucking pests

The present studies were conducted during 2013 on 28 year old Kinnow mandarin trees growing in the orchards of PAU Regional Research Station, Abohar. The efficacy of Horticulture Mineral Oil (HMO) @ 05, 0.75, 1.0 and 1.25% in comparison to already recommended pesticides *i.e*. ethion@ 0.20% + ziram @0.25% [1] against sooty mould was evaluated. In each treatment, three trees were treated by keeping single tree per unit replication. For all the treatments three sprays were given at fortnightly intervals during September and October. The data on sooty mould was recorded before spray and then 7 days after each spray. For this purpose, twenty leaves selected randomly from all the four geographical directions of a tree are observed. The data for sooty mould was presented as Percent Disease Index (PDI) [2]

Table 1. Efficacy of HMO against sooty mould on kinnow mandarin

Treatment	Percent reduction in sooty mould (PDI) incidence after seven days of		
	First spray	Second spray	Third spray
HMO @ 0.5%	38.66 (38.41)	53.75 (47.13)	61.25 (51.49)
HMO @ 0.75%	51.91 (46.08)	64.33 (53.33)	73.66 (59.14)
HMO @ 1.0%	61.91 (51.88)	74.08 (59.47)	81.83 (64.78)
HMO @ 1.25%	62.41 (52.17)	74.25 (59.53)	82.50 (65.33)
Ethion 50EC (0.20 %) +Ziram 27 SC (0..25%)	51.25 (45.70)	63.00 (52.52)	71.58 (57.77)
Control (Water Spray)	20.33 (26.74)	24.75 (29.79)	33.00 (35.02)
CD (p = 0.05)	3.72	4.81	3.24

*Figures within parenthesis are the mean arc sine transformed values.

The data presented in Table 1 revealed that HMO (1.25%) recorded highest (82.50%) reduction in sooty mould incidence, but it was at par with HMO@1.0% which caused 81.83% reduction in sooty mould incidence after 7 days of third spray. This was followed by HMO @ 0.75% and ethion+ziram which were found to be statistically at par with each other. The other treatments i.e. HMO@0.5% and control (water spray) also recorded 61.25 and 33.00% reduction in sooty mould incidence after 7days of third spray, respectively. The most effective treatment (HMO@1.25%) recorded highest reduction in sooty mould incidence after 7 days of first and second

spray also. This treatment (HMO@1.25%) remained at par with HMO@1.0% after 7 days of first, second and third spray.

References

1. Arora P. K., Thind S.K. and Aulakh P.S. 2005. Correlation of citrus whitefly population with sooty mould development and its control. Pest Management in Hort. Ecosystems, 11(1) : 61-64
2. Arora, P.K., Thind S.K. and Kumar A. 2012. Management of citrus sooty mould-whitefly syndrome in kinnow mandarin. In : Proceedings International Conference –Sustainable Agriculture for Food and Livelihood Security (Eds. S.K. Sandhu, N. Sidhu and Allah Rang) PAU, Ludhiana. November 27-29, 2012. Crop Improv., 39 (Special issue): 889-890.

PS-IV-48

In-vitro propagation of endangered medicinal herb *Chlorophytum borivilianum* Sant and Fern.

Nupur Jauhari[1], K. Lavanya[1], Navneeta Bharadvaja[1*], Neelam Sharma[2]

[1]Department of Biotechnology, Delhi Technological University, Delhi 110 042; [2]National Bureau of Plant Genetic Resources, Pusa Campus, New Delhi 110 012; e-mail: jauharinupur@gmail.com

Abstract

Safed musli, 'a golden root' is a unique gift of nature to mankind since time immemorial as an alternative to chemical aphrodisiac. National Medicinal Plants Board (NMPB) New Delhi has recognized safed musli as the sixth important herb among 28 medicinal plants to be protected, promoted and preserved. The fleshy roots of Safed musli have medicinal properties and are used to prepare the herbal drug which is considered as a valuable nervine and general tonic for strength and vigor. Recently the phytocompound present in the plant is utilized in cancer studies as it possesses the anti-tumor properties. This plant is endangered because of the difficulties in cultivating the roots and its long dormancy period. Safed musli commands great demand and it has exorbitant price for its processed products both in indigenous and global markets. In the present study we attempt *in vitro* tuberization with different concentrations of auxins and cytokines on the basal media in order to get higher number of roots. It is an important way to conserve and commercially utilize plant resource for the welfare of human health.

Key words: Safed musli, endangered, aphrodisiac, phytocompound, anti-tumor

Safed musli, botanically known as *Chlorophytum borivilianum* Sant and Fern., belongs to family Liliaceae. National Medicinal Plants Board (NMPB), New Delhi, has recognized Safed musli as the sixth important herb among 28 medicinal plants to be protected, promoted and preserved [1]. Among the medicinal plants, safed musli is a potential endangered with unparallel medicinal properties. Only the fleshy roots, which have medicinal properties, are used to prepare the herbal drug which is considered as a valuable nervine and general tonic for strength and vigor. There is a lot of demand for its processed products but the production is far behind the demand due to slow propagation rate in nature. There is a great demand for fleshy root of safed musti.

Greater emphasis needs to be given for *in-situ* conservation, where the plant species are adapted to the specialized environment. Amongst *ex-situ* methods, storage of seeds in seed gene banks the most popular and conventional strategy has limited application in this texa. In view of this, there is an urgent need to apply in vitro culture methods for the micropropagation and conservation of this valuable threatened plant species. *Chlorophytum* is threatened with extinction in India due to indiscriminate collection and over exploitation of natural resources for commercial purposes to meet the requirements of the pharmaceuticals industries, coupled with limited cultivation [2]. In the view of this there is an urgent need to apply in vitro culture methods for the micropropagation and

conservation of this valuable threatened plant species. There are a few reports in literature regarding micropropagation of the taxa. In vitro multiplication of *C. borivilianum* was achieved on MS medium supplemented with 2 mg l^{-1} BA. Among the different combinations involving auxins (IBA/NAA) tested for rooting, IBA (3 mg l^{-1}) was relatively better [3]. Our emphasis was to obtain higher number of shoots and shoot length in less time as compared to wild plant growing under natural habitat so as to conserve and commercially utilize plant resource for the welfare of human health.

The plant material was collected from Central Institute of Medicinal and Aromatic Plants, Lucknow and maintained in the agro net of the Delhi Technological University, Delhi. Healthy young plants taken from the net house were thoroughly washed under running water after soaking in detergents like teepol or tween-20 for 10 minutes. Explants were excised and surface sterilization was carried out with 0.1% (w/v) mercuric chloride ($HgCl_2$) and 0.2% streptomycin for 6-8 min. after treating with 0.1% (w/v) bavistin. Finally, treated explants were washed with sterilized distilled water for 3-4 times before inoculation. Explants were cultured on MS medium supplemented with different growth regulators. The pH of the medium was adjusted to 5.8 before autoclaving at 121°C and 1.06 kg cm-2 for 15 min. The cultures were kept at 25±2°C under 16/8h photoperiod (30 ìmol m^{-2} s^{-1}) light/dark provided by cool white fluorescent lamps.

Various concentrations of BA (1mg l^{-1} –5mg l^{-1}) were tested for its effect on multiplication of shoots. Shoot number and shoot length were recorded after 8 weeks of culture. Twelve explants were used per treatment and the experiments were repeated twice. Shoots were transferred to rooting media containing various concentrations of auxins. The rooted shoots, after 8 weeks of rooting, were transferred to pots for hardening. Agar was thoroughly washed under running tap water. Plantlets were transferred to planton (Tissue culture box, Tarson) containing autoclaved mixture of soil, sand and manure, and covered with perforated polythene bags having whole. Plants were watered every 2-3 days with MS broth (pH 5.8) for 2-3 weeks. Polythene bags were removed after 3 weeks and the plants transferred to earthen pots containing garden soil.

Attempts were made to standardize a procedure of *in-vitro* establishment and shoot multiplication. It is known that the plants growing in field become more prone to fungal and bacterial attack. Parts of these plants are difficult to sterilize. Effective sterilization procedure for aseptic establishment of cultures was standardized. Of the various media tested, MS containing different concentrations of BA was the most suitable for culture establishment. Shoot emergence was observed within 2 weeks of culture and by 4 weeks, good healthy shoots were formed in all the media. The difference in response to various treatments became noticeable by 8 weeks. Maximum shoot length and higher number of shoots was observed in 3 mg l^{-1} BA. Shoot length and number of shoots were reduced as the concentration of BA was increased further.

MS Supplemented with BA had enhancing effect on the number of shoots with 3 mg l^{-1} BA. The present study clearly demonstrates successful *in-vitro* multiplication with different concentration of BA. Significant rooting was observed with the addition of auxins viz. NAA (Naphthalene acetic acid) and IAA (Indole-3-acetic acid) on MS medium. However, type of rooting is different in the media consisting of NAA alone and in combination of NAA and IAA. The root proliferation was obtained on full strength of MS medium supplemented with increasing concentration for IAA at 1mg l^{-1} and NAA at 3mg l^{-1} [5]. The finding is significant in terms of the fact that *in vitro* clonal multiplication of Safed musli, a rare Indian medicinal herb, has been achieved on MS medium supplemented with 3mg l^{-1} BA using young shoot bases as explants. Significant success has been achieved in number of medicinal plants regarding standardization of various stages of *in vitro* propagation which is a prerequisite for applying *in-vitro* techniques for germplasm conservation. Rapid clonal multiplication leading to regeneration of plantlets through tissue culture is an important pre requisite for *in-vitro* conservation. Results of the present study compare well with the earlier reports and revealed that elite collection of *C.borivilianum* could be established and multiplied *in-vitro*. Thus generated *in-vitro* shoots will serve as source material for further *in-vitro* conservation studies.

References

1. National Medicinal Plants Board. 2004. Thirty two prioritized medicinal plants, National Informatics Centre, Ministry of Health and Family Welfare, Department of Ayush, Government of India. http://www.nmpb.nic.in.
2. Nayar M.P. and Sastry A.R.K. 1987. Red Data Book of Indian Plants, Vol 1, BSI, Calcutta.
3. Pudake R.N. and Dhumale D.B. 2003. *In vitro* multiplication of Chlorophytum borivilianum Sant and Fern. J. Maharashtra Agric. Univ., 28(3): 265-267.
4. Murashige T. and Skoog F. 1962. A revised medium for rapid growth and bio assays with tobacco tissue cultures. Physiol. Plant., 15: 473-497.
5. Latto S. K. Bamotra S. Sapru Dhar R. Khan S. and Dhar A. K. 2006. Rapid plant regeneration and analysis of genetic fidelity of *in vitro* derived plants of *Chlorophytum arundinaceum* Baker-an endangered medicinal herb. Plant Cell Rep 25: 499-506.

PS-IV-49

Effect of salicyclic acid and proline on seed germination of aged and fresh seeds of radish (*Raphanus sativus*)

Shruti, Namarta Gupta and Heera Singh[1]

Department of Botany, [2]Department of Vegetable Sciences, Punjab Agricultural University, Ludhiana 141 004; e-mail: shrutipau4@gmail.com

Abstract

Seed treatment of naturally aged and fresh seeds of radish with water, salicyclic acid and proline showed improved percent germination as compared to control. Seed germination is the growth of an embryonic plant within a seed and result in the formation of the seedling. During the ageing process, seeds become less viable due to oxidative damages. Under ambient seed storage conditions, radish seeds loose vigour and viability exhibiting signs of physical deterioration. Oxidative damage of membranes and of other cellular constituents has been invoked as a mechanism of seed ageing. Seed ageing mechanisms include bio-membrane degradation, protein denaturation, interference with DNA and protein synthesis, accumulation of toxic materials and destruction of electron transport system of oxidative phosphorylation. Proline accumulation has been reported to be important for tolerance of certain adverse environmental conditions [1]. Proline catabolism is an important regulator of cellular ROS balance and can influence numerous additional regulatory pathways. Another plant growth regulator that appears to be involved in the regulation of proline metabolism is salicyclic acid. Several recent studies reported a promoting effect of SA on proline accumulation even in the absence of stress [2]. The present investigation was planned with the objective to study the effect of water, salicyclic acid and proline on germination and vigour of naturally aged radish seeds.

Key words: Radish, salicyclic acid, proline and ageing

The seeds of radish (*Raphanus sativus)* cultivar Punjab Pasand were used for different seed treatments i.e water, salicyclic acid (50 mg/L and 100 mg/L) and proline (5 mM and 10 mM). The effect of these treatments on seed germination of fresh and aged seeds of radish was recorded at 25°C. Seed treatments replicated thrice each with fifty seeds were kept for 12 h and 24 h. After the seed treatment with different solutions, seedling were raised between the two layers of germination paper and kept in the seed germinator. The data on seed germination and vigour was recorded after 10 days of sowing.

The results exhibited that the fresh seeds of radish variety Punjab Pasand had more percent germination at 25°C than the aged seeds of radish. Hydration, Salicyclic acid and Proline treatments for 12 and 24 h increased the percent germination of seeds as compared to control . The hydration of seed for 12 h and 24 h had increased the germination in fresh as well as naturally aged seeds but the effect was more pronounced in fresh seeds of

radish when the seeds were hydrated for 24h than the aged seeds. Both the concentration of Salicylic acid (50 mg/L and 100 mg/L) significantly increased percent germination in fresh as well as aged seeds of radish but the effect was found to be more when fresh seeds of radish were treated with Salicylic acid at 100 mg/L for 24 h as compared to the treatment of aged seeds and fresh seeds with Salicylic acid for 12 h at 50 mg/L and 100 mg/L. Thus the seed treatment of fresh seeds with Salicylic acid for 24 hrs gave better results. Similarly, both the concentrations of Proline (5 mM and 10 mM) significantly increased the percent germination as in fresh seeds as compared to control and naturally aged seeds. Maximum improvement in percent germination was achieved in seeds treated with Proline at 10 mM for 24 h at 25°C as compared to 24 h in both aged and fresh seeds. Although all the treatments improved the final percent germination in fresh as well as aged seed, the germination of Proline 10 mM treated seeds was more. The physiological, biochemical mad molecular changes might be the possible basis of improved germination [3]. Similar results has been observed in earlier studies also where salicyclic acid and proline play important role in the improvement of germination and tolerance to different types of stress [4, 5].

References

1. Miller G., Honig A., Stein H., Suzuki N., Mittler R. and Zilberstein A. 2009. Unraveling delta1-pyrroline-5-carboxylate proline cycle in plants by uncoupled expression of praline oxidation enzymes. J. Biol. Chem., 284: 2682-92.
2. Misra N. and Saxena P. 2009. Effect of salicylic acid on proline metabolism in lentil grown under salinity stress. Plant Sci., 177: 181-89.
3. Farooq M., Basara S. M. A., Tabassum R. and Afzal L. 2006. Enhancing the performance of direct seeded fine rice by seed primig. Plant Prod. Sci., 9: 446-56.
4. Morvaghatian A. and Khorsanasand F. J. 2013. Effects of salicylic acid on wheat germination parameters under drought stress. J Agric. and Environ. Sci., 12: 1603-08.
5. Agami A. R. 2014. Applications of ascorbic acid or proline increase resistance to salt stress in barley seedlings. Biol. Plantarum, 2: 341-47.

PS-IV-50

Screening of QPM germplasm for multiple disease resistance

Ramesh Kumar[*], K. S. Hooda, Jyoti Kaul, D. P. Chaudhary, V. K. Malik[1], Harleen Kaur[2], S. S. Sharma[3], Robin Gogoi[4], R. Devlash[5] and N. Mallikarjuna[6]

Directorate of Maize Research, New Delhi 110 012 [1]CCSHAU,Uchani(Karnal), [2]PAU,Ludhiana, [3]MPUAT, Udaipur, [5]CSKHPKV, Bajaura, [6]ZARS, Mandya [4]Divison of plant pathology, IARI, New Delhi; e-mail: rk.phagna@gmail.com

Abstract

A set of 17 QPM genotypes was subjected to rigorous screening at hot spot locations against different diseases [maydis leaf blight (MLB) at Ludhiana, Karnal and Delhi; turcicum leaf blight (TLB) at Bajaura and Mandya; charcoal rot (CR) at Delhi and Ludhiana; and Fusarium stalk rot (FSR) and Rajasthan downy mildew (RDM) at Udaipur] following standard disease screening techniques during *kharif*, 2013. Nine lines have shown resistance against one or more diseases. DQL 2008-1 was resistant against FSR and moderately resistant (MR) to TLB; DQL 2010 resistant against MLB with moderate resistance to TLB and CR; DQL 2015 resistant against TLB with moderate resistance to MLB and CR; DQL 2024 resistant against TLB and moderate resistance to MLB; DQL 2025 resistant to MLB and TLB; DQL 2028 and DQL 2038 resistant against FSR and moderate resistance to MLB, TLB and CR; DQL 2048 resistant against TLB and moderate resistance to MLB and CR; and DQL 2071 was rated resistant against FSR and moderately resistant to MLB, TLB and CR. These resistant sources are under confirmation for multiple disease resistance so as to utilize them in conferring the same into potential maize hybrids.

Key words: QPM, resistance, MLB, TLB, FSR and CR

Maize is an important cereal crop of the world. It is called queen of cereals. Maize is affected by as many as 112 diseases on a global basis and out of these 35 has been reported from India. The loss in terms of harvested grain by different diseases per annum has been determined to be in the order of 13.2 per cent, amounting to 1459.6 million rupees [1]. The impact of diseases results not only in lower yields but also reduces the value and quality of the grain and may increase cost of cultivation. The disease spectrum varies in different agro-climatic zones but the more serious diseases are leaf blight, downy mildew, stalk rot and rust. However, QPM is very sensitive to various diseases like maydish leaf blight, turcicum leaf blight, post flowering stalk rot, charcoal rot, etc. Hence, QPM germplasm need to be screened against different diseases for development of resistant/ tolerant hybrids. In the present investigation, QPM inbred lines were screened against May dish Leaf Blight (MLB) and Charcol rot (CR), Fusarium Stalk Rot (FSR), Rajasthan Downey Mildew (RDM) in a multiloation trial to identify resistant/ tolerant inbreds for development of hybrids with multiple resistance.

Seventeen newly developed QPM inbred lines were sown in single row plot of 3 m length at Ludhiana and Karnal for MLB and Delhi and Ludhiana for Charcol rot, Bajaura and Mandya for TLB and for FSR and RDM at Udaipur during *kharif* 2013 by following standard techniques of artificial inoculation.The disease score was recorded by following the techniques given Payak and Sharma [2]. Susceptible checks were planted after every 10th row and on both sides of plot to create epiphytotic conditions.

Nine lines have shown resistance against one or more diseases. DQL 2008-1 was resistant against FSR and moderately resistant (MR) to TLB; DQL 2010 resistant against MLB with moderate resistance to TLB and CR; DQL 2015 resistant against TLB with moderate resistance to MLB and CR; DQL 2024 resistant against TLB and moderate resistance to MLB; DQL 2025 resistant to MLB and TLB; DQL 2028 and DQL 2038 resistant against FSR and moderate resistance to MLB, TLB and CR; DQL 2048 resistant against TLB and moderate resistance to MLB and CR; and DQL 2071 was rated resistant against FSR and moderately resistant to MLB, TLB and CR. These resistant sources are under confirmation for multiple disease resistance so as to utilize them in conferring the same into potential maize hybrids.

Table 1. QPM genotypes resistant to different diseases

S.No.	Genotype	Resistant	Moderately resistant
1.	DQL-2008-1	PFSR (FSR)	TLB
2.	DQL-2010	MLB	TLB, PFSR (C.ROT)
3.	DQL-2015	TLB	MLB, PFSR (C.ROT)
4.	DQL-2024	TLB	MLB
5.	DQL-2025	MLB, TLB	-
6.	DQL-2028	PFSR (FSR)	MLB, TLB, PFSR (C.ROT)
7.	DQL-2038	PFSR (FSR)	MLB, TLB, PFSR (C.ROT)
8.	DQL-2048	TLB	MLB, PFSR (C.ROT)
9.	DQL-2071	PFSR (FSR)	MLB, TLB, PFSR (C.ROT)

References

1. Sharma R C and Lal S. 1998. Maize diseases and their management. Indian Farm., 48: 92-96.
2. Payak, M. M. and Sharma, R. C. 1979. Resistance to diseases in maize : The Indian experience. Crop Improv., 6: 75-85.

PS-IV-51

Characterization of Indian barley (*H. vulgare*) for morphological descriptors and their implication in DUS testing

Vishnu Kumar*, R. P. S. Verma, S. R. Vishwakarma, Dinesh Kumar, A. S. Kharub and Indu Sharma

Directorate of Wheat Research, Karnal 132 001, [1]ICARDA, Morocco, [2]NDUA&T, Faizabad; e-mail: vishnupbg@gmail.com

Abstract

A total of 83 released Indian barley varieties were characterized for 32 morphological descriptors based on scale 1 to 9 to describe the state of each character. 79 genotypes were observed with erect growth habit and the genotypes Alfa93, Clipper, RD2668 and Sonu were classified semi-prostrate in nature. Stem basal, auricle and upper node pigmentations were exhibited in the genotypes viz. Alfa93, DL88, DWRB91, HBL113 etc. The varieties RD 2668 and UPB 1008 were having short and narrow flag leaf. For spike morphology, most of the varieties were classified with green, erect, medium long spikes with intermediated density. The varieties BH393 and NDB943 were bearing smooth awns, while rough awns were observed in rest of the varieties.

Key words: DUS, morphological descriptors, barley

Germplasm is the base of genetic diversity, valuable source of disease and pest resistance and the primary step for the development of a food and nutritionally secure country [1, 4]. India is signatory to Trade Related Aspect of Intellectual Property Rights (TRIPs), and formulated *sui generis* system for the protection of plant varieties. "Protection of Plant Varieties and Farmers Rights" (PPV&FR) boosts up research and protection of varieties *vis-à-vis* ensures rights of farmers and village communities, benefit sharing and growth of seed industry [2, 3]. Indian market is eye catching for barley based multi-national companies (beer, malt, multi grain etc.), hence Indian barley germplasm needs to be protected and registered under PPV&FR. Therefore, the present experiments were conducted and 32 morphological descriptors were recorded to fulfil DUS (distinctiveness, uniformity and stability) stipulations in barley.

The experiments were laid out in randomized complete block design (RCBD) with 3 replications during *rabi*, 2012-13 and 2013-14 at Karnal and Faizabad locations. In view of seed availability, the data for the new varieties namely BH 885, BH 946, BHS 400, DWRB 92, HUB 113, RD 2786, RD2794, VLB 118 etc. could be recorded only in *rabi,* 2013-14. The genotypes were evaluated for 32 morphological characters viz. growth habit, stem basal pigmentation, auricle anthocyanin pigmentation, upper node pigmentation, flag leaf attitude, flag leaf sheath waxiness, spike emergence, spike type, lateral florets, spike waxiness, spike colour, spike attitude, awn roughness, flag leaf length, flag leaf breadth, awn tip pigmentation, spike basal sterility, lemma pigmentation, spike length, plant height, peduncle length, presence of awns, awn type, awn length, spike density, hullness of grains, grain colour, grain shape, grain weight, grain surface, rachilla hairs and grain crease width. These observations were recorded on individual plant/plot basis, while mean of 10 random competitive plants per replication was considered for flag leaf length, flag leaf breadth, spike length, plant height, peduncle length and awn length. The two-digit code system was used to record the observations, where the first digit refers to the principal stage of development beginning with germination and ending with kernel ripening [5]. The second digit (between 0 and 9) subdivides each principal growth stage. The scale 1 to 9 was used to describe the state of each character for the purpose of digital data compilation.

In the present study, adequate variation was observed for all the characters, except growth habit, flag leaf sheath waxiness, awn roughness, spike basal sterility, presence of awns and awn type. The frequency distributions

Table 1. Frequency distribution for different characters in barley

Descriptor	Range	Scale	Frequency	Descriptor	Range	Scale	Frequency
Growth habit	Erect	3	79	Lemma pigmentation	Absent	3	50
	Semi-prostrate	5	4	Nerve pigmentation	5	31	
	Prostrate	7	-		pigmented	7	2
Stem basal pigmentation	Absent	1	52	Spike length	Small	3	17
	Present	9	31		Medium	5	61
Auricle pigmentation	Absent	1	66		Long	7	5
	Present	9	17	Plant height	Very short	1	-
Upper node pigmentation	Absent	1	51		Short	3	-
	Present	9	32		Medium	5	25
Flag leaf attitude	Erect	1	23		Tall	7	50
	Semi-erect	5	45		Very tall	9	8
	Drooping	9	15	Peduncle length	Short	3	2
Flag leaf sheath waxiness	Absent	1	1		Medium	5	57
	Present	9	82		Long	7	24
Spike emergence	Very early	1	-	Awns	Absent	1	-
	Early	3	8		Present	9	83
	Medium	5	27	Awns type	Hooded	1	-
	Late	7	39		Awnletted	3	-
	Very late	9	9		Normal	5	83
Spike type	Two-row	3	12	Awns length	Short	3	-
	Six-row	7	71		Medium	5	11
Lateral florets (2 row)	Rudimentary	1	4		Long	7	72
	Developed	9	8	Spike density	Lax	3	11
Spike waxiness	Absent	1	24		Intermediate	5	63
	Present	9	59		Dense	7	9
Spike colour	Pale green	1	10	Grain hullness	Hulless	1	6
	Green	2	71		Hulled	9	77
	Dark green	3	2	Grain colour	Amber	1	6
Spike attitude	Erect	3	61		Yellow	2	77
	Semi-erect	5	17		Purple	3	-
	Drooping	7	5		Black	4	-
Awn roughness	Smooth	1	2	Grain shape	oval	1	5
	Rough	9	81		oblong	5	42
Flag leaf length	Short	3	2		elongated	7	36
	Medium	5	24	Grain size	Small	1	2
	Long	7	57		Medium	3	43
Flag leaf breadth	Narrow	3	2		Large	5	32
	Medium	5	32		Very large	7	6
	Wide	7	49	Grain surface	Smooth	1	38
Awn tip pigmentation	Absent	1	61		wrinkled	9	45
	Present	9	22	Grain crease width	Narrow	3	59
Spike basal sterility	Absent	1	80		Intermediate	5	23
	Present	9	3		wide	7	1
Rachilla hairs	Rudimentary	1	74				
	Prominent	9	9				

of each descriptor of genotypes are depicted in Table 1. For growth habit, 79 varieties were recorded with erect plant type and 4 genotypes namely Alfa93, Clipper, RD2668 and Sonu were semi-prostrate in nature. Stem basal,

auricle and upper node pigmentations were exhibited in 31, 17 and 32 varieties, respectively. These three pigmentations were present collectively in the genotypes viz. Alfa93, DL88, DWRB91, HBL113, Himani, JB58, LSB2, NB1, NB2, NB3 and NDB1173, respectively. For the flag leaf characters, most of the Indian barley varieties were characterized with semi-erect (45) in nature with waxy flag leaf sheath (82), while 57 and 49 varieties were observed with long and wide flag leaf, respectively (Table 1). Two varieties viz. RD 2668 and UPB 1008 were having short and narrow flag leaf. Out of 83 barley varieties, 71 were six row type and rest 12 genotypes were two-row barley. In two row types 8 varieties were having developed lateral florets, while remaining 4 varieties viz. DWRB73, DWRUB52, RD2668 and UPB 1008 were classified with rudimentary lateral florets.

Out of 83 varieties, 50 were tall in stature and spike basal sterility was also unique feature for three varieties viz. HBL113, Kedar and RD2715. In this investigation, 59 genotypes were observed with waxy spikes and for other ear characters namely spike colour, attitude, length and density majority of the varieties were characterized as green (71), erect (61), medium long (61) and intermediated density (63), respectively (Table 1). All the varieties considered here were having normal awns with long awn length (72) and two varieties viz. BH393 and NDB943 were found with smooth awns. For grain characters, 6 varieties were hulless, 77 were yellow in colour and 42 genotypes were characterized with oblong grains. The grain surface of 45 varieties was observed as wrinkled and 59 genotypes were having narrow crease width (Table 1).

After perusal of data recorded in Indian barley, it was hypothesized that in general, the varieties with presence of basal stem/auricle/upper node/lemma pigmentation and lateral florets (two-row) are better general combiners for feed and malt barley. DWR28, DWRB 91, DWRB 92 etc. for malt and RD2035 and HBL113 for feed barley are excellent examples of the above said hypothesis. It was also assumed that the morphological descriptors viz. flag leaf sheath and spike waxiness, erect spikes and prominent rachilla hairs are more contributing towards stress resilient performances in barley. The present study is an evident of sufficient genetic diversity available in Indian barley germplasm, which would certainly help to pick better parents and to generate precise future breeding programmes. These descriptors would also be helpful to maintain the genetic purity of the genotypes. Beside this, in emerging need of intellectual property rights (IPR) regimes, this investigation would also facilitate as baseline DUS data of morphological descriptors for registration of extant barley varieties under PPV&FR Authority.

Acknowledgement

Authors express sincere thanks to PPV&FR Authority, New Delhi for financial supporting DUS barley project.

References

1. Brahmi P., Saxena S. and Dhillon B. S. 2004. The Protection of Plant Varieties and Farmers' Rights Act of India. Current Sci., 86: 392-398.
2. Katiyar P. K., Dixit G. P. and Singh B. B. 2008.Morphological characterization of green gram (*Vigna radiata*) varieties and their application for distinctness, uniformity and stability testing. Indian J. Agric. Sci., 78: 439-444.
3. Yadav A. K., Singh D. and Arya R. K. 2013. Morphological characterization of Indian mustard (*Brassica juncea*) genotypes and their application for DUS testing. Indian J. Agric. Sci., 83:1305-1316.
4. Yadav S., Verma N., Tyagi V., Singh S., Ranga S., Binda P. and Brahmi P. 2014. Exchange of plant genetic resources: Prospects in India. Indian J. Agric. Sci., 84: 616-623.
5. Zadoks J. C., Chang T. T. and Konzak C. F. 1974. A decimal code for the growth stages of cereals. Weed Res., 14: 415-421.

PS-IV-52

Screening of pea germplasm for resistance to powdery mildew and rust diseases

Rajinder Singh Bal* and Ashok Kumar

PAU, Regional Research Station, Gurdaspur 143 521; e-mail: rsbalgsp@gmail.com

Abstract

Present investigations was carried out to screen pea germplasm lines against powdery mildew and rust diseases. The symptoms of rust and powdery mildew appeared during last week of February and Ist week of March respectively. None of the entries were immune to both the diseases. Six entries *viz*., P128, P121, P139, P109, P154 and P105 were found to be resistant against powdery mildew while, five entries *viz*., P128, P106, P139, P123 and P127 showed resistance against rust.

Key words: Pea, screening, germplasm, powdery mildew, rust

Pea (*Pisum sativum* L.) is an important leguminous vegetable crop grown world wide mainly as a source of protein. Among various diseases which attack the crop, rust (*Uromyces viciae-fabae*) and powdery mildew (*Erysiphe polygoni*) are the major constraints in the production of peas. Powdery mildew can cause a yield loss of 58% [1] while rust can cause 20-100% yield losses. Also an effective economical control with fungicides is not possible. Keeping these points in view, some lines of field pea were screened to find some source of resistance to powdery mildew and rust diseases.

Table 1. Rating scale for powdery mildew

Score	Description	Reaction category
0	0 %foliage area infected	Immune
1	1-10 %foliage area infected	Resistant
2	11-30 %foliage area infected	Moderately Resistant
3	31-70 %foliage area infected	Moderately Susceptible
4	71-80 %foliage area infected	Susceptible
5	81-100 %foliage area infected	Highly Susceptible

Table 2. Rating scale for rust

Score	Description	Reaction category
0	No symptoms on leaf	Immune
1	Rust pustules covering <1% of leaf area	Resistant
3	Rust pustules covering 1-10% of leaf area	Moderately Resistant
5	Rust pustules covering 11-25% of leaf area	Moderately Susceptible
7	Rust pustules covering 26-50% of leaf area	Susceptible
9	Rust pustules covering >50% of leaf area	Highly Susceptible

The experiment was conducted at Regional Research Station, Gurdaspur during Rabi, 2012 season. 53 germplasm lines received from MULLaRP, Kanpur, were sown during first week of November. Each entry was sown in two rows each of 4m length alternated with susceptible check after two entries. The row length and row

spacing was maintained at 4m and 30cm respectively. A susceptible variety was sown in pots in polyhouse during first week of October. The pots showing powdery mildew symptoms were shifted to the field during mid February and shaken over the susceptible checks for development and spread of disease. For the spread of rust, the uredospores appearing on the plants in the pots were suspended in water and sprayed on the test entries during late evening hours. Disease reaction was recorded as per the following scoring scales:

The symptoms of rust appeared during last week of February while those of powdery mildew started during Ist week of March. None of the entries were immune to both diseases. The disease score of different entries varied between 1-4 for powdery mildew and 1-9 for rust. Six entries viz. P128, P121, P139, P109, P154 and P105 were found to be resistant while, eight entries were moderately resistant to powdery mildew. Twelve entries showed moderate susceptibility and the remaining entries were susceptible to powdery mildew. Similar results were reported by Davidson et al [3] who found that out of 88 lines tested, resistance to powdery mildew was shown by 19 lines. Shahid et al [4] also reported that four test entries were resistant, one moderately resistant and three were susceptible to powdery mildew.

Five entries viz. P128, P106, P139, P123 and P127 showed resistance against rust. Moderate resistance and moderate susceptibility was observed in seven and eleven entries respectively. The rest of the entries were susceptible to highly susceptible against rust. The results are in line with those of Xue and Warkentin [5] who evaluated 93 field pea varieties and recorded that eight were most resistant and the remaining were susceptible to rust. It was further observed that two entries were resistant to both powdery mildew and rust. Also, the rust developed very slowly on three out of the resistant entries. Rashid and Bernier [6] have recorded that slow rusting populations of *Vicia faba* (Broad bean) were more tolerant to rust than others. The findings are also supported by Sohi et al [7] who found that some cultivars were moderately resistant to powdery mildew and rust. The lines found resistant against either or both the diseases especially, the slow rusting entries can be used in the breeding programme.

References

1. Mahmood T., Ahmad I., Qureshi S.H. and Aslam M.1983. Estimation of yield losses due to powdery mildew in peas. Pak. J. Bot.15:113-115.
2. Amin K.S. and Ramachander P.R. 1989. Effect of saprol on epidemic development of rust and powdery mildew on pea and their influence on yield. J. Pulses Res. 2(2):140-146.
3. Davidson J.A., Krysinska-Kaczmarek M., Kimber R.B.E. and Ramsey M.D. 2004. Screening field pea germplasm for resistance to downy mildew (*Peronospora viciae*) and powdery mildew(*Erysiphe pisi*). Australasian Plant Pathology 33:413-417.
4. Shahid M., Shah S.F.A., Ali G.H. and Ishtiaq S. 2010. Resistance in pea germplasm/lines to powdery mildew under natural conditions. Mycopath.8(2):77-80.
5. Xue A.G. and Warkentin T.D. 2002. Reactions of field pea varieties to three isolates of *Uromyces fabae.* Can. J. Plant sci.82:253-255.
6. Rashid K.Y. and Bernier C.C. 1991. The effect of rust on yield of faba bean cultivars and slow rusting populations. Can. J. Plant Sci.71:967-972.
7. Sohi H.S., Sokhi S.S. and Rawal R.D. 1974. Varietal reaction of peas to powdery mildew(*Erysiphe polygoni* DC) and rust(*Uromyces fabae* Pers. De Bary). Mysore J. Agric. Sci.8:529-532.

PS-IV-53

Genetic resources of wild *Vigna* species – A treasure house for broadening the genetic base in cultivated *Vignas*

M. Latha, V. A. M. Nissar, Y. C. Roy, K. V. Bhat and S. Mani

National Bureau of Plant Genetic Resources Regional Station, KAU (P.O.), Vellanikkara, Thrissur, Kerala 680 656

Abstract

Systematic evaluation of 150 accessions belonging to 22 taxa of *Vigna* was done based on 48 qualitative and 24 quantitative characters. Variability in both qualitative and quantitative characters was observed between and within 22 different taxa. A new species was discovered from Western Ghats. Evaluation for susceptibility to storage pest, protein content, pollen morphology and crossability relationship among the taxa was studied.

Key words: Wild *Vigna* species, evaluation of genetic resources, crossability relationship

Vigna Savi belonging to the family Leguminoseae is a large genus comprising of seven sub-genera and over 150 species [1]. The seven sub-genera in the genus *Vigna* namely *Ceratotropis, Haydonia, Lasiopron, Macrorhyncha, Plectotropis, Sigmoidotropis* and *Vigna* were recognized . Most of the Asian *Vigna* species come under the sub-genus *Ceratotropis* and about half of them are either domesticated or cultivated [1]. The cultivated species under the sub-genus *Ceratotropis* include *Vigna radiata* (mung bean or green gram), *V.mungo* (urd bean or black gram), *V. umbellata* (rice bean), *V.aconitifolia* (moth bean) and *V.trilobata*. Out of the 21 species of Asian *Vigna*, 15-16 are found in India [2]. Tomooka [2] proposed a revised list of cultivated and wild taxa of Asiatic *Vigna* belonging to 3 sections distributed in Asia-Pacific region. Arora [3] reported 14 species of *Vigna* and their wild forms belonging to 4 sub-genera of the genus. Subsequently Babu [4] listed 23 *Vigna* species found in India including the 5 species which had their origin in other countries. The wild *Vigna* species/taxa that occur in southern Western Ghats (SWG) includes *V. sublobata*, *V. trilobata*, *V. umbellata* , *V. dalzelliana, V. minima, V. trinervia* var. *bourneae, V. khandalensis*, *V. pilosa, V. vexillata,* and *V. wightii. V. sublobata* and *V. silvestris* are the wild progenitors of green gram and black gram respectively and they are cross compatible [5] and can be a valuable sources for imparting biotic and abiotic stresses. A resistant strain of *V. sublobata* for YMV was reported by Singh and Ahuja[6]. Considering their potentiality to be used in breeding programme, a preliminary evaluation of the genetic resources of wild *Vigna* species assembled at NBPGR RS, Thrissur was taken up covering aspects like their crossability relationship, protein content and their susceptibility to storage pests.

One-hundred and fifty accessions of wild *Vigna* species raised in pots at the National Bureau of Plant Genetic Resources (NBPGR) Regional Station, Thrissur, Kerala were selected for the study. These accessions were raised in completely randomized design (CRD) with two replications as pot culture. Observations on 48 qualitative and 24 quantitative characters were taken at various phenophases of the crop from all the accessions. The descriptor list developed at NBPGR was used for recording the observations. Twenty-eight crosses were made involving 14 taxa belonging to 3 sections of *Vigna*. Emasculation and pollination was done on the same day between 8.00 a.m. to 10.00 a.m. All the 150 accessions were evaluated for susceptibility to *Callosobruchus* species under lab conditions. The petriplates were incubated in dark for further infestation. After two months of incubation observations on the number of seeds infested with the pest were recorded and expressed as percentage. Protein estimation was done in 27 accessions comprising 12 species by standard method.

Among the 48 qualitative characters studied, variability was observed in 23 characters namely type of seed germination, shape of primary leaf, nature of attachment of primary leaves, lobing of terminal leaflet, shape of

terminal leaflet tip, size of stipule, shape of stipule, presence of ligule, colour of flower, colour of corolla, shape of bracteole, colour of peduncle, nature of pod attachment to peduncle, colour of immature pod, colour of mature pod, curvature of pod, shape of pod beak, shape of seed, colour of seed, lustre on seed surface, mottling on seed surface and shape of hilum.

Qualitative characters such as type of seed germination, nature of attachment of primary leaves, size of stipule, shape of stipule, presence of ligule, shape of bracteole, nature of pod attachment to peduncle, curvature of pod, shape of seed and shape of hilum were very distinct for each taxa. Four different types of germination behaviour were noticed and the taxa were grouped based on it. Variability in size and shape of stipules and bracteoles were also observed. The 150 accessions were reclassified into 22 taxa based on the qualitative characters. One accession originally identified as *V.sublobata* was found to be a distinct taxa of *Vigna* and hence described and named as a new species *V*. *konkanensis* [7]. All the 24 quantitative characters studied exhibited wide range of variability. The keel pocket was present in all taxa but absent in *V.unguiculata, V.marina* and *V.pilosa*. The length of keel pocket varied from taxa to taxa. The percent of storage pest infestation recorded in 150 accessions of taxa of *Vigna* showed that the infestation ranged from 0-100 percent. Zero percent infestation was observed in 55 accessions belonging to different taxa except *V.aconitifolia*, *V.subramaniana* and the new species *V*. *konkanensis*. Crossability studies showed that even though maximum pod set was observed in crosses between taxa belonging to same section, there was no pod set in between two taxa of section Aconitifoliae. Moderate pod setting was also observed in crosses involving taxa belonging to different section. Crosses were attempted involving *V. hainiana* for the first time. The result showed that though cross compatibility exist between *V. hainiana* and *V. sublobata* F_1s failed to germinate indicating embryo abortion at some stage. Pod set was observed in crosses involving *Vigna trinervia* var. *bourneae* and *V. trinervia* var. *trinervia* with *V. radiata* as female parent. The F_1s were found to be robust resembling *V. trinervia* var. *bourneae* with bright yellow flowers but without any fertile pod formation. Premature fall of pods were also observed. Total Protein content analysed in 27 accessions showed that the maximum protein content (24.13%) was in *V*. *trinervia* var. *bourneae* (IC349885) and minimum (17.14%) in *V.dalzelliana* (IC406508). Considering the rich and valuable genetic resources in *Vigna* species, scope for their utilisation in improvement of pulse crops especially greengram, blackgram, ricebean and mothbean are immense. A systematic evaluation including screening of all the accessions assembled at this station in hot spots for biotic and abiotic stresses and genetic enhancement through pre-breeding will be useful for the breeders engaged in pulse crop improvement.

References

1. Verdcourt B. 1970. Studies in the Leguminosae-Papilionoideae for the flora of tropical East Africa. *IV Kew Bulletin*. 24: 502-569.
2. Tomooka N., Vauhan D.A., Moss H. and Maxted, N. 2003. The Asian *Vigna*: Genus *Vigna* Subgenus *Ceratotropis* Genetic Resources. Kluwer Academis Publishers, Dodrecht, Netherlands. 288p.
3. Arora, R.K. 1985. Diversity and collection of wild *Vigna* species in India. Plant Genetic Resources Newsletter. 63: 26-33.
4. Babu, C.R., Johri, B.M. and Sharma, S.K. 1985. Leguminosae -Papilionoideae: Tribe-Phaseoleae. Bull. Bot. Sur. India, 27: 1-28.
5. Audilakshmi B. and Chandel K.P.S., 1990. Interspecific hybridization and crossability studies among cultivated and closely related wild *Vigna* species in Indian Gene Centre. Indian J. Plant Genet. Resour. 3: 46-60.
6. Singh,B.V. and Ahuja, M.R.,1977. *Phaseolus sublobatus* Roxb. A source of resistance to yellow mosaic virus for cultivated mung. Indian J. Genet. 37: 130-132.
7. Latha M, Sheen Scariah, Krishnaraj M.V., Presannakumari K.T., Bhat K.V., Bisht I.S., and Joseph John K., 2014. *Vigna konkanensis* (Fabaceae: Papilionoideae)- a new species from the West Coast of India. Webbia: Journal of Plant Taxonomy and Geography 69: 49-52.

PS-IV-54

Crop species and their digitisation in the national herbarium of cultivated plants (NHCP)

E. Roshini Nayar*, Anjula Pandey, K. Pradheep, Rita Gupta, Deepali Upadhyay and Usha Jaiswal

Division of Plant Exploration and Germplasm Collection, National Bureau of Plant Genetic Resources, New Delhi 110 012; e-mail: roshini@nbpgr.ernet.in

Abstract

Crop plants and their wild relatives are the focus for digitisation at the National Herbarium of Cultivated Plants (acronym: NHCP). Forty major crop species, well represented by over 25 herbarium specimens each, and their wild relatives have been validated for their identity, diagnostic characters for quick identification. The database of information linked with digital images has been developed for use by researchers and collectors in the field and determining priorities for future collection.

Key words: Digitisation, specimens, diagnostic, crop, wild relatives

Species of crop plants and related representatives of the crop genepool are the focus for collection and augmentation in the National Herbarium of Cultivated Plants (NHCP). Digitisation of the specimens and, after validation of identity, working out diagnostic characters of species/ Groups (cultivar-groups) to be linked to images of specimens, is envisaged as a means of making the holdings available to a wide user base. Crop plants represented in the Indian region amounting to 479 crop species (Nayar *et al*., 2003) have been used as a basis for estimating the representation of crop species in the NHCP (Table 1) and for determining gaps for future additions of taxa belonging to the crop genepool. These reflect the collection and conservation priorities of major crop species, both native and introduced, as well as taxonomic and systematic study of crop genepools of Indian origin. Specimens were largely vouchers collected from farmer's fields or raised in experimental conditions. Herbarium specimens (one to several representing all parts and stages of growth of the species) which could be used to identify the material were selected and scanned to obtain digital images. Taxon sheets with taxonomic information, diagnostic features, phenology, cytological status and aspects contributing to its PGR value such as genepool, characters of differences from the wild taxa and its representation in the herbarium and genebank were linked to the digital images. Illustrative images of distinguishing characters were also added. Secondary data on source of germplasm, native or introduced, nature and extent of variation reported vis-a-vis observed through study of herbarium specimens were worked out.

A total of 403 crop species were represented in the NHCP by over 4000 specimens. Forty crop species were represented by more than 25 specimens each viz. Cereals and millets (7); grain legumes (11); vegetables (18); edible tubers (1); fibres (5); oilseeds (8); pseudocereals (1); spices and condiments (5); fruits (1) and medicinal plants (12). These reflected the collection and conservation priorities of major crop species, both native (Yadav *et al*., 2014) and introduced viz. rice (*Oryza sativa*), wheat (*Triticum aestivum*), oats (*Avena sativa*), pearl millet (*Pennisetum glaucum*), *Vigna* spp. including localised and minor ones (cowpea, green gram and moth bean), pigeon pea (*Cajanus cajan*), chick pea (*Cicer arietinum*), okra (*Abelmoschus esculentus*), brinjal (*Solanum melongena*), cucurbits (*Cucumis melo*, *Momordica charantia*, *Luffa cylindrica*, *Lagenaria siceraria* and *Coccinia cordifolia*), jute (*Corchorus capsularis*), *Brassica* spp. (oleiferous types of *Brassica rapa*, *B. juncea*,) sesame (*Sesamum indicum*), amaranths (both grain and leafy types), chenopods, black pepper (*Piper nigrum*), *Ziziphus* spp. (*Z. mauritiana*). Besides, native species of importance in the Indian region, such as Sawank (*Echinochloa colonum*), horse gram (*Macrotyloma uniflorum*), kesari dal (*Lathyrus sativus*) and lentil (*Lens culinaris*), lablab bean (*Lablab purpureus*) and linseed (*Linum usitatissimum*) were also among the better represented species.

A total of 240 wild species belonging to the crop genepools of the major crops were also represented.

Medik. species in India. National Bureau of Plant Genetic Resources, New Delhi.

Table 1. Crop species representation in NHCP

Crop category	Species in India	Species (NHCP)	Specimens (NHCP)	Specimens >25	Wild species (NHCP)
Cereals/ Millets	23	22	388	*Avena sativa* L., *Echinochloa colonum* (L.) Link., *Oryza sativa* L., *Pennisetum glaucum* (L.) R. Br., *Triticum aestivum* L.	72
Pseudocereals	3	3	35		
Grain legumes	15	14	366	*Vigna radiata* (L.) Wilczek, *Vigna aconitifolia* (Jacq.) Marechal, *Vigna umbellata* (Thunb.) Ohwi & Ohashi, *Vigna trilobata* (L.) Verdcourt, *Cicer arietinum* L., *Macrotyloma uniflorum* Roxb.	51
Fruits	86	66	420	*Ziziphus mauritiana* Lam.	5
Vegetables	76	69	966	*Coccinia cordifolia* (L.) Cogn., *Cucumis melo* L., *C. melo* var. *momordica* Duthie & Fuller, *Lablab purpureus* (L.) Sweet, *Luffa cylindrica* (L.) M. J. Roem., *Lagenaria ciceraria* (Molina) Standley, *Momordica charantia* L., *Solanum melongena* L., *Pisum sativum* L., *Solanum tuberosum* L.	71
Edible tubers	15	11	84	*Colocasia esculenta* (L.) Schott	
Oilseeds	24	20	243	*Brassica juncea* (L.) Czern. & Coss., *Brassica rapa* L. (=*B. campestris* L.), *Linum usitatissimum* L., *Sesamum indicum* L.	17
Spices/condiments/ flavouring	50	43	326	*Piper nigrum* L.	20
Fibre	23	15	137	*Corchorus capsularis* L.	4
Fodder & forages	38	33	455	*Prosopis cineraria* Druce, *Cenchrus ciliaris* L., *Heteropogon contortus (*L.) Beauv. ex Roem. & Schult.	
Medicinal/aromatic plants	82	70	567	*Andrographis paniculata* Wall. ex Nees., *Abelmoschus oschatus* Medik., *Mucuna prurita* Hk., *Ocimum basilicum* L., *Plumbago zeylanica* L.	
Miscellaneous	23	22	388		
Total	479	403	4131	40	240

Analysis of the holdings of these priority crop species in NHCP has been used to work out gaps in terms of additional species to be added (76 species mainly of vegetative propagated species, large sized plants such as sugarcane), as well as species with less representation but important for the Indian regions viz. *Echinochloa crus-galli* (L.) Beauv., *Hordeum vulgare* L., *Setaria italica* (L.) Beauv., *Triticum durum* Desf. among cereals and millets, *Cajanus cajan* (L.) Millsp., *Lathyrus sativus* L., *Lens culinaris* Medik., *Vigna mungo* (L.) Hepper and *Vigna unguiculata* (L.) Walp. among grain legumes, *Perilla frutescens* (L.) Britton an oilseed species, *Piper longum* L. *Abelmoschus esculentus* (L.) Moench, *Amaranthus dubius* Mart. ex Thell., *Amaranthus spinosus* L., *Capsicum annuum* var. *acuminatum* Fingh., *Cucumis melo* var. *utilissimus* Duthie & Fuller, *Cucumis sativus* L. and *Luffa acutangula* (L.) Roxb.among vegetables, and *Corchorus olitorius* L., *Crotalaria juncea* L. and *Hibiscus cannabinus* L. among fibres (all represented by 12 or less specimens). Another significant aspect for addition was characters/ parts of plants that are useful for identification and study of variation within species (dissections of floral parts in legumes, tubers, scales and outer layers in bulbous crops, perennating parts in grasses and tuberous crop), and habitat/ locations from which additional specimens are to be added, and especially in the wild species from the entire habitat range. The database of information along with linked images of the crop genepool (crop and wild species) were prepared for online use as well as in the field by collectors.

Voucher specimens from survey, collection and taxonomic studies on oleiferous *Brassica* spp. with a secondary centre of diversity in the Indian region, and biosystematic studies (Yadav *et al*., 2014; Pradheep *et al*., 2013; Pandey and Prakash, 2013) on *Abelmoschus*, *Vigna*, *Macrotyloma*, *Cucumis*, *Luffa* and *Momordica*, as well as introduced germplasm of cultivars, ecotypes and wild species of potential use in crop improvement work were some of the significant specimens authenticated for their identity available for use by researchers and explorers.

References

1. Nayar, E. Roshini, Anjula Pandey, Kamala Venkateswaran, Rita Gupta and BS Dhillon 2003 *Crop Plants of India. A Checklist of Scientific Names*. National Bureau of Plant Genetic Resources, New Delhi.
2. Pandey Anjula and Krishna Prakash 2013 A note on debatable taxonomic identity of *Luffa tuberosa* Roxb. (Cucurbitaceae): a potential wild edible vegetable in India. Indian J. Plant Genet. Resour. 26(2):124-127.
3. Pradheep K, ER Nayar and R. Srivastava 2013 Notes on the identification, taxonomic status and occurrence of *Ziziphus hysudricus* (Edgew.) Hole (Rhamnaceae) in India. In Abstracts, XXIII Annual Conference of Indian Association of Angiosperm Taxonomy and National Seminar on Recent Advances in Plant Taxonomy Research, Rashtrsant Tukadoji Maharaj Nagpur University, Nagpur, Maharashtra. Abst. pp 26.
4. Yadav, SR, KV Bhat, M Latha, JK John, SK Malik, M Aitwade, SR Rao, S Scariah, M Nissar, S Umdale, P Patil, G Krishnan and R Ghedsana 2014 An Illustrated Guide for the identification of *Vigna* Savi, *Cucumis* L. and *Abelmoschus* Medik. species in India. National Bureau of Plant Genetic Resources, New Delhi.

PS-IV-55

New sources of resistance for barley leaf blight caused by *Bipolaris sorokiniana* in India

R. Selvakumar*, S.S. Vaisu[1], S.P. Singh[2], R. P. S. Verma[3], Vishnu Kumar Goyal, Dineshkumar, Jogendra Singh, Rekha Malik, Anil Khippal, A. S. Kharub and Indu Sharma

Directorate of Wheat Research, Karnal, Haryana 132 001, [1]Banaras Hindu University, Varanasi, Uttar Pradesh, [2]Narenddra Dev University of Agriculture and Technology, Faizabad, Uttar Pradesh, [3]Rabat, International Center for Agricultural Research in the Dry Areas (ICARDA); e-mail: selvakumar2000@gmail.com

Abstract

Identification of resistant sources for various biotic stresses is helpful in breeding for disease resistance. In barley, the leaf blight resistant sources against *Bipolaris sorokiniana* are very limited thus screening of germplasm at multilocation will be an essential part of pre breeding programme. Three hundred and sixty exotic barley lines received from ICARDA were artificially screened for resistance against leaf blight at Faizabad and Varanasi consequently for two years under epiphytotic conditions. The leaf blight severity and Area under Disease Progress Curve (AUDPC) was also calculated and slow blighting lines were identified. Although no line was showing highly resistance to leaf blight, 24 lines were showing moderately resistance to leaf blight in both locations. The highly susceptible line RD 2503 showed the highest susceptibility to leaf blight with AUDPC score of 1404. The identified resistant germplasm lines are sources for leaf blight resistance in Indian barley breeding programme.

Key words: Barley, resistance, leaf blight

Barley (*Hordeum vulgare* L.) is an important cereal crop cultivated since ancient times in India and is considered as a sacred grain. In India, barley is cultivated on about 6.95 lacks ha area with production of 17.43 lacks tonnes and productivity of 2508 kg/ha (Anonymous, 2012-13). Barley is being used as animal feed, human food and in industry for malting and brewing. In India presently the productivity is below the world average and the diseases such as stripe rust, leaf rust and leaf blight play a major role in reducing the grain yield and quality of grains in the

major barley growing areas of the north-western plains. For developing disease resistant varieties the availability of donors harboring the resistance is very important but unfortunately the leaf blight resistant germplasm are very rare. Most of the released varieties are susceptible to leaf blight under favourable conditions and therefore search for leaf blight resistant germplasm is the priority of research.

Three hundred and sixty exotic barley lines were artificially screened for resistance against leaf blight at various locations viz., Faizabad and Varanasi during 2012-13 and 2013-14. The materials were grown in one metre length and 30 cm distance between rows. After every 20 lines of entries one line of infector (mixture of susceptible entries) was sown as well as surrounding four sides of test materials also. The initial leaf blight inoculums of *Bipolaris sorokiniana* was multiplied on sterilized wheat grains in laboratory. Fifteen days after incubation at 22+2°C with frequent shaking regularly the fully covered conidia were dislodged from the grains by adding water to the flask. The spore suspensions were filtered through muslin cloth and the filtrate containing conidia was adjusted to 1x10^{5} conidia per ml by mixing with more water. Spraying of water containing conidia was carried out using Knap sack sprayer over the test materials from tillering to flag leaf stage. The wheat grains surrounded by conidia were also added to the base of the seedlings to act as source of inoculum. The crop was grown as per recommended agronomic practices. Data on leaf blight was recorded at weekly interval starting from flowering stage till physiological maturity stage. For phenotyping, disease severity was recorded at three different growth stages using double-digit scale. The average of three stages for each genotype was calculated by taking mean of first and second digit separately and the infection responses were categorized as Immune, Resistant, Moderately resistant, Moderately susceptible, Susceptible and Highly susceptible. The Area under Disease Progress Curve (AUDPC) was calculated and lines exhibiting slow blighting phenomenon were sorted out.

Compared to Faizabad, Varanasi environment highly favours the leaf blight development (Fig. 1). Most of the entries started showing leaf blight symptoms in Varanasi comparatively earlier to Faizabad centre. Unfortunately there was no line showing highly resistance to leaf blight. However, 24 lines were showing moderately resistance to leaf blight in all locations. The Area Under Disease Progress Curve (AUDPC) was calculated and the lines were showing range between 393 and 1404. The highest AUDPC was observed in case of highly susceptible check RD2503. The lowest AUDPC was recorded for entries viz., Ana, AYAROSA/ BLLU//CALI92, Bella Union, Berolina, BLLU/ MINN DESC 2//PETUNIA 1, C 9173, C9609, C97073,CABUYA, CLE 203 INYA AROMO, Defra, Diamant, FNC 6-1, Haisa, Hiproly, Isaria, L94, MN 599, ND 19957, PAPELILLO, Peruvian,Sebastian, Weihenstephan Melthauresistente I and ZIGZIG/ BLLU// PETUNIA 1P.STO/3/LBIRAN/ UNA80//LIGNEE640/4/ BLLU/5/ PETUNIA 1. The highly susceptible line RD 2503 showed the highest susceptibility to leaf blight with AUDPC score of 1404. The identified resistant germplasm lines will be a good source for leaf blight resistance in Indian barley breeding programme (Fig. 2).

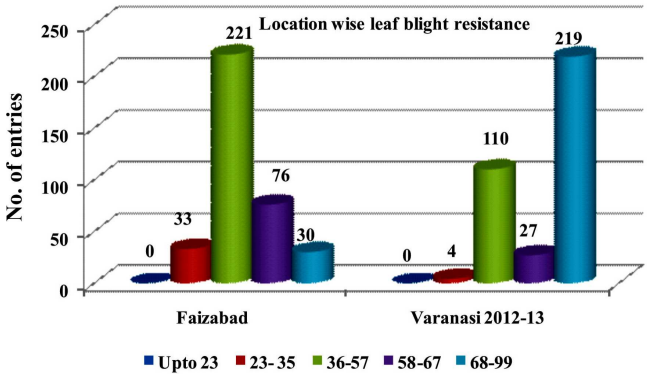


Fig. 1. Distribution pattern of blight presence of different locations

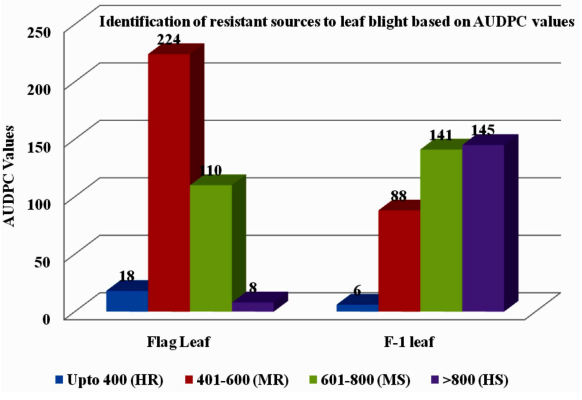


Fig. 2. Variation in bligh resistance in barley

Though leaf blight can be under check by spraying the chemical fungicides, use of resistant varieties is a viable option for poor farmers who cannot afford to buy the fungicides. Therefore identification of resistant sources for leaf blight and other biotic stresses is the only option for breeding new barley varities in India.

Reference

1. Anonymous (2013) *Progress report of All India Coordinated Wheat and Barley Improvement Project* 2012-13. Vol. VI. Barley Network. Directorate of Wheat Research, Karnal, India. P. 327.

PS-IV-56

Interspecific hybridization between *Vigna radiata* and *Vigna mungo* to transfer Mungbean Yellow Mosaic Virus (MYMV) resistance

R. K. Gill, T. S. Bains, Satinder Kaur[1], Asmita Sirari and Amandeep Kaur

Department of Plant breeding and Genetics, School of Agricultural Biotechnology, PAU, Ludhiana

Abstract

Interspecific crosses were attempted between different genotypes of *V. radiata* and *V. mungo* with an aim to transfer mungbean yellow mosaic virus (MYMV) resistance from *V. mungo* to *V. radiata.* The crossability percentage varied from 15.1 to 27.4. Five hybrid plants were easily identified on the basis of their leaf shape, pod size and branching pattern which did not resemble either of the two parents used in the crossing programme. The true hybrids will be selfed or backcrossed to map and transfer MYMV resistance gene(s) into susceptible mungbean cultivars.

Key words: *V. radiata*, *V. mungo*, interspecific hybridization, crossability

Mungbean (*Vigna radiata* (L.) Wilczek) is an important food legume in Asia particularly in the Indian subcontinent. Besides a short duration legume (maturing in 55 to 70 days), it fits well into many cropping systems and improves soil fertility as well as small farmer's income. The productivity of mungbean is very low in tropical and sub-tropical regions of Asia including India. This is due to inherent low yield potential of cultivars and their vulnerability to many foliar diseases such as; Mungbean yellow mosaic virus (MYMV), Cercospora Leaf Spot (CLS), Bacterial Leaf Spot (BLS), Anthracnose and pod rot. MYMV, transmitted by whitefly, *Bemisia tabaci,* is the most dreadful disease of mungbean crop. It attacks the crop in an epidemic form and in severe cases, there is yellowing of whole leaves and pods, leading to formation of shriveled grains or sometimes empty pods leading to complete yield loss. Thus, there is an immense need to introduce long term resistance for MYMV into mungbean in order to stabilize cultivation and production of this crop in north India. Urdbean (*Vigna mungo* L. Hepper) possesses higher degree of resistance to MYMV and other foliar diseases as compared to mungbean. Thus, present study was undertaken to transfer MYMV resistance from urdbean into mungbean and crosses were attempted between different susceptible mungbean genotypes and resistant urdbean genotypes .

Three genotypes of mungbean (SML 668, SML 832, TMB 37) and two genotypes of urdbean (Mash 114 and Mash218) were crossed in all the possible combinations. SML668 and SML 832 are high yielding varieties of summer mungbean recommended for cultivation through out Punjab state. TMB 37 is a high yielding variety developed from BARC (Bhabha Atomic Research Centre, Trombay). SML 668 and SML 832 varieties have now become susceptible to MYMV, if grown during kharif season. TMB 37 is also highly susceptible to MYMV under Punjab conditions. Mash 218 and Mash 114 are released varieties of urdbean recommended for cultivation in Punjab state during summer and *Kharif* seasons respectively. Both the urdbean genotypes are highly resistant to MYMV and other foliar diseases. A large number of crosses were attempted as the percentage of seed set has been reported to be low in interspecific crosses and germination of crossed seed is also poor. The emasculations

and pollinations were carried out as per the procedure given by Boiling *et al* [1] using *Vigna radiata* as female parent. To enhance the crossability and pod setting percentage 4ppm NAA (á- Naphthyl acetic acid) was applied to pedicel of emasculated bud as well as after pollination twice a day at least for ten days consecutively.

The crosses made between different genotypes of *V. radiata* and *V. mungo* showed high degree of flower abscission both after emasculation and pollination which might be due to flower injury, shock or physiological changes. Of the total 517 emasculated buds only 381 left for pollination, which yielded only 69 mature pods containing 140 seeds. The pod set percentage varied from 15.1 (SML 668 X Mash 218) to 27.4 percent (SML 668 X Mash 114) (Table 1).

Table 1. Crossability between *V. radiata* and *V. mungo*

S.No.	Cross	Total no. of flowers buds emasculated	Total no. of flower buds pollinated	No. of mature pods	Pod set percent age	No. of seeds sown	Germination percentage
1	SML 668 x Mash 218	146	126	19	15.1	33	**33.3**
2	SML 668 x Mash 114	71	51	14	27.4	24	**37.5**
3	SML 832 x Mash 218	89	67	13	19.4	28	**14.3**
4	SML 832 x Mash 114	45	25	6	24.0	15	**20.0**
5	TMB 37 x Mash 218	93	64	7	10.9	21	**47.6**
6	TMB 37 x Mash 114	73	48	10	20.8	19	**42.1**
	Total	**517**	**381**	**69**	**18**	**140**	

Low crossability and pod set percentage may be attributed to genetic diversity between the parents as well as embryo abortion after fertilization [2]. Of the 140 F_1 seeds only 45 germinated into complete F_1 plants indicating the low germination (32%) of these crosses. Five of these hybrid plants were easily identified as hybrids as their plant type such as, leaf shape, pod size and branching pattern plants did not resemble either of parents (Figure 1) but identification of other F_1s was not possible visually. DNA from all the F_1 plants has been extracted to validate F_1 true hybrids with molecular markers. The true F_1s will be selfed to develop F_2 and F_3 mapping populations to map the MYMV resistance gene(s) and transfer these into susceptible mungbean cultivars.

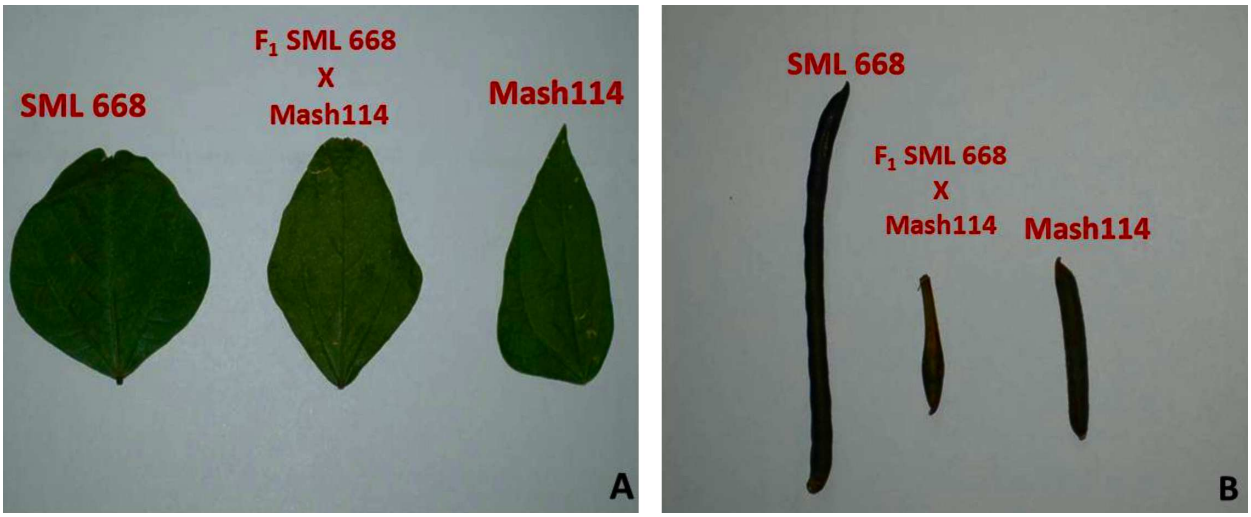


Fig. 1. A. Leaves and B. Pods of parental genotypes SML 668, Mash 114 and their F_1

A number of studies undertaken on crossability among different Vigna species indicate that *V. radiata* produced successful hybrids as seed parent with *V. mungo*, *V. umbellata* and *V. angularis*, although their reciprocal cross hybrids were not viable [3]. Thus in the present study an attempt was made to develop interspecific hybrids and in order transfer the MYMV resistance.

References

1. Boiling M., Sander D.A. and Matlock R.S. 1996. Mungbean hybridization technique. Agron.J., 53: 54-55.
2. Sharma J. and Satija C.K. 1996. In vitro hybridization in compatible crosses of *vigna* species. Crop Improvement, 23: 29-32.
3. Singh B.B. and Dikshit H.K. 2002. Possibilities and limitations of interspecific hybridization involving green gram and black gram. Indian J. agric. Sci., 72: 676-678.

PS-IV-57

Characterization of *Colletotrichum gloeosporioides* associated with blossom blight of *Uraria picta*

A. K. Srivastava*, A. Khaliq, N. Singh, A. Saroj, Nisha Raj, Birendra Kumar, S. C. Singh and A. Samad

Department of Plant Pathology, CSIR-Central Institute of Medicinal and Aromatic Plants (CSIR), P.O. CIMAP, Lucknow 226 015; e-mail: atulsrivastav.micro@gmail.com

Abstract

***Uraria picta* commonly known as the Prishniparni is one of the most important ingredients of Ayurvedic drug Dashmool. Roots and leaves are mainly used in the treatment ofr Alzheimer's disease. During August 2013, blossom blight, a new fungal disease was found on it in the farms of CSIR-CIMAP, Lucknow, India, and causes destruction of inflorescence. The causal agent of the disease was isolated and characterized as *Collectotrichum gloeosporioides* on the basis of its pathogenicity, morphology and molecular analysis.**

Key words: *Uraria picta, Collectotrichum gloeosporioides*, blossom blight

Uraria picta commonly known as the Prishniparni and Sankarjata belong to the family Fabaceae (Papilionaceae) has recorded as one of the important medicinal plant in Ayurveda School of medicine in India. *U. picta* is distributed in Southeast Asia, China, Taiwan, Australia and India (Fig. 1a). Its medicinal ingredients generally used for treating fatigue, oral sores and several gynecological disorders [1]. The extract of *U. picta* also helps in treating Alzheimer's disease. Earlier, leaf blight caused by *Phaeotrichoconis urariae* [2] and stem rot by *Fusarium thapsinum* [3] have been reported as fungal diseases on it.

During August 2013, appearance of brown color lesions were observed on the inflorescence of the *U. picta* at the CSIR-CIMAP experimental farms, Lucknow, which caused malformed, distorted and drying inflorescence. Severe infection caused poor seed setting and dry inflorescence (Fig. 1b). For investigation infected plant materials were cut into small pieces, surface sterilized with 1% sodium hypochlorite for one minute, followed by washing with autoclaved distilled water and blot with sterile filter paper. Subsequently small pieces were placed on to potato dextrose agar (PDA) and Petri plates were incubated at 28°C for 4 to 5 days. Consequently fungus was transferred into fresh PDA Plates. Single spore isolation technique (SSI) was used to get pure spore culture. Fungus was transferred into PDA slant with addition of paraffin liquid and kept at 4°C for preservation. Pathogenicity tests were carried out on detached as well as on attached healthy inflorescences by spraying spore suspension of 10^5 spores/ ml and subsequently with sterile distilled water which served as control. Inflorescence was kept at 25 $\pm$ 2°C under 75$\pm$ 3 % humidity for 10 days. Initial symptoms were observed after 4 days in all inoculated

inflorescence. Typical disease symptoms were observed after 8 days in all inoculated inflorescence while control remains free of infection. Morphological and microscopic studies were performed with SSI cultures. The small disc was taken from the edge of well grown culture plate and placed on PDA (potato dextrose agar). Colony diameter was recorded at 25°C up to 7 days. The 75 mm PDA plate was filled with full of mycelia within 6 days. The shape, length and width of 100 conidia were measured, and mean length and width were calculated. Colonies on PDA were well developed white to grey in color, having cottony aerial mycelium, orange sporulation and small black color dots on front side while black color dots were observed on reverse side of the Petri plates. Conidia were born singly on phialides cells. Conidia were straight, cylindrical and obtuse at the apex ranging from 3-6 x 12-14 µm (Fig. 1c). Appressoria were studied through slide-culture technique. The size and shape of appressoria were recorded after 5 to 7 days. Appressoria was irregular, without lobe brown to dark brown in colour ranges from 8-11 x 4-7 µm. Morphology and culture characteristic based studies revealed that causal organism is *Colletotrichum gloeosporioides*.

Genus *Colletotrichum* is a fungi, considered as causal agent of anthracnose disease. However, it is also reported as fatal pathogen of other diseases like blossom blight of Sarpgandha [6] and tip die back of Cassava. Anthracnose is the most common disease of the pre and post harvested fruits which drastically hampered the production, marketing and export of tropical fruits. The symptoms of anthracnose disease appear as necrotic lesions on stem, leaves, fruit and also on flower, in addition to crown and stem rots, seedlings blight etc. In India, *Colletotrichum* spp. has been reported on different plant as *C. chlorophytumi* on *Chlorophytum* species in Allahabad *C. capsici* leaf blight on French basil, *C. capsici* leaf blight on Safed musli, and *Colletotrichum capsici* on *Rauvolfia serpentina* [6].

To study rDNA ITS region, fungal genomic DNA was extracted using DNeasy Plant Mini Kit (Qiagen)/ NucleoSpin® DNA extraction Kit (Macherey-Nagel, Duren, Germany). The fungal culture was grown on PDA for 14 days at 27°C and were scraped with a sterile spatula and crushed to powder with the help of liquid nitrogen. All the extraction procedure accorded to the manual instructions. PCR reactions were carried out with universal primers ITS1 (5'- CCGTAGGTGAACCTGCGG-3') and ITS4 (5'-TCCTCCGCTTATTGATATGC-3') [9. Amplifications were carried out in a 25 ìl reaction mixture containing 2.5 ìl 10X buffer, 1 µl dNTP, 0.8 µl primers ITS1-forward and ITS4-reverse, 3 µl fungal genomic DNA (~50ng), 0.5 µl *Taq* polymerase and 16.4 µl mili-q water. The PCR setting were, initial denaturation for 5 min at 94°C followed by 30 sec at 94°C, annealing at 55°C for 30 sec and then extension for 2 min at 72°C, total 30 cycles were performed along with final extension at 72°C for 10 min. The PCR product was electrophoresed in a 1.2 % agarose gel with λ DNA ladder marker (Invitrogen, Barcelona,



Fig. 1. Healthy *Uraria picta* plant in field (a) Natural Infection on *U. picta* inflorescence (b) single spore (c)

Spain) and expected size, 600 bp of amplification visualized under UV light. The amplified product was cloned in pGEM-T vector (Promega) as per manufacturer's instructions. The Selection of right insert with correct orientation was done via restriction enzyme *Eco*-RI giving amplicons of approximately 600 bp and sequenced using ABI sequencer model 3730 (Perkin Elmer) at CIMAP. NCBI-BLASTn of the sequence showed 99% similarity with *Colletotrichum gloeosporioides* (HQ645073) and it was deposited in Genbank with accession number (KJ617392). This is the first report of blossom blight disease of *Uraria picta* caused by *C. gloeosporioides* in India. For the bio-security, plant breeding and integrated disease management, C*olletotrichum* spp. are most important and these information would be helpful in making the management strategies.

Acknowledgments

The authors are grateful to the Director, CSIR- CIMAP for providing facilities and encouragement.

References

1. Anonymous 2003. The Ayurvedic Formulary of India, 2nd ed. Govt. of India, Ministry of Health and Family Welfare, Department of AYUSH, New Delhi. 55.
2. Bharadwaj S.D. 1969. A new species of *Phaeotrichoconis* on *Uraria picta* from Varanasi, India. The Indian forester, 95: 24-26.
3. Bhattacharya A., Datta A.K., Saha A. 2011. Asiatic Fungal Weevil (*Eurymycter napinatus*)-transmitted *Fusarium thapsinum* Infection in *Uraria picta.* Pest Tech., 79-80.
4. Johnston P.R., Jones D. 1997. Relationships among *Colletotrichum* isolates from fruit-rots assessed using rDNA sequences. Mycologia, 89: 420-430.
5. Shukla R.S., Alam M., khaliq A., Bahl J.R., Singh H.N., Khanuja S.P.S. 2006. Blossom Blight, A New Disease of Rauvolfia serpentine. J. Mycol. Plant Pathol., 36: 427-430.
6. Sreenivasaprasad S., Talhinhas P. 2005. Genotypic and phenotypic diversity in *Colletotrichum acutatum*, a cosmopolitan pathogen causing anthracnose on a wide range of hosts. Mol Plant Pathol 6:361–378.

PS-IV-58

New report of citral rich *Ocimum* for tropical and sub tropical regions of India

S.C. Singh, Bhaskar Datt[1] A. Samad and Birendra Kumar*

CSIR-Central Institute of Medicinal and Aromatic Plants, Lucknow 226 015, [1]CSIR- National Botanical Research Institute, Lucknow 226 001; e-mail: birendrak67@rediffmail.com

Abstract

***Ocimum* is a highly cross pollinated genus due to inter and infra specific hybridaization, polyploidy and the existence of chemical races that do not differ significantly in morphology. *O. africanum* is intermixed with other species of *Ocimum* viz. *O. basilicum* and *O. americanum* (*O. canum*) in the same population. The taxonomy of *Ocimum* is in a state of confusion and the same species is often referred to by more than one name or *vice- versa*. The circumscription of *Ocimum* itself is also a matter of disputes among taxonomists. *O. basilicum* has fruiting calyx 6 – 8 mm long while in *O. africanum* up to 5.5 mm long. Furthermore, it is hoped the present report will attract other Indian taxonomists for the correct appraisal of *Ocimum* in India.**

Key words: Essential oil, *Ocimum africanum, O.basilicum*, citral

Ocimum is an important economic and medicinal herb due to presence of essential oils which consist of monoterpenes, sesquiterpenes and phenylpropanoids [1]. Its oil is the natural source of methyl chavicol, methyl cinnamate, camphor, neral, geranial, linalool, eugenol, etc. which are used in pharmaceutical, cosmetic and flavouring industries. In addition to these uses, *Ocimum* is widely cultivated as a pot herb for culinary uses, and for the fresh herb market, the export of *Ocimum* from Israel alone is worth 4 million US dollars per year [2]. In India as well it constitutes an important component of ever growing herbal market. Basil is an important essential oil crop with around 350 tonnes of essential oil being produced throughout the world annually. About half of this is produced from *Ocimum basilicum* L. and its close relatives.

The genus *Ocimum* L., collectively called basil, which is annual and perennial herbs and shrubs native to the tropical and subtropical regions of Asia, Africa, and Central and South America [1,2]. The taxonomy of *Ocimum* is in a state of confusion. In the literature concerning *Ocimum*, particularly the work pertaining to economic and industrial fields, same species is often referred to by more than one name or vice- versa. The circumscription of *Ocimum* itself is also a matter of dispute among taxonomists. Estimates of species in the world vary from 30 to 160 [3]. *Ocimum africanum* (Lemon basil) was described by Joao de Loureio in 1970. Over the next 50 years separate systematic botanists gave it two names, *O. citriodorum* Vis. and *O pilosum* willd. The same species is also found as *O. basilicum* var. *anisatum, O. americanum sensu* Pushpangadan & Sobti non L., etc. Although *O. americanum* is well known in Indian Floras, the following nomenclature (author citation), dichotomous key and description will facilitate to distinguish it from other closely related species. It is hoped that the present report will attract other Indian taxonomists for the correct appraisal of *O. africanum* in India.

Ocimum africanum Lour., Fl. Cochinch. 2; 270. 1790; Suddee, S. *et al*. in Kew Bull. 60: 28–29. 2005. *O. citratum* Rumph. in Herb. Amboin. 5: 266, t. 93, f.1. 1747. *O. pilosum* Willd., Enum. Pl. 2: 629. 1809. *O. basilicum* L. var. *anisatum* Benth., Labiat. Gen. Sp. 4. 1832. *O. basilicum* L. var. *pilosum* (Willd.) Benth., Prodr. 12:33. 1848. *Ocimum* × *citriodorum* Vis. in Linnaea 15: Litt. Ber. 102. 1841. *Ocimum americanum* L. var. *pilosum* (Willd.) A. J. Paton in Kew Bull. 47:426. 1992. *O. americanum sensu* Pushpangadan & Sobti non L. in Cytologia 47: 575. 583. 1982. 'Lemon basil'.

1a. Fruiting calyx up to 5 mm long; corolla 4 – 5.5 mm long

2a. Fruiting calyx 2 – 3 mm long; stem internodes with short adpressed

or retrorse hairs ...*O. americanum*

2b. Fruiting calyx 4 – 5.5 mm long; stem internodes with long, spreading and sometimes

retrorse hairs ... *O. africanum*

1b. Fruiting calyx 6 – 8 mm long; corolla 7 – 8 mm long ... *O. basilicum*

Ocimum africanum was described by Joao de Loureio in 1970. Over the next 50 years separate systematic botanists gave it two names, *O. citriodorum* Vis. And *O pilosum* willd. The same species is also found as *O. basilicum* var. *anisatum, O. americanum sensu* Pushpangadan & Sobti non L., etc. Aromatic, annual or short lived perennial herbs, up to 50 cm high; stems densely pubescent with long, spreading and sometimes retrorse hairs. Leaves elliptic-lanceolate or ovate-lanceolate, 0.8-3.5 x 0.6-2 cm, entire or shallowly serrate at margins, apex acute, base cuneate or obtuse, glandular punctuate, glabrescent above, hairy on veins beneath, sometimes pubescent on both surfaces with longer hairs on veins beneath; petioles 0.2-1.8 cm long, pubescent. Verticels up to 1 cm apart; axis densely pubescent with retrorse hairs; bracts ovate, up to 5 mm long; pedicels 1-2 mm long, recurved, finely pubescent. Calyx campanulate, 2-2.5 mm long, 4-5.5 mm long in fruit; posterior lip rounded, decurrent on tube; anterior lip with 2 median lanceolate teeth; tube with a ring of dense hairs at throat. Corolla white or light purple, 4-5.5 mm long; posterior lip with 4-lobed with oblong obovate villous lobes, anterior lip boat-shaped; tube straight, glabrous. Stamens 4, slightly exserted, posterior 2 shorter. Nutlets oblong, 1-1.5 mm long, black, minutely tuberculate.

Apart from taxonomic reasons, these differences are on account of high levels of both morphological and chemical variability exist within the genus due to inter-specific hybridization, polyploidy, and the existence of chemotypes or chemical races that do not differ signi?cantly in morphology [4]. To get better insight into intra- and inter-speci?c taxonomy, a variety of different approaches based on geographic origin, morphology, karyotype, chemical composition, and crossability have been used by some workers [5-7]. Despite these efforts, taxonomy and phylogenetic relationships within *Ocimum* genus are still in question.

The taxonomy of *Ocimum* in India is itself in confusion, with some Indian literature [8-9] providing detailed information on cytology and phytology using a different infrageneric classification from that used in recent taxonomic literature. Due to polymorphism, much confusion has still surrounding the identification of the species of *O. basilicum* and *O. americanum* which have a wide range of distribution in India with enormous diverse ecological settings. The confusion surrounding the name of *O. americanum* also arises because the type specimens of *O. americanum* and *O. canum* do not reveal the characters necessary to decide to which entity they belong. The Type of the former species is a young specimen lacking calyx, whereas the Type of the later species is an illustration [7].

After exhaustive survey and collection of *Ocimum* species in India, we have found various genetic and chemotypic diversities in natural population. Some species of *Ocimum* are citral rich, camphor rich, methyl cinnamate, methyl chavicol and linalool rich. On the basis of chemotypic variability various authorities named it as *Ocimum basilicum* and *O. americanum* (syn. *O. canum*). The populations of *O. americanum* and *O. afrinanum* are often intermixed and erroneously identified as *O. americanum* in most of herbaria in India. Chemical profiling worked out at CIMAP also indicates their distinctiveness. The results of chemical analysis of *O. africanum* essential oil by gas liquid chromatography exhibited the presence of neral (31.66%), geranial (40.23%), 1, 8 cineole (1.34%), ocimene (0.59%), linalool (2.29%), methyl chavicol (3.46%), citronellal (2.82%) and geraniol (2.26%) as major aroma chemicals. During the survey, the population of *O. africanum* in Lucknow and adjoining areas was also found infected with virus and showed mosaic, yellowing, deformation of leaves and over all stunted growth. The associated pathogen seems to be a begomovirus on the basis of molecular studies. From above studies it is revealed that this citral rich *O. africanum* or lemon basil can be commercially cultivated in tropical and sub tropical regions of India as an annual crop in two seasons (June-September and February-April).

Acknowledgements

The authors are grateful to the Directors, CSIR-CIMAP, and CSIR-NBRI, Lucknow for providing necessary facilities. We are thankful to Dr. Alan Paton, Royal Botanical Gardens, Kew, United Kingdom for critical suggestions. The study was financially supported by Uttar Pradesh State Biodiversity Board, and CSIR-CIMAP CHEM-BIO (BSC 0203), Lucknow, India.

Reference

1. Paton A., Harley M.R. and Harley, M.M. 1999. Ocimum: an overview of classi?cation and relationships. In: Basil: the genus *Ocimum* (eds. Hiltunen R., Holm Y.). Harwood, Amsterdam, pp. 1-38.
2. Darrah H. 1980. The cultivated basils. Thomas Buckeye, Independence, M.O.
3. Pushpangadan P. and Bradu B.L. 1995. Basil. In: Advances in Horticulture, Medicinal and Aromatic Plants (eds. Chadha, K.L., Gupta, R.). Malhotra Publishing House, New Delhi, pp. 627-657.
4. Simon J.E., Quinn J. and Murray R.G. 1990. Basil: a source of essential oils. In: Advances in new crops (eds. Janick J, Simon J.E.). Timber, Portland, pp. 484-989.
5. Grayer R.J., Kite G.C., Goldstone F.J., Bryan S.E., Paton A. and Putievsky E. 1996. Intraspecific taxonomy and essential oil chemotypes in sweet basil, *Ocimum basilicum*. Phytochemistry, 43: 1033-1039.
6. Khosla M.K. 1995. Study of inter-relationship, phylogeny and evolutionary tendencies in genus Ocimum. Ind. J. Genet., 55: 71-83.

PS-IV-59

Morpho-physiological evaluation of pearlmillet germplasm for summer season

Ejaz Ahmad Malik*, Ruchika Bhardwaj and R. S. Sohu

Department of Plant Breeding and Genetics, Punjab Agricultural University, Ludhiana 141 004 Punjab; e-mail: malik@ejaz14@gmmil.com

Abstract

The study was performed to evaluate grain-pearl millet germplasm for various morpho-physiological characters for the dry summer adaptability under Punjab conditions. The germplasm displayed considerable variability for all characters except days to maturity. Higher phenotypic coefficient of variance (PCV) than the genotypic coefficient of variance (GCV) was observed for all the traits. Strong positive association of grain yield with days to flowering and maturity (0.66, 0.15) suggests the selection of genotypes with early flowering and consequent early maturing is quiet effective for selecting the genotypes for summer cultivation. Significant positive association (0.17) between water soluble carbohydrates and grain yield depicted that WSC is good indicative for selecting heat tolerant genotypes.

Keywords: Pearlmillet, summer adaptability, PCV, heritability, WSC

Pearl millet (*Pennisetum glaucum* (L.) R. Br) is mainly grown in rainy (*kharif*) season (June-September) but is also cultivated during summer season (February-May) in India. Summer season pearl millet is cultivated as an irrigated crop under high level of agronomic management. It can be grown in areas chartered by low and erratic rainfall (200-600 mm of annual rainfall), high temperature and poor soil fertility and can address the emerging challenges of global warming and issues like water shortage. Morpho-physiological character evaluation and their association will help in identifying genotypes suitable for summer season cultivation. Therefore, in the present investigation an attempt was made to access the amount of variability and correlation among different yield contributing morpho-physiological traits. The material under study was obtained from Forage and Millet section, Department of Plant Breeding and Genetics, PAU Ludhiana. Seventeen male sterile (A-lines) and eighty three inbred lines of pearl millet were evaluated for different morpho-physiological traits *viz*., days to 50% flowering, number of productive tillers, spike sterility, days to maturity, chlorophyll content, cell membrane thermostability, water soluble carbohydrates, pollen viability, grain yield, 1000 grain weight and stover yield during *summer* 2013. The material was sown in randomized block design with two replications with row length =2m, row to row spacing =50cm and plant to plant spacing =15cm. The statistical analysis was carried out on the basis of mean of five plants using SAS 9.4 and genotypic and phenotypic coefficient of variance were estimated [1]. Heritablity, genetic advance (GA) and GA (% of mean) were calculated [2]. Correlation studies were carried out following the procedures [3] and significance of correlation coefficient was tested against tabulated 'r' values [4] at n-1 d.f. at 5% and 1% level of significance.

The analysis of variance revealed that all the germplasm lines were significantly different except days to maturity. The range of variability was very high in the characters like grain yield even after eliminating the CMS lines, there was significant variability for most of the characters. The genotypic and phenotypic coefficient of variance between all the traits (Table 1 clearly showed that the phenotypic coefficient of variance (PCV) was higher than the corresponding genotypic coefficient of variance (GCV) as also reported [5] earlier. Thus, the characters can be improved by careful selection so that the effect of phenotype is reduced in the later generations. Higher heritability was shown by the characters like grain yield, days to maturity, stover yield, chlorophyll content and water soluble carbohydrates, hence exhibiting high broad sense heritability and less environmental effect, [6] also reported high heritability for 1000 grain weight, days to maturity and grain yield. Thus, the direct selection

would be effective for further improvement of these traits. All the characters having higher heritability also had higher GA% clearly indicated the additive gene effect and selection of such characters would be effective. Correlation studies revealed that the grain yield/plot had significant and positive association with days to 50 % flowering, days to maturity, pollen viability, germination percentage, water soluble carbohydrate spike sterility and 1000 grain weight (Table 2). Both days to 50% flowering and days to maturity showed strong positive association (0.66, 0.15) with grain yield suggesting the selection of genotypes with early flowering and consequent early maturing is quiet effective for selecting the genotypes for summer cultivation. Under the field conditions, it was observed that the late flowering strains were very susceptible to downy mildew due to the onset of the monsoon rains (general observation). However, the earliness was found in genotypes that were having less number of effective tillers and number of effective tillers was negatively associated with earliness (-0.527). The strains with higher amounts of water soluble carbohydrates were better performing under summer conditions that is significant positive association (0.17) has been found between water soluble carbohydrates and grain yield. Thus the trait WSC is good indicative for selecting heat tolerant genotypes. Earlier it has been confirmed that WSC provide improved varieties with greater and more stable yields in stress environment [7].

Table 1. Estimate of genetic parameters in pearlmillet

Character	Range	GCV	PCV	h^2 (%)	GA	GA (% of mean)
Cell membrane stability	52.95-95.38	4.17	9.82	18.06	2.89	3.65
Water soluble carbohydrates	0.12-1.12	29.98	35.88	69.85	0.25	51.62
Chlorophyll content	8.50-42.55	25.71	29.46	76.16	9.72	46.22
Germination percentage	5-100	33.93	38.18	78.99	43.93	62.12
Number of effective tillers	1.5- 11	20.56	33.89	36.8	1.51	25.69
Percent spike sterility	0.71-10.02	35.31	42.93	67.67	3.21	59.84
Stover yield (kg/plot)	0.5-6	33.86	39.57	73.2	1.42	59.67
Pollen viability	32.9- 100	14.32	19.57	53.57	1.91	21.6
Days to maturity	100-133	18.58	19.86	87.53	30.13	35.82
Days to 50% flowering	50-71	2.32	5.39	18.54	2.51	2.06
1000grain weight (g)	3.67-14.21	3.22	4.96	42.27	2.69	4.32
Grain yield	10 -360	43.57	45.83	90.4	191.12	85.35

Table 2. Correlation coefficients among different traits in pearlmillet

	WSC	CHL	GERM	NTLS	SSTR	STOVR	POLLEN	DTM	DTF	1000GWT	GRAINY
WSC	-0.07	0.05	0.02	0.07	0.02	0.02	0.05	0.05	0.05	0.03	-0.03
CHL		-0.13*	0.08	-0.01	-0.19**	0.01	-0.06	0.18**	-0.16	-0.02	0.17**
GERM			-0.14*	0.06	-0.10	0.15**	0.17**	0.14*	0.08	0.06	0.03
NTLS				-0.05	-0.18**	0.05	0.10	0.14*	-0.14*	-0.01	0.20**
SSTR					0.17**	0.22**	-0.11	-0.16**	-0.03	-0.13*	-0.23**
STOVR						0.07	-0.25**	-0.60**	0.13*	-0.17**	-0.68**
POLLEN							-0.09	-0.22**	0.02	0.00	-0.18**
DTM								0.39**	0.12*	0.23**	0.32**
DTF									-0.05	0.26**	0.66**
1000GWT										0.31**	0.15**
GRAINY											0.16**

WSC water soluble carbohydrates, CHL chlorophyll content, GERM germination (%), NTLS number of productive tillers, SSTR spike sterility, STOVR stover yield (kg/plot) POLLEN pollen viability, DTM days to maturity, DTF days to flowering, 1000gwt 1000 grain weight (g) and GRAINY grain yield (g/plot)

References

1. Burton G. W. and DeVane E. H. 1953. Estimating heritability in tall fescue (Festucaarundinacea) from replicated clonal material. Agron. J., 45: 478-481.
2. Lush J. L. 1949. Heritability of quantitative characters in farm animals. Proceedings of the Eigth International Congress of Genetics (Hereditas, Suppl. Vol., 1949, 357-375).
3. Dewey D. R. and Lu K. H. 1959. A correlation and path-coefficient analysis of components of crested wheatgrass seed production. Agron. J., 51: 515-518.
4. Fisher, R. A. and F. Yates: Statistical Tables for Biological, Agricultural and Medical Research. 6th Ed. Oliver & Boyd, Edinburgh and London 1963. X, 146 P.
5. Sumathi P., Sumnath M. and Veerabadhiran P. 2010. Genetic variability for different biometrical traits in pearl millet genotypes. E Plt Breed J., 4: 437-440.
6. Mukesh S. S., Tara Satyavathi C., Madan P. S., Singh S. P. and Barthakur S. 2013. Genetic variability and association studies in pearl millet for grain yield and high temperature stress tolerance. Indian J Dryland Agrics., 28: 71-76.
7. McIntyre C. L., Seung D., Casu R. E., Rebetzke G. J., Shorter R. A. and Xue G. P. 2012. Genotypic variation in the accumulation of water soluble carbohydrates in wheat. Funct Plant Biol J., 39: 560-568.

PS-IV-60

Evaluation of randomized yield trial against brown planthopper, *Nilaparvata lugens* (Stal) population of Punjab, India

P. S. Sarao* and G. S. Mangat

Rice Section, Department of Plant Breeding and Genetics, Punjab Agricultural University, Ludhiana; e-mail: preetento@pau.edu; preetento@gmail.com

Abstract

A set of one hundred and fourteen randomized yield trial lines were evaluated against brown planthopper under glass house conditions at the rice research laboratories of the Department of Plant Breeding and Genetics as per the standard seed box technique. Six lines were viz., 6315-2, 6004, 6662, 6670-1, 6653 were moderately resistant to BPH and damage score of these lines varied from 3.53±0.68 to 5.42±0.36.

Key words: Rice, brown planthopper, biotic stress, plant genetic resources

Rice, *Oryza sativa* L. is a staple food for people in 39 countries. Among rice growing countries India has the largest area and it stands second in production. In Punjab, rice is cultivated over an area of 28.45 lakh hectare with total production of 113.74 lakh tones [1]. Due to warm humid crop environment, insect-pests are of prime importance and contribute substantially to yield loss. Yield loss due to insect pests of rice has been estimated at about 25 per cent [2]. In recent years, brown planthopper (BPH), *Nilaparvata lugens* (Stal) has caused a big loss to rice production in Asian countries. Rice plant suffer 40-70 per cent yield loss if attacked large number of first instar nymphs of brown planthopper [3]. Farmers applied numbers of sprays to control this pest, which again affect tri-trophic interactions of pest and natural enemies. The cultivation of resistant varieties is one of the major strategies to minimise insect-pests loss to achieve good rice yield. Keeping this in mind, the present study was conducted to find out promising material in randomized yield trial lines against brown planthopper, *Nilaparvata lugens* (Stal) population of Punjab, India. This phenotyping will help to find resistant or moderate resistant lines which will be further used for pre-breeding work to develop BPH resistant lines.

A set of 114 randomized yield trial lines (RYTs) were screened against BPH under glass house conditions

during *kharif* 2013 at the rice research laboratories of the Department of Plant Breeding and Genetics as per the standard seed box technique [4]. TN1and Ptb33 has been used as susceptible and resistanr checks to BPH. The germplasm lines were sown randomly in rows at spacing of 3.5 cm in seed box (45 x 35 x 10 cm) containing nutrient rich well puddled soil, each row having 10 seedlings. There were three replications for each line and these were infested at 12 day old age with 2nd-3rd instar nymphs @ 6-8 nymphs per seedling. Damage score on each seedling was scored on 0-9 scale when 90-100 per cent plants of TN1 were dead following Standard Evaluation System (SES) of rice [5]. Mean damage score of each line was classified as resistant (0 to 3.49), moderately resistant (3.50-5.49) and susceptible (5.50-9.00) following the scale developed by Heinrichs [4].

Table 1. Screening of randomized yield trial lines against brown planthopper, *Nilaparvata lugens* (Stal) population of Punjab, India

Mean damage score (0-9)	BPH reaction	Germplasm designation
0-3.49	R	Nil
3.50-5.49	MR	6315-2, 6004, 6662, 6670-1, 6653
5.50-9.00	S	108 lines

R= Resistant; MR= Moderately resistant; S= Susceptible

The BPH damage score among different germplasm lines varied from 3.53±0.68 to 9.00±0.00, while the damage score of resistant and susceptible check was 1.20±0.35 and 8.47±0.50, respectively (Table 1). Six lines were moderately resistant to BPH (Table 1). The damage cross of these moderately resistant lines varied from 3.53±0.68 to 5.42±0.36 (Table 1).

References

1. Anonymous. 2014. Package of practices for crops of Punjab (Kharif 2011). Directorate of Extension Education, PAU, 3 p.
2. Bae S. H. and Pathak M. D. 1970. Life history of *Nilavarpata lugens* (Homoptera: Delphacidae) and susceptibility of rice varieties to its attacks. Ann. Ent. Soc. Am., 63: 149-155.
3. Dhaliwal G. S., Jindal V. and Dhawan A. K. 2010. Insect pest problems and crop losses: changing trends. *Indian J. Ecol.,* 37: 1-7.
4. Heinrichs E. A., Medrano F. D. and Rapusas H. R. 1985. *Genetic evaluation for insect resistance in rice.* International Rice Research Institute, Los Banos, Philippines, 365pp.
5. Anonymous. 1996. Standard Evaluation System for Rice. 4th edition. International Rice research Institute, Philippines. 30-31 pp.

PS-IV-61

Differential expression of resistance in maize genotypes to shoot fly, *Atherigona naqvii* infestation in spring season

Jawala Jindal*, Dulcha Singh Brar[1] and M. S. Grewal

Department of Plant Breeding and Genetics,[1] Department of Entomology, Punjab Agricultural University, Ludhiana; e-mail: jawalajindal@pau.edu

Abstract

The host plant resistance holds a good potential for the management of shoot fly, *Atherigona naqvii* Steyskal in spring maize. The leaf injury incidence at 20 days after germination (DAG) the remaining genotypes did not give any clear cut differential host plant reaction. This might be due to the inherent capacity of different cultivars to recover from the leaf injury

i.e. tolerance. However, the differences were evident on the basis of deadhearts incidence in this regard that too at 20 DAG only. On this basis, genotypes were characterized as susceptible Parkash, PMH 2 and LM 16 (21.48–23.57 %); least susceptible JH 3459 and JH 3956 (10.49 & 10.95 %) and as intermediate CM 143, PMH 1 and JH 31244 (15.16–16.70 %) in terms of their susceptibility to *A. naqvii*.

Key words : *Atherigona*, maize, resistance, shoot fly, tolerance

The shoot fly, *Atherigona naqvii* Steyskal is the key pest of spring sown maize in Punjab. The large scale cultivation of spring maize emphasized the need to develop integrated pest management (IPM) strategies for shoot fly. The seed and soil application of insecticides is primarily adopted for its control but the exploitation of host plant resistant holds a good potential for the management of shoot fly. The maggots of shoot fly attack the emerging seedlings by feeding on the whorl leaves causing leaf injury and deadhearts [1]. The different cultivars are categorized for their reaction to shoot fly on the basis of leaf injury and deadhearts incidence. But the degree of deadhearts formation depends on the inherent capacity of different cultivars to recover from the leaf injury with time. The recording of shoot fly incidence at different times and type of injury observed may results in overlapping of resistant reaction of different genotypes to shoot fly at various locations. To develop crop cultivars with durable resistance to insect pests, it is important to identify germplasms with definite degree of resistance. So, the present studies were planned to study the variability in expression of resistance reaction in maize genotypes to shoot fly infestation with time and to find out the appropriate time and type of injury for categorization of different cultivars.

The eight maize genotypes including 6 hybrids (JH 3459, PMH 2, JH 31244, JH 3956, PMH 1 and Parkash) and 2 inbred lines (LM 16 and CM 143) with varying level of susceptibility to *A. naqvii* were screened to study their relative expression of resistance during spring season 2011 and 2012. The genotypes JH 3459 and CM 143 are reported as less susceptible, while PMH 2, Parkash and LM 16 as highly susceptible to shoot fly [2]. The test genotypes were sown in R.B.D. with 3 replications in plots of 5 rows with 3 meter length. The optimum shoot fly population in field was ensured by broadcasting the moistened fish-meal @ 50 g per m^2 on emergence of seedlings [2]. The leaf injury and deadhearts incidence was recorded on whole plot basis at 5, 10, 15 and 20 DAG to work out per cent infestation. The data on infestation parameters was analyzed using ANOVA and the different treatment means were separated by least significant differences test (LSD) at p=0.05.

At 5 days after germination (DAG) the deadhearts incidence was low. The leaf injury incidence was maximum in the hybrid Parkash and minimum in CM 143 during both the years (Table 1). However, leaf injury incidence in Parkash and CM 143 variably overlapped with other genotypes. At 10 DAG, leaf injury incidence was maximum in JH 31244 and Parkash during 2011 and 2012, respectively. It was again overlapping in different genotypes. The deadhearts incidence was maximum in susceptible hybrids Parkash and PMH 2 during both the test years. It was minimum in JH 3956 in 2011 and CM 143 in 2012. But the remaining genotypes formed a medium group. Hybrid PMH 1 was on par with less susceptible hybrid JH 3956 in 2011 and with susceptible hybrid Parkash during 2012, so no clear cut conclusions were drawn upto 10 DAG. The differential reaction in test genotypes to deadhearts incidence due to shoot fly attack started appearing at 15 DAG. The leaf injury was maximum in JH 31244, followed by susceptible hybrids Parkash and PMH 2. During 2011, it was minimum in hybrid JH 3459, JH 3956 and inbreds CM 143 and LM 16. The hybrid PMH 1 was on par with both the above groups. Similarly in 2012, less susceptible hybrids JH 3459 and JH 3956 were on par with the highly susceptible hybrids PMH 2 and Parkash. The deadhearts incidence was maximum in PMH 2, Parkash and LM 16; and minimum in JH 3956 and JH 3459 during both the years. But genotypes PMH 1, JH 31244 and CM 143 showed differential susceptible and overlapping reaction to both the groups during different test years. At 20 DAG, The leaf injury incidence was maximum in Parkash, JH 31244 and PMH 2; and minimum in JH 3459, CM 143 and JH 3956 during both the years. However, the leaf injury incidence in susceptible inbred LM 16 was on par with less susceptible genotypes. However, the clear cut differential reaction of the test genotypes in terms of deadhearts incidence became evident at 20 DAG. During both the years the deadhearts incidence being maximum in Parkash, LM 16 and PMH 2 formed a susceptible group. The hybrid JH 3956 and JH 3459 with minimum incidence formed the least

susceptible group. The hybrid PMH 1, CM 143 and JH 31244 were found to be intermediate in reaction to *A. naqvii* infestation.

In pooled analysis of 2011 and 2012 also, the leaf injury incidence revealed that except for the maximum susceptible hybrid Parkash, all the remaining genotypes did not give any clear cut differential host plant reaction (Table 1). However, the differences were evident on the basis of deadhearts incidence in this regard. The deadhearts incidence was maximum in susceptible genotypes Parkash, PMH 2 and LM 16 (21.48–23.57 %) ; and minimum least susceptible JH 3459 and JH 3956 (10.49 & 10.95 %). The other genotypes i.e. CM 143, PMH 1 and JH 31244 (15.16–16.70 %) formed the intermediate group in terms of their susceptibility to *A. naqvii*. In the present studies, even at 20 DAG the overlapping results with respect to leaf injury incidence were seemed to be due to the inherent capacity of different cultivars to recover from the leaf injury i.e. tolerance. However, the differences in deadhearts formation clearly indicated their relative susceptibility to shoot fly. Moreover, the deadheart counts is easy, quick and helpful in assessing the relative reaction of genotypes as it gives approximate idea about the total loss of plant population and yield [3]. So, during screening of maize germplasm against *A. naqvii* in spring season the categorization of germplasm should be based on deadhearts counted after 20 days of germination.

Table 1. Incidence of shoot fly, *Atherigona naqvii* on the different test maize genotypes during 2011 and 2012

Year: 2011	Per cent mean leaf injury and deadhearts incidence at								Pooled mean* LI
	5 DAG		10 DAG		15 DAG		20 DAG		
Genotype	LI	DH	LI	DH	LI	DH	LI	DH	
JH 3459	6.06	0.97	14.09	6.35	15.96	7.34	16.61	7.98	20.45
JH 3956	7.99	2.21	16.65	5.37	22.06	5.66	19.39	6.99	21.84
JH 31244	11.05	1.33	24.44	7.98	29.59	10.98	25.61	12.32	26.06
PMH 1	10.38	1.17	24.41	7.35	23.98	9.36	21.72	10.73	25.97
PMH 2	5.97	3.08	16.45	11.99	27.23	15.27	23.56	17.27	26.62
PARKASH	12.33	3.01	23.68	12.68	26.01	14.65	28.01	15.65	33.07
LM 16	3.34	1.97	8.96	10.75	19.37	14.65	21.01	16.33	23.13
CM 143	2.36	1.10	6.23	8.14	17.83	9.77	16.99	11.49	18.18
CD (p=0.05)	2.72	NS	6.04	3.03	6.48	2.83	5.77	3.32	4.47
Year: 2012	5 DAG		10 DAG		15 DAG		20 DAG		Pooled mean* DH
Genotype	LI	DH	LI	DH	LI	DH	LI	DH	
JH 3459	4.79	0.00	7.83	5.02	30.75	12.30	24.29	12.99	10.49
JH 3956	4.27	0.00	8.60	3.99	31.94	13.43	24.30	14.91	10.95
JH 31244	5.70	0.00	9.41	4.89	39.27	18.55	32.51	21.08	16.70
PMH 1	5.10	0.20	9.50	5.88	35.96	18.96	30.23	19.98	15.35
PMH 2	8.61	0.00	10.14	7.00	40.14	22.87	35.67	25.76	21.52
PARKASH	9.29	0.42	10.91	7.38	41.92	28.45	38.13	30.49	23.57
LM 16	8.28	0.65	7.07	4.85	26.52	23.08	25.26	26.64	21.48
CM 143	3.78	0.22	5.31	2.92	23.94	17.75	19.37	18.84	15.16
CD (p=0.05)	3.53	NS	3.27	1.85	11.70	5.99	7.37	5.00	2.87

*Mean incidence of both the years recorded at 20DAG; LI= leaf injury, DH= deadhearts

References

1. Kumar V. and Kanta U. 2012. Management of insect pest complex in maize. *In*: Theory and Practice of Integrated Pest Management. (eds. R. Arora, B. Singh and A. K. Dhawan). Scientific publishers, Jodhpur, 338-369.
2. Jindal J., Hari N. S., Grewal M. S. and Chawla J. S. 2007. Evaluation of different genotypes against shoot fly, *Atherigona naqvii* Steyskal in spring sown maize. Crop Improv., 34: 160-162.
3. Sharma V. K. and Singh J. M. 1975. Screening for resistance to *Atherigona* spp. in spring sown maize. Indian J. Ent., 37: 39-43.

PS-IV-62

Fusarium wilt resistance in wild derivative lines of chickpea from an interspecific cross

Amandeep Kaur[1], Vineet K. Sharma[1], Asmita Sirari, Livinder Kaur, Gursahib Singh[*] Sarvjeet Singh and Inderjit Singh

Department of Plant Breeding and Genetics, [1]Department of Plant Pathology, Punjab Agricultural University (PAU), Ludhiana 141 004, Punjab; e-mail: gursahibsingh@outlook.com

Abstract

A set of derivative lines from an interspecific cross between *Cicer arietinum* and *C. pinnatifidum* developed at our centre is an excellent pre-breeding material that needs further characterization for several other traits such as Fusarium wilt resistance. Out of 91 lines, 2 lines *i.e.* GLW-59 and GLW-107 were found free from wilt; 37 lines were found moderately resistant; 32 lines were found susceptible and 18 lines were found highly susceptible.

Key words: Chickpea, interspecific derivatives, resistance fusarium wilt

Fusarium wilt caused by *Fusarium oxysporum* f.sp. *ciceris* (Padwick) Matuo and K. Sato is major constraint in successful cultivation of chickpea in North western plains of India. The disease has potential to cause 10-100 per cent yield losses [1]. Persistence of pathogen in soil over the years even in the absence of host renders its control difficult [2]. Resistance breeding is the most effective method for management of chickpea wilt. Despite of extensive screening of chickpea germplasm for wilt resistance, few cultivars like WR- 315, with broad spectrum resistance have been utilized in several breeding programme. Keeping in view the narrow genetic base in chickpea, identification of genetically diverse sources of wilt resistance is urgently needed. A set of wild derivative lines from an interspecific cross between *Cicer arietinum* and *C. pinnatifidum* developed at our centre is an excellent pre-breeding material that needs further characterization for several other traits such as Fusarium wilt resistance.

A set of 91 wild derivatives lines from an interspecific cross between ICCV 96030 (*C. arietinum*) and *C. pinnatifidum* 188 was evaluated against Fusarium wilt following wilt sick plot method. Fifty seeds of each germplasm line were sown in the month of November along with susceptible check (JG-62), sown after every fourth derivative line. The sick plot showed uniform wilt sickness as susceptible check in whole plot started wilting one month after planting. The observations on the total number of plants germinated and the number of plants killed due to wilt was taken at regular intervals during the crop season and percentage wilt incidence was calculated. The disease reaction categories were assigned on the basis of per cent wilt incidence, following rating scale given earlier [3].

Table 1. Per cent wilt incidence of wild derivative lines

S.No.	Wild derivative lines	Wilt incidence %)	S.No.	Wild derivative lines	Wilt incidence %)
1.	GLW-3	-	48.	GLW-68	22.22
2.	GLW-4	40.00	49.	GLW-69	14.81
3.	GLW-5	100.00	50.	GLW-70	21.42
4.	GLW-6	33.33	51.	GLW-71	37.50
5.	GLW-7	30.00	52.	GLW-72	38.46
6.	GLW-9	21.05	53.	GLW-73	23.08
7.	GLW-10	37.50	54.	GLW-74	23.08
8.	GLW-11	15.38	55.	GLW-75	15.38
9.	GLW-14	27.27	56.	GLW-88	12.50
10.	GLW-15	53.85	57.	GLW-98	-
11.	GLW-16	80.00	58.	GLW-99	66.67
12.	GLW-17	100.00	59.	GLW-100	5.88
13.	GLW-19	71.43	60.	GLW-102	22.22
14.	GLW-21	35.71	61.	GLW-103	38.46
15.	GLW-22	33.33	62.	GLW-104	12.50
16.	GLW-23	38.46	63.	GLW-106	40.00
17.	GLW-24	19.05	64.	GLW-107	0.00
18.	GLW-25	18.18	65.	GLW-108	28.57
19.	GLW-26	30.43	66.	GLW-109	100.00
20.	GLW-27	33.33	67.	GLW-110	30.77
21.	GLW-28	7.14	68.	GLW-111	7.69
22.	GLW-29	20.00	69.	GLW-112	83.33
23.	GLW-30	11.76	70.	GLW-115	26.31
24.	GLW-31	21.43	71.	GLW-116	90.00
25.	GLW-32	22.22	72.	GLW-117	75.00
26.	GLW-33	28.57	73.	GLW-118	66.67
27.	GLW-35	18.18	74.	GLW-137	75.00
28.	GLW-36	35.29	75.	GLW-154	22.22
29.	GLW-38	15.79	76.	GLW-166	14.29
30.	GLW-39	33.33	77.	GLW-167	11.11
31.	GLW-41	41.18	78.	GLW-174	85.71
32.	GLW-42	25.00	79.	GLW-175	27.78
33.	GLW-44	6.25	80.	GLW-176	23.08
34.	GLW-48	19.05	81.	GLW-178	100.00
35.	GLW-51	9.09	82.	GLW-179	33.33
36.	GLW-53	40.00	83.	GLW-180	38.46
37.	GLW-57	15.79	84.	GLW-181	58.33
38.	GLW-58	5.88	85.	GLW-182	81.81
39.	GLW-59	0.00	86.	GLW-183	40.00
40.	GLW-60	27.78	87.	GLW-185	50.00
41.	GLW-61	14.29	88.	GLW-186	30.00
42.	GLW-62	15.38	89.	GLW-187	42.85
43.	GLW-63	26.67	90.	GLW-188	66.67
44.	GLW-64	6.67	91.	GLW-189	71.43
45.	GLW-65	22.22	92.	Control	100.00
46.	GLW-66	12.50			
47.	GLW-67	40.00			

- Not germinated

Out of 91 lines, 2 lines *i.e.* GLW-59 and GLW-107 were found free from wilt; 37 lines were found moderately resistant; 32 lines were found susceptible and 18 lines were found highly susceptible (Table 1). These lines have been previously evaluated against Ascochyta Blight (AB) and Botrytis Grey Mould (BGM) [4]. Few AB and BGM resistant lines *viz*., GLW 24, 28, 32, 51 and 69 showed moderate resistance to wilt. The identified wilt resistant derivative lines can serve as donors for further incorporation of wilt resistance into superior genetic background of chickpea.

References

1. Sharma K. D., Chen W. and Muehlbauer F. J. 2005. Genetics of chickpea resistance to five races of Fusarium wilt and a concise set of race differentials for *Fusarium oxysporum* f.sp. *ciceris*. Plant Dis., 89: 385-390.
2. Sharma K. D. and Muehlbauer F. J. 2007. Fusarium wilt of chickpea: physiological specialization, genetics of resistance and resistance gene tagging. Euphytica, 157: 1-4.
3. Nene Y. L., Haware M. P. and Reddy M. V. 1981. Chickpea diseases: Resistance screening technique. Information Bulletin No. 10, ICRISAT, Patancheru, India Pp 11.
4. Kaur L., Sirari A., Kumar D., Sandhu J. S., Singh S., Kapoor K., Singh I., Gowda C. L. L., Pande S., Gaur P., Sharma M., Imtiaz M. and Siddique K. 2012. Combining Ascochyta blight and Botrytis grey mould resistance in chickpea through interspecific hybridization. Phytopathologia mediterranea, 52: 163-172.

PS-IV-63

Assessment of genetic diversity In okra [*Abelmoschus esculentus* (L.) Moench]

Mamta Pathak* and Parbhat Kiran

Department of Vegetable Science, Punjab Agricultural University, Ludhiana 141 004; e-mail: mampathak@pau.edu

Abstract

The present was conducted to measure the genetic diversity among 28 diverse lines of okra. On the basis of D^2 values, 28 okra genotypes were classified into five groups (Table 1). Cluster II was the largest one with 20 genotypes, whereas, rest of the four clusters contained two genotypes each. The clustering of genotypes into different groups did not follow any specific pattern. For example, group I had genotypes originating from Ludhiana centre, whereas, entries originating from New Delhi and Uttrakhand were clustered together in group III. Cluster IV recorded highest average values for marketable yield, number of fruits per plant and protein content.

Key words: Okra, genetic diversity, YVMV, resistance

Okra [*Abelmoschus esculentus* (L.) Moench] is one of the most important vegetable crop grown for its tender fruits. It is a major summer and rainy season crop. For the improvement of yield and its contributing traits the information of genetic diversity available in germplasm is essential. Evaluation of germplasm lines for yield, its components traits and other economic attributes helps in the identification of lines which can be used as such in the development of superior cultivars or donors for the transfer of specific characters. For the want of an efficient procedure having high predictive potential, genetic diversity of parental lines is usually considered appropriate for the development of hybrids. Therefore the present was conducted to measure the genetic diversity among 28 diverse lines of okra.

Twenty eight lines of okra originating from diverse eco-geographical regions were grown in a randomized complete block design with three replications during rainy season at vegetable research farm of department of Vegetable Science. Plants were spaced 30cm in a row with row to row distance of 45cm. All the recommended

package of practices was followed to raise the crop. Data were recorded on five random plants per entry in each replication. The data recorded for 14 quantitative characters viz., days to first flowering, node at which the first flower appeared, days to first picking, marketable yield per plant (g), total yield per plant (g), number of fruits per plant, average fruit weight (g), plant height (cm), average fruit length (cm), days to first appearance of yellow vein mosaic virus (YVMV), YVMV incidence (%), protein content (%), total minerals (%), and mucilage content (%) were used to classify the okra lines based on Mahalanobis D^2 [1] statistics as explained by Rao [2].

On the basis of D^2 values, 28 okra genotypes were classified into five groups (Table 1). Cluster II was the largest one with 20 genotypes, whereas, rest of the four clusters contained two genotypes each. The clustering of genotypes into different groups did not follow any specific pattern. For example, group I had genotypes originating from Ludhiana centre, whereas, entries originating from New Delhi and Uttrakhand were clustered together in group III. Similarly, group II consisted of entries originated from diverse eco-geographical regions of the country. Therefore grouping of genotypes into different constellations were observed to be independent of their geographical origin. Similar results have been reported earlier [3-6]. Hence, it appears that geographical diversity may not be used as an index of genetic diversity.

Table 1. Inter and intra cluster values for 28 genotypes

Cluster	I	II	III	IV	V
I	**75.4**	640.97	1064.51	1273.98	1441.08
II		**156.81**	279.35	347.73	449.29
III			**57.1**	388.5	131.03
IV				**277.6**	443.88
V					**341.7**

Figures in the bold represent intra cluster distances.

Table 2. Cluster means for agronomic characters in okra

Characters	Days to 1st flowering	Node at which 1st flower appeared	Days to 1st picking	Marketable yield/ plant (g)	Total yield / plant (g)	Number of fruits/plant	Average fruit weight (g)
I	44.33	4.17	51.67	39.02	42.13	6.25	6.26
II	44.62	4.40	49.05	82.56	91.32	12.29	6.71
III	45.17	4.27	50.17	69.60	72.75	9.69	6.75
IV	43.17	4.43	47.84	139.21	155.08	20.35	6.80
V	43.67	3.93	47.50	76.81	81.41	11.76	6.74
Characters	Plant height (cm)	Average fruit length (cm)	Days to 1st appearance of YVMV	YVMV incidence (%)	Protein content (%)	Total mineral (%)	Mucilage content (%)
I	84.62	7.62	43.83	65.62	1.02	1.05	0.54
II	96.05	7.28	42.63	36.08	1.05	1.36	0.65
III	96.44	7.24	45.33	23.24	0.97	1.15	0.52
IV	93.43	7.38	39.83	25.65	1.26	0.96	0.63
V	93.11	7.12	44.67	17.98	0.93	1.03	0.65

This suggests that forces other than geographical separation are also responsible for divergence. Genetic drift and selection in different environments may cause greater diversity than geographical distance. Biotypes originating in particular habitat have different utility only for certain traits for which selection has been practiced. Therefore the varieties originating at the same place may have different genetic architecture or *vice versa* [5]. In

a previous study, some of the common genotypes exhibited the same clustering pattern as observed in the present investigation e.g. POS-1, POS-17, POS-9, Parbhani Kranti, VRO-22, VRO-21, Arka Abhay, KS-442, VRO-10, POS-27, Hissar Unnat, Selection-2 and Pusa-A-4. However some other entries displayed different clustering pattern like VRO-6, Punjab-8, IC-90185 and PB-266.

Inter and intracluster average D^2 values among the parental lines have been presented in Table 1. The maximum value for intercluster distance (1441.08) was observed between clusters I and V, followed by clusters I and IV (1278.98), I and III (1064.51), I and II (640.97), II and V (449.29) and so on. Genotypes POS-17 and POS-1 in the first cluster are likely to produce transgressive segregants upon hybridization with genotypes IC-90185 and Pusa Sawani belonging to cluster V. Minimum and maximum intracluster distances were observed within clusters III (57.1) and V (341.7), respectively. Cluster means for various traits studied in the present investigation have been depicted in Table 2. The range for cluster means for various traits is as follows: 43.0 to 45.17 (days to first flowering), 3.93 to 4.43 (node at which first flower appeared), 47.50 to 51.67 (days to first picking), 39.02 to 139.21 g (marketable yield per plant), 42.13 to 155.08 g (total yield per plant), 6.25 to 20.35 (number of fruits per plant), 6.26 to 6.80 g (average fruit weight), 84.60 to 96.44 cm (average plant height), 7.12 to 7.62 cm (average fruit length), 39.83 to 45.33 (days to first appearance of yellow vein mosaic virus disease), 17.98 to 65.62 % (YVMV incidence), 0.93 to 1.26 % (protein content), 0.96 to 1.36 % (total mineral content) and 0.52 to 0.65 % (mucilage content).

Cluster IV recorded highest average values for marketable yield, number of fruits per plant and protein content. Similarly cluster V exhibited lowest values for days to first picking and per cent virus incidence. Therefore, it may be rewarding to include VRO-6, Punjab-8, IC-90185 and Pusa Sawani in the breeding programmes for development of early, high yielding varieties with high protein and low per cent virus incidence.

References

1. Mahalanobis P. C. 1936. On the generalized distance in statistics. Proc. Nat. Inst. Sci., (India) 22: 49.
2. Rao C. R. 1952. Advanced Statistical Methods in Biometrical Research. Pp 390. John Wiley and Sons, Inc, New York.
3. Ariyo O. J. 1987. Multivariate analysis and the choice of parents for hybridization in okra (*Abelmoschus esculentus* (L.) Moench). Theor. Appl. Genet., 74:361-363.
4. Ghai T. R., Arora D., Jindal S. K. and Singh P. 2005. Assessment of genetic divergence based on nutritional quality and organic traits in okra [*Abelmoschus esculentus* (L.) Moench]. J. Genet. Breed., 59: 1-6.
5. Singh S. P. and Singh H. N. 1979. Genetic divergence in okra [*Abelmoschus esculentus* (L.) Moench]. Indian J. Hort., 51:166-170.
6. Singh S. P., Srivastva J. P., Singh H. N. and Singh N. P. 1977. Genetic divergence and nature of heterosis in okra. Indian J. agric. Sci., 47:546-549.

PS-IV-64

Feeding capacity of different larval instars of citrus leaf miner, *Phyllocnistis citrella* Stainton on Kinnow and rough lemon

Gurjeet Singh and D. R. Sharma*

Department of Entomology and *Fruit Science, Punjab Agricultural University, Ludhiana 141 004; e-mail: drajsharma@pau.edu

Abstract

The studies conducted at Punjab Agricultural University, Ludhiana during different seasons in 2013-14 on feeding capacity of citrus leaf miner on two hos plants namely *Citrus reticulate* (Kinnow) and Citrus jambhiri (rough lemon) indicated that overall nine length made by 3rd instar was maximum (2.93-3.17 cm) on both the hosts followed by 2nd (2.27-2.44 cm), 1st (1.35-1.41), 1st (1.35-1.41 cm) and 4th (0.88-1.23 cm) larval instar of Phyllocnistis citrella. Thus the larvae feed more during 2nd and 3rd instar duration but there was significant reduction in feeding during 4th instar.

Key words: Citrus, feeding, mine length, *Phyllocnistis citrella*

Citrus leaf miner is the most destructive pest which mostly attacks nurseries, young plantations and tender flushes with about 16 overlapping generations in a year and is reported in more than 80 per cent nurseries of India. The average infestation rate of citrus leaf miner varied from 17 to 57 per cent. Leaf miner feeds on epidermal tissues of the tender leaves by creating serpentine mines. These mines are shining silvery due to the entrapped air. As a result of mining, the leaves get distorted and crumpled. Newly hatched larvae mine into the leaf tissue and form galleries. The mature larvae settle down in enlargements of galleries near the leaf margin. By the time, they spin cocoons for pupation, the leaves get twisted or folded over and retarded the growth of plant, which caused reduction in yield of citrus. The growth of the seedlings was also checked considerably [1, 2]. Yield reduction in mature trees is uncommon, but has been reported in limes when heavily infested with citrus leaf miner. Mining of spring flush is more damaging than fall flush since the spring flush is primarily responsible for supporting fruit development. Young plants (three years of age or less) are especially susceptible to leaf miner damage. Severe damage to young trees may result in delayed maturity of 1 to 2 years. Its damage also encouraged the incidence and severity of citrus canker [3]. In addition to canker, the attacked leaves curled and provide shelter to various other insects of citrus (mealy bugs, dusky cotton bug and citrus psylla) against their natural enemies and adverse climatic conditions.

The mines made by the different larval instars in the leaves of *Citrus reticulata* (Kinnow) and *Citrus jambhiri* (rough lemon) were measured with the help of divider and scale. The observations were made from the hatching of eggs (in the form of dot mine) till the pupal formation. Ten leaves on each host were measured and data was recorded daily. The distance between two exuvial dots was considered as the feeding capacity of a particular instar. The larvae feed by making the mines into the leaves by killing the leaf tissues and which subsequently lead to curling

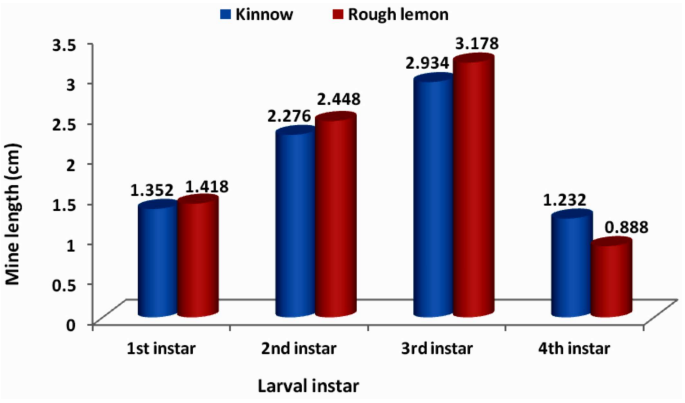


Fig. 1. Mine length fed by different larval instars of leaf miner on Kinnow and rough lemon

of leaves and stunted growth of young plants. Different instars made different mine lengths by feeding. It was observed that mine length made by 1st instar varied from 1.0- 1.5 cm on Kinnow and 0.9-1.6 cm on rough lemon during different seasons of the year i.e. spring (0.9-1.0 cm), summer (1.1-1.4 cm), rainy (1.3-1.6 cm), autumn (1.5 cm) and winter (1.4-1.8 cm) whereas the mine length of 2nd instar varied from 1.9-2.6 cm on Kinnow and 1.9-3.2 cm on rough lemon during different seasons of the year i.e. spring (1.9 cm), summer (2.5 cm), rainy (2.6-3.2 cm), autumn (2.1-2.3 cm) and winter (2.0-2.1 cm). The mean mine length of 3rd instar was minimum during winter season (2.3 cm) and maximum during rainy season (4.2 cm) (Table 1), whereas that of 4th instar varied from 0.86-1.5 cm on Kinnow and 0.6-1.1 cm on rough lemon. The average mine length made by different larval instars varied from 0.7-4.2 during different seasons of the year. The results indicated that larvae feed more during 2nd and 3rd instar duration (Fig. 1) but there was significant reduction in feeding during 4th instar.

Table 1. Feeding (based on mine length) by different instars of *P. citrella* on Kinnow and rough lemon during different months (2013)

Month	Larval instar	Mine length (cm) on host		
		Kinnow	Rough lemon	Mean
March-April	1st	1.05±0.05	0.90±0.08	0.98
	2nd	1.94±0.14	1.96±0.09	1.95
	3rd	2.53±0.13	2.46±0.18	2.50
	4th	0.86±0.12	0.64±0.08	0.75
Mean	1.60	1.50	1.65	
May-June	1st	1.40±0.05	1.16±0.07	1.28
	2nd	2.59±0.22	2.49±0.07	2.54
	3rd	2.88±0.23	2.94±0.25	2.91
	4th	1.16±0.16	0.87±0.25	1.02
Mean	2.00	1.86	1.94	
July-August	1st	1.34±0.20	1.63±0.04	1.49
	2nd	2.69±0.59	3.26±0.08	2.98
	3rd	3.90±0.82	4.63±0.09	4.26
	4th	1.50±0.31	1.13±0.14	1.32
Mean	2.35	2.66	2.51	
September-October	1st	1.53±0.30	1.59±0.35	1.56
	2nd	2.16±0.47	2.35±0.53	2.26
	3rd	3.03±0.62	3.52±0.78	3.27
	4th	1.51±0.25	0.96±0.21	1.24
Mean	2.05	2.11	2.08	
November-December	1st	1.44±0.32	1.81±2.11	1.63
	2nd	2.00±0.49	2.18±0.60	2.09
	3rd	2.33±0.58	2.34±0.56	2.34
	4th	1.13±0.29	0.84±0.26	0.99
Overall mean1.73	1.79	1.76		
Mean	1.95	1.98	2.00	

± SD= Standard deviation

References

1. Chadda R., Sharma D. R. and Dhaliwal H. S. 2008. Efficacy of neonicotinoids against leaf miner, *Phyllocnistis citrella* Stainton infesting nursery of rough lemon. J. Res. Punjab agric. Univ., 46: 37-40.
2. Sharma D. R. and Dhaliwal H. S. 2008. Efficacy and persistence of some new molecule against *Phyllocnistis citrella* on nursery plants. pp 246-55. *In*: Singh S, Shivankar V J, Srivastava A K, Vijaykumari N, Huchche A D, Singh I P, Ram L, Das A K and Rao C N (eds.) Proc Nat Symp Citriculture: Emerging Trends. National Research Centre for Citrus, Nagpur, Maharashtra.
3. Dhiman J. S., Batra R. C. and Sharma D. R. 2000. Synchronous attack of insect-pests and diseases in Kinnow nursery. pp 810-17. *In*: Shyam Singh and S P Ghosh (eds). *Proc Hi-Tech Citrus Mgmt*. National Horticulture Institute, Nagpur.

PS-IV-65

Host plants of citrus psylla, *Diaphorina citri* in Punjab

Hijam S. Devi*, D. R. Sharma[1] and H. S. Rattanpal[1]

Department of Entomology and *Fruit Science, Punjab Agricultural University, Ludhiana 141 004, Punjab; e-mail: shilahijam@gmail.com

Abstract

The studies on host plants of citrus psylla, Diaphorina citri Kuwayama were conducted at Punjab Agricultural University during 2012 amd 2013. A total of 129 citrus genotypes/cultivars and other plant species (annuals, and shrubs) were observed in the present study and out of these 47 plant species/genotypes had 0-5 individuals while 28, 49 and 5 plant species/ genotypes had 5-10, 10-20 and >20 individuals per shoot/leaf. The observations on the population of D. citri clearly indicated that citrus genotypes.cultivars were the main plant species to colonise the pests and >5 individuals per shoot/leaf were found on all Citrus species.

Key words: Citrus, host plants, Diaphorina citri

The psyllid, *Diaphorina citri* Kuwayama (Hemiptera: Psyllidae) is currently one of the most important pests of world citriculture. It was first reported in 1907 from Taiwan and is now well distributed across several countries. *Diaphorina citri* has been recorded on all the cultivated accessions of *Citrus* spp., *Murraya koenigii*, *Clausena lansium*, *Murraya exotica*, *Aegle marmelos*, *Limonia acidissima* and *Clausena excavate* [1]. It preferred to breed on *M. koenigii* (curry plant) when citrus cultivars were provided side by side [2].

The studies on the presence and abundance of *Diaphorina citri* populations were conducted from January to December during 2012 and 2013 on citrus genotypes/cultivars and other plant species available around the citrus orchards at Punjab Agricultural University, Ludhiana. The nymphal and adult populations of citrus psylla were recorded at 15 days interval. The nymphal population was recorded from 10 cm apical portion of a twig while the adult population of psyllid were recorded from underside of leaf lamina from 10 older leaves/plant. The plant species were identified. Nymphal and adult counts made at 15 days intervals were pooled annually. The citrus genotypes/cultivars and other plant species were then categorised as the population having 0, 1-5, 5-10, 10-20 and > 20 individual per shoot and leaf.

The results as revealed from Table 1 indicated that there were significant differences in abundance of *D. citri* on different genotypes/cultivars and other host plants. A majority of these annual host plants (Table 1) were found in the vicinity of citrus orchards and thus might not be preferred by *D. citri*. During the current studies, it was observed that psyllid population on *Murraya spp.* were observed only during spring season during both the years

when there was very high population on citrus species shoots and cannot be regarded as alternate host. Based on studies of *D. citri* in grapefruit and *M*. *paniculata,* it was reported that this pest did not prefer one host over the other [3, 4]. Other host plants such as *Murraya paniculata, Murraya exotica, Murraya paniculata, Aegle marmelos, Limonia acidissima* were found to be less colonised (1-5 nymphs and adults) by *D. citri*. Citrus psylla has been recorded on *M. koenigii* at Coimbatore and Pusa; *M. exotica* from Bangladesh, Punjab and Taiwan; on *Aegle marmelos* and *Limonia acidissima* from Maharashtra (George and Kandasamy, 1986) which corroborate the present study. During the current studies, it was observed that psyllid population on *Murraya* spp. were observed only during spring season during both the years when there was very high population on citrus species shoots and cannot be regarded as alternate host.

The observations on the population of *D. citri* (Table 1) clearly indicated that citrus genotypes/cultivars are the main plant species to colonise the pests and > 5 individuals per shoot/leaf were found on *Citrus* species only. Nova Mandarin, Brazilian Rangpur, Olinda Valencia, Texas Rangpur and Austrata were found highly susceptible. It has been observed that quality of the host plant can influence morphological and physiological variation. It has been observed that a total of 129 citrus genotypes/cultivars and other plant species were observed in the present study and out of these 47 plant species/genotypes had 0-5 individuals while 28, 49 and 5 plant species/genotypes had 5-10, 10-20 and >20 individuals per shoot/leaf.

Table 1. Average population of *D. citri* on citrus genotypes/cultivars and other plant species during 2012 and 2013

D. citri population/ 10 cm shoot and leaf*	Citrus genotypes/cultivars and other plant species
0	**Annuals:** *Acroclinum roseum, Althea roses, Alyssum maritimum, Calendula officinalis, Callistephus chinensis, Centaurea moschata, Delphinium ajacus, Dimorphotheca auriantiaca, Tropaeolum majus, Limonium sinuatum*.
	Shrubs: *Acalypha wilkinsiana, Artabotrys odorattissimus, Calliandra species, Cassia qlauca, Duranta repens/ D. plumeri, Hibiscus rosasinensis, Jasminum sarmbac, Jatropha pandurifolia*, *Lantana camara, Poinsettia pulchirrma, Thevetia peruviana*.
1-5	**Other plant species**: *Murraya paniculata, Murraya exotica, Aegle marmelos, Limonia acidissima*
	Citrus species
	Gou Tou, Benton, C-32, C-35, Rubidoux Doux, Volkamarina, Rangpur lime, NRCC-Rootstock, Falglo, Sunburst, Citron, Old Kinnow, Trovita, Pectinifera, Ruggopoda, South Africa Rangbue lima, Fortunella, Schaous Rough lemon, 58-III-IV-Rough lemon, KNRCC-Rootstock, Eureka Lemon, Ruby Nucellar.
5-10	**Citrus species**
	Kuharisha, U852, Carrizo, Star Ruby, C32A, Rhode Red, Calamondin, Ray Ruby, Cleopatra, Katazamir, Chetali Trifoliata, Florida rough lemon, Blood Red, Tharso, Lemon, Gonicoppae trifoliata, Hamlin, Lisbon lemon, Brazilian rough lemon, Khasi Mandarin, Okitsu wase, Indian Meyer Lemon, Long Kamquat, Mid-night Valencia, Rio Red Grapefruit, Fremont, Verna, Fukomoto.
10-20	**Citrus species**
	Sun Chu Sha Kat, Kinkoji, Rich 16-6, Troyer, Swingle, Valencia Salizonida, Valencia Late, Campbell Valencia, Abohar rough lemon, Kinnow, Rough lemon, Sohmyndong Rough lime, Nematanga Assam, Marisol, Clemenules, Nagpur rough lemon, Washington Navel, Rahuri Rangpur lime, Noreo Rangpur lime, Chase rough lemon, 14-9-13 Rough lemon, Assam Rough lemon, Hayer rough lemon, Coorg Mandarin, Mudhead Mandarin, Nagpur Seedless Mandarin, Nagpur Mandarin, Muscott, Ovari Mandarin, Pummelo, Miami Kumquat, Nagamo Kumquat, Pink Pummelo, White Pummelo, Ruby Red, Flame Grapefruit, Marsh Seedless, Pearl Tanglo, Foster, Dungan, Mosambi, Jaffa, Early Gold, Westin, Rocco Blood Orange, Cara Cara Navel, Saguni Blood Orange, Delta Valencia, Neo Hall Navel.
>20	**Citrus species**
	Nova Mandarin, Brazilian Rangpur, Olinda Valencia, Texas Rangpur, Austrata.

*Average population (adults and nymphs) of 2 years (2012-13) recorded at 15 days interval

References

1. Shivankar V. J., Rao C. N. and Singh S. 2000. Studies of citrus psylla, *Diaphorina citri* Kuwayama: A review. Agriculture review 21: 199-204.
2. George E. A. D. and Kandasamy C. 1986. Effect of various host plants on the biology of the psyllid, *Diaphorina citri* Kuwayama (Homoptera: Psyllidae). Pest Management 1:36-40.
3. Tsai James H., Wang Jin-jun and Lui Ying-Hong 2002. Seasonal abundance of the Asian citrus psyllid, *Diaphorina citri* (Homoptera: Psyllidae) in Southern Florida. Florida Entomologist 85: 446-51.
4. Tsai Y. P., Hwang M. T. and Wang H. C. 1984. *Diaphorina citri* on *Murraya paniculata*. Plant Protection Bulletin Taiwan 26: 285-87.

PS-IV-66

Selection and conservation of superior germplasm of *Eucalyptus tereticornis* Sm.

G. P. S. Dhillon*, Ashok Kumar and K. S. Sangha

Department of Forestry and Natural Resources, Punjab Agricultural University, Ludhiana 141 004 (Punjab); e-mail: dhillongps1@pau.edu

Abstract

In the present study, in the superior trees of *Eucalyptus* spp. were selected on the basis of three aspects: growth traits, stem traits and tolerance to gall insect by following the comparison tree method. Twenty six trees were selected and wood samples were collected at 2, 4, 6 and 8 meters from base. Various traits i.e. heartwood content, specific gravity, fibre length and fibre width, were also measured. The softwood cuttings from the coppice shoots were planted in rooting trays filled with vermiculite and placed in mist chamber having controlled conditions of humidity and temperature. Out of the selections, the cloning was possible only in 15 trees. Twelve ramets of each clone have been planted in hedge orchards for its conservation and one clone was planted in research trial at Bathinda. The present study revealed substantial variability among the genotypes. An examination of data revealed that genotype 4, 138 63, 81, 101, 137 and 143 ranked better growth for total height, whereas, genotype 57, 101, 142 and 143 showed higher growth for DBH. Genotype 55 and 67 were found very poor for height and DBH but they were found tolerant to gall wasp. These genotypes will be used for future breeding programme and for development of new clones.

Key words: Eucalyptus, selection, conservation, germplasm

Forests provide many benefits i.e. Timber, furniture wood, food, fuel wood, fibre, fodder, shelter etc. and serve man intangible benefits i.e. amelioration of environment, playing a vital role in carbon, hydrological and nutrient cycles. As per recent National Forest Policy has advocated to maintain 20 percent of geographic area in plains under tree cover. Agroforestry is promoted to enhance vegetative cover in Punjab. *Eucalyptus* has been adopted by farmers due to its adaptability, tolerance to harsh conditions, fast growth rate and variety of uses. Keeping in view the wide range of geographical distribution and the variation that exists, the genus provides ample scope for genetic improvement. There is a considerable genetic variation which can be exploited for the selection for fast growth, wood density, specific gravity and for adoptability to harsh growing conditions [1,2]. Selection of superior phenotypes, genetic testing and conservation of germplasm are the basis of any tree improvement programme.

The selections were made from 10 year old progeny trial (96 half-sib progenies) planted at PAU Ludhiana and from the farmer fields. The best trees from promising families of progeny trial were selected on the basis of three aspects: growth traits, stem traits and tolerance to gall insect but more attention was paid to tolerance characters. The selection from the farmer's field, were made by the comparison tree method. The observations

were recorded on candidate tree and also recorded on the next best five trees in the vicinity of the candidate tree. The superiority of candidate tree was calculated and compared over the mean of respective comparison trees.

The selected trees at Ludhiana were cut at stump height to promote coppice shoots. After felling of the selected trees at Ludhiana, wood samples were collected at 2, 4, 6 and 8 meters from base. Various traits i.e. heartwood content, specific gravity, fibre length and fibre width, were measured. The coppice shoots were used for the cloning. The softwood cuttings of length 8 to 10 cm were prepared and planted to rooting trays filled with vermiculite and placed in mist chamber having controlled conditions of humidity and temperature. The cuttings were kept under mist chamber for three weeks and were shifted in poybags. The plants were established in the hedge orchards.

On the visual basis, twenty six trees were identified. The data on morphology and stem traits *viz.* total height, diameter at breast height (DBH), straightness, and insect infestation of selected trees are given in Table 1. Genotype 57 recorded the maximum tree height (27.0 m) and the minimum was in genotype 67 (21.0 m). The maximum DBH was again found in genotype 57 (30.0 cm) and minimum was in genotype 55 (15.1 cm). The superiority for total height, and DBH were 12.5, and 42.9 per cent, respectively, in the genotype 57 than the control. From the straightness point of view genotype 57, 58, 98, 101, 127, 137 and 139 were found to be superior i.e. score 4 and genotype 59 and 62 were found to be inferior i.e. score 2. Seven genotypes *viz*. 57, 58, 98, 101, 127, 137 and 139 found more superior than control. Eighteen genotypes were found to be free from gall insect attack, however, genotypes 4, 58, 79, 99, 101, 130, 138 and 139 showed incidence of gall insect. Ten plus trees were selected from agricultural field plantations and from Research Station, Bathinda following comparison tree method. The superiority of selections over the adjoining trees varied from 12.24 to 49.38 per cent for tree height and from 1.87 to 61.50 per cent for diameter.

Table1. Variation in morphological characters of selected genotypes of *E. tereticornis* from progeny trial at PAU, Ludhiana

Genotype	Total height (m)	DBH (cm)	Straightness score	Insect attack
4	24.0	23.4	3	Moderate
7	25.5	21.3	3	Nil
26	25.0	20.0	3	Nil
55	22.5	17.1	3	Nil
57	27.0	30.0	4	Nil
58	24.5	21.0	4	Little
59	24.0	22.3	2	Nil
62	25.0	20.0	2	Nil
63	25.5	23.2	3	Nil
67	21.0	17.4	3	Nil
71	24.0	19.6	3	Nil
79	25.0	19.4	3	Little
80	23.0	19.9	3	Nil
81	25.5	19.1	3	Nil
82	24.0	22.0	3	Nil
98	23.0	21.3	4	Nil
99	23.0	17.3	3	Moderate
101	25.5	29.0	4	Little
127	25.0	20.8	4	Nil
130	25.0	22.6	3	Little
137	26.0	22.2	4	Nil
138	24.0	22.9	3	Moderate
139	25.0	19.2	4	Moderate
142	25.0	28.4	3	Nil
143	26.1	25.8	3	Nil
Control	24.0	21.0	3	Nil

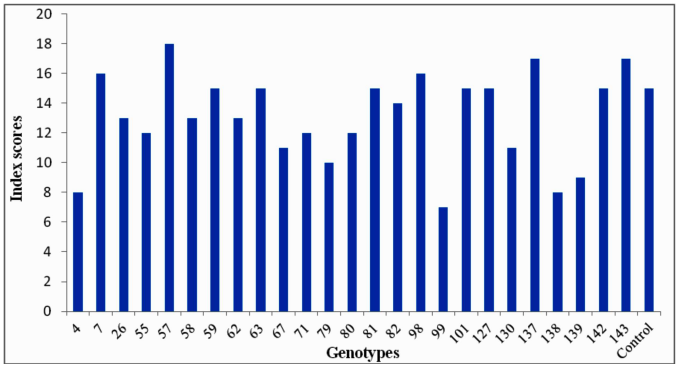


Fig. 1. Comparative index scores of 26 genotypes of *E. tereticornis*

Selection of plus trees has been accepted as preliminary and easy step in the development of progressive tree improvement programme. The perusal of the data showed that gall insect incidence was found across the state. The results were in accordance with early study [3]. Similar results for the selection of plus tree was reported in [4] and in *Dalbergia sissoo* Roxb. [5]. In the present study plus tree were selected through the comparison tree method from plantations.

The selected trees were classified on the basis of index scores Fig. 1. Index scores ranged from 7 to 18 among the genotypes. The highest index score (18) was observed in genotype 57 which indicated its overall superiority, closely followed by genotype 137, 143, 7 and 98. Seven genotypes *viz*., 59, 63, 81, 101, 127, 142 and control had got score 15. Minimum index score of 7 was found in genotype 99.

The total score of all selections were presented in Fig. 4.1. Similar study for index scoring analysis has been done in *Populus deltoides* [6] and in *Eucalyptus* clones [7].

The coppice shoots from the stumps of selected trees emerged after two months. Out of the selections, the cloning was possible only in 15 trees. After initial trials, the best season found was March-April and September-October. Twelve ramets of each clone have been planted in hedge orchards for its conservation and one clone was planted in research trial at Bathinda. The cloning of *E. grandis* and *Corymbia* spp was also successful.

References

1. Dhillon G. P. S. and Singh A. 2010. Variation in growth traits among progenies of *Eucalyptus tereticornis* Sm. Under flood plain conditions of Punjab. Indian J Agrofor 12: 91-94.
2. Sidhu D. S., Dhillon G. P. S. and Singh B. 2005 Study on the tree improvement of *Eucalyptus tereticornis* in Punjab. *Proc Exotics in Indian Forestry Symp.* Department of Forestry and Natural resources, PAU, Ludhiana, India.
3. Sangha K. S., Dhillon G. P. S. and Kumar V. 2011. *Leptocybe invasa* (Hymenoptera: Eulophidae), An invasive gall inducer of *Eucalyptus* in Punjab. In Dhawan, Sharma D R and Kumar R (eds) *Pest Management for Food Security and Environment Health*. Extended Abstracts 3rd Congress on Insect Science. Pp 32. PAU Ludhiana.
4. Sidhu D. S. 1993. Selection of plus tree and their progeny testing in *Eucalyptus* hybrid. Indian For 119: 744-52.
5. Yadav M. K, Dhillon R. S. and Singh V. P. 2005. Plus tree selection and progeny testing in Shisham (*Dalbergia sissoo* Roxb.). Legume Res 28: 55-58.
6. Dhillon G P. S. 2004. Studies on genotype x environment interaction of poplar (*Populus deltoides*) in Punjab. Ph. D. Thesis, Forest Research Institute University, Dehardun.
7. Kumar R, Bangarwa K S and Verma R C (2007) Genetic variability among different *Eucalyptus tereticornis* clones. Ann. For., 15: 201-06.

PS-IV-67

Evaluation of grape genotypes under North-Indian conditions

N. K. Arora*, M. I. S. Gill, Gagandeep Kaur and Navjot Gupta

Department of Fruit Science, Punjab Agricultural University, Ludhiana 141 004; e-mail: naresh_arora@pau.edu

Abstract

A range of grape varieties suitable for table and processing purpose were evaluated during the period under study. Yield was found to be maximum in grape variety Superior Seedless. The T.S.S was found to be highest in ISAB followed by Himrod.

Key words: Grapes, germplasm evaluation, N-Indian conditions.

Most of the commercial grape varieties grown in tropical regions of India are not suitable for commercial cultivation under N-Indian conditions. This primarily is due to extreme hot and cold weather conditions prevailing in this region of the country. The pre-monsoon rains especially in Punjab and its adjoining states followed by couple of hot humid months further limit commercial grape cultivation in these areas. The grape variety Perlette, which takes minimum number of days (90-100 days) from flowering to fruit harvest, is hence considered suitable and thus, is the only variety grown on commercial scale in N-India. Keeping in view, the limited gene pool vis-à-vis adaptability of grapes under N-Indian conditions, a strong need was felt to evaluate wide range of grape germplasm with respect to growth, yield and quality parameters.

Nine grape varieties trained on Y-system and planted in 2008 at Fruit Research Farm, Department of Fruit Science, PAU, were considered as plant material for the study. All the varieties/ hybrids were uniformly pruned at 3-4 bud level, during months of January-February. The recommended fertilizer doses and irrigation schedule was followed during the period of investigation. Four vines of each variety formed one replication. The treatment was replicated thrice in a randomized block design. The observations on ripening time, clusters/ vine, weight of cluster and on biochemical parameters like T.S.S and acidity were recorded as per standard procedure [4]. The data obtained was pooled and analyzed as per standard designs as described by Gomez and Gomez [2].

Among the different varieties, the maximum trunk girth was recorded in Merlot (18.7 cm), followed by Tannat (17.4cm) and Shiraz (17.4 cm). The minimum trunk girth (7.0 cm) was recorded in cultivar A35-1. The number of mature canes/vine varied from a minimum of 10.0 in A 35-1 to maximum of 40.0 in Merlot. The number of fruitful canes/vine was also maximum in Merlot. The period of panicle appearance ranged from 7 days in Cardinal and A 35-1 to 14 days in A 23-2 and Chardonny. The time of anthesis in different varieties ranged from end March (ISAB) to upto third week of April in A 23-2. Among the varieties evaluated, the earliest fruit set (5th April) was in ISAB and Superior Seedless followed by Chardonny (10th April). A 23-2 was last (23rd April) to have fruit set. The time of fruit ripening also varied among different varieties.

Himrod took minimum number of days (125) to ripen after pruning, while Tannat took maximum number of days (160) for ripening. The variability in ripening time of different varieties and hybrids during evaluation of grape germplasm has bveen described earleier [3, 4].

The significantly higher (68.0) number of bunches/ vine were obtained in ISAB. The least number of bunches/ vine (21.0) were obtained in A35-1. The grape variety A 23-2 had bunch number (28.0) which was significantly at par with Tannat (30.0). Similar type of variability with respect to yield and bunch weight was also been reported earlier [5, 6] in different grape varieties. The significantly higher bunch weight (486.6) was obtained in Superior Seedless. The least bunch weight (101.1) was obtained in cultivar Tannat. The maximum yield per

plant (23.8 kg) was obtained in Superior Seedless. The variety A 23-2 had minimum yield per plant (2.2 kg), which was at par with yield obtained in cv. A35-1 and Tannat. All varieties exhibited significant variation in their berry characteristics (Table I). The grape variety Cardinal had significantly higher weight of berries (575.0 g) as compared to other varieties/ hybrids. While the minimum berry weight (142.0 g) was recorded in variety Chardonny. Largest berry size was noted in the variety Cardinal(22.1 mm), whilst it was smallest (13.1 mm) in Chardonny.

The maximum T.S.S (17.9) was obtained in ISAB followed by Himrod (17.1). Significantly lowest T.S.S (14.0)was obtained in cv A35-1. These findings are in corroboration with findings of Thakur *et al* (2008), Ghosh *et al* (2008) who had also reported that different varieties of grapes show variation among T.S.S, acidity and T.S.S/ acid ratio. The average number of seeds/ berry ranged from no seeds in Superior Seedless to 3.5 seeds in ISAB.

Table 1. Fruit characteristics of new grape varieties at P.A.U, Ludhiana

Variety	Bunches/ vine (No.)	Bunch weight (g)	Yield/ plant (Kg)	Weight of 100 berries (g)	Berry diameter (mm)	T.S.S. (%)	Av. No. of seeds/ berry	Fruit ripening (DAP*)
Shiraz	55.0	190.8	10.5	168.8	13.0	15.0	2.4	138
Merlot	47.0	150.0	7.0	320.0	17.0	17.0	3.0	144
A 23/2	28.0	187.8	2.2	334.0	17.0	15.8	2.0	137
Chardonny	52.0	135.6	7.1	142.0	13.1	15.6	2.4	148
Convent Large Black	65.0	227.5	14.8	412.0	19.6	15.7	2.4	140
Tannat	30.0	101.1	3.0	207.3	14.8	14.1	2.9	160
ISAB	68.0	219.3	14.9	387.6	19.0	17.9	3.5	128
Himrod	64.0	180.0	11.5	190.0	14.9	17.1	2.2	125
Cardinal	49.7	157.1	7.7	575.0	22.1	14.1	1.8	137
Superior Seedless	49.0	486.6	23.8	378.0	17.6	17.0	0.0	130
A35-1	21.0	134.6	2.8	180.0	15.1	14.0	2.0	137
LSD (p=0.05)	7.3	21.8	2.1	32.2	3.2	1.7	0.78	7.4

* Days after Pruning

References

1. A.O.A.C. 1985. Official methods of analysis. Association of Official Agricultural Chemists, Washington D.C USA.
2. Gomez K.A and Gomez AA 1984. Statistical Proceeding for Agriculture Research (2nd edn.), John Wiley and sons Inc., New York
3. Kumar R and Rajan S 2008. Grape cultivars Flame Seedless and Pusa Navrang can be commercially grown in North Indian conditions. Acta Hort. 785: 69-72.
4. Ghosh SN, Tarai R and Pal PP 2008. Performance of eight grape cultivars in laterite soil of West Bengal. Acta Hort. 785: 73-78.
5. Gill MIS and Arora N K 2009. Performance of different grape varieties under N-Indian conditions. Indian J. Ecol. 36 (1): 15-17
6. Thakur A, Arora NK and Singh SP 2008. Evaluation of some grape varieties in the Northwest India. Acta Hort. 785: 79-83.

PS-IV-68

Collecting genetic resources of locally important potential species: Scope and future thrust

K. C. Bhatt*, Soyimchiten, N. S. Panwar and O. P. Dhariwal

Division of Plant Exploration and Germplasm Collection, National Bureau of Plant Genetic Resources, New Delhi 110012; e-mail: kcbhatt@nbpgr.ernet.in

Abstract

In India, agriculture is major source of livelihood of rural population while majority of them are not assured for food security due to small land holdings and poor soil productivity.There are a number of valuable plants consumed locally for various purposes growing in diverse agro-ecological regions could be important source to exploit. Keeping this in view, some of the region specific potential species identified are *Allium stracheyi* (Central Himalayan region); *Allium tuberosum, Parkia timoriana, Hodgsonia heteroclita* (north-eastern hill region); *Brassica tournefortii, Prosopis cineraria* (arid region); *Basella* spp.*, Canavalia ensiformis, Coccinia grandis, Ipomoea aquatica, Eurale ferox*, *Trapa natans*, *Moringa oleifera, Murraya koenigii,* (eastern and southern regions). So far limited collections have been made in these species; hence intensive collections of these resources from unexplored/ underexplored regions on priority are required.

Keywords: Collection, genetic resources, potential species

The number of plant species used by humans around the world is only one third of the number of species of crops that would meet specific needs. While there are many locally important plant(s)/crop(s) and wild species whose potential not been fully realized, grown traditionally for various purposes but are categorized under neglected species [1, 2]. In addition to this, over 9500 species of ethno-botanical importance have also been reported from Indian gene centre. Among these, some of them are restricted to a small region and are cultivated in small pockets and being consumed locally. Though these crops are not supposed to be competitive with well known crop species, however they play crucial role to sustain the food security, economy and food culture of the rural poor [3]. These species are also supposed to be more resilient than staple crops, because they are better adapted to grow in marginal land even under adverse soil and climatic conditions [4]. Besides, these are rich sources of nutrients and constitute an important part of the local diet of communities providing valuable nutritional components, which are often lacking in staple crops [5]. Decline of these important resources may erode the genetic base and can prevent the utilization of useful traits in crop improvement. Continued focus on crop diversification through exploitation of locally important potential species occurring in diverse regions of the country is need of the hour. Thus keeping in view the advantages of locally important species used as food at local level, their collection from diverse habitat is essential because they could become excellent source for useful gene source.

The locally important potential species were identified using personal experiences as well as observations by other explorers whosoever visited different agro-ecological regions for germplasm collecting. Tribal inhabited zones, rural and remote localities were visited during explorations to record the utilization pattern and local sale price of these resources. The germplasm of identified species was assembled through crop specific and multi-crop explorations either by independently or collaborative mode and information was gathered through interaction with farming, rural and tribal communities. To know the collection status, passport and other information were used from the database of Plant Exploration and Germplasm Collection Division/ plant collection reporter, annual reports of National Bureau of Plant Genetic resources, New Delhi, annual reports of All India Coordinated Research Project on Underutilized Crops and other published literature.

National Bureau of Plant Genetic Resources (NBPGR) being a nodal organization for management of genetic resources of different agri-horticultural crops and their wild relatives has collected over 2.75 lakhs accessions of different crops and wild species including many locally important potential species in collaborative mode from different agro-ecological regions of country. Some of the potential edible species identified are *Allium stracheyi* and *Cleome viscosa* in Central Himalayan region; *Allium tuberosum, Eryngium foetidum, Parkia timoriana, Hodgsonia heteroclita* and *Elaeocarpus floribundus* in north-eastern hill region; *Brassica tournefortii, B. Nigra* and *Prosopis cineraria* in arid region; *Basella alba, Canavalia ensiformis, Portulaca oleracea, Trichosanthes dioica, Coccinia grandis, Ipomoea aquatica, Mucuna pruriens* var. *utilis, Eurale ferox*, *Trapa natans*, *Moringa oleifera* and *Murraya koenigii* in eastern and southern region. Well documented information is available on genetic resources of less known cultivated food plants [6] but the number of accessions collected and areas surveyed in locally important food crops/species is limited, *viz. Coccinia grandis* (62 acc.) mainly from Kerala, Odisha and Tamil Nadu; *Lepidum sativum* (28 acc.) from Himachal Pradesh; *Moringa oliefera* (126 acc.) from Andhra Pradesh, Jharkhand, Karnataka and Himachal Pradesh; *Murraya koenigii* (46 acc) from Andhra Pradesh and Himachal Pradesh; *Portulaca oleracea* (19) from Maharashtra; *Trichosanthes dioica* (117 acc.) from Assam, Odisha, Uttar Pradesh and West Bengal; *Cleome viscose* (37 acc.) from Gujarat, Rajasthan and Uttarakhand; *Brassica tournefortii* (12 acc.) from Rajasthan and Haryana; *Allium tuberosum* (15) from Arunachal Pradesh.

The above account indicates that there is a need of intensive collection in *Allium stracheyi*, *Amaranthus spinosus, Cleome viscosa* and *Myrica esculenta* from Uttarakhand, Himachal, Sikkim and Jammu & Kashmir; *Allium tuberosum, Eryngium foetidum, Parkia timoriana, Hodgsonia heteroclita, Moghania vestita, Pachyrrhizus erosus, Elaeocarpus floribundus* from all states of NEH region; *Brassica tournefortii, B. nigra, Prosopis cineraria* from parts of Rajasthan, Haryana and Gujarat; *Basella alba, Canavalia ensiformis, Portulaca oleracea, Trichosanthese dioica, Coccinia grandis, Ipomoea aquatica, Mucuna pruriens* var. *utilis, Eurale ferox*, *Trapa natans*, *Moringa oleifera, Murraya koenigii* from parts of Bihar, Jharkhand, Andhra Pradesh, Madhya Pradesh, Odisha, West Bengal, wetern Ghats and NEH regions to enrich the germplasm base.

Reliability on a handful of major crops is probably unsustainable in the long run, especially in view of global climate change. Also as a result of Green Revolution, many locally important traditional crop species and varieties have been replaced by high-yielding crop cultivars. Moreover, traditional crops do not meet modern standards for uniformity and other characteristics as they have been neglected by breeders. Thus they tend to be less competitive in the marketplace compared with commercial cultivars. The aforesaid situation warrants for systematic collection of diverse germplasm of locally important species from unexplored and under-explored areas to widen the genetic base on priority. While *in situ* on farm conservation of these species in their original environment is needed for better maintenance of their resource base as well as to ensure sustainable use.

References

1. Padulosi S., Eyzaquirre P. and Hodgkin T. 1999. Challenges and strategies in promoting conservation and use of neglected and underutilized crop species (ed. J. Janick). Alexandria, Va, USA: ASHS Press.
2. Mal B. 2007. Neglected and underutilized crop genetic resources for sustainable agriculture. Indian Journal of Plant Genetic Resources, 22:1-16.
3. Magbagbeola JAO, Adetoso JA and Owolabi OA. 2010. Neglected and underutilized species (NUS): a panacea for community focused development to poverty alleviation/poverty reduction in Nigeria. Journal of Economics and International Finance, 2: 208-211.
4. Smith RW. 1988. The place of life support species in hostile or risk-prone environments: An overview, *In*: Life support species: diversity and conservation (eds., R.S. Paroda, P. Kapoor, R.K. Arora and Bhag Mal). NBPGR, New Delhi, 14-19.
5. Johns T and Eyzaguirre PB. 2006. Symposium on “wild-gathered plants: basic nutrition, health and survival” Linking biodiversity, diet and health in policy and practice. Proceedings of the Nutrition Society, 65:182-189.
6. Paroda, R.S. and Bhag Mal. 1989. New plant sources for food and industry in India. *In*: New crops for food and industry (eds., G.E. Wickens, N. Haq and P. Day). Chapman and Hall, London, 135-149.

PS-IV-69

In vitro conservation of exotic *Allium ramosum* L. germplasm

Ruchira Pandey[1], Neelam Sharma, K. S. Negi and R. K. Tyagi

National Bureau of Plant Genetic Resources, Pusa Campus, New Delhi 110 012; e-mail: ruchira@nbpgr.ernet.in

Amongst bulbous crops, alliums represent an important genus with species mostly used as a vegetable, spice or a medicine (Pandey *et al*., 2008) and these are propagated through seeds as well as bulbs. Being a cross-pollinated crop, propagation through seeds leads to a highly heterogenous progeny. To maintain the desired genotypes, species are thus selectively or exclusively vegetatively propagated by bulbs/cloves.

Allium ramosum (EC32898), an exotic *Allium* species, procured by National Bureau of Plant Genetic Resources (NBPGR) from USA, is commonly known as flowering Chinese chives or fragrant-flowered garlic. Bulbs and leaves are used for culinary and medicinal purposes. Maintained in the field genebank of NBPGR Regional Station at Bhowali, *A. ramosum* germplasm needs to be regenerated every year. Coupled with uncertain weather and prevalence of diseases, routine handling from one season to another incurs annual loss of germplasm under field conditions.

The aforementioned problems necessitate the usage of *in vitro* clonal propagation techniques for safe and pathogen-free conservation of *A. ramosum* germplasm for medium-to long-term. *In vitro* clonal propagation is an integral component of any *in vitro* conservation programme with emphasis on reducing the number of subculture cycles. Strategies have been investigated upon for enhancing the subculture duration under normal-growing conditions or under growth-limiting conditions in *A. ramosum*. A viable and promising option, cryopreservation at the temperature of liquid nitrogen (-196^{0}C) holds the key for long-term conservation of vegetatively propagated plant species (Reed 2008). There are no reports in the literature regarding cryopreservation of this important *Allium* species. Preliminary experiments have revealed that long-term conservation at the temperature of liquid nitrogen (-196^0 C) is feasible in *A. ramosum.* Present investigations highlight *in vitro* strategies for conservation of *A. ramosum* germplasm at NBPGR in India.

Plants of *A. ramosum*, procured from (NBPGR) Regional Station at Bhowali, Nainital, Uttarakhand were maintained in the net house at NBPGR, New Delhi and these served as the source of explants (bulbous shoot bases) for initiating cultures. Following removal of roots and leaves (cut off 1 cm above the shoot base), the outer scales were removed from the shoot bases. The bulbous bases were immersed in a solution containing tee pol (0.1% v/v), cetrimide (0.1% w/v), bavistin (0.5% w/v) and streptomycin (0.1% w/v) for 1h on a magnetic stirrer. Explants were then treated with 0.5% $HgCl_2$ for 40 min followed by rinsing with sterile distilled water five times. The bulbous bases were cut transversely at 5 mm height on a sterile surface and a few mm of basal plate tissue was removed. Following removal of outer two to three layers of foliage leaf bases, the resulting shoot bases were implanted onto Murashige and Skoog (1962) medium (MS) supplemented with NAA (0.1 mgl^{-1}), 2iP (0.5 mgl^{-1}), spermidine (10 mgl^{-1}) and 3% sucrose and solidified with 0.8% agar for culture initiation and proliferation (hereafter referred as MSP1). After 8-10 subcultures of 4-6 weeks each, the proliferated shoots provided sufficient material for conservation experiments. Except for cultures subjected to low temperature treatment, all the cultures were maintained under culture room conditions (25±.2^0 C, 16h/8h photoperiod with irradiance of 30 ìmol m^{-2}s^{-1}) provided by cool-white fluorescent tubes.

Six to eight week-old plantlets excised from the proliferating mass were trimmed to 5 mm height and all existing roots cut off. The shoots thus obtained were transferred to culture tubes (25 mm × 150 mm) containing 20 ml of media and served as explants for *in vitro* slow growth experiments. Irrespective of the slow growth strategy, all cultures were maintained for a week under culture room conditions, as stated above, to detect and eliminate contamination. They were then subjected to various slow growth strategies such as low temperature incubation, use of osmotic agents, minimal media and type of culture tube closure.

In the first set of experiments, effect of culture tube closure on storage of cultures, shoots were transferred to culture tubes containing MSP1 medium and closed with cotton plugs or polypropylene caps. These cultures were then incubated under culture room conditions as described above. For all subsequent experiments, polypropylene caps were used as culture tube closure.

In the next set of experiments, shoots were stored in the following media gelled with 0.8% agar. The details of media with their respective codes are given below:

AN: MS basal medium without sucrose

AS: Water+3% sucrose

A: Water

MSP10: MSP1 medium but with 10% sucrose

To investigate the effect of low temperature, a set of shoot cultures implanted on the above 4 media were shifted to low temperature (4^0 C, dark) in the module.

Seventy-two to one hundred replicates were used for each treatment and experiments were repeated two times.

At fixed interval, twelve cultures from each treatment were examined visually and then transferred to fresh medium under standard culture room conditions. Survival of *in vitro* cultures was assessed by the ability of explants to resume growth upon transfer to fresh medium.

Six to eight week old plantlets with well developed roots were washed free of agar and their leaves were trimmed to ca.4 cm from the base. These were subsequently transplanted in small plastic pots containing sterilized soil and covered with polythene bags to maintain high humidity. These pots were maintained in a nethouse at 25^0C. After two weeks, the polythene bags were removed and by six to eight weeks, plantlets were transferred to earthen pots.

Experimental material consisted of shoot bases (about 1-2 mm in length) obtained from 3 or 4 week-old *in vitro* plantlets of *A. ramosum.* Stock cultures were multiplied on MSP1 medium. They were sub cultured every six to eight weeks under culture room conditions on MSP1 or MSP10, depending upon the experiment. Excised shoot bases obtained from mother cultures were pre grown on MSP1 or MSP10 media, in Petri dishes containing 10 ml medium. They were then dehydrated with the PVS2 solution for 10-50 min at 25^0C. The dehydrated shoot bases were directly immersed into liquid nitrogen. After rapid warming in a water bath at 40^0C, the shoot bases were washed with 1.2M sucrose solution and then plated on MSP1 medium for regrowth.

Procedure for *in vitro* multiplication and conservation of *A. ramosum* L. was developed using shoot bases as explants. Multiple shoots were obtained on MS medium supplemented with NAA, 2iP and spermidine. Shoots were rooted on ½ or full strength MS basal medium and plantlets were established under net house conditions.

None of the cultures maintained under culture room conditions on MSP1 medium with cotton plugs as closures, survived after seven months. In comparison, the cultures covered with polypropylene caps remained

healthy for a longer period. Cultures maintained on MS basal medium lacking sucrose (AN) exhibited 33% survival, with 40% survival on A medium (agar+water) within 2 months of storage. Subsequently, the cultures turned yellow and none survived after 4 months in the former. Interestingly, on AS medium (agar+ sucrose+water), cultures exhibited 66% survival after 12 months of storage.

Shoot cultures could be conserved for 15 months on half-strength or full-strength MS basal medium as well as on MSP10 under standard culture conditions. Exposure to low temperature was beneficial across all treatments except in case of cultures maintained on AN medium. Cryopreservation experiments carried out with *A. ramosum* using vitrification technique revealed that shoot base explants, excised from mother cultures maintained on shoot multiplication (MSP1) medium and pre-grown on the same medium at 25^0C, exhibited 75-20% survival with 10-50 mins PVS2 dehydration. Following LN freezing, there was only 20% survival up to 50 mins PVS2. With inclusion of high sucrose in the preconditioning medium of mother cultures as well as in the pre growth medium at 25^0C, there was 20% post-thaw regrowth with 50 mins PVS2. The regrown shoots, however, turned white after 4 wks.

In vitro conservation techniques offer the possibility of conserving the germplasm of particularly vegetatively propagated crops wherein field maintenance is not only expensive but also risky. Among several slow growth strategies, low temperature incubation has been most successful with a large number of plant species. Cryopreservation of living tissues most commonly at the temperature of liquid nitrogen (LN;-196^0C) offers the advantage of preserving material for unlimited period without alteration.

In the present investigations, shoot cultures of *A. ramosum* could be successfully conserved for 15 months using a combination of slow growth strategies such as minimal media, low temperature and polypropylene caps as closures. With cotton plugs as closures, the death of cultures occurs mainly due to nutrient depletion and desiccation. Improvement in survival following replacement of cotton plugs with polypropylene caps could be attributed to a check in desiccation rate. These observations compare favorably with published results from various laboratories.

The present findings on conservation of *A. ramosum* are important because they offer the convenience of storing the germplasm for more than one growing season and also the feasibility of cryopreserving it for posterity.

Acknowledgement

The authors gratefully acknowledge the facilities provided by Director, NBPGR, New Delhi.

References

1. Murashige T. and Skoog F. 1962. A revised medium for rapid growth and bioassays with tobacco tissue culture. Physiol. Plant. 15: 473-497.
2. Pandey A., Pandey R., Negi K. S. and Radhamani J. 2008. Realizing value of genetic resources of *Allium* in India. Genet. Resourc. Crop Evol., 55: 985-994.

PS-IV-70

Physiological and agronomic characterization of international core set for drought and heat tolerance

Priyanka Vijay, Neha Rai, Manoj Pandey, Kavita, Anita Yadav, Vasudha Jadon, Sutapa Dutta, K. T. Ramya, Nivedita Sinha, P. Ramya, Neelu Jain*, P. K. Singh, G. P. Singh and K. V. Prabhu

Division of Genetics, Indian Agricultural Research Institute, New Delhi 110 012

Abstract

Wheat, one of the important cereal crops in India, is adversely affected by abiotic stresses such as drought and heat. Genetic gains associated with certain physiological traits adaptive to drought and heat stress have been measured in an international core set and in the present report we explored this variability under Indian conditions. Significant correlations were observed between photosynthetic pigments and yield. Multi-location yield trials revealed some promising lines that can be used as donors in the breeding programmes.

Key words: Drought, wheat, phenotyping, physiological, abiotic stress

Wheat is one of the most important cereal crops in India and is a major source of energy and nutrition in human diet. During past few decades, growth and productivity of wheat is adversely affected by major biotic and abiotic stresses. Among the various abiotic stresses, drought and heat are the major stresses that restrict wheat yields. Much emphasis is being given on breeding efforts to develop genotypes that can perform better in these stressful production environments. Certain physiological traits are known to be stress adaptive and may lead to variation in drought and heat stress responses. Genetic gains associated with these traits have been measured in a range of environments and a core set has been compiled by CIMMYT representing variability for various morpho-physiological traits. In this study, our objective was to explore this variability among the core set under Indian conditions and to select some promising lines to be used as donors in breeding programmes. An International core set for moisture and thermo stress adaptive traits received from CIMMYT under Generation challenge Programme was used in this study. These are genetically diverse parents of mapping populations, released varieties, landraces, advance lines and tails of mapping populations known internationally for drought and heat tolerance and characterized physiologically under Mexican and Australian conditions. The experiment was laid out in alpha-lattice design with two replications in one-meter rows each in rabi season of 2011-12 and 2012-13 under restricted irrigation conditions. The standard cultivation practices prescribed for wheat under irrigated conditions were followed precisely.

Table 1. Correlation coefficients among photosynthetic pigments and yield traits

	Mean yield	SPAD	Chla	Chlb	Carotenoid	Chla/Chlb	Carotenoids/Chl	TKW
Mean yield	1.000							
SPAD	0.29**	1.000						
Chla	0.054	0.142	1.000					
Chlb	0.091	0.103	0.863**	1.000				
Carotenoids	-0.011	0.165	0.881**	0.709**	1.000			
Chla/Chlb	-0.117	0.041	0.063	-0.445**	0.161	1.000		
Carotenoids/chl	-0.168	0.007	-0.424**	-0.540**	0.033	0.330**	1.000	
TKW	0.058	0.273**	0.032	-0.003	0.045	0.058	0.050	1.000

Table 2. Genotype performance based on AMMI analysis

Genotypes (codes)	Environments
Baviacora92/Seri (G88)	Delhi 2013, Ludhiana 2013, Powarkheda 2012, Powarkheda 2013, Pune 2013
Baviacora92/Seri (G87)	Delhi 2013, Ludhiana 2012, Powarkheda 2012, Powarkheda 2013, Pune 2013
Seri Babax line SB044 (G137)	Delhi 2013, Ludhiana 2013, Powarkheda 2012, Powarkheda 2013, Pune 2013
Kukri/RAC875(G64)	Delhi 2013, Ludhiana 2013, Powarkheda 2012, Pune 2013
HGO94.91(G4)	Delhi 2013, Ludhiana 2012, Powarkheda 2012, Pune 2013
Babax (G120)	Ludhiana 2012, Powarkheda 2012, Pune 2013
Excalibur (G80)	Ludhiana 2012, Powarkheda 2012, Pune 2013
QG-58-5.1 (G118)	Delhi 2012, Powarkheda 2013, Pune 2012

A trial was evaluated at four locations (IARI New Delhi, ARI Pune, JNKVV Powarkheda and PAU, Ludhiana) and phenotyping was carried out for a number of traits. Data on germination, days to heading, days to maturity, canopy temperature (CT), chlorophyll content (SPAD), flag leaf area, NDVI, yield and contributing traits was recorded. The chlorophyll contents were measured with the help of SPAD meter (Minolta SPAD-502) three times during the study at reproductive stage while chlorophyll pigments were extracted by incubating the leaf tissue in DMSO following the method of [1]. CT was measured using hand-held infra-red meter. Moisture stress significantly affected different physiological parameters. There were significant correlations between different photosynthetic pigments. Strong positive correlations were observed between chlorophyll a and chlorophyll b and with other chlorophyll contents (Table1). Carotenoids and chlorophyll contents were also positively correlated among the genotypes. Significant variation in SPAD values were observed among the core set genotypes. A positive correlation was observed between SPAD values at the time of anthesis and the mean yield (r = 0.29; p=0.01) and thousand kernel weight (r = 0.273; p=0.01). Higher total chlorophyll was observed in parents of internationally known mapping populations namely, Kukri/Excalibur, Kukri/Rac875, Bav92/Seri, Krichauff etc. Moisture stress observed significant negative correlations between yield and CT.

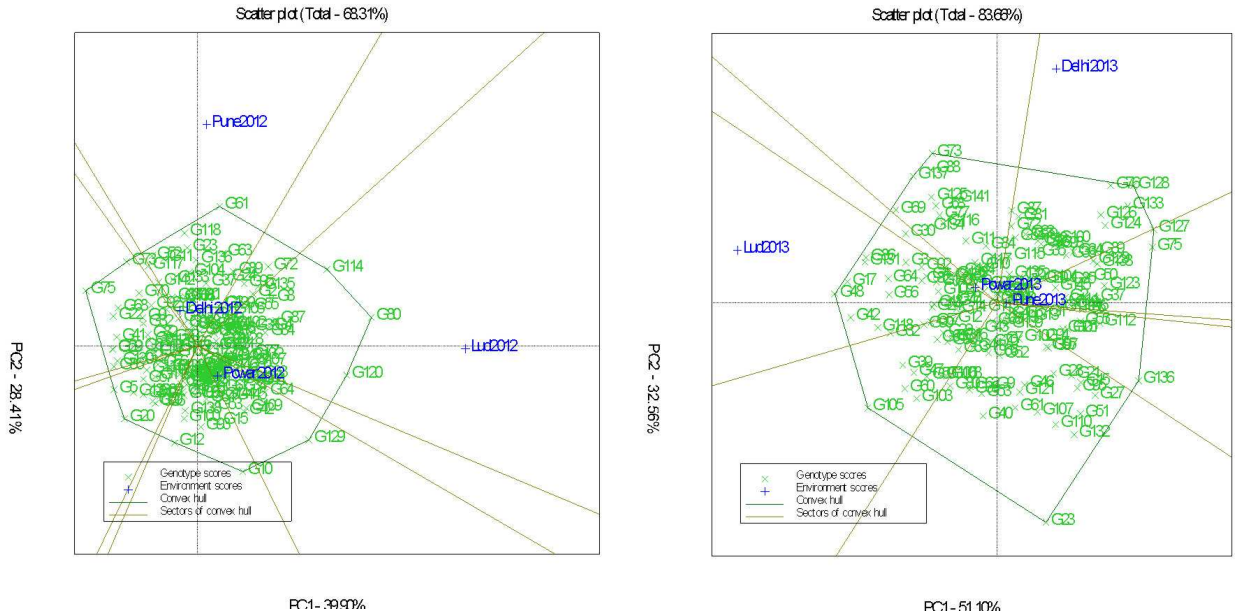


Fig. 1. GGE biplot for the four environments in year 2012 (A) and year 2013 (B)

The multi-location yield data was subjected to AMMI and biplot analysis to predict the performance of genotypes. Highest mean yield observed in pooled data was for Pune in 2012 and Delhi in 2013. Based on AMMI analysis, the best ten selections in each environment were compared. Some of the selections were consistently performing in more than one environment under moisture stress. Table 2 represents genotypes performing best in the multiple environments under stress. The best predicted genotypes on the basis of their significantly higher CD values for the photosynthetic pigment traits and yield trials data are used as potential donors for their utilization in our wheat breeding programme. The GGE biplot analysis indicated Ludhiana and Pune during 2012 and Delhi during 2013 to be more representative environment for genotypes (Fig. 1). The angles of the environment vectors Ludhiana and Pune in 2012 indicated that they are independent to each other which is also the case with Ludhiana and Delhi in 2013. Equal length of environment vectors represent their discriminating abilities among environments [2], hence in 2012 Ludhaiana and Pune were more discriminating. The shorter length of the environment vector suggested that it provided little or no information about the genotypic differences. The polygon view in figure 1 indicated that genotypes located on the vertices performed best in the respective environment sector. The four environments lie in four different sectors for both the years. The vertex genotypes include Kukri/ RAC875, Kukri/Excalibur, Babax, Excalibur, Aus30354 Cettia etc. in the year 2011-12 (Fig. 1A) and Seri/ Bav92/ WBLL1, Kukri/Excalibur, Bav92/Seri, during the year 2012-13 (Fig. 1B). Physiological parameters have not very explicitly used in breeding programmes, however recent advances in crop physiology has offered the breeders novel opportunity to combine adaptive traits. Several genomic regions underlying stress adaptive physiological traits for drought and heat tolerance have been reported [3]. Physiological characterization coupled with high-through-put phenotyping and genomics will provide the understanding about the network of tolerance related traits but also will give insights into the candidate genes and the underlying QTLs. The genotypes identified in the present international core set will help us in transferring the genomic regions in to novel varities in our breeding programmes.

References

1. Hiscox J. D. and Israelstam G. F. 1979. A method for the extraction of chlorophyll from leaf tissue without maceration. Canadian J. Bot., 57: 1332-1334.
2. Yan W. and Tinker N.A. 2006. Biplot analysis of multi-environment trial data: Principles and applications. Canadian J. Plant Sci., 86: 623-645.
3. Pinto R. S., Reynolds M. P., Mathews K. L., McIntyre C. L., Olivares-Villegas J. J., Chapman S. C. 2010. Heat and drought adaptive QTL in a wheat population designed to minimize confounding agronomic effects. Theor. Appl. Genet., 121: 1001-1021.

Atmospheric and Climate Sciences, 2015, 5, 13-22
Published Online January 2015 in SciRes. http://www.scirp.org/journal/acs
http://dx.doi.org/10.4236/acs.2015.51002

Variation in Parameters of Ambient Air Quality in National Capital Territory (NCT) of Delhi (India)

Anunay A. Gour[1], Santosh K. Singh[1], Sushil K. Tyagi[2], Anubha Mandal[1]

[1]Department of Environmental Engineering, Delhi Technological University (Formerly Delhi College of Engineering), Delhi, India
[2]Central Pollution Control Board (CPCB), Delhi, India
Email: anunaygour@live.in

Received 29 October 2014; revised 30 November 2014; accepted 16 December 2014

Copyright © 2015 by authors and Scientific Research Publishing Inc.
This work is licensed under the Creative Commons Attribution International License (CC BY).
http://creativecommons.org/licenses/by/4.0/
Open Access

Abstract

Air Pollution is an escalating problem worldwide fuelled by increasing anthropogenic activities, speedy development, rapid industrialization, transportation, superfluous use of fossil fuel consumption, increasing global power needs, etc. Also the diverse meteorological factors influence our environment to a great extent. Population explosion has led to remarkable increase in vehicular population. The use solely depends upon the lifestyle of the citizen. Any change in the lifestyle has a remarkable effect on the air we breathe. A comprehensive database for pollution levels from the year 2006 to 2010 was analyzed for a main traffic intersection and a non-traffic area in Delhi (India). The paper asserts that pollutant concentration levels on weekend are lower than those on weekdays (increase on Sundays with respect to weekdays is CO 2.98 times, PM2.5 1.18 times, NO 1.62 times, NO_2 5.76 times, SO_2 1.27 times and O_3 1.15 times). The pollution levels have been found to attenuate on public holidays and weekends. Pollution can hence be related to the weekly cycle of human activities. Pollutions due to vehicular emissions on roads, rails, air or water all serve as major sources of pollution. Hence, viably possible solutions for pollution control can also be achieved by controlling the magnitude of traffic flow on roads.

Keywords

Ambient Air Quality, Emission, Seasonal Variation, Weekend Effect, Delhi

How to cite this paper: Gour, A.A., Singh, S.K., Tyagi, S.K. and Mandal, A. (2015) Variation in Parameters of Ambient Air Quality in National Capital Territory (NCT) of Delhi (India). *Atmospheric and Climate Sciences*, **5**, 13-22.
http://dx.doi.org/10.4236/acs.2015.51002

1. Introduction

The temporal variation of concentration of pollutant throughout the day varies with the influence of local wind parameters such as direction, speed and other meteorological aspects. On the other hand, changing patterns of vehicular traffic and industrial activities also act as a factor for variation in pollution levels. Authors such as Blanchard *et al.* [1], Murphy (2008) *et al.* [2], Fujita *et al.* [3], Gour *et al.* [4], Murphy (2007) *et al.* [5] and Kakoli *et al.* [6] note that weekly cycle of activities of population explains divergent temporal variation in pollution levels from weekdays (Monday to Friday) to weekend (Saturday and Sunday). The paper attempts to carry out an assessment of 24 h daily average concentration of six major pollutants for a period of five years (from 2006 to 2010). It exhibits Weekly & Seasonal Variation, Weekday-Weekend differences in concentration of pollutants, Variation in ambient air quality on Public Holidays, *i.e.* the holiday effect, Comparison of Annual average concentration and National Ambient Air Quality Standards (NAAQS), and Comparison of pollutant levels at a Traffic Area and a Non-Traffic Area.

Pollution Emission

The human population explosion has led to a significant increase in the vehicular population. The urban population of India has tripled within a period from 1951 to 1991, from 62.5 million to 217.6 million; correspondingly the vehicle population has increased almost 124 times from 0.3 million to 37.2 million (Ministry of State Transport 2000). Fossil fuel driven vehicles are the significant contributors to pollution. A major section of population uses private vehicles (diesel, petrol and compressed natural gas driven) such as two-wheeled vehicles and cars including the high fuel consuming Sports Utility Vehicles (SUVs), Multiple Utility Vehicles (MUVs), trucks, etc. However, mass rapid transportation modes such as metro rail and buses and railways continue to be the most popular means of transportation for intra-city travel; they cater to about 60% of the total commuting requirements. Private vehicles account for 30% of the total demand for transportation, while the rest of the demand is met largely by auto-rickshaws and taxis. Reddy and Venkataraman [7] and Abera *et al.* [8] note that the pollutants like CO and NO_x emanate from automobile exhausts, whereas use of coal based fuels causes heavy emissions of SO_2. Murphy (2008) *et al.* [2] and Rosibeto *et al.* [9] find that the levels of O_3, NO_x and particulate matter are an issue of concern in the urban environment. The variation in concentration of such pollutants strongly relates to the pattern of human activities in the city. Khaiwal *et al.* [10] report that implementation of compressed natural gas (CNG) as fuel in public transport in Delhi has mitigated the major pollutants, but increased the emission of benzene and other organic compounds. Consumption of fuels for automobile and industrial purposes, factors related to individual's lifestyle, working and non-working environment, religious and cultural practices, festivities, etc. act as major factors for variation in ambient air quality in the metro. This explicitly expresses an idea about the magnitude by which the pollution can be mitigated by altering the lifestyle or some of the habits of the population. It can also be resolved that pollution mitigation is a function of public willingness and proper understanding by the masses without which it is impossible to tackle this threat.

Authors like Chhabra *et al.* [11], Maureen *et al.* [12], Barman *et al.* [13] and Ramalingaswami *et al.* [14] report that pollutants such as carbon monoxide (CO), particulate matter (10 μ and 2.5 μ size), nitrogen oxide (NO), nitrogen dioxide (NO_2) and sulphur dioxide (SO_2) cause health effects related to lungs, throat, cardiovascular disorders, etc. Blanchard *et al.* [1], Murphy (2008) *et al.* [2], Fujita *et al.* [3], Gour *et al.* [4], Murphy (2007) *et al.* [5], Kakoli *et al.* [6], Reddy and Venkataraman [7], Stephens *et al.* [15] and Debaje *et al.* [16] find that pollutant concentrations surge on weekdays and reduce on weekend. The data also reveal that ozone (O_3) increases on weekend especially on Sundays contrary to decreasing concentration of other pollutants like NO_x and some hydrocarbons which act as its precursors. Such observations are also referred to as "Weekend effect" by Blanchard *et al.* [1], Fujita *et al.* [3], Gour *et al.* [4], Murphy (2007) *et al.* [5], Rosiberto *et al.* [9], Stephens *et al.* [15], Debaje *et al.* [16] and Tan *et al.* [17]. On weekend, the reduced PM and aerosols result in more inward solar radiation accompanied with the precursor NO_x accumulated over the week aids the ozone production. At some instances, concentration of Ozone increases on weekend irrelevant of the concentrations of its precursors. Seasonal variations during summer, winter, North East Monsoon (NE Monsoon) and South West Monsoon (SW Monsoon) over weekday-weekend differences were also studied. Factors such as diurnal temperature range, daily maximum temperature, daily precipitation, annual precipitation and wind speed and seasonal maximum and minimum temperature influence the pollutant concentration.

2. Methodology

2.1. Description of Study Area

National Capital Territory of Delhi is one of the largest metropolises by area and population in the world. It has population more than 12.25 million inhabitants in the territory. There are nearly 22.2 million residents in the greater National Capital Region (NCR) urban area which includes Noida, Greater Noida, Ghaziabad, Gurgaon and Faridabad along with other smaller nearby towns. There are 6.5 million registered vehicles in the city, which is the highest in the world among all cities, while the NCR has 11.2 million vehicles. Public transport in the metropolis includes the Delhi Metro, the Delhi Transport Corporation mass transit bus system, auto-rickshaws, cycle-rickshaws and taxis.

The area of study, ITO Station at R.C. Aggarwal Square, Bahadur Shah Zafar Marg, is one of the prime commercial locations with numerous corporate and government offices in its vicinity, see **Figure 1**. Air quality here is greatly affected by the heavy vehicular traffic; hence it turns out to be a principle site for such comparative studies. Ambient air here is also influenced by emissions from two coal-fired power generation stations namely, Pragati Thermal Power Plant (Indraprastha) and Badarpur Thermal Power Plants (Badarpur). DCE Station located inside Delhi college of Engineering was selected as a non-traffic area for some more comparisons.

2.2. Data

The paper analyses 24 h daily average concentrations of six pollutants, namely, CO, NO, NO_2, SO_2, O_3, PM (10 μ and 2.5 μ) for the period of 5 years from 2006 to 2010 at the National Ambient Air Quality Monitoring Station (NAAQMS) of Central Pollution Control Board (CPCB) at R.C. Aggarwal Square near Income Tax Office (ITO) on Bahadur Shah Zafar Marg, New Delhi.

3. Results and Discussions

Statistical and graphical analysis of the 24 h data pertaining to the period of 2006 to 2010 are discussed in the following headings:

- Weekday and Weekend Comparison;
- Weekly Variation;
- 24 H Annual Average (Traffic vs. Non-Traffic Area);
- Average Annual Pollution Levels;
- Average Seasonal Variation;
- Public Holidays.



Figure 1. NAAQMS ITO station at R.C. Aggarwal Square, Bahadur Shah Zafar Marg, New Delhi, India (source: Google maps).

3.1. Weekday and Weekend Comparison

Figure 2 shows the 24 h average concentration of the parameters plotted on a time scale of consecutive seasons from years 2006 to 2010 on x-axis and concentration of the respective parameters represented by the graphs of weekdays (red) and weekends (cyan). Seasonal grouping of data facilitates analysis with similar meteorological conditions and hence can be useful in studying the season-induced variations in pollution. The observations are as follows:

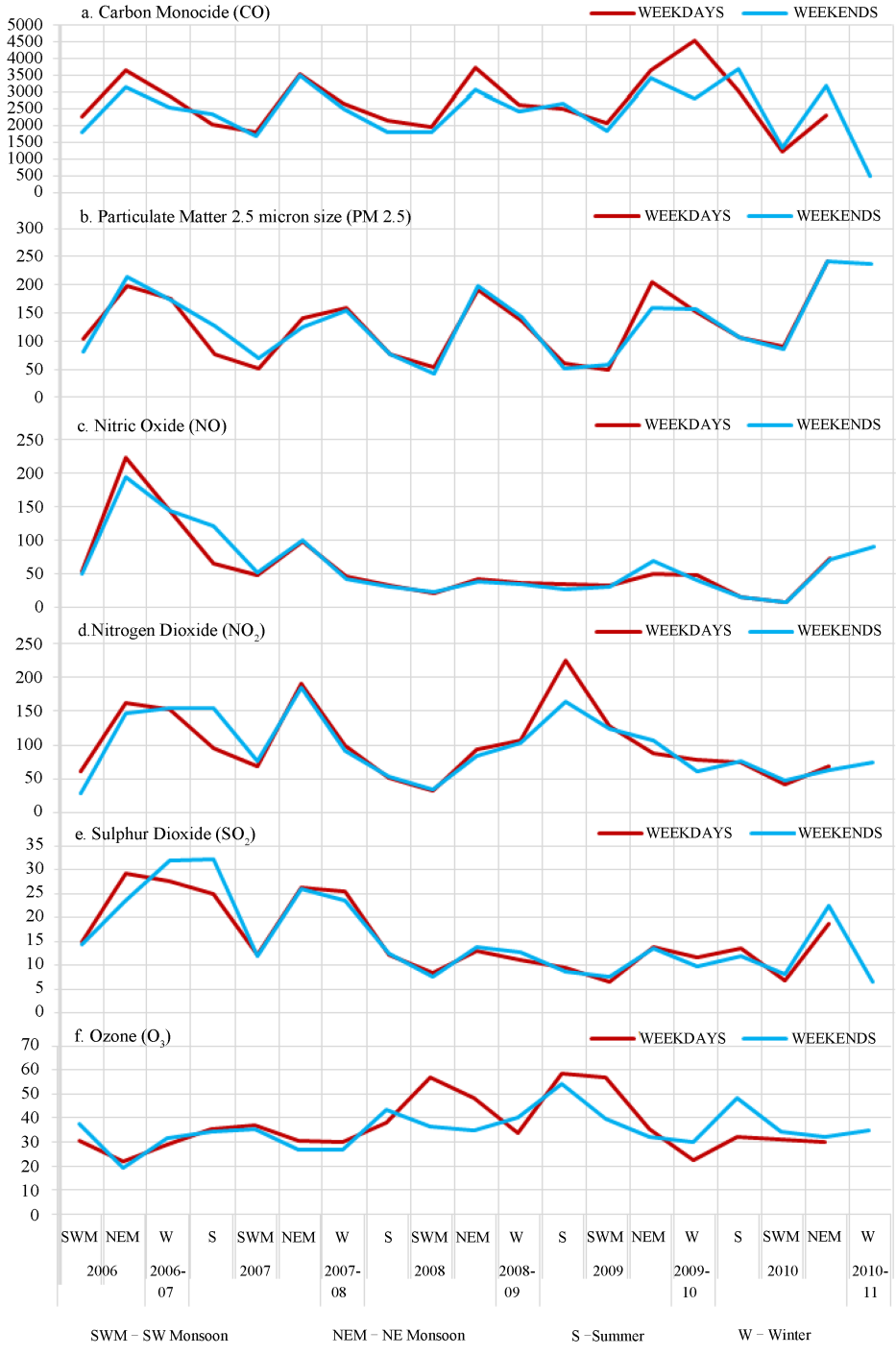


Figure 2. Weekday-weekend comparison w.r.t. seasons (Gour *et al.* [4]).

Carbon Monoxide: It is evident that average weekday concentration of carbon monoxide, as occurrence of co-ordinates of individual temporal ranges show a well defines sequence (cyan-red), *i.e.* pollution levels on Weekdays is more than that on Weekends. As substantiated by existing data from 2006 to 2010, on an average, concentration of CO as on weekdays is 1.75 times as that on Saturdays and is as much as 2.98 times as that on Sundays. CO being one of the substances that are agelessly related to vehicular exhausts very well demonstrated the impact of vehicles over the environment. A well-defined pattern exist, with highest concentration during NE Monsoon is seen which gradually falls through winter and summer and reaches its lowest in the season of SW Monsoon. Year 2010 shows CO with 1.5 times more concentration than that fixed for national ambient air. CO in automobiles is produced as a result of incomplete combustion of fuel; possible due to inadequate oxidation *i.e.* in shortage of oxygen. Mitigation of vehicular CO can be guaranteed by facilitating complete combustion of fuels.

Particulate Matter is the category of pollutants which causes major respiratory track related disorders like asthma, etc. Apart from the natural sources transportation, stationary combustion and industrial and traffic-related fugitive emissions, street dust etc. can be ways of particulate pollution. The concentration of particulate matter here, by and large, was found to be similar during weekends and weekdays under the influence of particulates like fly-ash and dust from the two thermal power generation plants nearby. As substantiated by existing data from 2006 to 2010, on an average, concentration of PM2.5 as on Weekdays is 1.12 times as that on Saturdays and is as much as 1.18 times as that on Sundays. Similar to CO, PM also shows a well-defined pattern with highest concentration during NE Monsoon is seen which gradually falls through winter and summer and reaches its lowest in the season of SW Monsoon. Particulates are seen to rise in year 2010. The average concentration of PM2.5 throughout the period (2006-2010) studied, had always been above by about 3.34 times the NAAQS permissible limit and hence can be said as an area of greater vitality for the need to mitigate pollution.

Oxides of Nitrogen are the precursors of both acid precipitation and ozone, each of which is blamed for injury to plants. It is nitrogen oxide that absorbs sunlight, initiating the photochemical processes that produce nitric acid, which may precipitate with the rainfall. As substantiated by existing data from 2006 to 2010, on an average, concentration of NO as on Weekdays is 1.56 times as that on Saturdays and is as much as 1.62 times as that on Sundays. Also the concentration of NO_2 as on Weekdays is 1.28 times as that on Saturdays and is as much as 5.76 times as that on Sundays. Similar to CO and PM, NO_x also shows a well-defined pattern with higher concentration during NE Monsoon is seen which gradually falls through winter and summer and reaches its lowest in the season of SW Monsoon. After the high of 2006, level of NO lowered from 2007 to 2009 but soared again in year 2010, whereas NO_2 had a high in summer of 2009.

Sulphur Dioxide, being an integrated component of fossil fuels, leads to emission amount of oxides of sulphur into atmosphere. Validated by the data from 2006 to 2010, on an average, concentration of SO_2 as on Weekdays is 1.31 times as that on Saturdays and is as much as 1.27 times as that on Sundays. Similar to CO, PM and NO_x, SO_x also shows a well-defined pattern with higher concentration during NE Monsoon is seen which gradually falls through winter and summer and shows steep fall with the onset of SW Monsoon reaches its lowest in this season. The pattern of SO_x from 2006 to 2010 is shows a falling trend.

Ozone shows somewhat unpredictable behavior as per the data from 2006 to 2010, on an average, concentration of O_3 as on Weekdays is 1.22 times as that on Saturdays and is as much as 1.15 times as that on Sundays. Compared to other pollutants, ozone shows contrary concentrations, which remain similar with some peaks at Sundays. Contrary to CO, PM and NO_x, SO_x which shows higher concentration in NE Monsoon gradually falls through winter and summer and attain their lowest in SW Monsoon, Ozone shows lowest levels in NE Monsoon increases through Winter and Summer and reaches its highest levels in SW Monsoon. Ozone shows significant influence of solar radiation and obliquity to sun. The rain-washed air during SW Monsoon gives way to increased insolation and causes increased photo-oxidation of NO_x and HCs. It has been observed that ozone shows higher levels where NOx shows lower levels and vice versa. Years 2008 and 2009 show higher levels of O_3.

3.2. Weekly Variation

It was observed that the concentration of the pollutants such as CO, NO, NO_2 drastically falls as we reach Sundays *i.e.* towards the end of the week. The changing pattern of vehicular usage of individuals in urban areas-shows a cyclic variation of pollutants with a periodicity of 1 week [14]. Sunday being a holiday becomes the day for rest and entertainment for the population; hence it is envisaged with clearer roads, lesser traffic flow, hence

less pollution as compared to that on other days. On Sundays, it is evident that the concentration of pollutants even at the normal peak times is far below the average weekday's level of pollutants. Similar trend can be observed as most of the government offices and private offices observe a half-day at work on Saturday; hence rendering a pollution level slightly above than that on Sundays but assertively below the pollution levels on Weekdays.

3.3. 24 H Annual Average (Traffic vs. Non-Traffic Area)

Figure 3 shows the effect of the vehicular emission over the concentration of pollutants, taking into consideration the Income Tax Office (ITO) station, which is located at the main traffic intersection, is under heavy traffic flow throughout the day. Whereas, **Figure 4** shows DCE Station is located inside Delhi College of Engineering campus where a negligible traffic with very restricted entry of vehicles exists and a low influence of some small scale industries nearby. The principal emissions from vehicles include CO and SO_2, combustion and heating also cause formation of NO_2. It was found that level of CO is alarmingly high at ITO whereas below permissible limit at DCE. Differences exists in concentration of ozone, which shows higher pollution levels at the DCE station whereas the heavy traffic area shows relatively low levels of ozone. This can be explained as; a highly polluted area has an envelope of dust and pollutant gases which retards the solar radiation which in turn slows down photo-oxidation of NO_x. Hence, rather being below NAAQ Standard's permissible value, DCE shows higher levels of ozone than that at ITO. A general falling trend is visible in 24 h annual average from 2006 to 2010.

3.4. Average Annual Pollution Levels

The pattern showed by the annual daily averages shows increasing levels of CO and PM, whereas a falling trend in terms of SO_2, NO_2 and O_3, despite of increasing number of vehicles on road. This can be due to new motor regulations, use of CNG, catalytic convertors, etc. Increased influence of the surrounding (e.g. coal powered power stations) leads to rise in level of particulates and CO, although, a general fall of consecutive year's pollution levels is evident from the data studied.

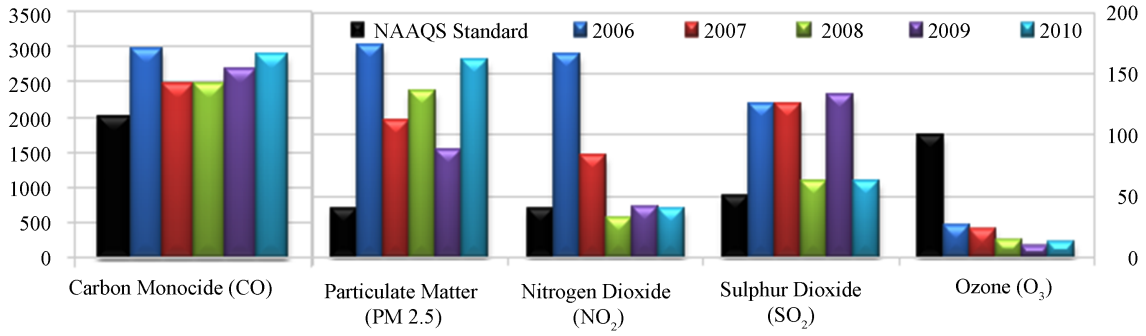


Figure 3. 24 h annual average concentration of pollutants at a traffic intersection (ITO Station).

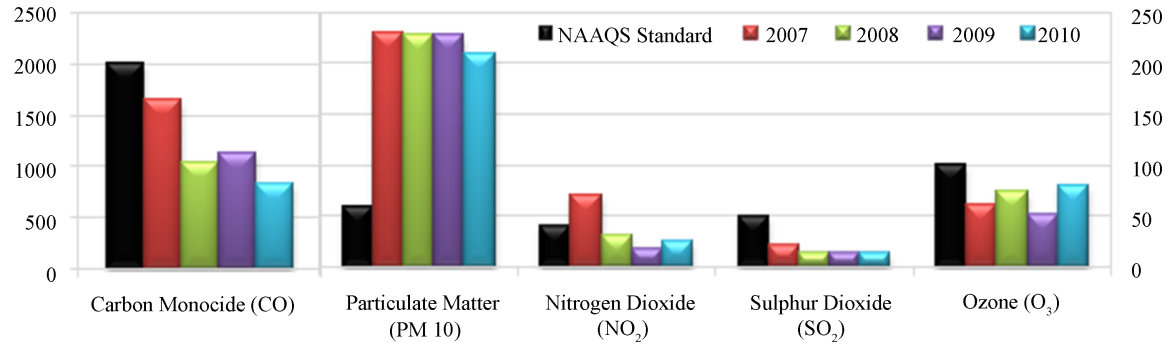


Figure 4. 24 h annual average concentration of pollutants at a non-traffic area (DCE Station).

Average concentration of pollutants from 2006 to 2010 shows levels of CO, PM and NO_2 persistently violating the permissible limits as assumed in the National Ambient Air Quality Standard (NAAQS) as shown in **Table 1**. CO exceeds by 30% more than NAAQS, similarly, PM2.5 shows 220% excess concentration. The concentration of NO is in excess by more than 50% of its permissible value, concentration SO_2, O_3 and PM10 were found to be lower than limits.

3.5. Average Seasonal Variation

Figure 5 observes that maximum concentrations of pollutants occur during winter season, as the atmosphere is quite dry in the winter and also due to the lowered mixing height; because the atmospheric lid, *i.e.* tropopause or the zone of temperature inversion, is formed at the lower level as compared to any other seasons. Similarly it can be stated that since the tropopause is formed at a relatively higher altitude during summers, the atmosphere gets an increased volume of air for dispersion of pollutants. The data, as studied, show near concentration of pollutants between winter and summer seasons.

This demonstrates that in reality, summers have higher level due to greater dispersion of pollution than in winters. The inter-annual seasonal daily averages confirms that season of SW Monsoon shows a significant fall in concentrations of pollutants as compared to higher concentrations in winter. It also shows similar levels during summer and NE Monsoon seasons. This can be explained on the grounds that pollutants possibly get absorbed and precipitated with rain-water during the SW Monsoon season. On a divergent note, the concentration of ozone shows slight increase in level during SW Monsoon, this increase can be related to clarity of atmosphere and fair insolation. Sunlight splits the nitrogen dioxide into nitric oxide and atomic oxygen, which combines with molecular oxygen to yield ozone, as in Reactions 1 and 2 as followings:

$$NO_2 + \text{sunlight} \rightarrow NO + O \qquad \text{Reaction 1}$$

$$O + O_2 \rightarrow O_3 \qquad \text{Reaction 2}$$

These reactions are rather fast so NO and NO_2 cycle, but the sum of their concentration ([NO] + [NO_2]) tends to remain fairly constant. Because of this cycling, it is convenient to consider the two chemicals as a group; hence the term NO_x.

3.6. Public Holidays

A public holiday (PH) marks the day-off for the Govt. Offices; Central Public Sector Undertaking companies (CPSUs) and other such institutions. The effect of such a leave can be well demonstrated as gazetted holidays

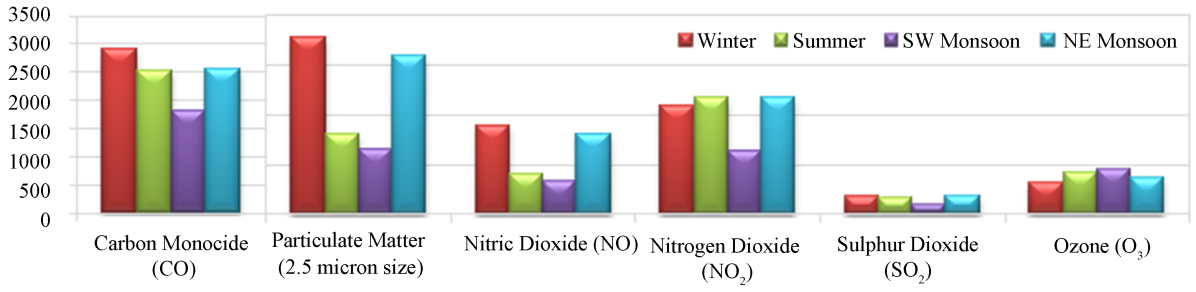


Figure 5. Average seasonal variation of pollutant concentration.

Table 1. 4 h averages for the period of 2006-2010.

Parameter	CO#	PM2.5*	NO*	NO_2*	SO_2*	O_3#
NAAQS	2000	40	-	40	50	100
Average	2608.93	127.68	61.79	97.62	16.19	38.14

#Annual 8 h average; *Annual 24 h average.

for the period of 2006 to 2010 (18 gazetted holidays per year) were analyzed and found that if pollution earlier was unity (1) the pollution reduces by at least 4% for O_3 and PM11 to 14 % for NO, CO and NO_2 from the pollution levels of the respective parameters in the same week. The pollution levels falls on the PH and again starts rising from the next day.

Figure 6 gives a general idea about the effect of a holiday on pollution; but if the effect of the weekly cycle of human activities over the pollution levels near public holidays is intended to study; it can be done so by grouping the parameters on the PH by the day on which it occurs. Hence all PH were grouped and their averaged 24-h pollution concentration was analyzed. **Table 2** analyses the data by representing the factor (<1 = "decrease" and vice versa) after comparing the pollution levels for 3 days (*i.e.* taking earlier level = 1 or unity) before the PH on a particular day.

4. Conclusions

Comparison of annual average concentration of parameters with respect to NAAQ Standards shows violation from the standard of CO, PM and NO_2 persistently from 2006 to 2010. It is observed that CO exceeds by more than 30% of its permissible value, PM2.5 by 220%; NO is excess by more than 50%; SO_2, O_3 and PM10 are found to be within limits. The pattern of the 24 h annual averages shows increasing levels of carbon-monoxide and particulates, whereas sulphur dioxide, nitrogen dioxide and ozone show a falling trend.

Weekend-Weekday Analysis validates that the emission from vehicular usage by individuals in urban areas shows a cyclic behavior with a periodicity of 1 week. As substantiated by the data from 2006 to 2010, concentration of CO on weekdays is as 1.75 times as that on Saturdays and is as much as 2.98 times as that on Sundays. Concentration of parameters in the year 2010 shows CO with 1.5 times more concentration than the NAAQ Standard. Particulates are seen to rise in Year 2010 and their average concentration on Weekdays is as 1.12 times as that on Saturdays and is as much as 1.18 times as that on Sundays. The average concentration of PM2.5 throughout the period (2006-2010) had been found to be 3.34 times more than the NAAQS Standard. NO on weekdays shows as 1.56 times concentration as that on Saturdays and is as much as 1.62 times as that on Sundays. Also the concentration of NO_2 on weekdays is as 1.28 times as that on Saturdays and is as much as 5.76 times as that on Sundays. Average concentration of SO_2 on weekdays is as 1.31 times as that on Saturdays and is as much as 1.27 times as that on Sundays. The pattern of SO_x from 2006 to 2010 shows a falling trend. The concentration of ozone on weekdays is 1.22 times as that on Saturdays and is as much as 1.15 times as that on

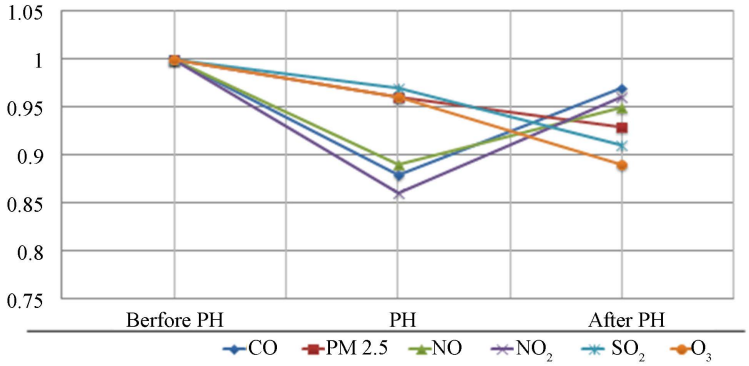


Figure 6. Comparison of pollutant concentration during public holidays.

Table 2. Pollution level comparison on public holidays.

Aspect	CO	PM2.5	NO	NO_2	SO_2	O_3
Before PH	1	1	1	1	1	1
On PH	0.88	0.96	0.89	0.86	0.97	0.96
After PH	0.97	0.93	0.95	0.96	0.91	0.89
% reduction	12	4	11	14	3	4

Sundays. It has been observed that ozone shows higher levels where NO_x shows lower levels and vice versa. Years 2008 and 2009 show higher levels of O_3.

Seasonal Variation Analysis infers an annual cycle in monthly concentration as the trend starts falling from February, gradually extending till the month of August. It attains a rising gradient from August till it reaches the highest in November, then the trend again falls till February. The season of winter in 2010 shows pollutants with higher levels of concentration than those during the preceding years. Parameters such as CO, PM, NO_x and SO_x generally show higher concentration in NE Monsoon; the concentration gradually falls throughout winter and summer seasons and attains lowest levels in SW Monsoon season. On a contrary note, Ozone shows lowest levels in NE Monsoon, increases throughout winter and summer seasons, and reaches its highest levels in SW Monsoon. Concentration of the parameters in winter can increase by almost 1.61 to 2.69 times concentration in SWM, and similarly by 1.23 to 1.4 times in summer and 1.41 to 2.47 times in NEM. Contrarily, ozone show its minimum levels in winter due to obliquity to sunrays, whereas reaches its maximum in SWM.

Analysis of pollutant concentration on public holidays shows that the pollution levels reduce by at least 4% for O_3 and PM, and up to 11% to 14% for NO, CO and NO_2 from the pollutant concentration levels of the same week. If PH occurs in the start of the week (*i.e.* on Monday or Tuesday), pollution levels show lower than even weekends. Most pollution is observed if PH occurs on mid-week (Wednesday) or on weekends (Saturdays).

The paper differentiates air pollutant concentration between weekdays and weekends. The observed phenomena of weekend effect and holiday effect provide evidence of impact of human activity on ambient air. Pollution variation corresponds to the pattern of working on weekend and weekdays. Comparative analysis from different aspects shows that vehicular emission largely increases on weekdays and drops down on weekends. Such weekend effect or holiday effect is also seen on public holidays. A general trend of fall in concentration has been found during the season of SW Monsoon. The study also shows, in particular, higher levels of Ozone during weekends. Hence, the cycle of human activities at different periodicities shows their deep influence over environmental health. It can hence be stated that vehicular pollution mitigation is a function of public willingness and understanding without which it is impossible to tackle this menace.

References

[1] Blanchard, C.L. and Shelley, T. (2006) Weekday/Weekend Differences in Ambient Air Pollutant Concentrations in Atlanta and the Southeastern United States. *Journal of Air & Waste Management*, **56**, 271-284. http://dx.doi.org/10.1080/10473289.2006.10464455

[2] Murphy, D.M., Capps S.L., Daniel, J.S., Frost, G.J. and White, W.H. (2008) Weekly Patterns of Aerosol in the United States. *Atmospheric Chemistry and Physics*, **8**, 2729-2739. http://dx.doi.org/10.5194/acp-8-2729-2008

[3] Fujita, E.M., Campbell, D.E., William, S., Keislar, R.E., Barbara, Z., Sagebiel, J.C., Wendy, G., Michael, K. and Bowen, J.L. (2002) Weekend/Weekday Ozone Observations in the South Coast Air Basin: Volume II—Analysis of Air Quality Data. Report, National Renewable Energy Laboratory, Desert Research Institute, Division of Atmospheric Sciences, Nevada, USA.

[4] Gour, A.A., Singh, S.K., Tyagi, S.K. and Mandal, A. (2012) Weekday/Weekend Differences in Air Quality Parameters in Delhi, India. *IMPACT*: *International Journal of Research in Engineering & Technology*, **1**, 69-76.

[5] Murphy, J.G., Day, D.A., Cleary, P.A., Wooldridge, P.J., Millet, D.B., Goldstein, A.H. and Cohen, R.C. (2007) The Weekend Effect within and Downwind of Sacramento: Part 1: Observations of Ozone, Nitrogen Oxides, and VOC Reactivity. *Atmospheric Chemistry and Physics*, **7**, 5327-5339. http://dx.doi.org/10.5194/acp-7-5327-2007

[6] Karar, K., Gupta, A.K., Kumar, A., Biswas, A.K. and Devotta, S. (2006) Statistical Interpretation of Weekday/Weekend Differences of Ambient Particulate Matter, Vehicular Traffic and Meteorological Parameters in an Urban Region of Kolkata, India. *Indoor and Built Environment*, **15**, 25-245.

[7] Reddy, M.S. and Venkataraman, C. (2002) Inventory of Aerosol and Sulphur Dioxide Emissions from India: I—Fossil Fuel Combustion. *Atmospheric Environment*, **36**, 677-697. http://dx.doi.org/10.1016/S1352-2310(01)00463-0

[8] Kume, A., Charles, K., Berehane, Y., Anders, E. and Ali, A. (2010) Magnitude and Variation of Traffic Air Pollution as Measured by CO in the City of Addis Ababa, Ethiopia. *Ethiopian Journal of Health Development*, **24**, 156-166.

[9] Da Silva Júnior, R.S., De Oliveira, M.G.L. and De Fátima Andrade, M. (2009) Weekend/Weekday Differences in Concentrations of Ozone, NOx, and Non-Methane Hydrocarbon in the Metropolitan Area of São Paulo. *Revista Brasiliera de Metrologia*, **24**, 100-110.

[10] Ravindra, K., Wauters, E., Tyagi, S.K., Mor, S. and Van Grieken, R. (2006) Assessment of Air Quality after the Implementation of Compressed Natural Gas as Fuel in Public Transport in Delhi, India. *Environmental Monitoring and*

Assessment, **115**, 405-417. http://dx.doi.org/10.1007/s10661-006-7051-5

[11] Chhabra, S.K., Pande, J.N., Joshi, T.K. and Kumar, P. (2001) Air Quality and Health. *Workshop on Land Use*, *Transportation and the Environment*, Pune, 3-4 December 2001, 1-24. http://www.deas.harvard.edu/TransportAsia/workshop_papers/ChhabraetalFinal2.pdf

[12] Cropper, M.L., Simon, N.B., Anna, A. and Sharma, P.K. (1997) Policy Research Working Paper No. 1860: The Health Effects of Air Pollution in Delhi, India. Development Research Group, The World Bank.

[13] Barman, S.C., Kumar, N., Singh, R., Kisku, G.C., Khan, A.H., Kidwai, M.M., Murthy, R.C., Negi, M.P.S., Pandey, P., Verma, A.K., Jain, G. and Bhargava, S.K. (2010) Assessment of Urban Air Pollution and It's Probable Health Impact. *Journal of Environmental Biology*, **31**, 913-920.

[14] Ramalingaswami, V., Aggarwal, P., Chhabra, S.K., Desai, P., Ganguly, N.K., Gopalkrishnan, K., Kacker, S.K., Kalra, V., Kamat, R., Kochupillai, V., Nag, D., Pande, J.N., Raina, V., Ray, P.K., Saiyed, H., Seth, P.K., Trehan, N. and Wasir, H.S. (1999) Urban Air Pollution. *Current Science*, **77**, 334-336.

[15] Stephens, S., Madronich, S., Wu, F., Olson, J., Ramos, R., Retama, A. and Munoz, R. (2008) Weekly Patterns of Mexico City's Surface Concentrations of CO, NOx, PM10 and O_3 during 1986-2007. *Atmospheric Chemistry and Physics*, **8**, 5313-5325. http://dx.doi.org/10.5194/acp-8-5313-2008

[16] Debaje, S.B. and Kakade, A.D. (2006) Weekend Ozone Effect over Rural and Urban Site in India. *Aerosol and Air Quality Research*, **6**, 322-333.

[17] Tan, P.-H., Chou, C., Liang, J.-Y., Chou, C.C.-K. and Shiu, C.-J. (2009) Air Pollution "Holiday Effect" Resulting from the Chinese New Year. *Atmospheric Environment*, **43**, 2114-2124. http://dx.doi.org/10.1016/j.atmosenv.2009.01.037

Scientific Research Publishing (SCIRP) is one of the largest Open Access journal publishers. It is currently publishing more than 200 open access, online, peer-reviewed journals covering a wide range of academic disciplines. SCIRP serves the worldwide academic communities and contributes to the progress and application of science with its publication.

Other selected journals from SCIRP are listed as below. Submit your manuscript to us via either submit@scirp.org or Online Submission Portal.

